

TRANSPORTATION RESEARCH
RECORD

No. 1388

*Pavement Design, Management,
and Performance*

**Rigid and Flexible
Pavement Design and
Rehabilitation**

A peer-reviewed publication of the Transportation Research Board

**TRANSPORTATION RESEARCH BOARD
NATIONAL RESEARCH COUNCIL**

NATIONAL ACADEMY PRESS
WASHINGTON, D.C. 1993

Transportation Research Record 1388
Price: \$45.00

Subscriber Category
IIB pavement design, management, and performance

TRB Publications Staff
Director of Reports and Editorial Services: Nancy A. Ackerman
Senior Editor: Naomi C. Kassabian
Associate Editor: Alison G. Tobias
Assistant Editors: Luanne Crayton, Norman Solomon,
Susan E. G. Brown
Graphics Specialist: Terri Wayne
Office Manager: Phyllis D. Barber
Senior Production Assistant: Betty L. Hawkins

Printed in the United States of America

Library of Congress Cataloging-in-Publication Data
National Research Council. Transportation Research Board.

Rigid and flexible pavement design and rehabilitation: a peer-reviewed publication of the Transportation Research Board/Transportation Research Board, National Research Council.
p. cm.—(Transportation research record ISSN 0361-1981; no. 1388)

ISBN 0-309-05457-5

1. Pavements—Design and construction. 2. Pavements—Maintenance and repair. I. National Research Council (U.S.). Transportation Research Board. II. Series: Transportation research record; 1388.

TE7.H5 no. 1388

[TE251]

388 s—dc20

[627.8]

93-9033
CIP

Sponsorship of Transportation Research Record 1388

GROUP 2—DESIGN AND CONSTRUCTION OF TRANSPORTATION FACILITIES

Chairman: Charles T. Edson, Greenman Pederson

Pavement Management Section

Chairman: Joe P. Mahoney, University of Washington

Committee on Rigid Pavement Design

Chairman: Gary Wayne Sharpe, Kentucky Transportation Cabinet
Don R. Alexander, Brian T. Bock, Larry J. Butler, Kathleen Theresa Hall, Ira J. Huddleston, John E. Hunt, Anastasios M. Ioannides, Walter P. Kilareski, Starr D. Kohn, Roger M. Larson, Jo A. Lary, Brian R. McWaters, Theodore L. Neff, William Albert Nokes, Mauricio R. Poblete, Robert J. Risser, Jr., Mark B. Snyder, Shiraz D. Tayabji, Mang Tia, John P. Zaniewski, Terrence L. Zoller, Dan G. Zollinger

Committee on Flexible Pavement Design

Chairman: Newton Jackson, Washington State Department of Transportation

Secretary: Stephen B. Seeds, Nichols Consulting Engineers
Douglas I. Anderson, Uno Arebratt, Chris A. Bell, Jacques Bonnot, Elton R. Brown, James L. Brown, Stephen F. Brown, Albert J. Bush III, George R. Cochran, N. F. Coetzee, Raymond A. Forsyth, C. R. Freeme, W. Charles Greer, Jr., Jerry J. Hajek, John P. Hallin, W. N. Lofroos, Kenneth H. McGhee, Carl L. Monismith, William Albert Nokes, Cesar A. V. Queiroz, Lufi Raad, John L. Rice, Cheryl A. Richter, Peter Sebaaly, Gary Wayne Sharpe, Marshall R. Thompson

Committee on Pavement Rehabilitation

Chairman: David E. Newcomb, University of Minnesota

Secretary: Roger C. Olson, Minnesota Department of Transportation

Paul Autret, Michael C. Belangie, Thomas L. Boswell, James L. Brown, Martin L. Cawley, Denis E. Donnelly, Wade L. Gramling, Kathleen Theresa Hall, Joseph B. Hannon, Don M. Harriott, Ira J. Huddleston, Thomas J. Kazmierowski, Walter P. Kilareski, Aramis Lopez, Jr., Joe P. Mahoney, Richard W. May, William G. Miley, Louis G. O'Brien, Gary Wayne Sharpe, James F. Shook, Eugene L. Skok, R. N. Stubstad, Shiraz D. Tayabji, Robert L. White

Daniel W. Dearasaugh, Jr., Transportation Research Board staff

Sponsorship is indicated by a footnote at the end of each paper. The organizational units, officers, and members are as of December 31, 1992.

Transportation Research Record 1388

Contents

Foreword	vii
Performance of Interlocking Concrete Pavements in North America <i>Gonzalo R. Rada, Peter J. Stephanos, and Shiraz D. Tayabji</i>	1
Rigid Pavement Design for Ports in Chile <i>Jacob Greenstein and Chaim J. Poran</i>	11
Maximum Bearing Stress of Concrete in Doweled Portland Cement Concrete Pavements <i>Hua Guo, Thomas J. Pasko, Jr., and Mark B. Snyder</i> DISCUSSION, A. M. Ioannides, 26 AUTHORS' CLOSURE, 27	19
Comparison of Four Different Methods for Measuring Deflections in Jointed Reinforced Concrete Pavements <i>Andrew Bodocsi, Issam A. Minkarah, Charles S. Young, Richard A. Miller, and Rajagopal S. Arudi</i>	29
Effects of Temperature on Early Crack Formation in Portland Cement Concrete Pavements <i>Yeou-Shang Jenq, Chwen-Jang Liaw, and Sang-Chel Kim</i>	35
Load Equivalency Concepts: A Mechanistic Reappraisal <i>Anastasios M. Ioannides and Lev Khazanovich</i>	42
Examination of Pure Environmental Effects on Pavement Condition <i>Turki I. Al-Suleiman, Adnan A. Basma, and Khaled Ksaibati</i>	52
Use of a Three-Dimensional, Dynamic Finite Element Program for Analysis of Flexible Pavement <i>Sameh Zaghoul and Thomas White</i>	60

Estimation of Axle Loads of Heavy Vehicles for Pavement Studies <i>T. F. Fwa, B. W. Ang, H. S. Toh, and T. N. Goh</i>	70
Analytical and Experimental Investigations of Operating Mechanisms in Reinforced Asphalt Pavements <i>Hozayen Hozayen, M. Gervais, A. O. Abd El Halim, and R. Haas</i>	80
Development of Strategic Highway Research Program Long-Term Pavement Performance Climatic Data Base <i>S. D. Rabinow, G. R. Rada, S. D. Tayabji, and C. A. Richter</i>	88
Remaining Fatigue Life Analysis: Comparison Between Dense-Graded Conventional Asphalt Concrete and Gap-Graded Asphalt-Rubber Hot Mix <i>Lutfi Raad, Stephan Saboundjian, and John Corcoran</i>	97
Theoretical Analysis of the Effects of Wide-Base Tires on Flexible Pavements Using CIRCLY <i>Dario Perdomo and Bill Nokes</i>	108
Development and Implementation of a Mechanistic, Empirically Based Overlay Design Procedure for Flexible Pavements <i>Linda M. Pierce, Newton C. Jackson, and Joe P. Mahoney</i>	120
Performance Monitoring of Joint Load Transfer Restoration <i>Kathleen T. Hall, Michael I. Darter, and Jamshid M. Armaghani</i>	129
Major Factors Explaining Performance Variability of Seal Coat Pavement Rehabilitation Overlays <i>Mohamed-Asem U. Abdul-Malak, D. W. Fowler, and A. H. Meyer</i>	140
Application of Cracking and Sealing and Use of Fibers To Control Reflective Cracking <i>Yi Jiang and Rebecca S. McDaniel</i>	150

Analysis of Crack Resistance of Asphalt Concrete Overlays—A Fracture Mechanics Approach	160
<i>Yeou-Shang Jenq, Chwen-Jang Liaw, and Pei Liu</i>	
Analytical Considerations for Thin Concrete Overlays on Asphalt	167
<i>James W. Mack, Lawrence W. Cole, and J. P. Mohsen</i>	
Breaking and Seating of Concrete Pavements: Kentucky's Experience	174
<i>R. Clark Graves, David L. Allen, and Gary W. Sharpe</i>	
Direct Tension and Simple Stiffness Tests—Tools for the Fatigue Design of Asphalt Concrete Layers	182
<i>James M. Matthews and Carl L. Monismith</i>	
Rehabilitation Procedures for Faulted Rigid Pavement	200
<i>Luis Julian Bendaña and Wei-Shih Yang</i>	



Foreword

TRB Committees on Rigid Pavement Design, Flexible Pavement Design, and Pavement Rehabilitation sponsored four sessions dealing with pavement design and rehabilitation during the 1993 Annual Meeting. The first six papers in this Record were presented in a session entitled Rigid Pavement Design. Rada et al. discuss the performance of concrete pavements constructed of interlocking concrete blocks, or pavers. Greenstein and Poran present rigid pavement design concepts for ports in an area of Chile that is subject to high seismic risk. Guo et al. use a component model recently developed to challenge the current computational methods used to predict the maximum bearing stress of concrete under the critical dowel. Bodocsi et al. compared deflection data in jointed reinforced concrete pavements measured with the linear voltage displacement transducer, the geophone, the falling weight deflectometer, and the Dynaflect. Jenq et al. look at the formation of cracks in the early life of portland cement (PC) concrete pavements and show that peak temperature differentials play an important role. Ioannides and Khazanovich take a look from a mechanistic point of view at the concepts of equivalent single-axle load, equivalent single-wheel load, and equivalent single-axle radius.

The following six papers were presented in a session entitled Flexible Pavement Design. Al-Suleiman et al. examine pavement deterioration caused purely by environmental effects. Zaghoul and White analyze flexible pavement with ABAQUS, a three-dimensional, dynamic finite element program. Fwa et al. present a statistical approach to estimate and characterize axle loads of heavy vehicles for pavement design and performance analysis. Hozayen et al. analyze the operating mechanisms of flexible pavements reinforced with grids. Rabinow et al. summarize the development of the Long-Term Pavement Performance climatic data base developed under the Strategic Highway Research Program. Raad et al. compare conventional dense-graded asphalt concrete versus gap-graded asphalt rubber hot mix using remaining fatigue life analysis. Perdomo and Nokes describe their analysis of how wide-base tires affect flexible pavements.

The next seven papers were presented at a session entitled Pavement Rehabilitation. Pierce et al. discuss the Washington State Department of Transportation's development and implementation of a mechanistic, empirically based overlay design procedure for flexible pavements. Hall et al. describe and present performance data on a major experiment in restoration of joint load transfer on I-10 in Florida. Abdul-Malak et al. explain the variability in performance of seal coats by experimenting with various causal factors. Jiang and McDaniel present a study on two methods of mitigating reflective cracking in asphalt overlays of rigid pavements: cracking and seating prior to overlay and fiber reinforcement in the overlay mixture. Jenq et al. use fracture mechanics theory to analyze crack resistance of asphalt overlays. Mack et al. present an analytical study to account for the performance of an experimental, very thin PC concrete overlay of an asphalt pavement. Graves et al. describe Kentucky's experience with breaking and seating of PC concrete pavements.

The final two papers in this Record stem from presentations at the 1992 TRB Annual Meeting. Matthews and Monismith present a design strategy for asphalt concrete layers using results of the direct tension and simple stiffness tests. Bendaña and Yang describe an 8-year study of rehabilitating faulted rigid pavements along I-84 in New York State.



Performance of Interlocking Concrete Pavements in North America

GONZALO R. RADA, PETER J. STEPHANOS, AND SHIRAZ D. TAYABJI

When compared with use in other parts of the world, the use of interlocking concrete pavements in North America is a rather new development. As a result, little information about their performance is available to verify or calibrate existing design methods or develop new ones. Toward overcoming this limitation, the performance of interlocking concrete pavements at three sites was evaluated. Record searches along with field investigations—deflection testing, visual condition surveys, and transverse profile surveys—were conducted as part of this effort. A brief description of each site is provided and the field and office data obtained, along with the interpretation of these data, are summarized. Particular emphasis is placed on the performance of these pavements in terms of structural capacity, distresses, and rut depths. However, other performance considerations for interlocking concrete pavements are also discussed.

The concept of tightly fitted paving units or pavers set on a flexible granular base is as old as the roads of the Roman Empire. The modern version, interlocking concrete pavements, originated in The Netherlands in the late 1940s as a replacement for clay brick streets. This technology quickly spread to Germany and Western Europe as a practical and attractive method useful for both pedestrian and vehicular pavement. Concrete pavers were introduced in the United States in the mid-1970s and have been successfully used in many pavement applications. To date, over 100 million m² of interlocking concrete pavements has been placed in this country, at an average cost of \$9 to \$18/m² (pavers only).

A typical pavement cross section is shown in Figure 1a. In this pavement structure, both the base and subbase are composed of unbound granular material. Granular base and subbase layers stabilized with asphalt or cement also can be used, as shown in Figure 1b. Restraints are required along the edges of interlocking concrete pavements to prevent the outward migration of blocks from the force of traffic, which would result in the opening of joints and loss of interlock between the paver blocks. These restraints can be developed from any construction that prevents the lateral movement of the blocks along the periphery of the paved area.

Typical block laying patterns are illustrated in Figure 2. Regardless of the pattern used, concrete pavers are first placed, mechanically or manually, on a bedding sand layer and vibrated with a high-frequency plate vibrator. Sand is then spread and swept into the joints and the pavers are again vibrated until the joints are full of sand so that the interlocking of blocks (full shear transfer), so critical to the performance of interlocking concrete pavements, is obtained.

Research studies have shown that the load distribution and failure modes of an interlocking concrete pavement are very similar to those of any other flexible pavement system (i.e., the main failure mode is increasing roughness due to repetitive shear deformations). Understandably, most existing interlocking concrete pavement design methods rely on modified flexible (or asphaltic concrete) pavement design procedures.

Because the use of concrete pavers in pavement construction is a rather new development in North America, little information about their performance is presently available to verify or calibrate existing design methods or to develop new ones. Toward overcoming this limitation, a study was undertaken to document the performance of streets in North America constructed with concrete pavers.

Three projects were selected for use in this study—Main Street in North Bay, Ontario; Third, Pine, and Cedar Streets in Timmins, Ontario; and Hay Street in Fayetteville, North Carolina. At each site, extensive field investigations were conducted to assess the functional and structural condition of the pavements. They included (a) nondestructive deflection testing, (b) visual condition surveys, and (c) transverse profile or rut depth surveys.

The results of the field investigations, coupled with available construction, traffic, and climatic data, served as the basis for this study. First a description of each site and a summary of the field and office data obtained are provided, along with the interpretation of these data. Then other performance considerations for interlocking concrete pavements are discussed. Finally, the major findings and conclusions are presented.

PROJECT SITES

Center City of North Bay, Ontario

The reconstruction of Main Street with an interlocking concrete pavement was part of a complete renovation plan for the North Bay city center. The project covers an area of approximately 150,000 ft² (13,935 m²), including sidewalks, and extends along 3,300 ft (1,006 m) of Main Street (see Figure 3). The first block—Sherbrooke to Wyld—was opened to traffic in late July 1983, but had to be closed because of a substantial number of corner “pop-offs” caused by the wrong gradation of the joint sand. The damaged pavers were replaced, the surface was resanded, and the block was successfully reopened to traffic. The last block—Algonquin to Cassells—was opened to traffic in early November 1983.

A schematic diagram of the pavement cross section and laying pattern is also given in Figure 3. The pavement consists

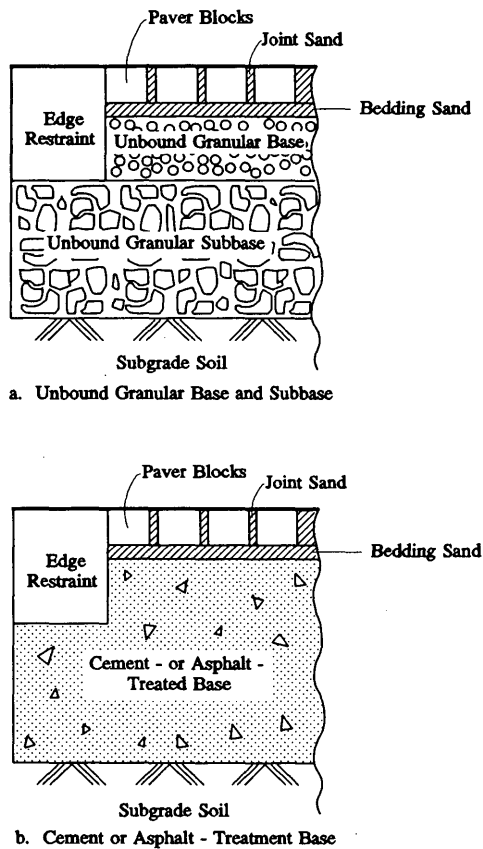


FIGURE 1 Typical interlocking concrete pavement cross sections.

of 3.2-in. (80-mm) concrete pavers over 1.2 in. (30 mm) of bedding sand. Except for the crosswalks, where a stretcher bond pattern was used, the concrete pavers are laid in a herringbone pattern. A 5.9-in. (150-mm) granular base and 7.9-in. (200-mm) granular subbase provide support for the concrete pavers and bedding sand layer. The pavement structure rests on a sandy subgrade, with shattered rock or bedrock at shallow depths. Surface water is directed to a catch basin and storm sewer outlet. Subdrains were not installed in this project because of the free-draining subbase material.

Two-way traffic along Main Street consists of approximately 8,000 vehicles per day, with 13,300 vehicles per day at the intersection of Algonquin and Main Streets. Although no breakdown by weight class is available, traffic includes automobiles, buses, and trucks. It has been estimated from field observations that most of the traffic consists of automobiles, with approximately 4 to 5 percent delivery trucks and buses.

In addition to traffic, the pavements are subjected to very severe weather conditions. Temperatures range from -40°F (-40°C) to 96°F (35°C), with an average daily temperature of 38°F (3°C). North Bay also receives an average of 39 in. (990 mm) of precipitation each year, which consists of both rain and snow.

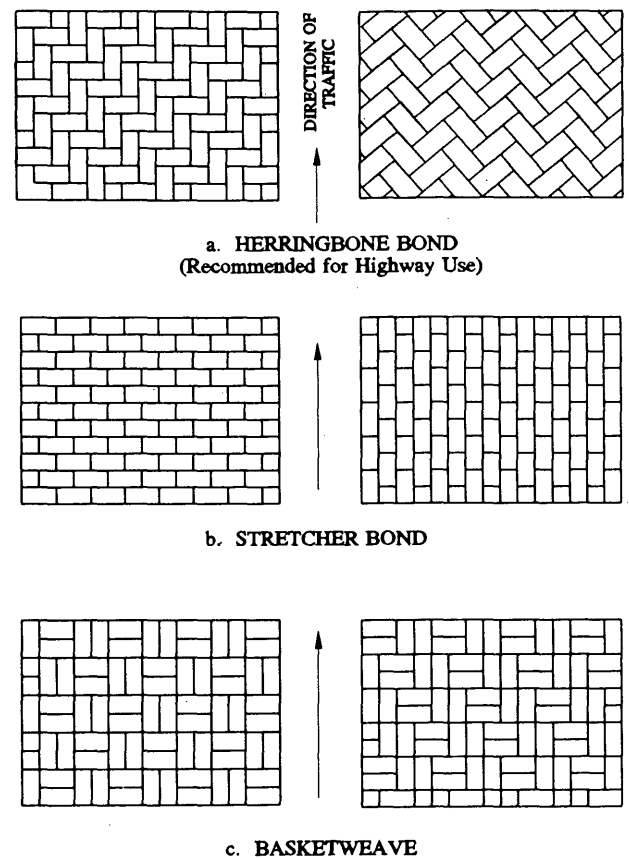


FIGURE 2 Typical block laying patterns.

Center City of Timmins, Ontario

Timmins, a city in the northern reaches of Ontario, underwent a downtown renovation program that utilized over 120,000 ft^2 (11,120 m^2) of pavers. The phased project, beginning in 1984, included the reconstruction of 10 streets in the city center with interlocking concrete pavements. Figure 4 shows the layout of the study area (Third, Cedar, and Pine streets).

The pavements consist of 3.2-in. (80-mm) concrete pavers over a 1.2-in. (30-mm) bedding sand layer. The pavers are laid in a herringbone pattern and are supported by a 5.9-in. (150-mm) gravel base and a granular subgrade. Both the pavement cross section and laying pattern of the pavers are also illustrated in Figure 4. Storm sewers and drains provide an outlet for surface water off the interlocking concrete pavement.

Two-way traffic on Third Street has been estimated to be 6,000 vehicles per day and includes automobiles, buses, and trucks. Although a breakdown by weight class is not available, it is estimated from field observations that most of the traffic consists of automobiles, with approximately 4 to 5 percent buses and delivery trucks.

As at North Bay, the climate at this site is very severe. Temperatures range from -46°F (-43°C) to 100°F (38°C), with an average daily temperature of 34°F (1°C). Timmins

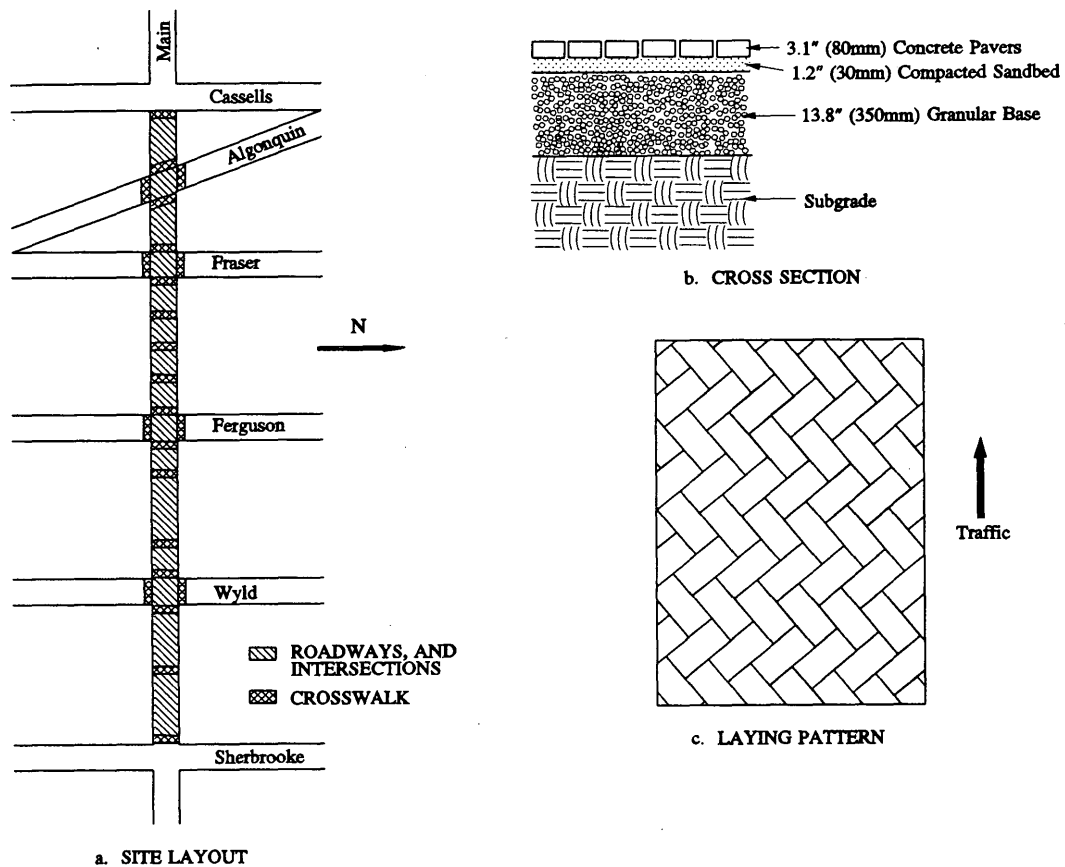


FIGURE 3 Timmins, Ontario: site layout, pavement cross section, and laying pattern.

also receives an average of 34 in. (860 mm) of precipitation each year, which consists of both rain and snow.

Transit Mall in Fayetteville, North Carolina

The Transit Mall in Fayetteville, North Carolina, is located on Hay Street between Ray Avenue and Market House Circle. Hay Street was reconstructed as an interlocking concrete pavement in an effort to revitalize the downtown district. The mall is intended for city bus access to transport citizens to and from the many shops that line Hay Street. The mall is three blocks long, 24 ft (7.3 m) wide, and covers an area of 41,400 ft² (3,850 m²), not including sidewalks (see Figure 5).

The Transit Mall pavements were constructed in summer 1984 and opened to traffic in May 1985. Figure 5 shows the pavement cross section and laying pattern used. The pavement system consists of 3.2-in. (80-mm) concrete paver blocks over 1.5 in. (38 mm) of bedding sand. A 2-in. (51-mm) asphalt concrete layer over 8 in. (200 mm) of unbound granular base provides support for the concrete pavers and bedding sand layer. The top of the subgrade was removed and replaced with select fill during the excavation process because of the discovery of archeological artifacts. Storm sewers and drains provide an outlet for surface water off the interlocking concrete pavement.

The mall is intended for bus access only. Buses typically have a curb weight of 24,680 lb (110 kN) and ride on two axles. Weekly bus schedules result in traffic counts as follows: 348 buses per day during weekdays, 152 buses per day on Saturdays, and no buses on Sundays.

Compared with the climate of the two previous sites, the climate in Fayetteville is considerably milder. Although temperatures range from -29°F (-34°C) to 110°F (43°C), the average daily temperature is 61°F (16°C). The average annual precipitation is 19 in. (480 mm), with very little snowfall.

PERFORMANCE EVALUATION

Pavement Structural Capacity

Several procedures are presently available for use in pavement structural evaluation. They range from destructive procedures such as borings and cores to nondestructive testing methods such as static-creep (e.g., Benkelman beam), steady-state (e.g., Dynaflect), and impulse [falling weight deflectometer (FWD)] deflection devices. In this study, a Dynatest model 8002 FWD device was used to assess the structural capacity of the interlocking concrete pavements. Deflection basin tests were conducted using nominal impulse loads of 5,000 and 9,000 lbf (22 to 40 kN). The response of the pavements to these loads was

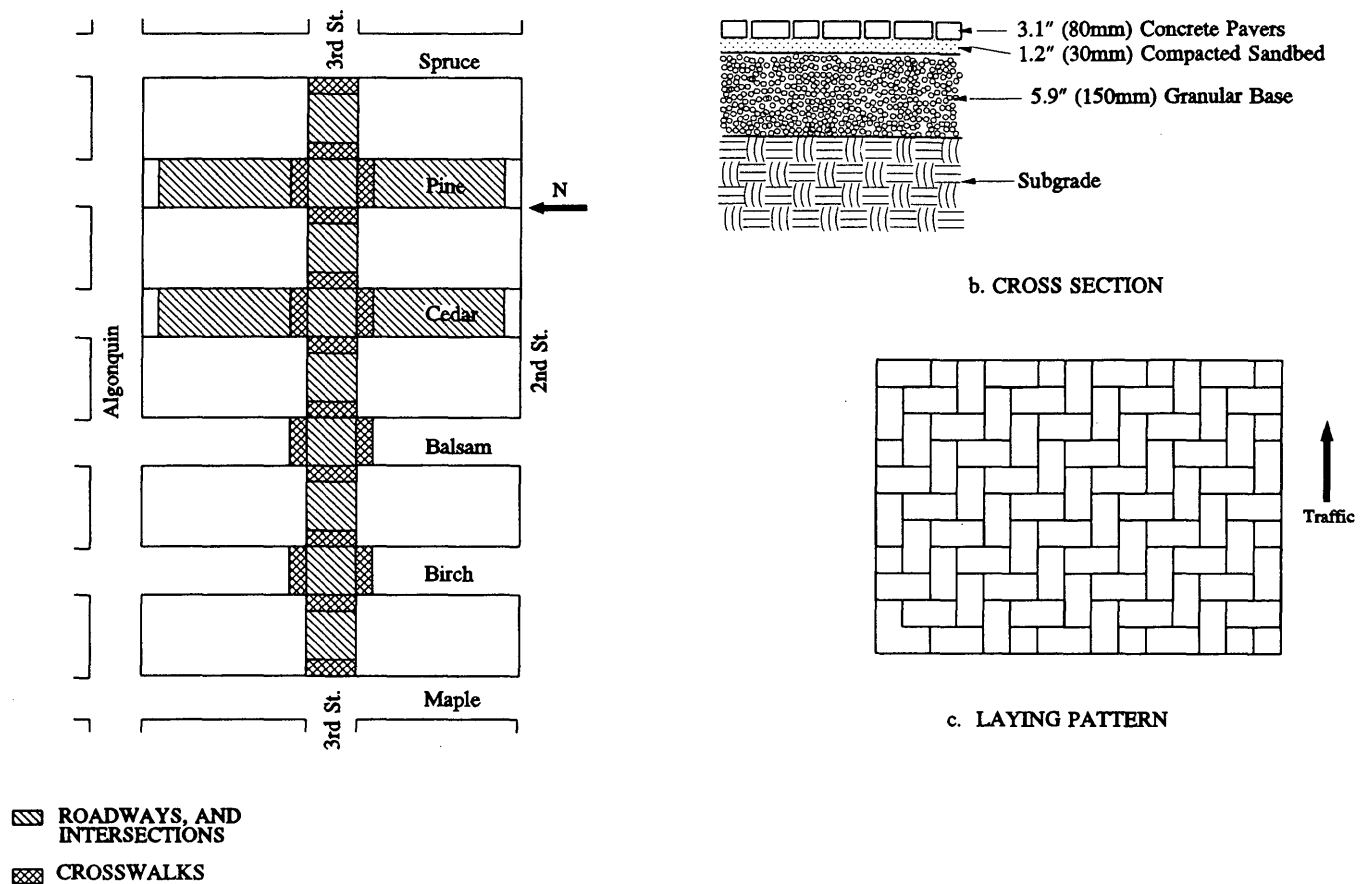


FIGURE 4 Fayetteville, North Carolina: site layout, pavement cross section, and laying pattern.

measured by means of deflection sensors located at 0, 8, 12, 18, 24, 36, and 48 in. (0, 20.3, 30.5, 45.8, 61.0, 91.4, and 121.9 cm) from the load center. A total of 652 deflection tests were performed, 242 in North Bay, 232 in Timmins, and 178 in Fayetteville. Table 1 is a statistical summary of the measured deflections at each site.

To analyze the measured deflections, a multilayer elastic solution was used because of its simplicity and general acceptance [finite element methods produce a better fit, but their complexity is a major limitation (1)]; both paver blocks and bedding sand are modeled as a composite layer. In particular, in situ pavement layer moduli were backcalculated using a program called MODULUS (2). The MODULUS program, developed by the Texas Transportation Institute, utilizes a forward calculation scheme, WESLEA [elastic solution (3)], to build a deflection basin data base for a given pavement. A pattern search technique is then used to determine the set of layer moduli that best fits the measured basin.

The North Bay and Timmins pavements were modeled as three-layer structures: a composite layer of concrete pavers and bedding sand surface, a layer of unbound granular base, and the subgrade soil. In the evaluation of the Fayetteville pavements, a two-layer structure was used because preliminary analysis of the deflection data yielded very similar moduli for both the base and subgrade layers. No attempt to backcalculate the modulus of the thin asphalt concrete layer below

the bedding sand was made because current technology is not sufficiently advanced to accurately and consistently do otherwise.

The results of the moduli backcalculation analysis are summarized in Table 2. These results have been grouped into three major categories—roadways, intersections, and others (parking lanes, sidewalks, bus stops)—on the basis of traffic. In the case of the Transit Mall in Fayetteville, North Carolina, the moduli backcalculated at the intersections have been grouped with those corresponding to the roadways, because cut-through traffic across the Hay Street intersections is not allowed. Table 2 also shows the layer moduli obtained for asphaltic concrete pavements adjacent to the project sites.

Several major conclusions can be drawn from the results presented in Table 2. First, there is a clear relationship between the amount of traffic the interlocking concrete pavement receives and the modulus of the composite paver blocks and bedding sand layer. In all cases, the modulus of this composite layer decreases as one goes from the high (“intersections”) to the low (“other”) traffic areas; average modulus values range from 420 to 560 ksi for the intersections; 300 to 377 ksi (2067 to 2598 MPa) for the roadways; and 118 to 207 ksi (813 to 1426 MPa) for the low traffic areas.

This finding is consistent with the results from other similar studies found in the literature. Modulus values for the composite paver and sand layer, developed by researchers in sev-

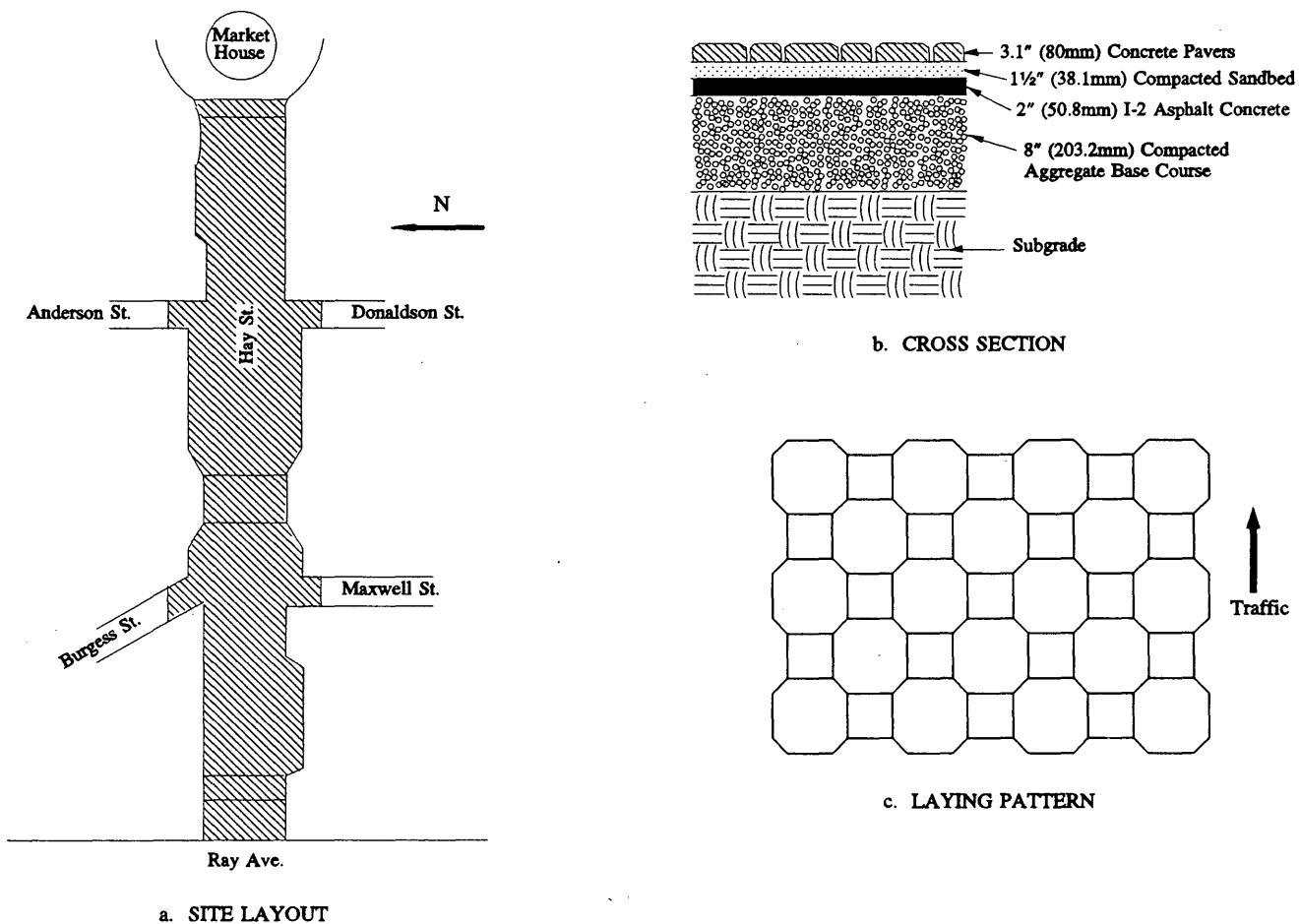


FIGURE 5 North Bay, Ontario: site layout, pavement cross section, and laying pattern.

eral countries, are summarized below (1 ksi = 6.89 MPa):

Country	Modulus (ksi)	Reference
United Kingdom	130.5 290.0	(7)
Japan	243.9 627.9	(13)
New Zealand	60.2	(15)
Australia	50.8 464.0	(11)
Netherlands	92.7 402.1	(10)
United States	450.0	(14)

Although a wide range of values is reported, it is apparent that initial modulus values are significantly lower than those measured after many traffic repetitions, revealing a time/traffic dependence of the layer strength. Thus, the paver blocks initially act as individual units and gradually lock together and share the load.

Although the concept of progressive stiffening is widely accepted, significant differences exist in the literature as to when full lock-up of the pavers occurs (4). Values generally ranging from 5,000 to 100,000 equivalent 18-kip (80-kN) axle

loads (EALs), but as high as 1,000,000 EALs, have been suggested. For the sites investigated, the number of EALs since construction was determined on the basis of field estimates and information provided by the responsible agencies to be in the 100,000 to 120,000 range (i.e., very similar for all three sites). This similarity, coupled with the fact that data from earlier years are not available, prohibited the authors from shedding further light on this issue.

A comparison of the values presented in Table 2 and those from other researchers also reveals that there is excellent agreement between the composite moduli derived in this study [118 to 560 ksi (813 to 3858 MPa)] and those found in the literature [50 to 628 ksi (345 to 4327 MPa)]. Because the use of interlocking concrete pavements in North America is a relatively new development when compared with countries such as The Netherlands and Australia, where they have been used for several decades, these results are encouraging.

Table 2 also shows that the moduli of the composite block and sand layer are similar to those of asphalt concrete (AC). This is particularly true for the high traffic areas (intersections), where in all likelihood full lock-up has already occurred. Modulus values range from 420 to 560 ksi (2894 to 3858 MPa) for the pavers and sand layer versus 408 to 568 ksi (2811 to 3914 MPa) for the AC layer. More importantly,

TABLE 1 Measured Deflections

Project Site	Pavement Category	Number of Points	Parameter	Sensor						
				r=0"	r=8"	r=12"	r=18"	r=24"	r=36"	r=48"
North Bay	Roadways	95	Average (mils)	15.44	11.45	8.68	5.70	4.19	2.82	2.08
			Std. Dev. (mils)	2.13	1.43	1.11	0.96	0.83	0.65	0.52
			C.O.V. (%)	13.79	12.49	12.74	16.91	19.69	23.24	25.07
	Intersections	14	Average (mils)	14.93	11.16	8.60	5.86	4.28	2.81	2.05
			Std. Dev. (mils)	1.60	1.68	1.56	1.36	1.11	0.79	0.58
			C.O.V. (%)	10.69	15.03	18.13	23.17	25.98	28.27	28.10
	Others	6	Average (mils)	49.00	34.38	21.80	12.02	8.23	5.08	3.52
			Std. Dev. (mils)	18.30	12.64	9.19	4.71	3.09	1.46	0.87
			C.O.V. (%)	37.35	36.76	42.14	39.17	37.47	28.79	24.82
	AC Pavements	6	Average (mils)	7.77	6.17	5.10	3.72	2.83	1.73	1.18
			Std. Dev. (mils)	0.93	0.71	0.60	0.48	0.39	0.27	0.22
			C.O.V. (%)	11.93	11.59	11.70	12.89	13.88	15.34	18.83
Timmins	Roadways	89	Average (mils)	15.62	11.73	8.97	6.20	4.78	3.29	2.49
			Std. Dev. (mils)	1.93	1.58	1.25	0.94	0.77	0.54	0.41
			C.O.V. (%)	12.38	13.49	13.90	15.22	16.04	16.52	16.31
	Intersections	24	Average (mils)	15.57	11.78	9.14	6.28	4.80	3.33	2.50
			Std. Dev. (mils)	1.91	1.55	1.25	0.94	0.73	0.54	0.46
			C.O.V. (%)	12.29	13.13	13.66	14.96	15.10	16.17	18.41
	AC Pavements	3	Average (mils)	19.10	15.50	13.70	11.37	9.17	6.40	4.20
			Std. Dev. (mils)	6.76	4.52	3.44	2.16	1.17	0.53	0.17
			C.O.V. (%)	35.40	29.17	25.11	18.98	12.74	8.27	4.12
Fayetteville	Roadways	44	Average (mils)	19.23	13.89	9.88	5.95	4.05	2.67	2.00
			Std. Dev. (mils)	3.18	2.12	1.48	0.82	0.52	0.30	0.24
			C.O.V. (%)	16.53	15.27	14.97	13.74	12.77	11.06	12.03
	Others	36	Average (mils)	20.49	14.24	9.58	5.68	4.00	2.73	2.05
			Std. Dev. (mils)	2.59	2.07	1.62	0.73	0.47	0.32	0.25
			C.O.V. (%)	12.66	14.56	16.96	12.89	11.65	11.67	11.99
	AC Pavements	5	Average (mils)	16.68	13.10	10.88	8.28	6.16	3.76	2.62
			Std. Dev. (mils)	2.09	1.93	1.40	0.89	0.61	0.38	0.29
			C.O.V. (%)	12.55	14.72	12.86	10.71	9.85	10.06	11.26

Notes: (1) 1 inch = 25.4 mm; 1 mil = 25.4 micron
 (2) Deflections shown correspond to a 9,000 lb. load, measurements were also taken at a nominal 5,000 lb. load but are not shown here.

TABLE 2 Backcalculated Layer Moduli

Project Site	Pavement Category	Number of Points	Layer Type	Layer Thickness (in.)	Layer Modulus		
					Mean (ksi)	Std. Dev. (ksi)	C.V. (%)
North Bay	Roadways	190	Pavers/Sand	4.3	377.0	164.3	44.2
			Granular Base	13.8	39.5	10.7	27.7
			Subgrade	Variable	14.9	4.6	30.6
	Intersections	28	Pavers/Sand	4.3	559.9	191.9	35.0
			Granular Base	13.8	28.7	7.1	24.7
			Subgrade	Variable	17.9	2.6	14.2
	Others	12	Pavers/Sand	4.3	118.3	18.5	11.8
			Granular Base	13.8	14.5	1.8	13.6
			Subgrade	Variable	7.8	4.6	45.4
	AC Pavements	12	Asph. Conc. (*)	5.5	567.8	184.5	31.8
			Granular Base	14.8	34.3	4.6	14.0
			Subgrade	Variable	13.8	2.1	15.3
Timmins	Roadways	178	Pavers/Sand	4.3	300.3	103.4	35.0
			Granular Base	5.9	86.3	23.6	30.3
			Subgrade	Variable	17.7	3.1	17.9
	Intersections	48	Pavers/Sand	4.3	420.6	147.8	35.7
			Granular Base	5.9	64.2	25.9	43.6
			Subgrade	Variable	19.1	3.9	20.1
	AC Pavements	6	Asph. Conc. (*)	3.5	566.0	233.0	39.0
			Granular Base	6.0	91.9	39.8	43.3
			Subgrade	Variable	9.5	0.6	6.1
Fayetteville	Roadways	88	Pavers/Sand	4.6	344.5	124.4	35.1
			Base/Subgrade	Variable	12.5	1.7	13.7
	Others	72	Pavers/Sand	4.6	206.6	68.0	30.2
			Base/Subgrade	Variable	12.1	2.0	15.2
	AC Pavements	10	Asph. Conc. (*)	5.0	408.0	151.0	37.0
			Granular Base	8.0	42.6	26.7	62.6
Subgrade	Variable	11.1	1.3	11.1			

Notes: (1) 1 inch = 25.4 mm; 1 ksi = 6.89 MPa
 (2) Modulus of this layer has not been temperature corrected as surface gradient temperature data were not available

this finding illustrates that the load distribution of interlocking concrete pavements is similar to that of flexible pavements.

Pavement Distress

Because not all pavement distress is traceable to structural mechanisms, accurate condition surveys that assess a pavement's physical distress are vital to the performance evaluation effort. Condition survey results not only provide a measure of pavement condition, but also assist in defining probable causes of the distress. To accomplish this, however, the condition survey must provide for certain minimum information requirements: (a) identification of the distress types existing in the pavement, (b) measure of the severity level for each distress type present, and (c) measure of area affected by each combination of distress type and severity.

Because interlocking concrete pavements are a relatively new development, a well-established and generally accepted procedure for carrying out visual distress surveys does not presently exist. In view of this, information regarding distress types and their measurement was extracted from various sources in the literature to develop an interim condition survey procedure. The primary sources of information were Shahin and Kohn (5) and a Dutch Study (6), as well as unpublished information provided by the Concrete Paver Institute. Table 3 shows the final list of distress types selected for interlocking concrete pavement evaluation along with their units of measure and possible severity levels.

Sampling plans for evaluation of the interlocking concrete pavements under investigation were then developed. The pavements were first subdivided into sample units according to area [2,400 ft² (223 m²) per sample unit]. Individual sample units were then selected at random for use in the field surveys—24 sample units covering 57,600 ft² (5351 m²) in North Bay, 18 sample units covering 43,200 ft² (4013 m²) in Timmins, and 12 sample units covering 27,120 ft² (2520 m²) in Fayetteville (in all cases, the sample unit coverage exceeded 50 percent of the total pavement area). Finally, for each sample unit selected, the pavement distress types present as well as their severity and extent were determined. Table 4 summarizes the results of these visual condition surveys on a site-by-site basis. From these data, the following observations were made.

The predominant pavement distress types at North Bay are depressions and corner or edge spalling of the blocks. Depressions were found over 4.17 percent of the area surveyed, but this is somewhat misleading because they are very localized; all occur within one sample unit. Furthermore, these depressions are over an area where excavation of the pavement surface was necessary to gain access to underground utilities, and the subsequent pavement repairs were carried out with less than satisfactory results. Corner and edge spalling of the blocks was found to be a problem in 3.59 percent of the area surveyed. It appears that two factors are contributing to this distress: (a) inferior-quality pavers supplied by one of the manufacturers, as evidenced by their frequent replacement over the last 5 years, and (b) a combination of harsh winter conditions and snow removal operations.

At Timmins, the predominant pavement distress types are snowplow damage and block spalling, which were found over 18.82 and 2.82 percent of the area surveyed. Snowplow damage refers to scratch marks on the surface of the paver blocks resulting from snow removal operations using plows. Block spalling appears to be related to the same two factors as in North Bay, that is, quality of some of the pavers as well as winter conditions and snow removal operations.

In the case of the Fayetteville interlocking concrete pavements, the predominant distress types are surface staining, swell/heave, and depressions. These distresses were found over 3.02, 2.95, and 1.25 percent of the area surveyed, respectively. The first distress type is primarily associated with oil spillage from buses, which account for most of the traffic at this site. The other two distress types—swell/heave and depression—are of low severity and are likely caused by a combination of bus loadings and wet soil. Furthermore, the swell and heave distress is very localized (i.e., within one sample unit). In this area a water main broke, requiring removal and replacement of the paver blocks.

Overall, it was concluded that with the exception of localized areas, the interlocking concrete pavements at the three North American sites are providing excellent performance. After 6 to 8 years, the pavements are still in very good to excellent condition. If localized distresses are not included in the analysis, surface deformation, which is the primary failure mode in interlocking concrete pavements, occurs in less than

TABLE 3 Interlocking Concrete Pavement Distress Types

Distress Type	Unit of Measure	Severity Levels
Surface Irregularities:		
Rutting	square feet	Low, Medium, High
Swell and Heave	square feet	Low, Medium, High
Depression	square feet	Low, Medium, High
Transition to Utility	square feet	Low, Medium, High
Transition to Curb	square feet	Low, Medium, High
Block Distress:		
Corner or Edge Spalling	percent	Low, Medium, High
Cracked Blocks	percent	Low, Medium, High
Polished Aggregate	square feet	not applicable
Stained or Contaminated Surface	square feet	not applicable
Horizontal Creeping	square feet	Low, Medium, High
Joint Distress:		
Deformed Joint (Joint Width)	square feet	Low, Medium, High
Loss of Sand in Joint	square feet	Low, Medium, High
Miscellaneous:		
Snow Plow Damage	square feet	not applicable
Others	not applicable	not applicable

Note: 1 square foot = 0.09 square meter

TABLE 4 Visual Distress Survey Results

A. North Bay (Area surveyed: 57,600 s.f.)							
Distress Type	Severity Level			Density (%)			Total Dens. (%)
	Low	Medium	High	Low	Medium	High	
Surface Irregularities							
Rutting (s.f.)	---	---	---	---	---	---	---
Swell/Heave (s.f.)	---	---	---	---	---	---	---
Depression (s.f.)(**)	---	2400	---	---	4.17%	---	4.17%
Transition to Utility (s.f.)	25	15	---	0.04%	0.03%	---	0.07%
Transition to Curb (s.f.)	50	---	---	0.09%	---	---	0.09%
Block Distress							
Corner or Edge Spalling (%)	3.47%	0.12%	---	3.47%	0.12%	---	3.59%
Cracked Blocks (%)	0.12%	---	---	0.12%	---	---	0.12%
Stained Surface (s.f.)(*)	---	---	---	---	---	---	---
Joint Distress							
Deformed Joints (s.f.)	40	---	---	0.07%	---	---	0.07%
Miscellaneous							
Snow Plow Damage (s.f.)	---	---	---	---	---	---	---
B. Timmins (Area Surveyed: 43,200 s.f.)							
Distress Type	Severity Level			Density (%)			Total Dens. (%)
	Low	Medium	High	Low	Medium	High	
Surface Irregularities							
Rutting (s.f.)	---	270	---	---	0.63%	---	0.63%
Swell/Heave (s.f.)	---	160	---	---	0.37%	---	0.37%
Depression (s.f.)	---	---	---	---	---	---	---
Transition to Utility (s.f.)	---	---	---	---	---	---	---
Transition to Curb (s.f.)	---	4	---	---	0.01%	---	0.01%
Block Distress							
Corner or Edge Spalling (%)	2.61%	0.21%	---	2.61%	0.21%	---	2.82%
Cracked Blocks (%)	0.27%	0.04%	---	0.27%	0.04%	---	0.31%
Stained Surface (s.f.)(*)	---	---	---	---	---	---	---
Joint Distress							
Deformed Joints (s.f.)	---	---	---	---	---	---	---
Miscellaneous							
Snow Plow Damage (s.f.)	7990	140	---	####	0.32%	---	18.82%
C. Fayetteville (Area surveyed: 27,120 s.f.)							
Distress Type	Severity Level			Density (%)			Total Dens. (%)
	Low	Medium	High	Low	Medium	High	
Surface Irregularities							
Rutting (s.f.)	---	---	---	---	---	---	---
Swell/Heave (s.f.) (**)	800	---	---	2.95%	---	---	2.95%
Depression (s.f.)	200	140	---	0.74%	0.52%	---	1.25%
Transition to Utility (s.f.)	34	22	---	0.13%	0.08%	---	0.21%
Transition to Curb (s.f.)	---	6	---	---	0.02%	---	0.02%
Block Distress							
Corner or Edge Spalling (%)	<0.01%	---	---	<0.01%	---	---	<0.01%
Cracked Blocks (%)	---	---	---	---	---	---	---
Stained Surface (s.f.)(*)	820	---	---	3.02%	---	---	3.02%
Joint Distress							
Deformed Joints (s.f.)	60	---	---	0.22%	---	---	0.22%
Miscellaneous							
Snow Plow Damage (s.f.)	---	---	---	---	---	---	---

Note: 1 square foot (s.f.) = 0.09 square meter

(*) No severity level associated with this distress type

(**) Only identified in one sample unit

1.5 percent of the pavement areas surveyed (see Table 4). Besides localized pavement deformations, distresses associated with individual paver blocks are the next major problem at the sites. This problem is largely one of aesthetics and can be easily resolved by the replacement of the affected blocks (3 to 4 percent by total area at each site).

Pavement Rut Depths

The primary failure mode in interlocking concrete pavements is increasing roughness as a result of repetitive shear deformations. The results of the visual condition surveys provided some insight about the extent and severity of this distress type,

but not an accurate measurement of their magnitude. Accordingly, transverse profile surveys were conducted at multiple locations within each site to determine rut depths.

A Dipstick Auto-Read Profiler was used in this effort. This device measures the relative elevation of two points that are 1 ft (0.30 m) apart. Measurements were taken at 1-ft intervals from the edge of the pavement to the centerline. From these data, rut depths were determined using commercially available software and an assumed 6-ft (1.83-m) straight edge. Table 5 summarizes the results of the rut depth analysis. The following observations were made from these data.

At all three sites, rut depths in the right wheelpath are larger than those in the left wheelpath. These differences are

TABLE 5 Rut Depth Measurements

Project Site	Number of Lines	Statistic	Rut Depth Measurements (inches)		
			Wheel Path:		
			Left	Right	Average
North Bay	21	Mean	0.210	0.230	0.220
		Std. Dev.	0.176	0.148	0.118
		Minimum	0.047	0.010	0.061
		Maximum	0.927	0.662	0.569
Timmins	18	Mean	0.242	0.426	0.334
		Std. Dev.	0.145	0.162	0.142
		Minimum	0.000	0.014	0.007
		Maximum	0.449	0.706	0.551
Fayetteville	22	Mean	0.090	0.133	0.112
		Std. Dev.	0.062	0.072	0.048
		Minimum	0.014	0.008	0.034
		Maximum	0.253	0.313	0.208

Note: 1 inch = 25.4 mm

small for the North Bay and Fayetteville pavements but quite significant in Timmins: 0.20 in. (5.1 mm) on average. It is hypothesized that these differences are caused by the lower degree of block confinement, and hence lock-up, achieved at the pavement edge (right wheelpath) during the construction process (i.e., related to the construction of the edge restraints as well as the placement and vibration of the pavers and sand at the pavement edge).

Table 5 also shows large rut depths for the North Bay and Timmins pavements: 0.45 to 0.93 in. (11.4 to 23.5 mm). These large measurements occur in just a few localized areas, which correspond with those few distressed areas identified from the visual condition surveys. For example, the 0.93-in. (23.5-mm) reading in North Bay was taken in the repair area alluded to earlier.

Overall, however, the results in Table 5 clearly indicate the excellent performance of the interlocking concrete pavements. After 6 to 8 years in service, average pavement rut depths range from 0.11 in. (2.8 mm) in Fayetteville to 0.22 in. (5.6 mm) in North Bay and 0.33 in. (8.5 mm) in Timmins. These are well below the 0.50 to 0.75-in. (12.7- to 19.1-mm) level typically considered as a failure by most highway agencies.

OTHER CONSIDERATIONS

Data reported in the literature (1,4,7-19) indicate that the performance of concrete paver pavements depends on the interlocking of the individual units and, to a lesser degree, on the shape and thickness of the block. The interlocking of the paver blocks is in turn influenced by laying pattern and thickness of the bedding sand.

Block shape has more of an effect on the mechanical behavior of concrete blocks (i.e., a uniform cross section will not crack as easily as a variable cross section). Block thickness primarily affects the mechanical behavior, but an increase in thickness also produces an increase in structural capacity. The performance of the herringbone laying pattern is much better than that of the stretcher or basketweave patterns, which tend to creep in the direction of traffic movement and adversely affect the interlocking of the pavers. Also, as thickness of the bedding sand layer decreases, the overall performance improves. Very thin layers [less than 1 in. (25.4 mm) after compaction], however, will not produce the locking-up action

obtained by sand migration upward into the joints during the initial vibration phase in construction.

Because the pavements under investigation were all constructed with 3.2-in. (80-mm) paver blocks and 1.2 to 1.5 in. (30.5 to 38.1 mm) of bedding sand, the impact of these factors on the performance of the pavements could not be assessed. With regard to block shape and laying pattern, rectangular concrete pavers were laid at the two Ontario sites in a herringbone pattern, whereas irregular-shaped blocks were used at the North Carolina site, also laid in a herringbone pattern. However, the results do not clearly indicate that one is performing better than the other. The pavements at all three sites are structurally sound, have similar moduli for the composite paver block and sand layer, show little distress (mostly localized), and have small rut depths.

Furthermore, because these pavements were constructed at around the same time (1983 to 1985) and pavement condition data other than those collected in this study are not available, little can be said about the long-term performance of these pavements. Although they are presently in excellent condition, future monitoring will be required to establish their long-term performance. Additional sites with varying factors—for example, block shape and thickness, thickness of bedding sand, and laying pattern—must also be monitored over long periods of time, preferably since the time of initial construction, to better ascertain the influence of these factors on the performance of interlocking concrete pavements.

CONCLUSIONS

When compared with use in other parts of the world, the use of interlocking concrete pavements in North America is a relatively new development. As a result, little information about their performance is available to verify or calibrate existing design methods or develop new ones. Toward overcoming this limitation, the performance of interlocking concrete pavements at three sites was evaluated. Record searches along with field investigations—deflection testing, visual condition surveys, and transverse profile surveys—were conducted as part of this effort.

From the analysis and interpretation of the data collected, the following observations and conclusions were made:

- A definite relationship exists between the amount of traffic the pavement receives and the modulus of the composite paver blocks and bedding sand layer; as traffic increases, the modulus also increases.

- There is excellent agreement between the backcalculated composite moduli and those found in the literature for other parts of the world where these pavements have been used for several decades.

- The backcalculated composite moduli are very similar to those of asphalt concrete, thus confirming that the load distribution of interlocking concrete pavements is very similar to that of flexible pavements once lock-up has occurred.

- After 6 to 8 years in service, the pavements at the three sites are in excellent condition. All are structurally sound, very little distress is present (mostly localized areas), and very small rut depths were measured.

- If localized distresses are not included in the analysis, then surface deformation, which is the primary failure mode in interlocking concrete pavements, occurs in less than 1.5 percent of the areas surveyed.

- Rut depths along the right wheelpath are larger than those in the left wheelpath; this difference is likely to be related to the construction of the edge restraints or the placement and vibration of the pavers and sand at the pavement edge.

Finally, although much valuable information was obtained from this initial study, additional effort is still required to better define the performance of interlocking concrete pavements. Additional sites, covering a wider range of factors such as laying patterns, bedding sand thickness, block thickness, traffic, subgrade, and environment must be evaluated. Only through such monitoring studies will the influence of these factors on the performance of the pavement be adequately established.

REFERENCES

1. G. R. Rada, D. R. Smith, J. S. Miller, and M. W. Witzak. Structural Design of Concrete Block Pavements. *Journal of Transportation Engineering*, ASCE, Vol. 116, No. 5, 1990, pp. 615-635.
2. J. Uzan, R. L. Lytton, and F. P. Germann. *General Procedure for Backcalculating Layer Moduli*. STP 1026, ASTM, pp. 217-228, 1989.
3. F. J. Van Cauwelaert, D. R. Alexander, T. D. White, and W. R. Barker. Multilayer Elastic Program for Backcalculating Layer Moduli in Pavement Evaluation. STP 1026, ASTM, pp. 171-188, 1989.
4. K. G. Sharp, and P. J. Armstrong. Testing of Concrete Block Pavements by the Australian Road Research Board. *Proc., 2nd International Conference on Concrete Block Paving*, Delft, The Netherlands, 1984, pp. 40-49.
5. M. Y. Shahin, and S. D. Kohn. *Pavement Maintenance Management for Roads and Parking Lots*. CERL-TR-M-294. U.S. Army, Construction Engineering Research Laboratory, 1981.
6. Studie Centrum Wegenbouw. *Manual and Catalogue of Defects for the Visual Inspection of Roads* (in Dutch). 1982.
7. R. J. Armitage. Concrete Block Pavement Evaluation with the Falling Weight Deflectometer. *Proc., 3rd International Conference on Concrete Block Paving*, Rome, Italy, 1988, pp. 203-208.
8. J. M. Clifford. Some Considerations Which Affect the Modelling of Segmental Block Pavements for Industrial Applications. *Proc., 3rd International Conference on Concrete Block Paving*, Rome, Italy, 1988, pp. 170-177.
9. F. Dutruel and J. Dardare. Contribution to the Study of Structural Behavior of a Concrete Block Pavement. *Proc., 2nd International Conference on Concrete Block Paving*, Delft, The Netherlands, 1984, pp. 29-39.
10. L. J. M. Houben, A. A. A. Molenaar, G. H. A. M. Fuchs, and H. O. Moll. Analysis and Design of cpb's. *Proc., 2nd International Conference on Concrete Block Paving*, Delft, The Netherlands, 1984, pp. 86-99.
11. *Interlocking Concrete Road Pavements*. Cement and Concrete Association of Australia, Brisbane, 1986.
12. S. Lekso. The Use of Concrete Block Pavements for Highways. *Proc., 1st International Conference on Concrete Block Paving*, United Kingdom, 1982, pp. 101-103.
13. Y. Miura, M. Takaura, and T. Tsuda. Structural Design of Concrete Block Pavements by CBR Method and Its Evaluation. *Proc., 2nd International Conference on Concrete Block Paving*, Delft, The Netherlands, 1984, pp. 152-157.
14. R. S. Rollings, Corps of Engineers Design Method for Concrete Block Pavements. *Proc., 2nd International Conference on Concrete Block Paving*, Delft, The Netherlands, 1984, pp. 147-151.
15. P. A. Seddon. The Behaviour of Concrete Block Paving Under Repetitive Loading. *Proc., 1st International Conference on Concrete Block Paving*, United Kingdom, 1982.
16. B. Shackel. The Evolution and Application of Mechanistic Design Procedures for Concrete Block Pavements. *Proc., 3rd International Conference on Concrete Block Paving*, Rome, Italy, 1988, pp. 114-120.
17. B. Shackel. A Study of the Performance of Block Paving Under Traffic Using a Heavy Vehicle Simulator. *Proc., 10th ARRB Conference*, Vol. 10, No. 2, 1980, pp. 19-30.
18. B. Shackel. An Experimental Investigation of the Roles of the Bedding and Jointing Sands in the Performance of Interlocking Concrete Block Pavements Subjected to Traffic. *Concrete Beton*, No. 19, 1980, 09, pp. 5-15.
19. B. Shackel. The Design of Interlocking Concrete Block Pavements for Road Traffic. *Proc., 1st International Conference on Concrete Block Paving*, United Kingdom, 1982.

Publication of this paper sponsored by Committee on Rigid Pavement Design.

Rigid Pavement Design for Ports in Chile

JACOB GREENSTEIN AND CHAIM J. PORAN

A case study of rigid pavement design for two ports located in the central zone of Chile, which is an area of high seismic risk, is presented. Special considerations were required to address the problem of liquefiable subgrade soils that were the cause of severe damage to existing pavements during the large earthquake of March 3, 1985. Rational design charts were developed for rigid pavements on the basis of tensile stresses induced by critical edge loads. Slab stresses were evaluated by using two computer codes, and tensile stress-slab thickness relationships were developed for various values of composite modulus of subgrade reaction and for several modes of port pavement loads, including container stacks and loading equipment, such as front lift truck and straddle carrier. Results indicated that container stacking on the slab edge is the critical load and would require substantial strengthening of existing pavements and large investments in new ones. To overcome this problem it was decided to restrict container stacking to a minimum distance of 38 cm (15 in.) from the edge. Consequently, new pavements were designed on the basis of the loads of the container-handling equipment, and existing pavements were strengthened to meet the same criteria. A design chart was developed to assess the risk of liquefaction of loose sandy subgrade soils during future large earthquakes. The chart is based on expected ground motion levels and standard penetration test N -values. Finally, remedial measures were recommended to improve density and the liquefiable deposits in new pavement areas.

A case study of rigid pavement design is presented for the ports of Valparaiso and San Antonio located in the central region of Chile, as shown in Figure 1. A large earthquake occurred in the Pacific coast area near the ports on March 3, 1985, as reported by Poran et al. (1,2). The earthquake had a surface wave magnitude of $M_s = 7.8$ on the Richter scale and its intensity was rated as VII and VIII (on the modified Mercalli scale) at the Valparaiso and San Antonio ports, respectively. Both ports suffered severe damage from the earthquake. The rehabilitation plan for these ports includes the addition of substantial container-handling facilities as described in the report on development program of ports of the Fifth Region (3). The existing pavements in the ports are rigid. Several alternatives for new pavements were considered in a preliminary life cycle cost analysis on the basis of design criteria (4-6). Results of the study indicated that new rigid pavements are most economical primarily because of the operational constraints in the ports where the new facilities are also designated for general cargo.

Evaluation of existing pavements in the ports indicated that the solid and uncracked slabs are 30 cm (12 in.) thick with a

modulus of elasticity of over 34 500 MPa (5 million psi) and have a flexural strength of over 4620 kPa (670 psi). The concrete slabs are supported by cement-stabilized granular base placed on high-quality compacted subbase overlying hydraulic fill that varies in thickness between 3 and 12 m (10 and 40 ft). Large-scale liquefaction was induced by the 1985 earthquake in the areas in which the hydraulic fill consisted of loose sandy soils. As a result, many existing rigid pavement areas suffered severe damage and were rendered inoperable (2).

Performance observations of rigid highway pavements and numerical methods (7) have shown that edge stresses are more critical than corner or interior stresses in pavement slabs. Experience with rigid airport pavements is similar, as reported by FAA (8). A computer code H51 that was developed for FAA on the basis of the work by Kreger (9) was used for this analysis. The program permits accurate computation of tensile stresses at the edge of a concrete slab under any local configuration. This program was used to develop the design charts and personal computer programs for most standard aircraft, including the largest 747s and DC-10s (8). Comprehensive design charts for port pavements were published by the British Port Association (6). However, these charts were not applicable for the evaluation because the existing pavement structure in Chilean ports is not included. The computer program CORNER, which is based on Westergaard's corner equations published by Ioannides et al. (10), was used to compute stresses in the slab corner.

Special consideration was given to improvement and densification of sandy subgrade soils for new pavement in hydraulic fill areas on the basis of a liquefaction risk evaluation procedure outlined by Seed et al. (11,12). The criteria are based on standard penetration test (SPT) N -values and expected peak ground acceleration (PGA) at the ports during a future large earthquake in the central region of Chile.

The results of these case studies are outlined as follows.

EXISTING PAVEMENT SYSTEMS

Design Specifications

Available design reports indicate that the existing rigid pavements at the Chilean ports of Valparaiso and San Antonio were designed to specifications similar to those for a pavement structure that consists of the following layers:

- Concrete slabs
 - Thickness, 30 cm (12 in.);
 - Minimum compressive strength, 36.2 MPa (5,250 psi);

J. Greenstein, Interamerican Development Bank, 1300 New York Ave., N.W., Washington, D.C. 20577. C. J. Poran, Department of Civil Engineering, University of North Carolina at Charlotte, Charlotte, N.C. 28223.

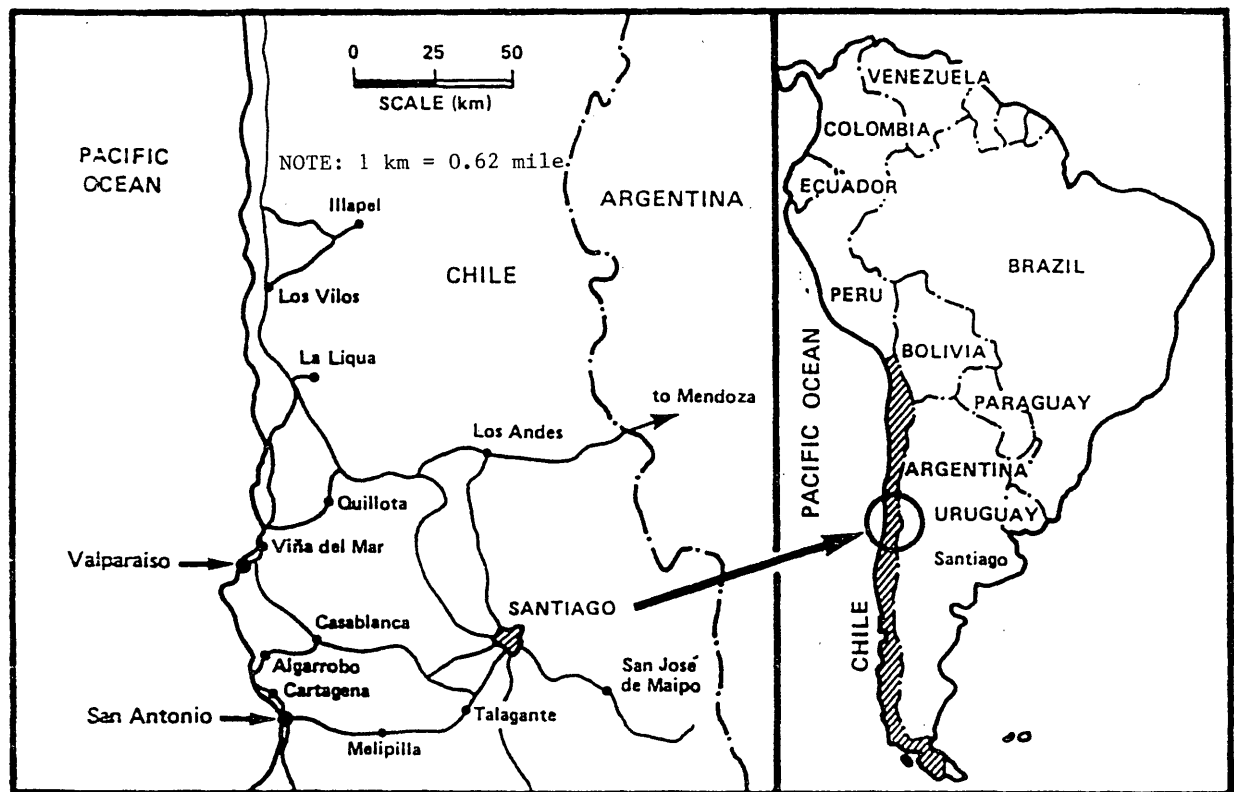


FIGURE 1 Port locations.

- Minimum flexural strength, 4590 kPa (665 psi);
- Minimum modulus of elasticity, 27 580 MPa (4×10^6 psi);
- Estimated Poisson's ratio, 0.15.

- Cement-stabilized base: The thickness of the existing cement-stabilized base (CSB) varies in different port areas between 25 and 38 cm (10 and 15 in.). The CSB was stabilized with 6 percent portland cement by weight and was required to have a minimum elastic modulus of 690 MPa (100,000 psi).

- Subbase: Under the CSB there is a high-quality subbase material 41 to 61 cm (16 to 24 in.) thick. The subbase material was required to have a minimum California bearing ratio (CBR) of 40 percent.

- Fill: The subbase overlies areas of hydraulic or local fill with thickness of 3 to 12 m (10 to 40 ft) above the natural dense granular soil deposit and bedrock (in several locations at the port of Valparaiso). Mean sea level is generally 2.8 m (9 ft) below the top of the fill.

Evaluation of Existing Pavement Systems

Nondestructive testing (NDT) based on deflection measurements can be effective in the evaluation of existing conditions of both rigid and flexible pavements, as discussed by Greenstein (13) and numerous other authors. Although NDT was initially considered for these ports' pavements, no such tests were conducted because of budgetary constraints. However, available plate load test results conducted on a subbase layer

of a similar pavement indicated that the minimum composite subgrade reaction of subbase and fill was 200 lb/in.³ These results were used for correlations (3). On the basis of boring logs and test results from the ports' pavements, it was concluded that the actual properties of the existing pavements were as follows:

- Concrete slabs
 - Thickness, 30 cm (12 in.);
 - Minimum flexural strength, 4620 kPa (670 psi);
 - Minimum modulus of elasticity, 34,500 MPa (5×10^6 psi).
- Cement-stabilized base: The minimum elastic modulus was estimated to be 1030 MPa (150,000 psi). Figure 2 (14) was used to evaluate the composite modulus of subgrade reaction for the CSB, subbase, and fill material. Using a minimum subgrade reaction modulus of 54 MN/m³ (200 lb/in.³) on the subbase, the estimated result on the CSB is 136 MN/m³ (500 lb/in.³).
- Subbase: Soil testing data indicated that the ASTM D-2487 classification of the subbase is SP-GP or SM-GM with a CBR of more than 40 percent. Test results indicated that the composite elastic modulus of the subbase and fill materials varies between 145 and 386 MPa (21,000 and 56,000 psi) and the composite modulus of subgrade reaction (k) is in the range of 54 to 95 MN/m³ (200 to 350 lb/in.³).
- Fill: Many SPT N -value profiles were compiled for the fill material and were used in the liquefaction risk evaluation as subsequently described in this paper.

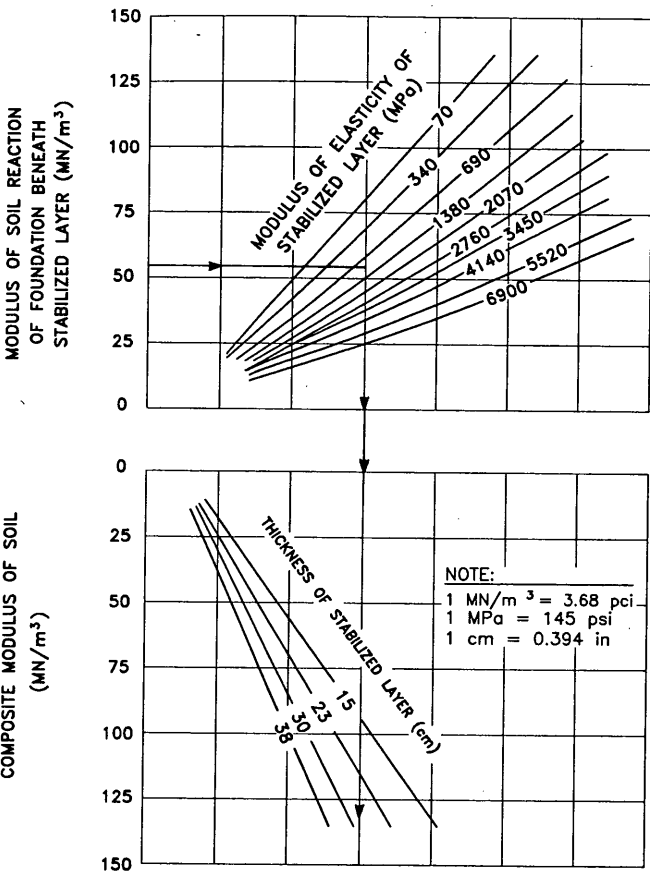


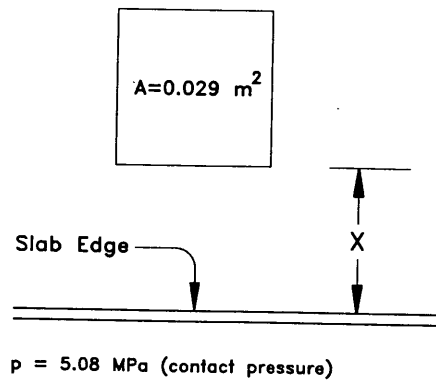
FIGURE 2 Nomogram to determine the composite subgrade reaction modulus for stabilized base overlying subgrade.

DESIGN LOADS

Design load calculations for the container stack loads and handling equipment (including dynamic factors) generally were based on the procedures outlined (6). The following representative loads were considered for these port pavements:

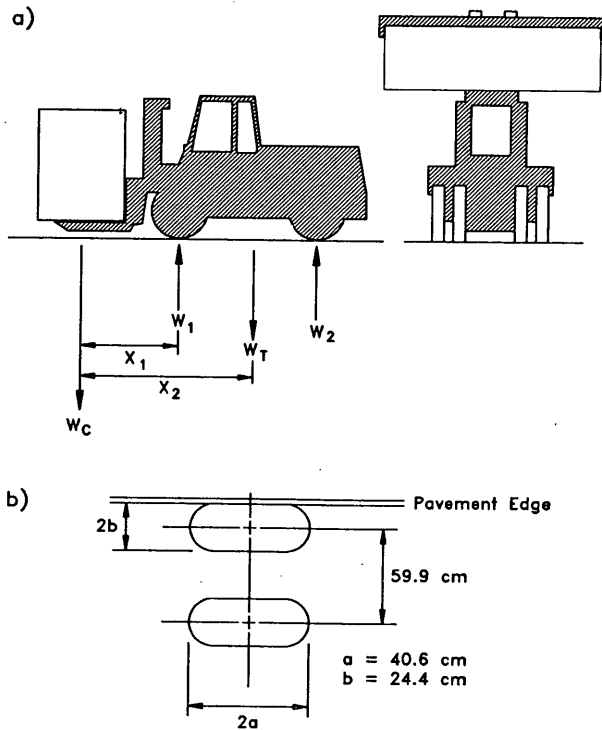
- Container stack loads: The most commonly used containers in Chilean ports are 12.2 m (40 ft) long. On the basis of Chilean statistics, a maximum weight of 214 kN (24 tons) was considered for a single container. According to the Chilean specifications, the design loads were based on stacking in three levels, one on top of the other. Therefore, the total load was 642 kN (72 tons) and the design load was reduced by 20 percent according to the design recommendations (6) because it is unlikely that all three containers in the stack will be fully laden. These loads are transferred to the rigid pavements through four corner supports (castings). Each support has a contact area of 289 cm² (44.8 in.²). Therefore, the design contact pressure for each support is equal to 5080 kPa (737 psi). Figure 3 shows the critical container load configuration on the slab edge. Obviously, the distance from the slab edge (X) significantly affects the tensile stresses in the slab. These stresses reach their maximum value for X = 0.

- Front lift truck: The front lift truck is a common type of container-handling equipment in multipurpose port facilities.



NOTE:
 1 MPa = 145 psi
 1 m² = 1,550 in²

FIGURE 3 Layout of container stack castings near the slab edge.



NOTE:
 1 cm = 0.394 in

FIGURE 4 Front lift truck: a, dimensions and weights; b, critical edge loading layout.

A front lift truck is shown in Figure 4a. It has two dual wheels, as shown in the assembly configuration of Figure 4b. The critical front end design load (W_1) is distributed on two wheels; the load on each wheel is 246 kN (55,000 lb), with a contact pressure of 783 kPa (113.6 psi) and a contact area of 0.31 m² (484.4 in.²).

• **Straddle carrier:** The straddle carrier, also container-handling equipment, is shown in Figure 5. Under critical operating conditions the design loads were considered for a single wheel parallel to the slab edge (the adjacent wheel has a negligible effect on these stresses) and all wheel loads are considered equal. Two different types of straddle carriers were specified with wheel loads of 195 and 342 kN (44,000 and 77,000 lb) and contact pressures of 1077 and 783 kPa (156.2 and 113.6 psi), respectively.

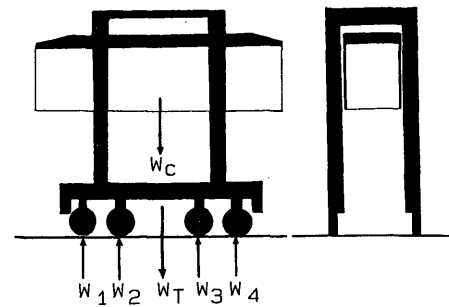


FIGURE 5 Layout of a straddle carrier and acting loads.

EVALUATION OF PAVEMENT STRESSES

The effects of various load configurations and slab thicknesses on tensile stresses in the slab were investigated for both edge and corner loading. Edge loading stresses were computed with the H51 computer code, and stresses at the slab corner were computed with the CORNER computer program, as follows.

Stresses Caused by Container Stack Loads

Figure 6 shows the relationship between the tensile stress at the slab bottom and the slab thickness for container stack loads. Lines 1A and 1B represent free edge loading for com-

posite subgrade reaction modulus of 136 and 95 MN/m³ (500 and 350 lb/in.³). It is well established that adequately constructed joints transfer loads between the jointed slabs. According to Chilean experience this load transfer is at least 25 percent (i.e., 25 percent of the edge load is transferred to the jointed slab). Therefore it is necessary to look at 25 percent stress reduction at jointed slab edges. Line 2 represents the stress-thickness relationship for a jointed edge and k -value of 136 MN/m³ (500 lb/in.³). Line 3 represents the stress-thickness relationship at the corner of the slab.

On the basis of operational forecasts (3), 10,000 load repetitions were considered for container stacking during the design life of these pavements. On the basis of the literature (10,15), the allowable stress/strength ratio (SSR) for 10,000 load repetitions is 0.64. Therefore, the allowable tensile stress in the slabs is 2965 kPa (430 psi, computed as 0.64 × 670 psi). Finally, Line 2 in Figure 6 was used to determine the

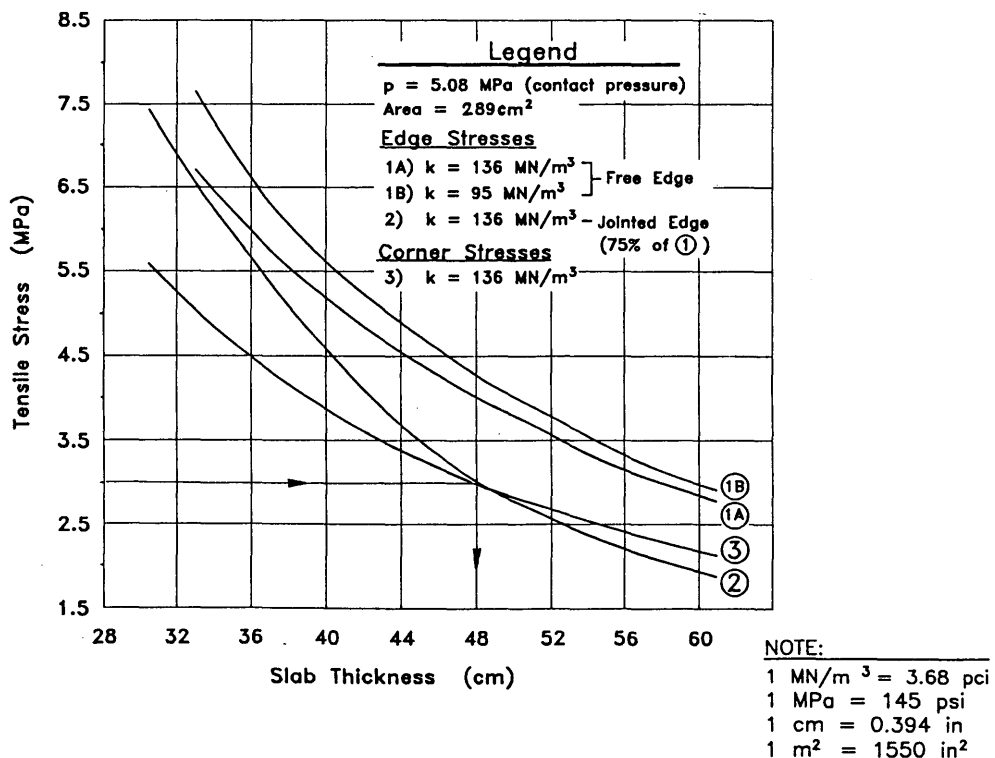


FIGURE 6 Tensile stress versus slab thickness relationship for container stack load ($X = 0$).

required slab thickness to support container stacks at the edge. For allowable stress of 2965 kPa (430 psi) the required slab thickness is 48 cm (19 in.). This also implied that an additional overlay concrete slab with a minimum thickness of 18 cm (7 in.) will be needed to support 10,000 repetitions of these loads provided that there is a monolithic bond between the overlay and the existing slab and that the joints overlap. In many areas of the ports the existing slabs are cracked and shattered. Based on FAA (8), these areas will require concrete overlays of up to 33 cm (13 in.). This requirement was rendered economically infeasible, as subsequently discussed.

Stresses Caused by Container-Handling Equipment

Figures 7 and 8 show stress-thickness relationships for front-lift truck and straddle carrier, respectively. These relationships were computed with the H51 and CORNER computer programs for edge and corner stresses, respectively.

Figure 7 clearly shows that edge stresses are much higher than corner stresses and therefore are considered critical. Based on operational forecasts (3), 100,000 load repetitions were considered for the front lift truck during the design life of these pavements. In this case an SSR = 0.56 was used, and therefore the allowable stress was reduced to 2586 kPa (375 psi). Finally, Line 4 was used for thickness design under front lift truck loads. This line represents 25 percent of the load transfer of the jointed slab and a composite modulus of subgrade reaction of 136 MN/m³ (500 lb/in.³). Figure 7 indicates that

the required slab thickness for front lift truck operations is 45 cm (17.5 in.).

Figure 8 shows a stress-thickness relationship caused by straddle carrier operations. Again, slab edge stresses are higher than corner stresses (which were not plotted on this figure). The graph is based on the required 100,000 load repetitions for this type of equipment during the design life of the pavement (3). Lines 4 and 5 are used for design with the 342- and 195-kN (77,000- and 44,000-lb) wheel loads, respectively. For an allowable stress of 2965 kPa (430 psi), these lines indicate that the required slab thicknesses are 35 and 30 cm (14 and 12 in.), respectively.

DESIGN RECOMMENDATIONS

On the basis of the evaluation mentioned earlier, the design recommendations were as follows.

Container Stack Loads

The evaluation indicated that a 48-cm (19-in.) slab is needed to support the container stacks. This was previously determined for the worst case, in which the container castings are placed on the slab edge (X = 0). If the stacking is restricted to a certain short distance from the edge (X > 0), these stresses are significantly reduced. The Chilean Port Authority requested an evaluation of the alternative to restricting the

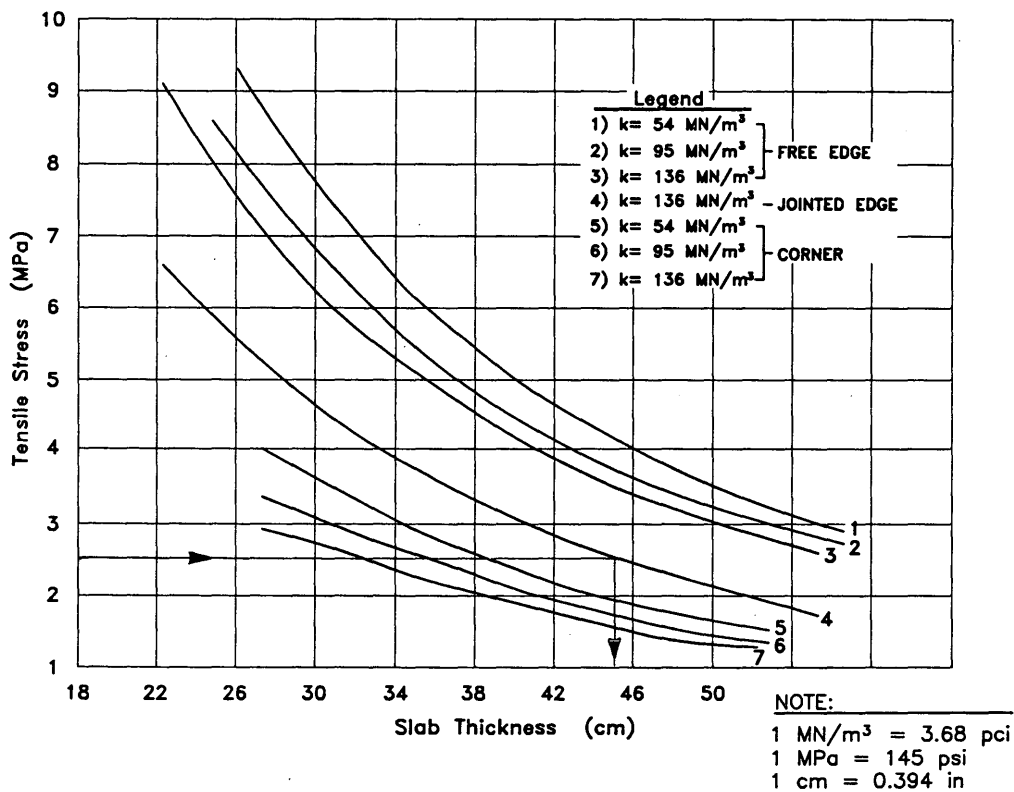


FIGURE 7 Tensile stress versus pavement thickness for front lift truck.

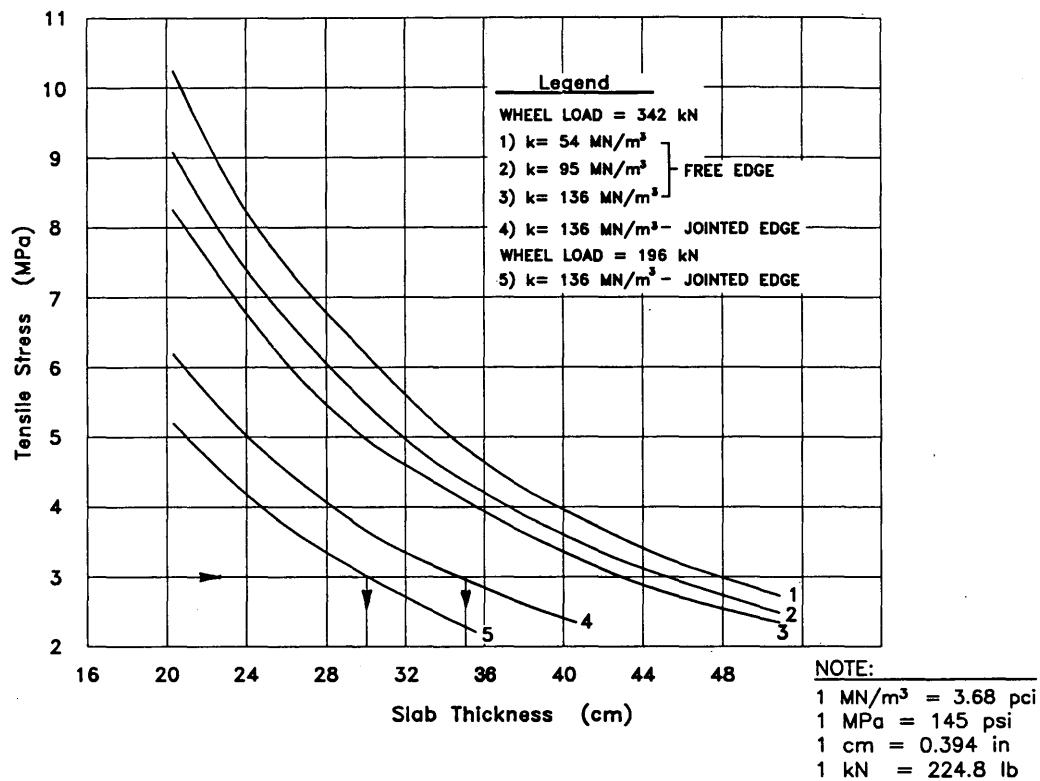


FIGURE 8 Tensile stress versus pavement thickness for straddle carrier.

container stacking at slab edges. This required that the appropriate distance (X) be determined to ensure that the edge stresses would not exceed 2965 kPa (430 psi). The H51 program was used for this evaluation, and the results are shown in Figure 9. For example, Line 3 represents the stress-thickness relationship that occurs when the container support is located 40.6 cm (16 in.) from the edge. This line yields edge tensile stresses of 2070 and 2830 kPa (300 and 410 psi) for slab thicknesses of 41 and 30 cm (16 and 12 in.), respectively. Line 1 represents the worst case ($X = 0$), in which these tensile stresses reach their maximum value. According to Figure 9, with the existing slab thickness of 30 cm (12 in.) the stresses will be equal to the allowable stress of 2965 kPa (430 psi) when the container stack is located 38 cm (15 in.) from the slab edge. The policy of controlling the container stack location was found more economical and practical than strengthening the existing pavement structure with a minimum concrete overlay of 18 cm (7 in.).

Front Lift Truck

As previously evaluated, the required slab thickness for the front lift truck is 45 cm (17.5 in.). Because this handling equipment is going to be used only in defined and channelized lanes, only a limited area needs to be strengthened (3). The recommendations specified that in these areas a monolithic concrete overlay of 15 cm (6 in.) be constructed on solid and uncracked existing slabs only and that the cracked and shattered slabs be replaced with new slabs 45 cm (17.5 in.) thick.

Straddle Carrier

No strengthening was recommended for the areas in which the lighter equipment is used [195 kN (44,000 lb) per wheel load]; the uncracked slabs 30 cm (12 in.) thick were judged adequate. On the other hand, it will be necessary to construct an 8-cm (3-in.) monolithic concrete overlay for the straddle carrier with a load of 342 kN (77,000 lb) per wheel (based on a minimum overlay thickness) and construct slabs 35 cm (14 in.) thick for the new pavement.

EARTHQUAKE CONSIDERATIONS

The massive earthquake that took place on March 3, 1985, in the central region of Chile had a surface wave magnitude of $M_s = 7.8$ on the Richter scale. Its epicenter was located in the Pacific Ocean approximately 39 km (24 mi) from the port of San Antonio. The earthquake intensity was rated as VII and VIII on the modified Mercalli scale at the ports of Valparaiso and San Antonio, respectively. The damage to the port facilities was extensive (3). Large settlements occurred in backfill and pavement areas where loose sandy deposits liquefied and some existing pavement areas were destroyed.

Liquefaction risk analysis was conducted on the basis of the procedure described previously (11,12), and the results are presented in Figure 10. The critical envelope shown is a convenient method for evaluating liquefaction potential based on SPT N -values for a large number of soil borings performed in the sandy hydraulic fill deposits before and after the earth-

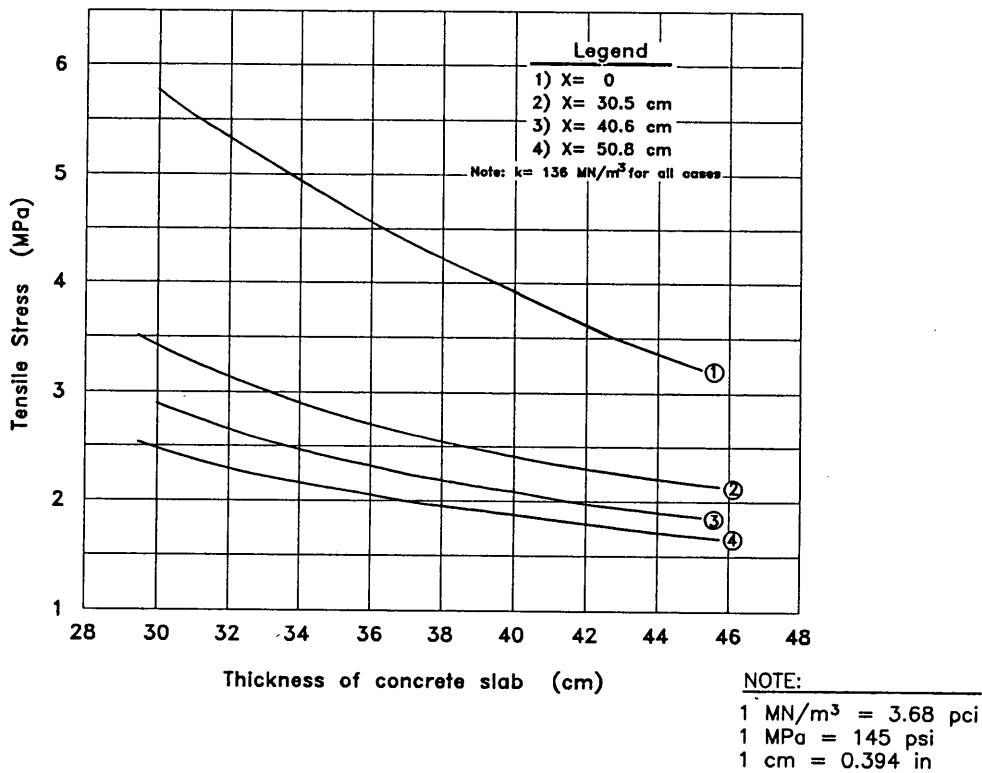


FIGURE 9 Stress-thickness relationship of a jointed edge for container stack load.

quake. The limits indicated are based on the range of PGA values recorded at the port of San Antonio during the March 3, 1985, earthquake (1,2). The earthquake design considered for the ports is expected to result in PGA values within this critical range. The range shown on the left side of Figure 10 is the lower limit. It corresponds to sandy soils in which liquefaction is likely to occur. The range located between the two limits is defined as the critical range or the zone of uncertainty. This critical range corresponds to PGA values of 0.67 and 0.43 g for the upper and lower limits, respectively. The upper limit may be applied to sandy soils with D_{50} larger than 0.25 mm (0.01 in.), and the lower limit may be better suited for silty sands with 15 percent fines.

The upper limit in Figure 10 was recommended as the design curve for the minimum required density of the fill material under water level. In the Chilean ports the water level is approximately 3.95 m (13 ft) from the ground surface. For example, at a depth of 4.5 and 9 m (15 and 30 ft) from ground surface, the SPT N -value should be a minimum of 30 and 40, respectively, to resist liquefaction during an earthquake similar to the one in 1985.

These criteria are recommended for hydraulic fill deposits under water level in new rigid pavement areas and in areas in which existing pavements were badly damaged from liquefaction induced by the 1985 earthquake. The damaged pavements will be reconstructed to the new specifications. Dynamic compaction, sand piles, or vibroflotation were recommended as effective soil improvement methods for these loose sandy deposits (3) to mitigate the risk of liquefaction.

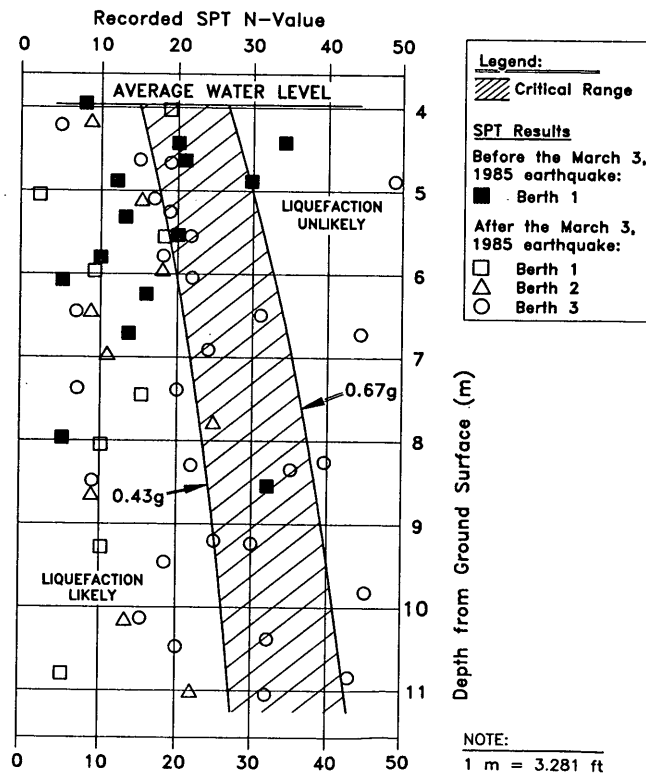


FIGURE 10 Critical liquefaction range for sandy soils in the Port of San Antonio.

In addition, it was shown (2) that loose sandy fill above the water level may also undergo considerable settlement during strong earthquakes. Therefore, it was recommended that the fill material above water level be compacted to a minimum of 95 percent of AASHTO-T 99-90.

SUMMARY AND CONCLUSIONS

1. A rational methodology for rigid pavement design was developed for the Chilean Port Authority. Tensile stress-thickness relationships were computed at slab edge and corner for various levels of composite modulus of subgrade reaction and representative loads associated with container operations. Two computer programs were used for this evaluation. Generally, it was concluded that edge loading governs pavement thickness.

2. The representative design loads used in this analysis were container stack castings, front lift truck, and straddle carrier. The loads were computed on the basis of Chilean specifications with the procedures outlined (6). A total load of 514 kN (58 tons) was used for a stack of three containers with contact pressure of 5080 kPa (737 psi) and a contact area of 289 cm² (44.8 in.²). The front lift truck was considered with two dual wheel assemblies, a wheel load of 246 kN (55,000 lb), and contact pressure of 783 kPa (113.6 psi). Two types of straddle carriers were considered with wheel loads of 195 and 342 kN (44,000 and 77,000 lb) and contact pressure of 1077 and 783 kPa (156.2 and 113.6 psi), respectively.

3. Design charts of required slab thickness that are based on load repetitions during the design life are presented. It was concluded that a slab 30 cm (12 in.) thick is adequate if the container stacking areas are arranged in such a way that the castings are restricted to a minimum distance of 38 cm (15 in.) from the edges of the slabs. This arrangement will result in substantial savings in the new pavement areas and will not require overlays on the existing ones. A rigid pavement 45 cm (17.5 in.) thick will be required in the channelized areas of front lift truck operations. The straddle carrier with a 195-kN (44,000-lb) wheel load will require slabs 30 cm (12 in.) thick. However, the heavier straddle carrier with 342-kN (77,000-lb) wheel load will require a minimum overlay of 8 cm (3 in.) on existing slabs, for a total of 38 cm (15 in.), and a thickness of 35 cm (14 in.) for new pavements.

4. Deep soil improvement and densification were recommended to minimize liquefaction settlements and pavement failures. The liquefaction risk evaluation procedure is based on SPT *N*-values. For the pavement areas, a minimum *N*-value is specified for any given depth of the sandy fill material below water level. Dynamic compaction, vibroflotation, or

sand piles were recommended for deep soil improvement. Conventional compaction was also recommended to minimize subgrade settlement of loose sandy soils above water level.

REFERENCES

1. C. J. Poran, J. Greenstein, and L. Berger. Geotechnical Problems in Port Design in Chile. In *ASCE Specialty Conference Proc., Ports '89*, Boston, May 1989, pp. 583-592.
2. C. J. Poran, J. Greenstein, and L. Berger. Earthquake Induced Settlements in Port Facilities in Chile. *Proc., 12th International Conference on Soil Mechanics and Foundation Engineering*, Rio de Janeiro, Brazil, Vol. 3, Aug. 1989, pp. 1991-1994.
3. Louis Berger International-Inecon. *Development Program of Ports of the 5th Region and Feasibility, 1st Stage*. Ministry of Transportation and Telecommunication of Chile and the World Bank, 1988.
4. M. Meletiou and J. Knapton. *Container Terminal Pavement Management*. UNCTAD Monographs on Port Management: Monograph 5, Report UNCTAD/SHIP/494(5) GE. 87-55225/6982E, 1987.
5. M. Meletiou. The Task of Container Terminal Pavement Selection. In *ASCE Specialty Conference Proc., Ports '89*, Boston, May 1989, pp. 124-133.
6. *The Structural Design of Heavy Duty Pavements for Ports and Other Industries*. British Port Association, London, England, 1987.
7. M. T. Darter. *WESTY V4.0-Computerized Version of the Westergaard Equations for Interior, Edge, and Corner Stresses and Deflections*. ERES Consultants, Inc., Champaign, Ill., May 1987.
8. *Airport Pavement Design and Evaluation*. Advisory Circular AC 150/5320-6C. FAA, U.S. Department of Transportation, Dec. 1978.
9. W. C. Kreger. *Computerized Aircraft Ground Floatation Analysis—Edge Loaded Rigid Pavements*. Research Report ERR-FW-572. General Dynamics, Jan. 1967.
10. A. M. Ioannides, M. R. Thompson, and E. J. Barenberg. *The Westergaard Solutions Reconsidered*. Presented at 64th Annual Meeting of the Transportation Research Board, Washington, D.C., Jan. 1985.
11. H. B. Seed, I. M. Idriss, and I. Arango. Evaluation of Liquefaction Potential Using Field Performance Data. *Journal of the Geotechnical Engineering Division*, ASCE, Vol. 109, No. 3, March 1983, pp. 458-482.
12. H. B. Seed, K. Tokimatsu, L. F. Harder, and R. M. Chung. *The Influence of SPT Procedures in Soil Liquefaction Resistance Evaluation*. Report UBC/EERC-84/15. National Science Foundation, Washington, D.C., 1984.
13. J. Greenstein. Using Nondestructive Testing in the Semi-Arid Zone of Peru. In *Transportation Research Record 1137*, TRB, National Research Council, Washington, D.C., 1987.
14. *Rigid Pavements for Airfields Other than Army*. Report T.M. 5-824-3 and Report AFM 88-6, Chapter 3, U.S. Army, U.S. Air Force, Aug. 1979.
15. R. G. Packard. *Design of Concrete Airport Pavement*. Portland Cement Association, 1973.

Publication of this paper sponsored by Committee on Rigid Pavement Design.

Maximum Bearing Stress of Concrete in Doweled Portland Cement Concrete Pavements

HUA GUO, THOMAS J. PASKO, JR., AND MARK B. SNYDER

Hundreds of numerical calculations were conducted using the component model developed recently to test the accuracy of existing design procedures. It has been found that the maximum bearing stress of concrete, under the critical dowel, cannot be accurately predicted by the "effective length" assumption that is currently used in engineering analysis. A detailed discussion to analyze the potential problems and the causes of the problems is presented. Errors in computed values of maximum bearing stress can also affect the prediction of joint faults in pavement performance models.

Smooth round dowel bars have been employed as load transfer devices in jointed concrete pavements for a long time. Many experimental and analytical studies have been conducted to develop and improve the design procedure for dowels. Before the 1960s, the most influential analytical models were developed by Timoshenko et al. (1) and Friberg (2), and some significant experimental studies of dowelled slabs were conducted by Teller et al. (3,4), Finney et al. (5), and Keeton et al. (6). The complete review of these studies and the application in engineering design can be found in the thesis by Snyder (7) and the report by Heinrichs et al. (8).

Researchers have concluded that the maximum concrete bearing stress is the most important parameter to be determined in portland cement concrete (PCC) pavement joint design. Currently the maximum bearing stresses of concrete under dowels are required to be equal to or smaller than the concrete bearing strength. Furthermore, the level of the bearing stress has direct effects on the accumulation of joint faulting, which is a very important parameter in the performance of PCC pavements (8).

The procedure of Friberg (2) can be generally divided into two steps to determine the maximum bearing stress. The first step is to predict the maximum shear force acting on the critical dowel bar. The second step is to calculate the maximum bearing stress on the concrete under the critical bar by using the maximum shear force obtained in the first step.

The first step is based on three assumptions:

1. A certain percentage of the total load is transferred across the dowelled joint. The range varies from 0 to about 50 percent, depending on the quality of the joint, pavement struc-

tural parameters, and the load type. Because 50 percent would be a maximum bearing stress, Heinrichs et al. (8) suggest using 45 percent.

2. The dowel shear forces are linearly distributed along the joint (see Figure 1).

3. An "effective load transfer length" (L_1) was assumed to be 1.81 by Friberg (2), and all dowels located farther than L_1 from the load center do not contribute to transferring load. The radius of relative stiffness of the slab was determined to be l by the formula

$$l = \left[\frac{Eh^3}{12(1 - \mu^2)k} \right]^{1/4} \quad (\text{in.}) \quad (1)$$

where

E = elasticity modulus of concrete (psi),
 μ = Poisson's ratio of the concrete,
 h = thickness of the concrete slab (in.), and
 k = modulus of the subgrade.

Using these assumptions, the maximum shear force acting on the critical dowel bar can be calculated. As mentioned above, $L_1 = 1.81$ was proposed by Friberg (2). In the second step, the shear force on the dowel is assumed known. The model of Timoshenko et al. (1) gives a procedure to predict the behavior of a steel bar embedded in "pure elastic" concrete. On the basis of the Timoshenko theory, Friberg (2) derived the maximum bearing stress (σ_{\max}) formula:

$$\sigma_{\max} = \psi \delta_0 \quad (2)$$

where

$$\delta_0 = \frac{P_1(2 + \beta J_0)}{4\beta^3 E_s I} \quad (3)$$

in which

P_1 = "maximum" shear force acting on the dowel, predicted in the first step (lb);

J_0 = width of the joint opening (in.);

E_s = modulus of elasticity of the dowel bar (psi);

I = moment of inertia of dowel bar cross section = $0.25 \times \pi (D/2)^4$ (in.²);

D = diameter of the dowel bar (in.);

β = $(\psi D/4E_s I)^{0.25}$ (1/in.); and

ψ = dowel-concrete interaction coefficient (lb/in.³).

H. Guo, Galaxy Scientific Corporation, 1413 Cantillion Blvd., Suite 100, Mays Landing, N.J. 08330. T. J. Pasko, Jr., FHWA, 6300 Georgetown Pike, McLean, Va. 22101. M. B. Snyder, Department of Civil Engineering, Michigan State University, East Lansing, Mich. 48824.

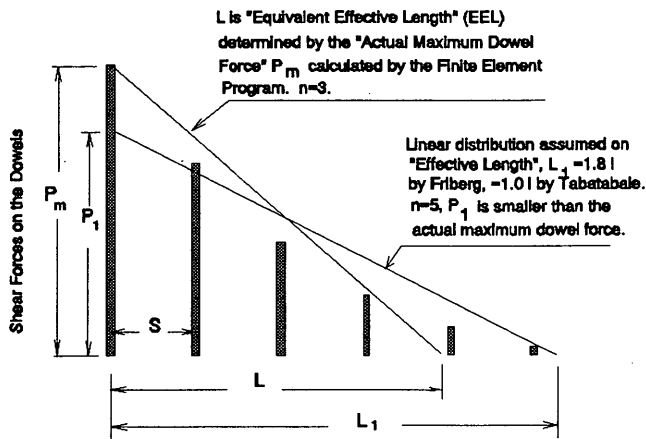


FIGURE 1 Effective length (L_1) and equivalent effective length (L).

After conducting a three-dimensional finite element analysis for a dowel embedded in an elastic concrete space, Tabatabaie et al. (9) proposed to use the following formula to determine the maximum bearing stress directly:

$$\sigma_{\max} = \frac{(800 + 0.068E)}{D^{4/3}} (1 + 0.355J_0)P_1 \quad (\text{psi}) \quad (4)$$

where E is concrete elastic modulus in kpsi and P_1 is the maximum shear force acting on the critical dowel as determined previously (9,10) by using the ILLISLAB program as follows:

$$P_1 = \alpha SP_t \quad (5)$$

in which

- $\alpha = 0.0091$, for edge load;
- $\alpha = 0.0116$, for protected corner load (with tie bar on shoulder);
- $\alpha = 0.0163$, for unprotected corner load (without tie bar on shoulder);
- S = dowel spacing (in.); and
- P_t = total load (kp).

On the basis of the results produced by using the finite element program ILLISLAB, Tabatabaie et al. (9) concluded, "Only the dowels within a distance 1.01 from the center of the load are effective in transferring the major part of the load." It is obvious that this assumption is more conservative than that of Friberg. Heinrichs et al. (8) proposed to use $L_1 = 1.01$ instead of 1.81 in the first step to predict the maximum shear force acting on the critical dowel; then he used Friberg's model (Equation 3) to determine the maximum bearing stress.

SOME COMMENTS

The Effective Length

As summarized earlier, the determination of the maximum bearing stress can be divided into two steps. First, the effective length (EL) was introduced to determine the maximum shear

force acting on the critical dowel. However, the only purpose of the first step is to determine the maximum shear force on the dowel. If the effective length assumption is good, the maximum shear force P_1 predicted by using the assumed effective length should be identical or close to the actual maximum shear force P_m . Figure 1 indicates that when the distribution of the dowel shear forces is very nonlinear, the procedure could cause significant error ($P_1 < P_m$ in most cases).

Comparison of a Few Numerical Examples

Table 1 presents the maximum bearing stresses calculated by using Friberg's model (Equations 2 and 3, effective length $L_1 = 1.81$ and $L_1 = 1.01$), the model of Tabatabaie et al. (Equation 4), and the component dowel bar model [Guo et al. (11,12)], which have been installed in computer program JSLAB-92 on the basis of the original JSLAB (13). The pavement analyzed is presented in Figure 2. The parameters used are $h = 25.4$ cm (10 in.), $\Psi = 0.4065 \times 10^6$ MPa/m (1.5 million psi/in.), $E = 31.005$ GPa (4.5 million psi), and $J_0 = 0.635$ cm (0.25 in.).

Table 1 demonstrates that the results acquired by using different models are different. It is important to understand what would cause these discrepancies.

Effects of the Subgrade Modulus

Figure 3, taken from Figure 44 of Heinrichs et al. (8), indicates that the maximum bearing stress increases when the subgrade modulus k increases. The same conclusion can also be obtained by analyzing Equations 2 and 3 (see also Table 1). However, this conclusion is difficult to interpret. It does not seem logical that as subgrade support at the joint increases, all other factors being equal, the maximum bearing stress would also increase.

Effects of Concrete Modulus E

Equation 4 indicates that the maximum bearing stress increases as the concrete modulus increases when the other parameters remain the same. This conclusion does not agree with the results obtained from Friberg's model. As discussed earlier, the higher concrete modulus means that the loaded side has greater load resistance capability, so that the total load and the maximum load transferred by the critical dowel should be reduced, not increased as suggested by Equation 4.

Since development in the 1940s, the effective length concept has been widely used in PCC pavement design. It may be worthwhile to reinvestigate the concept to possibly improve the design procedure.

EQUIVALENT EFFECTIVE LENGTH

Based on the EL assumption, if the total load is known and the percent of the total load transferred is assumed, the maximum shear force can be calculated by the following formulas.

TABLE 1 Calculated Maximum Bearing Stresses by Various Models

Friberg's model, L = 1.8 l			
k \ D	1.905 cm (0.75 in)	3.175 cm (1.25 in)	4.445 cm (1.75 in)
13.55 MPa/m(50 pci)	16.4/2387	6.51/945	3.56/516
54.2 MPa/m(200 pci)	22.1/3208	8.75/1270	4.78/694
135.5 MPa/m(500 pci)	26.65/3868	10.56/1532	5.77/837
Friberg's model, L = 1.0 l			
13.55 MPa/m(50 pci)	26.91/3907	10.66/1547	5.82/845
54.2 MPa/m(200 pci)	35.44/5143	14.03/2037	7.67/1113
135.5 MPa/m(500 pci)	41.08/5962	16.27/2361	8.89/1290
Component dowel bar model			
13.55 MPa/m(50 pci)	35.54/5158	19.4/2815	13.53/1964
54.2 MPa/m(200 pci)	30.72/4459	17.07/2478	11.66/1692
135.5 MPa/m(500 pci)	26.5/3846	15.36/2229	10.5/1524
Tabatabaie's model			
k=any values	21.43/3111	10.84/1574	6.92/1005

Note: Values are in MPa (psi).

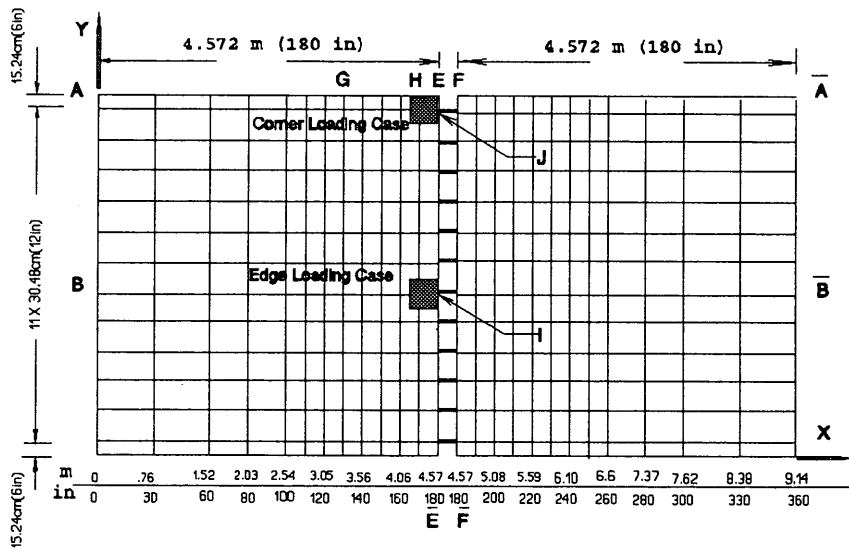


FIGURE 2 Finite element mesh and two load cases.

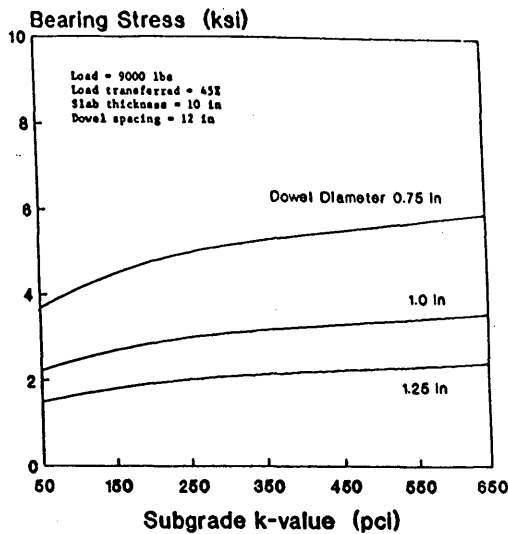


FIGURE 3 Effects of subgrade modulus on maximum bearing stress (δ).

When the load is located in the middle of the joint (defined as edge loading),

$$P = \frac{P_i C}{2n + 1 - \frac{Sn(n + 1)}{L}} \quad (6)$$

When the load is located at an end of the joint (defined as corner loading),

$$P = \frac{P_i C}{n + 1 - \frac{n(n + 1)S}{2L}} \quad (7)$$

where

- P = maximum shear force and is equal to P_1 in Friberg's model (Figure 1);
- n = number of effective dowels on one side of bar under load (number of total active bars is $2n + 1$ for the edge loading case and $n + 1$ for the corner loading case);
- S = dowel spacing;
- C = percent of total load transferred across joint; and
- P_i = total load.

Some of the above parameters are shown in Figure 1.

Because the most important parameter in the first step of the current design procedure is maximum shear force, the EEL may be defined as a length L that can be determined by Equation 6 or 7, depending on the edge or corner loading case. The maximum shear force and the percent of the total load transferred can be calculated by an appropriate finite element program as discussed by Guo et al. (11,12). According to definition, n is not the total number of the effective dowels on one side of the bar under the load; it is only the number of the dowels that significantly transfer load. As shown in Figure 1, n is 5 under the EL definition but is only 3 under the EEL definition.

The EEL formulas can be obtained by solving L in Equations 6 and 7 as follows (P is equal to P_m when the EEL definition is applied). When the load is located at the edge of the joint,

$$\frac{L}{l} = \frac{P_m n(n + 1) S}{l[(2n + 1)P_m - P_i C]} \quad (8)$$

When the load is located at the corner of the joint,

$$\frac{L}{l} = \frac{P_m n(n + 1) S}{2l[(n + 1)P_m - P_i C]} \quad (9)$$

In any case the following formula must be satisfied:

$$n \leq \frac{L}{S} \leq (n + 1) \quad (10)$$

There exists a significant difference between the concept of the EL and the EEL. The EL is an assumed value for predicting the maximum shear force that may be either more or less than the actual value. The EEL is the value calculated by using the "actual maximum shear force" predicted by the finite element method so that when it is substituted back in Equation 6 or 7 the predicted maximum shear force must be equal to the actual force calculated by the finite element program. Friberg (2) proposed $L_1/l = 1.8$ and Tabatabaie et al. (9) suggested $L_1/l = 1.0$, whereas both assumed L/l constant. However, Equations 8 and 9 indicate that L/l , where L is corresponding to the actual maximum shear force of the dowels, is a function of n , S , P_m , P_i , and C , as well as the radius of relative stiffness l .

Some Characteristics of EEL

JSLAB-92 [a computer program modified from the JSLAB version 1986 developed by Tayabji et al. (13)] was employed to calculate the maximum shear force on the dowel bar. The finite element mesh is given in Figure 2. The numerical analyses were conducted for two loading cases. The first is a 40-kN (9,000-lb) load with tire pressure of 344.5 kPa (50 psi) acting at Node I in Figure 2. The loading area is $30.5 \times 38.1 \text{ cm}^2$ ($12 \times 15 \text{ in.}^2$), and this case is defined as edge loading. The second is the same type of load acting at Node J in Figure 2, and this case is defined as corner loading. Using the calculated maximum shear forces and the percentage of total load transferred across the joint, L/l may be calculated by using Equations 8 through 10.

By using the EL assumption, the higher subgrade modulus always reduces the l -value (Equation 1) and then reduces L_1 ($L_1 = 1.81$ or $L_1 = 1.01$) and the number of effective dowels n (Equation 10). Because the percent of the total load transferred is assumed constant, the maximum shear force and bearing stress will always increase as shown in Table 1. However, Figure 4 indicates that L/l increases when the k -value increases. Figure 5 shows that the total load transferred decreases as the k -value increases. Figures 4 and 5 explain that the increase of subgrade modulus does not have to increase the maximum bearing stress.

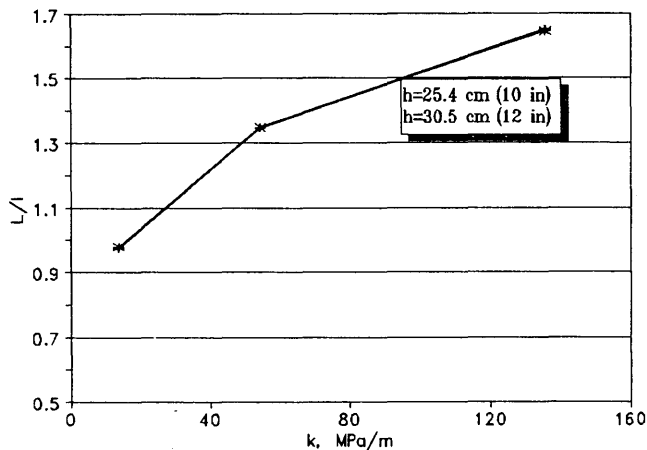
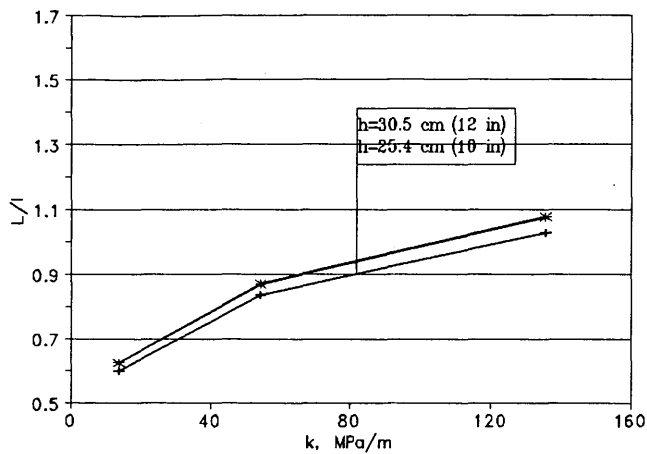


FIGURE 4 Effects of subgrade modulus on EEL: *top*, load at corner; *bottom*, load at edge.

Relation Between EEL and *l*

Figure 6 plots the 12 examples with the same dowel-concrete interaction coefficient (0.407×10^6 MPa/m = 1.5×10^6 psi/in.), dowel diameter (3.175 cm = 1.25 in.), and joint opening (0.635 cm = 0.25 in.), but with different slab thickness and subgrade modulus for both edge and corner loading cases. For the same radius of the relative stiffness value *l*, the *L* value could be very different. Therefore, the rather wide bandwidth suggests that the assumptions of $L/l = 1.8$ or 1.0 might not be an appropriate assumption to accurately predict the maximum shear forces on the critical dowel and the maximum bearing stress of the concrete.

EFFECTS ON MAXIMUM BEARING STRESS

When Friberg (2) developed the dowel bar analytical model in 1940s, it was impossible to analytically predict the maximum shear force acting on the critical dowel precisely; hence, he proposed the approximate but simple procedure for the dowel bar design. Since development of the finite element method and the application of high-speed computers, more options now exist for analyzing the load transfer mechanism. For

example, it is not necessary to divide the entire analysis procedure into two steps. As discussed by Guo et al. (11,12), the component model of a dowel bar can be installed into a finite element program to calculate the responses of each dowel, including the distribution of bending moments, shear forces, the relative displacements of the beam, and the bearing stresses of the concrete. The results are calculated with comprehensive consideration of all inputs simultaneously and without additional assumptions such as effective length and percent of total load transferred. In this section, more numerical examples will be given to analyze the effects of different variables on the maximum bearing stress of the critical dowel. All results presented in this section were calculated for a single tire with 40 kN (9,000 lb) acting at the corner of the slab (Figure 2).

Effects of Slab Thickness and Subgrade Modulus

Figure 7 shows that the bearing stress decreases when the slab thickness increases. Four curves showing the effects of the subgrade modulus on the maximum stress are presented in Figure 8 and indicate that the maximum stress decreases when the subgrade modulus (*k*-value) increases. This conclusion is different from the results presented previously (8,9) (see also

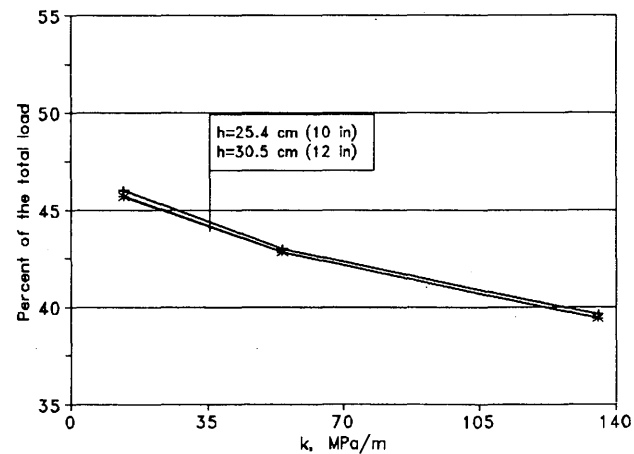
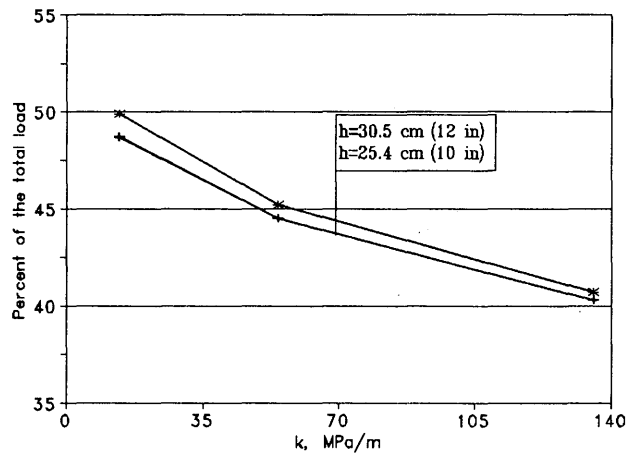


FIGURE 5 Effects of subgrade modulus on load transfer efficiency: *top*, load at corner; *bottom*, load at edge.

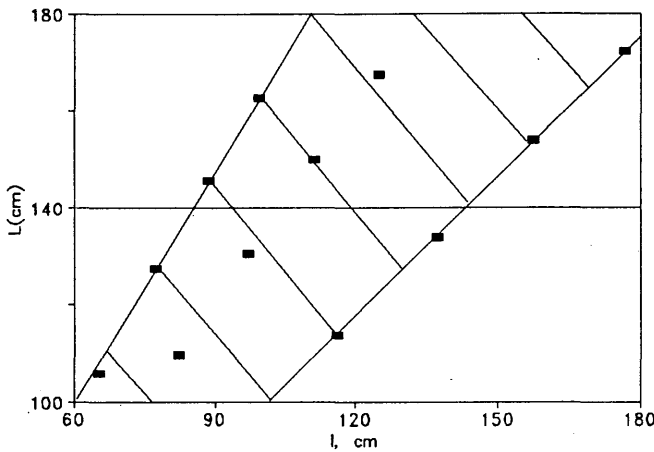
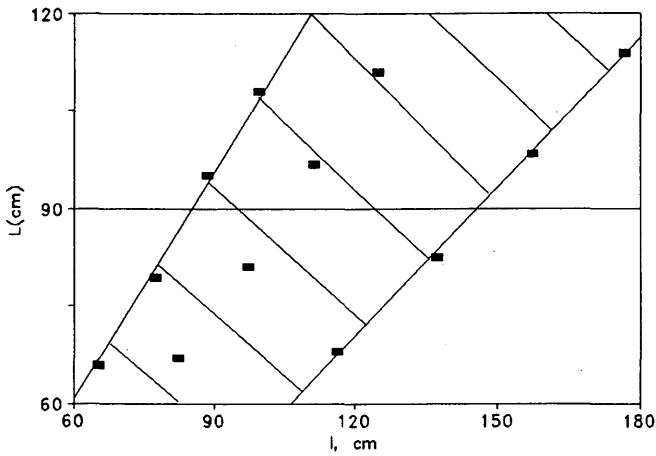


FIGURE 6 Relationship between EEL and l (radius of relative stiffness): top, load at corner; bottom, load at edge.

Figure 3 and Table 1). It is believed that the historical discrepancy was caused by using the effective length assumption, which sometimes cannot accurately describe the maximum bearing stress characteristics.

Effects of Dowel Diameter and Width of Joint Opening

Figure 9 indicates that the maximum bearing stress of the concrete is very sensitive to the dowel's diameter (D), which might be the most sensitive parameter of all. The smaller diameter can cause a dramatic increase in the maximum stress. This finding qualitatively has good agreement with those found in previous formulas (2,9) (Equations 2 through 4). Both Figures 9 and 10 indicate the insensitivity of the maximum bearing stress due to the variation of width of the joint opening. Using Equation 4 to predict the maximum bearing stress, the increase of joint opening from 0.635 cm (0.25 in.) to 1.905 cm (0.75 in.) yields about a 16 percent increase in the maximum bearing stress, $[0.355 \times (0.75 - 0.25)/(1 + 0.355 \times 0.25)] \times 100 = 16.3$. However, by using the dowel bar component model in JSLAB-92, the increase is only 1.2 percent for the $D = 1.905$ -cm (0.75-in.) dowel, 3.3 percent for the

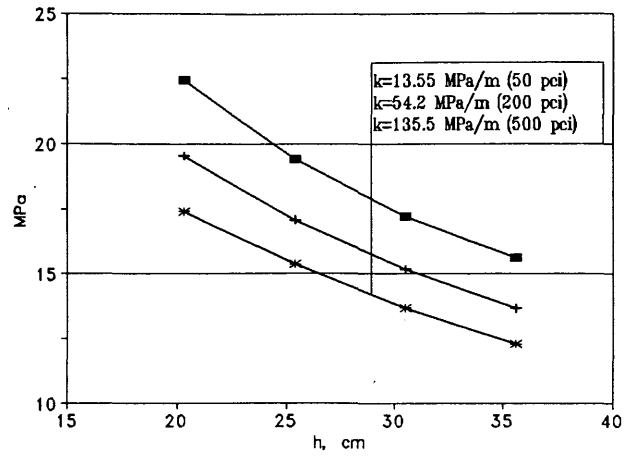


FIGURE 7 Effects of slab thickness on maximum bearing stress.

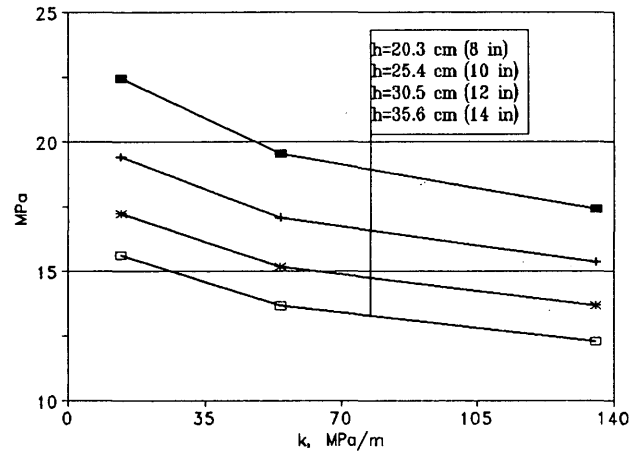


FIGURE 8 Effects of subgrade modulus on maximum bearing stress.

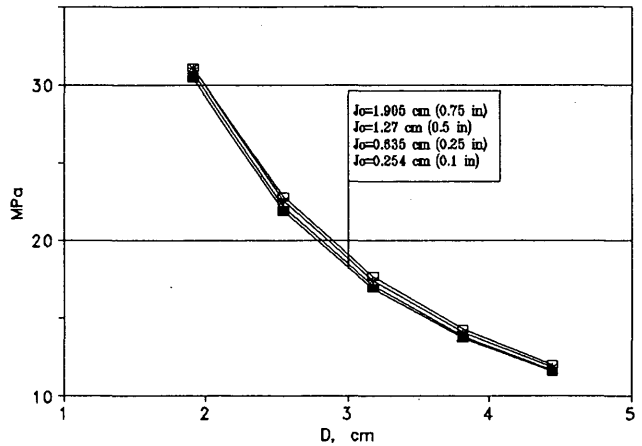


FIGURE 9 Effects of dowel diameter on maximum bearing stress.

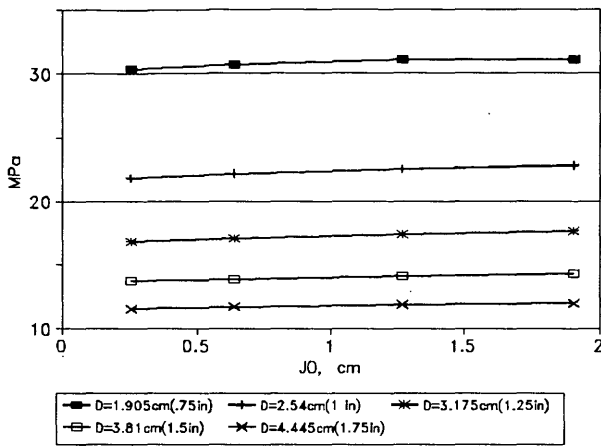


FIGURE 10 Effects of width of joint opening on maximum bearing stress.

$D = 3.175$ -cm (1.25-in.) dowel, and 2.7 percent for the $D = 4.445$ -cm (1.75-in.) dowel.

Effects of Concrete Elasticity and Dowel-Concrete Interaction Coefficient

Figure 11 presents the maximum stress curves versus the dowel-concrete interaction coefficient Ψ . As summarized previously (5), the values of Ψ measured by various investigators varied from 81.3 to 2331 GPa/m (0.3×10^6 to 8.6×10^6 lb/in.³). In practice, 406.5 GPa/m (1.5×10^6 lb/in.³) is often used. However, Ψ is a function of such variables as concrete properties, dowel bar diameter, slab thickness, dowel length, and dowel looseness. Figure 11 shows that the higher Ψ corresponds to the higher maximum bearing stress and implies that the dowel in a deteriorated joint or with significant looseness would have a smaller maximum bearing stress.

Figure 12 shows that the maximum bearing stress decreases when the concrete elasticity modulus increases. As discussed earlier, this is understandable because the higher E -value in-

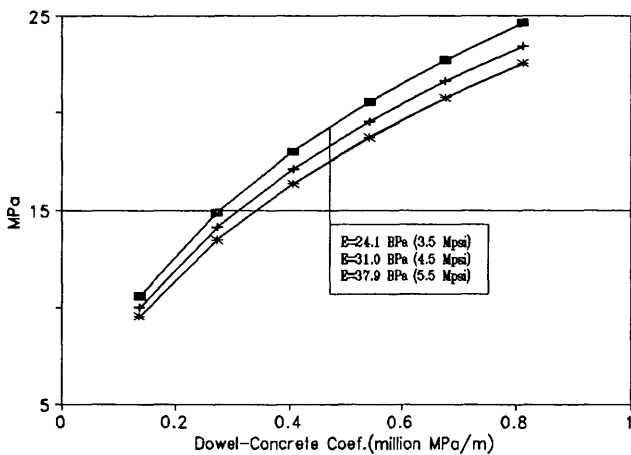


FIGURE 11 Effects of dowel-concrete interaction coefficient on maximum bearing stress.

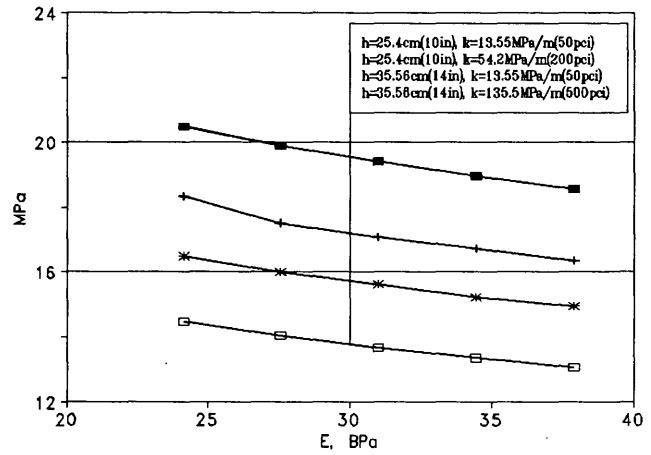


FIGURE 12 Effects of concrete elasticity modulus on maximum bearing stress.

dicates that the stronger loaded slab can withstand more of the load and will distribute less load across the dowels to the unloaded slab. Because the role of the higher E -value is similar to that of the higher k -value of the subgrade, both should reduce the amount of load transferred across the joint. However, Equation 4 indicates that the higher E -value would cause higher maximum bearing stress. The discrepancy might be partially caused by the application of the dowel stiffness matrix in ILLISLAB and the component stiffness matrix in JSLAB-92 (11,12). The former produces a nonequilibrium element, which occasionally leads to unreasonable results.

SUMMARY

A general principle has been drawn from analyzing the results of hundreds of numerical examples: The higher values of dowel diameter, slab thickness, concrete modulus, and subgrade modulus can reduce the maximum bearing stress of the concrete under the critical dowel. The maximum bearing stress is not sensitive to the width of joint opening but is very sensitive to the dowel-concrete interaction behavior (which is difficult to control).

The discovery of an error in the stiffness matrix of dowel bars used in some finite element programs and of the inappropriate utilization of the joint effective length made it necessary to reevaluate some design procedures for the dowel system. The following are the major findings in this paper.

- Equation 4 could yield some questionable results. The maximum bearing stress does not increase proportionately with the increase in concrete elasticity E , and it is also not sensitive to the width of joint opening, as indicated in Equation 4.
- The maximum bearing stress of the critical dowel increases as the subgrade modulus decreases. This finding, different from the conclusion presented in the historical literature, suggests that the most critical season in the year for the maximum bearing stress is spring because the thawing reduces the subgrade modulus in the wet-frozen region. The thawing

effect (subgrade softening) could cause a 10 to 20 percent difference in the maximum bearing stress.

- The use of the effective length, which began in the 1940s and was modified at the end of the 1980s, underestimates the maximum bearing stress in some cases. The equivalent effective length concept presented herein has been developed to prove that the EL assumption needs more study.

- The most critical dowel is the one under a tire load nearest the corner. The maximum bearing stress could be two times that of the critical dowel stress under the tire load at the edge of the joint.

- Because of the significant difference between the results obtained from the existing and the developed models in predicting the maximum bearing stresses, it is suggested that all empirical models that use Equation 4 to calculate the maximum bearing stress, and then to predict the joint faulting, should be reevaluated before being employed in engineering projects.

ACKNOWLEDGMENT

The authors gratefully acknowledge the valuable support of FHWA.

REFERENCES

1. S. Timoshenko et al. *Strength of Materials, Part II, Advanced Theory and Problems*, 2nd ed. D. Van Nostrand Company, Inc., 1941.
2. B. F. Friberg. Design of Dowels in Transverse Joints of Concrete Pavements. *Transactions ASCE*, Vol. 105, 1940.
3. L. W. Teller et al. A Study of Structural Action of Several Types of Transverse and Longitudinal Joint Designs. *Public Roads*, Vol. 17, No. 7-8, 1936.
4. L. W. Teller et al. Performance of Dowels under Repetitive Loading. *Public Roads*, Vol. 30, No. 1, April 1958.
5. E. A. Finney et al. Progress Report on Load Deflection Tests Dealing with Length and Size of Dowels. *HRB Proc.*, Vol. 27, 1947.
6. J. R. Keeton et al. Load Transfer Characteristics of a Doweled Joint Subjected to Aircraft Wheel Loads. *HRB Proc.*, Vol. 36, 1957.
7. M. B. Snyder. *Dowel Load Transfer Systems for Full-Depth Repairs of Jointed Portland Cement Concrete Pavements*. Ph.D. thesis. University of Illinois, Urbana, 1989.
8. K. W. Heinrichs et al. *Rigid Pavement Analysis and Design*. Report FHWA-RD-88-068. FHWA, U.S. Department of Transportation, 1988.
9. A. M. Tabatabaie et al. *Analysis of Load Transfer System for Concrete Pavements*. Report FAA-RD-79-4, FAA, U.S. Department of Transportation, 1979.
10. A. M. Ioannides et al. *Analysis of Slab-on-Grade for a Variety of Loading and Support Conditions*. Report AFOSR-83-0143, Dec. 1984.
11. H. Guo et al. Dowel Bar Modeling of Finite Element Program for PCC Pavement Analysis. *Workshop on Load Equivalency, Mathematical Modeling of PCC Pavements*, Feb. 1992.
12. H. Guo. *Mathematical Modeling for Dowel Load Transfer Systems*. Ph.D. dissertation. Michigan State University, East Lansing, July 1992.
13. S. D. Tayabji et al. *Analysis of Jointed Concrete Pavements*. Report FHWA-RD-86-041. FHWA, U.S. Department of Transportation, Feb. 1986.

DISCUSSION

A. M. IOANNIDES

University of Illinois, Urbana, Ill.

In the pursuit of improved mechanistic design procedures for doweled PCC pavements, the "component" dowel formulation introduced by the authors (3,4) is certainly a rigorous and well-founded contribution. Furthermore, results presented in the paper are invaluable in clarifying several crucial issues related to the design of doweled joints. Intense research activities at the University of Illinois (UI) in the last 5 years have also focused on unraveling the complex interactions arising at such joints (14,15). The purpose of this discussion is to complement the authors' work by providing some additional information from the UI studies.

An important conclusion reached by the authors is that "the maximum bearing stress (σ_{max}) . . . increases as the subgrade modulus (k) decreases," thereby contradicting "the historical literature." The authors correctly point out that the finite element (FE) program J-SLAB does not confirm the trend presented in a sensitivity plot (Figure 2) by Heinrichs et al. (8). However Figure 2 was compiled using computer program PFAULT, and not the UI FE program ILLI-SLAB. Whereas the latter is primarily an analytical tool, PFAULT was intended to facilitate the application of a mechanistic-empirical design algorithm. As such, PFAULT incorporates a number of reasonable and necessary—at the time—assumptions, including two alluded to by the authors, that is, that the transferred load efficiency (C) is assumed to be 45 percent and that the "effective length" (L) is assumed to be equal to the radius of relative stiffness (l) of the slab-subgrade system. From a design point of view (14), another significant assumption pertains to the value of the "dowel-concrete interaction coefficient" (Ψ) which is set to 1.5 million lb/in.². When ILLI-SLAB is used to verify the authors' results in Table 1, it is found that, indeed, as k increases, σ_{max} decreases. The source for the discrepancy in trends noted by the authors is, therefore, not the result of a difference between the J-SLAB and ILLI-SLAB FE programs, but rather the consequence of the semiarbitrary assumptions made in PFAULT to incorporate knowledge obtained using the FE method into a practical design algorithm, which would not necessitate the execution of any demanding FE code. Table 2 clearly indicates that neither the C - nor the L -assumptions in PFAULT are satisfied in the cases considered by the authors. The contradiction identified by the authors points to the need to exercise caution when empirical (or even mechanistic-empirical) algorithms are used in sensitivity analyses, particularly concerning variables for which they afford little resolution. As Heinrichs et al. (8) pointed out, "the (PFAULT) solution is more sensitive to those variables related to the dowel bars used (i.e., dowel diameter, spacing, and modulus of support) than to pavement system characteristics (e.g., slab modulus and thickness, subgrade modulus, and joint width)."

It is also observed in Table 2 that ILLI-SLAB results can be considerably different from those obtained using J-SLAB. It is not readily apparent, however, that such differences are exclusively due to the "component" dowel formulation introduced in J-SLAB. Similar discrepancies had been observed in comparisons with results from an earlier version of J-SLAB

and were ascribed to "differences in the FE idealizations adopted in each of these programs" (15). J-SLAB was found to accentuate "the relative importance of the bending load transfer mechanism compared to the shear mechanism by 5 to 20 times." Note that the ILLI-SLAB results in Table 2 were obtained assuming that the dowels are pure shear load transfer devices (no moment transfer), which is consistent with the prevailing understanding of in situ phenomena (16). It would be very enlightening as to the net effect of the introduction of the "component" dowel formulation if the authors presented a comparison between results obtained using the original and their modified versions of J-SLAB.

The authors do not address the development of a design algorithm that would dispense with the need to execute an FE code on a case-by-case basis. Setting $L = nS$ in Equations 6 and 7, these become identical to the formulas presented by Ioannides et al. (17); that is, an assumption about the size of L is still required. Equations 8 and 9 cannot be used for this purpose because they involve the maximum dowel shear force (P_m), which would be available only if the FE code were executed. Such an execution would, of course, determine L precisely as well, thus dispensing with the need for an assumption about its size. The authors note that (L/l) "is a function of n , S , P_m , P_r , and C , as well as the radius of relative stiffness, l ." The large number of variables warrants the use of dimensional analysis as done by Ioannides and Korovesis (14). A much simpler solution to this problem was recently proposed by Khazanovich and Ioannides (18), who suggested estimating P_m by the following expression:

$$P_m = B \frac{1 - LTE_\delta}{1 + LTE_\delta} \Delta_f \quad (11)$$

In this expression LTE_δ is the load transfer efficiency in terms of deflections, B is set equal to the composite (springs-

in-series) shear stiffness of the composite dowel [given by Equation 2 previously (14)], and Δ_f is the free-edge (or free-corner) deflection at the critical location. LTE_δ may be measured in the field or may be estimated using the S-shaped curve in Figure 1 (14) for edge loading; a similar curve may also be compiled for corner loading. Δ_f may be calculated using the appropriate Westergaard equation (19) or simply set equal to the sum of the deflections measured in the field on the loaded and unloaded sides of the joint at the critical location. The last column in Table 2 confirms that this method applies, assuming that dowels are pure shear load transfer devices.

REFERENCES

14. A. M. Ioannides and G. T. Korovesis. Analysis and Design of Doweled Slab-On-Grade Pavement Systems. *Journal of Transportation Engineering*, ASCE, Vol. 118, No. 6, Nov./Dec. 1992, pp. 745-768.
15. A. M. Ioannides and G. T. Korovesis. Backcalculation of Joint Related Parameters in Concrete Pavements. *Proc., 3rd International Conference on the Bearing Capacity of Roads and Airfields*, Trondheim, Norway, July 3-5, 1990, Vol. 1, pp. 549-558.
16. A. M. Tabatabaie and E. J. Barenberg. Finite-Element Analysis of Jointed or Cracked Concrete Pavements. In *Transportation Research Record 671*, TRB, National Research Council, Washington, D.C., 1978, pp. 11-19.
17. A. M. Ioannides, Y. H. Lee, and M. I. Darter. Control of Faulting Through Joint Load Transfer Design. In *Transportation Research Record 1286*, TRB, National Research Council, Washington, D.C., 1990, pp. 49-56.
18. L. Khazanovich and A. M. Ioannides. *Glasnost and Concrete Pavement Engineering: Insights Concerning Slabs-On-Grade from the Former Soviet Union. Proc., 5th International Conference on Concrete Pavement Design and Rehabilitation*, Purdue University, West Lafayette, Ind., April 20-22, 1993.
19. A. M. Ioannides, M. R. Thompson, and E. J. Barenberg. Westergaard Solutions Reconsidered. *Transportation Research Record 1043*, TRB, National Research Council, Washington, D.C., 1985, pp. 13-23.

TABLE 2 Verification of Authors' Results for Corner Loading

RUN	k pci	D in.	P _T lb	P _m lb	ILSL		JSLAB		C %	f _{dc}	L/l	δ _L mils	δ _U mils	LTE _δ	B lb/in.	P _m * lb
					σ _{max} psi	σ _{max} psi	σ _{max} psi	σ _{max} psi								
1	50	0.75	3957	2273	5987	5158	43.96	0.574	0.565	37.17	33.04	0.889	5.51E+05	2273		
2	200	0.75	3616	2086	5494	4459	40.17	0.576	0.795	16.52	12.73	0.770	5.51E+05	2086		
3	500	0.75	3278	1900	5004	3846	36.42	0.579	0.993	10.18	6.737	0.661	5.51E+05	1900		
4	50	1.25	4010	2743	2861	2815	44.55	0.684	0.438	36.09	34.13	0.945	1.40E+06	2743		
5	200	1.25	3751	2584	2695	2478	41.67	0.688	0.613	15.55	13.70	0.881	1.40E+06	2584		
6	500	1.25	3509	2430	2535	2229	38.98	0.692	0.765	9.332	7.592	0.813	1.40E+06	2430		
7	50	1.75	4027	3033	1728	1964	44.74	0.753	0.377	35.70	34.52	0.966	2.56E+06	3033		
8	200	1.75	3794	2882	1642	1692	42.15	0.759	0.526	15.18	14.06	0.925	2.56E+06	2880		
9	500	1.75	3586	2742	1562	1524	39.84	0.764	0.655	8.997	7.927	0.881	2.56E+06	2741		

Note: P_T = total transferred load by all dowels;

C = transferred load efficiency = (P_T/P_t) × 100%;

f_{dc} = critical distribution factor = (P_m/P_T);

Δ_L = deflection on the loaded side of the joint at the critical location;

Δ_U = deflection on the unloaded side of the joint at the critical location;

LTE_δ = (Δ_U/Δ_L);

P_m* = Value of P_m predicted by Eq. (11).

AUTHORS' CLOSURE

It is a pleasure to read the discussion by Ioannides, who corroborates the findings through his own research; in particular he states that ILLISLAB has been used to verify that as subgrade modulus k increases, the maximum bearing stress σ_{\max} decreases.

The authors agree with the statement in the discussion: J-SLAB (13) "was found to accentuate 'the relative importance of the bending load transfer mechanism compared to the shear mechanism by 5 to 20 times.'" It has also been found that the maximum dowel bending moments calculated by the original J-SLAB could differ from the modified JSLAB-92 by more than 10 times. This discrepancy was caused by the nonequilibrium stiffness matrix employed in the J-SLAB program. It is believed that the component model (11,12) installed in JSLAB-92 has the ability to more appropriately consider the contribution of shear and bending in the dowel design (11,12).

Equation 11 could be a very good form for estimating the maximum shear force in the dowels. When test data are avail-

able (δ_v , δ_L , and then LTE_δ), the equation can be used to estimate the maximum shear force in a straightforward manner. However, it seems that Equation 11 should be used with special care where the dowels exhibit significant looseness, which is often the condition in the field. For example, one limit case is the joint that has entirely lost its load transfer capability, namely, $\delta_v = 0$, then $LTE_\delta = 0$ and $P_m = B\Delta_j$; this result is greater than the shear force of any dowel in perfect condition. In fact, P_m should be zero in this case, not the maximum.

The considerable difference between the results by ILLI-SLAB and JSLAB-92 in Table 2 might be caused by the various dowel bar models used in the two programs. As discussed previously (11,12), the dowel stiffness matrix used in ILLI-SLAB cannot satisfy the equilibrium conditions [see Equations 3 through 43 in Tabatabaie et al. (9)]. Further study is needed to quantitatively evaluate the effects of using the nonequilibrium stiffness matrix in a computer program.

Publication of this paper sponsored by Committee on Rigid Pavement Design.

Comparison of Four Different Methods for Measuring Deflections in Jointed Reinforced Concrete Pavements

ANDREW BODOCSI, ISSAM A. MINKARAH, CHARLES S. YOUNG,
RICHARD A. MILLER, AND RAJAGOPAL S. ARUDI

A total of 107 dynamic deflection tests on a jointed reinforced concrete pavement were conducted to compare the performance of four measuring instruments: the linear voltage displacement transducer (LVDT), the geophone, the falling weight deflectometer (FWD), and the Dynaflect. The deflections were measured at six joints of the test pavement in the southbound roadway on Route 23 in Chillicothe, Ohio. The deflections measured by LVDT and geophone were produced by the axle loads of a fully loaded two-axle truck. Thus, this test program allowed the comparison of not only the performance of the four types of instruments, but also the deflections caused by "real-life" truck loading with those caused by "artificial" FWD and Dynaflect test loadings. Furthermore, the deflection measurements at the joints due to truck load were compared at four different speeds: static (0 mph or 0 km/hr) and moving at 10, 35, and 50 mph (16, 56, and 80 km/hr). Another important aim of this test program was to determine whether the geophone measurements were reliable and how truck speeds affected them. It was found that the LVDT and geophone deflection measurements agreed well, provided that the truck speed was equal to or exceeded 35 mph (56 km/hr). Also, the static deflection test results closely agreed with those from the moving load tests. Furthermore, it was found that the normalized FWD test results yielded the highest deflections, approximately 13 percent higher than the deflections caused by the moving truck. On the other hand, the results from the normalized Dynaflect tests agreed well with the deflections caused by the moving truck.

In 1972 the Ohio Department of Transportation (ODOT) built a jointed reinforced concrete pavement test section 3,225 ft (983 m) long in the southbound roadway on Route 23 in Chillicothe, Ohio. The pavement slab is 9 in. (0.229 m) thick. Some portions of the slab were built on granular base 12 in. (0.305 m) thick; others on asphalt-treated base 4 in. (0.102 m) thick. This test section was studied from 1972 to 1980 (1-3), and again from 1989 to 1992 by researchers at the University of Cincinnati for joint behavior, such as horizontal movements and vertical joint deflections, and for various signs of deterioration. The pavement in Chillicothe is exceptionally suited for experimental studies because several key variables were incorporated into the pavement, namely, joint spacing, type of base, type of dowel bar, and configuration of the sawcut. Table 1 shows the joints that were tested in this pro-

Department of Civil and Environmental Engineering, University of Cincinnati, ML 0071, Cincinnati, Ohio 45221-0071.

gram and the characteristic properties of the pavement segment straddling each joint.

In the early and mid-1970s joint deflections were measured under a fully loaded truck with a rear axle load of approximately 18 kips (80.06 kN) and moving at speeds of 10, 35, and 50 mph (16, 56, and 80 km/hr). When the pavement research was resumed in 1989, it was decided that the vertical joint deflections would again be measured under a moving truck so that the new results could be compared with the old ones. Also in this test program, the pavement was surveyed for longitudinal and transverse cracking, faulting of joints, and pavement and corner cracking. The most significant damage was transverse cracking. The pavement condition index (PCI) in 1991 ranged from a high of 80 to a low of 41. A weighted average PCI of 59 was obtained for the entire pavement.

Furthermore, in 1989 geophones were used as additional instruments for measuring vertical joint deflections. Also, in the fall of 1990, ODOT conducted falling weight deflectometer (FWD) and Dynaflect measurements at the same time and on the same joints as the truck tests.

In summary, the fundamental purpose of the test program was to compare joint deflections from truck tests with those from FWD and Dynaflect tests, and to compare geophone measurements with those from the linear voltage displacement transducer (LVDT). Specifically, the program aimed at answering the following questions:

- How do results from truck load tests relate to those from FWD and Dynaflect tests?
- How closely matched are the deflections measured by the various methods, and specifically, do geophone measurements agree with those from the LVDT?
- How do static deflections relate to the deflections under the moving truck load?
- Does truck speed affect the accuracy of geophone deflection measurements?

In this phase of the program, a total of six different joints were tested for vertical deflections. This paper presents a summary of the instrumentation, the calibration procedures, the test methods used, and the final results.

TABLE 1 Joint Designation and Test Pavement Information

Joint No.	Joint Spacing, m	Type of Base	Type of Dowel
21	6.4	Stabilized	Standard (Uncoated)
29	12.2	Stabilized	Standard (Uncoated)
49	6.4	Granular	Coated
59	12.2	Granular	Coated
69	12.2	Granular	Standard (Uncoated)
89	6.4	Granular	Standard

INSTRUMENTATION AND CALIBRATION

Four different deflection measuring instruments were used during this test program, namely LVDT, geophone, FWD, and Dynaflect.

LVDT

The LVDT is a well-known and proven device used to measure relative displacements. Its drawback is that it requires a fixed reference point. The LVDT yields a voltage-time history directly proportional to the displacement-time history of its core-to-coil position. Table 2 gives the manufacturer's specifications for the LVDT used in these tests. Note that the only error listed by the manufacturer is that due to nonlinearity. For this transducer the error band is ± 0.0025 in. (0.0635 mm). Because it is a bias error, the error band can be reduced by proper calibration techniques to yield an accuracy of ± 0.0006 in. (0.0152 mm). Calibration of the LVDT was performed before each test to determine the appropriate calibration factor. The calibration curve for LVDT is shown in Figure 1.

Geophone

The geophone is a device that measures an output voltage proportional to the velocity of the base of the unit. This response is frequency dependent, particularly at lower frequencies (less than 15 Hz). Care must be taken to properly calibrate the geophone and to appropriately process its response to obtain velocity versus time and, in this test series, to obtain the deflections-versus-time history of the pavement joint to which the base of the geophone was attached. One great advantage of the geophone is that it does not need a fixed reference point to make a measurement. However, the deflection must take place at a relatively high velocity; in addition, static deflection measurements cannot be made by a geophone. Table 3 gives the manufacturer's specifications for the geophone used in this project.

Thorough presentations on the characteristics of the geophone and its various uses can be found in papers by Nazarian (4), Nazarian and Bush (5), Nazarian and Alexander (6), and Graves and Drnevich (7).

To obtain the displacement-time history of the vertical deflection of a joint with a geophone, the frequency domain

TABLE 2 LVDT Specifications

Model Number	0242-0000
Range (working)	± 0.250
Maximum (usable)	± 0.375
Input Volts, DC	6.0 to 30.0
Input Current	8.3 ma @ 6V Input to 52 ma @ 30V Input
Linearity % Full Scale Over Total Working Range	± 0.5
Over Maximum Usable Range	± 1.0
Internal Carrier Frequency (Hz), Nominal Greater Than	3600
% Ripple (rms) Nom.	0.8
Output Impedance (Ohms)	5200
Frequency Response 3 db Down	115 Hz
Temperature Range	-65 °F to +250 °F
Resolution	Infinite

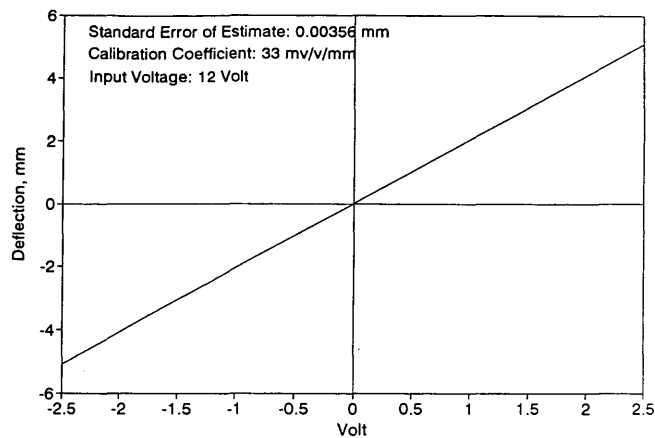


FIGURE 1 Calibration curve for LVDT 4.

solution, as described by Nazarian (4), was implemented. Specifically, before the geophone was used in the field, its frequency response function was determined through calibration. After the field measurements were taken, each velocity-time response was transformed to the frequency domain, using a fast Fourier transform. Next, this was divided by the frequency response function of the geophone to obtain the velocity spectrum. Division of the velocity spectrum by the angular frequency yielded the displacement spectrum. Finally, this signal was inverse Fourier transformed to obtain the displacement-time history of the deflected geophone (the same as the pavement joint to which it was attached).

The calibration of the geophone used in this project was performed at the Structural Dynamics Research Laboratory of the University of Cincinnati. The equipment for the calibration is shown schematically in Figure 2. The shaker, or exciter, was put in motion over a range of frequencies, and the output of the geophone and the LVDT was measured and

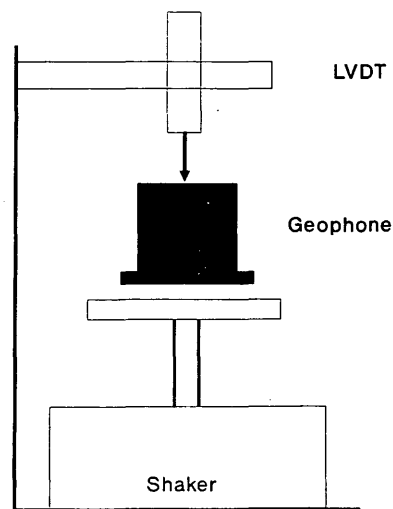


FIGURE 2 Geophone calibration equipment.

recorded. The frequency response function of the geophone was obtained by coupling the geophone output voltage to the actual displacement measured by the LVDT. An HP35660 signal analyzer was used for this purpose.

Two HP35660 signal analyzers were used to gather the field data. The reduction of the data was performed on a 386-based personal computer (PC), using the MATLAB analysis software.

FWD and Dynaflect

The FWD and the Dynaflect, both commercial road-testing devices, were provided by the Ohio Department of Transportation and operated by ODOT personnel. The falling weight

TABLE 3 Geophone Specifications

Model Number	L-10B
Standard Frequency Range, Hz	4.5 - 10
Frequency Tolerance	± 0.5 Hz
Standard Coil Resistance, Ohms	138/215/374
Resistance Tolerance, %	5 5 6.5
Maximum Distortion @ .7in/s @ 12 Hz or Resonance	0.2%
Transduction Constant, V/in/s $\pm 10\%$	$0.041 * \text{SQRT}(R_c)$
Open Circuit Damping, $\pm 10\%$	$1.908/f$
Coil Current Damping	$12.15 (R_c)/f(R_c + R_s)$
Suspended Mass, Grams	17.00
Power Sensitivity, mW/in/s	1.67
Case-to-Coil Motion, in. p-p	0.080
Basic Unit Diameter, in.	1.25
Basic Unit Height, in.	1.4
Basic Unit Weight, oz.	5.0

deflectometer device was a Dynatest model and was operated with a dynamic force output of between 14,968 and 15,826 lb (66.58 and 70.39 kN). The load was transmitted by a circular plate with a radius of 5.9 in. (0.150 m). The deflections were picked up by geophones.

The Dynaflect device was operated with the standard 1,000-lb (4.448-kN) peak-to-peak dynamic force range. The load was transmitted by two 16-in.-diameter (0.406-m) by 2-in.-wide (0.051-m) urethane-coated steel wheels. The deflections were sensed by geophones.

Both devices were calibrated each morning by their operators, using standard procedures, before leaving the ODOT garage.

TEST PROCEDURE

A total of 107 dynamic tests, which included a moving fully loaded two-axle ODOT truck and the FWD and Dynaflect devices, were performed on southbound State Route Ross 23 in Chillicothe, Ohio, the site of an ODOT test pavement. The tests were conducted during the fall of 1990. A geophone and an LVDT were placed at the various joints of the pavement, as shown schematically in Figure 3 for a typical joint.

The required fixed reference point for the LVDT measurements was provided by driving a steel rod 10 ft (3.048 m) long and 1 3/8 in. (0.035 m) in diameter approximately 4 in. (0.102 m) away from the edge of the pavement in a 9-in.-deep (0.229-m) cutout hole, adjacent to each of the six joints tested. The tip of the rod was driven to be flush with the bottom of the 9-in.-thick (0.229-m) pavement slab. For each test sequence the coil assembly of the LVDT was attached to the side of the pavement at a point directly above the reference rod. The core of the LVDT was attached to the top of the reference

rod. Deflection of the pavement at one side of the joint caused the coil assembly to move in relation to the fixed core. An output voltage proportional to the pavement movement was produced and recorded. Power to the LVDT was supplied by a 12-V battery.

The geophone was glued to the top surface of the pavement, approximately 3 in. (0.076 m) from both the joint and the edge of the pavement. The sudden deflection of the pavement from truck loading caused the geophone to record the velocity changes, producing an output voltage directly proportional to this velocity. Both geophone and LVDT signals were recorded by HP35660 signal analyzers.

For each of the six joints, the tests began by placing the rear axle of the fully loaded two-axle truck, with front and rear axle loads of 7,600 and 20,450 lb (33.80 and 90.96 kN), respectively, on the leave side of the instrumented joint to measure the static slab deflection. Afterward the truck was driven across the joint consecutively at speeds of 10, 35, and 50 mph (16, 56, and 80 km/hr), and the vertical deflection of the joint was again measured. Lines were placed on the pavement to guide the truck so as to maintain a constant 12-in. (0.305-m) distance from the pavement edge.

The data recorded were uncalibrated geophone and LVDT voltages. The LVDT voltage was converted to displacement by multiplying the data by a constant scale factor that was derived earlier during the calibration procedure. The geophone data were converted from a raw voltage (that was proportional to velocity) to a displacement, using

$$\text{IFFT} = \text{FFT}(\text{DATAFILE}) \cdot \text{FRF} \cdot \text{K1} \quad (1)$$

where IFFT is the displacement function and FFT is the recorded voltage function from the data file. The frequency response function (FRF) was established previously for the geophone during the calibration procedure. K1 is a constant of the LVDT that was used in calibrating the geophone.

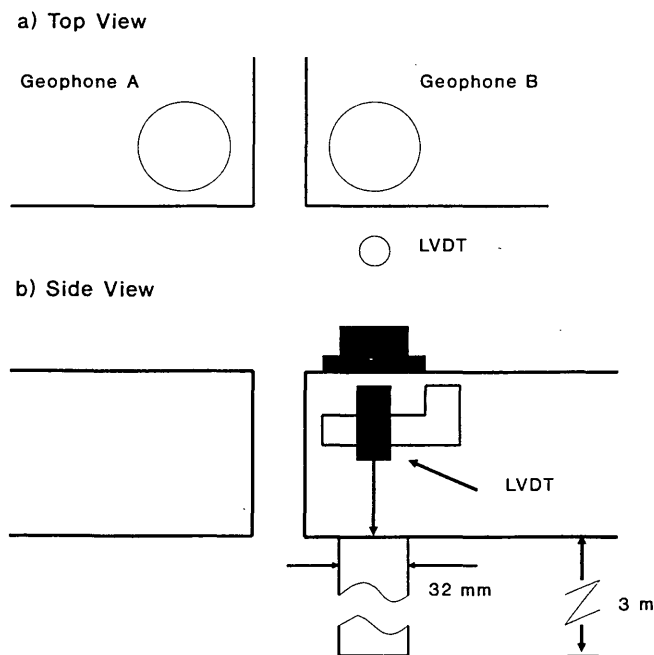


FIGURE 3 Placement of geophone and LVDT on pavement.

RESULTS

The LVDT and geophone measurements were analyzed, digitized, and then plotted for each of the six joints and for each of the three truck speeds (two or three trials each). Because the values from the trials agreed well with each other, only the average value was reported in Table 4. Typically, for each test, the LVDT and geophone deflection-versus-time plots were printed on the same sheet, and to the same scale, for ease of comparison. Of course, for the static tests only LVDT data were taken. As an example, Figure 4 presents the LVDT (solid curve) and geophone (dashed curve) plots of deflections for Joint 59 caused by the fully loaded two-axle truck moving across the joint at a speed of 35 mph (56 km/hr). There are two peaks on each curve, the first caused by the passing of the front axle of the truck over the joint, and the second caused by the passing of its rear axle. The net deflection of the joint from either of the plots, and caused by either of the axles, can be obtained by reading the deflection at the peak point and adjusting this reading by the zero offset at the beginning of the plot.

TABLE 4 Summary of Peak Deflection Measurements

Date: October 31/November 1, 1990 Rear Truck Axle: 90.96kN

Joint #	Static Load	LVDT			Geophone			FWD, Normalized	Dyna-flect, Normalized	AM/PM	Pavement Surface Temperature, °C
		16 km/h	56 km/h	80 km/h	16 km/h	56 km/h	80 km/h				
21	0.1016	0.0610	0.0584	0.0940	0.0356	0.0635	0.0737	0.0965	0.0762	PM	19
29	---	0.1321	0.1118	0.1041	0.0686	0.0991	0.1016	0.1092	0.0864	AM	17
49	---	0.0965	0.1092	0.1143	0.0406	0.1219	0.1067	0.1397	0.1219	PM	21
59	0.1422	0.1854	0.1778	0.1651	0.0813	0.1422	0.1549	0.1346	0.1219	AM	13
69	0.1321	0.0914	0.0991	0.0940	0.0584	0.1168	0.1245	0.1321	0.1168	PM	19
89	0.0991	0.0813	0.0914	0.0940	0.0533	0.1016	0.1143	0.1422	0.1270	PM	21
Mean	0.1067	0.1080	0.1080	0.1110	0.0564	0.1074	0.1125	0.1257	0.1085		

Note: All tabulated deflections are net average deflections. The range of temperature gradient during testing was from -0.04°C/mm to -0.01°C/mm, where the bottom of slab was permanently warmer than the top.

The FWD and Dynaflect measurements were processed by the on-board computers in the ODOT vans, and the printouts of the results were provided by ODOT to the researchers.

The composite of all results from the measurements taken during the fall of 1990 is presented in Table 4. Here, for each tested joint, the peak deflections from the LVDT and geophone measurements under the moving rear axle of the truck are tabulated, together with the normalized FWD and Dynaflect measurements. The FWD and Dynaflect measurements were normalized using one level of dynamic force for each (see the section on instrumentation and calibration) and linearity. In addition, the deflection of the same joints caused by the static application of the rear axle of the truck is also

presented. Also shown are the pavement surface temperature and the time of day each test was conducted.

ANALYSIS AND CONCLUSIONS

The results from the extensive investigation of the vertical deflections of six joints in the ODOT test pavement in Chillicothe, Ohio, are summarized in Table 4. After analyzing this table and other accumulated data, the following conclusions can be drawn:

- The overall means of the results from the static tests, the 10-, 35-, and 50-mph (16-, 56-, and 80-km/hr) LVDT tests,

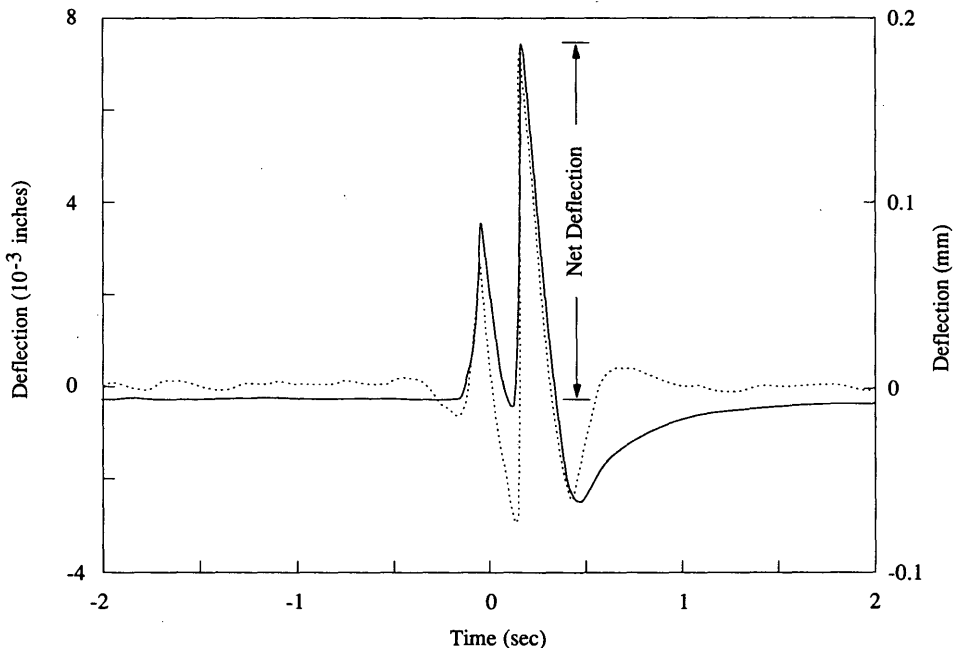


FIGURE 4 LVDT and geophone plots of deflections for Joint 59.

the 35- and 50-mph (56- and 80-km/hr) geophone tests, and the normalized Dynaflect test results all compared well.

- The joint-by-joint comparison of LVDT deflections with geophone deflections at 50 mph (80 km/hr) showed good agreement in three out of six cases. The spread of deviation was 2 to 32 percent. Also, for afternoon (p.m.) measurements, the LVDT deflections at 10 mph (16 km/hr) were all found to be smaller than at 50 mph (80 km/hr). Furthermore, all FWD deflections were slightly higher than the LVDT and geophone deflections at 50 mph (80 km/hr), except at Joint 59.

- Truck speed had relatively little effect on the deflection results from LVDT measurements in this test series. Specifically, the mean deflections increased from 0.0042 to 0.0044 in. (0.00011 to 0.00012 m) as the truck speed increased from zero (static test) to 50 mph (80 km/hr). However, at four out of the six joints tested, the joint deflections were found to be large at higher speeds. In general, increasing truck speed should result in increased joint deflections on concrete pavements, especially on older and rougher pavements, because of the dynamic interaction between the pavement and the truck tires, as shown by Gillespie et al. (8). The comparison of a large number of joint deflections on the same pavement from another phase of testing during four seasons of measurements by LVDT and at truck speeds of 10 and 50 mph (16 and 80 km/hr) showed generally larger deflections at the higher speed [see report by Minkarah et al. (9)].

- Truck speed had a pronounced effect on the results obtained from geophone measurements. Specifically, at a truck speed of 10 mph (16 km/hr), the overall mean deflections were only approximately 50 percent of the mean deflections from the 50-mph (80-km/hr) tests. Also, there was a small (4.5 percent) decrease in the mean deflections obtained from geophone measurements as the truck speed decreased from 50 to 35 mph (80 and 56 km/hr). The reason for this may have been the working mode of the geophone, which requires fast deflection of the pavement slab for accurate measurement. Namely, at lower speeds the low frequency of deflection vibrations would result in a nonlinear relationship between the velocity of deflection and the voltage output by the geophone.

- It appears from the limited data that the overall mean of the morning (a.m.) deflections of the joints was greater than the mean of the afternoon (p.m.) deflections. This may be explained by the upward curling of the slab corners during the morning hours, as shown by Poblete et al. (10). The curling results in reduced support and larger deflection under wheel loading.

- Both the normalized FWD and Dynaflect measurements gave reliable joint deflections for a variety of slab dimensions, base conditions, and types of dowels, even though the FWD deflection measurements were slightly higher than the "true deflections" (LVDT). However, all FWD tests were run only at one load level; therefore, more tests will be needed to justify the linear normalization used.

- From another phase of testing on this pavement, the mean of joint deflections on granular base was found to be greater than the mean of joint deflections on stabilized base [see report by Minkarah et al. (9)].

- Finally, more field testing will be needed to enlarge the data base and substantiate the findings of this test program.

ACKNOWLEDGMENTS

The funding for this study was provided by an Ohio Department of Transportation (ODOT) contract.

The authors gratefully acknowledge the assistance of William F. Edwards, Engineer of Research and Development of ODOT, in providing the FWD and Dynaflect devices for the test program, and for his support throughout this project. Sincere thanks are due to the staff of ODOT's District 4 for their continued assistance in the field, to the Structural Dynamics Research Laboratory of the University of Cincinnati for their assistance in calibrating the geophones and lending their HP signal analyzers, and to S. Nazarian of the University of Texas at El Paso for his advice at the initial stages of the project.

REFERENCES

1. I. A. Minkarah, J. P. Cook, and J. F. McDonough. *Determination of Importance of Various Parameters on Performance of Rigid Pavement Joints*. FHWA; Ohio Department of Transportation, Aug. 1981.
2. I. A. Minkarah and J. P. Cook. The Vertical Movement of Jointed Concrete Pavements. In *Transportation Research Record 990*, TRB, National Research Council, Washington, D.C., 1984, pp. 9-16.
3. I. A. Minkarah, J. P. Cook, and I. Ahmad. Recommended Static and Dynamic Limits of Vertical Movements for Testing Joint Sealants. *Proc., 2nd World Congress on Joint Sealing and Bearing Systems for Concrete Structures*, San Antonio, Tex., Sept. 1986.
4. S. Nazarian. *Calibration Process for Determination of Surface Deflections of Pavement Systems Using Velocity Transducers*. Research Report GR87-2. Geotechnical Engineering Center, University of Texas at Austin, 1987.
5. S. Nazarian, and A. J. Bush III. Determination of Deflection of Pavement Systems Using Velocity Transducers. In *Transportation Research Record 1227*, TRB, National Research Council, Washington, D.C., 1989, pp. 147-158.
6. S. Nazarian and D. R. Alexander. Determination of Surface Deflection of Pavements under Moving Loads. Presented at 68th Annual Meeting of the Transportation Research Board, Washington, D.C., Jan. 1989.
7. R. C. Graves and V. P. Drnevich. Calculating Pavement Deflections with Velocity Transducers. Presented at 70th Annual Meeting of the Transportation Research Board, Washington, D.C., Jan. 1991.
8. T. D. Gillespie, S. M. Karamihas, D. Cebon, M. W. Sayers, M. A. Nasim, W. Hansen, and N. Ehsan. *Effects of Heavy Vehicle Characteristics on Pavement Response and Performance*. Final Report, NCHRP Project 1-25(1). TRB, National Research Council, Washington, D.C., 1992.
9. I. A. Minkarah, A. Bodocsi, R. A. Miller, and R. S. Arudi. *Final Evaluation of the Field Performance of Ross 23 Experimental Concrete Pavement*. Draft Report. Ohio Department of Transportation, 1992.
10. M. Poblete, R. Salsilli, R. Valenzuela, A. Bull, and P. Spratz. Field Evaluation of Thermal Deformations in Undoweled PCC Pavement Slabs. In *Transportation Research Record 1207*, TRB, National Research Council, Washington, D.C., 1988.

Publication of this paper sponsored by Committee on Rigid Pavement Design.

Effects of Temperature on Early Crack Formation in Portland Cement Concrete Pavements

YEYOU-SHANG JENQ, CHWEN-JANG LIAW, AND SANG-CHEL KIM

Major distress problems of concrete pavements generally start with crack formation caused by the combined effects of traffic load and service temperature. Water and salt can easily infiltrate into pavement at the location of cracks and create durability and structural problems. Although crack formation has an important effect on the durability and structural capacity of concrete pavements, studies on the crack formation mechanisms in concrete are still limited to conventional stress-based or strain-based elasticity analysis because of the complexity of the problem. Recently because of the promising features of fracture mechanics-based models, fracture mechanics analysis on concrete structures is receiving more attention from researchers. A cohesive crack model was used to study the effect of temperature on crack formation in concrete pavements and to demonstrate the feasibility of fracture mechanics analysis on concrete pavement systems. It was found that the peak temperature differential that causes formation of random cracks in the pavement is sensitive to the age of the pavement; to properly control the occurrence of random cracking, saw-cut grooves should be introduced at the earliest possible age of the concrete pavement.

Major distress problems of concrete pavements generally start with crack formation caused by the combined effects of traffic load and service temperature. Water and salt can easily infiltrate into the pavement at the location of cracks and create durability and structural problems. Crack formation in concrete pavements can be a progressive development caused by, for example, traffic-induced fatigue or even a single-occurrence overloaded truck or thermal stress resulting from a large temperature change. Although crack formation has an important effect on the durability and structural capacity of concrete pavements, studies on the crack formation mechanisms in concrete pavements are still limited to the conventional stress-based or strain-based elasticity analysis. It has been shown that conventional models are not able to capture some widely observed size effect and notch sensitivity behavior on concrete structures and that models developed on the basis of fracture mechanics theories are more suitable for describing crack development in concrete materials (1). Because of the promising features of fracture mechanics-based models, the application of these models to analyzing actual concrete structures is receiving more attention from researchers. One of the advantages of using the fracture mechanics-based models is that the extrapolation capability of these models is much better than that of conventional models in terms of dynamic loading con-

ditions and various geometrical configurations of the concrete structures.

In the present paper, the effects of temperature on the crack formation mechanisms caused by an artificially introduced groove are analyzed to demonstrate the feasibility of fracture mechanics analysis on concrete pavement systems. A saw-cut groove is generally introduced to confine crack formation at the location of the groove at a controlled spacing—for example, 3.66 m (12 ft). A better design for the optimum groove depth calls for better understanding of how the artificially introduced groove affects crack formation in the pavement.

COHESIVE CRACK MODEL

In modeling crack formation and crack propagation in concrete, a crack can generally be modeled as a Griffith-type traction-free cracks (2) or a Dugdale-Barenblatt type of cohesive crack (3–6). In this paper, the cohesive crack concept proposed by Hillerborg et al. (5) will be used. The cohesive crack concept assumes that when a crack starts to develop in a material, this crack is still able to transfer some forces. The crack zone that is bridged by this cohesive force, which is generally termed the “process zone” (see Figure 1), is governed by the applied load, structure and sample geometries, and the basic properties of the material. The cohesive crack concept was originally proposed by Dugdale (3) and Barenblatt (4) for metals and by Hillerborg et al. (5) for portland cement concrete (PCC) to characterize progressive crack development in these materials.

Several assumptions were made in the cohesive crack model (5):

1. The process zone is assumed to initiate when the first principal stress reaches the tensile strength (f_t , as defined in Figure 2a and b).
2. The direction of the process zone will be perpendicular to the direction of the first principal stress.
3. The properties of the materials outside the process zone are governed by a stress-strain relationship (Figure 2a). The stress-strain curve does not have to be linear. However, for simplicity, a linear relationship can be assumed.
4. The material in the process zone is able to transfer stress, and the stress-transferring capability depends on its opening displacement according to the stress-separation relationship shown in Figure 2b.

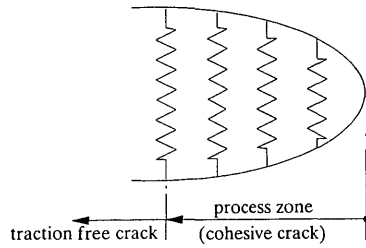


FIGURE 1 Cohesive crack modeled by nonlinear spring.

On the basis of these assumptions, the size of the process zone, the magnitude of the bridging stress, and the applied load can be determined (5,6). The proposed stress-separation curve concept is the key factor that separates the proposed fracture mechanics model from the conventional strain-based or stress-based models. Since strain cannot be defined objectively when there are displacement discontinuities (e.g., a crack), a fracture mechanics model is more suitable in characterizing the fracture mechanisms in a material.

NUMERICAL FORMULATION

For simplicity, a notched beam is used to demonstrate the numerical formulation for the proposed cohesive crack model. Consider a notched beam with a preexisting crack up to Node *n* subjected to a load *P* in the midspan, as indicated in Figure 3 (top). It was assumed that the process zone would develop along a straight plane, which is reasonable for Mode I crack propagation. When the beam is loaded, by introducing the closing stresses over the crack, one can analyze the progressive crack development in the beam.

In the calculation process, the stresses acting across a cohesive crack are replaced by equivalent nodal forces. These forces can be determined according to the stress-separation curve when the width at the cohesive crack zone is known. As indicated in Figure 3 (top), when the first node reaches its tensile strength, the opening displacement at the first node is still equal to zero, that is, $\sigma_1 = f_t, w_1 = \dots = w_{n-1} = 0$. From this, one can determine the first point, which corresponds to the crack initiation point, of the load-load line

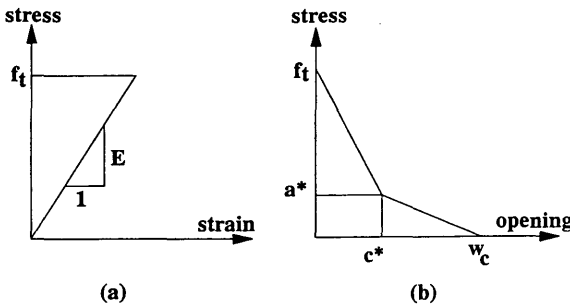


FIGURE 2 (a) Deformation properties of the material outside the fracture zone can be obtained from a $\sigma-\epsilon$ curve; (b) those of the fracture zone can be obtained from a $\sigma-w$ curve.

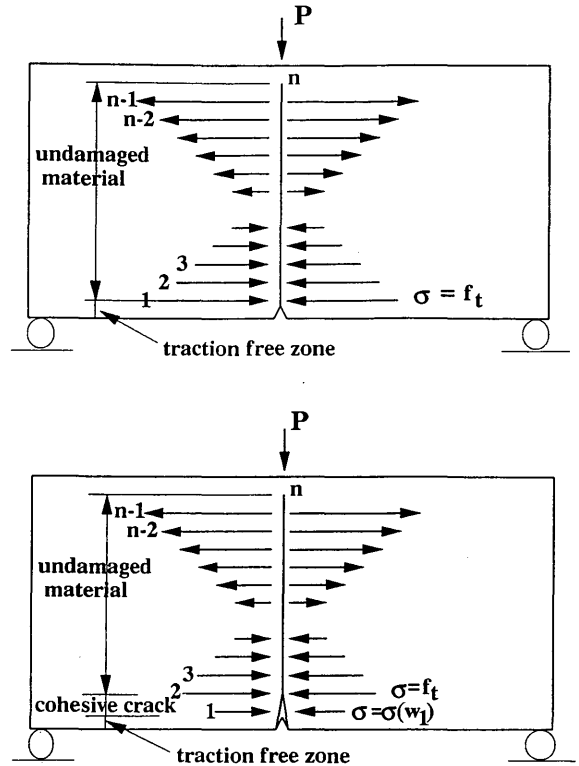


FIGURE 3 Notched beam subjected to three-point bending: top, at crack initiation; bottom, schematic illustration of the second step.

deflection ($P - \delta$) curve and the load-crack mouth opening displacement (P -CMOD) curve.

When the crack starts to propagate as shown in Figure 3 (bottom), the first node is opened and the second node is assumed to reach the tensile strength. At this point the boundary conditions can be expressed as $\sigma_2 = f_t, w_2 = w_3 = \dots = w_{n-1} = 0, w_1 \neq 0$, and $\sigma_1 = \sigma(w_1)$. The system of equations is nonlinear because of the stress-separation constraint. Therefore, an iteration process is needed for this step.

Following the same principle, the progress of the crack propagation can be analyzed, and complete $P - \delta$ and $P - \text{CMOD}$ curves can be generated. The driving force for crack propagation in a pavement system is not limited to the applied load (*P*). Service temperature differential (*T*), which is defined as the temperature difference from the surface to a certain depth of the pavement, can also be the driving force for crack propagation. The principle involved in the numerical formulation, however, is the same for the applied load and service temperature. Thus, one can derive the numerical formulation for temperature loading by replacing the effect of applied load with that of temperature. To obtain the theoretical results using the proposed cohesive crack model, a numerical method such as a finite element method must be applied.

CRACK CONTROL

Under ideal conditions a pavement slab will respond to temperature differentials across its thickness as follows. Assuming

no-curl (flat) condition at the reference temperature, a negative temperature differential—which means that the surface temperature is lower than the temperature at the bottom slab—makes the slab curl upward at the edges, with the corners exhibiting the greatest curling, whereas the center stays in contact with the subgrade. In contrast, a positive temperature differential causes reverse results. Thus, a high thermal tensile stress will occur at the center of the slab at negative temperature differential, whereas a high thermal compressive stress may occur at the center at positive temperature differential. In either case, part of the concrete slab is not in direct contact with the subbase, and bending action caused by the applied traffic load can further increase the magnitude of tensile stresses in the pavement. Since concrete has a very low tensile strength compared with its compressive strength, a combined tensile stress induced by temperature gradient and traffic loads can easily crack the pavement. Furthermore, for a long concrete slab, formation of these cracks can occur randomly.

To control random cracking in plain concrete pavements, current practice requires the introduction of a saw-cut groove of about one-third or one-fourth of the concrete pavement thickness when the pavement is about 1 to 3 days old. After the groove is introduced and before the pavement is open to traffic, a natural crack may or may not develop at the location of the groove, depending on the magnitude of the thermal stress caused by temperature change and the concrete's properties. Adequate groove depth must be provided to ensure that the transverse cracks will be confined at the location of the groove. If the groove is not deep enough, cracks may form outside the groove (7), which will cause costly maintenance and repair work later. However, a groove depth that is too deep may not be economical, because it will require more work during the cutting and sealing processes. The adequacy of the groove depth is also highly dependent on the age of the concrete pavements; in some cases timing of the cut is more important than the depth of the cut in terms of crack control, especially if a high shrinkage deformation is expected at a very early concrete pavement age.

To better understand factors affecting crack formation in grooved (or notched) concrete pavements, a parametric study was performed and an experimental program was designed to evaluate the material properties needed for the theoretical model.

EXPERIMENTAL PROGRAM

Because the artificial groove generally is introduced to the pavements within 3 days after placement of concrete, it is important to evaluate the concrete fracture properties at an early age. The fracture parameters evaluated are the tensile strength, the fracture energy, and the shape of the stress-separation curve. An experimental program was designed to assess these fracture properties at various ages. Determination of these parameters is discussed in the following section.

Preparation of Concrete Specimen

Sand and pea gravel with maximum aggregate size of 0.95 cm (3/8 in.) were used to fabricate the concrete samples. All the

aggregates were dried in the oven for 24 hr and then exposed to air at room temperature to maintain a constant water content in the aggregates. The mix proportion for cement, sand, pea gravel, and water was 1.0:2.6:2.6:0.5, which was used by Jenq and Shah (2). Beam specimens and cylinder specimens were prepared for the study. The beams were used for three-point bending tests and indirect tensile tests, whereas the cylinders were for compressive tests. Some of the beams were saw-cut with a notch-depth ratio of 1:3. The dimensions of the beam specimen were 30.48 cm (12 in.) long, 7.62 cm (3 in.) high, and 2.54 cm (1 in.) thick. The dimensions of the cylinder specimen were 7.62 cm (3 in.) in diameter and 15.24 cm (6 in.) high. Specimens were tested at 16 hr, 1 day, 3 days, 7 days, 14 days, and 28 days. Each series consisted of 11 samples, which included four notched beams, four unnotched beams, and three cylinders.

Three-Point Bending Tests

Notched beam tests and unnotched beam tests were conducted using three-point bending tests. During the test, the applied load, the CMOD, and the load-point deflection (δ) were monitored and stored in a digital form. The rate of loading was controlled by a constant increment of CMOD. Various loading rates for notched beams were applied, with a range of 0.46 to 0.66 mm/min (0.018 to 0.026 in./min) depending on the ages, whereas a constant loading rate of 0.25 mm/min (0.01 in./min) was given for unnotched beams. Typical load-load line deflection and load-CMOD curves obtained from the test are given in Figure 4. From these two curves, Young's modulus, fracture energy (G_f), and shape of the stress-separation curve can be evaluated.

Indirect Tensile Tests

To calculate the tensile strength, splitting tensile tests were conducted by loading one-half of the broken beam tested in the three-point bend tests. The test was performed under displacement control (load-line deflection control). The loading rate was fixed at 0.25 mm/min for all ages of concrete.

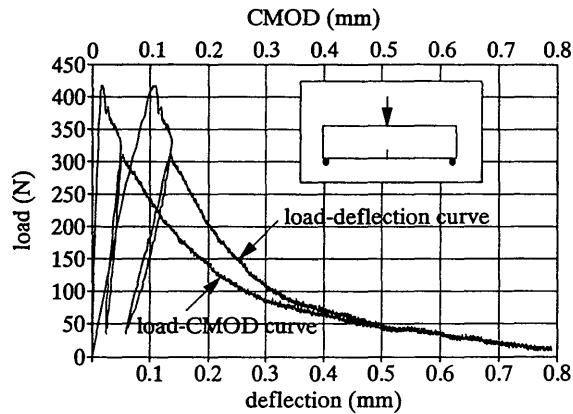


FIGURE 4 Typical load-load line deflection and load-CMOD curves.

TABLE 1 Material Properties of Concrete Obtained from Experiments

Age	16-hrs	1-day	3-days	7-days	14-days	28-days
Young's modulus, E (GPa)						
- from load-CMOD curve	8.34	14.69	21.03	25.45	26.90	30.28
- from load-deflection curve	6.21	8.97	20.01	22.07	24.14	26.90
Fracture energy, G_f (N/m)	10.16	30.13	52.21	44.68	61.85	85.85
Indirect tensile strength, f_t (MPa)	0.33	0.88	1.32	1.63	1.57	2.06
Modified tensile strength, f_t (Mpa)	0.58	1.44	2.40	2.86	3.65	3.81
Poisson's ratio, ν	0.2	0.2	0.2	0.2	0.2	0.2
Coefficient of thermal expansion, k ($10^{-6}/^{\circ}\text{C}$)	3.09	3.09	3.09	3.09	3.09	3.09

1 GPa=0.1450x106 psi, 1 MPa=145 psi, 1 N=0.225 lb, 1 N/m=0.00571 lb/in, $1/^{\circ}\text{C}=1.8/^{\circ}\text{F}$

EXPERIMENTAL RESULTS

Material parameters of concrete evaluated at various ages from the tests are summarized in Table 1. As expected, Young's modulus increases with the age of the concrete. However, the Young's modulus values calculated from the load-CMOD curves are higher than those obtained from the load-deflection curves. Lower modulus values obtained from the load-deflection curves may be caused by additional settlement deflection at supporting points. Similar results were also reported by other researchers.

Fracture energy is defined as the area under the load-line deflection curve divided by the initial uncracked ligament area (δ). Although the area under the load-CMOD curve does not have a direct physical meaning, the fracture energy calculated from the area under load-CMOD curves seems to be comparable with that obtained from load-deflection curves, as indicated in Figure 5. This suggests that the P -CMOD curve should be used to determine the fracture energy, since CMOD value is less sensitive to support settlements. Fracture energy was found to increase as the age of concrete increases.

Since the shape of a softening stress-separation curve also has a major influence on the calculated results, it is necessary to find a stress-separation curve that best describes (or fits)

the material behavior. The shape of the stress-separation curve is dependent on the tensile strength (f_t), a^* , and c^* , as defined in Figure 2, provided that the fracture energy, which is the same as the area under the stress-separation curve, is kept constant. On the basis of the fracture energy and indirect tensile strength determined from the experimental program and assuming different values of a^* and c^* , theoretical predictions on the load-CMOD curves can be obtained. After a lengthy numerical experiment, it was concluded that the splitting tensile strength obtained from the beam samples was too low to yield a reasonable prediction. As a result, modified tensile strengths (see Table 1) along with various shape factors were used. Some theoretical P -CMOD curves were plotted in Figure 6 along with the experimental results for 16-hr-old concrete. On the basis of these numerical experiments, modified tensile strengths for concrete of various ages along with constant shape factors of $a^* = 0.25$ and $c^* = 0.1$ were used as the input material properties for the proposed model.

NUMERICAL ANALYSIS

Concrete pavements with various slab thicknesses and a known temperature distribution were analyzed. The thicknesses of

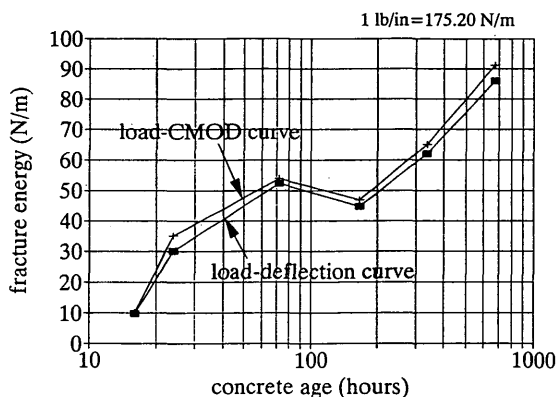


FIGURE 5 Fracture energy calculated from load-CMOD curve and load-deflection curve (notched beam).

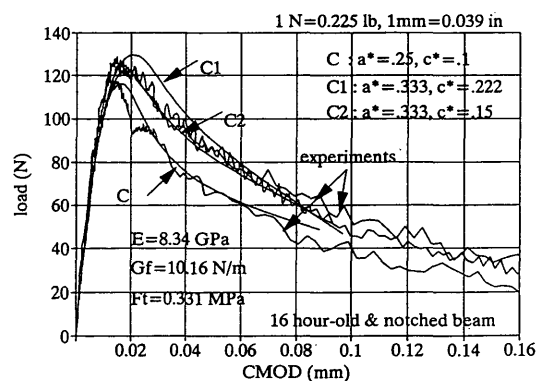


FIGURE 6 Experimental results and numerical results obtained from various combinations of a^* and c^* for 16-hr-old concrete.

the subbase and the subgrade are 22.86 cm (9 in.) and 203.2 cm (80 in.). The span of the slab is 7.32 m (24 ft). In this analysis, the material properties of concrete at 16 hr, 1 day, and 3 days were based on experimental results (Table 1). Young's modulus, Poisson's ratio, and coefficient of thermal expansion are 0.35 GPa (5.0×10^4 psi), 0.3, and $2.22 \times 10^{-6}/^\circ\text{C}$ ($4.0 \times 10^{-6}/^\circ\text{F}$) for subbase, and 0.21 GPa (3.0×10^4 psi), 0.4, and $2.0 \times 10^{-6}/^\circ\text{C}$ ($3.6 \times 10^{-6}/^\circ\text{F}$) for subgrade, respectively (9). For the present analysis, only temperature effect is considered, since no traffic load is expected for concrete pavements at this early age (i.e., less than 3 days old). Shrinkage deformation, which can be indirectly incorporated into the temperature analysis, is not explicitly considered in the present analysis.

The pavement system was analyzed in a three-layer system as indicated in Figure 7. Because of the symmetry of the pavement, only half of the slab was analyzed. It was also assumed that the subbase and subgrade (or soil) cannot resist any tensile stress, which is why free boundary conditions were prescribed on the left part of the pavement. The finite element mesh used in the analysis is given in Figure 8. A finer mesh was used at the location of crack formation for better numerical accuracy. ABAQUS finite element package was used in all the finite element analyses.

Because the driving force in the present study is temperature, temperature distribution in the pavement should be prescribed first. A parabolic equation was used to describe the temperature distribution along the depth of the pavement. This assumption was based on the results of field temperature measurement (8,11). A uniform temperature distribution below 38.1 cm (15 in.) of the pavement surface was also assumed. A typical unit temperature differential profile is given in Figure 9. The relative temperature difference below 38.1 cm (15 in.) deep was assumed to be zero. Knowing the temperature profile, the effects of temperature differential (T) on the crack formation in the pavement system can be evaluated. Stress analysis was first performed on the pavement system without any crack formation. It was found that the highest tensile stress occurred at the top of the midspan of the concrete pavement. Thus, it was assumed that a crack will initiate at the top of the midspan of the pavement and propagate downward to the subgrade.

On the basis of the same numerical formulation principle discussed earlier, the opening displacement of the crack at

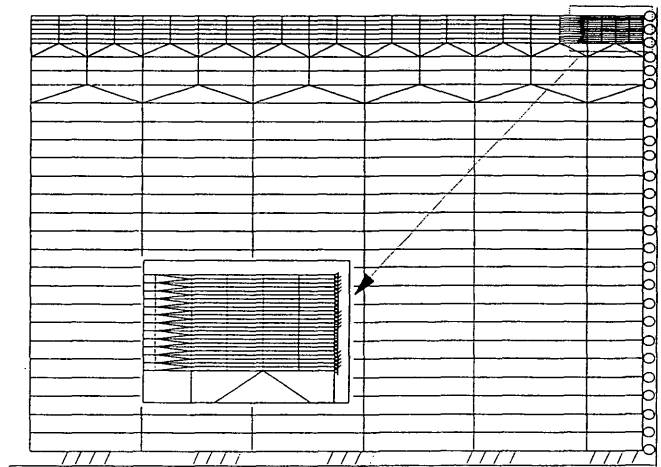


FIGURE 8 Finite element mesh.

each node and at the reference point can be calculated from the following equations:

$$w_i = \sum_{j=1}^{n-1} a_j \sigma_j + c_j T \tag{1}$$

$$w_R = \sum_{j=1}^{n-1} b_j \sigma_j + d_T T \tag{2}$$

$$\begin{bmatrix} a_{11} & a_{12} & \dots & a_{1(n-1)} & c_1 \\ a_{21} & a_{22} & \dots & a_{2(n-1)} & c_2 \\ \dots & \dots & \dots & \dots & \dots \\ a_{(n-1)1} & a_{(n-1)2} & \dots & a_{(n-1)(n-1)} & c_{n-1} \\ b_1 & b_2 & \dots & b_{n-1} & d_T \end{bmatrix} \times \begin{bmatrix} \sigma_1 \\ \sigma_2 \\ \dots \\ \sigma_{n-1} \\ T \end{bmatrix} = \begin{bmatrix} w_1 \\ w_2 \\ \dots \\ w_{n-1} \\ w_R \end{bmatrix} \tag{3}$$

or

$$\{C\}[F] = [\Delta] \tag{4}$$

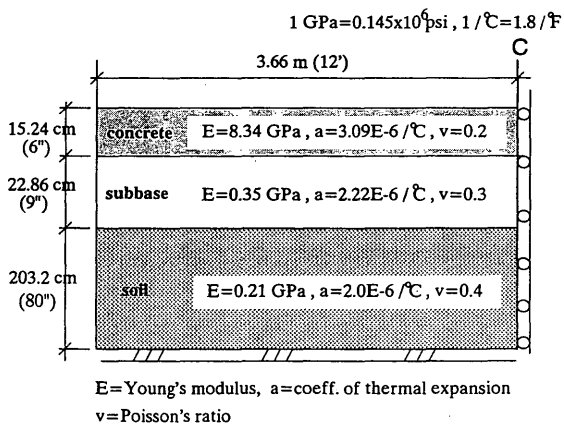


FIGURE 7 Boundary conditions.

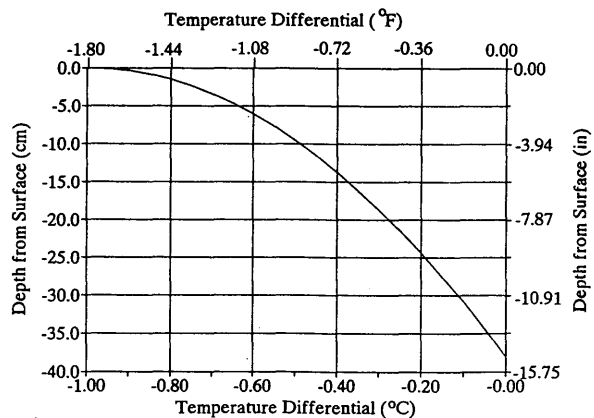


FIGURE 9 Unit parabolic temperature differential in concrete pavements.

where

- a_{ij} = opening displacement of the crack at Node i when an equivalent closing force is acting at Node j ,
- c_j = opening displacement of the crack at Node i when a unit negative temperature differential is applied,
- b_j = opening at the reference point when an equivalent closing force is acting at Node j ,
- d_T = opening at the reference point when a unit negative temperature differential is applied,
- σ_j = closing pressure at Node j ,
- w_i = opening of the crack at Node i , and
- w_R = opening of the reference point.

The square matrix, $\{C\}$, in Equation 4 is referred to as the influence matrix. In the influence matrix, except for the last column, the i th column represents the opening displacement at each node and at the reference point when a pair of equivalent unit closing forces acts at the i th node point. The reference point can be an arbitrary point that is of interest to the engineers. For example, for a three-bend point loading configuration, the load point can be chosen to be the reference point. The selection of the reference point, however, does not affect the numerical results. The last column represents the openings at each node and the opening at the reference point when a negative unit temperature differential is applied at the reference point. The vector $[F]$ represents the closing pressure at each node and the applied temperature differential and the vector $[\Delta]$ represents the opening displacement at each node and the reference point.

Thus, on the basis of the calculation procedures discussed in earlier sections, a complete temperature differential versus CMOD curve and crack growth development due to temperature differential can be generated. The definition of CMOD used here is the same as that for the crack opening displacement at the top of the concrete slab.

DISCUSSION OF RESULTS

Figure 10 gives the development of crack formation with respect to the change of temperature differential. Each data

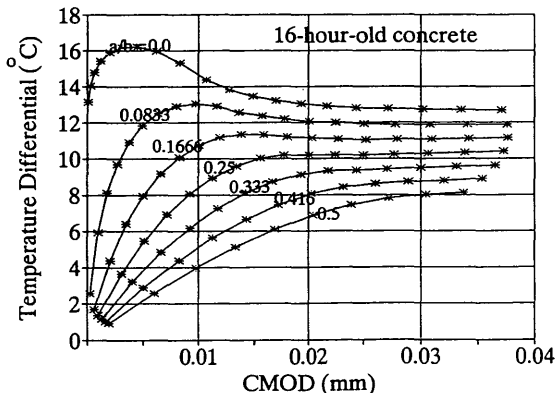


FIGURE 10 Development of temperature differential with various notch-depth ratios for 16-hr-old concrete pavement.

point represents an element-length crack advancement in the concrete slab. Stable crack formation was first observed, because further crack advancement requires a higher temperature differential, as can be seen in Figure 10. However, when the peak temperature differential is reached, crack advancement becomes unstable (especially for an a/b ratio less than 0.25) because further crack propagation requires a lower temperature differential. Thus, when the peak temperature differential is reached, one can conclude that a through crack is formed in the concrete pavement. Figure 10 also indicates that the peak temperature differential decreases as the notch-depth ratio increases. Therefore, if the temperature differential in the field is lower than usual, a deeper groove is needed to ensure proper crack control. A value of $a/b = 0$ represents the temperature differential that may cause the formation of a random crack in the plain concrete pavement. For this particular case, this temperature differential is about 16.67°C (30°F) for a 16-hr-old pavement. This peak temperature will be even lower if the effect of shrinkage is included. If the expected temperature differential is higher than 16.67°C (30°F), then the groove (or cut) has to be introduced before the concrete is 16 hr old to prevent the occurrence of random cracking. Once random cracks form, the introduction of a saw-cut groove to control crack formation will not be very effective.

Effects of groove-depth ratio (or notch-depth ratio) and age on crack formation at various temperature differentials are given in Figures 11 and 12. As indicated, the thicker the concrete pavement, the lower is the groove-depth ratio (or notch-depth ratio) necessary for crack control. This also confirms the fact that concrete pavements also exhibit similar size-effect and notch sensitivity behavior (1), as observed in other types of concrete structures. Figures 11 and 12, however, reflect only the effect of groove-depth ratio. Timing is also critical for the overall final crack control; that is, the groove has to be introduced before random cracks occur, as discussed earlier. Thus, for better crack control, the groove should be introduced at the earliest allowable age without damaging the pavement.

On the basis of the proposed approach and with the knowledge of the expected temperature differential and the pave-

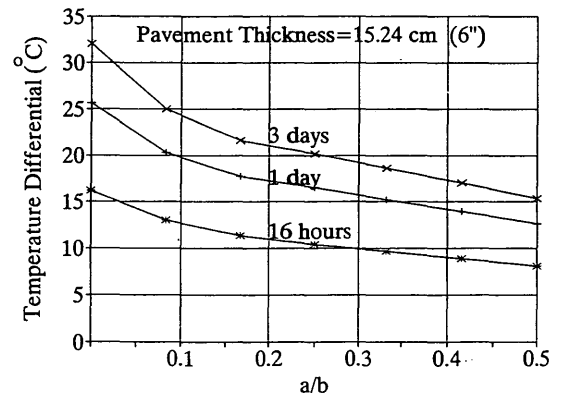


FIGURE 11 Temperature differential versus notch-depth ratio curves for concrete pavement 15.24 cm (6 in.) thick at various ages.

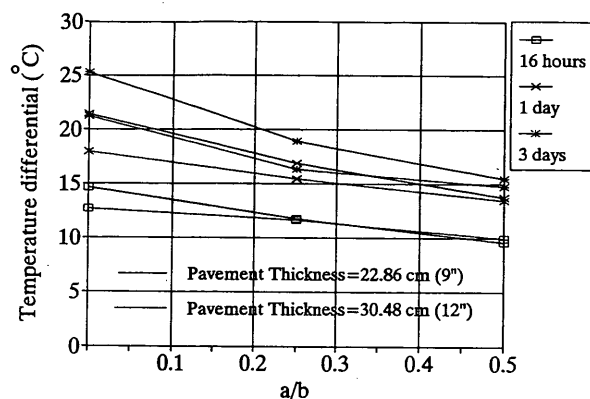


FIGURE 12 Temperature differential versus notch-depth ratio curves for concrete pavement 22.86 cm (9 in.) and 30.48 cm (12 in.) thick.

terms of crack control will be drastically reduced no matter what the depth.

REFERENCES

1. Y. S. Jenq and S. P. Shah. Feature of Mechanics of Quasi-Brittle Crack Propagation in Concrete. *International Journal of Fracture*, Vol. 51, 1991, pp. 103-120.
2. Y. S. Jenq and S. P. Shah. Two Parameter Fracture Model for Concrete. *Journal of Engineering Mechanics*, Vol. 3, No. 10, 1985, pp. 1227-1241.
3. D. S. Dugdale. Yielding of Steel Sheets Containing Slits. *Journal of the Mechanics and Physics of Solids*, Vol. 8, 1960, pp. 100-108.
4. G. I. Barenblatt. The Mathematical Theory of Equilibrium of Crack in Brittle Fracture. *Advances in Applied Mechanics*, Vol. 7, 1962, pp. 55-129.
5. A. Hillerborg, M. Modeer, and P. E. Petersson. Analysis of Crack Formation and Crack Growth in Concrete by Means of Fracture Mechanics and Finite Elements. *Cement and Concrete Research* 6, 1976, pp. 773-782.
6. J. D. Perng. *Analysis of Crack Propagation in Asphalt Concrete Using a Cohesive Crack Model*. M.S. thesis. Ohio State University, June 1989.
7. C. L. Saraf and B. F. McCullough. Controlling Longitudinal Cracking in Concrete Pavements. In *Transportation Research Record 1043*, TRB, National Research Council, Washington, D.C., 1985.
8. J. M. Armaghani, T. J. Larsen, and L. L. Smith. Temperature Response of Concrete Pavements. In *Transportation Research Record 1121*, TRB, National Research Council, Washington, D.C., 1987, pp. 23-33.
9. G. M. Jones, M. I. Darter, and G. Littlefield. Thermal Expansion-Contraction of Asphalt Concrete. *Proc., Association of Asphalt Paving Technologists*, Vol. 37, 1968, pp. 56-100.
10. RILEM Draft Recommendation: Determination of the Fracture Energy of Mortar and Concrete by Means of Three-Point Bend Tests on Notched Beams. *Materials and Structures*, Vol. 18, 1985, pp. 287-290.
11. J. M. Richardson and J. M. Armaghani. Stress Caused by Temperature Gradient in Portland Cement Concrete Pavements. In *Transportation Research Record 1121*, TRB, National Research Council, Washington, D.C., 1987, pp. 7-13.

Publication of this paper sponsored by Committee on Rigid Pavement Design.

ment thickness, one can determine proper timing and optimum depth of the groove to control the formation of cracks in plain PCC pavements. Studies on the effects of shrinkage, different geometrical configurations, service loads, and concrete properties are ongoing.

CONCLUSIONS

It can be concluded from the present study that crack formation and propagation in concrete pavements can be properly analyzed using fracture mechanics. Results of crack control by introduction of a saw-cut groove are dependent on the age of the concrete, the temperature differential, and the depth of the groove. Knowing the expected temperature differential and the thickness of the pavement, one can determine the timing and groove depth that are needed to ensure proper crack control in plain concrete pavements.

It can also be concluded that timing of the saw cut is actually more important than its depth. If the saw cut is introduced after the formation of random cracking, its effectiveness in

Load Equivalency Concepts: A Mechanistic Reappraisal

ANASTASIOS M. IOANNIDES AND LEV KHAZANOVICH

The history and evolution of load equivalency concepts are traced and discussed, in view of the fact that accommodation of mixed traffic consisting of multiwheel load assemblies is of cardinal importance in any pavement design. It is explained that the equivalent single-axle load concept is considerably different from the equivalent single-wheel load (ESWL) approach, inasmuch as the former is statistical-empirical and is based on the assumption of linear pavement damage accumulation, whereas the latter is soundly mechanistic, if relatively crude, and is merely an innovative means of computing responses under multiwheel gears. A third concept, namely, the equivalent single-axle radius (ESAR), is also mechanistic in nature and dispenses with the arbitrary constant pressure or constant radius assumptions of the ESWL approach. According to the ESAR concept, it is possible to determine with reasonable accuracy a primary structural response, such as the maximum bending stress that occurs in a concrete pavement system, through the use of available closed-form equations for a single-wheel load, into which an equivalent single-wheel radius of a multiple-wheel assembly is substituted. The ESAR concept is currently considered for incorporation in an improved mechanistic "limit state" design procedure for concrete pavements. Because of the far-reaching implications of these proposals, rigorous engineering mechanics derivations are used to verify the applicability of the concept for both the dense liquid and the elastic solid foundation.

Before the AASHO Road Test (1958–1960), the development of pavement design procedures relied heavily on the theoretical investigations of two well-known researchers. With respect to portland cement concrete (PCC) pavement systems, the prominent name is that of Westergaard (1), who idealized the PCC slab as a plate resting on a Winkler, or dense liquid, foundation. A couple of decades later, Burmister (2) extended Boussinesq's concept of the semiinfinite elastic half-space to develop the layered elastic theory, which has formed the basis for the design of bituminous pavement systems. The solutions derived by Westergaard and Burmister were intended for practical applications, despite the fact that their scope was restricted by a number of limiting assumptions and idealizations. A most important shortcoming common in the derivations of both of these pioneers stemmed from the assumption that the load consisted of a single tire print.

A number of subsequent studies attempted to eliminate the limiting assumptions introduced by Westergaard and Burmister, including the one pertaining to the configuration of the applied loading. Thus, a graphical extension of Westergaard's plate-on-dense-liquid theory to multiple-wheel loads was provided by Pickett and Ray (3), who developed the very popular charts, now known under their names. These may be

used to determine a specific response (e.g., deflection or slab bending stress) at a specific location (e.g., interior or edge) for a specific pavement system (i.e., of known radius of relative stiffness, l). Note that, in addition to the dense liquid foundation considered by Westergaard, Pickett and Ray derived solutions for the elastic solid idealization. Their charts were patterned after the charts developed some 15 years earlier by Newmark (4), which had extended the Boussinesq solution (single wheel on homogeneous foundation) to multiple-wheel loads.

With the advent of the computer, computerized versions of the Pickett and Ray charts were also prepared. Program AIRPORT (earlier name: PDLIB) was coded by Packard (5) for the Portland Cement Association (PCA) and may be used for the determination of the maximum dense liquid interior stress under any single- or multiple-wheel load configuration. Similarly, Kreger (6) developed the H-51 program for the dense liquid edge loading stress. This program was later expanded by Ioannides (7), and the resulting version, H51-ES, may be used to determine the edge stress, assuming either a dense liquid or an elastic solid subgrade. A similar evolution occurred with respect to Burmister's layered elastic theory. The development of the BISAR computer code in the early 1960s enabled engineers to determine the response of any specified multilayered system under a prescribed multiwheel load (8).

These computer codes, however, do not address the need for a comprehensive solution applicable to a range of practical problems, which would be incorporated in a design guide in a suitable form, that is, as an equation, chart, or nomogram. In an effort to provide such a solution, Yoder and Witzak (9) employed the principles of dimensional analysis in presenting a graphical summary of numerous results obtained using the Pickett and Ray charts. Three dimensionless ratios were introduced for this purpose, namely, (L/l) , (x/l) , and (d/l) , where L is the length of the elliptical tire prints, and x and d are the longitudinal and transverse wheel spacings, respectively. The resulting graphs may be used to determine the edge or interior bending stress under single, dual, or dual tandem wheel loads.

Similarly, a chart for the determination of the dense liquid interior bending stress under dual-wheel loads was prepared by researchers at PCA, using a data base consisting of results from AIRPORT (10). Application of the principles of dimensional analysis in the interpretation of the same data base resulted in an even simpler, more concise nomogram (11). The dimensionless ratios used in the latter were (a/l) and (S/a) , in which a is the radius of each tire print and S is the spacing between the duals. The spacing ratio (S/a) had also

been used in the early 1970s in an Asphalt Institute design procedure (9). In contrast, an approach dating to the 1950s pertaining to the Federal Aviation Agency employed the spacing ratio (S/l) instead (12). Because $(S/l) = (S/a) * (a/l)$, the two spacing ratio forms are interchangeable, although (S/a) is preferable because it is based exclusively on the tire configuration characteristics.

Notwithstanding the contributions made previously, the most prevalent approach in assessing the effect of multiple-wheel loads on pavement systems has been to transform the actual applied multiple-wheel load into some equivalent loading system consisting only of a single wheel, which could then be accommodated in available single-wheel analysis or design procedures. In this paper load equivalency concepts are reviewed, especially as they might apply to the development of an improved mechanistic design procedure. It is demonstrated that despite being relatively crude, the equivalent single-wheel load (ESWL) concept is soundly mechanistic in nature, whereas the very popular equivalent single-axle load (ESAL) concept is entirely statistical-empirical and possibly inappropriate for use in mechanistic design. A less common approach, namely, the equivalent single-axle radius (ESAR) concept, is discussed in detail and a mechanistic justification for its use is developed. This justification is in the form of closed-form equations for a dual wheel load applied on a slab-on-grade concrete pavement system.

ESWL CONCEPT

The earliest documented application of a load equivalency approach in accommodating multiple-wheel loads was devised by the U.S. Army Corps of Engineers in the 1940s. Boyd and Foster (13) developed a method that was aimed at accommodating the B-29 aircraft in the existing single-wheel California-bearing-ratio-based design procedure by reducing the dual-wheel gear of that aircraft to a single tire print. By today's standards, their method was crude, employing as it did Boussinesq's solution for the homogeneous elastic half space, thereby ignoring the layered nature of the pavement system. Yet the Boyd and Foster method was distinguished by the following two characteristics, which remain desirable features of any design procedure to this day:

1. It was mechanistic in nature, being based on a rigorous—
if simple—theoretical solution; and
2. It was calibrated and verified using field measurements.

The significance of their method lay in its originality, and, rather unexpectedly for its authors, it begot one of the most pervasive and influential concepts in pavement design history, namely, the concept of the ESWL. As explained in more detail below, this concept should be distinguished from the entirely statistical-empirical ESAL concept, proposed in the 1960s after the AASHO Road Test. Boyd and Foster were, in fact, looking for a method that could “be used to find axle spacings and loads that will produce no greater detrimental effect than is produced by a given load on a single axle.” In current conventional terminology, this meant that they sought

combinations of total applied load and dual-wheel spacing that would result in a load equivalency factor (LEF) of unity when compared with any “given” single axle. In contrast, the AASHO LEFs developed later were assigned values other than 1 and aimed at converting any arbitrary load to an 18-kip equivalent single axle.

Boyd and Foster were the first to recognize that any load equivalency depended on wheel spacing and repeatedly refer to the “efficiency of variations” in this geometric gear characteristic. Furthermore, they recognized that the equivalency relationship depended on the mechanistic response, for example, stress, strain, or deflection, selected to quantify the “detrimental effect” on the pavement. Also contained in their paper is the earliest acknowledgment that load equivalencies are sensitive to the thickness of the constructed pavement layers and presumably also to their individual moduli. Consequently, these authors appeared to be concerned about the generality of their finding and noted that their comments apply to “this case [alone].” To enhance the generality of the ESWL approach, Boyd and Foster (13) expressed the design thicknesses as dimensionless quantities by “resolving them into ratios of appropriate dimensions of the assembly.” They postulated that “the dimension of the assembly that governs the depth at which the dual wheel loads act as independent units is the spacing between the contact areas of the tires,” which they designated d . Similarly, “the depth at which the dual wheels act as a single wheel load is governed by the distance between the centers of the wheels,” which they designated s . From the geometric configuration of the B-29, design thicknesses were obtained on the basis of $(d/2)$ and $(2s)$. This is the earliest documented use of the principle's dimensional analysis in the development of a load equivalency concept.

It is significant to note that Boyd and Foster (13) did not consider their method to be a rigorous theoretical solution, but only an approximation whose agreement with “actual observation” was “reasonably close” and “slightly conservative.” They never intended the method to be a final solution, but to merely serve as an interim approach until “time and economic considerations permitted the direct development” of design criteria for multiple-wheel assemblies. It appears, however, that the savings in effort that were afforded by the load equivalency approach simply were too attractive, because in the 40 years that have passed since then, no attempt has been made toward such “direct development” of multiple-wheel criteria. Rather, a substantial amount of energy has been devoted to refining an equivalency method that would reduce multiple-wheel gears to an equivalent single-wheel load. In these efforts, however, a number of considerations present in the original Boyd and Foster paper were gradually abandoned or forgotten, so that subsequent “refined” methods were—at least in some respects—less comprehensive and theoretically less rigorous. In addition, each of the later investigators introduced new assumptions, which yet other researchers ignored or forgot as they tried to “re-refine” the already “refined” proposals.

An excellent case in point is offered by the Corps of Engineers study published in 1958 by Foster himself and Ahlvin, whose approach was still mechanistic in nature, and retained Boussinesq's homogeneous foundation assumption (14). Dimensional analysis concepts were adhered to in its derivation: the spacing between the wheels (S) was expressed in terms

of the radius of each wheel (a) as the dimensionless ratio (S/a). Similarly, the geometric coordinates for offset (r , and depth (z), were also expressed in dimensionless forms as (r/a) and (z/a). Yet Boyd and Foster's multiple response considerations were abandoned, and, presumably for simplicity's sake, Foster and Ahlvin (14) retained only the criterion of equivalency of deflections. Thus, the strong dependence of any resulting equivalency relationship on the primary structural response considered was gradually forgotten by many subsequent investigators. A notable exception to this trend is the study performed by the Australian researchers Gerrard and Harrison (15). Interestingly, Foster and Ahlvin (14) recognized that equating the magnitude of the maximum deflection alone would not be adequate, even if one could dispense with all other primary responses (such as stresses and strains), and noted that the shape of the deflection basin should also be considered.

As far as can be ascertained, Foster and Ahlvin (14) were the first to coin the term equivalent single-wheel load. It should also be noted that the ESWL method relied on the use of the principle of superposition, applicable under conditions of elasticity and of similarity of boundary and support conditions. Thus, the extension of their equivalency concept to distresses of a nonrecoverable nature, such as rutting and cracking, is theoretically unjustified. Their main "refinement" consisted of the fact that in obtaining the complete curve of depth (or thickness) versus ESWL, it was no longer necessary to resort to Boyd and Foster's simplistic assumption of an "orderly" (i.e., linear) variation when log-log scales were used. In addition, Foster and Ahlvin (14) abandoned the original constant pressure assumption and equated instead the contact area of the ESWL to that of one wheel of the multiple-wheel assembly. No justification was provided for this choice, but, as Huang (16,17) later showed, the constant radius assumption makes the ESWL calculation easier.

The main contribution of Huang (16) was the introduction of Burmister's layered elastic theory (implemented on an IBM-360 computer) into the computation of ESWLs, an approach adopted also by Gerrard and Harrison (15). Huang presented his results in a "simplified chart such that EDWLs for any combinations of pavement thickness, modulus ratio, wheel spacing, and contact radius could easily be found." This was achieved by using dimensional analysis concepts in the form of dimensionless ratios, for example, (E_1/E_2), (S/a), and (h/a), in which E_1 and E_2 are the moduli of the constructed layer and of the natural subgrade, respectively, whereas h denotes the thickness of the constructed layer. Huang had hoped that "the simplicity of the chart will encourage its use so that more field data will be collected to check the validity of the chart." Following Foster and Ahlvin (14), Huang (16), and later Gerrard and Harrison (15), assumed that the ESWL and each wheel of the dual assembly had the same contact area radius (a). The equivalency relation was based on equality of the maximum vertical deflection at the interface between the two layers in the system, that is, at the top of the subgrade. In addition, because Huang's method is mechanistic, it allocates due importance to a variable ignored in many other pavement investigations, namely, the radius of the applied load (a). In fact, this parameter is so important that it appears in two of Huang's three dimensionless ratios, (h/a) and (S/a).

THE ESAL CONCEPT

In the interpretation of the AASHO Road Test results in the early 1960s, the concept of the equivalent single-axle load (ESAL) was employed. The origins of this concept can also be traced to the early 1940s in a procedure adopted by the California Division of Highways (18,19). However, since its inception the ESAL concept has been drastically different from the ESWL concept: whereas the latter constitutes an attempt to accommodate multiple-wheel loads in the mechanistic determination of pavement responses (i.e., of stresses, strains, or deflections), the original California suggestion was introduced "for the reason that it is necessary to determine some common denominator to which we reduce our axle load determinations" so that distresses due to the "fatigue effect" may be defended against. The historical coincidence between the development of the ESAL concept and the increased interest of highway engineers in the phenomenon of fatigue is extremely significant and must not be overlooked.

The ESAL concept as adopted in the interpretation of the AASHO Road Test data was not entirely faithful to the original California suggestion. Rather than considering solely the "fatigue effect" as Grum (18,19) had suggested, the AASHO statistical regression methodology was based on the equivalency of the empirical and subjective present serviceability index (PSI). This index was later correlated statistically with the combination of several pavement distresses, the primary one being roughness, not fatigue. Nonetheless, AASHO's entirely statistical-empirical ESAL concept is based on the assumption that the destructive effect of a number of applications of a given axle group (defined in terms of load magnitude and configuration) can be expressed in terms of a different number of applications of a standard or base load. Therefore, the ESAL concept presupposes and is based on a concept of linear cumulative damage (quantified in terms of a drop in the PSI), a popular, if arbitrary, extrapolation of Miner's fatigue hypothesis (20).

In the first decade following the AASHO Road Test and the novel application of exclusively statistical concepts that it ushered in, engineers remained skeptical, as witnessed by the discussion comments from several forums at that time. A paper by Deacon published in 1969 (21) appears to mark a turning point in highway engineering history, because it purported to provide much needed intellectual underpinnings for the ESAL concept. This was in the form of a "proof" of the validity of the concept, which also illustrated its intimate connection with the linear cumulative fatigue hypothesis. A closer review of this proof reveals that the validity of the ESAL concept is proven on the basis of the assumption that the concept is valid in the first place, rendering Deacon's exercise an argument in a circle and therefore of little value. Furthermore, the validity of the ESAL concept is based on the assumption of the validity of the linear cumulative fatigue hypothesis, and vice versa. Given the scatter in experimental fatigue data, as well as the specimen size effect involved in any correlation of individual material laboratory test results with the performance of multilayer pavement systems, it is hard to accept that a rigorous theoretical proof of the validity of the ESAL concept can be derived at all. It is worth recalling at this point that the developers of the ESWL concept desisted from providing such proofs for their own, more mechanistic, construct.

An interesting and fortuitous by-product of the statistical manipulations of the AASHO Road Test data has become one of the principles most widely used by practicing pavement engineers. This is the so-called fourth-power law, whose historical origins can be traced to a relatively obscure National Cooperative Highway Research Program (NCHRP) report by Irick and Hudson (22), in which it was attributed to "work that was done at the HRB subsequent to the AASHO Road Test." Its definitive statement, however, did not appear until 1970, when Scala (23) presented it as the "simplest formula" to describe the results of the AASHO Road Test for each given "arrangement of load." He suggested that "accepting that the deflection of a pavement is proportional to the load, the LEF values for a given loading system vary by the fourth power of the ratio of the deflections under the loads." Scala (23) justifies the use of the vertical (elastic) deflection, either measured in the field or calculated from theory, in establishing LEFs by stating that this response "has been proven to be a good indication of the performance of a pavement under various loading systems." The adequacy of deflection as a universal, single indicator of all pavement distresses is certainly debatable. In any case, however, Scala's suggestion would lead to drastically different LEFs than, for example, Deacon's suggestion of using a strain ratio raised to the power 5.5.

The fourth-power approximation represents the simplest "best-fit" equation through data that invariably had a considerable scatter. Scala considered this variation negligible and concluded: "It appears that the LEF values are independent of the road structure [i.e., whether the pavement is rigid or flexible, or what its structural number or slab thickness may be]. Hence, in considering the effect of altering the regulations limiting axle-loads on the life of the highway surface the nature of actual road structure can be ignored." Independent of the validity of this statement vis-à-vis Scala's stated reason for deriving and using the fourth-power approximation (namely, to "advise" with respect to the effect of altering the Australian Motor Vehicle Standards), his comments cannot be interpreted as meaning that the LEFs (and still less the ESWLs) are independent of factors relating to the pavement structure. Certainly earlier investigators have pointed out the influence of such input parameters as layer thicknesses and moduli. Even Scala presents and discusses in detail a long list of such factors and in several instances refers to previous literature, showing that they are indeed important.

The existence of a fourth-power law was recently refuted by theoretical and field investigations conducted by the Organization for Economic Cooperation and Development (OECD) (24). That study "demonstrated that from a strict theoretical viewpoint, it is not possible to prove the existence of a law of equivalence between loads in terms of their damaging effects on pavements." In addition, it was noted that

in view of the statistical nature of [the] supporting equations, [the load equivalence law] is necessarily also a statistical law . . . and the exponent γ has a different value for each type of pavement structure, i.e., flexible, semi-rigid, rigid. For fatigue phenomena and permanent deformation of flexible pavements, it is usual to set $\gamma = 4$. For semi-rigid and rigid pavements and in regard to fatigue of hydraulically bound materials, the γ values are between 11 and 33, depending on the material concerned. From the point of view of behavior of these types of structures, it is important to note that such high γ values reflect the pre-

dominant role of heavy loads even if they are infrequent. In fact the actual value of the exponent γ does not play a major role if the standard load is well chosen, this choice being dependent on the actual load distribution. (24)

Data presented from field tests in Italy, France, and Finland show that γ varies between 1.2 and 8 when fatigue cracking and rutting of bituminous pavements are considered. To assess the significance of such differences, a typical flexible pavement design problem was submitted to Belgium, France, the Netherlands, the United Kingdom, and the United States. In accommodating mixed traffic, "all five participating countries used the notion of equivalent traffic." The four European countries used $\gamma = 4$, whereas the United States used this only for single axles and a modified equivalence law for multiple axles. Nevertheless, from the responses received "it emerges that there are as many solutions proposed as countries proposing them" (24).

A final comment needs to be made with respect to another practice that has gained considerable popularity in the last 25 years, namely, the use of mechanistic tools such as computerized layered elastic analysis in the determination of LEFs. An early example of this approach is provided by the aforementioned study by Deacon (21), who noted that "empirical determinations [of LEFs] are impractical," since they require "extensive, controlled experiments such as the AASHO Road Test." Therefore, Deacon argued, "theoretical determination of these factors can be of immense significance" provided "suitable analytical techniques" are employed. The approach followed by Deacon, and later by several other investigators, involves the use of Burmister's three-layer theory, implemented in the CHEVRON computer code. Such an exercise, however, constitutes a mechanistic extension introduced into an entirely statistical/empirical framework, a process that "rarely leads to reliable conclusions" (25). As a consequence of the statistical-empirical nature of the ESAL concept and of Miner's fatigue hypothesis, it is impossible to derive reliable and general LEFs using mechanistic tools or measurements of particular pavement structural responses. This is because entirely statistical-empirical concepts cannot be combined with mechanistic procedures in a meaningful way, primarily because of the difference in the understanding of a pavement system inherent in these two approaches. More specifically, exclusively statistical-empirical methods consider the pavement system as the sum of individual, "independent" components and fail to discern the engineering interactions between the geometry of the applied loads, the constructed layers, and the supporting subgrade, which form the basis of a mechanistic understanding of the pavement system (25). In addition, because the distresses considered in the determination of the PSI are permanent and largely irreversible, it is clear that the ESAL concept is in violation of the principles of elasticity and superposition, which are of fundamental significance in mechanistic approaches. The failure of several previous studies to develop LEFs of general applicability, the exclusive use of the AASHTO LEFs in all design procedures that employ the load equivalency approach, as well as the refutation of the fourth-power law by OECD (24), provides ample evidence of the futility of mechanistic LEF development exercises. A good summary of the pertinent literature is provided by Papagiannakis and Haas (26).

THE ESAR CONCEPT

The development of an improved load equivalency concept requires the return to mechanistic principles to which only the ESWL was found to adhere in the preceding review. However, both the equal contact radius and equal contact pressure assumptions made in determining an ESWL are arbitrary and unnecessarily restrictive, imposed only for reasons of expediency. A more general approach would require neither, but would determine instead the radius of an equivalent single wheel that would lead to the same response if loaded by the same total load as the dual-wheel assembly. Such an approach to load equivalency is termed the equivalent single-axle radius (ESAR) concept. The basic idea is already evident in a 1934 paper by Bradbury (27) and was suggested again recently (28) as a means of establishing more reliable mechanistic load equivalency procedures. The importance of load geometry in general and of the load radius (a), in particular may be noted in connection with the governing independent variable (all) (29). This dimensionless ratio implies that the sensitivity of the pavement system response to changes in load radius (a) is just as pronounced as the effect of variations in the radius of relative stiffness (l).

As noted earlier, a major step toward an improved load equivalency concept was taken in a published discussion in which application of the principles of dimensional analysis showed that the effect of dual-wheel loads may be quantified by (S/a), where S is the spacing of the two loads (11). Furthermore, during the present investigation it was found that it is possible to determine with reasonable accuracy the maximum bending stress occurring in a slab on grade under interior loading through the use of Westergaard's equation for a single-wheel load, into which the equivalent single-wheel radius (a_{eq}) of a multiple-wheel assembly is substituted. Statistical regression techniques applied to the interior loading maximum bending stress data presented by Tayabji and Halpenny (10) resulted in the following expression of a_{eq} :

$$\frac{a_{eq}}{a} = 1.00 + 0.241683 \left(\frac{S}{a} \right) \quad (1)$$

This formula implies that once the primary structural response is chosen, it is possible to derive with reasonable accuracy an equivalent radius (a_{eq}) for any arbitrary loading gear configuration simply as a function of its geometry (size and spacing of tire prints). The loss of accuracy involved in such a transformation from a multiple- to a single-wheel load has been assessed with reference to data bases compiled at the University of Illinois and elsewhere and has been found to be negligible in many cases when competent slab-subgrade systems are considered.

Investigations into the applicability of the ESAR concept to airport and highway pavement design have been presented in two Ph.D. theses submitted recently to the University of Illinois. In the first, Seiler (30) examined the variation of the equivalent radius (a_{eq}) with the pavement radius of relative stiffness (l) for six multiple-wheel aircraft types, of which three were military and three were commercial. It was shown that for competent pavement sections (a_{eq}) is largely insensitive to l . A similar application of the ESAR concept to highway

pavements was presented in the thesis by Salsilli-Murua (31). Truck configurations consisting of dual, tandem, and tridem axles were examined, and predictive formulas were developed describing the effect of such multiple-wheel loads on the critical tensile bending stress arising in the concrete pavement slab. This approach has recently been used in the evaluation of the detrimental effect of "super-single" or wide-base tires (32).

Unlike the ESAL approach, the ESAR concept addresses all three components of a pavement system, namely, the constructed layers, the supporting natural subgrade, and the geometry of applied loads, primarily the size and spacing of tire prints. Furthermore, in contrast to the ESWL approach, the ESAR concept imposes no a priori assumptions as to the total applied load, contact pressure, or size of tire print, and leads to a reasonably precise estimate of the chosen primary structural response under a multiple-wheel load. This estimate is achieved through the use of available closed-form equations for a single-wheel load into which the equivalent single-wheel radius (a_{eq}) of a multiple-wheel assembly is substituted. Thus, the application of the ESAR concept is akin to Odemark's "method of equivalent thicknesses" (33).

The ESAR concept may be used to address one of the major factors contributing to the complexity of the problem of accommodating the effects of mixed traffic on highway pavements, namely, the very large number of types of trucks that use the national network. Trucks differ from one another not only in terms of size and gross weight, but also in terms of number and spacing of axles, number and spacing of tires per axle, tire type (e.g., radial or bias ply), inflation pressure, and applied contact pressure. Recent collaborative efforts between pavement and truck (mechanical) engineers have indicated that suspension stiffness and damping as well as static and dynamic equalization may also need to be considered (34). The most extensive of such studies was conducted by Gillespie et al. (35) under the sponsorship of NCHRP. These investigators indicated that it is possible to establish a short "baseline matrix" of 13 truck configurations to provide an adequate description of the entire traffic stream. This finding makes much more manageable the problem of mixed traffic. The ESAR concept may now be applied to each of these (and other) truck configurations to provide a mechanistic assessment of their relative damaging effect leading to the development of more efficient and reliable pavement design algorithms. Such algorithms must describe the structural response of the pavement under a number of different loading and support conditions in the context of a new "limit state" design procedure.

Current design methodologies are based on the assumption that pavement distresses accumulate slowly with repeated application of stress or strain cycles at amplitudes significantly smaller than the material's ultimate strength. Consequently, Miner's linear cumulative fatigue hypothesis is often used for distresses such as rutting and erosion, in addition to fatigue cracking. The major highways of the nation, however, which receive not only millions of legally loaded trucks but also relatively fewer heavily overloaded trucks, may not fail in fatigue at all. This possibility becomes even more important when one considers the variation in structural capacity experienced by the pavement system during the annual cycle. Thus, a "limit state" may be expected to occur when heavily

overloaded trucks are applied during periods of considerable loss in pavement strength, such as during spring thaw or partial contact conditions due to a temperature differential through the thickness of the slab. Because of the far-reaching implications of these proposals, a mechanistic justification for the ESAR concept is provided below, where the statistical regression Equation 1 is reproduced from first principles using engineering mechanics, for both the dense liquid and elastic solid foundations.

VERIFICATION OF ESAR CONCEPT

Dense Liquid Foundation

Consider a plate consisting of a linear elastic, homogeneous, and isotropic material resting on a dense liquid foundation. Under a single-wheel load distributed uniformly over a circular area of radius (a), the distribution of deflections [$w(s)$] may be written as follows (36):

$$w(s) = \frac{Pl_k^2}{\pi D} \left(\frac{1}{a_k}\right)^2 [1 - C_1 \text{ber } s - C_2 \text{bei } s] \quad \text{for } 0 < s \leq a_k \quad (2)$$

$$w(s) = \frac{Pl_k^2}{\pi D} \left(\frac{1}{a_k}\right)^2 [C_3 \text{ker } s + C_4 \text{kei } s] \quad \text{for } s \geq a_k \quad (3)$$

in which

$a_k = (a/l_k)$, which is the dimensionless radius of the applied load;

$s = (r/l_k)$, which is the normalized radial distance measured from the center of the load;

$l_k = (D/k)^{1/4}$, which is the radius of relative stiffness of plate-subgrade system for the dense liquid foundation;

$D =$ flexural rigidity of the plate, which is equal to $Eh^3/12(1 - \mu^2)$;

$E =$ plate elastic modulus;

$\mu =$ plate Poisson's ratio;

$h =$ plate thickness;

$k =$ modulus of subgrade reaction;

$P =$ total applied load, which is $p\pi a^2$; and

$p =$ applied load intensity (pressure).

Note that ber, bei, ker, and kei are Kelvin Bessel functions that may be evaluated using appropriate series expressions available in the literature (37). Constants C_1 through C_4 have been evaluated by Ioannides (38). In the present study, the following simplified expressions have been derived for these constants, valid in the interval $0 < a_k < 0.6$:

$$C_1 = 1 - \frac{\pi}{8} a_k^2 + \left[\frac{5}{4} - \gamma + \ln \left(\frac{a_k}{2} \right) \right] \left(\frac{a_k}{2} \right)^4 \quad (4)$$

$$C_2 = \frac{1}{2} a_k^2 \ln \left(\frac{2}{a_k} \right) + \left(\frac{1}{4} - \frac{\gamma}{2} \right) a_k^2 + \frac{\pi}{64} a_k^4 \quad (5)$$

$$C_3 = - \left(\frac{a_k}{2} \right)^4 \quad (6)$$

$$C_4 = - \frac{a_k^2}{2} \quad (7)$$

in which γ is Euler's constant = 0.577 215 664 90.

The distribution of deflections given by Equations 2 and 3 may be used to obtain the corresponding distribution of bending stresses. Graphs presented by Losberg 36 indicate that the tangential stress (σ_ϕ) is more critical than the radial stress (σ_r). Using the mathematical software package MATHEMATICA, the following expression has been derived for σ_ϕ :

$$\sigma_\phi(s) = \frac{6P}{\pi h^2} \left(\frac{1}{a_k}\right)^2 (C_1 J + C_2 K) \quad (8)$$

for $0 < s \leq a_k$, and

$$\sigma_\phi(s) = - \frac{6P}{\pi h^2} \left(\frac{1}{a_k}\right)^2 (C_3 L + C_4 M) \quad (9)$$

for $a_k < s \leq 1$, in which

$$J = \frac{(1 + 3\mu)s^2}{16} \quad (10)$$

$$K = - \frac{(1 + \mu)}{2} \quad (11)$$

$$L = \frac{\pi}{8} (\mu + 1) + \frac{1}{s^2} (\mu - 1) + \frac{s^2}{16} \left[\gamma - \frac{5}{4} + \mu \times \left(3\gamma - \frac{11}{4} \right) + (1 + 3\mu) \ln \left(\frac{s}{2} \right) \right] - \frac{\pi s^4}{1,536} (1 + 5\mu) \quad (12)$$

$$M = \frac{1}{4} [1 - 2\gamma - \mu(1 + 2\gamma)] - \frac{1}{2} (1 + \mu) \ln \left(\frac{s}{2} \right) + \frac{\pi s^2}{64} (1 + 3\mu) + \frac{s^4}{384} \left[\frac{-5}{3} + \gamma \right] + \mu \left(5\gamma - \frac{22}{3} \right) - (1 + 5\mu) \ln 2 \quad (13)$$

Consider now the same elastic plate resting on a dense liquid subgrade but loaded by two circular loads, each of radius a , spaced at distances S center to center. Once again, it is assumed that the loads are applied at the plate's interior, that is, far from any edges or corners. Under these conditions, the bending stress distribution along a line (O_1-O_2) connecting the centers of the two circular loads may be expected to be a function of the following three dimensionless parameters: $a_k = (a/l)$, the nondimensional radius of the applied loads; $s = (r/l)$, the nondimensional radial distance from the center (O_1) of the first of the two loads; and $\xi = [(S - r)/l]$, the nondimensional radial distance from the center (O_2)

of the second loaded area. The bending stress from both loads, $\sigma_{II}(a_k, s, \zeta)$ at any point along O_1-O_2 may be obtained by superposition of the contributions of each of the two loads, as given by Equations 8 and 9. Examination of the complete stress distribution during this study revealed that the maximum stress always occurs under each of the two wheel loads. Therefore, for the range $s < a_k$, the combined bending stress is obtained from

$$\sigma_{II}(a_k, s, \zeta) = -\frac{6P/2}{\pi h^2} \left(\frac{1}{a_k}\right)^2 [C_1 J + C_2 K + C_3 L + C_4 M] \quad (14)$$

in which

$$J = \frac{(1 + 3\mu)s^2}{16} \quad (15)$$

$$K = -\frac{(1 + \mu)}{2} \quad (16)$$

$$L = \frac{\pi}{8}(\mu + 1) + \frac{1}{\zeta^2}(\mu - 1) + \frac{\zeta^2}{16} \left[\gamma - \frac{5}{4} + \mu \left(3\gamma - \frac{11}{4} \right) + (1 + 3\mu) \ln \left(\frac{\zeta}{2} \right) \right] - \frac{\pi \zeta^4}{1,536} (1 + 5\mu) \quad (17)$$

$$M = \frac{1}{4} [1 - 2\gamma - \mu(1 + 2\gamma)] - \frac{1}{2} (1 + \mu) \times \ln \left(\frac{\zeta}{2} \right) + \frac{\pi \zeta^2}{64} (1 + 3\mu) + \frac{\zeta^4}{384} \left[-\frac{5}{3} + \gamma + \mu \left(5\gamma - \frac{22}{3} \right) - (1 + 5\mu) \ln 2 \right] \quad (18)$$

Note that in keeping with the definition of P as the total applied load, the wheel load applied over each area in Equation 14 is $P/2 = p\pi a^2$. The magnitude of the maximum combined stress, $\sigma_{II\max}$, may be obtained by differentiating Equation 14 with respect to s and setting the derivative to zero. The following expression has been found to yield a reasonable estimate of the location of the maximum stress (r_{\max}):

$$\frac{r_{\max}}{l} \approx -\frac{f(0) * (a_k)}{f(a_k) - f(0)} \quad (19)$$

where

$$f(a_k) = \frac{\partial}{\partial s} \sigma_{II}(a_k, s, \zeta) \Big|_{s=a_k} \quad (20)$$

and

$$f(0) = \frac{\partial}{\partial s} \sigma_{II}(a_k, s, \zeta) \Big|_{s=0} \quad (21)$$

Truncated series expressions for $f(a_k)$ and $f(0)$ can be derived by differentiating Equation 15 through 18 and setting $s = a_k$, $\zeta = [(S - a)/l]$, and $s = 0$, $\zeta = (S/l)$, respectively.

The validity of the proposed approximate method for determining $\sigma_{II\max}$ has been verified by comparison with the exact numerical solution obtained using MATHEMATICA.

A simpler expression may be derived for the bending stress, σ_{II0} , arising under the center of one of the two wheel loads. This stress is expected in most cases to be an adequate approximation of $\sigma_{II\max}$. Setting $s = 0$ and $\zeta = S/l = S_k$ in Equation 14, the formula for $\sigma_{II\max}$ may be simplified by truncation into

$$\sigma_{II0} \approx \frac{P}{h^2} \frac{3(1 + \mu)}{2\pi} \left\{ \frac{1}{2} - \gamma + \frac{1}{4} \times \left[\frac{1 - 2\gamma - \mu(1 + 2\gamma)}{(1 + \mu)} \right] + \frac{1}{2} \ln \left(\frac{2}{a_k} \right) - \frac{1}{2} \ln \left(\frac{S_k}{2} \right) + S_k^2 \frac{\pi}{64} \frac{1 + 3\mu}{1 + \mu} \right\} \quad (22)$$

Having obtained $\sigma_{II0} \approx \sigma_{II\max}$, it is desirable to determine the equivalent radius of a single-wheel load, which would reproduce this maximum stress using available closed-form equations. In this case, the following interior loading equation (39,40) may be used:

$$\sigma_0 = \frac{P}{h^2} \frac{3(1 + \mu)}{2\pi} \left[\ln \left(\frac{2}{a_k} \right) + \frac{1}{2} - \gamma + a_k^2 \left(\frac{\pi}{32} \right) \right] \quad (23)$$

A first estimate (b), say, of the load radius may be obtained from

$$b_k = \exp \left(R - \frac{\sigma_0}{T} \right) \quad (24)$$

in which $b_k = (b/l) \approx a_k$, and

$$T = \frac{P}{h^2} \frac{3(1 + \mu)}{2\pi} \quad (25)$$

$$R = \ln 2 + \frac{1}{2} - \gamma \quad (26)$$

An improved estimate of the radius (a) may then be obtained using the following expression:

$$a_k = \frac{\frac{2}{b_k} - \left(\frac{1}{b_k^2} - \frac{3\pi}{16} \right)^{1/2}}{\frac{\pi}{16} + \frac{1}{b_k^2}} \quad (27)$$

Returning now to Equation 22, a first estimate of the equivalent radius can be written as

$$b_k = R^* (a_k S_k)^{1/2} \left[1 - S_k^2 \frac{\pi}{64} \frac{1 + 3\mu}{1 + \mu} \right] \quad (28)$$

in which

$$R^* = \exp \left[R - \frac{1}{2} - \gamma - \gamma\mu - \ln 2 \right] \quad (29)$$

Setting $\mu = 0.15$, Equation 28 results in the following approximate expression for a_{eq} :

$$\frac{a_{eq}}{a} = 1.0674 \left(\frac{S}{a} \right)^{1/2} [1 - 0.0619S_k^2] \quad (30)$$

Equation 30 shows that a first approximation of the equivalent radius may be obtained merely as a function of the geometry of the applied loads, namely, of the spacing ratio (S/a), provided S_k is not much greater than unity. Equation 30 may also be rewritten in the form of Equation 1 obtained by statistical regression. This is accomplished by considering the minimum (S/a) value of 2 (the two tire prints touch with no clear space between them) and an arbitrary upper limit of (S/a) = $2a + 0.6l$ (corresponding to $S_k \approx 1$). For $S = 2a$, the S_k^2 term in Equation 30 is negligible, resulting in

$$\frac{a_{eq}}{a} \approx 1.50952 \quad (31)$$

Setting $S = 2a + 0.6l$, Equation 30 results in a quasi-linear relationship between (a_{eq}/a) and a_k for values of the latter between 0.05 and 0.3. This relationship may be approximated by

$$\frac{a_{eq}}{a} \approx 1.50952 + \frac{0.1390}{a_k} \quad (32)$$

Therefore, within the range prescribed here,

$$a_{eq} = a_{eq|S=2a} + \frac{a_{eq|S=2a+0.6l} - a_{eq|S=2a}}{0.6l} * (S - 2a) \quad (33)$$

from which

$$\frac{a_{eq}}{a} = 1.046 + 0.2316(S/a) \quad (34)$$

This equation compares favorably with Equation 1, thus verifying mathematically the ESAR concept for the dense liquid foundation.

Elastic Solid Foundation

The corresponding tangential bending stress distribution under a single-wheel load applied on a plate resting on an elastic solid foundation was found in this study to be

$$\sigma_\phi = \frac{6D}{h^2} \frac{P}{\pi a} \frac{2}{C} \left[\frac{1-\mu}{r} \int_0^\infty \frac{J_1(\alpha r) J_1(\alpha a)}{1+\alpha^3 l_e^3} d\alpha + \mu \int_0^\infty \frac{\alpha J_0(\alpha r) J_1(\alpha a)}{1+\alpha^3 l_e^3} d\alpha \right] \quad (35)$$

where

C = elastic solid foundation parameter [$E_s/(1 - \mu_s^2)$];
 E_s = Young's modulus for subgrade;
 μ_s = Poisson's ratio for subgrade;
 l_e = radius of relative stiffness of plate-subgrade system for the elastic solid foundation

$$= \sqrt[3]{2 D/C} \quad (36)$$

J_0, J_1 = Bessel functions of the first kind, order 0 and 1, respectively; and
 α = dummy variable.

The combined stress (σ_{II}) due to two circular loads at any distance (r) along the line joining the centers of the two wheel loads (O_1-O_2) is obtained by superposition as

$$\sigma_{II} = \frac{6}{h^2} \frac{P/2}{\pi a_e} \left[\frac{1-\mu}{s} \int_0^\infty \frac{J_1(\beta s) J_1(\beta a_e)}{1+\beta^3} d\beta + \mu \int_0^\infty \frac{\beta J_0(\beta s) J_1(\beta a_e)}{1+\beta^3} d\beta + \frac{1-\mu}{Z} \int_0^\infty \frac{J_1(\beta \zeta) J_1(\beta a_e)}{1+\beta^3} d\beta + \mu \int_0^\infty \frac{\beta J_0(\beta \zeta) J_1(\beta a_e)}{1+\beta^3} d\beta \right] \quad (37)$$

where

$Z = S - r$,
 $\beta = \alpha l$,
 $s = r/l_e$,
 $a_e = a/l_e$, and
 $\zeta = Z/l_e$.

In view of the complexity of Equation 37, a simpler expression may be derived once again for the bending stress (σ_{II0}) occurring under the center of one of the two circular loads. This is achieved by superposition, using the formula presented by Losberg (36) for the stress under the center of one wheel [$\sigma(a_e)$] and the solution for the stress due to a point load, arising at a normalized distance $S_e = S/l_e$ from the load [$\sigma(S_e)$] presented by Hogg (41). Both of these important contributions were verified during this study using MATHEMATICA, and the following general expressions were derived:

$$\sigma(a_e) = \frac{P}{h^2} \frac{3(1+\mu)}{2\pi} \left[\ln \left(\frac{2}{a_e} \right) + \frac{1}{2} - \gamma + a_e^2 \left(\frac{\pi}{12\sqrt{3}} \right) \right] \quad (38)$$

$$\sigma(S_e) = \frac{6P}{h^2} \left[\frac{1}{8\pi} - \frac{\gamma}{4\pi} - \frac{\mu}{8\pi} - \frac{\gamma\mu}{4\pi} + \frac{(1+3\mu)S_e^2}{48\sqrt{3}} - \frac{1+\mu}{4\pi} \ln \left(\frac{S_e}{2} \right) \right] \quad (39)$$

Thus, by superposition:

$$\sigma_{110} = \sigma(a_e) + \sigma(S_e) \quad (40)$$

Equation 40 corresponds to Equation 22 derived above for the dense liquid subgrade. Proceeding in the manner outlined above, the following expression may be written for the approximate equivalent radius $b_e = b/l_e$:

$$b_e = R^* (a_e S_e)^{1/2} \left(1 - S_e^2 \frac{\pi}{24\sqrt{3}} \frac{1 + 3\mu}{1 + \mu} \right) \quad (41)$$

in which R^* is as defined by Equations 29 and 26. It is apparent that the only difference between this expression and the corresponding Equation 28 derived earlier for the dense liquid foundation is that $24\sqrt{3}$ replaces 64 in the latter. Thus, Equation 30 becomes

$$\frac{a_{eq}}{l_e} = 1.0674a_e \left(\frac{S}{a} \right)^{1/2} \left(1 - 0.0953S_e^2 \right) \quad (42)$$

whence Equation 34 becomes

$$\frac{a_{eq}}{a} = 1.066 + 0.2218(S/a) \quad (43)$$

confirming the validity of the ESAR concept for the elastic solid foundation and by implication for any subgrade type. A similar derivation could verify the validity of the ESAR concept on the basis of deflection considerations.

CONCLUSIONS

Accommodation of mixed traffic consisting of a wide variety of single- and multiple-wheel gear configurations is one of the most critical considerations in pavement design. Closed-form analytical solutions based on the theory of elasticity have hitherto been formulated in terms of a single tire print, whereas graphical and computerized approaches that can accommodate multiple-wheel loads are generally too cumbersome for incorporation in a design guide. For this reason, a number of load equivalency concepts have been promulgated over the last 50 years, with the general aim to transform complex load assemblies into single-wheel loads, which could be accommodated in existing design procedures developed for single-wheel loads.

In this paper, three such load equivalency concepts are reviewed. A critical reexamination of the pertinent literature leads to the conclusion that the ESWL concept is significantly different from the ESAL concept. The ESWL concept constitutes an attempt to provide a general mechanistic solution to the problem posed by multiple-wheel loads on airport and highway pavements using the theory of linear elasticity and the principle of superposition, as well as field measurements for verification purposes. In contrast, the ESAL concept is entirely statistical/empirical and violates fundamental precepts of elasticity, as well as the principle of superposition. It seeks to establish "relative damage" effects, quantified as a drop in the PSI, between a standard (base) load level and config-

uration, and any other load level and configuration. In doing so, it fails to recognize the interactions between the characteristics of the three main components of the pavement system, namely, the constructed layers, the supporting natural subgrade, and the geometry of the applied loads. In addition, an intimate connection between the ESAL concept with another statistical-empirical concept, namely, Miner's linear cumulative fatigue hypothesis, has been established. In view of these findings, it is considered inappropriate to continue using ESAL counts as a primary design input. ESAL counts may be retained as indirect inputs to the design process, that is, as indicators of the relative amount of traffic services by any given pavement. As such, they may be used to classify pavements in terms of traffic level and may serve as one of the criteria for selecting the allowable working stress, strain, or deflection level in a pavement system.

A third, less-known load equivalency approach, the ESAR concept, is discussed in this paper, and its advantages over both the ESAL and the ESWL concepts are explained. According to this concept, it is possible to determine with reasonable accuracy a chosen primary structural response occurring in a PCC pavement system through the use of available closed-form equations for a single-wheel load, into which an equivalent single-wheel radius of a multiple-wheel assembly is substituted. Through rigorous engineering mechanics derivations, the concept is verified for both the dense liquid and elastic solid foundation. The ESAR concept can be incorporated into an improved mechanistic "limit-state" design approach and can be instrumental in accommodating the wide variety of load configurations imposed on modern pavements. This may be accomplished through the development of a rating scale based on the level of stress caused by and the probability of occurrence of each of the truck configurations examined. Such a scale will enable pavement designers to select their design-loading configuration as a percentile of the load spectrum, much like a geotechnical engineer selects the flood level for the design of a dam (e.g., the 95th percentile of damaging effect, compared with the 95-year flood). Efforts toward the development of such a design procedure are continuing at this time.

ACKNOWLEDGMENTS

This material is based on work supported by the National Science Foundation. The government has certain rights to this material. Additional funding was provided by NCHRP.

REFERENCES

1. H. M. Westergaard. Stresses in Concrete Pavements Computed by Theoretical Analysis. *Public Roads*, Vol. 7, No. 2, April 1926.
2. D. M. Burmister. The Theory of Stresses and Displacements in Layered Systems and Applications to the Design of Airport Runways. *HRB Proc.*, Vol. 23, 1943.
3. G. Pickett, and G. K. Ray. Influence Charts for Concrete Pavements. *Transactions, ASCE*, Vol. 116, 1951.
4. N. M. Newmark. *Influence Charts for Computation of Stresses in Elastic Foundations*. Bulletin 338. University of Illinois Engineering Experiment Station, Urbana, 1942, pp. 5-25.
5. R. G. Packard. Computer Program for Airport Pavement Design. PCA, SR029.02P, Skokie, Ill., 1967.

6. W. C. Kreger. *Computerized Aircraft Ground Flotation Analysis-Edge Loaded Rigid Pavement*. Research Report ERR-FW-572. General Dynamics Corporation, Fort Worth, Tex., Jan., 1967.
7. A. M. Ioannides. *Analysis of Slabs-On-Grade for a Variety of Loading and Support Conditions*. Ph.D. thesis. University of Illinois, Urbana, 1984.
8. M. G. F. Peutz, H. P. M. Van Kempen, and A. Jones. Layered Systems Under Normal Surface Loads. In *Highway Research Record 228*, HRB, National Research Council, Washington, D.C., 1968.
9. E. J. Yoder and M. W. Witzczak. *Principles of Pavement Design*, 2nd ed. Wiley-Interscience, New York, N.Y., 1975.
10. S. D. Tayabji and D. Halpenny. Thickness Design of Roller-Compacted Concrete Pavements. In *Transportation Research Record 1136*, TRB, National Research Council, Washington, D.C., 1987, pp. 23-31.
11. A. M. Ioannides. Discussion: Thickness Design of Roller-Compacted Concrete Pavements, by S. D. Tayabji and D. Halpenny. In *Transportation Research Record 1136*, TRB, National Research Council, Washington, D.C., 1987, pp. 31-32.
12. E. J. Yoder. *Principles of Pavement Design*. John Wiley and Sons, Inc., New York, N.Y., 1959.
13. W. K. Boyd and C. R. Foster. Design Curves for Very Heavy Multiple Wheel Assemblies. In Development of CBR Flexible Pavement Design Method for Airfields: A Symposium. *Transactions, ASCE*, Vol. 115, Paper 2406, pp. 534-546, 1950.
14. C. R. Foster and R. G. Ahlvin. Development of Multiple-Wheel CBR Design Criteria. *Journal of the Soil Mechanics and Foundations Division, ASCE*, Vol. 84, No. SM2, May 1958, pp. 1647-1-1647-12.
15. C. M. Gerrard and W. J. Harrison. A Theoretical Comparison of the Effects of Dual-Tandem and Dual-Wheel Assemblies on Pavements. *Proc., 5th Conference of the Australian Research Board*, 1970.
16. Y. H. Huang. Chart for Determining Equivalent Single-Wheel Loads. *Journal of the Highway Division, ASCE*, Vol. 94, No. HW2, Nov. 1968, pp. 115-128.
17. Y. H. Huang. Computation of Equivalent Single-Wheel Loads Using Layered Theory. In *Highway Research Record 291*, HRB, National Research Council, Washington, D.C., 1969, pp. 144-155.
18. F. J. Grumm. Designing Foundation Courses for Highway Pavements and Surfaces. *California Highways and Public Works*, Vol. 19, No. 11, Nov. 1941, pp. 4-23.
19. F. J. Grumm. Designing Foundation Courses for Highway Pavements and Surfaces. *California Highways and Public Works*, Vol. 20, No. 3, March 1942, pp. 6-20.
20. M. A. Miner. Cumulative Damage in Fatigue. *Transactions, American Society of Mechanical Engineers*, Vol. 67, 1945, pp. A.159-A.164.
21. J. A. Deacon. Load Equivalency in Flexible Pavements. *Proc., Association of Asphalt Paving Technologists*, Vol. 38, 1969, pp. 465-494.
22. P. E. Irick and W. R. Hudson. *NCHRP Report 2A: Guidelines for Satellite Studies of Pavement Performance*. HRB, National Research Council, Washington, D.C., 1964.
23. A. J. Scala. Comparison of the Response of Pavements to Single and Tandem Axle Loads. *Proc., 5th Conference of the Australian Research Board*, 1970.
24. *Heavy Trucks, Climate and Pavement Damage*. Organization for Economic Cooperation and Development, Paris, 1988.
25. A. M. Ioannides. Theoretical Implications of the AASHTO 1986 Nondestructive Testing Method 2 for Pavement Evaluation. In *Transportation Research Record 1307*, TRB, National Research Council, Washington, D.C., 1991, pp. 211-220.
26. A. T. Papagiannakis and R. C. G. Haas. *Wide-Base Tires: Industry Trends and State of Knowledge of Their Impact on Pavements*. Ministry of Transportation and Communications, Ontario, Canada, Dec. 1986.
27. R. D. Bradbury. Evaluation of Wheel-Load Distribution for the Purpose of Computing Stresses in Concrete Pavements. *HRB Proc.*, Vol. 14, 1934, pp. 225-254.
28. A. M. Ioannides and R. A. Salsilli-Murua. Temperature Curling in Rigid Pavements: An Application of Dimensional Analysis. In *Transportation Research Record 1227*, TRB, National Research Council, Washington, D.C., 1989, pp. 1-11.
29. A. M. Ioannides. Discussion: Responses and Performance of Alternate Launch and Recovery Surfaces (ALRS) Containing Stabilized-Material Layers, by R. R. Costigan and M. R. Thompson. In *Transportation Research Record 1095*, TRB, National Research Council, Washington, D.C., 1987.
30. J. S. Seiler. *A Knowledge-Base for Rehabilitation of Airfield Concrete Pavements*. Ph.D. thesis. University of Illinois, Urbana, 1991.
31. R. A. Salsilli. *Calibrated Mechanistic Design Procedure for Jointed Plain Concrete Pavements*. Ph.D. thesis. University of Illinois, Urbana, 1991.
32. A. M. Ioannides, R. A. Salsilli, I. Vinding, and R. G. Packard. 'Super-Singles': Implications for Design. *Proc., 3rd International Symposium on Heavy Vehicle Weights and Dimensions*, Queens' College Cambridge, United Kingdom, June 28-July 2, 1992.
33. N. Odemark. Investigations as to the Elastic Properties of Soils and Design of Pavements According to the Theory of Elasticity (in Swedish). *Meddelanden fran Statens Vaginstitut* (Sweden) 1949 [English Translation by M. A. Hibbs and J. Silfwerbrand (A. M. Ioannides, ed.), 1990].
34. M. S. Mamlouk. *Vehicle-Pavement Interaction: State of the Art*. Final Report FHWA-AZ90-340. Arizona State University, Tempe, Jan. 1990.
35. T. D. Gillespie, S. M. Karamihas, D. Cebon, M. W. Sayers, M. A. Nasim, W. Hansen, and N. Ehsan. *Effects of Heavy Vehicle Characteristics on Pavement Response and Performance*. Preliminary Draft Final Report, NCHRP Project 1-25(1). University of Michigan Transportation Research Institute, Dec. 1991.
36. A. Losberg. Structurally Reinforced Concrete Pavements, *Doktorsavhandlingar vid Chalmers Tekniska Hogskola*, 1960.
37. N. W. McLachlan. *Bessel Functions for Engineers*, 2nd ed. Clarendon Press, Oxford, United Kingdom, 1955.
38. A. M. Ioannides. Dimensional Analysis in NDT Rigid Pavement Evaluation. *Journal of Transportation Engineering, ASCE*, Vol. 116, No. 1, Jan./Feb. 1990, pp. 23-36.
39. H. M. Westergaard. New Formulas for Stresses in Concrete Pavements of Airfields. *Transactions ASCE*, Vol. 113, 1948.
40. A. M. Ioannides, M. R. Thompson, and E. J. Barenberg. Westergaard Solutions Reconsidered. In *Transportation Research Record 1043*, TRB, National Research Council, Washington, D.C., 1985.
41. A. H. A. Hogg. Equilibrium of a Thin Plate, Symmetrically Loaded, Resting on an Elastic Foundation of Infinite Depth. *The London, Edinburgh & Dublin Philosophical Magazine and Journal of Science*, Series 7, Vol. 25, 1938.

Publication of this paper sponsored by Committee on Rigid Pavement Design.

Examination of Pure Environmental Effects on Pavement Condition

TURKI I. AL-SULEIMAN, ADNAN A. BASMA, AND KHALED KSAIBATI

A study was undertaken to examine pure environmental effects on the condition of pavements. The road network within the campus of Jordan University of Science and Technology was utilized. More than half of this road network was untrafficked because of delays in several construction projects to which these roads lead. The condition of 71 primary and secondary pavement sections was evaluated periodically for 7 years. A methodology was proposed to investigate the pure environmental effects, pure traffic effects, and their interaction on pavement deterioration. The first order-second moment Taylor series expansion was used to estimate the variations in pavement service life under each of these effects. The results of the analysis showed that most of the pavement deterioration in lightly trafficked roads was caused by environmental factors. Heavily trafficked roads showed the widest range of pavement service life expectancy. To further improve the obtained results, continuous pavement monitoring is needed.

Pavement deterioration usually is caused by a combination of factors such as traffic load, environment, initial design, and quality of construction. Therefore, pavement deterioration may result from traffic-induced distress, environmentally associated distress, and the interaction of these two. For example, rutting and alligator cracking are regarded as traffic-induced distresses, whereas longitudinal and transverse cracking are viewed as environmental or non-load-related distresses (1). The relationship between traffic loading and pavement performance was developed through the AASHO Road Test in the early 1960s. This relationship is summarized in the *AASHTO Interim Guide for the Design of Pavement Structures* (2).

The pure effects of environmental factors such as moisture, soil conditions, and temperature on pavement deterioration were not investigated in the AASHO Road Test because it was conducted over a short period (2 years). The determination of respective proportions of traffic and environmental responsibilities is an old problem in highway pavement evaluation and cost allocation studies. There is not enough information to separate traffic-related effects from environmentally related effects during physical measurements of pavement condition. As a result, the responsibilities of these two effects have been determined subjectively in most cost allocation studies, and thus there has not been an acceptable solution to this problem. Indeed, researchers (3,4) have attempted to collect data on pavement performance to quantify relationships and propose mathematical models. Although the findings of these studies shed some light on the relative effect

of pure environment on pavement performance, the number of pavement sections used to arrive at the results was limited. Consequently, there seems to be a need to improve and refine existing procedures dealing with this problem.

The basic objective of this study is to investigate and evaluate purely environmental effects on pavement performance. To accomplish this goal, the road network within the campus of Jordan University of Science and Technology (JUST) was utilized. Among the pavements examined, more than half were untrafficked because of delays in several major construction projects to which these roads lead. The untrafficked pavements were compared with similar trafficked pavements. A total of 71 sections of primary and secondary trafficked and untrafficked roads were considered. A complete description of the site and the road network follow.

SITE DESCRIPTION

JUST lies in the northern part of Jordan about 20 km east of the city of Irbid. The campus occupies approximately 13 km². Work on the road network started in September 1981 and was completed in April 1984 with an estimated cost of 11,870,000 Jordanian dinars (about \$34,000,000 U.S.). Approximately 60 percent of this cost was for paving the roads and 40 percent was for the infrastructure services such as sewer systems, water treatment plant, and electricity. The overall length of the road network is about 30 km. Of this, 20 km is primary roads, and 11.5 km is secondary roads, with the rest being service roads used for various purposes.

The special conditions and financial difficulties that Jordan was experiencing caused delays in and postponement of many vital construction projects within the campus. Because of these difficulties, several parts of the road network were not being used, with the result that maintenance was limited to trafficked roads only. Untrafficked roads (exceeding half the total length of the road network), on the other hand, were neglected and not maintained, which caused serious damage to the pavements. These conditions provided an excellent opportunity to fulfill the objectives of this study.

ROAD NETWORK CHARACTERISTICS

Most of the information about the road network at JUST was obtained from the Department of Maintenance and Operation and the Department of Engineering Projects. The compiled information included the master plan of the road network and the materials used in the construction of the pavement layers.

T. I. Al-Suleiman and A. A. Basma, Department of Civil Engineering, University of Science and Technology, Irbid, Jordan. K. Ksaibati, Department of Civil Engineering, University of Wyoming, Laramie, Wyo. 82071.

The average annual rainfall and temperature variation data were also collected.

Pavement Characteristics

The road network at JUST can be divided into three types: primary or main roads, secondary roads, and cycle paths. Figure 1 shows the thickness and materials used in the first two types. As indicated, primary and secondary roads are basically similar, with the exception of the additional 5 cm thickness in the subbase in primary pavements.

Daily Traffic Volume

The traffic volume was obtained by using traffic counters on the main ring road between 7:00 a.m. and 8:00 a.m. (peak hours). The traffic volume was found to range between 30 and 210 vehicles per hour, with most of the vehicles being small passenger cars. This volume was assumed to be half the daily volume because the traffic is not continuous. The reason behind this was that only university employees were allowed to enter the campus by automobile. Consequently, the daily traffic volume was found to range between 60 and 420 vehicles. On the basis of this information, the trafficked roads can

be considered low volume. Accordingly, most of the existing damage to the pavement of the trafficked roads cannot be considered purely traffic related.

Rainfall

Figure 2 shows the average rainfall between 1984 and 1990, with a minimum of 124 mm in 1985 and a maximum of 376 mm in 1988. This range is relatively high when compared with those in other parts of the world. Most of the damage to the pavement (mostly in the form of potholes and cracks) became apparent after 1988 when the rainfall was at its maximum.

Temperature Variation

Figure 3 presents the maximum and minimum monthly ambient temperatures for 1983. It is unfortunate that complete temperature data for other years were not available. From Figure 3 it can be seen that the minimum recorded temperature was 1°C (January) and the maximum was 34°C (July), whereas the maximum monthly temperature variation was 20°C (May). These temperature variations, along with the variation in the amount of rainfall, are believed to be the major causes of pavement distress.

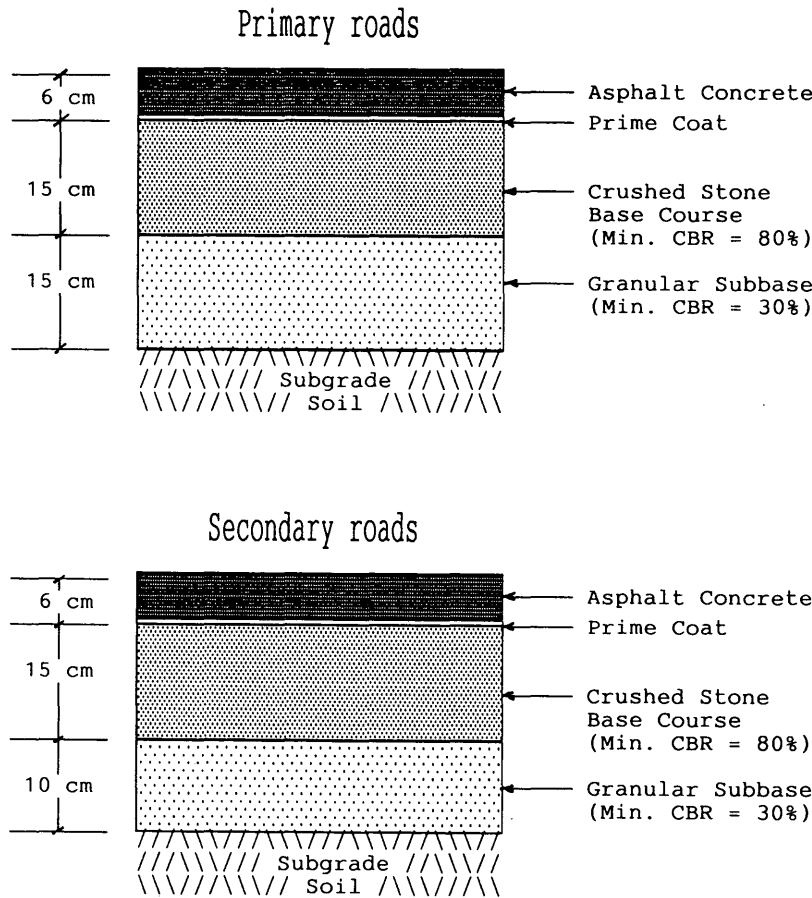


FIGURE 1 Pavement layer thicknesses and materials used in primary and secondary roads.

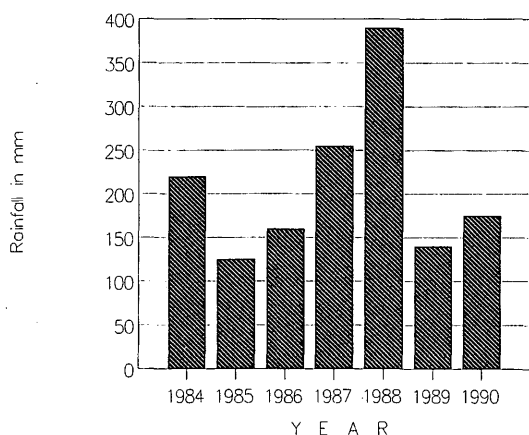


FIGURE 2 Annual rainfall during the period 1984-1990.

SOIL PROPERTIES

The objective of this part of the work was to provide a complete laboratory study of the subgrade soil. The intention of such a study is to provide insight into whether the soil was indeed a contributing factor to the pavement damage. To accomplish this task, soil specimens from two untrafficked pavement sections (about 200 m apart) were extracted and tested. The first section showed severe cracking, whereas the other section showed none. A thorough laboratory investigation was conducted on the soil samples, and the experimental data were compared. The experimental tests consisted of

- Field water content and field unit weight,
- Grain size distribution,
- Consistency limits determination,
- Compaction tests,
- Swell measurements, and
- Collapse measurements.

Table 1 summarizes the experimental results obtained on the soils beneath both the cracked and the uncracked pave-

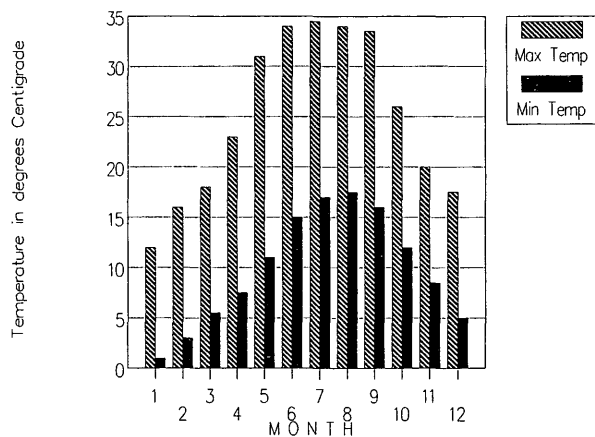


FIGURE 3 Minimum and maximum temperatures during 1983.

ment sections. From these results the following observations were made (see Table 1):

1. Both soils contain low percentages of clay and in general a relatively high percentage of sand.
2. Both soils are low in plasticity; however, the soil under the cracked pavement has a higher activity.
3. The relative compaction of the soil under the cracked pavement was well below the required standards for pavement construction. The usual minimum required degree of compaction is 90 to 95 percent.
4. Both soils have a low potential for expansion.
5. The soil beneath the cracked pavement shows a higher tendency to collapse.

PAVEMENT CONDITION EVALUATION

To determine the pavement condition it was necessary to use a rating technique that is not costly and does not require much instrumentation. For this reason the PAVER method, developed by the U.S. Army Corps of Engineers (5), was adopted. The condition rating used in this method is the pavement condition index (PCI). It is an objective numerical indicator ranging from 0 (failed pavement) to 100 (excellent pavement) on the basis of the measured quantity and severity of each type of distress present in the pavement.

Evaluation Results

The evaluation of the road network entailed both trafficked and untrafficked primary and secondary roads. The entire road network was divided into 18 branches. The branches were further divided into a total of 71 sections, with each section divided into sample units. This resulted in a total of 487 sample units.

The pavement evaluation results revealed that 69 percent of the sections were in excellent condition, 26 percent in very good condition, 4 percent in good condition, and 1 percent in fair condition. In general, therefore, the pavement network at JUST would seem to require only routine maintenance.

Types of Pavement Distresses

The pavement survey showed a wide variation in the density and severity of distresses. The distresses encountered were

- Longitudinal and transverse cracks,
- Alligator cracks,
- Rutting,
- Depressions,
- Potholes,
- Weathering and raveling,
- Polished aggregate,
- Bleeding, and
- Patching.

Figure 4 shows the extent of damage to some of the untrafficked pavement sections. It is important to note that the

TABLE 1 Summary of Subgrade Soil Properties

Property	Cracked Pavement	Uncracked Pavement
Date of sampling	July 8, 1991	July 8, 1991
Depth of sampling, m	0.55	0.60
Field water content, %	5.10	4.90
Field unit weight, kN/m ³	17.17	16.93
Grain size distribution		
Percent Sand (S)	56.0	40.0
Percent Silt (M)	32.0	44.0
Percent Clay (C)	12.0	16.0
Percent Fines (F=M+C)	44.0	60.0
Consistency Limits		
Liquid limit, (LL) %	36.0	36.8
Plastic limit, (PL) %	20.5	25.6
Plasticity index, (PI) %	15.5	11.2
Activity, A = PI/C	1.29	0.70
Compaction		
Optimum water content, %	12.0	16.0
Max. dry unit weight, kN/m ³	19.6	17.3
Relative compaction, %	83.2	93.1
Expansion		
Swell potential [*] , (SP) %	0.41	1.23
Swell pressure [†] , (p _s) kPa	47.0	56.0
Percent Collapse [#] under an applied pressure of		
50 kPa	2.36	1.60
100 kPa	3.40	1.86
200 kPa	5.45	4.61
400 kPa	10.36	8.05
800 kPa	12.47	11.40
1600 kPa	14.43	13.60
Unified soil classification	Sandy-silt (SM)	Low plastic silt (ML)

* Specimen tested at field water content and unit weight

† Values obtained by zero swell test

Values obtained by single odometer collapse test

distresses in most of the untrafficked pavement sections were in the form of longitudinal and transverse cracks. Some of these cracks were 10 m long, 5 cm wide on the surface, and deep enough to reach the subgrade soil (see Figure 4, top).

PREDICTING PAVEMENT CONDITION

Predicting pavement condition aids not only in assessing the pavement service life but also in estimating the cost and the most effective maintenance strategy. It is well recognized that pavement performance is affected by several factors, such as traffic loads, environment, age, initial design, and construction materials. Generally speaking, however, pavement performance is a result of the combined effects of pavement characteristics and the imposed conditions. Hudson and Flan-

agan (4) attempted to estimate separately the relative effects of pure traffic and pure environment and their interaction on pavement performance. However, their study included only 14 pairs of sections (trafficked and untrafficked). They stated that, to solve this problem, one must have access to unused (untrafficked) pavements and "the results will be 5 to 10 years, or longer, in coming." Clearly, the existence of such pavements is very rare. That more than half of the road network at JUST was untrafficked provided an opportunity for such a study.

Description of Methodology

The methodology followed was based on the assumption that pavement distresses after n number of years are a result of three factors:

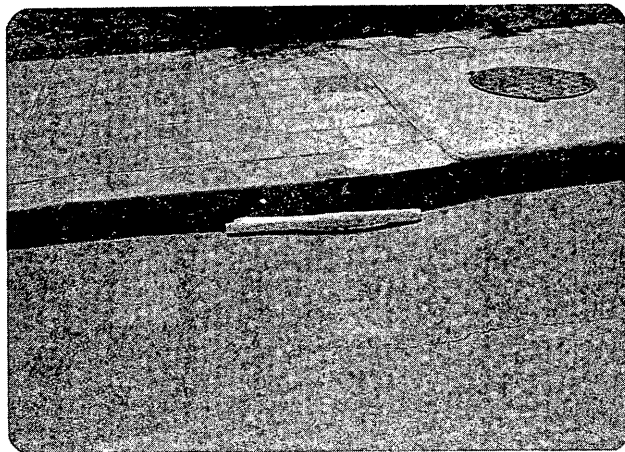


FIGURE 4 Pavement distresses in untrafficked roads: *top*, longitudinal cracking; *bottom*, cracking associated with depression.

1. Environmentally related effects,
2. Traffic-related effects, and
3. Interaction between traffic and environment.

Consequently, pavement deterioration or the change in pavement condition index (ΔPCI) after n years can be mathematically expressed as

$$\Delta PCI = \Delta PCI_e + \Delta PCI_{te} + \Delta PCI_t \tag{1}$$

where

- ΔPCI = total loss in PCI,
- ΔPCI_e = loss in PCI due to environment,
- ΔPCI_t = loss in PCI due to traffic, and
- ΔPCI_{te} = loss in PCI due to the interaction between traffic and environment.

Figure 5 shows a schematic representation of Equation 1. Figure 6 presents the general relationship between pavement age and the loss in PCI under the aforementioned effects. An earlier study (6) indicated that such a relationship can be mathematically expressed as

$$PCI = 100 - a(\text{age})^b \tag{2}$$

or

$$\Delta PCI = 100 - PCI = a(\text{age})^b \tag{3}$$

where PCI is the pavement condition index (0 to 100), ΔPCI is the loss in PCI after age of n years, a is the slope coefficient, and b is the parameter controlling the degree of curvature of performance curve. The values of a and b vary depending on the affecting factors, as indicated in Figure 6.

Application of Methodology

To study the effect of pavement initial design on its performance level, the above-mentioned approach was applied to both primary and secondary roads. Furthermore, to investi-

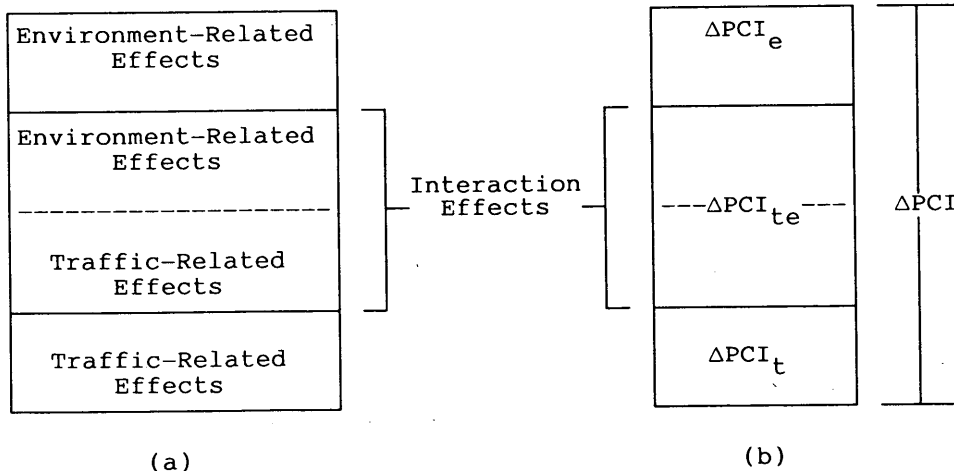


FIGURE 5 Schematic diagram: (a) traffic-related and environmentally related effects; (b) corresponding pavement deterioration.

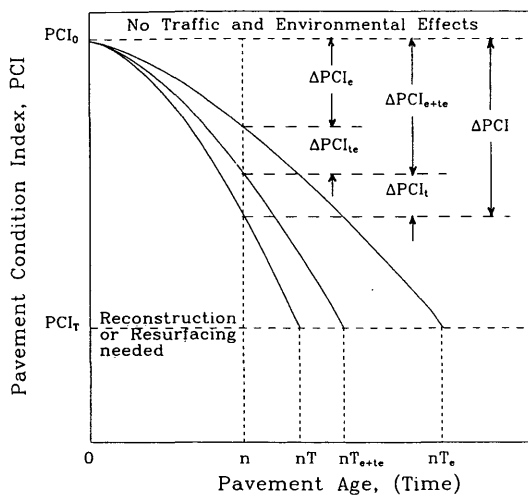


FIGURE 6 Schematic diagram showing pavement conditions over time under traffic-related and environmentally related effects.

gate the effects of traffic and environment and the interaction between them, the road network was divided into five groups on the basis of their service status:

1. Untrafficked primary,
2. Lightly trafficked primary,
3. Untrafficked secondary,
4. Lightly trafficked secondary, and
5. Heavily trafficked secondary.

Table 2 presents the average and standard deviation of PCI (7 years after construction) for each road group. These results show that, for primary untrafficked and lightly trafficked pavement sections, the average loss in PCI was 7.36 and 8.38, respectively. This loss indicates that most of the deterioration in primary roads was caused by environmental factors. Secondary pavements, on the other hand, show similar results for untrafficked and lightly trafficked pavements. However,

in these sections, most of the damage was caused by heavy traffic, resulting in a loss of 13.05 in PCI compared with a loss of 9.65 in PCI caused by the environment. In both cases, though, environmental effects on the condition of the pavement were substantial. To determine the values of *a* and *b* in Equation 2 (or Equation 3) the road groups in Table 2 were monitored periodically for 7 years (1984–1990). The average loss in PCI (Δ PCI) versus age (in years) for the five road groups can be seen in Figure 7. These data are used to estimate the values of *a* and *b* (Table 3); the general form of the equation is that of Equation 3. These values can be used to predict the service life of the pavement, that is, when PCI reaches its terminal value. Columns 3 and 4 of Table 4 show the expected number of years required for PCI to reach 70 and 40, respectively. Between these two values, the pavement might require an overlay or reconstruction. However, because the plots in Figure 7 are for the average values of PCI, the predicted numbers of years to terminal PCI in Table 4 are

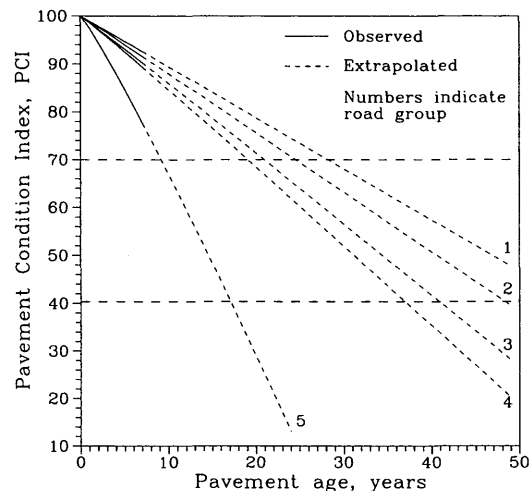


FIGURE 7 Expected pavement service life for each road group.

TABLE 2 Averages and Standard Deviations of PCI for Each Road Group

Road Class	Service Status	Pavement Deterioration	PCI 7 years after construction	
			Average	Standard Deviation
Primary	Non-Trafficked	Δ PCI _e	92.64	7.45
	Light-Trafficked	Δ PCI _e + Δ PCI _{te}	91.62	5.00
Secondary	Non-Trafficked	Δ PCI _e	90.35	1.63
	Light-Trafficked	Δ PCI _e + Δ PCI _{te}	89.43	4.48
	Heavy-Trafficked	Δ PCI _e + Δ PCI _{te} + Δ PCI _t	77.30	11.8

TABLE 3 Values of a and b for Monitored Road Groups

Road Class	Service Status	Road Group	a	b
Primary	Non-Trafficked	1	1.043	1.0054
	Light-Trafficked	2	1.160	1.016
Secondary	Non-Trafficked	3	1.305	1.029
	Light-Trafficked	4	1.405	1.037
	Heavy-Trafficked	5	2.602	1.104

averages. In other words, the average (or expected) number of years to terminal PCI (70) for primary untrafficked roads is 28.3 years. Clearly, this value is not constant and will vary from section to section because PCI of the surveyed sections is a variable (see Table 2). Consequently, the interest here is the predicted range of the pavement service life. This matter is treated in the following section.

VARIATION IN PAVEMENT SERVICE LIFE

Because PCI values vary, the age to reach terminal PCI will vary. To evaluate this variation the first order-second moment Taylor series expansion was used. An explanation of this technique follows.

Consider the following relationship:

$$y = g(x) \quad (4)$$

Expanding this function in a Taylor series about the mean and truncating at the linear term yields

$$\text{Var}[y] = (dy/dx)^2 \text{Var}[x] \quad (5)$$

or

$$\text{SD}[y] = (dy/dx) \text{SD}[x] \quad (6)$$

where $\text{Var}[\cdot]$ and $\text{SD}[\cdot]$ are, respectively, the variance and standard deviations, whereas (dy/dx) is the derivative of y with respect to x evaluated at the mean of x .

Rewriting Equation 3 to become $\text{Age} = g(\Delta\text{PCI})$ and applying Equation 6 gives

$$\text{SD}[\text{age}] = \text{SD}[\Delta\text{PCI}] \left(\frac{1}{ba} \right) \left[\frac{E(\Delta\text{PCI})}{a} \right]^{(1/b)-1} \quad (7)$$

where $E[\cdot]$ is the expected value. The range of the pavement service life can be evaluated as an interval estimate using the following equation:

$$E[\text{age}] = \overline{\text{age}} \pm D \quad (8)$$

where

- $E[\text{age}]$ = expected age
- $\overline{\text{age}}$ = average age (from Equation 3),
- $D = t_{1-\alpha/2,d}(\text{SD}[\text{age}]/N)$,
- $t = t$ - value,
- α = significance level,
- N = number of pavement sections, and
- d = degrees of freedom or $N - 1$.

TABLE 4 Pavement Age to Terminal PCI for Each Road Group

Road Class	Service Status	Pavement Age (years)	
		PCI _T = 70	PCI _T = 40
Primary	Non-Trafficked	$nT_e = 28.3$	56.5
	Light-Trafficked	$nT_{e+te} = 24.6$	48.6
Secondary	Non-Trafficked	$nT_e = 21.0$	41.3
	Light-Trafficked	$nT_{e+te} = 19.1$	37.4
	Heavy-Trafficked	$nT = 9.2$	17.2

TABLE 5 Values of D in Equation 8 for Monitored Roads at Various Significance α -Levels

Road Class	Service Status	Average age, years		Sign. α	D years
		PCI=70	PCI=40		
Primary	Non-Trafficked	28.3	56.5	0.1	13.4
				0.05	16.7
	Light-Trafficked	24.6	48.6	0.1	7.0
				0.05	8.4
Secondary	Non-Trafficked	21.0	41.3	0.1	7.2
				0.05	14.6
	Light-Trafficked	19.1	37.4	0.1	5.0
				0.05	6.3
	Heavy-Trafficked	9.2	17.2	0.1	20.7
				0.05	25.1

The results for Equation 8 are given in Table 5, which shows that lightly trafficked secondary roads have the narrowest range of life expectancy. At $\alpha = 0.1$ and by Equation 8, the time for PCI to reach 40 is between 32.4 and 42.4 years (37.4 ± 5.0). In other words, 90 percent ($1 - \alpha$) of pavements in this group of roads might require overlay or reconstruction between 32.4 and 42.4 years. In untrafficked pavements in the same road class and with the same α -value, the PCI will drop to 40 between 34.1 and 48.5 years. The widest range is observed in heavily trafficked secondary pavements. This result is not surprising because secondary pavements are 5 cm thinner in the subbase than are primary pavements. Consequently, heavy loading will cause a wider variation in PCI (see Table 2), resulting in a wider range of expected life.

SUMMARY AND CONCLUSIONS

The basic objective of this study was to investigate purely environmental effects on pavement condition. The road network at JUST was utilized. Of this road network, more than half of the roads were untrafficked because of construction delays in structures to which these roads lead. A total of 71 primary and secondary pavement sections were considered. These sections were divided into five groups, depending on their class and service status. The sections were surveyed periodically for 7 years to determine the pavement condition index on the basis of this monitoring period, the results of this study warrant the following main conclusions.

1. Most of the deterioration in primary and secondary roads was caused by environmental factors, especially for lightly trafficked pavements.
2. The effect of traffic loading on pavement performance becomes more evident in heavily trafficked roads.

3. Heavily trafficked secondary roads showed the widest range of life expectancy. The narrowest range was observed in secondary lightly trafficked pavements.

It is important to note that this is a continuing study. Most of the untrafficked roads within the JUST campus are expected to remain so for at least the next 10 years. All the sections included in this study will be continuously monitored to further improve the data.

REFERENCES

1. M. Riggins, R. L. Lytton, and A. Garcia-Diaz. Developing Stochastic Flexible Pavement Distress and Serviceability Equations. In *Transportation Research Record 1048*, TRB, National Research Council, Washington, D.C., 1985, pp. 1-7.
2. *Interim Guide for the Design of Pavement Structures*. AASHTO, Washington, D.C., 1986.
3. T. F. Faw and K. C. Sinha. Estimation of Environmental and Traffic Loading Effects on Highway Pavements. *Journal of the Australian Road Research Board*, No. 17, Vol. 4, Dec. 1987, pp. 256-264.
4. W. R. Hudson and P. R. Flanagan. An Examination of Environmental Versus Load Effects on Pavements. In *Transportation Research Record 1121*, TRB, National Research Council, Washington, D.C., 1987, pp. 34-39.
5. M. Y. Shahin and S. D. Kohn. *Pavement Maintenance Management for Roads and Parking Lots*. Technical Report M-294. U.S. Army Corps of Engineers, Oct. 1981.
6. E. A. Sharaf, M. Y. Shahin, and K. C. Sinha. Analysis of the Effects of Differing Pavement Maintenance. In *Transportation Research Record 1205*, TRB, National Research Council, Washington, D.C., 1988, pp. 29-35.

Publication of this paper sponsored by Committee on Flexible Pavement Design.

Use of a Three-Dimensional, Dynamic Finite Element Program for Analysis of Flexible Pavement

SAMEH ZAGHLOUL AND THOMAS WHITE

Predominantly flexible pavement structural response to loads is predicted by using an elastic multilayer analysis. This type of analysis is based on the assumption that pavements are subjected to static loads and that paving and subgrade materials are linear elastic materials. In this paper, ABAQUS, a three-dimensional, dynamic finite element program (3D-DFEM), was used to analyze flexible pavements subjected to moving loads at various speeds. A number of material models were used to represent actual material characteristics such as viscoelasticity and elastoplasticity. The validity and then the application of 3D-DFEM to flexible pavement analysis were examined. Validation was accomplished by analysis of both static and dynamic cases. The static and dynamic verification studies indicated that 3D-DFEM can be used with confidence to predict actual pavement response from moving loads.

A predominantly flexible pavement structural response to loads is predicted by using an elastic multilayer analysis. This type of analysis is based on the assumption that pavements are loaded only statically (1), whereas in reality pavements are subjected to both static and moving loads. Also, this analysis assumes that paving and subgrade materials are linear or piecewise linear elastic materials. However, asphalt mixtures are viscoelastic materials, and clays exhibit plasticity. The inability of multilayer analysis to represent actual loading conditions and pavement materials is significant. This significance is reflected in differences between predicted and measured pavement response. The simplicity and speed of multilayer analysis have been used as justification for the relative results obtained. However, a three-dimensional, dynamic finite element method (3D-DFEM) is available and provides a more realistic analysis for predicting pavement response.

ABAQUS, a three-dimensional, dynamic finite element program (2), has the capability to simulate actual pavement loading conditions. A number of material models can be used to represent material characteristics such as elasticity, viscoelasticity, and plasticity.

The purpose of this paper is to examine the validity and then the application of 3D-DFEM to flexible pavement analysis. Validation was accomplished by analysis of both static and dynamic cases. First, because of industry acceptance, elastic multilayer analysis was used as a basis of comparison for the static case. Static loads were assumed to be applied on a pavement section with linear elastic material properties. The pavement response was predicted using 3D-DFEM and

an elastic multilayer analysis program, Bitumen Structures Analysis in Roads (BISAR) (3). It was found that the results obtained using 3D-DFEM and BISAR are highly correlated. Second, a nonlinear dynamic analysis was conducted of pavements in which actual pavement response had been measured under moving trucks. In a Canadian study (4), pavement response was measured for 14 pavement sections subjected to moving trucks of varying speeds. Selected pavement cross sections from this study were modeled with 3D-DFEM. Loads were applied to the modeled pavement sections at the actual field test speed. The predicted pavement response was found to agree with the measured pavement response. These static and dynamic verification studies showed that 3D-DFEM can be used with confidence to predict actual pavement response from moving loads. Using the 3D-DFEM nonlinear dynamic analysis capabilities, a sensitivity analysis was conducted. Factors ignored by elastic layer analysis were addressed, such as moving loads, system damping, and viscoelastic and plastic behavior of pavement and foundation materials.

FEATURES OF THE FINITE ELEMENT MODEL

Model Geometry

Conventional flexible pavements consist of layers, that is, surface, base, and subbase on a subgrade. At some depth the subgrade can be considered as a deep foundation. The deep foundation may be an extension of the subgrade soil or another soil type. In some cases the subgrade or deep foundation is bedrock.

The finite element mesh (FEM) dimensions have to be small enough to allow detailed analysis of the pavement section. However, small mesh dimensions increase the number of elements. As a result, memory and computational time increase. On the other hand, a coarse FEM will not allow detailed analysis. A compromise is to use a fine FEM for a detailed analysis and a coarse mesh for other analyses. An example of the mesh used in this study is shown in Figure 1. This FEM consists of two equally spaced meshes in the horizontal (xy) plane. A coarse mesh with a 22.2-in. spacing was used in both the transverse (x) and longitudinal (y) directions. In the region of the load path, finer mesh with a 4.44-in. spacing was used in the x -direction. Mesh dimensions in the vertical direction were selected to match the pavement layer thicknesses (i.e., surface, base, and subbase). The number of layers re-

quired to model the subgrade depends on the detail desired in predicting the vertical pavement response. In this study, the surface and base course were each modeled as a single layer, whereas the subgrade was modeled as a set of five layers. The FEM presented in Figure 1 has 5,670 nodes and 5,278 three-dimensional elements. Adhesion between layers was considered a function of friction and normal pressure on the layers (Mohr-Coulomb theory).

Boundary Conditions

Boundary conditions for the finite element model have a significant influence on the predicted response. Therefore, potential boundary conditions for pavements need to be considered.

Edges Parallel to Traffic Direction (Parallel to Y-Axis)

At the pavement edge, two forces exist between the pavement edge and the adjacent soil; vertical friction (*F*) and lateral, passive pressure (*P*). Boundary conditions representing these forces were included in the analysis.

Edges Perpendicular to Traffic Direction (Parallel to X-Direction)

The analysis model should represent adequate length to reduce any edge effect error. However, analysis of an extended

length increases the size of the problem and the analysis time. An evaluation of section length was conducted with lengths ranging from 200 to 1,400 in. For sections longer than 400 in., no significant effect on the pavement response was found. The length of various sections included in this study was 600 in., and the load was applied to the middle 200 in. only.

Pavement-Shoulder Modeling

Three conditions for the degree of continuity at the pavement-shoulder joint were considered:

1. No crack.
2. Narrow crack; pavement and shoulder are in contact with friction.
3. Wide initial crack (1 in.) with possible interaction because of deformation.

Material Properties

It is assumed that paving materials are linear elastic in multilayer analysis. In the 3D-DFEM analysis, paving materials were divided into three groups: asphalt mixtures, granular materials, and cohesive soils. The actual material behavior for each group was considered.

Asphalt mixtures were modeled as viscoelastic materials. This type of material is time and temperature dependent (*I*). The time-dependent properties were represented by instantaneous and long-term shear moduli (*5*). Instantaneous shear modulus was selected at a loading time of 0.1 sec, which is equivalent to a speed of 40 mph. Long-term shear modulus was selected at a loading time of 1.0 sec, which is equivalent to a speed of 1.5 mph. The temperature effect was considered through the shear modulus values. Figure 2a shows the effect of loading time and temperature on asphalt mixture stiffness.

Granular materials, which could consist of base course, subbase, and subgrade in some cases, were modeled using the Drucker-Prager model (*5,6*). This is an elastic-plastic model in which granular materials are assumed to behave as elastic materials for low stress levels. When the stress level reaches a certain yield stress, the material will start to behave as an elastic-plastic material. Figure 2b shows the assumed stress-strain curve for granular materials.

The Cam-Clay model (*5,7-9*) was used for clays. This model uses a strain rate decomposition in which the rate of deformation of the clay is decomposed additively into an elastic and a plastic part. Figure 2c shows the assumed soil response in pure compression.

Other material and layer characteristics required in the analysis include modulus of elasticity, Poisson's ratio, damping coefficient, and bulk density.

LOADING CYCLES

The 3D-DFEM analysis can be used to simulate truck loads moving at highway speeds. A truncated sawtooth load function is used at speeds less than 20 mph, whereas a step load function is used for speeds greater than 20 mph. Figure 3

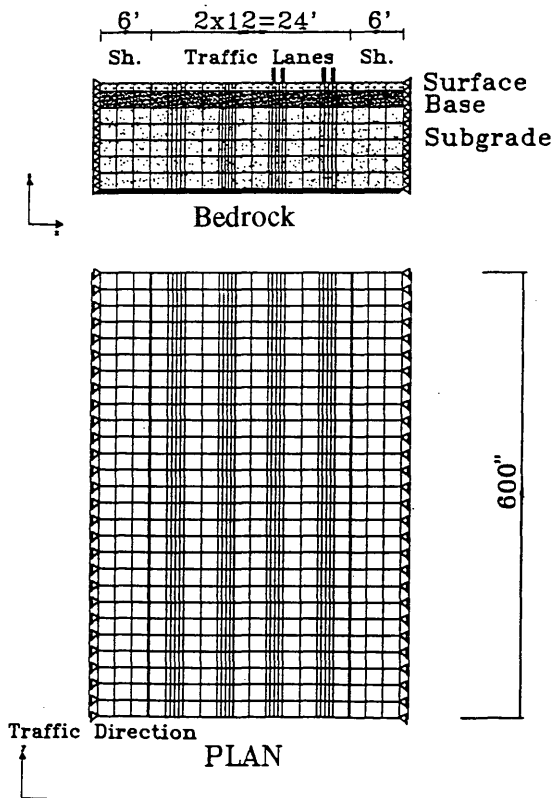


FIGURE 1 Finite element mesh.

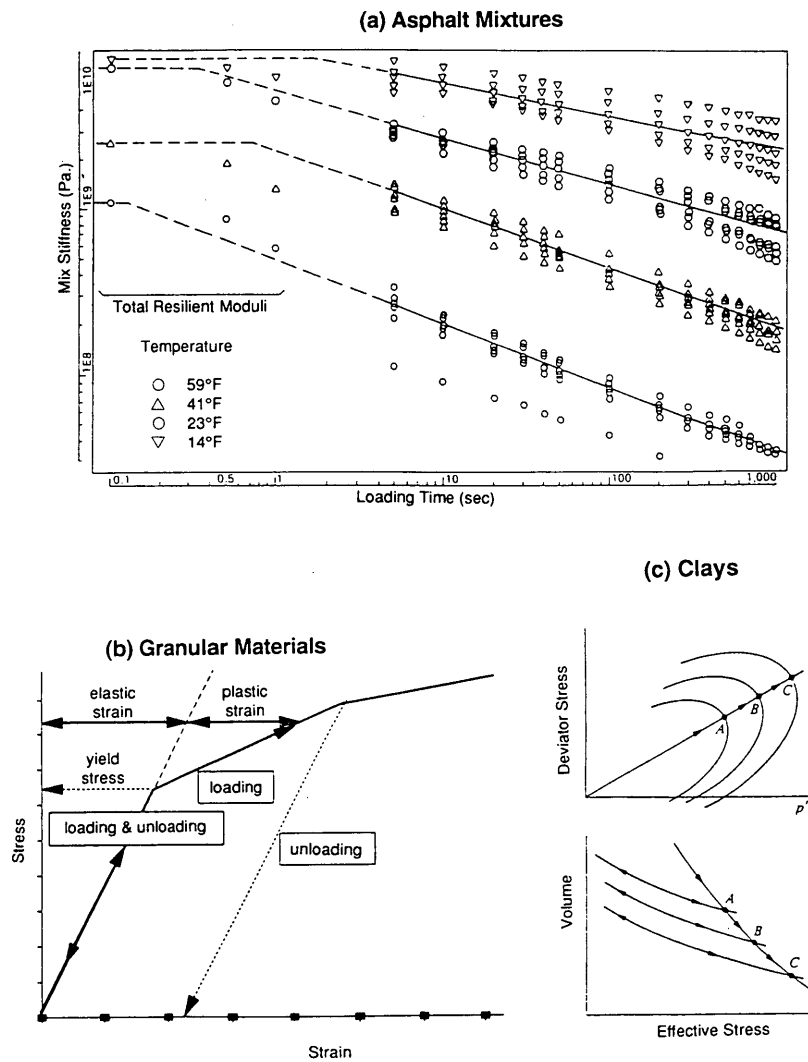


FIGURE 2 Material models.

shows the truncated sawtooth load cycle used in the analysis. The load cycle begins with a load magnitude equal to zero at time T_0 . After time T_0 , the load is increased linearly to a maximum value at time T_1 . The load magnitude remains constant between time T_1 and T_2 . After time T_2 , the load is decreased linearly to zero at time T_3 . The length of time from T_0 to T_1 , T_1 to T_2 , and T_2 to T_3 is a function of speed and the length of the contact area between the truck tire and pavement surface. The length of the contact area or tire print was calculated by assuming the area to be a combination of a central rectangle with semicircles at the ends, as shown in Figure 3 (1).

$$L = \left(\frac{A}{0.5226} \right)^{1/2}$$

where A is the contact area in square inches.

In the step function load cycle $T_0 = T_1$ and $T_2 = T_3$. Load cycle application in the 3D-DFEM analysis considers that no load is applied at a point (n) on a pavement before time T_0 . After T_0 the load cycle is applied at point n and to subsequent points at increments of time equal to the distance between the axles.

Times T_0, \dots, T_3 were calculated as follows:

$$T_i = j \frac{L}{V}$$

where

- L = length of the tire print (in.);
- V = speed (in./sec);
- $i = 0, 1, 2, \text{ and } 3$, respectively; and
- $j = 0.0, 0.3, 0.7, \text{ and } 1.0$, respectively (for $V < 20$ mph) and $0.0, 0.0, 1.0 \text{ and } 1.0$, respectively (for $V > 20$ mph).

In initial studies an 18-kip single axle with dual wheel was assumed.

FINITE ELEMENT MODEL VERIFICATION

Before general application, 3D-DFEM was verified in a two-step process. These two steps included evaluation of its ca-

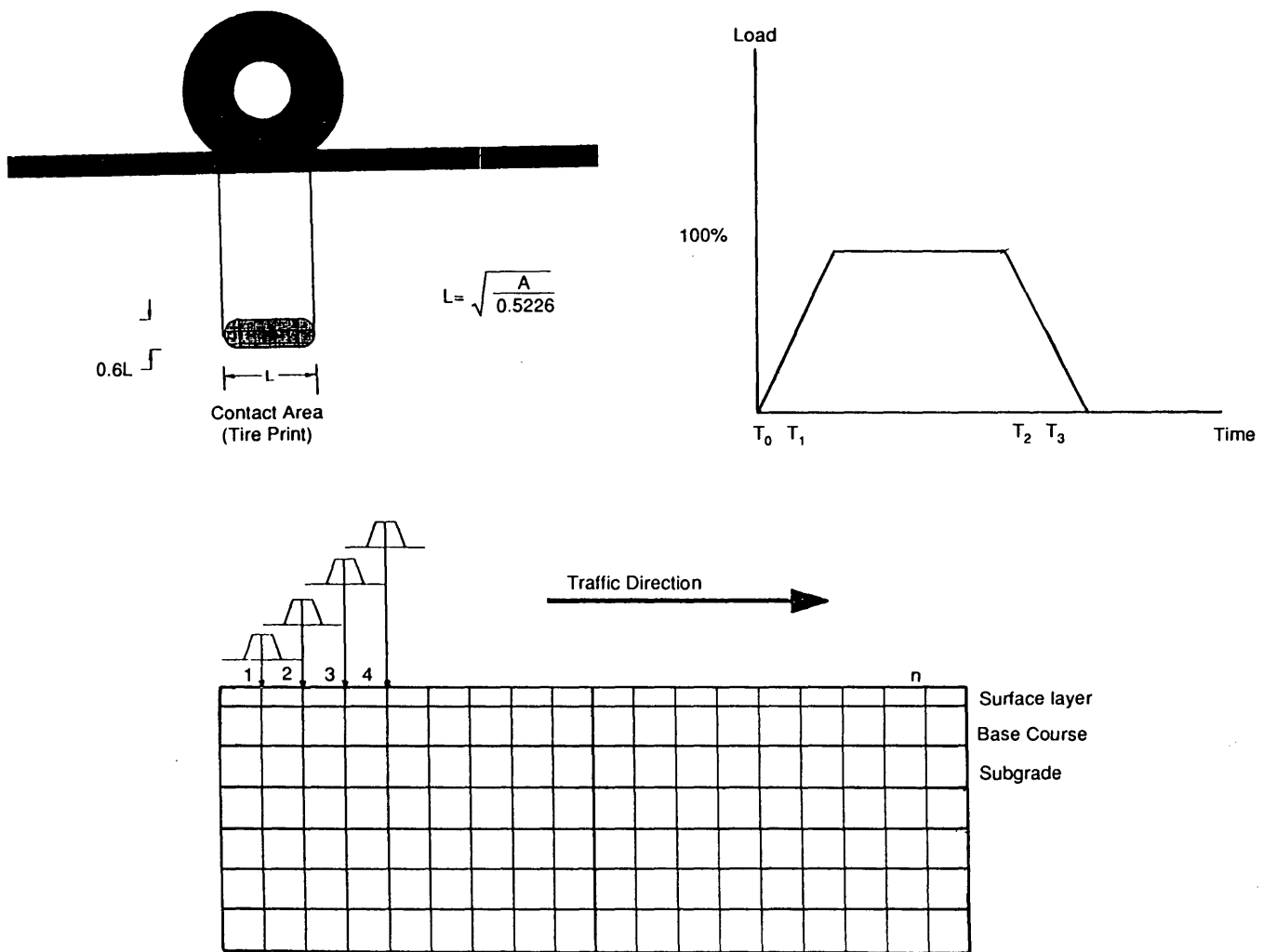


FIGURE 3 Assumed loading cycle.

capabilities to predict pavement response for both static and dynamic cases.

Static Analysis Verification

For the elastic static case, a design of the experiment was developed. Subsequently, analyses of sections with factor combinations satisfying the design of the experiment were conducted with both a layered elastic analysis (BISAR) and the 3D-DFEM analysis. In the latter case elastic material properties were used for the various layers as well as for static loading.

Three factors were included in the design of the experiment:

- Surface layer thickness (T_s) = 4 and 8 in.
- Base course thickness (T_b) = 10 and 20 in.
- Subgrade modulus of elasticity (E_{sg}) = 5,000 and 30,000 psi.

Eight different pavement cross sections were analyzed using the multilayer procedure and 3D-DFEM. Pavement deflec-

tion at various lateral distances (x) as well as at various depths (z) were predicated using BISAR and the 3D-DFEM for the eight pavement cross sections. A regression analysis of the results included three variables, deflection predicted using BISAR (DB), deflection predicted using ABAQUS (DF), and the cross-section number ($PTYPE$). Because the sections analyzed represent significantly different pavement sections, the section number was included in the analysis as a dummy variable. DB was considered the dependent variable, whereas the other two variables, DF and $PTYPE$, and their interaction, $DF*PTYPE$, were considered the independent variables. The interaction term, $DF*PTYPE$, was used to check whether the linear correlation between DB and DF depends on the range of pavement cross sections. From the regression analysis, a high linear correlation between DB and DF was found ($R^2 = 0.96$). Also, both variables DF and $PTYPE$ show a significant effect on DB . The interaction term, $DF*PTYPE$, shows an insignificant effect on DB , which means that this linear correlation is independent of pavement cross section, that is, this relationship can be generalized for the flexible pavement cross sections included in the analysis.

Dynamic Analysis Verification

A study was also conducted to evaluate the time-dependent dynamic analysis feature of 3D-DFEM. Since there is no standard dynamic analysis method for the dynamic case as there is for the static case, a decision was made to compare the predictions with the measured dynamic response of pavements due to moving loads.

A study in Canada (4) involved measuring horizontal tensile strain and surface deflection for asphalt pavements at 14 sites across Canada. Field measurements were made at three nominal speeds—6, 12, and 50 mph—for a number of load levels and load configurations. The structural numbers (SN) were estimated for the 14 sections. A total of 3 of the 14 sections with low, medium, and high values of SN were selected for analysis. These three sections are located in the Provinces of Quebec (Sections 3a and 4) and Alberta (Section 10). A finite element mesh was created for each site to match the pavement cross section given by the CanRoad report (4). Reasonable material properties were assumed for each layer on the basis of the material description given in the CanRoad report (4). Table 1a shows the assumed material properties for the three

sites. For the three selected sites, the surface deflections were predicted for two load levels of 9182 kg and 11 127 kg and for the low (6-mph), and high (50-mph) speeds. Table 1b shows the measured and predicted deflection values for the three sites. An analysis was made to check whether there was a linear correlation between the predicted and measured deflections. As can be seen from Figure 4, the deflections were found to be highly correlated ($R^2 = 99.9$ percent). This high correlation implies that 3D-DFEM can be used to predict the dynamic response of pavements subjected to moving loads.

SENSITIVITY ANALYSIS

After verification of the 3D-DFEM analysis, a sensitivity analysis was conducted to investigate the effect of various factors on pavement response. These factors were divided into two groups:

- Cross-section attributes:
 - Deep foundation type and location,
 - Shoulder width and pavement-shoulder joint, and
 - Asphalt mixture properties.

TABLE 1 Dynamic Analysis Verification

(a) Assumed Material Properties

Material	Layer	Site # 3a	Site # 4	Site # 10
Modulus of Elasticity (ksi)	Surface	200	150	200
G-Ratio		0.75	0.75	0.75
Bulk Density (pcf)		150	150	150
Poisson's Ratio		0.3	0.3	0.3
Modulus of Elasticity (ksi) [^]	Base	50	30	20
Bulk Density (pcf)		140	140	140
Angle of Internal Friction		38	38	38
Cohesion (pcf)		0	0	0
Poisson's Ratio		0.35	0.35	0.35
Modulus of Elasticity (ksi) [^]	Subbase	15	7.5	no subbase
Bulk Density (pcf)		130	130	
Angle of Internal Friction		35	33	
Cohesion (pcf)		0	0	
Poisson's Ratio		0.35	0.35	
Modulus of Elasticity (ksi) [^]	Subgrade	10	3	3
Bulk Density (pcf)		130	125	125
Angle of Internal Friction		35	0	0
Cohesion (pcf)		0	750	750
Poisson's Ratio		0.35	0.4	0.4

[^]Based on $E = 1500^{\circ}$ CBR

(b) Comparison Between Measured and Predicted Pavement Surface Deflections

CanRoad Section Number [^]	Load (kg)	Speed (km/h)	Measured Deflection (mils)	Predicted Deflection (mils)
3A	9,182	6.0	20.91	20.97
3A	9,182	50.0	19.29	20.3
3A	11,127	6.0	19.49	18.1
3A	11,127	50.0	17.91	17.31
10	9,182	6.0	29.88	30.16
10	9,182	50.0	24.8	23.56
10	11,127	6.0	25.2	24.9
10	11,127	50.0	22.0	23.4
4	9,182	6.0	52.0	51.61
4	9,182	50.0	46.81	45.99
4	11,127	6.0	44.8	42.59
4	11,127	50.0	40.5	37.95

[^]See Canroad Report (4).

- Load attributes:
 - Load repetitions and
 - Speed.

Cross-Section Attributes

Effect of Deep Foundation Type

Pavement response is affected by the deep foundation type and condition. An analysis was conducted to investigate the effect of deep foundation type on pavement response predicted by the 3D-DFEM analysis. The pavement section was analyzed with each of the following deep foundations:

1. Shallow bedrock, starts at 64 in. below the pavement surface.
2. Shallow, soft to medium clay layer (cohesion = 500 psf), starts at 64 in. below the pavement surface.

Material and Layer Characteristics

The characteristics of the basic cross section considered earlier and in the subsequent sensitivity study are indicated in Table 2 (5,10-13). The base course and subgrade moduli of elasticity were taken as 1,500 times the California bearing ratio. The asphalt layer properties used in this example are based on the annual average temperature in Indiana (57°F, approximately). These properties are used in the balance of the sensitivity analysis unless noted.

Dependent Variable: MEASURED DEFLECTION

R-Square	C.V.	Root MSE	DM Mean
0.998691	4.054384	1.2284444	30.299167

Parameter	Estimate	T for H0: Parameter=0	Pr > T	Std Error of Estimate
DF	1.020945219	91.60	0.0001	0.01114537

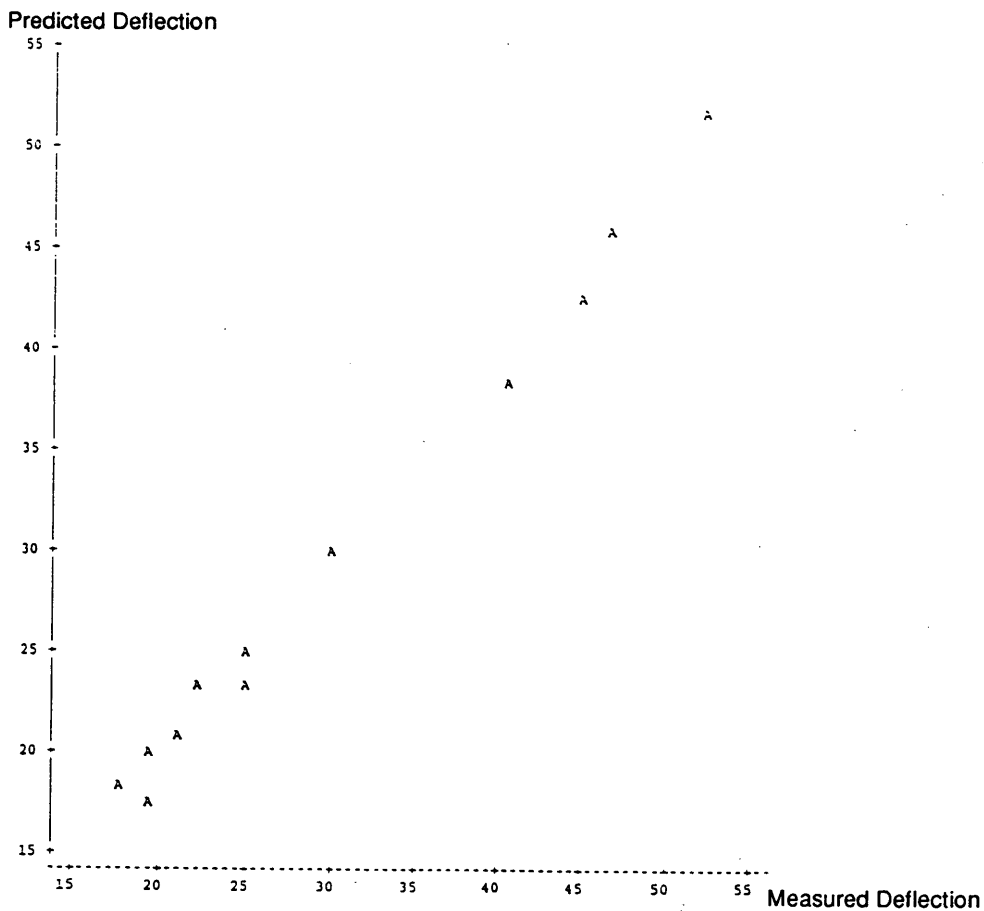


FIGURE 4 Dynamic analysis verification.

TABLE 2 Characteristics of Basic Cross Section

Characteristic	Value
Asphalt concrete surface layer	
Thickness	4 in.
Modulus of elasticity	600,000 psi
Poisson's ratio	0.3
G-ratio	0.8
Damping coefficient	0.05
Bulk density	150 pcf
Granular base course	
Thickness	10 in.
Modulus of elasticity	60,000 psi
Poisson's ratio	0.3
Damping coefficient	0.05
Bulk density	140 pcf
Angle of internal friction	38
Cohesion	0
Sandy subgrade	
Modulus of elasticity	30,000 psi
Poisson's ratio	0.3
Damping coefficient	0.05
Bulk density	125 pcf
Angle of internal friction	30
Cohesion	0

Note: $G\text{-ratio} = 1 - \frac{\text{Long term shear modulus}}{\text{Instantaneous shear modulus}}$

3. Shallow, stiff clay layer (cohesion = 1,000 psf), starts at 64 in. below the pavement surface.
4. Deep bedrock, starts at 164 in. below the pavement surface.

The subgrade above these deep foundations was assumed to be sandy silt subgrade. Load was applied as an 18-kip single-axle load moving at a speed of 1.75 mph. Figure 5 shows the variation in surface deformation with lateral distance (x). The cross section with soft to medium clay foundation showed a higher deflection than that of the other cross sections. Therefore, it is important to consider the deep foundation type in pavement design and evaluation.

Effect of Shoulder Width and Pavement-Shoulder Joint

Shoulders provide lateral support to pavement structures (14). Multilayer elastic analysis cannot be used to examine the questions of shoulder versus no shoulder and degree of disconti-

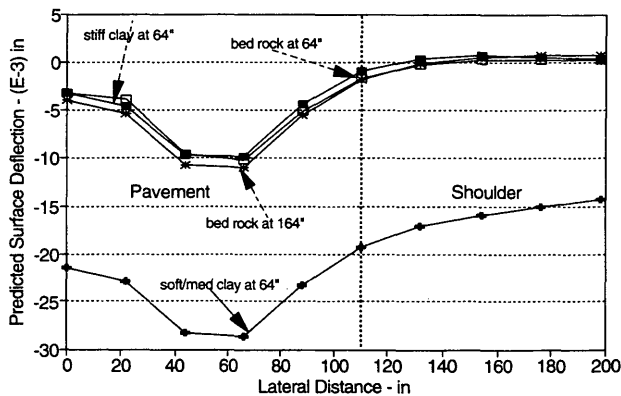


FIGURE 5 Effect of deep foundation type on pavement deflection.

nuity at the pavement-shoulder joint. 3D-DFEM readily accounts for these conditions. An evaluation was conducted for two shoulder conditions. One analysis included a cross section with an 8-ft shoulder. The other analysis was for the condition with no shoulder. The shoulder structure for the 8-ft width was assumed to be the same as the traffic lane of the basic section. Load was applied as an 18-kip single-axle load, 1 ESAL, moving at a speed of 1.75 mph. The outer wheel centerline of this load was positioned approximately 3 ft from the outer edge of the traffic lane. As shown in Figure 6 (top), the surface deflection of the no-shoulder cross section is 33 percent higher than that of the section with the 8-ft shoulder.

Effect of Pavement-Shoulder Joint

To study the effect of pavement-shoulder joint conditions on pavement response, three pavement cross sections were analyzed. The three cross sections assumed 8-ft shoulders with the same structure as the traffic lanes. The first condition analyzed was a wide longitudinal crack extending to the base course. Even with a wide crack there is the possibility of interaction between the pavement and shoulder with significant deflection. Friction will develop with interaction. The second condition analyzed was a narrow crack with friction assumed. The friction force at the pavement and shoulder interface is a function of normal pressure and the coefficient of friction. Complete continuity at the interface was assumed for the third condition. As before, load was applied as an 18-kip single-axle load moving at a speed of 1.75 mph. The centerline of the outer wheelpath was positioned approxi-

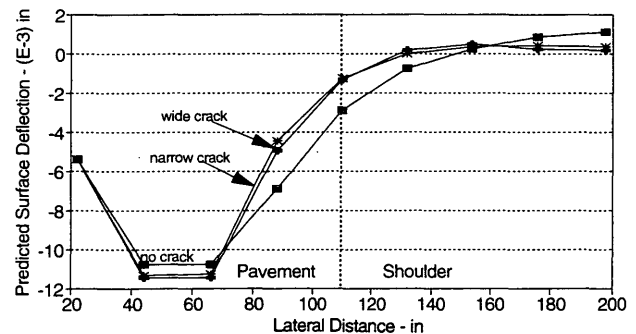
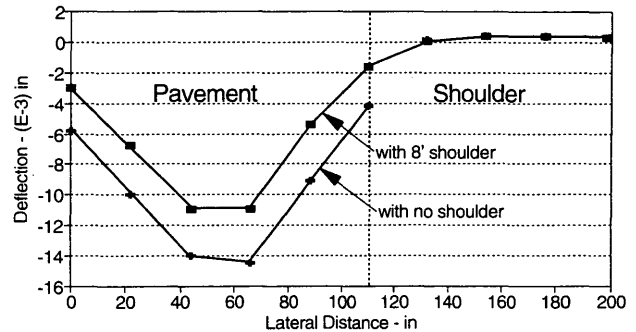


FIGURE 6 Effect of shoulders on pavement response: *top*, effect of shoulder width; *bottom*, effect of pavement-shoulder crack.

mately 3 ft from the pavement-shoulder joint. Deflection basins for the three cross sections are presented in Figure 6 (bottom). A greater deflection occurs as a result of the wide crack. The deflection basin also has a different slope at the crack. In general, the deflection basin shape for the narrow crack is similar to that for the wide crack but with lower maximum deflection. Deflection for the case with no crack is lower than for conditions with cracks. However, because of the moment transfer, the deflection at the shoulder is higher than those of the cross sections with cracks. The difference in maximum surface deflection for the three conditions was found to be small because in all three the shoulder provides lateral support to the pavement. This shows the importance of shoulders, even earth shoulders.

Effect of Asphalt Mixture Properties

The asphalt layer was modeled in this analysis as a viscoelastic material. Elastic as well as viscoelastic properties are required to define asphalt mixtures. Loading time and temperature are two significant parameters for this type of material.

To study the temperature effect on asphalt mixture stiffness and pavement response, two analyses were made of the basic pavement structure. One analysis was made with asphalt layer properties measured at 59°F (approximate annual average temperature in Indiana), whereas the other analysis was made with the asphalt layer properties at 120°F (12,15). The vertical plastic compression strain at the pavement surface for the two analyses is presented in Figure 7, in which it is indicated that as the temperature increases the asphalt mixture becomes less viscous and hence the plastic strain increases.

Load Attributes

Effect of Load Repetitions

3D-DFEM predicts the effects of load repetitions on the pavement plastic and elastic response. When a pavement is subjected to a moving load, a horizontal tensile strain develops at the bottom of the asphalt layer. This strain is associated

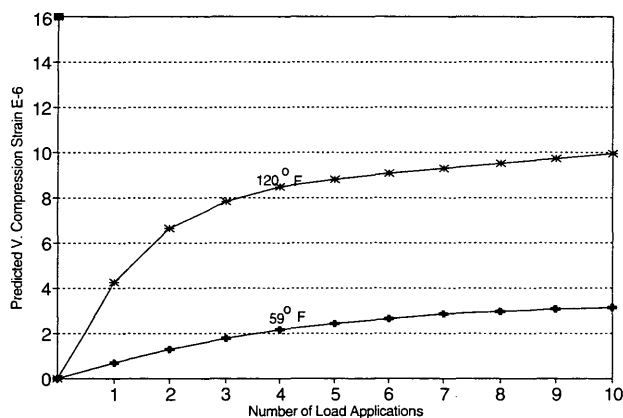


FIGURE 7 Effect of temperature on vertical plastic compression strain.

with fatigue cracking. The horizontal tensile strain has two components—elastic and plastic. The elastic component of this strain is fully recovered after the load is released, whereas the plastic component remains. The basic cross section was analyzed for effect of repetition of an 18-kip single-axle load. Figure 8 shows the effect of these load repetitions on the horizontal tensile strain at the bottom of the asphalt layer, in which it is indicated that, after the first loading cycle, the elastic strain is almost constant. However, the plastic strain accumulates with each loading cycle.

Effect of Moving Load Speed

Previous studies (1b) have shown that static loads are more damaging to pavements than moving loads. A comparison was made of the effect on the pavement response of trucks moving at a creep speed (1.75 mph), a slow speed (10 mph), and a relatively high speed (30 mph). These results are presented in Figure 9, in which it is indicated that the pavement deflection at 10 mph is significantly less than that at 1.75 mph. However, the difference between the pavement deflection at speeds of 10 mph and 30 mph is relatively small. It should be noted that multilayer analysis cannot account for the effect of speed on pavement response.

RUT DEPTH PREDICTION

3D-DFEM has the capability to predict pavement rutting. In this analysis rut depth is defined as the total permanent deformation that accumulates at the pavement surface. This total deformation is the sum of the permanent deformation of various pavement layers, including the subgrade.

Granular subgrades and untreated granular layers can be considered elastoplastic materials. The behavior of these types of material depends on the imposed stress level. When these materials are subjected to stress higher than their yield stress, elastic as well as permanent plastic deformation will occur. The permanent plastic deformation accumulates as pavement rutting.

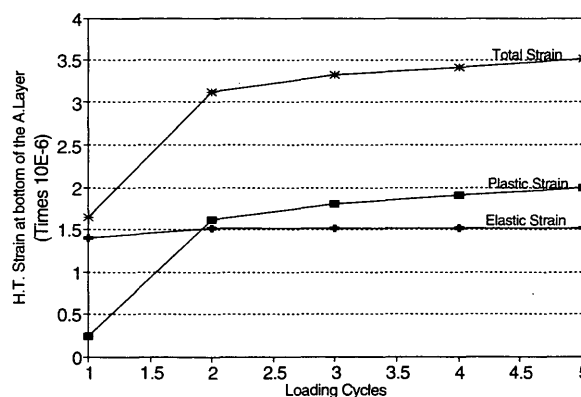


FIGURE 8 Effect of load repetitions on horizontal tensile strain.

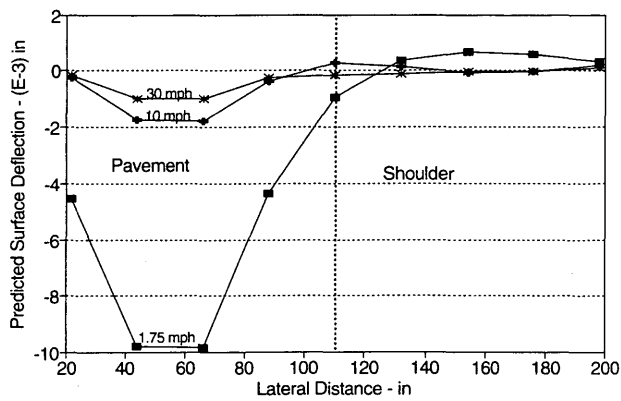


FIGURE 9 Effect of speed on pavement deflection.

Asphalt mixtures are viscoelastic materials. Viscoelastic material response is more complex than that of elastoplastic materials. The behavior depends not only on the stress level, but also on factors such as temperature, rate of loading, and loading time.

Flexible pavement rutting was predicted for two single-axle loads with dual wheels (18-kip and 58-kip). These loads were applied to the basic pavement section at a speed of 1.75 mph. Results are shown in Figure 10. The predicted rut depth of the 58-kip load was found to be approximately 100 times higher than that of the 18-kip load. To show why the 58-kip load caused this severe rutting, the permanent deformation of each layer was plotted for both loads and presented in Figure 11. Permanent deformation for the 18-kip load developed primarily in the asphalt layer, whereas 85 percent of the permanent deformation for the 58-kip axle load developed in the subgrade layer. This occurred because the 58-kip axle load subjected the subgrade to a stress level higher than its yield stress. Permanent deformation in the base course and asphalt surface as a result of the 58-kip axle load was about 10 and 5 percent of the total permanent deformation, respectively. A few passes of such heavy loads can cause considerable pavement rutting.

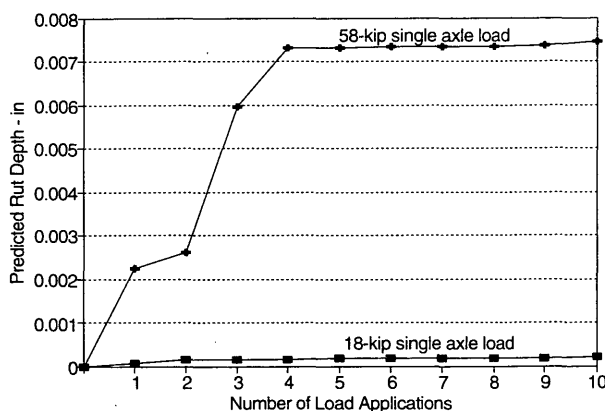


FIGURE 10 Effect of axle loads on pavement rutting.

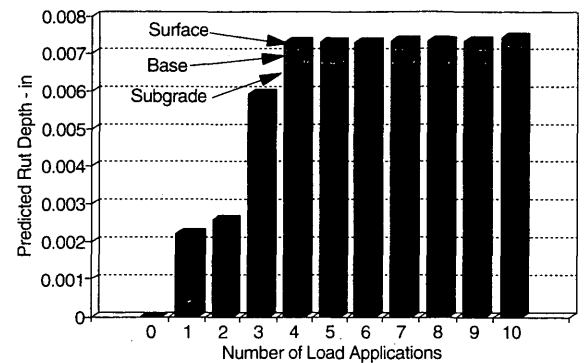
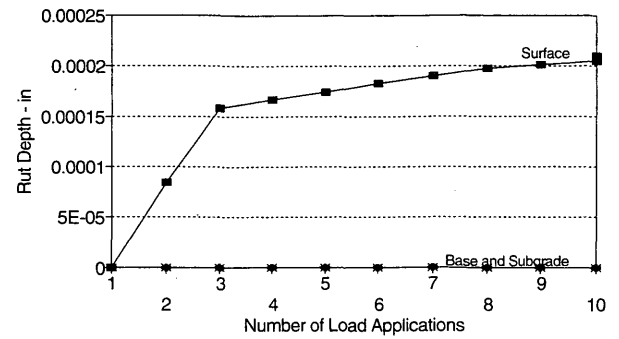


FIGURE 11 Predicted pavement rutting: top, 18-kip single-axle load; bottom, 58-kip single-axle load.

SUMMARY AND CONCLUSIONS

A truck moving over a pavement creates a load pulse that is transmitted through the pavement layers. The magnitude of the load pulse varies with time. The pavement layers respond differently to this load pulse, depending on the material characteristics of each layer. In a multilayer elastic analysis, the load is assumed to be a static load and the materials of different layers, including subgrade, are assumed to be linear elastic materials, even asphalt mixtures. The difference in the multilayer elastic analysis assumptions and the actual loading conditions and material characteristics leads to an inaccurate prediction of pavement response.

In this paper a three-dimensional, dynamic finite element model was used to analyze flexible pavements. 3D-DFEM has the capability to simulate actual truck loads moving at various speeds and can include linear and nonlinear material properties. Three material models were used to model various paving materials and subgrades. The Drucker-Prager model was used to model granular and silty materials, whereas the Cam-Clay model was used for clayey soils. Asphalt mixtures were modeled as viscoelastic materials. 3D-DFEM has the capability to predict both elastic and plastic pavement response. This capability helps to predict and explain pavement response under various loading conditions and for different material characteristics.

3D-DFEM was verified by comparing its predictions with a multilayer elastic analysis, assuming static loads and linear elastic material properties. A high linear correlation was found between the results obtained by 3D-DFEM and those obtained by the multilayer elastic analysis. To verify the dynamic, non-

linear analysis capabilities of 3D-DFEM, the 3D-DFEM predictions were compared with actual pavement deflection measurements. It was found that with a 99 percent confidence level, there is no difference between the predicted and measured deflections.

A sensitivity analysis was conducted using 3D-DFEM to study the effect of cross-section parameters and load parameters on pavement response. It was found that the moving load speed has a significant effect on elastic and plastic pavement response. The confinement effect of shoulders and degree of continuity at the pavement-shoulder joint were found to reduce pavement deflection. Temperature, loading time, and rate of loading were found to have a significant effect on pavement response. Loads that generate stresses higher than yield stresses will increase rutting significantly.

The effect of various load attributes, axle load and spacing, number of axles and number of wheels, as well as cross-section attributes, subgrade type, various material properties, and deep foundation type, was investigated and found to be significant to pavement response.

ACKNOWLEDGMENT

The research presented in this paper is part of a study sponsored by the Indiana Department of Transportation and FHWA.

REFERENCES

1. E. J. Yoder and M. W. Witzczak. *Principles of Pavement Design*, 2nd ed., John Wiley and Sons, Inc., New York, 1975.
2. ABAQUS, Finite Element Computer Program. Version 4.9. Hibbitt, Karlsson and Sorensen, Inc., 1989.
3. *Bitumen Structures Analysis in Roads (BISAR)*, Computer Program. Koninlilijke/Shell-Laboratorium, Amsterdam, July 1972.
4. *Vehicle Weight and Dimension Study*. Canroad Transportation Research Corporation, Ottawa, Canada, 1986.
5. ABAQUS, Finite Element Computer Program. Theory Manual, Version 4.9. Hibbitt, Karlsson and Sorensen, Inc., 1989.
6. D. C. Drucker and W. Prager. Soil Mechanics and Plastic Analysis or Limit Design. *Quarterly of Applied Mathematics*, Vol. 10, 1952, pp. 157-165.
7. A. Schofield and C. P. Worth. *Critical State Soil Mechanics*. McGraw Hill, New York, 1968.
8. R. H. Parry, ed. *Stress-Strain Behavior of Soils*. G. T. Foulis and Co., Henley, England, 1972.
9. D. Wood. *Soil Behaviour and Critical State Soil Mechanics*. Cambridge University Press, Cambridge, England, 1990.
10. K. P. George. Resilient Testing of Soils Using Gyrotory Testing Machine. In *Transportation Research Record 1369*, TRB, National Research Council, Washington, D.C., 1992.
11. D. Kim and K. H. Stokoe. Characterization of Resilient Modulus of Compacted Subgrade Soils Using Resonant Column and Torsional Shear Test. In *Transportation Research Record 1369*, TRB, National Research Council, Washington, D.C., 1992.
12. R. Roque, M. Tia, and B. E. Ruth. Asphalt Rheology to Define the Properties of Asphalt Concrete Mixtures and the Performance of Pavements. In *Asphalt Rheology: Relationship to Mixture*. (O. E. Briscoe, ed.), ASTM STP 941, ASTM, Philadelphia, 1987, pp. 3-27.
13. K. Derucher and G. Korfiatis. *Materials for Civil and Highway Engineers*, 2nd ed. Prentice Hall, Englewood, N.J., 1988.
14. *A Policy on Geometric Design of Highway and Streets*. AASHTO, Washington, D.C., 1990.
15. *Presentation at Peer Review No. 2*, Atlantic City, N.J., Battelle Resource International, June 1991.
16. A. Papagiannakis, R. Hass, J. Woodrooffe, and P. Leblanc. *Impact of Roughness-Induced Dynamic Load on Flexible Pavement Performance*. ASTM STP 1031, ASTM, Philadelphia, 1990, pp. 383-397.

Publication of this paper sponsored by Committee on Flexible Pavement Design.

Estimation of Axle Loads of Heavy Vehicles for Pavement Studies

T. F. FWA, B. W. ANG, H. S. TOH, AND T. N. GOH

A statistical approach was used to characterize axle loads of heavy vehicles for use in highway pavement design and performance analysis. On the basis of actual axle loads of 12,638 vehicles measured on Singapore roads, the characteristics of variations of vehicle gross weights and axle loads were investigated. Vehicles were grouped into various classes according to their axle configurations. Weibull functions were used to model distributions of vehicle weights by vehicle class. Various models of axle load distributions were examined, and it was found that a second-order polynomial regression model offered the best estimates of axle loads. On the basis of the analysis of the axle load data, there is a need to conduct axle load studies to provide reliable estimates of traffic loading for effective management of the existing road network and the economical design of new pavements.

It is generally accepted that structural damage of road pavements caused by traffic is mainly a result of the axle loads imposed by trucks. This observation is clearly reflected in the equivalent traffic load computations used by pavement researchers and highway agencies in pavement design and pavement performance analysis (1-4). For example, in terms of the AASHTO equivalent single-axle load (ESAL) (5), one tractor-semitrailer combination is equivalent to about 2.0 ESALs, one bus to about 0.39 ESAL, and one passenger car to only 0.0004 ESAL.

In view of the importance of heavy vehicles in traffic load computation for pavement design and analysis, studies have been conducted by many highway agencies to quantify the axle load distributions of these vehicles (6-8). This paper is a report of a recent study in Singapore to characterize the axle loads of heavy vehicles for use in pavement design and performance analysis. Currently local highway agencies apply conversion factors obtained from design practice in the United Kingdom (9) and the United States (2) to compute equivalent standard axle loads. This study was undertaken with the aim of providing an improved analytical tool to quantify traffic loadings for pavement studies.

METHODOLOGY

A common practice in characterizing heavy vehicle loadings is to determine the ESAL (sometimes also known as the truck factor) for each vehicle type (2,9,10). Another method of characterization is by calculating axle load distributions. The first method provides a speedy means of computing the total design ESAL from traffic volume data. However, by not pre-

senting the axle load distributions used to derive the ESAL, the first method is not usable for more elaborate analysis of traffic loading effects on pavements. For example, the load equivalency factors used for computing the ESAL vary with the type and design of the pavement. In addition, there exist pavement distresses that cannot be explained by ESAL alone (4,11). Axle load data are also required for the design of concrete pavements and for the selection of appropriate design loads for highway bridges (12,13). Knowing axle load distributions also allows engineers to have a better understanding of the loading patterns produced by heavy vehicles and the relative damaging effect of various axles. This study therefore characterizes vehicle loading of various vehicle types by axle load distributions.

The main steps involved in the traffic loading characterization procedure adopted in this study are shown in Figure 1. Vehicle weight modeling and axle load modeling were the two key elements in the procedure. A vehicle weight distribution model was developed for each vehicle class, and an axle load distribution model was proposed for each axle of a vehicle class. Statistical techniques were employed to formulate both the vehicle weight and the axle load distribution models.

Weigh-in-motion equipment was used to measure axle weights as vehicles passed instrumented sites at normal traveling speeds. The equipment had piezoelectric weight sensors and a loop vehicle detector, enabling it to record axle weights as well as axle spacings for vehicle classification purposes. The accuracy of the weigh-in-motion measurements was checked against axle weight measured by static weighbridges at selected sites: these values were found to be within 15 percent of the static weights 95 percent of the time.

CLASSIFICATION OF VEHICLE TYPES

The data recorded by the weigh-in-motion equipment were classified into nine classes according to the number of axles, as shown in Table 1. This system was similar to the classification scheme adopted by the vehicle registration authority of Singapore. Because the loading impact of the first three classes is small compared with that of the heavier vehicles in the other classes, the present study focused on vehicles classified under Classes 4 through 9. The total number of these heavy vehicles recorded at 45 sites was 12,638. An initial attempt to formulate axle load models based on the above classification, however, did not produce satisfactory results for some of the classes. Further, subclassifications were found necessary.

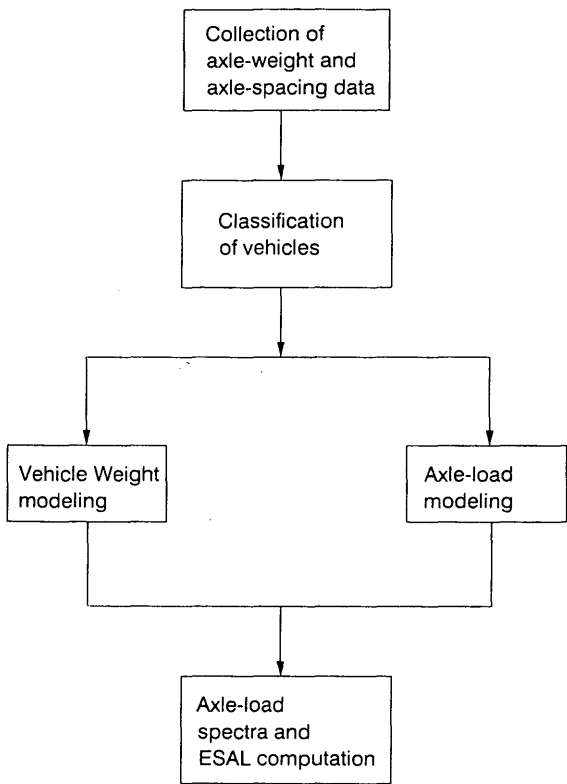


FIGURE 1 Traffic loading characterization procedure.

The classification system in Table 1 was made on the basis of the number of axles alone. On the basis of the reasoning that the spacings between axles and the relative positions of axles would also affect the distribution of loads among axles, a refinement to the classification system in Table 1 was made by considering the detailed pattern of axle arrangement. In addition, a distinction between single, tandem, and tridem axles was also made. Following the definition by AASHTO (5), a tandem axle consists of two axles that are positioned within a distance of 101.6 cm (40 in.) and 243.8 cm (96 in.), and a tridem axle consists of a group of three axles

that are positioned within the same distance. The revised classification system is presented in Table 2 in which the ranges of axle spacing between all adjacent axles are indicated. Classes 4, 8, and 9 were each broken into two subclasses.

The two subclasses of buses in Class 4 were the short wheelbase type, for which the spacing between the front and rear axles is less than 610 cm (20 ft), and the long wheelbase type for which the axle spacing is greater than 610 cm (20 ft). The two subclasses of Class 8 vehicles were also differentiated on the basis of wheelbase length. Class 8A vehicles were used for carrying 20-ft (6.1-m) containers, and Class 8B vehicles were used for carrying 40-ft (12.2-m) containers. The two subclasses of Class 9 represented vehicles with different axle configurations. Subclass 9A had two single front axles and a rear tridem axle, whereas Subclass 9B had a single front axle followed by two rear tandem axles.

DEVELOPMENT OF VEHICLE WEIGHT DISTRIBUTION MODELS

The gross operating weight of a heavy vehicle, whether it is a bus or a truck, is a function of the number of passengers and the amount and type of goods it carries. The loads carried, which may be considered to be randomly distributed, may vary from a minimum value equal to or close to zero to the full capacity of the vehicle. However, because of the constantly present dead weight of the vehicle, the vehicle weight distribution tends to be skewed to the higher load range (i.e., having a longer tail on the heavy load end) as illustrated in Figure 2a. Another form of vehicle weight distribution with two peaks, as shown in Figure 2b, was also found in the recorded data. The Weibull distribution function (14) has the ability to describe the trends of vehicle weight variation shown in Figure 2, and was thus used in the present study to model the weight distribution in each vehicle class. The density distribution of the Weibull function is given by










$$f(W) = ab(W - c)^{b-1}e^{-a(W-c)^b} \tag{1}$$

where *a*, *b*, and *c* are constants that define the shape of the

TABLE 1 Vehicle Classification by Number of Axles

VEHICLE CLASS	VEHICLE TYPE	NUMBER OF AXLES
1	motorcycles	-
2	passenger cars	2
3	pickups, vans	2
4	buses	2
5	single unit trucks	2
6	single unit trucks	3
7	tractor-trailer combination trucks	3
8	tractor-trailer combination trucks	4
9	tractor-trailer combination trucks	5 or more

TABLE 2 Vehicle Classification for Present Study

VEHICLE CLASS	VEHICLE TYPE	AXLE SPACING(m)	VEHICLE CONFIGURATION
4A	2 AXLE BUSES (long wheelbase)	5.5-6.1	
4B	2 AXLE BUSES (short wheelbase)	6.1-7.0	
5	2 AXLE TRUCKS SINGLE UNIT	4.0-6.0	
6	3 AXLE TRUCKS SINGLE UNIT	3.0-5.0 ⁽¹⁾	
7	3 AXLE TRUCKS TRACTOR-TRAILER COMBINATION	6.0-7.0 ⁽²⁾	
8A	4 AXLE TRUCKS TRACTOR-TRAILER COMBINATION	3.0-6.0 ⁽³⁾	
8B	4 AXLE TRUCKS TRACTOR-TRAILER COMBINATION	8.5-10.0 ⁽³⁾	
9A	5 AXLE TRUCKS TRACTOR-TRAILER COMBINATION	7.5-11.0 ⁽⁴⁾	
9B	5 AXLE TRUCKS TRACTOR-TRAILER COMBINATION	7.5-9.0 ⁽⁴⁾	

Note: (1) Spacing between front single axle and rear tandem axle
 (2) Spacing between middle single axle and rear single axle
 (3) Spacing between middle single axle and rear tandem axle
 (4) Spacing between middle single (or tandem) axle and rear tridem (or tandem) axle

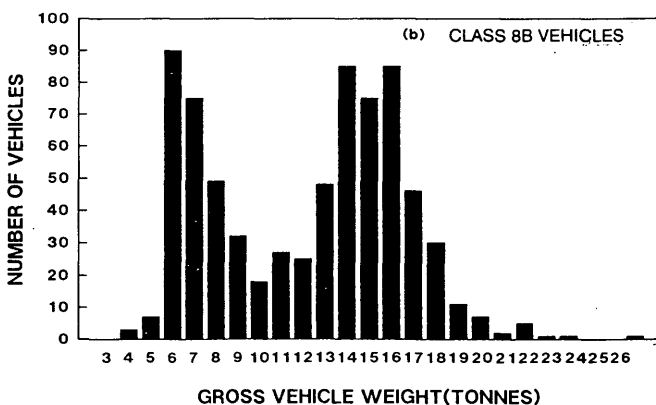
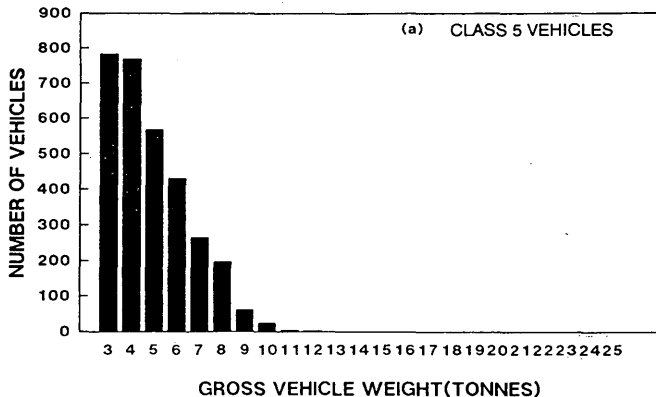


FIGURE 2 Examples of vehicle weight distribution.

distribution and W is the gross vehicle weight of individual vehicles. The corresponding Weibull cumulative function is

$$F(W) = 1 - \exp[-a(W - c)^b] \quad (2)$$

Vehicle Weight Distribution Models

A vehicle weight distribution model for each vehicle class was developed for this study. Together with axle load distribution models, the ESAL contribution from various vehicle classes could be calculated. For each vehicle class, the Weibull cumulative function of Equation 2 was used for the purpose of model calibration. The Weibull constants a , b , and c were obtained by the following steps: (a) extract vehicle weight data for all vehicles in the vehicle class of interest from field survey records; (b) arrange vehicle weight data in increasing order; (c) construct cumulative vehicle weight distribution from Item b; and (d) determine constants a , b , and c by fitting Equation 2 to the cumulative distribution of Item c using the method of least squares.

Table 3 gives all the vehicle weight distribution models derived for the various vehicle classes. For distributions with two peaks, it was necessary to fit the data using two Weibull functions. This happened for vehicle Classes 6, 7, 8A, and 8B. The goodness of fit of the models was examined by the Kolmogorov-Smirnov test (14). As shown in the last column of Table 3, all tests accepted the Weibull distribution at the 99 percent confidence level. Figure 3 shows examples of the cumulative distribution plots of actual vehicle weight data and predicted weight values.

DEVELOPMENT OF AXLE LOAD MODELS

Two methods for specifying the axle load distribution of a vehicle were examined in the study. One expresses axle load distribution in terms of percentages of gross vehicle weight; the other estimates the individual axle loads directly. Both methods of representing axle load distribution are examined in this section.

Variables in Axle Load Models

Statistical regression techniques were adopted for developing the axle load prediction models. The analyses involved identification of parameters that affect the load transmitted to each axle and the determination of statistically significant mathematical forms that could predict axle load distribution satisfactorily.

Assuming the body of a vehicle to be rigid, the parameters that affect the magnitude of load carried by each axle of the vehicle include the following: (a) axle configuration of the vehicle, including the number of axles, type of axle, and arrangement of the axles; (b) dead weight of the vehicle and its center of gravity; and (c) the weight of goods and passengers carried by the vehicle and their distributions along the length of the vehicle. Theoretically it might be possible to develop an overall axle load model having the three forms of parameters identified above as the independent variables. This

TABLE 3 Vehicle Weight Distribution Models

VEHICLE CLASS	WEIBULL CUMULATIVE DISTRIBUTION MODEL	WEIBULL DENSITY DISTRIBUTION MODEL
4A	$1 - \text{EXP}(-0.2481 * (W-4)^{2.4819})$	$0.6158 * (W-4)^{1.4819} * \text{EXP}(-0.2481 * (W-4)^{2.4819})$
4B	$1 - \text{EXP}(-0.0610 * (W-3.3)^{3.0962})$	$0.1889 * (W-3.3)^{2.0962} * \text{EXP}(-0.0610 * (W-3.3)^{3.0962})$
5	$1 - \text{EXP}(-0.1574 * (W-1.5)^{1.5971})$	$0.2514 * (W-1.5)^{0.5971} * \text{EXP}(-0.1574 * (W-1.5)^{1.5971})$
6	$0.1413(1 - \text{EXP}(-0.0774 * (W-3)^{3.8214}))$ + $0.8587(1 - \text{EXP}(-4.6E-5 * (W-3)^{5.0824}))$	$0.1413(0.2958 * (W-3)^{2.8214} * \text{EXP}(-0.0774 * (W-3)^{3.8214}))$ + $0.8587(2.338E-4 * (W-3)^{4.0824} * \text{EXP}(-4.6E-5 * (W-3)^{5.0824}))$
7	$0.3891(1 - \text{EXP}(-0.1132 * (W-3)^{2.8656}))$ + $0.6181(1 - \text{EXP}(-6.3E-5 * (W-3)^{4.5790}))$	$0.3819(0.6244 * (W-3)^{1.8656} * \text{EXP}(-0.1132 * (W-3)^{2.8656}))$ + $0.6181(5.436E-6 * (W-3)^{3.5790} * \text{EXP}(-6.3E-5 * (W-3)^{4.5790}))$
8A	$0.5227(1 - \text{EXP}(-0.0363 * (W-3)^{2.3399}))$ + $0.4773(1 - \text{EXP}(-9.8E-8 * (W-3)^{6.7198}))$	$0.5227(0.0849 * (W-3)^{1.3399} * \text{EXP}(-0.0363 * (W-3)^{2.3399}))$ + $0.4773(6.585E-7 * (W-3)^{5.7198} * \text{EXP}(-9.8E-8 * (W-3)^{6.7198}))$
8B	$0.3379(1 - \text{EXP}(-0.0103 * (W-3)^{3.4652}))$ + $0.6621(1 - \text{EXP}(-9.8E-7 * (W-3)^{5.5470}))$	$0.3379(0.0357 * (W-3)^{2.4652} * \text{EXP}(-0.0103 * (W-3)^{3.4652}))$ + $0.6621(5.436E-6 * (W-3)^{4.5470} * \text{EXP}(-9.8E-7 * (W-3)^{5.5470}))$
9A	$1 - \text{EXP}(-0.0487 * (W-4.5)^{1.4268})$	$0.0695 * (W-4.5)^{0.4268} * \text{EXP}(-0.0487 * (W-4.5)^{1.4268})$
9B	$1 - \text{EXP}(-0.0099 * (W-4.5)^{2.4489})$	$0.0242 * (W-4.5)^{1.4489} * \text{EXP}(-0.0099 * (W-4.5)^{2.4489})$

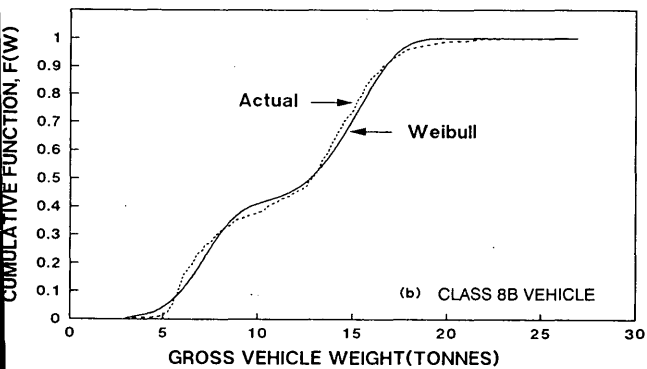
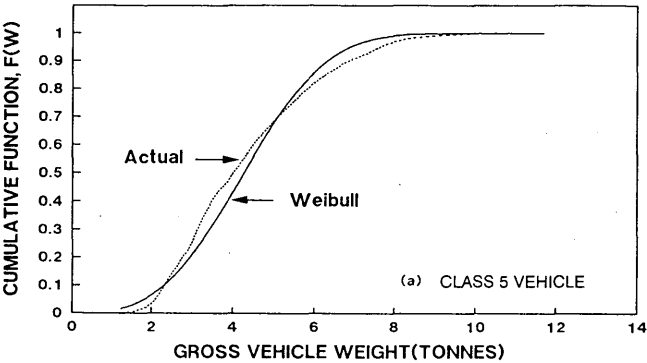


FIGURE 3 Examples of cumulative distribution of vehicle weights.

is, however, impractical for pavement studies because it would not be easy to obtain all the information required to use the model. This problem can be overcome by choosing to develop separate models for individual vehicle classes, such as those in Table 2, and using the total vehicle weight as the independent variable.

After a preliminary analysis that examined various forms of mathematical models, two forms of models were found to produce satisfactory results. One was the polynomial regression model; the other was a nonlinear model that expressed the magnitude of an axle load as a function of a power term of gross vehicle weight.

Polynomial Regression Models

The polynomial regression models take the following form:

L-model:

$$L = a_0 + a_1W + a_2W^2 + \dots + a_nW^n + \epsilon_a \tag{3}$$

P-model:

$$P = b_0 + b_1W + b_2W^2 + \dots + b_nW^n + \epsilon_b \tag{4}$$

where *L* is the magnitude of an axle load, *P* is the percentage share of the axle load expressed as a percentage of gross vehicle weight *W*, subscripted coefficients *a* and *b* are regression constants, and ϵ_a and ϵ_b are error terms. Statistical analyses showed that all the *L*-models, but not all the *P*-models, were statistically significant at the 99 percent confidence level. Figure 4a shows that the coefficients of multiple determination

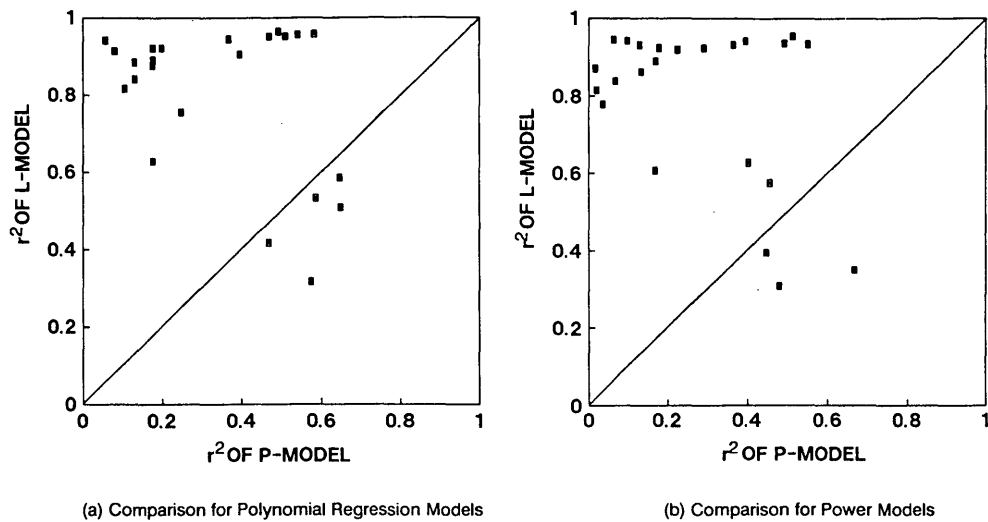


FIGURE 4 Comparison of *L*- and *P*-models for axle loads.

(r^2) of the *L*-models were much higher than the r^2 of the corresponding *P*-models. It is apparent that the *L*-models were superior to the *P*-models in their ability to estimate axle loads.

Table 4 presents the *L*-models with those terms that are statistically significant at the 99 percent confidence level. In

the case of Classes 4A and 4B, instead of identifying their two axles as front and rear axles, it was found that better axle load models could be developed by differentiating the two axles as heavy (HMAX) and light (HMIN) axles. This procedure was effective in accounting for the two different bus designs commonly found in Singapore—some with engines

TABLE 4 Polynomial Regression Models for Axle Loads

VEHICLE CLASS	POLYNOMIAL FUNCTION	r^2	PROB. > F
4A	HMAX = $0.3851 + 0.6284*W - 0.0049*W^2$	0.9216	0.0001
	HMIN = $-0.3851 + 0.3716*W + 0.0049*W^2$	0.8904	0.0001
4B	HMAX = $0.9208 + 0.2037*W + 0.0295*W^2$	0.8850	0.0001
	HMIN = $-0.9208 + 0.7963*W - 0.0294*W^2$	0.8410	0.0001
5	X1 = $0.7262 + 0.1707*W + 0.0159*W^2$	0.6293	0.0001
	X2 = $-0.7264 + 0.8292*W - 0.0159*W^2$	0.8759	0.0001
6	X1 = $1.9279 - 0.0053*W + 0.0090*W^2$	0.4177	0.0001
	X23 = $-1.9280 + 1.0053*W - 0.0090*W^2$	0.9514	0.0001
7	X1 = $2.1481 - 0.1918*W + 0.0157*W^2$	0.5852	0.0001
	X2 = $-0.9945 + 0.6510*W - 0.0135*W^2$	0.9419	0.0001
	X3 = $-1.1536 + 0.5408*W - 0.0021*W^2$	0.9572	0.0001
8A	X1 = $0.6488 + 0.2783*W - 0.0084*W^2$	0.5092	0.0001
	X2 = $-0.0496 + 0.2845*W + 0.0015*W^2$	0.9271	0.0001
	X34 = $-0.5991 + 0.4373*W + 0.0069*W^2$	0.9635	0.0001
8B	X1 = $1.2051 + 0.1375*W - 0.0013*W^2$	0.5326	0.0001
	X2 = $-0.3525 + 0.3623*W - 0.0023*W^2$	0.9139	0.0001
	X34 = $-0.8526 + 0.5002*W + 0.0036*W^2$	0.9513	0.0001
9A	X1 = $0.9816 + 0.1870*W - 0.0048*W^2$	0.3166	0.0001
	X2 = $0.0450 + 0.2852*W - 0.0028*W^2$	0.8169	0.0001
	X345 = $-1.0267 + 0.5277*W + 0.0076*W^2$	0.9556	0.0001
9B	X1 = $-0.3808 + 0.3715*W - 0.0081*W^2$	0.7555	0.0001
	X23 = $-0.3176 + 0.3246*W + 0.0054*W^2$	0.9444	0.0001
	X45 = $0.6984 + 0.3040*W + 0.0027*W^2$	0.9047	0.0001

Note:

- (1) *W* is gross vehicle weight in tonnes.
- (2) HMAX refers to the load of heavy axle, and HMIN the lighter axle in tonnes.
- (3) X_i = load on the *i*th axle from the front in tonnes.
- (4) X_{ij} = load on the tandem axle comprising the *i*th and *j*th axles from the front in tonnes.
- (5) X_{ijk} = load on the tridem axle comprising the *i*th, *j*th and *k*th axles from the front in tonnes.

located in the front and others with engines located in the rear of the vehicle.

Table 4 also shows that the r^2 of the models for front axles was significantly lower than the r^2 of the models for other axles, that is, while the load on most front axles was not highly correlated to the gross vehicle weight. To determine the axle load distribution of a vehicle, it is therefore reasonable to compute first the estimated loads of other axles using the A -models (see the following section) and then subtract these loads from the gross vehicle weight to obtain an estimate of the front axle load.

Power Models

Power models express axle load A or percentage axle load P in terms of gross vehicle weight raised to a power as follows:

A -model:

$$A = c(W^d) \quad (5)$$

P -model:

$$P = e(W^f) \quad (6)$$

where c , d , e , and f are model coefficients. The model coefficients were determined using the linear regression technique

by taking the logarithmic transformation of Equations 5 and 6.

As in the case of polynomial regression models, Figure 4b shows that L -models were superior to P -models. Table 5 presents the L -models obtained. The results also confirmed the earlier finding concerning the relationship between gross vehicle weight and the load on the front axle.

Comparison of Axle Load Models

The relative accuracy of the two forms of axle load models derived above, namely, the polynomial L -models and the power L -models, was compared using the actual field survey data collected in this study. The comparison was carried out for each vehicle class as follows: (a) from the gross weight of a vehicle, the load on each axle of the vehicle was computed using the two models respectively; (b) Step a was repeated for all the vehicles in the survey records; (c) for the results obtained from each model, the coefficient of multiple determination and the root-mean-square difference between the actual and predicted axle loads were computed.

The results of the comparison, as shown in Table 6, indicate that both models gave predicted axle loads that were highly correlated with the actual loads. Judging from the relative values of r^2 and root-mean-square differences, the polynomial L -models appeared to be marginally better than the power L -models.

TABLE 5 Power Models for Axle Loads

VEHICLE CLASS	POWER MODELS	r^2	PROB. > F-STATISTIC
4A	HMIN = $0.2416 * W^{1.1787}$ HMAX = $0.7883 * W^{0.9050}$	0.8671 0.9310	0.0001 0.0001
4B	HMIN = $0.4097 * W^{1.0706}$ HMAX = $0.5809 * W^{0.9526}$	0.8142 0.8700	0.0001 0.0001
5	X1 = $0.6098 * W^{0.7330}$ X2 = $0.4264 * W^{1.1912}$	0.6066 0.8890	0.0001 0.0001
6	X1 = $0.9361 * W^{0.4726}$ X23 = $0.3655 * W^{1.2913}$	0.3945 0.9539	0.0001 0.0001
7	X1 = $0.8752 * W^{0.3411}$ X2 = $0.3458 * W^{1.0666}$ X3 = $0.1505 * W^{1.4160}$	0.3494 0.9457 0.9338	0.0001 0.0001 0.0001
8A	X1 = $0.6842 * W^{0.5600}$ X2 = $0.2386 * W^{1.0901}$ X34 = $0.2417 * W^{1.2574}$	0.5746 0.9411 0.9320	0.0001 0.0001 0.0001
8B	X1 = $0.5856 * W^{0.6125}$ X2 = $0.2033 * W^{1.1555}$ X34 = $0.2826 * W^{1.1926}$	0.6272 0.9237 0.9181	0.0001 0.0001 0.0001
9A	X1 = $0.8745 * W^{0.4103}$ X2 = $0.3260 * W^{0.8936}$ X345 = $0.2196 * W^{1.3487}$	0.3079 0.8385 0.9354	0.0001 0.0001 0.0001
9B	X1 = $0.1887 * W^{1.1119}$ X23 = $0.1926 * W^{1.2539}$ X45 = $0.5784 * W^{0.8434}$	0.7785 0.9410 0.9228	0.0001 0.0001 0.0001

Note: See Table 4 for definitions of symbols.

TABLE 6 Comparison of Axle Load Models

CLASS	AXLE * LOAD (Tonnes)	POLYNOMIAL L-MODEL		POWER L-MODEL	
		r ²	root-mean- square of difference (tonnes)	r ²	root-mean- square of difference (tonnes)
4A	HMIN	0.9436	0.1707	0.9442	0.1761
	HMAX	0.9600	0.1707	0.9602	0.1761
4B	HMIN	0.9171	0.1752	0.9088	0.1866
	HMAX	0.9407	0.1752	0.9348	0.1866
5	X1	0.7933	0.4400	0.7802	0.4533
	X2	0.9359	0.4401	0.9324	0.4533
6	X1	0.6216	0.4770	0.4621	0.5421
	X23	0.9740	0.4770	0.9679	0.5421
7	X1	0.7650	0.3191	0.5564	0.5350
	X2	0.9705	0.3345	0.9579	0.4041
	X3	0.9784	0.3486	0.9723	0.4048
8A	X1	0.7136	0.4429	0.7218	0.4592
	X2	0.9629	0.3481	0.9629	0.3486
	X34	0.9816	0.4409	0.9820	0.4592
8B	X1	0.7284	0.4686	0.7369	0.5025
	X2	0.9553	0.4459	0.9536	0.4698
	X34	0.9749	0.6110	0.9760	0.6568
9A	X1	0.5329	0.4993	0.5635	0.5009
	X2	0.9021	0.4780	0.9033	0.4776
	X345	0.9763	0.7272	0.9778	0.7082
9B	X1	0.8575	0.3288	0.8636	0.3283
	X23	0.9705	0.2914	0.9721	0.2841
	X45	0.9507	0.3154	0.9493	0.3236

* See Table 4 for definitions of symbols

ESAL COMPUTATION USING PROPOSED MODELS

A verification test of the applicability of the approach developed in this study was carried out by comparing the ESAL values computed using the derived models with the ESAL values calculated on the basis of actual axle data, and with ESAL values calculated using the following three other methods:

1. *U.K. Road Note 29 conversion factor method (9)*: In this method the total ESAL is obtained by multiplying the volume of commercial vehicles (U.K. term for heavy vehicles) by a constant ESAL conversion factor. For public roads, the conversion factor given is 0.45.

2. *Asphalt Institute truck factor method (2)*: This method is similar to the U.K. Road Note 29 method in that truck factors are multiplied by truck volumes to arrive at the design ESAL. The main difference is that this method provides truck factors for various vehicle classes as shown in Table 7.

3. *The constant-percentage axle load method (15)*: This method assumes constant-percentage shares among the various axles for a given vehicle type. In the present comparative study, the constant-percentage shares were taken as the mean percentage values computed from axle load data collected. Table 8 gives the mean axle load percentage shares for various vehicle classes.

Comparisons of all the above computational methods were made for the overall ESAL, including contributions from all heavy vehicle classes, as well as for ESALs of individual vehicle classes. The values of computed ESAL are given in Table 9 and plotted in Figure 5. The following observations can be made:

1. The Asphalt Institute method and the U.K. Road Note 29 method both are volume-based methods that compute ESAL directly by multiplying heavy vehicle volume by certain factors, producing highly conservative ESAL values for Singa-

TABLE 7 ESAL Computation: Asphalt Institute Method

Single-unit trucks			Tractor semi-trailers		
2-axle 4-tire	2-axle 6-tire	3-axle or more	3-axle	4-axle	5-axle or more
0.01-0.07	0.15-0.32	0.29-1.59	0.33-0.78	0.43-1.32	0.63-1.53

Note: Equivalent axle load = \sum (Truck traffic volume x Truck factor)

TABLE 8 ESAL Computation: Constant-Percentage Axle Load Method

Vehicle Class	Axle Load as a Percentage of Gross Vehicle Weight
4A	HMAX = 0.67 W ; HMIN = 0.33 W
4B	HMAX = 0.54 W ; HMIN = 0.46 W
5	X1 = 0.44 W ; X2 = 0.56 W
6	X1 = 0.31 W ; X23 = 0.69 W
7	X1 = 0.24 W ; X2 = 0.40 W ; X3 = 0.36 W
8A	X1 = 0.28 W ; X2 = 0.29 W ; X34 = 0.43 W
8B	X1 = 0.25 W ; X2 = 0.30 W ; X34 = 0.45 W
9A	X1 = 0.23 W ; X2 = 0.26 W ; X345 = 0.51 W
9B	X1 = 0.24 W ; X23 = 0.35 W ; X34 = 0.41 W

Note: (i) ESAL factor is obtained from AASHTO table [5] after axle load is computed.

(ii) Definitions of all symbols are given in Table 4.

por traffic. The total ESAL values obtained from these two methods were each more than three times the actual values.

2. The three methods that made use of axle load distributions, namely, the constant-percentage method, the polynomial regression model, and the power model, all yielded ESAL estimates of the same order of magnitude as the actual value. In order of decreasing accuracy in their predictions, the polynomial method produced the best results, followed by the power model, and the constant-percentage method.

3. The actual ESAL for buses (Classes 4A and 4B) and two-axle, single-unit trucks (Class 5) fell within the range given by the Asphalt Institute method. For all other classes of heavy vehicles, the actual ESAL values were much lower than the lower limits of the Asphalt Institute method. The

big differences in ESAL values in Classes 6 and 9 could possibly be explained by the fact that the Asphalt Institute method classifies these two classes under three axles or more and five axles or more, respectively, thereby tending to overestimate the ESAL by including the effects of other multiple-axle vehicles not included in Classes 6 and 9. In general, the large discrepancy between the ESAL loading on Singapore roads and those predicted by the U.S. and the U.K. methods can be attributed to the differences in the operational characteristics of the freight industry. Being a small island state, Singapore does not have large volumes of long-haul truck fleets. The trip distances of freight movements are very short compared with those in the United States and the United Kingdom.

TABLE 9 Values of ESAL Computed by Various Methods

CLASS	NUMBER OF VEHICLES	ACTUAL ESAL	ESAL BY AXLE LOAD DISTRIBUTION METHOD			ESAL BY VOLUME BASED METHOD		
			CONSTANT PERCENTAGE METHOD	POLYNOMIAL REGRESSION L-MODEL	POWER L-MODEL	ASPHALT INSTITUTE METHOD		U.K. ROAD NOTE 29 METHOD
						LOWER LIMIT	UPPER LIMIT	
4A	1418	79.88	89.23	72.35	73.58	14.18	99.26	-
4B	852	20.51	19.81	18.46	18.52	8.52	59.64	-
5	3103	87.26	64.74	59.86	59.56	31.03	217.21	-
6	4040	217.01	191.26	231.24	224.13	1171.6	6423.6	-
7	870	107.71	80.27	101.43	124.78	287.1	678.6	-
8A	1049	59.37	55.73	69.06	68.25	451.07	1384.7	-
8B	747	78.46	70.25	121.01	146.89	321.21	986.04	-
9A	323	38.39	29.29	31.997	32.37	203.49	494.2	-
9B	236	4.68	4.62	5.345	5.544	148.68	361	-
TOTAL	12638	693.27	605.2	710.752	753.62	2636.88	10704.3	5687

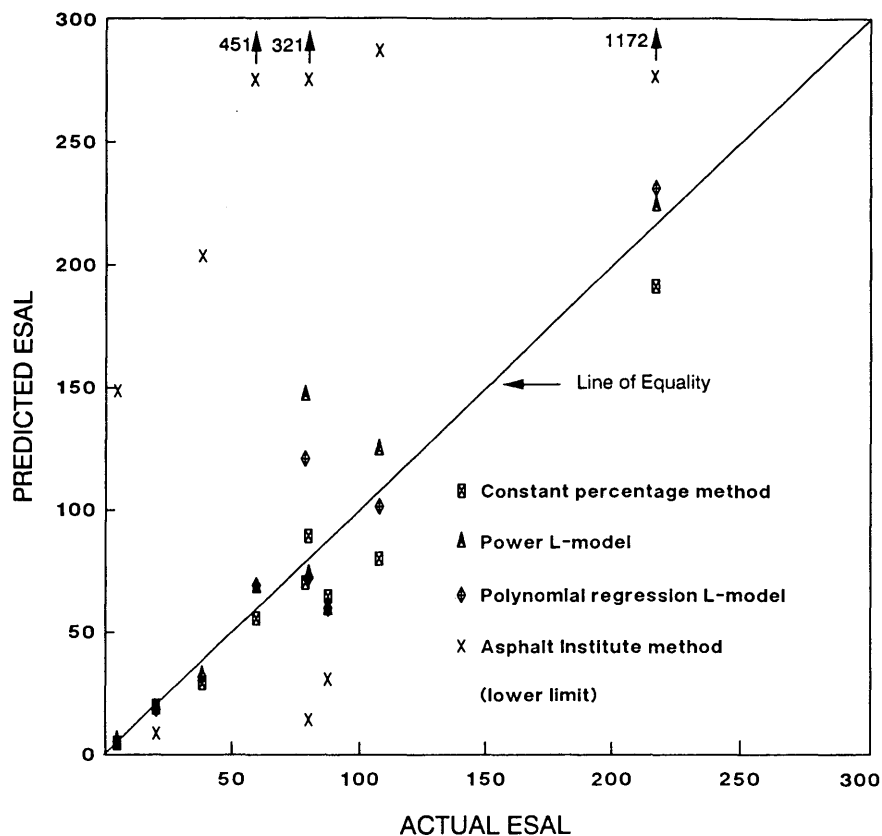


FIGURE 5 Comparison of ESAL values computed by various methods.

These results clearly demonstrate the need to conduct axle load studies to evaluate traffic loading in countries or regions not covered by established pavement design manuals such as the Asphalt Institute manual or the U.K. Road Note. This is because the characteristics of freight transportation are likely to vary from country to country. Overestimation of traffic loading leads to wasteful design in terms of layer thickness for new pavements and to underestimation of remaining pavement life in road network management systems.

CONCLUSIONS

On the basis of field data on axle loads of heavy vehicles, mathematical models were derived for vehicle weight and axle load distributions for the major vehicle classes in Singapore. It was shown that the vehicle weight distributions of individual vehicle classes could be described closely by Weibull distribution functions. In the case of axle load distributions, either second-order polynomial regression models or power models could be used. Second-order polynomial regression models were found to give the closest estimation of the actual ESAL of the measured axle loads. The use of general-purpose, volume-based procedures developed for U.S. or U.K. traffic loading conditions resulted in grossly overestimated ESAL values for Singapore.

The approach adopted in this study can be easily applied elsewhere to characterize vehicle weight and axle load distri-

butions for use in pavement or bridge design, and in traffic loading estimation for pavement performance monitoring. The coefficients in the vehicle weight and axle load models can be calibrated to suit local traffic conditions.

REFERENCES

1. E. J. Yoder and M. W. Witzak. *Principles of Pavement Design*, 2nd ed. John Wiley and Sons, Inc., New York, 1975.
2. *Thickness Design—Full Depth Asphalt Pavement Structures for Highways and Streets*. Manual Series MS-1, The Asphalt Institute, 1981.
3. M. E. Dwiggin, M. I. Darter, J. P. Hall, and J. B. DuBose. Pavement Performance Analysis of the Illinois Interstate Highway System, *Proc., 4th International Conference on Concrete Pavement Design and Rehabilitation*, Purdue University, 1989, pp. 447–453.
4. J. Verstraeten. The Consideration of Traffic in the Design and Maintenance of Bituminous Pavements—Practical Consequences. *Proc., 7th Conference of the Road Engineering Association of Asia and Australasia*, Vol. 2, Singapore, 1992.
5. *Guide for Design of Pavement Structures*. AASHTO, Washington, D.C., 1986.
6. *Highway Performance Monitoring System: Field Manual*. FHWA, Washington, D.C., 1987.
7. T. E. Jones. *Axle-Loads on Paved Roads in Kenya*. TRRL Laboratory Report 763. U.K. Transport and Road Research Laboratory, Crowthorne, Berkshire, England, 1977.
8. M. C. Tai. In Search of Optimum Axle Loadings for Commercial Vehicles—The Malaysian Experience. *Proc., REAAA/PIARC*

- Workshop on Truck Loads on Roads*, Kuala Lumpur, Malaysia, 1990.
9. Road Research Laboratory. *A Guide to the Structural Design of Pavements for New Roads*. Road Note 29. Department of the Environment, United Kingdom, 1970.
 10. *Analysis of Traffic Loadings on Interstate Highways in Illinois*. Report FHWA-IL-UI-222, Illinois Department of Transportation, Springfield, 1989.
 11. D. Kinder and J. Brown. Road Demand and Road Wear. *Proc., REAAA/PIARC Workshop on Truck Loads on Roads*, Kuala Lumpur, Malaysia, 1990.
 12. D. J. Harman and A. G. Davenport. A Statistical Approach to Traffic Loading on Highway Bridges. *Canadian Journal of Civil Engineering*, Vol. 6, 1979.
 13. I. Konishi, H. Kameda, and T. Matsumoto. Traffic Load Measurement and Probabilistic Modelling for Structural Design of Urban Expressways. *Proc., ICSSAR '85, 4th International Conference on Structural Safety and Reliability*, Vol. 3, Kobe, Japan, 1985, pp. 141–150.
 14. L. L. Lapin. *Probability and Statistics for Modern Engineering*, 2nd ed. PWS-KENT Publishing Company, Boston, 1990.
 15. T. Ruenkairergsa. Problems of Truck Overloading in Thailand. *Proc., REAAA/PIARC Workshop on Truck Loads on Roads*, Kuala Lumpur, Malaysia, 1990.

Publication of this paper sponsored by Committee on Flexible Pavement Design.

Analytical and Experimental Investigations of Operating Mechanisms in Reinforced Asphalt Pavements

HOZAYEN HOZAYEN, M. GERVAIS, A. O. ABD EL HALIM, AND R. HAAS

Reinforcement of asphalt pavements has become a feasible alternative within the past decade, largely because of grids. Whether reinforcement is an effective alternative for any given situation, however, must be established on a performance and economic basis. Potential performance benefits include reductions in rutting, cracking, and layer thickness, plus extended pavement life. The effectiveness of reinforced pavements depends on the interaction between reinforcement and the asphalt mix. Such interaction is provided by a number of mechanisms including interlock, bond, confinement, and membrane effects. The extent to which a mechanism dominates the operation of a given reinforcement depends on the geometry, strength, and the elastic properties of the grid involved. The effects of various geometric properties of reinforcements on the effectiveness of grids through the mechanisms under which they operate are discussed. The test results showed that the interlock operating mechanism is governed mainly by the grid opening size and the thickness of strand. The bond operating mechanism is governed mainly by the grid surface area.

The notion of reinforcing asphalt pavement has existed for many years. A few attempts have been made to use metallic and other materials to minimize pavement cracking (1,2). These attempts were not based on fundamental considerations, however, and they were not cost- and performance-effective (3).

The advent in the late 1970s of a new generation of high-strength polymer meshes, known as "grids," indicated that under certain circumstances reinforcement could be a viable option for reducing pavement rutting, cracking, and layer thickness. Results of the early research (4) showed that the use of grids to reinforce asphalt pavements can result in reducing surface rutting by a factor of 2 or more and increasing fatigue life by four to five times. These laboratory results were subsequently supported by data and observations gathered from field trials in many parts of the world. However, with the availability of many types of grids on the market and a wide variety of design conditions, pavement engineers are faced with having to determine whether reinforcement is an effective option under any given situation.

H. Hozayen and M. Gervais, National Research Council of Canada, Ottawa, Ontario, Canada K1A 0R6. A. O. Abd El Halim, Center for Geosynthetics Research Information and Development, Department of Civil Engineering, Carleton University, Ottawa, Ontario, Canada K1S 5B6. R. Haas, Department of Civil Engineering, University of Waterloo, Waterloo, Ontario, Canada N2L 3G1.

With the advances in chemical products technology, more polymer materials that can be used for asphalt pavement reinforcement have become available. These include textiles, fiberglass, and grids. Because of their low modulus, high elongation, and sheet structure, the use of textiles in heavy-duty asphalt pavements does not appear to be feasible (5). Although fiberglass-reinforced plastic seems to have some advantages compared with other reinforcement materials, it is a relatively expensive material and, therefore, its use in pavement reinforcement may not be cost-effective. The process for selecting the best alternative and implementing it involves the following stages (6):

1. Identification of critical design factors,
2. Selection of the best reinforcement for the application,
3. Economic analysis,
4. Determination of the appropriate installation or construction method, and
5. In-service monitoring.

OBJECTIVES OF THE PAPER

This research has been carried out to investigate the effects of various reinforcement types and properties on the effectiveness of their operating mechanisms. The following are the specific objectives of this paper:

1. To briefly review reinforcement alternatives (types and locations in the pavement structure), major variables (pavement layer and reinforcement properties, etc.), and functions (rutting, fatigue cracking, and reflection cracking).
2. To identify the grid operating mechanisms (interlock, bond, confinement, and membrane effect) to provide behavior that is compatible with the asphalt layer.
3. To experimentally verify the operating mechanisms identified in Objective 2 above, so that a basic understanding of the reinforcement behavior can be provided.
4. To determine the most important parameters that govern the performance of grid-reinforced asphalt pavements.

The work presented in this paper deals with the two main reinforcing mechanisms, that is, interlock and bond. Quantifying confinement and membrane mechanisms requires more

complex test facilities and therefore it is not discussed in this work.

ASPHALT PAVEMENT REINFORCEMENT

The term "reinforcement" generally means the inclusion of certain materials with some desired properties within other materials that lack these properties. Many reinforcement applications have been used to enhance the tensile strength of other media such as retaining walls, portland cement concrete, slope stability measures, embankments, and asphalt pavements (4).

If reinforcement is to be considered, two basic needs must be established (7,8):

1. Intended function of the reinforcement; one or more of (a) reduced rutting, (b) reduced cracking (fatigue, reflection), (c) reduced layer thickness (asphalt, base, subbase), or (d) extended pavement life or reduced maintenance, or both.
2. Reinforcement alternatives: (a) types and possible locations in the pavement structure, and (b) major variables (pavement layer and reinforcement properties, traffic loads and volumes, etc.).

Figure 1 is a schematic illustration of the location alternatives and the major variables. Although only one location would normally be chosen for reinforcements, Figure 1 illustrates several possible ones, depending on the variables listed. The best location for any given set of conditions is determined

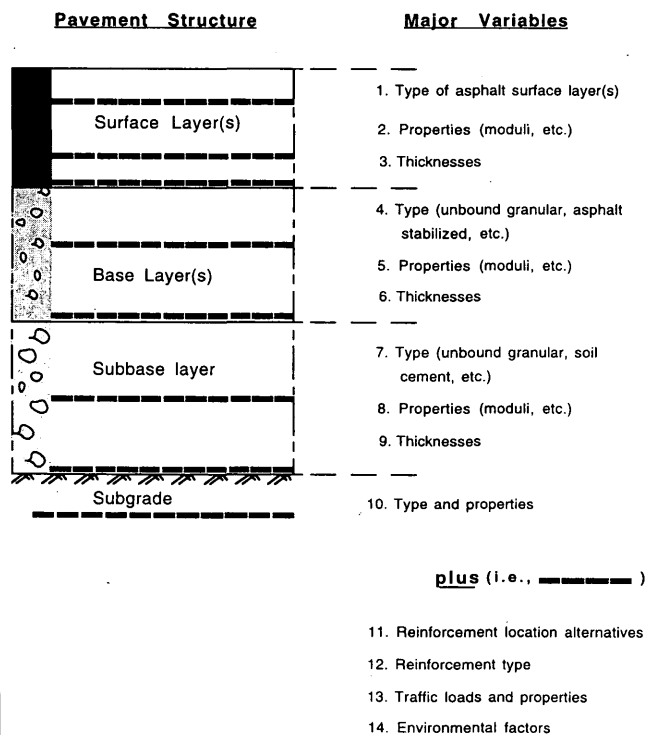


FIGURE 1 Reinforcement location alternatives and some of the major variables.

through a proper structural design, plus construction practicalities.

Examples of how different locations for reinforcement can have a major effect on reduced rutting or extended life, or both, are provided for a very weak subgrade (9), for granular base reinforcement on weak to strong subgrades (10), and for asphalt reinforcement on weak to strong subgrades (11).

Within the entire pavement structure, the asphalt concrete layer receives most of the load- and non-load-induced tensile stresses. However, it is well known that asphalt concrete lacks the ability to resist such tensile stresses, which makes it an ideal medium for reinforcement.

Grids have become more acceptable for pavement reinforcement. The grid bond and interlock with the asphalt matrix (provided by the open mesh structure) and their high modulus and tensile strength (which are comparable with mild steel) make them the most promising materials for asphalt pavement reinforcement applications. Two grid types have been considered for this study: polyethylene and polyester. Properties of the two grid types and their effects on the operating mechanisms are discussed.

OPERATING MECHANISMS OF REINFORCEMENT

Identification of Mechanisms

The effectiveness of reinforced asphalt pavements is governed by the ability of the reinforcement to mobilize a number of mechanisms. These mechanisms can be identified as (a) interlock, (b) bond, (c) confinement, and (d) membrane effect. The presence and contribution of each mechanism depend on the characteristics of the asphalt mixture, the reinforcement, and their interaction. The definition of each mechanism and the extent to which a mechanism can dominate the behavior of the reinforcement are discussed.

Interlock is defined as the portion of the mobilized strength of the reinforced layer through anchorage resistance provided between the mesh opening and the aggregates of the asphalt mixture. Optimum interlock can be achieved when the ratio between the dimensions of the opening and the aggregate size is 3:1 to 4:1; this ratio has been observed in this investigation and will be discussed in a subsequent section.

Bond is defined as the portion of the mobilized strength of the reinforced layer provided by the adhesion between the surface of the reinforcement and the asphalt cement of the mixture. As the surface area of the reinforcement increases, higher bond resistance can be obtained, provided that the other geometric properties are constant, that is, same strand thickness and geometry of openings and joints. Also, increasing the asphalt content of the mix will increase the bond developed at the interface between the asphalt and the reinforcement (4,11).

The confinement mechanism is provided through the compatibility between the overall properties (physical and geometric properties) of the reinforcement and the characteristics of the asphalt layer. In other words, the confinement mechanism depends on the width of the overall reinforcement in relation to the width of the paved lane. For example, if the width of the reinforcement is significantly less than that of

the paved lane, the strength mobilized by the confinement mechanism will be less than the strength mobilized if both widths were identical.

The fourth mechanism that contributes to the overall strength of the reinforced layer is the membrane effect. This mechanism depends on the elasticity of the reinforcement, its position within the asphalt layer, the type of underlying layer (i.e., base, subbase, or subgrade), and the length of the reinforced layer beyond the influence of the loaded area. The membrane mechanism acts to redistribute the applied stresses into a larger area of the base, subbase, or subgrade of the pavement structure.

Factors Affecting the Operating Mechanisms

To enhance the development of the operating mechanisms for a given reinforcement, the selected grid should have properties that are compatible with those of the layer material and particularly the asphalt mixture under a wide range of temperatures. The compatibilities between the aggregate and the opening of the grid, the thermal properties, and the stiffness of the grid relative to the asphalt layer are the key parameters that contribute to the realization of the potential of a reinforced asphalt pavement.

In essence, the factors that affect the reinforcement operating mechanisms can be categorized into three types:

1. Factors related to the geometry of the grid and its physical properties,
2. Factors related to the material properties of the asphalt pavement layer (asphalt content, maximum aggregate size, layer thickness, etc.), and
3. Factors related to installation or construction procedure (paving train interaction with grid, interaction between asphalt layer and compactor, etc.).

It is beyond the objectives of this paper to discuss how the operating mechanisms are affected by the factors related to the properties of the asphalt pavement layer or those related to the installation or construction process. The emphasis instead is on the effects of the grid geometry on mobilizing the various mechanisms.

Table 1 summarizes the factors related to the geometry of a grid reinforcement that can affect the operating mechanisms. The interlock mechanism is affected mainly by the size of the grid openings with respect to the maximum aggregate size, the ratio of strand area to the total area of the grid, and the strand thickness. The bond mechanism is affected by the grid surface area, the geometry of the opening (square or curved corners), and the strand width. The confinement mechanism depends on the dimensions of the grid with respect to the dimension of the reinforced layer, whereas the membrane effect mechanism is a function of the geometry of the grid joints.

The testing program presented in this paper was carried out to investigate the effects of the above-mentioned geometric properties of the grid on the operating mechanisms. Details of the experimental investigation and analysis of test results are discussed next.

EXPERIMENTAL INVESTIGATION

The experimental investigation was carried out at two different testing facilities: Carleton University and the Institute for Research in Construction of the National Research Council of Canada in Ottawa. The laboratory tests consisted of fastening an asphalt concrete slab to steel plates—one fixed and the other mobile (see Figure 2). The slabs were laid flat horizontally and were fully supported by the plates. A tensile load could be applied to the sample by horizontal movement of the mobile plate (no eccentric loading or bending movement was applied).

An actuator driven by a variable-speed electric motor was used to apply the horizontal loads, and a precalibrated load cell, located between the mobile plate and the actuator, measured the loads required to pull the asphalt slab apart. Also, a direct current differential transducer (DCDT) was used to measure the displacements. Both of the measuring devices were connected to a data acquisition unit.

Selection of Grids

To demonstrate the effects of the grid geometric properties (Table 1) on the reinforcement operating mechanisms, two

TABLE 1 Factors of Grid Geometric Properties Affecting Operating Mechanisms

Operating Mechanism	Factors of Grid Geometric Properties Affecting the Mechanism
Interlock	<ul style="list-style-type: none"> - Size of openings with respect to max. aggregate particle size, - Ratio of strands area to the total area of the grid, - Strand thickness.
Bond	<ul style="list-style-type: none"> - Grid surface area, - Geometry of opening (square or curved corners), - Strand width.
Confinement	<ul style="list-style-type: none"> - Dimension of grid with respect to the dimension of the asphalt layer.
Membrane Effect	<ul style="list-style-type: none"> - Grid joints (i.e., overlapped, cemented strands or continuous merging materials).

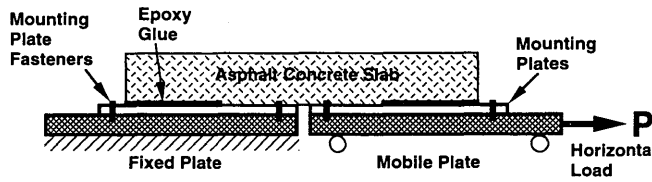
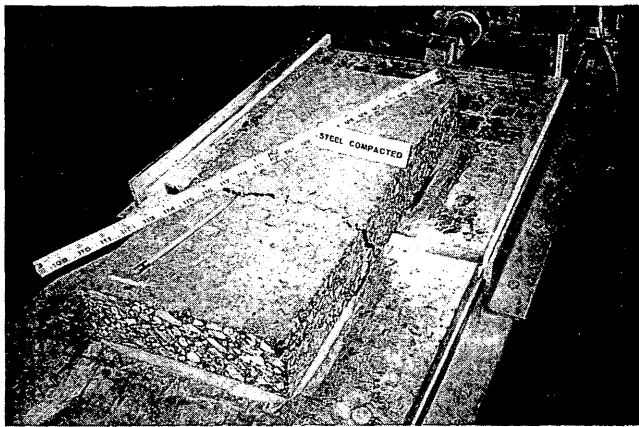


FIGURE 2 Reinforced slab testing machine for selection of grids.

types of grids were selected. These are polyethylene and polyester, which have a variety of geometric properties. Table 2 shows the properties of the grids utilized in the testing program.

The grids shown in Table 2 were selected only on the basis of varying geometric properties and not to demonstrate that one type of grid is ideal for asphalt pavement reinforcement. For example, Grids G3 and G5 were modified (by eliminating every second strand in the longitudinal direction, yielding Grids G4 and G6, respectively) during the experimental in-

vestigation to evaluate specific characteristics of the grids and to alter their performance (see Table 2). These modifications resulted in removing between one-third and one-half the number of strands.

Testing Program

Table 3 presents a summary of the testing program, which involves two series of tests. The objective of the first series was to evaluate the effect of various geometric properties on the bond operating mechanism. To achieve maximum bond while minimizing the interlock mechanism, the specimens were constructed in the field as follows:

1. Placement and compaction of the first asphalt lift,
2. Placement of grid reinforcement on top of the compacted surface of the first asphalt lift, and
3. Placement and compaction of the second asphalt lift on top of the grid reinforcement.

The purpose of compacting the first asphalt lift was to ensure that no interlock between this asphalt lift and the grid reinforcement was developed. Hence, the main mechanism mobilized from this construction procedure was bond.

After examination of the results from the first test series, it was decided to include additional variations on the geometric properties for the next series of tests. The variation on geometric properties was achieved by modifying Grids G3 and G5 (see Table 2). Subsequently, a total of five grids were tested to evaluate the interlock operating mechanism. For this series, samples were compacted in the laboratory. The first asphalt lift was not compacted before placing the grid. Rather, the entire slab (i.e., first asphalt lift, the grid, and the second asphalt lift) was compacted as a unit by a vibratory plate. The main mobilized mechanism, therefore, was interlock.

TABLE 2 Properties of Selected Grids Used in the Testing Program

Grid		Property									
		Opening			Strand		Ratio of Grid Open. Width to Max. Agg. Size	% Openings Area to Total Grid Area	% Surface Area to Total Grid Area	Geometry* of Grid Joints	Tensile Strength (KN/m)
No.	Polymer	Area (mm ²)	Min. Width (mm)	Corner Geometry	Width (mm)	Thick (mm)					
G1	polyethylene	3064	46.8	rounded	4.34	1.47	3.6	83.6	16.4	C.M.	16.0
G2	polyester	339	17.7	square	2.89	1.04	1.3	75.2	24.8	O.S.	30.0
G3	polyester	657	17.0	square	2.77	0.82	1.3	80.7	19.3	O.S.	32.0
G4	polyester	1512	36.8	square	2.77	0.82	2.8	87.9	12.1	O.S.	19.2
G5	polyester	723	25.4	square	6.25	1.3	1.9	48.0	52.0	O.S.	51.6
G6	polyester	3952	62.5	square	6.25	1.3	4.7	71.4	28.6	O.S.	31.0
G7	polyester	2159	48.3	square	8.74	0.96	3.7	64.5	35.5	O.S.	41.0

* C.M. = Continuous Materials
O.S. = Overlapped Strands

TABLE 3 Summary of the Testing Program and Variables Considered

Sample Grid No.	No. of Samples Tested	Sample Dimensions (mm)	MTO Asphalt Mix Type	Site Fabrication	Operating Mechanism Evaluated
Unreinforced G1 G2 G3 G5	12 8 3 8 6	1200x1200 x75	HL3	Field compaction	Bond
Unreinforced G1 G4 G5 G6 G7	4 2 2 3 4 2	300x600 x75	HL3	Laboratory compaction	Interlock

ANALYSIS OF TEST RESULTS

Typical test results for the first test series (evaluation of bond operating mechanism) and the second test series (evaluation of interlock operating mechanism) are illustrated in Figures 3 and 4, respectively. Figure 3 shows that the tensile stresses that are resisted by the bond mechanism decrease rapidly to a very low level. After the grid is fully mobilized and the applied stresses are higher than the grid bond strength, splitting cracks along the interface between the reinforcement and the asphalt mix start to propagate to the ends of the sample, causing a separation that results in a rapid decrease in the tensile stresses (see Figure 3).

It is interesting that the use of Grid G2 or G3 resulted in a decrease in the maximum tensile strength of the reinforced asphalt when compared with the strength of the unreinforced asphalt (see Figure 3). This result would suggest that under certain circumstances (i.e., if bond were the only operating mechanism to be mobilized) a grid can weaken instead of strengthen the asphalt pavement. One should expect no significant increase in the tensile strength of the reinforced asphalt pavements. Similar to the reaction in steel-reinforced concrete, the tensile strength provided to the composite is mobilized after the concrete itself is cracked. In the case of reinforced pavements subjected to horizontal stresses or displacements, the grid will act to provide sufficient strength to maintain and preserve the integrity of the asphalt layer.

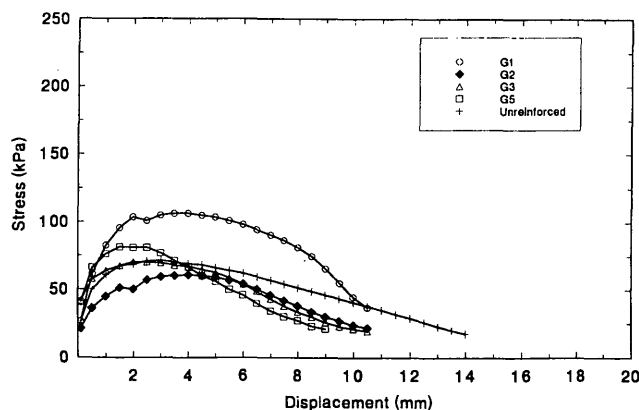


FIGURE 3 Typical stress displacement curves for the evaluation of bond operating mechanism.

Unlike the bond strength (which decreases rapidly), the interlock strength can still be provided by the reinforcement even after the peak stresses have been reached (see Figure 4). The grids of Figure 4 mobilized an effective interlock operating mechanism controlling the tension cracks and resisting stresses to a large degree (i.e., the tensile stresses did not decrease rapidly after the peak stress). The failure was caused by tension (transverse) cracks rather than splitting cracks that had propagated a bit earlier before reaching the peak stresses.

The results shown in Figure 4 emphasize the importance of the grid geometry to its tensile strength. As discussed earlier, Grid G6 is a modified version of Grid G5. In fact, the tensile strength of Grid G6 is approximately 40 percent less than that of Grid G5 because of the removal of every second strand. However, in spite of the lower tensile strength of Grid G6, its reinforced slab resulted in about a 30 percent tensile strength increase when compared with the strength of Grid G5 reinforced slab (see Figure 4). This result is further supported by the fact that asphalt slabs reinforced with Grid G1 gave the best overall performance in spite of the lower tensile strength of G1 (see Table 2).

Figures 3 and 4 also show that the peak stresses resisted by the interlock operating mechanism are much higher than those resisted by the bond operating mechanism. To achieve an effective interlock operating mechanism, the reinforcement grid has to be placed on an uncompacted asphalt lift and

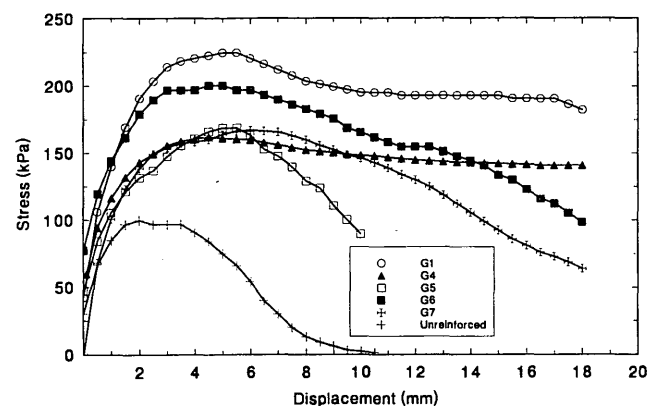


FIGURE 4 Typical stress displacement curves for the evaluation of interlock operating mechanism.

sandwiched between the two asphalt lifts (which was the construction procedure followed for Figure 4 specimens).

Effect of Grid Surface Area

Figure 5 illustrates the effect of grid surface area (area of strands) on the bond operating mechanism evaluated in the first test series. As the grid surface area increases, the peak stress decreases to a point after which it starts to increase.

It is postulated that the effect of the interlock operating mechanism (which cannot be completely eliminated even though the objective of the construction procedure for these samples was to develop bond only) influences the measured strength at lower values of grid surface area. For example, although the surface area of Grid G2 is larger than that of Grid G3, the Grid G2 bond strength is lower. This difference can be explained by Figure 6, which characterizes the measured peak stresses as a function of the grid opening size, showing that the interlock operating mechanism has been developed and is smaller for Grid G2 than for Grid G3.

For grid surface areas greater than 25 percent (of total grid area), however, the bond operating mechanism increases as the grid surface area increases (see Figure 5). For example, Grid G5 has a surface area of 52.5 percent and exhibits a high bond operating mechanism. If the surface area reached 100 percent (which is the case with a fabric sheet), the dashed curve in Figure 5 demonstrates that the bond operating mechanism would have provided the total measured strength and no interlock would have existed.

Effect of Opening Size

Figure 7 shows the relationship between the opening size (areas of opening) and the peak stress developed mainly by the interlock operating mechanism (second test series). As the opening size increases, the mobilized interlock operating mechanism increases and resists higher tensile peak stresses. Because more asphalt materials can be accommodated into a larger opening size, higher anchorage resistance can be developed. The anchorages then provide the interlock operating

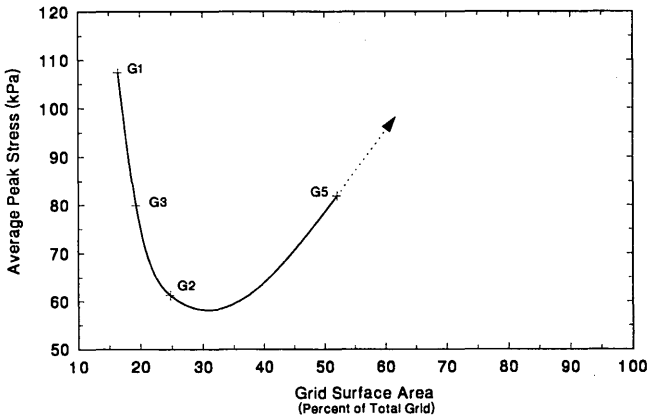


FIGURE 5 Effect of grid surface area on bond operating mechanism.

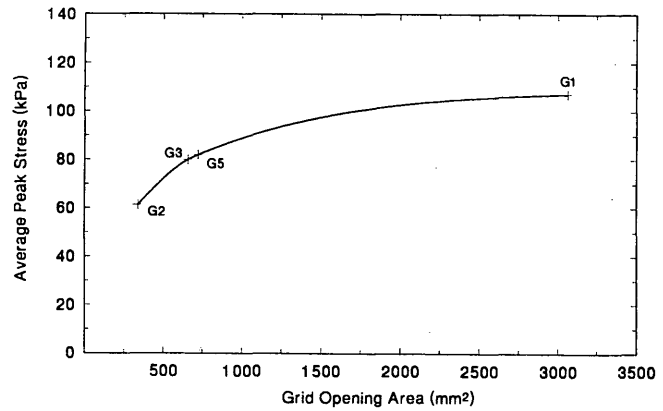


FIGURE 6 Effect of interlock operating mechanism on measured bond operating mechanism of first test series.

mechanism. This phenomenon is applied for a given strand shape (i.e., rounded or flat), as well as grid joint geometry (i.e., continuous materials or overlapped strands). For example, the polyester grids (G4, G5, G6, and G7) have the same strand shape and the same joint geometry and can be characterized by a Figure 7 curve. The polyethylene Grid G1, however, has a different strand shape and joint geometry and exhibits high peak stress for the following reasons:

1. Grid G1 strands have a rounded shape and smooth surface, whereas Grid G6 strands have a flat shape and sharp edges that cause localized shear stress at the interface between the strands and the asphalt mix.
2. The joints of Grid G1 are of continuous materials (merging between transverse and longitudinal strands), whereas the joints of Grid G6 are of crossed-overlapped strands. The continuous joints provide a biaxial resistance, which in turn provides a better confinement during the interlock operating mechanism.

Figure 7 also shows that no significant gain on the interlock operating mechanism can be achieved for opening sizes larger than about 2000 mm² (i.e., the peak stress curve has a flatter slope for large opening sizes). Grids G1, G6, and G7 provide

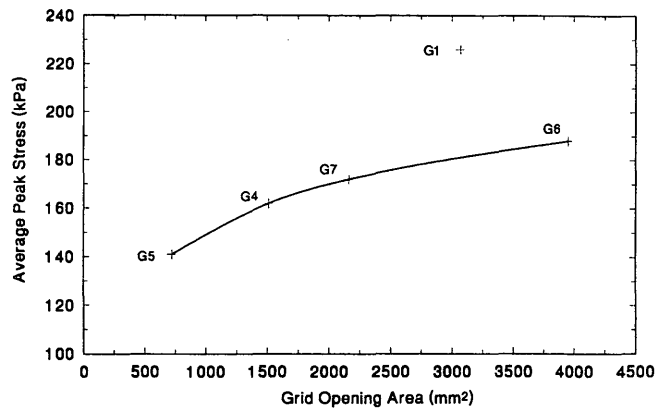


FIGURE 7 Effect of grid opening size on interlock operating mechanism.

higher tensile strength than that provided by the rest of the grids. These three grids have a ratio of opening width to maximum aggregate size of more than 3 (see Table 2). Grid G7, for example, has a ratio of opening width to maximum aggregate size of 3.7. This ratio is 4.9 for Grid G6, but no significant increase in the tensile strength is achieved. It can be concluded, therefore, that the appropriate value for the ratio of grid opening width to maximum aggregate size is 3.6 or a range of 3 to 4 (i.e., 3:1 to 4:1).

Effect of Strand Thickness

The relationship between the strand thickness and the peak stress developed mainly by the interlock operating mechanism (second test series) is shown in Figure 8. As the strand thickness increases, the mobilized interlock operating mechanism increases. A larger strand thickness would allow anchorages that are formed by the asphalt material. The thicker the anchorage, the higher the mobilized interlock operating mechanism.

Figure 8 shows that Grid G5 does not follow the peak stress curve. Because of the very small opening size of this grid (compared with the other Grids G4, G6, and G7), the mobilized interlock operating mechanism is low. This is also supported by a Figure 7 relationship, which illustrates that the interlock operating mechanism is sensitive to small opening sizes that have areas less than 1500 mm² (i.e., the slope of the peak stress is steep for small opening sizes; see Figure 7). Therefore, it is expected that Grid 5 will have a much lower interlock operating mechanism and that the peak stress curve should be fitted to the other grids as shown in Figure 8.

CONCLUSIONS

The following conclusions can be drawn from the results of the analytical and experimental investigations presented in this paper.

1. The effectiveness of reinforced asphalt pavements depends to a large extent on the geometric properties of the

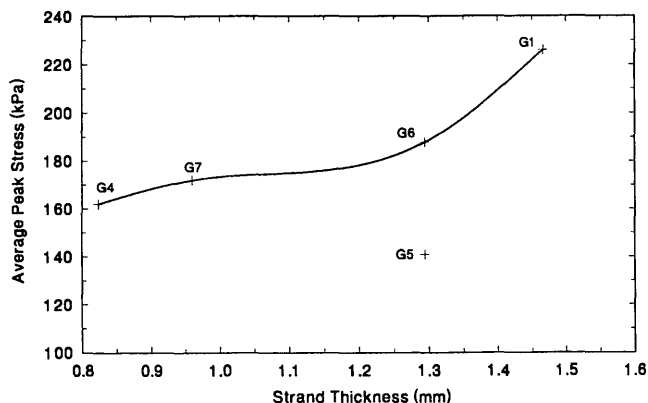


FIGURE 8 Effect of grid strand thickness on interlock operating mechanism.

grid. An interlock mechanism provides the main component of the reinforcing mechanisms.

2. The grid opening size is the most important geometric property that governs the interlock operating mechanism. A larger opening size would accommodate more asphalt materials to provide anchorages, which increase the interlock operating mechanism.

3. The strength mobilized by the interlock operating mechanism can still be provided even after the peak stresses are reached (i.e., even after cracks develop).

4. The bond operating mechanism is governed mainly by the grid surface area. For grid surface areas greater than about 25 percent (of total grid area), the bond mechanism increases as the grid surface area increases.

5. Grids with thicker strands can mobilize a more effective interlock operating mechanism because of thicker anchorages developed between the strands.

6. The small increase in the slab peak strength is primarily due to the bond operating mechanism, whereas the resistance to large deformation is due to the interlock operating mechanism.

7. To achieve the most effective interlock operating mechanism, the reinforcement grid has to be placed on an uncompacted asphalt lift and sandwiched between the two asphalt lifts.

Finally the research work presented in this paper addresses the main parameters that govern the performance of grid-reinforced asphalt pavements. The testing program followed; although it does not simulate traffic loadings, it does approximate stresses induced by temperature. The test results suggest that when the selected reinforcing grid meets certain geometric characteristics, the reinforced pavement resists the thermal stresses and maintains its integrity.

REFERENCES

1. E. Zube. Wire Mesh Reinforcement in Bituminous Resurfacing. *Bulletin 131*, HRB National Research Council, Washington, D.C., 1956.
2. F. C. Brownridge. An Evaluation of Continuous Wire Mesh Reinforcement in Bituminous Resurfacing. *Proc., AAPT*, Vol. 33, 1964.
3. A. O. Abdelhalim and R. Haas. *Flexible Pavement Reinforcement: Assessment of Available Materials and Models and a Research Plan*. Interim Report for Project 21130. Ontario Joint Transportation and Communication Research Program, March 31, 1981.
4. A. O. Abd El Halim, R. Haas, J. Walls, R. Bathurst, and W. Phang. A New Method for Effective Reinforcement of Asphalt Pavements. *Proc., Roads and Transportation Association of Canada*, Halifax, Nova Scotia, Canada, Vol. 2-1, Sept. 1982, pp. 29-41.
5. Q. Robnett, J. Lai, J. Lavin, L. Murch, and C. Murray. Use of Geotextiles in Road Construction. *1st Canadian Symposium on Geotextiles*, Calgary, Alberta, Canada, Sept. 1980, pp. 113-136.
6. A. O. Abd El Halim, R. Haas, H. Hozayen, and M. Gervais. Effective Reinforcement of Asphalt Pavements, *Proc., of the Canadian Technical Asphalt Association 36th Annual Conference*, Montreal, Quebec, Canada, Nov. 1991, pp. 171-192.
7. R. Haas. *A New Technology to Increase Pavement Life and Reduce Maintenance*. Report prepared for Project 21140. Ontario Joint Transportation and Communication Research Program, Jan. 31, 1984.

8. R. Haas and P. Joseph. Design Oriented Evaluation of Alternatives for Reflection Cracking Through Pavement Overlays. *Proc., Conference on Reflective Cracking in Pavements*, Université de Liège, Belgium, March 1989, pp. 23-46.
9. G. Kennepohl, N. Kamel, J. Walls, and R. Haas. Geogrid Reinforcement of Flexible Pavements: Design Basis and Field Trials. *Proc., AAPT*, 1985, pp. 45-47.
10. R. Penner, R. Haas, J. Walls, and G. Kennepohl. Geogrid Reinforcement of Granular Bases. *Proc., Roads and Transportation Association of Canada*, Vancouver, British Columbia, Canada, Vol. 1, Sept. 1985, pp. 263-294.
11. A. O. Abd El Halim, R. Haas, and W. Phang. Geogrid Reinforcement of Asphalt Pavements and Verification of Elastic Layer Theory. In *Transportation Research Record 949*, TRB, National Research Council, Washington, D.C., 1983, pp. 55-65.

Publication of this paper sponsored by Committee on Flexible Pavement Design.

Development of Strategic Highway Research Program Long-Term Pavement Performance Climatic Data Base

S. D. RABINOW, G. R. RADA, S. D. TAYABJI, AND C. A. RICHTER

Although the effects of climatic factors on pavement performance have long been recognized as important, those effects remain largely unquantified because individual pavement research projects to date generally have been restricted to limited geographic areas with more or less uniform climatic conditions and relatively short time spans, making it difficult to separate the effects of climatic factors from those of loading. By virtue of the relatively broad geographic and climatic distribution of the test sections involved and the long-term nature of the study, the Long-Term Pavement Performance (LTPP) program will rectify this situation. The Strategic Highway Research Program (SHRP) climatic data base is intended to provide the weather and climatic information needed to characterize the environment in which each LTPP test section has existed from the time of construction through the LTPP monitoring period. The development of SHRP's LTPP climatic data base, including the identification and sources of data, selection and verification of weather stations, actual data retrieval from available sources, and data quality assurance, is summarized. Future activities, such as updates and expansion of the data base and the collection of ground-truth data, are also discussed.

The Strategic Highway Research Program (SHRP) long-term pavement performance (LTPP) research is a 20-year study to determine pavement performance and the factors that affect it. To meet these goals, two series of experiments were established within the LTPP research program. The General Pavement Studies (GPS) involve test sections on existing pavements, whereas the Specific Pavement Studies (SPS) involve specially constructed pavement test sections. Both sets of test sections are, or will be, located on in-service highways throughout the United States and Canada and hence subjected to "real" nonidealized traffic loadings and a wide range of environmental conditions.

The data to be collected for SHRP LTPP research can be divided into five categories: (a) inventory data describing the location, geometry, and construction history of the test section; (b) monitoring data such as distress, profile, and deflection, which are collected to monitor changes in the pavement over time; (c) traffic data, which describe the loading to which the pavement is subjected; (d) climatic data, describing the environmental conditions to which the pavement is subjected; and (e) maintenance and rehabilitation data, describing and defining any and all maintenance applied to

the pavement. This paper focuses on the collection and storage of climatic data for SHRP LTPP test sections.

Although the effects of climatic factors on pavement performance have long been recognized as important, those effects remain largely unquantified because individual pavement research projects to date generally have been restricted to limited geographic areas with more or less uniform climatic conditions and relatively short time spans, making it difficult to separate the effects of climatic factors from those of loading. By virtue of the relatively broad geographic and climatic distribution of the test sections involved, and the long-term nature of the study, the LTPP program will rectify this situation.

Over the past several years, SHRP has mounted an effort to identify, obtain, and store climatic data for LTPP GPS test sections (1). This effort culminated in the development of SHRP's LTPP climatic data base, which contains the weather and climatic information needed to characterize the environment in which each GPS test section has existed from the time of construction through the LTPP monitoring period. In this paper the development of the LTPP climatic data base, the actual data collection and quality assurance process, and future activities related to climatic data are reviewed.

Although not discussed in the paper, climatic data, along with other LTPP information, are currently being used by the SHRP analysis contractor to verify and calibrate the existing AASHTO pavement performance models. It is anticipated that in coming years, these data will be used to better quantify the effects of climatic factors on pavement performance, to verify and calibrate other existing performance models, or to develop new ones. In addition, these data conceivably can support an unlimited number of research and development efforts that address the impact of climate on pavement performance.

DATA BASE DEVELOPMENT

Identification of Weather Stations

Details on the development of plans for the collection of climatic data have been documented elsewhere (1,2). Those plans centered around the use of National Climatic Data Center (NCDC) and Canadian Climatic Center (CCC) data. Technical direction was provided by SHRP's Environmental Data Expert Task Group (ETG) composed of pavement and weather professionals.

S. D. Rabinow, G. R. Rada, and S. D. Tayabji, PCS/Law Engineering, 12240 Indian Creek Court, Suite 120, Beltsville, Md. 20705-1242. C. A. Richter, FHWA-LTPP Division, 6300 Georgetown Pike, HNR-40, McLean, Va. 22101-2296.

The development of plans began with the definition of a "perfect" weather station: it must be close to the pavement test section and the types of data collected and their accuracy must be equivalent to at least a first-order weather station. Although an attempt to establish proximity guidelines was made, it became apparent from the start (as was expected) that weather stations could not be found close to most SHRP/STP test sites. Consequently, the plans were developed around the concept that data from up to five nearby weather stations would be used to estimate site-specific climatic conditions, that is, by development of a statistical or "virtual" station.

The choice of five weather stations to represent climatic conditions at a given site was somewhat arbitrary and may yield a misleading impression of data coverage for a given site. In fact, one "good" station is all that is needed for a given site. In terms of the virtual station, an "interpolation" algorithm using a $1/R$ weighting scheme was originally recommended, where R is the distance from the weather station to the site. This scheme was later modified to $1/R^2$ on the basis of the recommendations of the ETG. In any case, the closer the weather station is to the site, the greater its effect is on the calculated values for the virtual station. For example, any weather station three times farther from the GPS site than the closest weather station carries only one-ninth the

weight in the calculation of the closest station. Figure 1 shows an example of a GPS site and the five weather stations selected for describing its environmental conditions.

The criteria established for the identification of weather stations in the vicinity of the pavement test section are as follows. For each GPS test site, identify

- At least one active first-order weather station with 50 percent data coverage for the record length to be used (a wider range of data elements is collected by these stations and a higher level of quality assurance is exercised by NCDC on the data);

- The closest active cooperative weather stations that satisfy the following criteria (data elements collected by these stations generally are limited to temperature and precipitation):

- At least 50 percent data coverage for the record length to be used,

- Record length at least equal to the pavement age or 5 years after the pavement construction date,

- The following data elements recorded as a minimum: minimum daily temperature; maximum daily temperature; daily precipitation; and daily snowfall (if applicable); and,

- The three closest active or inactive (with at least part of the record length covering years after the pavement construc-

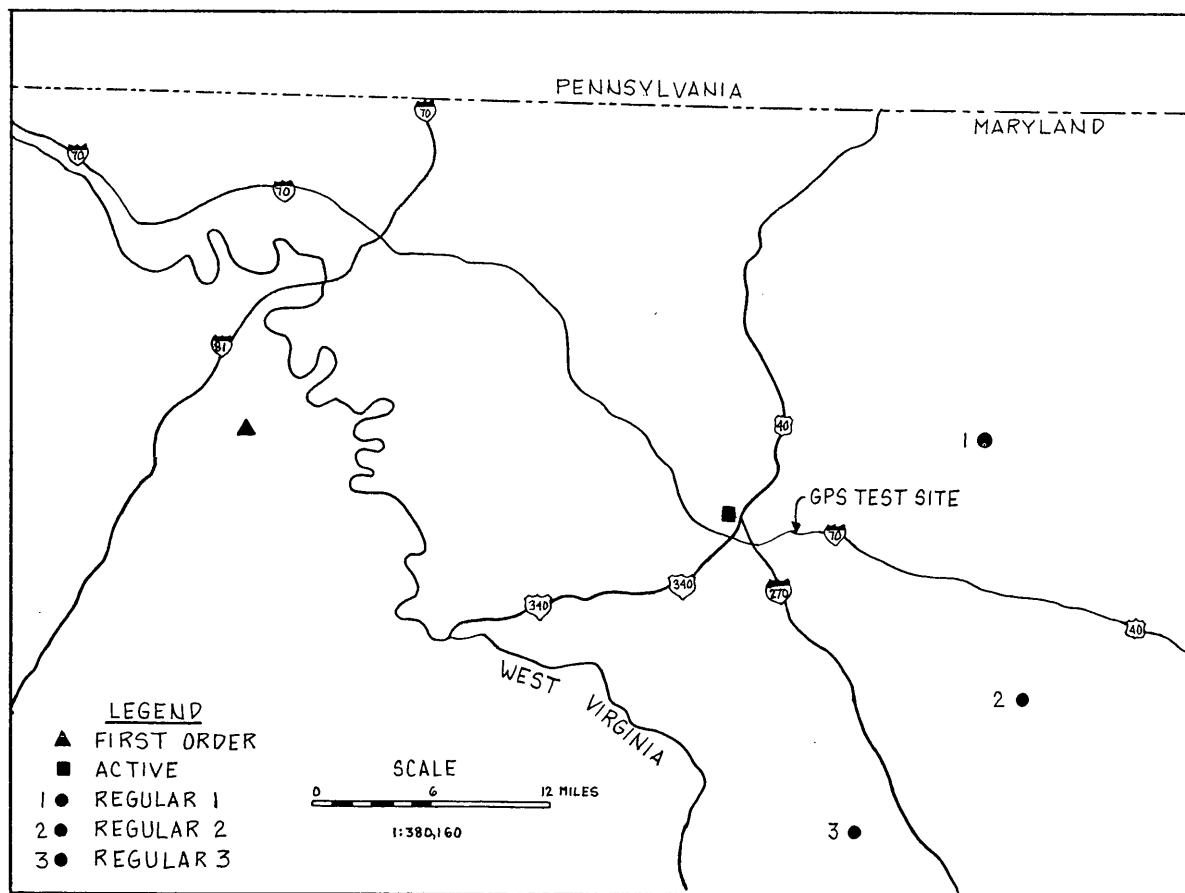


FIGURE 1 Sample GPS site and related weather stations.

tion date), first-order or cooperative weather stations other than those included in the first and second items.

The identification process was to be global—not limited by state or provincial borders to allow the consideration of weather stations close to a site but located in a neighboring state or province.

Climatic Data Elements

On completion of the weather station identification process, the data elements shown in Table 1 were acquired from NCDC and CCC files, where available, for each station. Because of limitations associated with the NCDC data collection procedure, however, only the first six data fields listed in Table 1 are available from cooperative weather stations, and the rest are available only from first-order weather stations. Also, the first five elements in this list generally are available for the entire time span, whereas the remaining eight are predominantly available only after 1984.

In addition, the monthly average, standard deviation, skewness, and kurtosis were determined for all data elements shown in Table 1, except daily occurrences of weather, for each year. The equations used in these computations are summarized below:

$$\bar{x} = \frac{\sum_{i=1}^n X_i}{n}$$

$$S^2 = \frac{\sum_{i=1}^n (X_i - \bar{x})^2}{n}$$

$$\alpha_3 = \frac{\frac{\sum_{i=1}^n (X_i - \bar{x})^3}{n}}{S^3}$$

$$\alpha_4 = \frac{\frac{\sum_{i=1}^n (X_i - \bar{x})^4}{n}}{S^4}$$

where

- \bar{x} = monthly average;
- S = monthly standard deviation;
- α_3 = monthly kurtosis;
- α_4 = monthly skewness;
- X_i = value of a data element on the i th day; and
- n = number of days with records in a month.

Where some daily data were missing, the monthly statistical parameters were to be calculated using the available data only, without substitution for missing data. In addition, the following "derived" data were to be calculated and ultimately stored in the LTPP climatic data base:

- Total monthly precipitation,
- Total monthly snowfall,
- Number of air freeze-thaw cycles (monthly),
- Mean daily temperature range (monthly),
- Number of wet days (precipitation > 0.01 in.),
- Number of high-intensity precipitation days (precipitation > 0.5 in.),
- Air freezing index,
- Number of days with maximum temperatures above 90°F (monthly), and
- Number of days with minimum temperature below 32°F (monthly).

It should be clearly noted that the average monthly values to be stored within the data base were to be average daily values for that parameter for that month. For example, the average precipitation field for a particular month would contain the average daily precipitation for that month.

Of these calculated parameters, only the air freezing index and air freeze-thaw cycles are complex. For the air freezing index, each day's minimum temperature is compared with 32°F (0°C for Canadian GPS sites), and if it is below freezing, the number of degrees below freezing is added to both the current month's air freezing index and the current year's air freezing index. If the daily minimum temperature is missing, the missing data count is incremented for both the monthly count and the yearly count. Air freeze-thaw cycles are calculated by comparing daily minimum (TMIN) and daily maximum (TMAX) temperatures to the freezing point and to each other. Each air freeze-thaw cycle consists of one sequence of a TMIN below freezing followed by a TMAX above freezing followed by a TMIN below freezing.

In addition to the climatic data elements, it was recommended that the following information be stored in the climatic data base to characterize the weather stations: weather station name, number, and type (first order or cooperative); distance from applicable SHRP test site; elevation; bearing with respect to test site; and data coverage for temperature and moisture.

Several other data elements were considered for inclusion in the climatic data base but were rejected for one or more reasons. Thornthwaite moisture index (TMI) was not included because of the lack of pan evaporation data needed to calculate values, and because it was believed that storage of values derived from contour maps, which are widely available, was not warranted.

Another example of a data element initially intended to be included is solar radiation. Solar radiation data were indeed collected by NCDC until 1984 at a few sites. At some point before that date, however, it was discovered that the measured values were highly unreliable, and NCDC terminated their collection. There have been several efforts since that date to correct the collected data, but they have thus far proven ineffective. Consequently, SHRP elected not to store these suspect values.

Climatic Data Base

Once the climatic data elements and sources of information had been established, the last step in the development of the

TABLE 1 Climatic Data Elements

Data Element	NCDC Designation
1. Maximum Daily Temperature	TMAX
2. Minimum Daily Temperature	TMIN
3. Mean Daily Temperature	MNTP
4. Daily Precipitation	PRCP
5. Daily Snowfall	SNOW
6. Daily Occurrence of Weather	DYSW
7. Daily Average Wind Speed	AWND
8. Peak Gust Wind Speed and Direction	PKGS
9. Percent of Possible Sunshine	PSUN
10. Average Sky Coverage - Sunrise to Sunset	SCSS
11. Average Sky Coverage - Midnight to Midnight	SCMM
12. Daily Minimum Relative Humidity	MNRH
13. Daily Maximum Relative Humidity	MXRH

data base dealt with the formulation of the data base. In view of the massive data storage requirements (estimated at 3 gigabytes) and after much deliberation, a data base structure composed of three levels was recommended. Details of the recommended data base organization are as follows.

- *Raw climatic data:* The lowest level of the data base (referred to as the "low-level" data base) would consist of daily NCDC and CCC data cleansed of unnecessary codes and flags and stored "off-line" on long-term storage media. The data would be stored in the original system of units [U.S. customary for NCDC data and International System (SI) for CCC data] for individual weather stations, without direct linkage to individual pavement test sites. Statistical parameters would not be stored at this level.

- *Daily data, statistical parameters, and derived data:* The second level of the data base (referred to as the "middle-level" data base) would include daily data for individual weather stations and a virtual weather station corresponding to each test section, as well as the calculated statistical parameters and derived data for all of these stations. Data for the virtual station would be created using the following interpolation algorithm:

$$V_m = \frac{\sum_{i=1}^k \left(\frac{V_{mi}}{R_i^2} \right)}{\sum_{i=1}^k \left(\frac{1}{R_i^2} \right)}$$

where

- V_{mi} = value of a data element on day m , station i ;
- R_i = distance of weather station i from the site;
- V_m = calculated data element for Day m for the virtual weather station; and
- k = number of weather stations for the site (up to five).

All data at this level would be stored in U.S. customary units for U.S. GPS sites and SI units for Canadian GPS sites. Also, the data would be stored off-line and would be associated with specific test sites for easy recovery.

- *Monthly summary data:* The final level of the data base (referred to as the "top-level" data base) would contain monthly summary data (calculated statistical parameters and derived data) from the individual weather stations as well as the virtual station. This portion of the climatic data base would be included in the National Pavement Performance Data Base (NPPDB).

As the storage scheme outlined above was being developed, consideration was given to processing the data and retaining only the final "virtual" values in NPPDB, with the thought that researchers desiring more detailed data could always go to NCDC and CCC for the original data. However, the members of the Environmental Data ETG believed strongly that this was not an appropriate course because a significant number of researchers were likely to want the raw data and should not have to duplicate SHRP's efforts to acquire the information. They also believed that it was important to have the real weather station data alongside the virtual data, so that researchers could evaluate the viability of the virtual data for themselves, in light of the individual weather station values. Also, it was suggested that the use of data from the closest weather station would be preferable to the use of virtual data in some instances. Thus, it was recommended that both measured and virtual data be stored in the NPPDB.

DATA COLLECTION AND QUALITY ASSURANCE

Upon approval of the plans, work began in earnest toward the physical development of the LTPP climatic data base. To make this process as efficient and cost-effective as possible, it was decided to subcontract the actual data collection and data base population effort to a company experienced with

this type of work. The major objectives of the subcontractor's work effort were

- To identify weather stations in the vicinity of pavement test sites included in the GPS study, and
- To acquire and process data from various weather stations for each of the above sites and to develop the climatic data base following specifications established by SHRP.

In essence, the end product of this effort was to be the development of the climatic data base for 777 GPS test sites.

To accomplish these objectives, three separate phases were undertaken. Under Phase I, the subcontractor was required to identify weather stations in the vicinity of the GPS pavement test sites using the criteria detailed earlier and approved by the Environmental Data ETG and to provide the list of weather stations to SHRP for review and approval. The Phase II work effort addressed the likely need for the identification of additional weather stations as a result of the addition of more pavement test sites to the GPS experiments or to replace, for one reason or another, those previously identified. Finally, under Phase III, the subcontractor was required to obtain and process the data for the final list of weather stations. It was initially estimated that 300 first-order and 2,000 cooperative weather stations would be used in the development of the climatic data base for the GPS experiments.

Selection of Weather Stations and Data Base Population

Formal development of the LTPP climatic data base began with the submission of the list of GPS test sites to the subcontractor. Using the latitude and longitude data provided for each test site on this list, the subcontractor identified the required five weather stations in the vicinity of the GPS test sites that satisfied the criteria discussed earlier.

After the initial weather station identification (and during the course of the necessary reselections), the four SHRP Re-

gional Coordination Office (RCO) contractors were asked to assist in an evaluation of the degree to which the five weather stations identified for each GPS test site in their region were believed to represent conditions at the site. Each RCO was provided with the list of GPS test sites and the corresponding weather stations. In addition, guidelines were prepared to aid the RCO in this evaluation—for example, input from the state climatologists, weather-station-to-site distance, elevation difference, and terrain considerations.

The degree to which the selections were reviewed varied significantly from region to region according to whether the review was done directly by the RCO or whether the RCO relied on the state climatologists to perform the review. When the state climatologists were relied on, results were often delayed until long after the data collection had been completed; thus relatively few weather stations were rejected as being nonrepresentative of the weather conditions at the GPS site.

In the western region, however, an extensive in-house review was undertaken because of concerns regarding the rough terrain and long distances between weather stations and the GPS sites; this region represents the worst case in terms of the relationship between weather station and test sections. All GPS sites and their selected weather stations were located on large-scale topographical maps. All weather stations determined to be on opposite sides of a mountain ridge from the GPS site were deemed nonrepresentative. Similarly, weather stations at elevations significantly different from those at the GPS site were also deemed nonrepresentative.

All in all, the review of weather stations by the RCOs resulted in the rejection of more than 200 (of a total of more than 3,000). Also, a few additional GPS test sites were added to the original list. As a consequence, a follow-up effort was undertaken to identify new or alternative weather stations. Tables 2 through 4 give the final distribution of weather stations by distance and elevation difference to the site, categorized by type of weather station. The distribution of accepted weather stations per site is shown below (only 24 GPS sites are represented by fewer than three weather stations):

TABLE 2 First-Order Weather Station Distance and Elevation Difference Distribution

Elevation Difference (feet)	Distance (miles)							rejected	Grand total
	0 - 10	10 - 20	20 - 30	30 - 40	40 - 50	50+			
0 - 100	66 (8.5%)	70 (9.0%)	45 (5.8%)	31 (4.0%)	29 (3.7%)	69 (8.9%)	0 (0.0%)	310 (39.9%)	
100 - 200	8 (1.0%)	29 (3.7%)	27 (3.5%)	25 (3.2%)	13 (1.7%)	34 (4.4%)	0 (0.0%)	136 (17.5%)	
200 - 300	5 (0.6%)	9 (1.2%)	7 (0.9%)	14 (1.8%)	11 (1.4%)	27 (3.5%)	0 (0.0%)	73 (9.4%)	
300 - 400	5 (0.6%)	7 (0.9%)	5 (0.6%)	11 (1.4%)	3 (0.4%)	14 (1.8%)	0 (0.0%)	45 (5.8%)	
400 - 500	3 (0.4%)	1 (0.1%)	2 (0.3%)	2 (0.3%)	5 (0.6%)	15 (1.9%)	0 (0.0%)	28 (3.6%)	
500+	1 (0.1%)	4 (0.5%)	16 (2.1%)	10 (1.3%)	8 (1.0%)	41 (5.3%)	0 (0.0%)	80 (10.3%)	
rejected	0 (0.0%)	0 (0.0%)	0 (0.0%)	0 (0.0%)	0 (0.0%)	0 (0.0%)	105 (13.5%)	105 (13.5%)	
Grand total	88 (11.3%)	120 (15.4%)	102 (13.1%)	93 (12.0%)	69 (8.9%)	200 (25.7%)	105 (13.5%)	777 (100.0%)	

TABLE 3 Active Cooperative Weather Station Distance and Elevation Difference Distribution

Elevation Difference (feet)	Distance (miles)							Grand total
	0 - 10	10 - 20	20 - 30	30 - 40	40 - 50	50+	rejected	
0 - 100	329 (42.3%)	121 (15.6%)	18 (2.3%)	0 (0.0%)	0 (0.0%)	1 (0.1%)	0 (0.0%)	469 (60.4%)
100 - 200	70 (9.0%)	59 (7.6%)	12 (1.5%)	2 (0.3%)	0 (0.0%)	0 (0.0%)	0 (0.0%)	143 (18.4%)
200 - 300	44 (5.7%)	17 (2.2%)	2 (0.3%)	0 (0.0%)	0 (0.0%)	0 (0.0%)	0 (0.0%)	63 (8.1%)
300 - 400	17 (2.2%)	13 (1.7%)	2 (0.3%)	1 (0.1%)	0 (0.0%)	0 (0.0%)	0 (0.0%)	33 (4.3%)
400 - 500	8 (1.0%)	7 (0.9%)	1 (0.1%)	0 (0.0%)	0 (0.0%)	0 (0.0%)	0 (0.0%)	16 (2.1%)
500+	24 (3.1%)	22 (2.8%)	4 (0.5%)	0 (0.0%)	0 (0.0%)	0 (0.0%)	0 (0.0%)	50 (6.4%)
rejected	0 (0.0%)	0 (0.0%)	0 (0.0%)	0 (0.0%)	0 (0.0%)	0 (0.0%)	3 (0.4%)	3 (0.4%)
Grand total	492 (63.3%)	239 (30.8%)	39 (5.0%)	3 (0.4%)	0 (0.0%)	1 (0.1%)	3 (0.4%)	777 (100.0%)

No. of Accepted
Weather Stations

5
4
3
2
1

No. of Sites

634
86
33
18
6

On completion of the weather station selection process, the focus shifted to the retrieval of the climatic data for each selected weather station (see Table 1 for a list of the data elements extracted from the NCDC and CCC files). Processing of the raw data also yielded various monthly statistics and other "derived" data elements for inclusion in the climatic data base. These additional data elements and their derivations were discussed earlier.

Concurrent with the above effort, various activities were undertaken to finalize the structure of the climatic data base. Following the recommendations provided in the plans, the data base was defined as being made up of three levels: (a) raw

climatic data (low level); (b) daily data, statistical parameters, and derived data (middle level); and (c) monthly summary data (high level). A description of each level was provided earlier. Next, the structure of each level and that of individual records within each level were finalized as were the formats for the various data elements. Finally, the computer code required to calculate the monthly statistics and other derived data was developed.

In all, 37 nine-track tapes containing over 3 gigabytes of climatic data were generated. The low-level data base contains 17 tapes with a total of 1.5 gigabytes of data. The middle-level data base also contains 17 tapes, with a total of 1.4 gigabytes of data. The top level of the data base contains three tapes with a total of 0.22 gigabyte of data. To ensure the quality of the data contained in these tapes, a series of checks was performed on them. These quality assurance checks and their outcome are discussed in the next section. After the successful completion of the quality checks, all three levels of the climatic data base were turned over to TRB, where

TABLE 4 Regular Cooperative Weather Station Distance and Elevation Difference Distribution

Elevation Difference (feet)	Distance (miles)							Grand total
	0 - 10	10 - 20	20 - 30	30 - 40	40 - 50	50+	rejected	
0 - 100	105 (4.5%)	423 (18.1%)	372 (16.0%)	78 (3.3%)	7 (0.3%)	3 (0.1%)	0 (0.0%)	988 (42.4%)
100 - 200	43 (1.8%)	160 (6.9%)	215 (9.2%)	37 (1.6%)	5 (0.2%)	0 (0.0%)	0 (0.0%)	460 (19.7%)
200 - 300	23 (1.0%)	104 (4.5%)	108 (4.6%)	25 (1.1%)	2 (0.1%)	2 (0.1%)	0 (0.0%)	264 (11.3%)
300 - 400	10 (0.4%)	50 (2.1%)	58 (2.5%)	19 (0.8%)	1 (0.0%)	0 (0.0%)	0 (0.0%)	138 (5.9%)
400 - 500	9 (0.4%)	34 (1.5%)	35 (1.5%)	19 (0.8%)	0 (0.0%)	0 (0.0%)	0 (0.0%)	97 (4.2%)
500+	16 (0.7%)	106 (4.5%)	107 (4.6%)	27 (1.2%)	5 (0.2%)	0 (0.0%)	0 (0.0%)	261 (11.2%)
rejected	0 (0.0%)	0 (0.0%)	0 (0.0%)	0 (0.0%)	0 (0.0%)	0 (0.0%)	123 (5.3%)	123 (5.3%)
Grand total	206 (8.8%)	877 (37.6%)	895 (38.4%)	205 (8.8%)	20 (0.9%)	5 (0.2%)	123 (5.3%)	2331 (100.0%)

the NPPDB is now located. Both the low- and middle-level data bases are being stored off-line, whereas the top-level data base is stored in the NPPDB. Only data for the closest and virtual weather stations are currently in the NPPDB for each GPS test site because of storage limitations. An example of a portion of the top-level data is contained in Table 5.

Data Quality Assurance

To ensure the reliability of the data stored in the climatic data base, only data flagged as valid from NCDC and CCC were used in the development process. Additional quality control procedures included verification that all ordered and available data had been obtained and a thorough checking and review of the software used in the development of the data base. Furthermore, because there is a substantial amount of data in each level of the data base, quality assurance checks were performed separately on each level; for example, all tapes were checked for readability and completeness.

Readability checks included verifying that the data areas of the tapes contain only numeric characters. Any nonnumeric data found there indicated that either the tape was corrupted or the hardware had failed. Many of the checks described above were performed in a random fashion, with data observed throughout the entire data set. Where appropriate, virtual weather station data were compared with data from

the nearest available weather station when they were in close proximity, to evaluate whether the calculated data were reasonably close to the measured data. Where both U.S. and Canadian weather stations were selected, samples of data were checked to determine whether unit conversions were performed appropriately. Also, for a small group of GPS sites and their selected weather stations, the entire set of data was entered on the data collection forms to verify that the forms and the computerized data collection process matched.

Finally, an additional set of NPPDB data checks is currently under way. These checks generally take several different forms. From the point of view of completeness of the data base, some data elements are checked simply to ensure their presence. Other data elements are checked against a range of values for that type of parameter to flag those that are out of the range of normal values. Still other data elements are checked against values contained in other data tables to maintain internal consistency. The climatic data base will not be released to the public until it has passed these quality assurance checks.

FUTURE ACTIVITIES

Although significant effort has been spent on the development of SHRP's LTPP climatic data base, the work is far from complete. First, the climatic data currently available in the data base end somewhat before the writing of this paper. Because the majority of LTPP sections will be monitored for many years to come, future updates of the climatic data base will be required periodically. Also, despite the data base development effort to date, there are gaps in the data for a number of weather stations and some weather stations may not be representative of on-site weather conditions. To address both of these concerns, the feasibility of obtaining ground truth (actual or on-site) weather data through on-site weather stations needs to be investigated. Finally, it is important that an effort similar to the one discussed in this paper be undertaken to expand the LTPP climatic data base to include SPS tests sites. These three issues are discussed further.

Data Base Updates

The majority of SHRP sections, both GPS and SPS, will be monitored for many years. However, the climatic data currently stored in the LTPP data base includes information only through February 1991 for U.S. sites and through December 1989 for Canadian sites. Thus, future updates of the climatic data base will be required periodically. Current recommended plans call for these updates to be performed ever 2 years for each active GPS test site. As part of these updates, weather stations that have become inactive would be replaced by other weather stations of the same order (first order or cooperative) or higher. At the same time, a check would be made to verify whether any new stations have been established closer to the site than stations already included in the data base. In case such stations are identified, these stations will be added to the data base and new data for other existing weather stations

TABLE 5 Sample Top-Level Virtual Data for GPS Site 480001

Max Temperature					
(degrees F)	Jan	Feb	Mar	Apr	May
Average	68.06	69.57	70.00	79.06	87.90
Std Dev	8.326	7.946	8.858	6.601	5.889
Skewness	-0.617	-0.424	-1.390	-0.390	-0.541
Kurtosis	2.640	2.062	4.291	3.025	2.089
Frz/Thw	1	0	0	0	0
Miss Cnt	0	0	0	0	0
# >90	0	0	0	1	15
Min Temperature					
(degrees F)	Jan	Feb	Mar	Apr	May
Average	45.93	47.28	52.12	59.06	67.67
Std Dev	9.121	5.912	9.545	7.277	6.905
Skewness	0.569	0.185	0.089	-0.277	-0.448
Kurtosis	2.678	2.805	1.688	2.080	1.942
Frz Index	0	0	0	0	0
Miss Cnt	0	0	0	0	0
# <32	0	0	0	0	0
Precipitation					
(inches/100)	Jan	Feb	Mar	Apr	May
Average	4.26	12.32	8.55	10.76	11.80
Std Dev	8.644	24.310	21.110	34.510	38.120
Skewness	2.166	2.067	4.048	4.314	4.246
Kurtosis	6.393	6.080	20.160	21.700	21.340
Total	132	345	265	323	366134
# >0.5	0	3	1	1	3
# >0.01	12	11	15	11	11
Snowfall					
(inches/10)	Jan	Feb	Mar	Apr	May
Average	0	0	0	0	0
Std Dev	0	0	0	0	0
Skewness	-9999	-9999	-9999	-9999	-9999
Kurtosis	-9999	-9999	-9999	-9999	-9999
Total	0	0	0	0	0

will not be collected. Historic data will be maintained in the data base even after a station has been dropped.

As the analysis of the LTPP data progresses, it may become necessary to collect and store additional data elements. Likewise, additional activities may be necessary in the future, depending on the result of the climatic data base verification study discussed below.

Collection of Ground Truth Data

Despite the effort that went into the development of the LTPP climatic data base, there are gaps in the data for a number of the weather stations selected. Furthermore, data obtained from the selected weather stations may not be representative of the actual, on-site weather conditions for a number of sites. To overcome these shortcomings, it is planned to obtain ground truth weather data to achieve the following:

- Evaluate the degree to which estimates derived from NCDC and CCC weather data are representative of actual, on-site weather conditions and
- Provide weather data for those sites for which no representative weather stations have been identified or to fill in gaps in the available data.

To analyze the uniformity in the weather pattern in the area of the test sites, the weather information from each of the selected weather stations will be compared statistically with virtual data derived from the others. Depending on the results of this analysis, the correlation between the weather stations and the location of the test site can be estimated. This analysis will consider only temperature and moisture, represented by mean temperature and total precipitation. It is further anticipated that the above analysis will be supplemented (and validated) by weather data obtained from weather stations installed at or near a limited number of GPS test sites.

On completion of the analysis of degree of representativeness, it is likely that on-site or ground truth weather stations will be required at a number of GPS test sites. As an absolute minimum, these weather stations would collect temperature, precipitation, and snowfall data. Other data elements such as wind speed and relative humidity would also be considered, but their inclusion would depend on a number of factors, including financial constraints.

Expansion to SPS Experiments

The availability of climatic data is as critical for SPS experiments as for the GPS experiments. The data elements given in Table 1 are also considered essential for each SPS site. In general, it is anticipated that a procedure similar to that described for the GPS sites will be followed to obtain climatic data for SPS sites. These data will be collected at a later date because the SPS experiments are very young. Also, in some cases, a more rigorous data collection effort may be required—that is, installation and operation of a weather station at the sites if a weather station is not located in the

proximity of the test site. State climatologists will be requested to provide input regarding adjacent weather stations and the extent of their representativeness of the climate conditions at the test site before the data collection approach is selected.

Tentatively, the following guidelines have been established to assess the representativeness of the weather stations:

- Mean daily temperature (monthly) should be within 10 percent of that at the weather station.
- Daily precipitation (monthly) and daily snowfall (monthly) at the test site should be within 20 percent of that at the weather station.

If the weather station data do not meet these requirements, or if other reasons exist for not considering adjacent weather stations (poor quality of data, potential closure, etc.), a cooperative-type weather station will likely be established for these test sites. It is anticipated that since many of the test sites will be in remote locations, use will be made of commercially available weather stations capable of measuring the necessary climatic data. The use of these weather stations will also permit collection of solar radiation data at a few test sites.

SUMMARY AND CONCLUSIONS

This paper presents details on the development of the climatic data base for LTPP test sections. For the GPS test sites that have been in service, generally for a large number of years, past climatic data had to be collected from in-service weather stations in both the United States and Canada. Thus, the data base provides the best available estimate for the climatic data at each GPS test section. Efforts are currently under way to determine the reliability of the data base and to identify the need for ground truth weather stations at a small number of test sections.

The resulting data base is one of the most comprehensive climatic data bases developed; it contains climatic data applicable to each GPS test section from the date of construction of that section. The data base will be regularly updated as the LTPP program continues for another 15 years. A similar data base also will be developed for the SPS test sites. In addition, a more rigorous data collection effort (i.e., installation and operation of on-site weather station) will be implemented at a number of GPS and SPS sites to ensure that climatic data collected for these sites are truly representative.

ACKNOWLEDGMENTS

The work described in this paper was performed by PCS/Law Engineering under contract to the Strategic Highway Research Program, National Research Council. The authors gratefully acknowledge the cooperation and assistance of the SHRP staff; the SHRP Expert Task Group on Environmental Data, chaired by Richard Berg; the SHRP regional coordination contractors; and EarthInfo, Inc., the LTPP climatic data base subcontractor.

REFERENCES

1. *Development of SHRP's LTPP Climatic Database*. Draft Technical Report. Strategic Highway Research Program, National Research Council, Washington, D.C., 1992.
2. *Data Collection Guide for Long-Term Pavement Performance Studies*. Operational Guide SHRP-LTPP-OG-001. Strategic Highway Research Program, National Research Council, Washington, D.C., Jan. 1990.

The publication of this paper does not necessarily indicate approval or endorsement by the National Academy of Sciences, the United States government, or AASHTO or its member states of the findings, opinions, conclusions, or recommendations either inferred or specifically expressed herein.

Publication of this paper sponsored by Committee on Flexible Pavement Design.

Remaining Fatigue Life Analysis: Comparison Between Dense-Graded Conventional Asphalt Concrete and Gap-Graded Asphalt-Rubber Hot Mix

LUTFI RAAD, STEPHAN SABOUNDJIAN, AND JOHN CORCORAN

A procedure for estimating the remaining fatigue life of existing bituminous pavements has been developed. This procedure incorporates laboratory fatigue data for tensile strain or surface curvature in terms of repetitions to failure. It also utilizes laboratory data on reduction of flexural stiffness with load repetitions. The proposed method was applied to investigate the remaining fatigue life of a dense-graded conventional asphalt concrete mix (CAC-DG) and a gap-graded asphalt-rubber hot mix (ARHM-GG) using laboratory flexure fatigue data and multilayer elastic analysis of typical pavement sections. Results show that for a given initial state of fatigue damage, the remaining fatigue life of ARHM-GG could be significantly longer than that of CAC-DG. It is also illustrated that thinner sections of ARHM-GG, compared with CAC-DG, will exhibit the same remaining fatigue life. This reduction in thickness becomes more significant with increasing foundation support under the pavement surface layer.

The use of asphalt-rubber binder in pavements has progressed from its application in asphalt-rubber and aggregate membranes (ARAM), also referred to as stress-absorbing membranes (SAM), and ARAM interlayers, also referred to as stress-absorbing membrane interlayers (SAMI), which began in 1968, to the incorporation of asphalt-rubber hot mix (ARHM) in pavement overlays, which began in 1975 (1-3). In addition to overlays, asphalt-rubber mixtures have been used as a surface course in reconstructed pavement sections (4). Field performance data on ARHM pavements indicate significant improvement in resistance to fatigue, abrasion, and aging compared with conventional asphalt concrete mixtures (5,6). These field data support laboratory fatigue test results that illustrate improved fatigue and fracture properties of asphalt-rubber mixtures compared with conventional asphalt concrete (7-9). Results of a recent study by Raad et al. (8) show that overlay thickness determinations using laboratory fatigue data support recommendation guidelines proposed by the California Department of Transportation (Caltrans) on overlay thickness equivalencies between gap-graded ARHM (ARHM-GG) and dense-graded conventional asphalt concrete (CAC-DG). Although asphalt-rubber overlays seem to provide a cost-effective option for pavement rehabilitation (2,7), the determination of the remaining fatigue life of the existing

pavement needs to be assessed for the purpose of improved overlay thickness selection. This assessment would be essential particularly in lieu of research presented by Seebaly et al. (10) indicating a lag between structural capacity reduction and surface cracking of field test sections. In this case, the back-calculated moduli of the asphalt layer were reduced by 50 percent before lineal cracking, or before AASHO Class 2 and 3 cracking was observed on the pavement surface. Structural damage in terms of reduction of the modulus of the bituminous surface therefore occurs before any visual fatigue cracking in the pavement. Such deterioration could be assessed through nondestructive testing using, for example, the falling weight deflectometer (FWD).

In this paper, a procedure for estimating the remaining fatigue life of existing bituminous pavements is summarized. The proposed method utilizes flexure fatigue data for ARHM-GG and CAC-DG. The remaining life is expressed in terms of the reduction of the modulus of the pavement surface and the applied wheel load and does not require knowledge of previous wheel load magnitudes and repetitions. In this respect, the proposed method provides a definite advantage over current procedures that use Miner's cumulative damage hypothesis (11) to estimate remaining life. Fatigue criteria are expressed in terms of (a) flexure tensile strains and (b) surface curvature. Results are used to compare the fatigue behavior of ARHM-GG and CAC-DG pavements. Specifically, the number of load repetitions required to induce a given degree of fatigue damage are compared. In addition, the remaining fatigue life of ARHM-GG and CAC-DG pavements is determined for similar sections with the same degree of fatigue damage (i.e., equal reduction in surface layer modulus). Thickness equivalencies between ARHM-GG and CAC-DG pavements associated with fatigue performance are also established using both strain and curvature criteria.

EXPERIMENTAL WORK

Materials

CAC-DG and ARHM-GG beam specimens were obtained from new pavement sections that were constructed in California for the purpose of comparing the field performance of CAC-DG and ARHM-GG materials. The crumb rubber ma-

L. Raad and S. Saboundjian, Transportation Research Center, Institute of Northern Engineering, University of Alaska Fairbanks, Fairbanks, Alaska 99775. J. Corcoran, Manhole Adjusting Inc., 2300 Greenwood Ave., P.O. Box 250, Monterey Park, Calif. 91754.

material used is scrap tire, vulcanized, with a specific gravity of 1.15 to 1.20, containing a minimum of 25 percent natural rubber. All materials meet Caltrans specifications. A summary of specifications for aggregate gradations, asphalt-rubber binder properties, and CAC-DG and ARHM-GG properties is presented in Tables 1 and 2.

Fatigue Testing

The fatigue behavior of CAC-DG and ARHM-GG was investigated using controlled strain flexure beam testing. A detailed description of the testing procedure and equipment is presented elsewhere (8). The beam specimens were cut to about 2 in. by 2 in. by 15 in. and were loaded at 5-in. interval third points. The density of the CAC-DG specimens varied between 152 lb/ft³ and 153 lb/ft³, whereas the density of ARHM-GG specimens varied in the range of 146 lb/ft³ and 148 lb/ft³. All tests were conducted using MTS Systems Corporation closed-loop hydraulic testing equipment and a haversine displacement pulse with a width of 0.10 sec and a frequency of 60 cpm. Fatigue tests were performed in an environmental chamber, and the temperature of the specimens was main-

tained between 70°F and 73°F. For a given displacement pulse, the variation of applied load and tensile and compressive strains across the center of the beam specimen was monitored with a number of pulse applications. Fatigue failure was assumed to occur when the flexure stiffness (E) determined from the central beam deflections and the applied load using simple beam theory assumptions was reduced by 50 percent.

Results

Fatigue criteria were developed in terms (a) maximum tensile strain in the middle beam section and (b) central beam curvature, with number of load repetitions to failure. These criteria are shown in Figure 1. The strain criterion is expressed as follows. For CAC-DG

$$N_f = 1.471 \times 10^{-10} \left(\frac{1}{\epsilon_t} \right)^{4.55} \quad (r^2 = 0.93) \quad (1)$$

For ARHM-GG

$$N_f = 2.350 \times 10^{-12} \left(\frac{1}{\epsilon_t} \right)^{5.41} \quad (r^2 = 0.93) \quad (2)$$

TABLE 1 Mix Aggregate Gradation Specification Limits for CAC-DG and ARHM-GG

Sieve Size	Percent Passing			
	Per Specification		Actual Field Results	
	CAC Dense Graded	ARHM Gap Graded	CAC Dense Graded	ARHM Gap Graded
3/4 in.	100	100	100	100
1/2 in.	95-100	90-100	97	96
3/8 in.	80-95	78-92	91	78
No. 4	59-66	28-42	68	39
No. 8	43-49	15-25	53	28
No. 30	22-27	5-15	35	16
No. 200	0-11	2-7	13	4.7
Asphalt Binder %	5.2 - 6.5	7.5 - 8.7	6.2	7.9

Note:
 Asphalt Cement (AR-4000) in CAC-DG
 Components of Asphalt-Rubber Binder:
 AR-4000 Asphalt Cement
 2% - 6% Asphalt Modifier (by total weight of Asphalt-Rubber binder)
 78% - 82% Asphalt Cement and Modifier
 18% - 22% Rubber

CAC-DG Caltrans Standard Specifications, 1988 Edition, Section 39-2.02
 ARHM-GG Proposed Standard Specifications for Public Works Construction, Section 203-11.3

TABLE 2 Properties of Asphalt-Rubber Binder

Property	Specification Limits	Actual Average Results of Binder Tested
Field Viscosity, Haake at 375 °F in Centipoise (ASTM D2669)	1350 - 3050	1775
Penetration, Cone at 77 °F in 1/10 mm (ASTM D217)	20 - 70	51
Resilience 77 °F in Percent Rebound (ASTM D3407)	15 Minimum	27
Field Softening Point in °F (ASTM D36)	125 - 165	142

where ϵ_t is the tensile strain and N_f is the number of repetitions to failure.

The curvature criterion, on the other hand, can be written in terms of curvature (ρ) or the inverse of the radius of curvature ($1/R$) at the center of the beam as follows. For CAC-DG

$$N_f = 8.232 \times 10^{-12} \left(\frac{1}{\rho}\right)^{4.94} \quad (r^2 = 0.90) \quad (3)$$

For ARHM-GG

$$N_f = 4.205 \times 10^{-13} \left(\frac{1}{\rho}\right)^{5.68} \quad (r^2 = 0.92) \quad (4)$$

where ρ is $(\epsilon_t + \epsilon_c)/h$; h is beam thickness in inches; ϵ_t , ϵ_c are tensile and compressive strains at the top and bottom of the middle beam section, respectively.

It is interesting to note that the curvature criterion incorporates the thickness of the beam in the fatigue equation. This implicitly implies that, for a given strain condition, thicker beam sections will exhibit longer fatigue life. This finding is consistent with fatigue fracture propagation described by the Paris law and applied to asphalt concrete and asphalt-rubber hot mix (7).

Fatigue damage associated with a given number of load applications can be described as a loss in flexural stiffness. The reduction in flexural stiffness, tensile stiffness, and compressive stiffness for both CAC-DG and ARHM-GG as deduced from the fatigue tests is shown in Figure 2. Tensile and compressive stiffness in this case are determined from the applied load and the measured tensile and compressive strains at the top and bottom of the middle section of the beam specimen. As shown, the loss in stiffness seems to proceed at

a much faster rate after 10^3 repetitions for CAC-DG compared with ARHM-GG, in which the decrease proceeds at a slower rate. Best-fit correlations of the stiffness reduction defined as the ratio of flexural stiffness E after N load applications to the initial flexural stiffness E_i are developed in terms of tensile strain ϵ_t and beam curvature ρ as follows. For CAC-DG

$$\left(\frac{E}{E_i}\right) \cdot (\epsilon_t)^{1/4} = 0.19056 - 0.01964 \cdot \log N \quad (r^2 = 0.74) \quad (5)$$

$$\left(\frac{E}{E_i}\right) \cdot (\rho)^{1/4} = 0.18832 - 0.01919 \cdot \log N \quad (r^2 = 0.73) \quad (6)$$

For ARHM-GG

$$\left(\frac{E}{E_i}\right) \cdot (\epsilon_t)^{1/4} = 0.17226 - 0.01509 \cdot \log N \quad (r^2 = 0.76) \quad (7)$$

$$\left(\frac{E}{E_i}\right) \cdot (\rho)^{1/4} = 0.17288 - 0.01501 \cdot \log N \quad (r^2 = 0.77) \quad (8)$$

The results of stiffness reduction E/E_i are shown in Figures 3 and 4. These results indicate that for a given repetition of ϵ_t or ρ , the reduction in E will be slightly higher for CAC-DG compared with ARHM-GG, thereby exhibiting more fatigue damage.

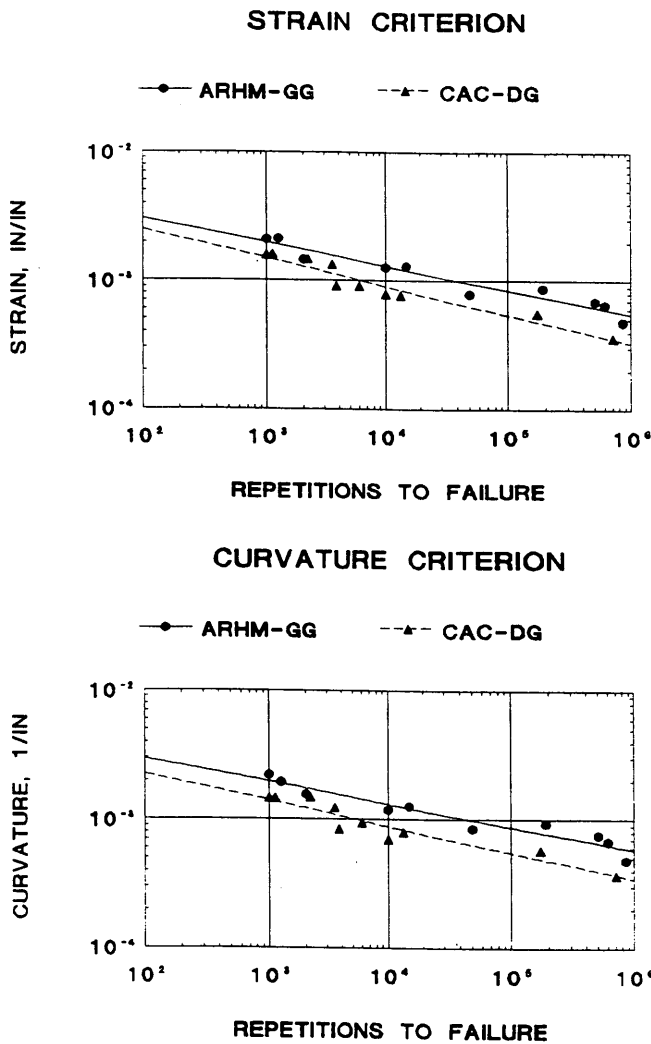


FIGURE 1 Fatigue failure criteria for CAC-DG and ARHM-GG.

REMAINING LIFE ANALYSIS

The remaining fatigue life for a pavement with a given E/E_i is defined as the number of repetitions of a given load (expressed in terms of tensile strain or surface curvature) required to induce ultimate fatigue damage by reducing E/E_i to 0.50. The remaining fatigue life can be estimated using the laboratory-determined relations for E/E_i in terms of load repetitions and applied tensile strain or surface curvature (Equations 5 through 8). For a given fatigue damage, expressed as E/E_i , these equations can be used to determine the equivalent number of repetitions (N_e) of a given load provided the corresponding load-induced strain or curvature is known. In this case, a remaining fatigue life factor (R_f) could be defined as

$$R_f = 1 - \frac{N_e}{N_f} \tag{9}$$

where N_e and N_f are both determined from Equations 5 through 8, depending on the mix type (CAC-DG or ARHM-GG) and

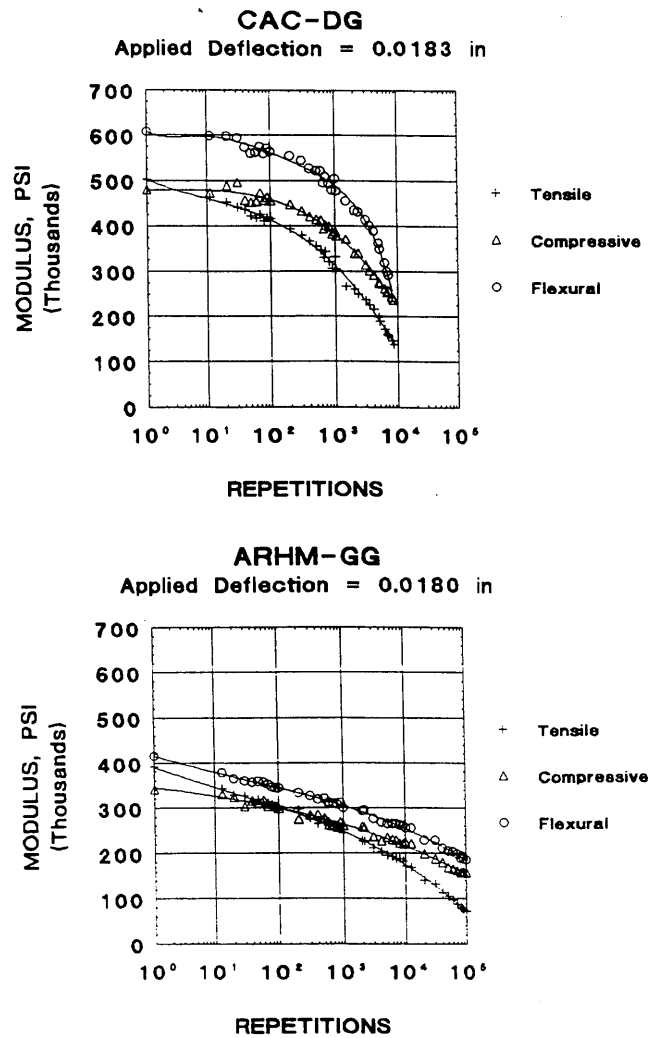


FIGURE 2 Variation of stiffness with load repetitions for CAC-DG and ARHM-GG.

strain or curvature criterion applied. N_f is the number of repetitions to failure for a new pavement estimated by substituting $E/E_i = 0.50$. For CAC-DG

$$R_f = 1 - 10^{-[(E/E_i - 0.50)/0.01964] \cdot \epsilon_i^{1/4}} \tag{10}$$

$$R_f = 1 - 10^{-[(E/E_i - 0.50)/0.01919] \cdot \rho^{1/4}} \tag{11}$$

For ARHM-GG

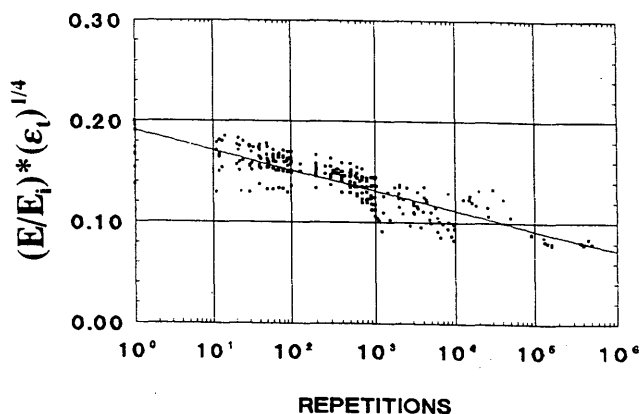
$$R_f = 1 - 10^{-[(E/E_i - 0.50)/0.01509] \cdot \epsilon_i^{1/4}} \tag{12}$$

$$R_f = 1 - 10^{-[(E/E_i - 0.50)/0.01501] \cdot \rho^{1/4}} \tag{13}$$

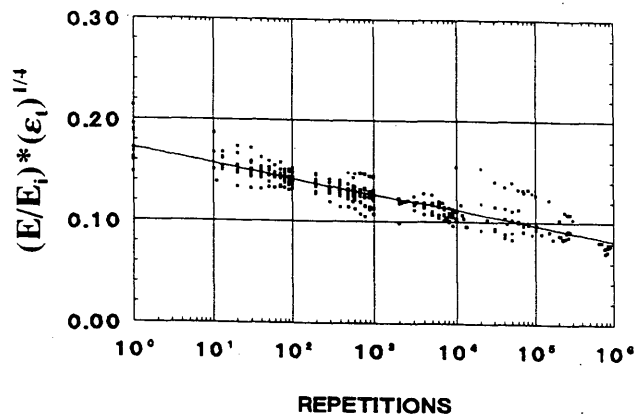
The corresponding remaining fatigue life N_{rf} can then be expressed as follows. For the strain criterion

$$N_{rf} = R_f \cdot (A1) \cdot \left(\frac{1}{\epsilon}\right)^{A2} \tag{14}$$

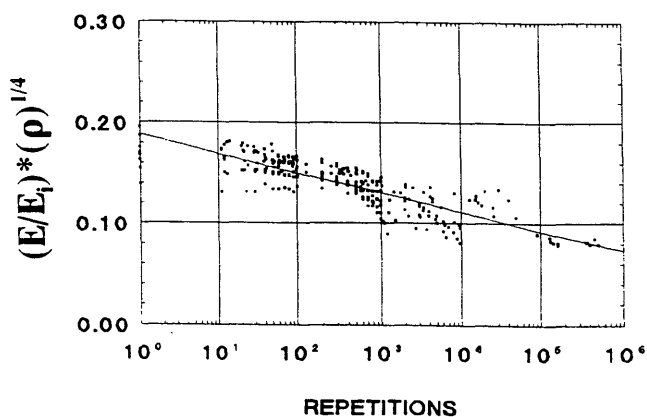
CAC-DG
STRAIN CRITERION



ARHM-GG
STRAIN CRITERION



CAC-DG
CURVATURE CRITERION



ARHM-GG
CURVATURE CRITERION

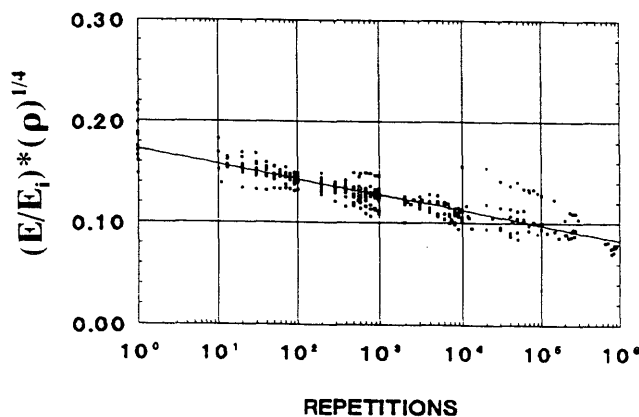


FIGURE 3 Stiffness reduction as a function of tensile strain and curvature for CAC-DG.

FIGURE 4 Stiffness reduction as a function of tensile strain and curvature for ARHM-GG.

For the curvature criterion

$$N_{rf} = R_f \cdot (B1) \cdot \left(\frac{1}{\rho}\right)^{B2} \quad (15)$$

where $A1$, $A2$, $B1$, and $B2$ are material constants defined in Equations 1 through 4.

The variation of the remaining life factor R_f with E/E_i , ϵ_i , and ρ is shown in Figures 5 and 6. Results indicate that R_f increases with an increase in E/E_i , ϵ_i , and ρ and attains slightly larger values for ARHM-GG compared with CAC-DG. The limits of variation are between 0 and 1 by definition.

Remaining fatigue life prediction requires the assessment of E/E_i at any given period during the service life of the pavement. E/E_i could be determined through backcalculation procedures using nondestructive pavement deflection equipment such as the FWD. Response parameters in terms of strains or surface curvature associated with a given wheel load are then used, together with E/E_i , to determine the remaining fatigue life as described in Equations 10 through 15. Surface

curvature can be easily estimated from surface deflection data. This calculation could provide a direct estimation of pavement remaining life following FWD measurement of a simulated wheel load. The estimation of load repetitions required to induce a given fatigue damage in CAC-DG or ARHM-GG in terms of stiffness reduction E/E_i could also be obtained by substituting $(1 - R_f)$ for R_f in Equations 14 and 15.

Remaining fatigue life analysis has been investigated using multilayer elastic theory and the proposed material models. Typical three-layer pavements with CAC-DG and ARHM-GG surfaces were analyzed using the ELSYM5 (12) computer program. A summary of the cases considered is presented in Table 3. A standard 9,000-lb wheel load with tire pressure equal to 100 psi was used. The analysis aimed at comparing the fatigue performance of CAC-DG and ARHM-GG pavements. Specifically, the number of load repetitions required to induce a given reduction in surface layer modulus, the number of load repetitions associated with remaining fatigue life for a given state of fatigue damage E/E_i , and the equivalent thickness correlation between CAC-DG and ARHM-GG were investigated.

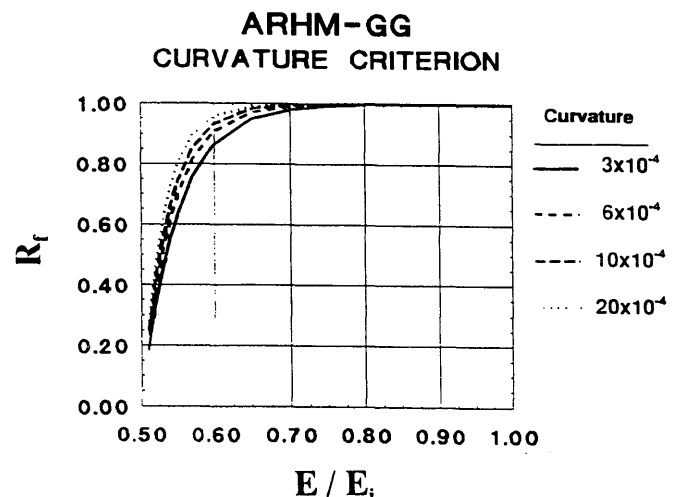
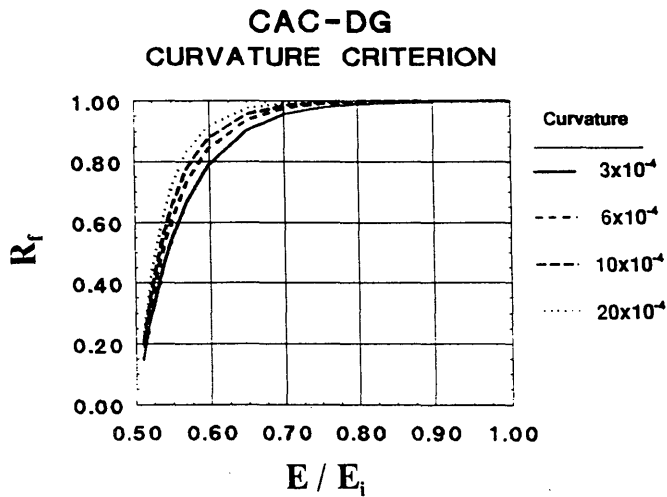
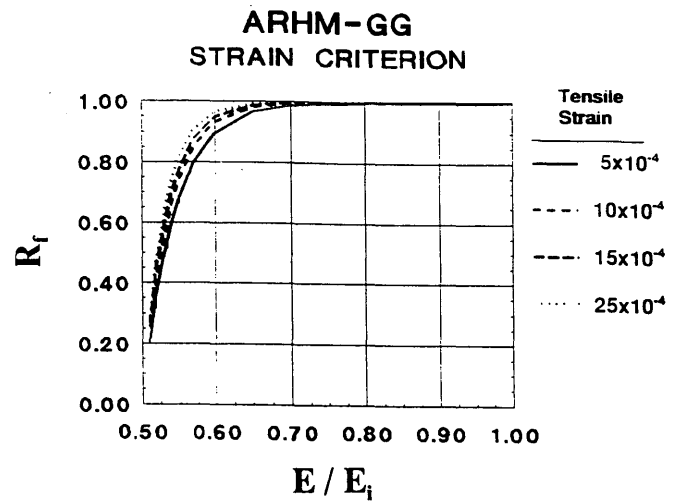
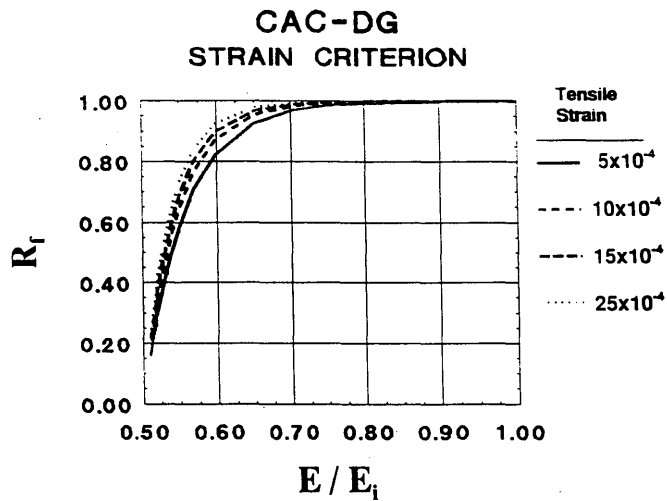


FIGURE 5 Variation of remaining fatigue life factor with stiffness reduction for CAC-DG.

FIGURE 6 Variation of remaining fatigue life factor with stiffness reduction for ARHM-GG.

TABLE 3 Summary of Material Properties and Pavement Cases Studied

PROPERTY	MATERIAL		
	CAC-DG	ARHM-GG	BASE/SUBGRADE
Modulus, ksi	$E_i = 550$ $E/E_i = 1, .85, .75, .65, .55$	$E_i = 350$ $E/E_i = 1, .85, .75, .65, .55$	$E_b/E_s = 80/20, 60/20, 40/20, 20/10$
Poisson's Ratio	0.40	0.40	0.30/0.45
Thickness, in.	2, 3, 4, 6, 8, 10	2, 3, 4, 6, 8, 10	8 in. Base over Infinite Subgrade
Note : E_i = Initial Modulus of Surface Layer E = Modulus of Surface Layer after N Repetitions E_b = Modulus of Base Layer E_s = Modulus of Subgrade			

Results of the analysis are presented in Figures 7 through 15. The number of wheel load repetitions (N_d) required to cause a given fatigue damage represented by stiffness reduction E/E_i is generally larger for ARHM-GG than for CAC-DG. This difference increases with an increase in surface layer thickness, underlying base and subgrade support and degree of fatigue damage (i.e., decreasing E/E_i) (Figures 7 through 10). A similar trend is observed for the variation of remaining fatigue life for a pavement with a given E/E_i . In this case, the difference in remaining fatigue life between CAC-DG and ARHM-GG pavements increases with increasing thickness and underlying pavement support but decreases with the increase in initial degree of fatigue damage (Figures 11 through 14). Results of the analysis were also used to establish thickness equivalencies between CAC-DG and ARHM-GG layers. In this case, the two materials are assumed to have initially the same fatigue damage state (i.e., E/E_i). Layer thicknesses for both CAC-DG and ARHM-GG are then selected to provide equal remaining fatigue life. As illustrated in Figure 15, thinner sections of ARHM-GG will exhibit the same remain-

ing fatigue life compared with CAC-DG pavements. The reduction in thickness is more significant for pavements with higher base and subgrade moduli. For example, assuming the base and subgrade moduli equal to 80 and 20 ksi, respectively, and a CAC-DG surface layer with a thickness in the range of 6 and 10 in., then the corresponding equivalent ARHM-GG thickness will be between 2 and 5 in., respectively. In case of overlay applications, more support will be provided by the underlying pavement compared with that provided by the base and subgrade in a typical new pavement structure. It is therefore expected that the equivalent ARHM-GG overlay thickness could be significantly smaller, as demonstrated by Raad et al. (8).

SUMMARY AND CONCLUSIONS

In this paper a method is proposed for predicting the remaining fatigue life of existing bituminous pavements. This method incorporates laboratory fatigue data for tensile strain

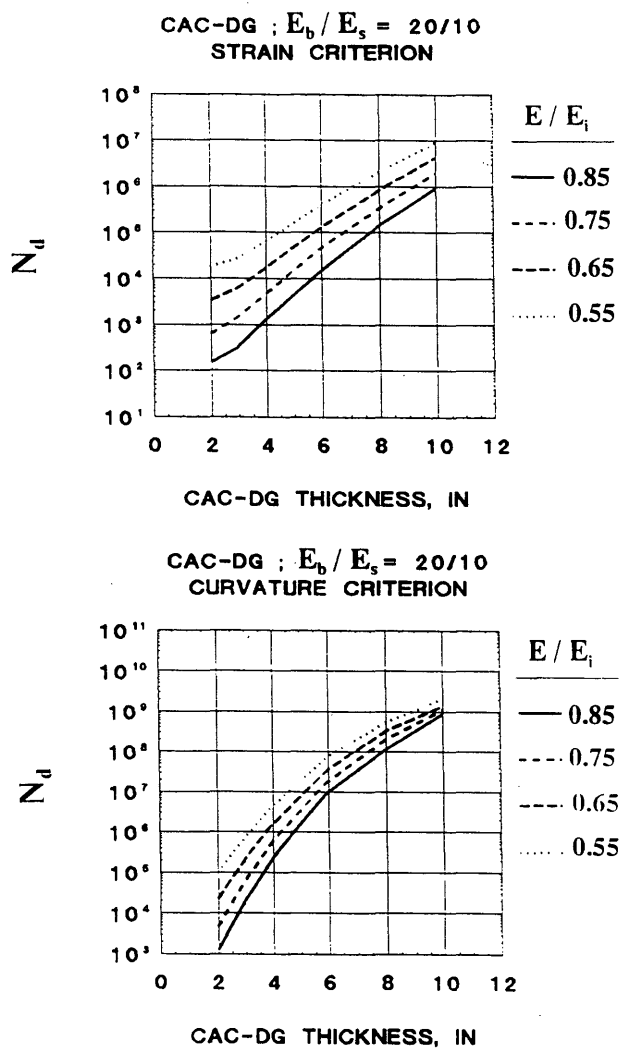


FIGURE 7 Variation of N_d with CAC-DG surface layer thickness for $E_b/E_s = 20/10$.

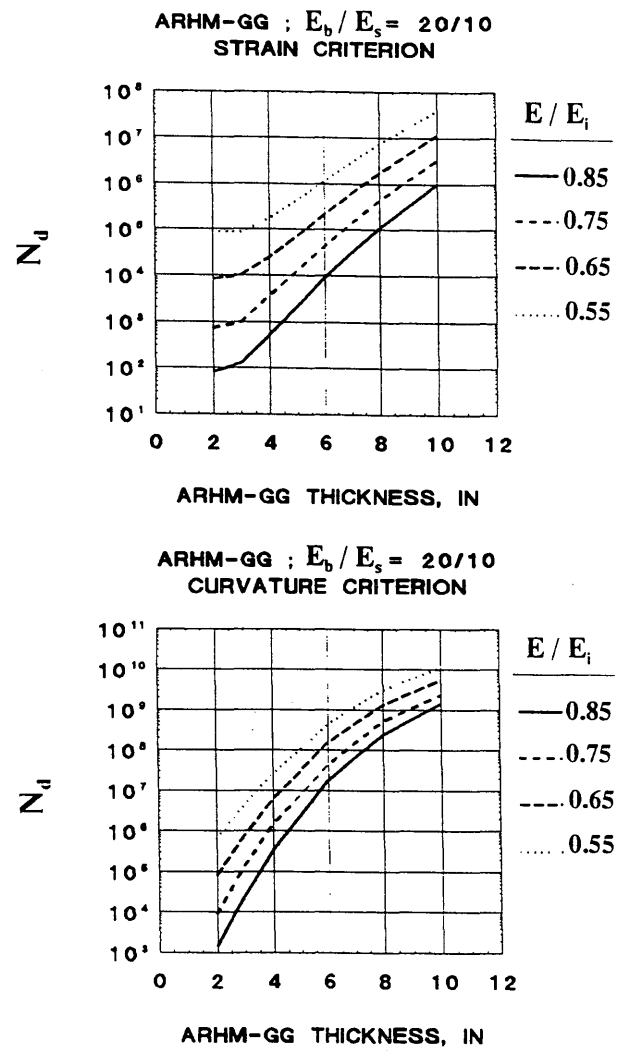


FIGURE 8 Variation of N_d with ARHM-GG surface layer thickness for $E_b/E_s = 20/10$.

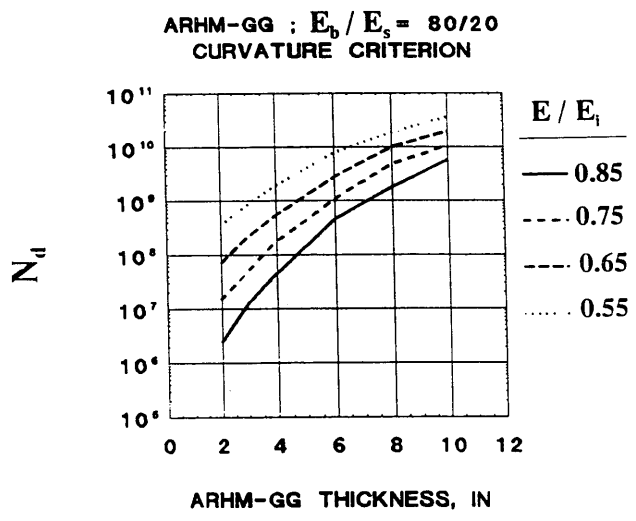
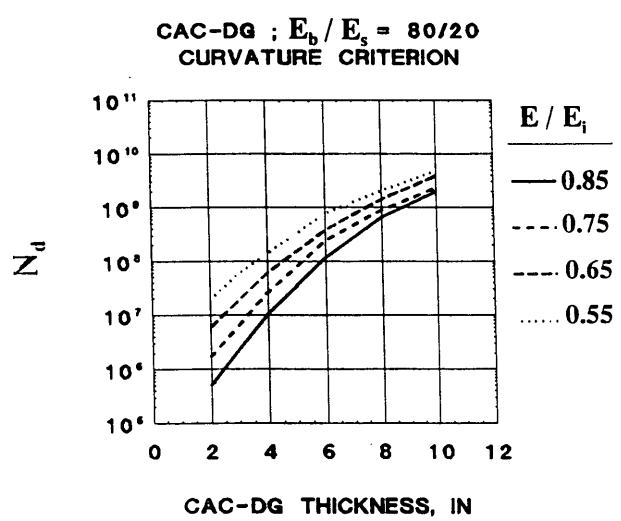
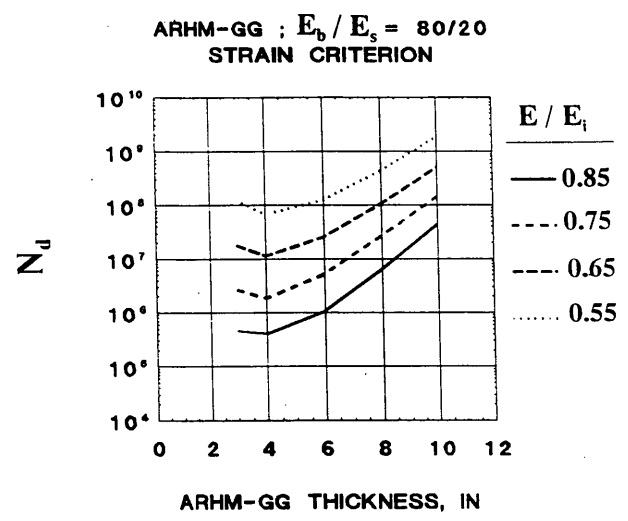
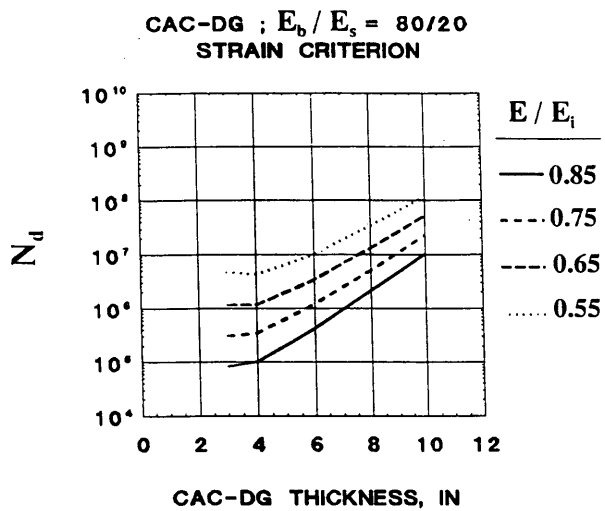
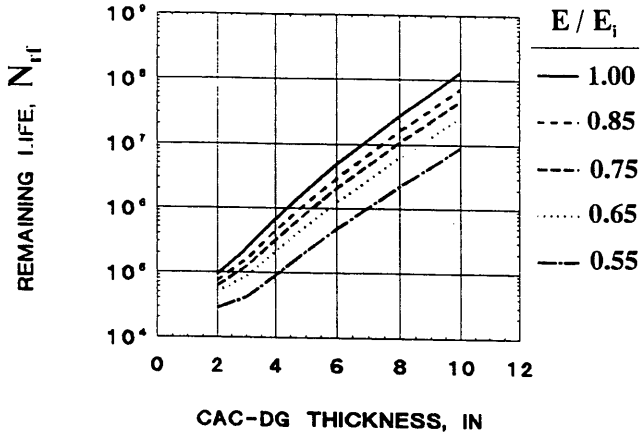


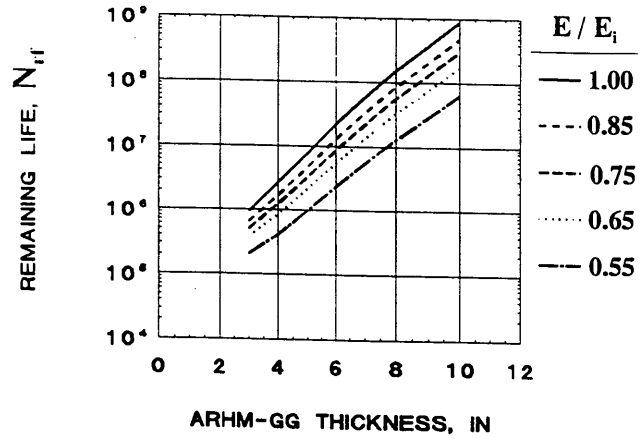
FIGURE 9 Variation of N_d with CAC-DG surface layer thickness for $E_b/E_s = 80/20$.

FIGURE 10 Variation of N_d with ARHM-GG surface layer thickness for $E_b/E_s = 80/20$.

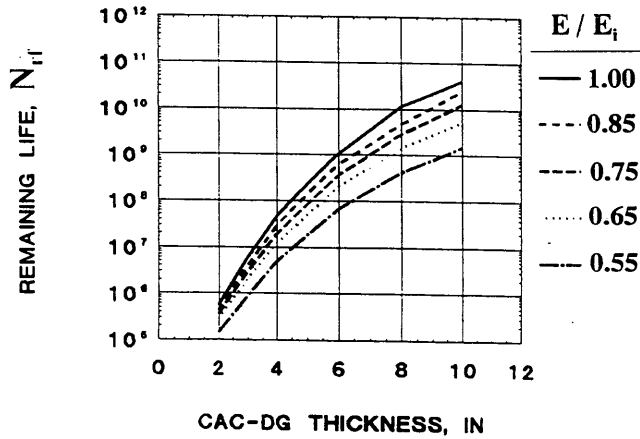
CAC-DG ; $E_b/E_s = 20/10$
STRAIN CRITERION



ARHM-GG ; $E_b/E_s = 20/10$
STRAIN CRITERION



CAC-DG ; $E_b/E_s = 20/10$
CURVATURE CRITERION



ARHM-GG ; $E_b/E_s = 20/10$
CURVATURE CRITERION

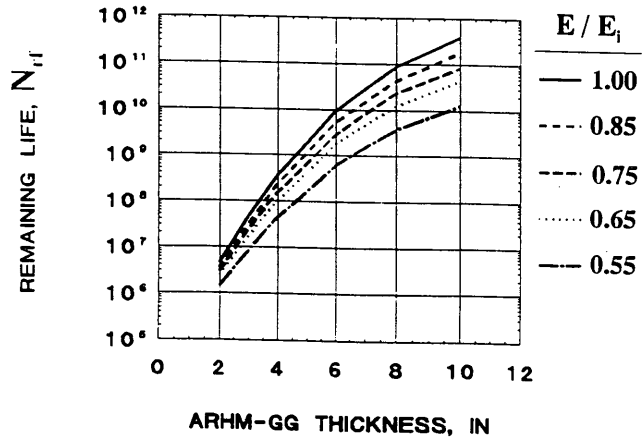


FIGURE 11 Variation of N_{rl} with CAC-DG surface layer thickness for $E_b/E_s = 20/10$.

FIGURE 12 Variation of N_{rl} with ARHM-GG surface layer thickness for $E_b/E_s = 20/10$.

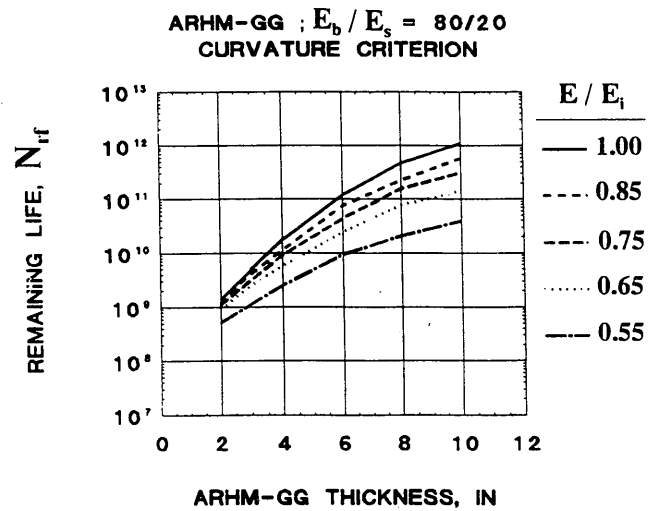
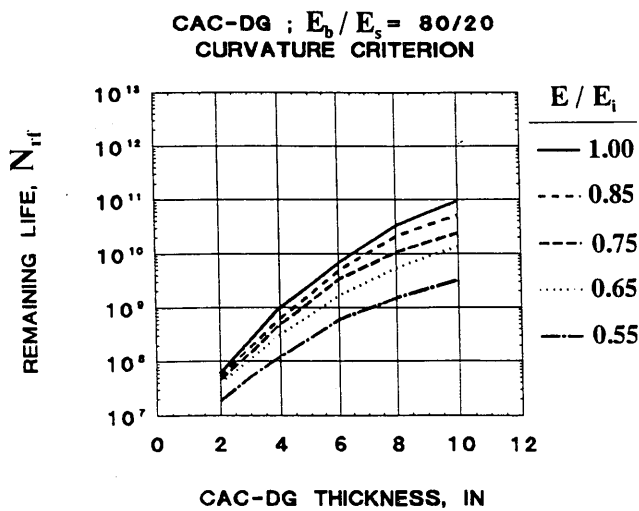
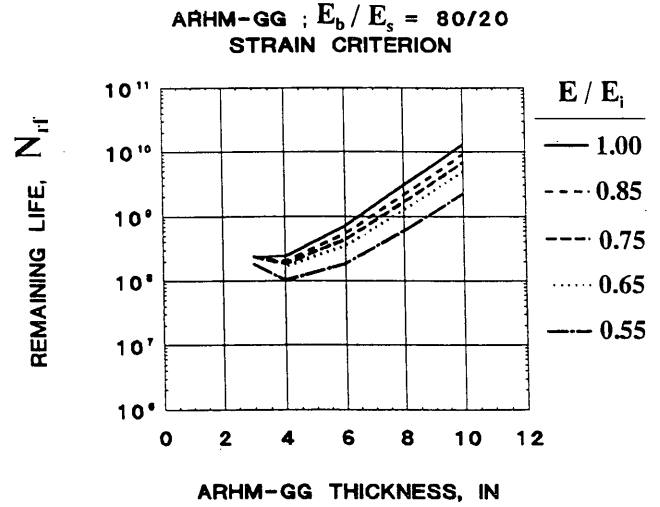
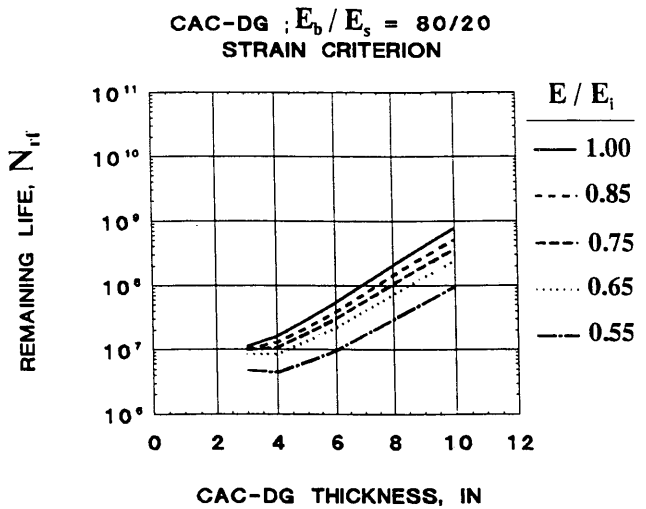


FIGURE 13 Variation of N_{rf} with CAC-DG surface layer thickness for $E_b/E_s = 80/20$.

FIGURE 14 Variation of N_{rf} with ARHM-GG surface layer thickness for $E_b/E_s = 80/20$.

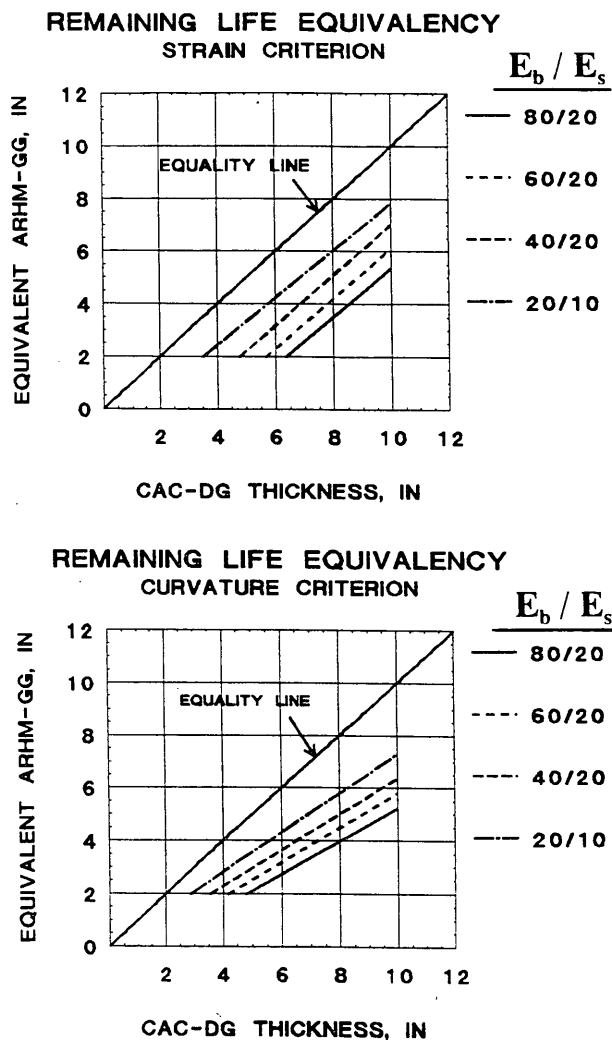


FIGURE 15 Thickness equivalencies for CAC-DG and ARHM-GG associated with a given remaining fatigue life.

under the pavement surface layer, which warrants consideration of using ARHM-GG in pavements and particularly in overlays.

The results presented in this paper are based on laboratory tests and simple multilayer elastic analysis covering limited loading and temperature conditions. Field research is needed to calibrate the proposed models and to verify the conclusions and trends obtained.

ACKNOWLEDGMENTS

This work has been supported by a research grant from Manhole Adjusting, Inc. This help is gratefully acknowledged. The authors would like to thank Nick Coetzee, who reviewed the research work and provided feedback and guidance.

REFERENCES

1. J. O. Kano and E. Charania. The Phoenix Experience Using Asphalt-Rubber. *Proc., National Seminar on Asphalt Rubber*, Kansas City, Mo., Asphalt Rubber Producers Group, Oct. 1989, pp. 366-393.
2. J. L. Van Kirk. Caltrans Experience with Asphalt-Rubber Concrete—An Overview and Future Direction. *Proc., National Seminar on Asphalt Rubber*, Kansas City, Mo., Asphalt Rubber Producers Group, Oct. 1989, pp. 418-431.
3. L. Schofield. The History, Development and Performance of Asphalt Rubber at ADOT. *Proc., National Seminar on Asphalt Rubber*, Kansas City, Mo., Asphalt Rubber Producers Group, Oct. 1989, pp. 328-365.
4. C. M. Turgeon. The Use of Asphalt-Rubber Products in Minnesota. *Proc., National Seminar on Asphalt Rubber*, Kansas City, Mo., Asphalt Rubber Producers Group, Oct. 1989, pp. 311-327.
5. A. Sainon. Advantages of Asphalt Rubber Binder for Porous Concrete. In *Transportation Research Record 1265*, TRB, National Research Council, Washington, D.C., 1990, pp. 69-81.
6. R. N. Doty. Flexible Pavement Rehabilitation Using Asphalt-Rubber Combinations. In *Transportation Research Record 1196*, TRB, National Research Council, Washington, D.C., 1988, pp. 212-223.
7. D. L. Hoyt and R. L. Lytton. Laboratory Behavior, Performance Prediction and Cost-Effectiveness of Asphalt-Rubber Concrete in Airport Pavements. *Proc., National Seminar on Asphalt Rubber*, Kansas City, Mo., Asphalt Rubber Producers Group, Oct. 1989, pp. 191-250.
8. L. Raad, S. Saboundjian, and R. Briggs. *Fatigue Behavior of Asphalt Rubber Hot Mix and Conventional Asphalt Concrete: A Comparative Study*. Final Report. Manhole Adjusting, Inc.; Transportation Research Center, Institute of Northern Engineering, University of Alaska, Fairbanks, Sept. 1992.
9. H. Al-Abdul-Wahab and G. Al Amri. Laboratory Evaluation of Reclaimed Rubber Asphaltic Concrete Mixes. *Journal of Materials in Civil Engineering*, Vol. 3, No. 3, Aug. 1991, pp. 189-203.
10. P. Seebaly, N. Tabatabaee, R. Bonaquist, and D. Anderson. Evaluating Structural Damage of Flexible Pavements Using Cracking and Falling Weight Deflectometer Data. In *Transportation Research Record 1227*, TRB, National Research Council, Washington, D.C., 1989, pp. 44-52.
11. M. A. Miner. Cumulative Damage in Fatigue. *ASME Transactions, Journal of Applied Mechanics*, Vol. 12, 1945, pp. A159-A164.
12. *ELSYM5. A Computer Program for the Analysis of Elastic Layered Systems with Normal Loads*. Coded by G. Ahlborn, ITTE, University of California, Berkeley, 1972.

or radius of curvature in terms of repetitions to failure. It also uses laboratory data on reduction of flexural stiffness with load repetitions. The proposed method is applied in the analysis of dense-graded conventional asphalt concrete (CAC-DG) and gap-graded asphalt-rubber hot mix (ARHM-GG) pavements. Controlled-strain fatigue test data for CAC-DG and ARHM-GG were incorporated in the analysis. Results indicate that the number of load repetitions required to induce a given fatigue damage, expressed in terms of the ratio of layer modulus after a given period of service to its initial modulus before the incurrence of any fatigue damage, could be significantly larger for ARHM-GG than for CAC-DG. Similar observations are made for the remaining fatigue life of CAC-DG and ARHM-GG, assuming a given initial state of fatigue damage. Thickness equivalencies are developed between CAC-DG and ARHM-GG on the basis of equal remaining fatigue life of pavement sections with similar initial fatigue damage. It is illustrated that thinner sections of ARHM-GG will be required for a given remaining fatigue life compared with CAC-DG pavements. This reduction in thickness becomes more significant with increasing foundation support

Theoretical Analysis of the Effects of Wide-Base Tires on Flexible Pavements Using CIRCLY

DARIO PERDOMO AND BILL NOKES

Many state highway agencies across the nation are concerned with the effects of wide-base tires on flexible pavements. This concern is supported, in many cases, by legislative regulations that try to limit the extent of damage caused by wide-base tires. A study was done by the California Department of Transportation to characterize and predict the effects of wide-base tires and to evaluate a tentative regulatory limit. The primary objectives were (a) to provide an extensive literature review summary about previous research in the area, including the wide range of regulatory limits, and (b) to perform an improved mechanistic analysis that includes effects of actual temperature gradients and nonuniform contact stress (normal and shear) distributions. The literature review summary indicates that the overall wide-base tire issue cannot be quantified reliably with a single regulatory limit. The reason for this lies in the various factors and assumptions involved in any experimental or theoretical evaluation (e.g., temperature and load conditions). Previous studies assume simple and incomplete loading conditions that are known to differ from actual circumstances. The mechanistic analysis, using a computer program called CIRCLY, shows that the effects of these simplifications significantly alter predicted pavement response. Future evaluations should continue to model the actual nonuniform vertical and shear forces that tires exert on pavement structures. The full influence of these factors should be verified by laboratory and field measurements.

By definition, wide-base (super-single or flotation) tires have rim widths of 356 mm (14 in.) or greater with nominal rim diameters between 560 and 610 mm (22 to 24 in.) (1). The most common rims are the 16R22.5 and the 18R22.5 (2).

Expected benefits from the use of wide-base tires include decreased fuel consumption and operating costs and increased payload. These larger tires are replacing conventional truck dual tires in all axle configurations (single, tandem, and tri-dem). This change is of great concern to the California Department of Transportation (Caltrans) because research during the past years, based on theoretical and experimental studies, suggests considerably more pavement deterioration from the use of wide-base tires (3-15).

Regulations based on limiting the weight per inch of tire width for steering and regular axles have been adopted in 28 states around the nation (as of 1990).

Division of New Technology, Materials, and Research, California Department of Transportation, 5900 Folsom Blvd., P.O. Box 19128, Sacramento, Calif. 95819-0128.

States (no.)	Limit	
	Newtons per Millimeter	Pounds per Inch
3	96	550
15	105	600
4	114	650
1	123	700
5	140	800

The scientific background behind these "pounds-per-inch" limits is uncertain.

In this paper, a literature review summary is first presented showing the wide range of factors involved in the analysis and comparison of the effects of wide-base tires versus conventional dual tires. Subsequently, the paper presents a mechanistic analysis for a typical California pavement structure. The analysis is based on layered elastic theory using a state-of-the-art computer program called CIRCLY (16). Capabilities of the program include modeling of nonuniform contact shear and vertical stresses as well as temperature gradients within the pavement structure.

LITERATURE REVIEW

An extensive literature review was done to collect and evaluate findings pertinent to the effects of wide-base tires and dual tires on flexible pavement structures. The following components were used to establish a basis for evaluation:

1. Primary response parameters: strains or deflections, or both.
2. Analytical methods: layered elastic or finite element analysis, or both.
3. Load equivalency: load equivalent factors based on either empirical or theoretical methods.
4. Available data bases based on measured primary responses.

Little information was found on actual testing to failure, influence of axle configuration (for wide-base tires), and effect of contact shear pressure.

Summary

General characteristics and findings from previous studies are summarized, respectively, in Tables 1 and 2. Figure 1 illus-

TABLE 1 Literature Review Summary

AUTHOR(S)	RESPONSE PARAMETERS (Measured-M, Calculated-C)	AXLE CONFIGURATIONS		BASIS FOR ANALYSIS		ANALYTICAL METHOD OR THEORY	STRUCTURAL SECTIONS	SURFACE TEMPERATURES
		Type	Axle Load, Tire Size, Inflation Pressure	Single primary response	Load equivalent factors			
Zube, et al (3) (California, USA)	Surface TS ⁽¹⁾ (M) TS at bottom of AC ⁽²⁾ (M) Surface Deflection (M)	SINGLE	WB ⁽³⁾ : 53 kN, 18x19.5, 515 kPa Duals : 80 kN, 10x20, 480 kPa	YES	NO	Elastic (Boussinesq) - used to estimate comparable WB load for field testing.	Wide range Surface layer : 50 to 95 mm	15 to 50 °C
Emery, et al (4) (Canada)	Surface Deflection (M) Deflection Bowl (M)	SINGLE	WB : 80 kN, 6.5x19.5, 580 kPa Duals : 80 kN, 9x20, 550 kPa	YES	NO	None	Wide range Surface layer : 50 to 115 mm	NF ⁽⁴⁾
Terrel, et al (5) (Washington, USA)	TS at bottom of AC (C) CS ⁽⁵⁾ at top of Subgrade(C)	SINGLE	Several loads and tire widths were modelled	NO	YES	Chevron (CHEV5L) program - used to calculate strains for life predictions	Wide range Surface layer : 75 to 230 mm	Mean : 20 °C
Christison (6) (Canada)	TS at bottom of AC (M) Surface Deflection (M)	SINGLE	WB : several, 18x22.5, 600 kPa Duals : 80 kN, 10x20, 550 kPa	YES	NO	None	2 structures Surface layer : 195 and 280 mm	5 to 25 °C
Christison, et al (7) (Canada)	TS at bottom of AC (M) Surface Deflection (M)	SINGLE TANDEM	WB : several, 16.5x22.5 / 18x22.5 Duals : 80 kN, 10x20, 550 kPa	NO	YES	None	2 structures Surface layer : 195 and 280 mm	5 to 25 °C
Snelgrove (8) (Canada)	Surface Deflection (M)	SINGLE	WB : several, 18x22.5, 550 kPa Duals : 80 kN, 10x22.5, 550 kPa	YES	NO	None	2 structures	NF
Southgate, et al (11) (Kentucky, USA)	Strain Energy Density (C)	TANDEM TRIDEM	Tire loads : 25-45 kN at 515 kPa	NO	YES	Chevron (CHEV5L) - modified for calculation of strain energy	Wide range Surface layer: 50 to 150 mm	NF
Sharp, et al (12) (Australia)	Surface Deflection (M)	SINGLE TANDEM TRIDEM	WB : several, 18x22.5, 690 kPa Duals : 80 kN, 10x22.5, 690 kPa	YES	NO	None	1 structure Surface layer : 75 mm	Reference : 32 °C
Huhtala, et al (13) (Finland)	TS at bottom of AC (M) (both longitudinal and transversal)	SINGLE	Loads : 75-120 kN WB : 355, 380, and 445 mm wide Duals : 255 and 305 mm wide Pressures : 480- 1050 kPa	NO	YES	None	2 structures Surface layer : 75 and 150 mm	5 to 10 °C
Bonaquist (14) (Virginia, USA)	TS at bottom of AC (M) CS in all layers (M)	SINGLE	Loads : 80-150 kN WB : 16.5x22.5 Duals : 11x22.5 Pressures : 515, 700, and 960 kPa	YES	NO	None	2 structures Surface layer : 89 and 178 mm	Mean : 14 °C and 23 °C

- (1) Tensile Strain
- (2) Asphalt Concrete
- (3) Wide Base Tire
- (4) Not Found
- (5) Compressive Strain

TABLE 2 Wide-Base Tire Limits

AUTHOR(S)	AXLE TYPE	ESTIMATES FOR WIDE BASE LIMITS			OTHER SPECIFICS (tensile strain-TS or compressive strain-CS, thin or thick section, tire width)	BASIS FOR LIMITS
		AXLE LOAD (kN)	WIDTH LIMITS			
			(N/mm)	(lbs/in)		
Zube, et al (3)	SINGLE	54	58	333	TS & Deflection	MEASURED primary response
Terrel, et al (5)	SINGLE	80	85	486	TS, thin, 470 mm	CALCULATED life using predictive equations for fatigue and rutting
		62	66	378	TS, thick, 470 mm	
		63	67	383	CS, thick, 470 mm	
		56	73	416	TS, thin, 380 mm	
		47	62	356	TS, thick, 380 mm	
		57	75	426	CS, thick, 380 mm	
Christison (6)	SINGLE	76	83	472	Bottom AC TS	MEASURED primary response
		64	70	397	Deflection	
Christison, et al (7)	SINGLE	72	79	450	TS & Defl, 457 mm	LEF's ⁽¹⁾ from average of two MEASURED primary responses
		66	79	452	TS & Defl, 419 mm	
	TANDEM	120	66	375	TS & Deflection	
Snelgrove (8)	SINGLE	75	82	469	Deflection	MEASURED primary response
Southgate, et al (11)	TANDEM	115	63	361	Strain energy	CALCULATED LEF's using work strain
	TRIDEM	200	73	417	Strain energy	
Sharp, et al (12)	SINGLE	59	64	367	Deflection	MEASURED primary response
	TANDEM	108	59	338	Deflection	
Huhtala, et al (13)	SINGLE	82	93	529	TS, thin	CALCULATED LEF's based on tensile strains
		80	90	514	TS, thick	
Bonaquist (14)	SINGLE	52	62	354	TS, thin	MEASURED primary response ⁽²⁾
		45	53	303	TS, thick	
		60	72	409	CS subgrade, thin	
		80	96	545	CS subgrade, thick	

(1) Load Equivalent Factor

(2) Failure Observed but not basis for limits

trates the findings presented in Table 2. Following are general observations regarding the findings.

1. Theoretical and measured results, using either single primary response or load equivalency factors, show that wide-base tires cause substantially more damage to the pavement structure than conventional dual tires under all axle configurations (single, tandem, and tridem) and conditions.

2. Previous studies suggest limits for single-axle configurations ranging between 53 and 96 N/mm (300 and 550 lb/in.) of tire width (Figure 1). Limits for tandem-axle configurations range between 53 and 70 N/mm (300 to 400 lb/in.) of tire width (Figure 1). Insufficient data were found for tridem axles. Most responses are below 79 N/mm (450 lb/in.).

3. Differences were found among the various analyses (Table 2) because all limits, those based on either single primary response or load equivalency factors, presented variations of one or more of the following factors: temperature, pavement structure, tire pressure, tire type and condition (age), tire load, axle configuration, axle spacing, selected response, and load duration.

4. The summation methods used for adding peak responses under tandem and tridem axle configurations affect the comparisons between various axle spacings and load distributions.

5. With respect to mechanistic analysis, none of the reviewed studies accounts for factors such as variable material response (e.g., caused by temperature gradients), pavement response to dynamic axle load variation, and tire-pavement

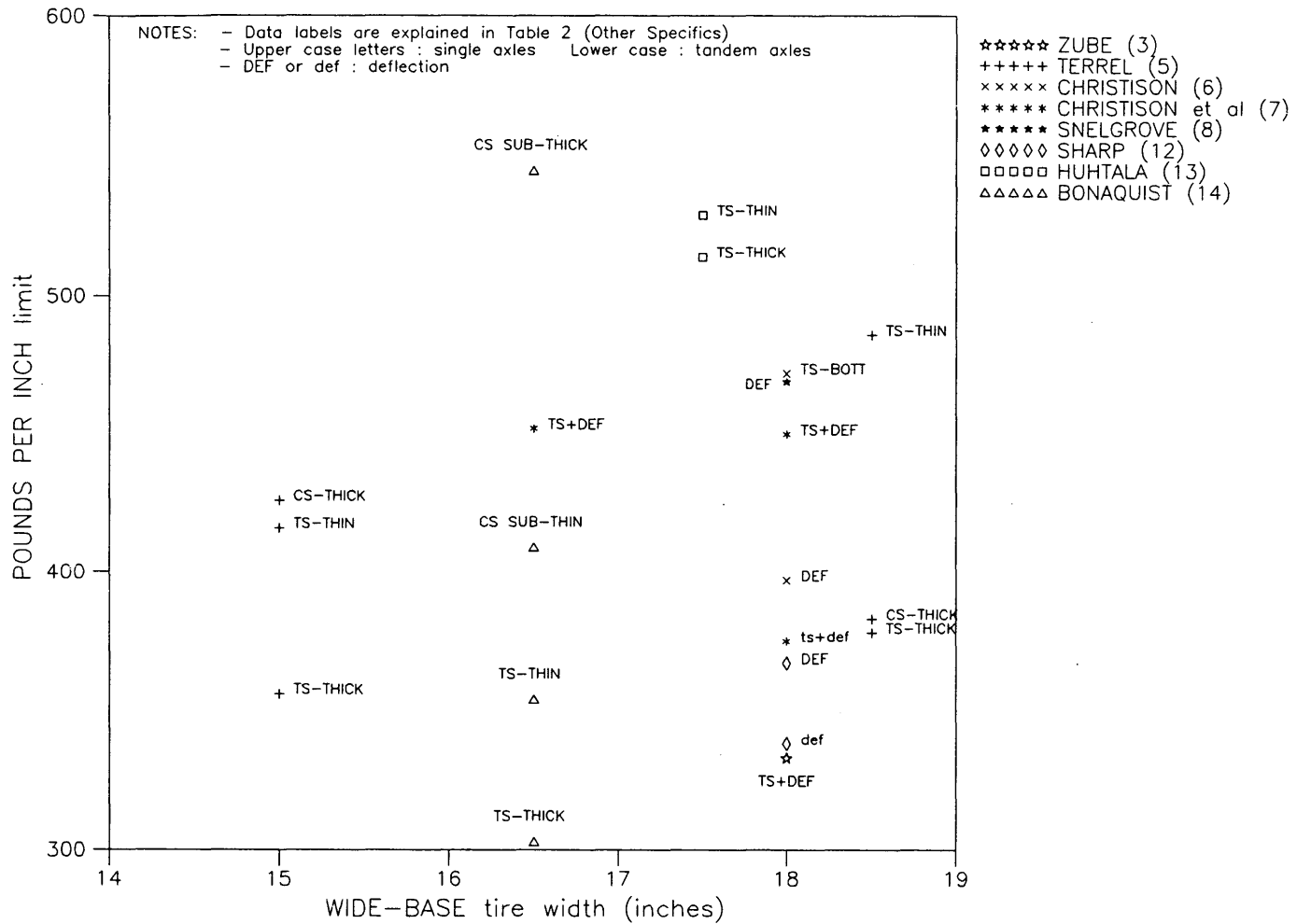


FIGURE 1 Pounds-per-inch limits based on Table 2.

interface effects. Some of these factors can be studied using the numerical method presented in this paper.

Significance

The information discussed previously suggests the need to reexamine the type of criterion or criteria by which to determine increased damage from wide-base tires. Selection of a reliable pounds-per-inch limit to protect flexible pavements is not possible using available information. In addition, the selection of a limit requires understanding the limitations of the method(s) used and augmenting or adjusting for factors that have not been adequately addressed by previous researchers. Some of these factors are mentioned in the summary section above.

Perhaps most significant is that previous studies of measured pavement response did not attempt to validate a mechanistic approach that subsequently could be used to evaluate different conditions. Conversely, other studies based on a mechanistic analysis did not validate fully their predictions by comparing primary response results with actual measurements. These facts imply a difficulty in setting a practical limit. More important, a criterion of pounds per inch may correlate

weakly with other attributes of wide-base tires, such as tire construction, condition, and pressure. Such factors may contribute substantially to accelerated pavement damage.

In the following section, an analytical method is used to compare dual and wide-base tires by addressing shear effects at the pavement-tire interface, nonuniform contact pressure distributions, and temperature gradients within the surface layer.

THEORETICAL ANALYSIS

This section presents an analytical evaluation of a typical California pavement structure using a computer program (CIRCLY) (16) that uses multilayered elastic theory and is capable of solving cases with multiple loads, several load types (i.e., vertical and shear loading), and anisotropic material characterization. Some of these capabilities are important in the design of surface layers when conditions of high stresses and loads at the tire-pavement interface exist, as in the case of wide-base tires.

Any theoretical evaluation requires thorough experimental supporting work to validate and calibrate the analytical model. In the absence of this work, this paper intends to highlight

main factors to consider when the surface effects of wide-base tires are studied and to indicate directions for further theoretical and experimental investigation. Among the main factors are the realistic modeling of surface stresses and the explicit use of energy principles for predicting failure potential.

Analytical Model

The CIRCLY program (16) is capable of analyzing multilayered anisotropic media subjected to multiple circular loads. Several load conditions can be modeled, including horizontal and vertical loads, shear stresses, and moments about horizontal and vertical axes (Figure 2). All loading conditions can be simulated using polynomial-type distributions.

Each layer is assumed to be of infinite extent in the horizontal direction. The layer interfaces can be modeled to be smooth (fully frictionless) or rough (fully continuous), and

the bottom layer may be assumed to have infinite or finite depth (resting on a rigid base). All layer interface planes are assumed to be horizontal, and the elasticity in each layer is homogeneous and of cross-anisotropic or isotropic symmetry. Compressive strains and stresses are denoted as positive.

Pavement Structure

The selected pavement structure, as shown in Figure 3, consists of a thick surface layer, an asphalt-treated permeable layer, an aggregate base, and a weak subgrade (*R* value around 15). All layers were assumed to be isotropic for this analysis, even though other findings (17,18) indicate anisotropy in some granular layers. Further investigation of this anisotropy is beyond the scope of this paper.

The surface layer was divided into sublayers to account for a temperature gradient that is reflected in the assumed mod-

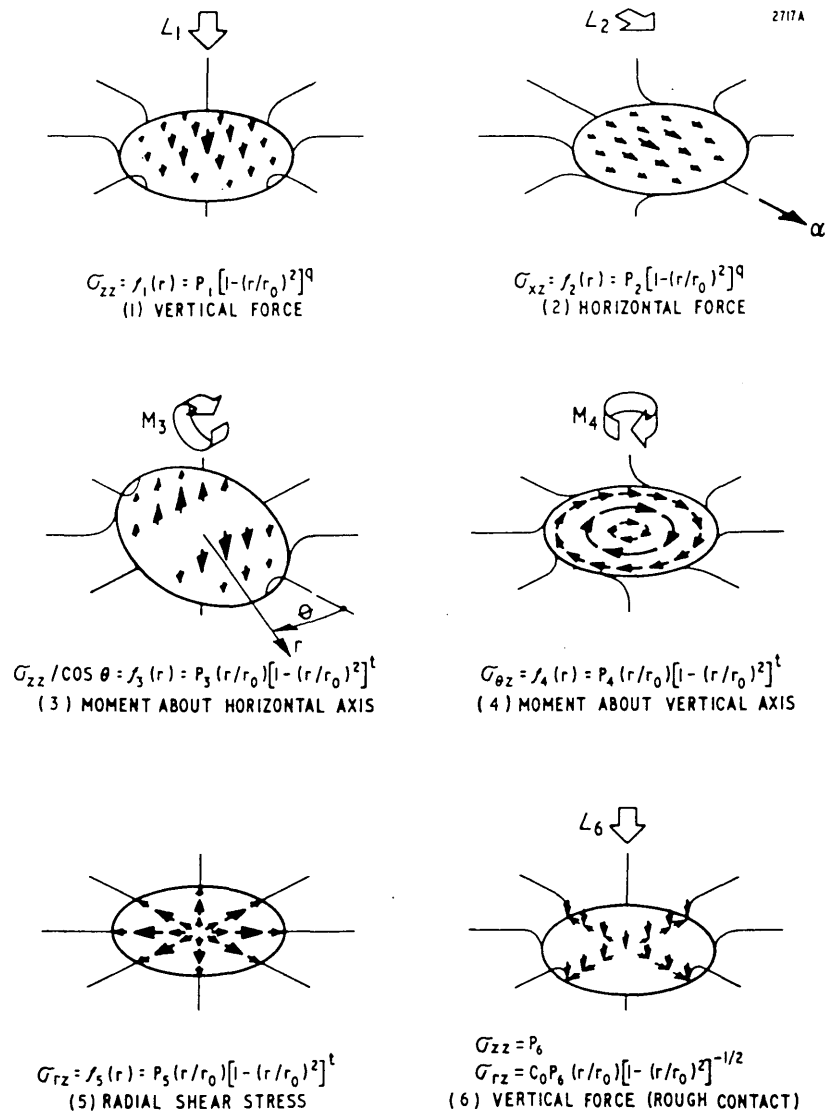


FIGURE 2 Loading types [after Wardle (16)].

	Thickness (mm)	Poisson's Ratio	Modulus (MPa)
DGAC	56	0.45	689
	56	0.40	827
	56	0.40	965
ATPB	76	0.35	1033
AB			
	427	0.35	207
SG	INF	0.40	24

FIGURE 3 Selected pavement structure.

uli. Selected moduli values attempt to represent critical day summer conditions. The section and materials are typical of Highway 99, north of Sacramento in California's Central Valley.

Loading Conditions

Two loading cases applied to the pavement structure were considered along with the effects of multiple loads. The two cases consisted of (a) nonuniform vertical stresses only and (b) nonuniform vertical stresses accompanied by nonuniform inward shear stresses. Both loading cases were assumed to be applied over circular contact areas.

The first loading case, under uniform conditions, is the most commonly assumed case in pavement analysis and design. The second loading case includes the observed and measured inward shear stresses for static and moving pneumatic tires (19,20) that have been ignored in most previous studies. These shear stresses develop from inward lateral tread movement caused by side-wall deflection within the contact area (21).

The following maximum legal axle loadings were analyzed: 89kN (20 kips) total load for the single axle, 151 kN (34 kips) total load for the tandem axle having 1.22-m (4-ft) spacing between axles, and 151 kN (34 kips) for the tridem axle having the same 1.22-m (4-ft) spacing between axles. In general, the legal axle loadings vary with axle spacing according to the California Vehicle Code (22). The typical nonuniform loading distributions used are shown in Figure 4. Evidence (23) in-

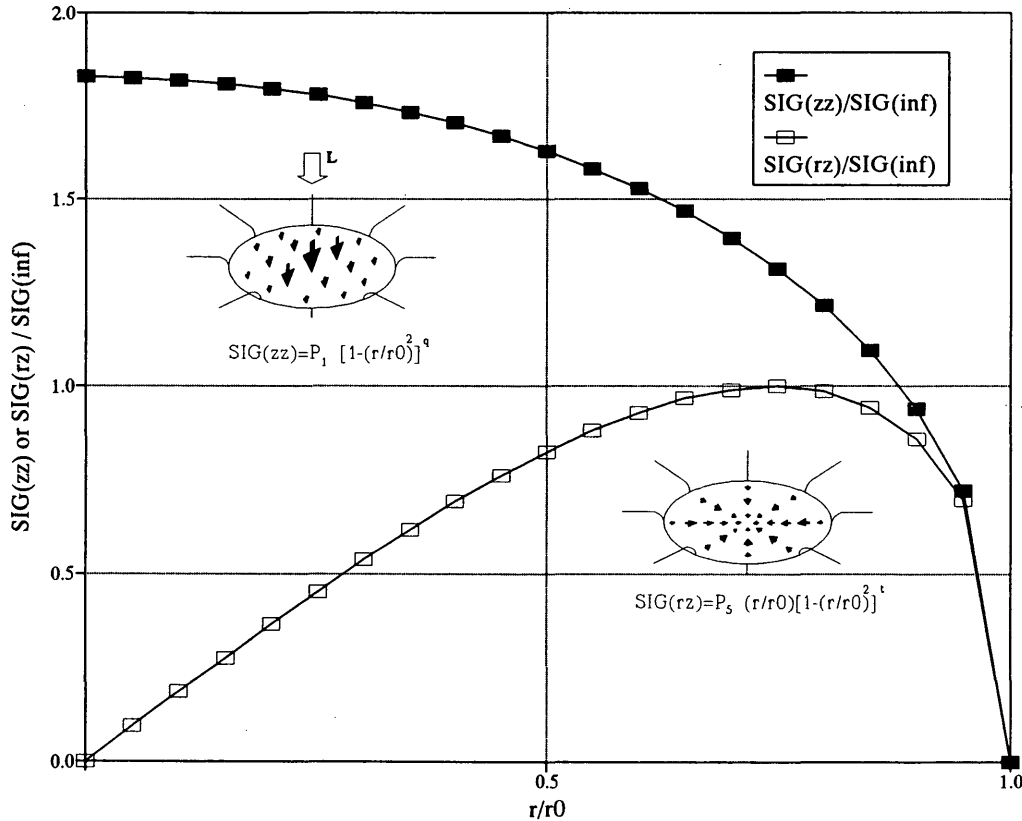


FIGURE 4 Typical nonuniform vertical and inward shear load distributions.

dicates that both vertical and shear stress distributions are parabolic in shape for the tire loadings and pressures commonly used in practice. In this analysis, the q -exponent for vertical stress distributions [Figure 2 (1)] varied between 0.15 and 0.30, whereas the t -exponent for inward shear stress distributions [Figure 2 (5)] maintained a constant value of 0.40. These values were selected on the basis of actual measured data from dual and wide-base tires (23).

The various radii used for all axle configurations were calculated from the following equation [derived from the parabolic vertical stress distribution equation presented in Figure 2 (1)]:

$$r_0 = \frac{L(q + 1)}{P_1 \pi}$$

where

- q = parabolic exponent,
- P_1 = maximum contact stress (160 psi for duals, 220 psi for wide-base),
- L = resultant force on tire (varies with axle configuration), and
- r_0 = calculated radius.

Performance Criteria

The selection of representative response parameters is a key factor in assessing unusual loading conditions and their effects on pavements. Surface response (top layer) is important when comparing the influence of wide-base and dual tires. This importance derives from the fact that vertical and shear forces have a significant effect at the tire-pavement interface.

This paper is limited to the evaluation of tensile strains (fatigue life determinant) and strain energies of distortion (failure criteria) within the surface layer. Tensile strains (at the bottom of the surface layer) have been linked to fatigue failure using an extended concept of Miner's hypothesis for damage (24). Strain energy (SE) is the work done on an element and stored within it and under elastic conditions is defined as follows (25):

$$\begin{aligned} SE/\text{volume} = & \frac{1}{2} (\sigma_x \epsilon_x + \sigma_y \epsilon_y + \sigma_z \epsilon_z \\ & + \tau_{xy} \gamma_{xy} + \tau_{yz} \gamma_{yz} + \tau_{xz} \gamma_{xz}) \end{aligned}$$

where σ_i , τ_{ij} are elastic stress components and ϵ_i , γ_{ij} are elastic strain components. The strain energy can be divided into two parts—one caused by distortion and the other caused by volume change. The part caused by distortion, called the strain energy of distortion, has been correlated with failure conditions (25). Strain energy of distortion (SED) is defined as follows:

$$SED/\text{volume} = SE/\text{volume} - \frac{1 - 2\nu}{6E} (\sigma_x + \sigma_y + \sigma_z)^2$$

where ν is the Poisson's ratio and E is the elastic modulus.

Results

Figure 5 shows all the axle configurations studied. Figure 6 shows typical results from the mechanistic analysis in the form of contour plots. All the results (26,27) were plotted using contour lines to draw conclusions with respect to both critical (peak) values and overall trends. Tensile strains were calculated in both the longitudinal (direction of travel) and transverse directions. Units for the strain energy of distortion are given in megapascals per unit volume (cubic meters). Tables 3 through 11 summarize the results for all axle configurations.

Tire Type

The main reason for this analytical evaluation was to compare the effects of wide-base tires and dual tires under more realistic loading conditions (nonuniformity and shear). Tables 5, 8, and 11 give us good insight into this part of the analysis. Wide-base tires produced 15 to 40 percent higher critical strain values than dual tires, and 30 to 115 percent higher critical strain energy of distortion values.

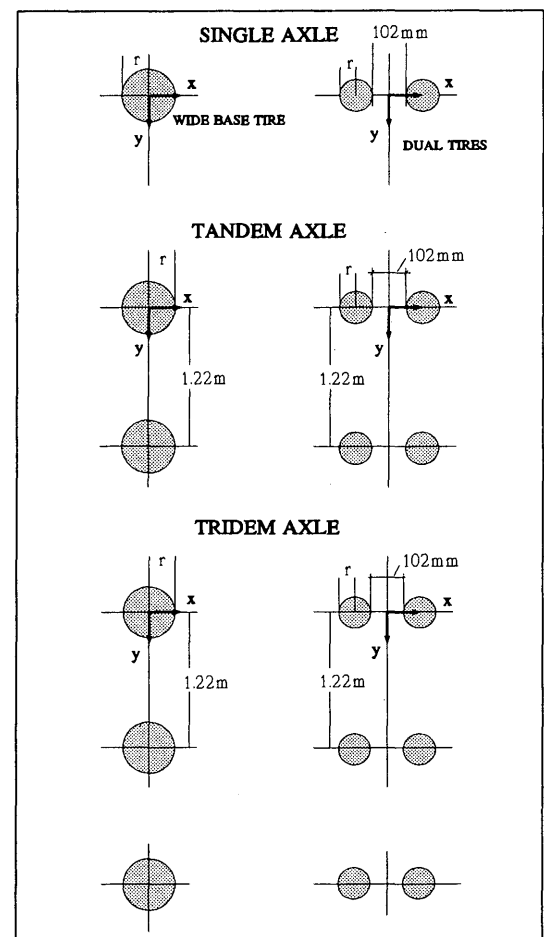


FIGURE 5 Axle configurations.

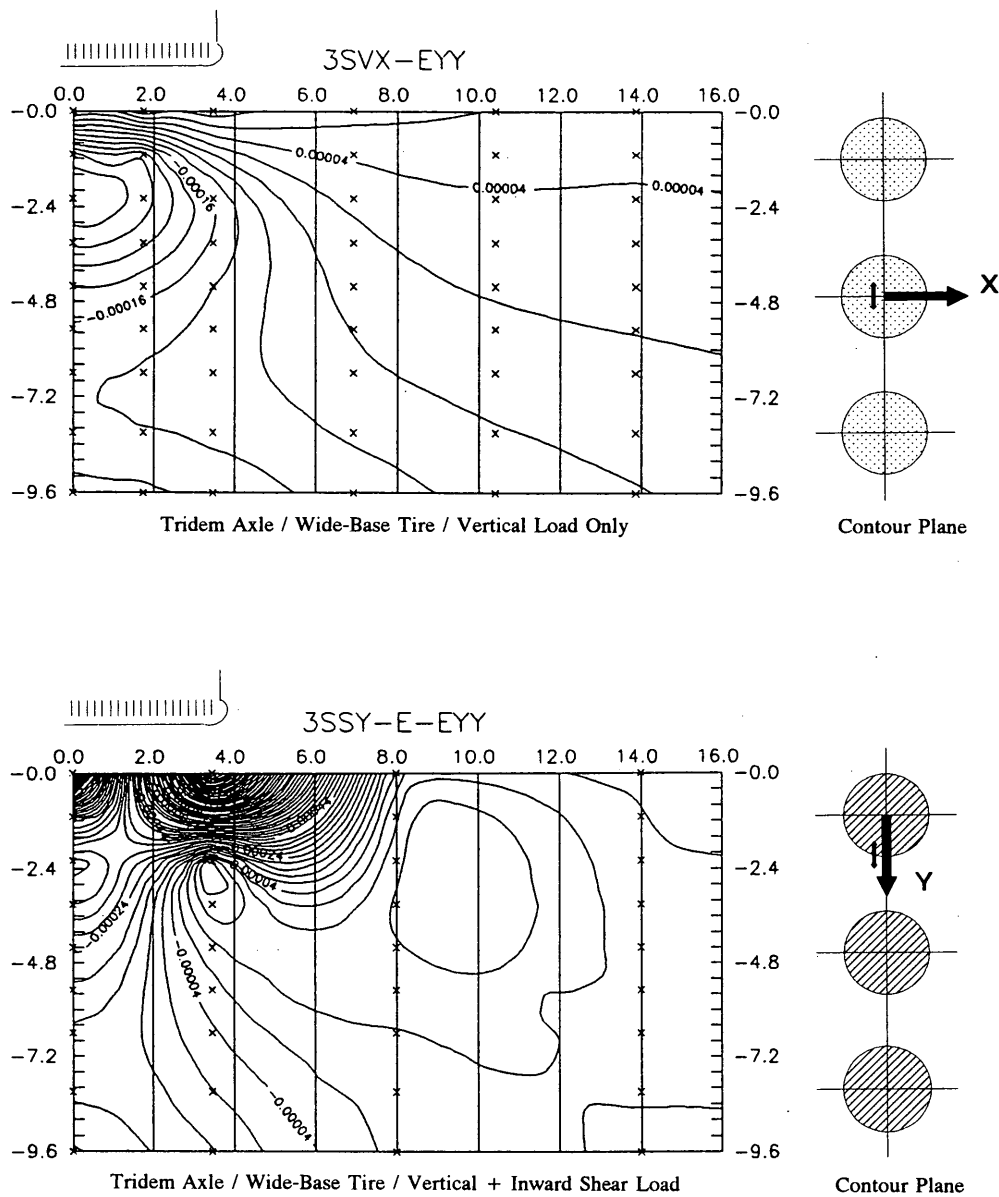


FIGURE 6 Typical contour plots. [Note: The contour plots presented are for peak tensile strains. The "contour plane" plots show planes where maximum strains occur (and directions). All values are in inches.]

Response Distribution

The typical contour plots presented in Figure 6 describe unique response distributions. Contour plots for all the cases analyzed are presented in other technical reports (26,27). In general, for the cases of vertical loading only, all the predicted responses (tensile strains and strain energies of distortion) present the greatest contour line variation (i.e., highest contour density) under the center of the tire for both wide-base and dual tires. In contrast, the cases of normal plus inward shear loading show the greatest contour line variation under the edges of the tire for the tensile strain and under the center of the tires for the strain energy of distortion. High contour line variations of strain energy of distortion imply potential areas where failure can originate.

Inward Shear Stresses

The presence of inward horizontal shear stresses as part of the pavement loading has a very important effect on pavement response. When inward shear loads are considered in the analysis, as they should, the critical (maximum) tensile strains for wide-base tires increase by factors between 6 and 6.7 (Tables 4, 7, and 10), depending on the axle configuration. As for dual tires, the multipliers are between 6.5 and 8.2. All these new maximum tensile stains occur on the surface of the pavement at the edges of the tires. On the other hand, the strain energies of distortion for wide-base tires increase by factors between 5.5 and 5.8 (Tables 4, 7, and 10), depending on the axle configuration. As for dual tires, the multipliers are between 8.9 and 9.2. In general, the results clearly indicate

TABLE 3 Single-Axle Critical Values

TIRE TYPE	LOADING STRESSES	MAXIMUM TENSILE STRAIN (ϵ_{xx} or ϵ_{yy} in microstrains)	MAXIMUM SED ⁽¹⁾ (MPa/m ³)	LOCATION OF MAXIMA (x,y,z) ⁽²⁾ in mm	
				ϵ_{xx} or ϵ_{yy}	SED
WB tire	Vertical only	-320 ($\epsilon_{xx}/\epsilon_{yy}$)	24	0,0,-56	0,0,-56
	Vertical plus shear	-2140 (ϵ_{xx})	132	r ⁽³⁾ ,0,0	0,0,0
Dual tires	Vertical only	-230 (ϵ_{yy})	11	50+r,0,-56	50+r,0,-56
	Vertical plus shear	-1880 (ϵ_{xx})	102	50+2r,0,0	50+r,0,0

- (1) SED is strain energy of distortion
 (2) See Figure 5 for location convention
 (3) r = radius of tire (in mm)

TABLE 4 Ratios of Maxima: Constant Tire Type

TIRE TYPE	ϵ_{max} for (VERT+SHEAR) / ϵ_{max} for (VERT only)	SED _{max} for (VERT+SHEAR) / SED _{max} for (VERT only)
WB tire	6.7	5.5
Dual tires	8.2	9.2

Note: WB is Wide Base

TABLE 5 Ratios of Maxima: Constant Loading Stress

LOADING STRESSES	WB ϵ_{max} / DUAL ϵ_{max}	WB SED _{max} / DUAL SED _{max}
Vertical only	1.4	2.15
Vertical plus shear	1.15	1.3

Note: WB is Wide Base tires, DUAL is Dual tires

that ignoring the shear stress effects leads to overestimating the life of the surface layers under actual conditions of contact stresses, regardless of the failure criterion being used (critical tensile strain or strain energy of distortion).

Another important observation is that primary response (tensile strain) and strain energy equivalencies between wide-base and dual tires are lower when inward shear stresses are considered (Tables 5, 8, and 11). This observation has direct implications in the analysis of fatigue load equivalency factors (power ratios of peak tensile strains) and it should be further investigated before any final conclusions are made.

Temperature Gradient

Consideration of a temperature gradient has a significant effect on predicted pavement response. The location of the critical tensile strains and strain energies of distortion is partly associated with the fact that the three surface sublayers have different modulus values. In all cases, the peak response values shifted in location to either the surface of the structure or within the first sublayer (Tables 3, 6, and 9). This finding may be relevant in explaining some actual observed surface distresses (28, 29).

TABLE 6 Tandem-Axle Critical Values

TIRE TYPE	LOADING STRESSES	MAXIMUM TENSILE STRAIN (ϵ_{xx} or ϵ_{yy} in microstrains)	MAXIMUM SED ⁽¹⁾ (MPa/m ³)	LOCATION OF MAXIMA (x,y,z) ⁽²⁾ in mm	
				ϵ_{xx} or ϵ_{yy}	SED
WB tire	Vertical only	-340 ($\epsilon_{xx}/\epsilon_{yy}$)	22	0,0,-56	0,0,-56
	Vertical plus shear	-2110 (ϵ_{xx})	129	r ⁽³⁾ ,0,0	0,0,0
Dual tires	Vertical only	-250 (ϵ_{yy})	11	50+r,0,-56	50+r,0,-56
	Vertical plus shear	-1870 (ϵ_{xx})	101	50+2r,0,0	50+r,0,0

- (1) SED is strain energy of distortion
- (2) See Figure 5 for location convention
- (3) r = radius of tire (in mm)

TABLE 7 Ratios of Maxima: Constant Tire Type

TIRE TYPE	ϵ_{max} for (VERT+SHEAR) / ϵ_{max} for (VERT only)	SED _{max} for (VERT+SHEAR) / SED _{max} for (VERT only)
WB tire	6.2	5.8
Dual tires	7.5	8.9

Note: WB is Wide Base

TABLE 8 Ratios of Maxima: Constant Loading Stress

LOADING STRESSES	WB ϵ_{max} / DUAL ϵ_{max}	WB SED _{max} / DUAL SED _{max}
Vertical only	1.4	2
Vertical plus shear	1.15	1.3

Note: WB is Wide Base tires, DUAL is Dual tires

Axle Configurations

Comparisons are possible among all axle configurations from the results presented in Tables 3, 6, and 9. In general, similar critical tensile strains occur for both tire types (duals and wide-base) among all axle configurations, being slightly higher for the tridem axle case. The critical strain energies of distortion are also similar for all axle configurations, being slightly higher for the single-axle case.

In all cases, the ratios of maxima presented in Tables 3 through 11 are similar under all axle configurations, being slightly higher for the single axle.

An important observation was made regarding the predicted peak responses (tensile strains and strain energies of distortion) for the tridem axle configuration. Peak response locations change (center or extreme tire), and sometimes peak tensile strain directions (x or y) as well (27), when inward shear stresses are present. Experimental work is needed to

TABLE 9 Tridem-Axle Critical Values

TIRE TYPE	LOADING STRESSES	MAXIMUM TENSILE STRAIN (ϵ_{xx} or ϵ_{yy} in microstrains)	MAXIMUM SED ⁽¹⁾ (MPa/m ³)	LOCATION OF MAXIMA (x,y,z) ⁽²⁾ in mm	
				ϵ_{xx} or ϵ_{yy}	SED
WB tire	Vertical only	-360 (ϵ_{yy})	22	0,1220,-56	0,0,-56
	Vertical plus shear	-2190 (ϵ_{yy})	123	0,r ⁽³⁾ ,0	0,1220,0
Dual tires	Vertical only	-290 (ϵ_{yy})	11	50+r,1220,-38	50+r,0,-38
	Vertical plus shear	-1900 (ϵ_{xx})	97	50+2r,0,0	50+r,1220,0

- (1) SED is Strain Energy of Distortion
 (2) See Figure 5 for location convention
 (3) r = radius of tire

TABLE 10 Ratios of Maxima: Constant Tire Type

TIRE TYPE	ϵ_{max} for (VERT+SHEAR) / ϵ_{max} for (VERT only)	SED _{max} for (VERT+SHEAR) / SED _{max} for (VERT only)
WB tire	6	5.5
Dual tires	6.5	9

Note: WB is Wide Base

TABLE 11 Ratios of Maxima: Constant Loading Stress

LOADING STRESSES	WB ϵ_{max} / DUAL ϵ_{max}	WB SED _{max} / DUAL SED _{max}
Vertical only	1.25	2
Vertical plus shear	1.15	1.3

Note: WB is Wide Base tires, DUAL is Dual tires

carefully address and analyze this finding. The analysis of damage accumulation models for tridem axle configurations is another issue that merits further investigation. This paper, however, concentrated only on the analysis of primary responses.

CONCLUSIONS

1. On the basis of the literature review, a definitive tire load limit (pounds per inch) does not exist that will enable one to reliably predict the pavement effects from wide-base

tires compared with dual tires under any axle configuration. Despite this, the data show that if a tire load limit is required for wide-base tires it should be substantially less than values that are typical for dual tires. A limit greater than 88 N/mm (500 lb/in.) is not justified using available literature cited in this study. Limits between 60 and 80 N/mm (350 and 450 lb/in.) are justifiable on the basis of published investigations.

2. Previous studies assume simple and incomplete loading conditions that differ from actual circumstances. The mechanistic analysis in this paper shows that the effects of these simplifications significantly alter the predicted pavement response. Future mechanistic evaluations should continue to

simulate the nonuniform vertical and inward shear loadings exerted by tires on the pavement. Laboratory and field measurements should verify the influence of these factors.

3. The mechanistic analysis presented in this paper shows that peak tensile strains may occur in a more shallow part of the surface layer. This finding derives from the use of sublayers for modeling temperature gradients and from the inclusion of inward shear contact stresses. In addition, the use of strain energy of distortion to characterize failure potential leads to substantial differences among the conditions studied. Future studies should expand the use of sublayers to predict spatial distribution and critical values of both strain and strain energy.

4. The study of anisotropy is another subject that demands further attention, as well as specific loading conditions such as braking and turning stresses. CIRCLY can model such cases, being a unique characteristic of this analytical tool.

5. Further investigations should be focused on specific pavement response in well-designed and controlled experiments. These efforts will help establish a sound scientific basis for predicting the pavement effects from wide-base tires. Related research is part of an on-going project conducted by the Caltrans Division of New Technology, Materials, and Research, and other researchers at the PACCAR (parent company of Kenworth Trucking Company) test track in Washington State.

ACKNOWLEDGMENT

This work was supported by the California Department of Transportation.

REFERENCES

1. R. Backlund. *Issue 1 - Super Single Tires*. Highway Planning Technical Report HPN-21, FHWA, U.S. Department of Transportation, March 17, 1989.
2. T. L. Ford and J. Zekoski. Impact of Truck Tire Selection on Contact Pressures. *Proc., 25th Paving and Transportation Conference*, University of New Mexico, 1988.
3. E. Zube and R. Forsyth. An Investigation of the Destructive Effects of Flotation Tires on Flexible Pavements. *Highway Research Record 71*, HRB, National Research Council, Washington, D.C., 1965.
4. J. J. Emery and W. G. Heslop. A Comparison of Flexible Pavement Behaviour Under Dual and Flotation Tires for Static and Moving Loads. *Proc., Canadian Good Roads Association*, Vancouver, British Columbia, 1967.
5. R. L. Terrel and S. Rimstrong. Pavement Response and Equivalencies for Various Truck Axle and Tire Configurations. In *Transportation Research Record 602*, TRB, National Research Council, Washington, D.C., 1976.
6. J. T. Christison. *Evaluation of the Effects of Axle Loads on Pavements From In Situ Strain and Deflection Measurements*. Internal Report HTE-78/02. Transportation and Surface Water Engineering Division, Alberta Research Council, 1978.
7. J. T. Christison and B. P. Shields. Evaluation of the Relative Damage Effects of Wide-Base Tire Loads on Pavements. *RTAC Forum 1980*, Vol. 4, No. 1, 1980.
8. F. B. Snelgrove. *The Fuel Economy, Stability and Pavement Effects of the Wide-Base Radial Tire*. CVOS-TR-80-01. Ontario Ministry of Transportation and Communications, 1980.
9. K. R. Peattie. *The Influence of Axle Spacing on Flexible Pavement Damage*. Research Report 54. Department of Civil Engineering, University of Newcastle upon Tyne, 1984.
10. W. Gorge. *Evaluation of Research Efforts Concerning the Influence of Commercial Vehicle Development on the Road Fatigue*. German Automotive Technical Research Association, Technical University of Munich, 1984.
11. H. F. Southgate and R. C. Deen. *Effects of Load Distributions and Axle and Tire Configurations on Pavement Fatigue*. Research Report UKTRP-85-13. Kentucky Transportation Research Program, 1985.
12. K. G. Sharp, P. F. Sweatman, and D. W. Potter. *A Comparative Study of the Effects of Wide Single and Dual Tires on Rebound Pavement Deflection*. Internal Report AIR 1137-1. ARRB, 1986.
13. M. Huhtala, J. Pihlajamaki, and M. Pienimaki. The Effects of Tires and Tire Pressures on Road Pavements. In *Transportation Research Record 1227*, TRB, National Research Council, Washington, D.C., 1989.
14. R. Bonaquist. An Assessment of the Increased Damage Potential of Wide-Base Single Tires. *Proc., 7th International Conference on Asphalt Pavements*, 1992.
15. J. J. Hajek and A. C. Agarwal. Influence of Axle Group Spacing on Pavement Damage. In *Transportation Research Record 1286*, TRB, National Research Council, Washington, D.C., 1990.
16. L. J. Wardle. *Program CIRCLY - User's Manual*. Australia, 1977.
17. C. M. Gerrard and J. R. Morgan. Anisotropy and Non-linearity in Sand Properties. *Proc., 8th International Conference on Soil Mechanics and Foundation Engineers*, pp. 287-292, 1973.
18. J. Onas. *Anisotropy and Stress-Strain Behaviour of Soil*. M. Eng. Sc. thesis, University of Melbourne, Melbourne, Australia, 1970.
19. O. Bode. *Deutsche Kraftfahrforchung and Strassenverkehrstechnik Heft 146*. 1961.
20. N. Seitz and A. W. Hussman. Forces and Displacement in Contact Area of Free Rolling Tires. *SAE Transactions*, 710626, 1971.
21. D. F. Moore. *The Friction of Pneumatic Tyres*. Elsevier Publishers, 1975.
22. *California Vehicle Code*. Department of Motor Vehicles, Jan. 1992.
23. P. Yap. A Comparative Study of the Effect of Truck Tire Types on Road Contact Pressures. *SAE Transactions*, 881846, 1988.
24. M. A. Miner. Cumulative Damage in Fatigue. *Journal of Applied Mechanics*, Sept. 1945.
25. S. Timoshenko. *Strength of Materials*, Vol. 2, New York, 1956.
26. D. Perdomo and W. Nokes. *Preliminary Investigation of the Effects of Wide-Base Tires on Flexible Pavements*. EA 32131. March 31, 1992.
27. D. Perdomo, and W. Nokes. *Preliminary Investigation of the Effects of Wide-Base Tires on Flexible Pavements: Phase II*. EA 32147. Oct. 1, 1992.
28. A. H. Gerritsen et al. Prediction and Prevention of Surface Cracking in Asphaltic Pavements. *Proc., 6th International Conference on Structural Design of Asphalt Pavements*, 1987.
29. M. Dazats and R. Linder. A Method for the Evaluation of the Structural Condition of Pavements with Thick Bituminous Road Bases. *Proc., 5th International Conference on Structural Design of Asphalt Pavements*, 1982.

Publication of this paper sponsored by Committee on Flexible Pavement Design.

Development and Implementation of a Mechanistic, Empirically Based Overlay Design Procedure for Flexible Pavements

LINDA M. PIERCE, NEWTON C. JACKSON, AND JOE P. MAHONEY

In the early 1980s the Washington State Department of Transportation (WSDOT) implemented a new pavement management system (WSPMS) that is project specific and contains detailed construction history and performance data for all projects throughout the state. With the new WSPMS, all resurfacing designs were made with more detailed knowledge of the past performance of each project, and conflicts between design expectations and actual past performance of each project were more obvious. Using the information contained in the WSPMS and deflection data obtained from the falling weight deflectometer, WSDOT decided to develop a mechanistic, empirically based flexible pavement overlay design method and contracted with the University of Washington and the Washington State Transportation Center to cooperatively develop such a method. A general overview of this mechanistic, empirically based overlay design procedure describes subsequent implementation activities and demonstrates the application of the design procedure using a case study in which the WSDOT mechanistic, empirical design procedure is compared with other standard overlay design procedures.

The Washington State Department of Transportation (WSDOT), like most western state DOTs, has been designing all new flexible pavements by a rational, empirically based pavement design method for over 40 years. By the late 1940s, Washington State had adopted a flexible pavement design method that was based on the California bearing ratio (CBR) test. In 1951 the CBR test procedure was abandoned in favor of a method that utilizes the Hveem stabilometer. The design procedure was essentially that originated by Hveem and Carmany (1). The principal differences between Washington's design procedure and the original California procedure were modifications in test procedures and in factors used for the base and pavement courses. The modifications were incorporated in the design to reflect field conditions and pavement performance experienced in Washington State. These design procedures and processes were first described by LeClerc in a presentation at the annual Highway Research Board meeting in 1956 (2). The basic design procedures were modified in 1957 and in 1966 to provide more detail in the design charts, which resulted in thicker asphalt pavement sections.

In 1974 Washington State established a formal 4-R pavement design process in response to the FHWA requirement for a determination of structural adequacy to qualify for federal aid for resurfacing projects. A component design pro-

cedure was adopted similar to that contained in the AASHTO Interim Pavement Design Guide and the Asphalt Institute's design procedures, except that Washington's was based on their Hveem design method. Benkleman beam deflections were collected in some districts and a comparison was made using the Asphalt Institute's rebound deflection-based design.

In the early 1980s WSDOT implemented its new pavement management system (WSPMS), which was project specific and had detailed construction history and performance data for all pavement sections throughout the state. With the WSPMS, all resurfacing designs were made with more detailed knowledge of the past performance of each project; thus, conflicts between design expectations and the actual past performance of each project became more obvious. Also at about this same time WSDOT obtained a falling weight deflectometer (FWD) as part of a federal research study on long-term pavement monitoring. Being somewhat dissatisfied with the adequacy of the current component and deflection-based procedures, plus having a current data base with detailed pavement performance data and a modern field pavement testing device, WSDOT decided to develop a mechanistic, empirically based flexible pavement overlay design method. Further, the general rehabilitation philosophy of WSDOT was to "fix it early, fix it thin." In this regard it was believed that the mechanistic, empirical approach would best provide overlay thicknesses that reflect the "early" treatment of small amounts of fatigue cracking (which is the dominant rehabilitation "trigger" distress for WSDOT). This work began in the mid-1980s when WSDOT contracted with the University of Washington and the Washington State Transportation Center to cooperatively develop a flexible pavement overlay design procedure. The resulting mechanistic, empirically based overlay procedure as developed was described in the final report dated January 1989 (3). When the development process began in 1985, the mechanistic, empirical design approach had been developed by other researchers; however, the issues of seasonal moduli changes, appropriate field failure criteria, and backcalculation of layer moduli were still at an early stage. The research team spent considerable effort on these basic issues and placed the entire system into personal computer compatible software.

This paper will provide an overview of the mechanistic, empirically based overlay design procedure, describe subsequent implementation activities, and demonstrate the application of the design procedure using a case study in which the WSDOT mechanistic, empirical design procedure is compared with other standard overlay design procedures.

L. M. Pierce and N. C. Jackson, Washington State Department of Transportation, P.O. Box 167, Olympia, Wash. 98507. J. P. Mahoney, University of Washington, 121 More Hall, FX-10, Seattle, Wash. 98195.

DEVELOPMENT OF THE PROCEDURE

The development of a mechanistic, empirical overlay design procedure requires a pavement response model, material characterization, and failure criteria. The associated tasks for the development of the overlay procedure are as follows.

Test Site Selection

To examine specific pavement performance in Washington State, 16 test sites were selected. These test sites were typical flexible pavement sections and were selected both for their uniformity (construction, distress, and subgrade soil) within each test site and for their variety (age, climate, traffic, structural section, and distress).

Laboratory Testing

Field asphalt concrete cores and unbound disturbed material samples were collected from each test site with the WSDOT Materials Laboratory performing the associated laboratory tests. To determine the modulus of elasticity of the asphalt concrete, the diametral resilient modulus test (ASTM D4123) was conducted at 5°C, 25°C, and 40°C (41°F, 77°F, and 104°F) with a load duration of 100 msec. To determine the resilient modulus of the unbound materials, the samples were re-molded and recompactd at a moisture content and density similar to those observed in the field at the time of sampling. A triaxial test was performed on each sample with confining pressures of 7, 14, and 28 kPa (1, 2, and 4 psi) and deviator stresses of 7, 14, 28, 41, and 55 kPa (1, 2, 4, 6, and 8 psi), in accordance with AASHTO T274. Asphalt concrete layer thicknesses were also determined from core samples.

Nondestructive Testing

WSDOT collected pavement surface deflection measurements with the FWD. These measurements were collected in the outer wheelpath nearly every season from 1985 to 1988.

Characterization of Pavement System

Pavement Model

Of several pavement models, the multilayered elastic system has been shown to provide reasonable pavement response solutions, in terms of deflection, stress, or strain caused by an applied load. The multilayered elastic model requires the following assumptions:

1. The material properties of each layer are homogeneous and isotropic;
2. Each layer has a finite thickness, except for the lower layer, and all layers are infinite in the lateral direction, and
3. The materials are characterized by the modulus of elasticity (resilient modulus) and Poisson's ratio (4).

Some contradictions to these assumptions include the variability in traffic load intensity; the elliptical or rectangular, rather than the assumed circular, shape of the tire footprint; dynamic rather than static loading; pavement material behavior that is not fully elastic; material properties of a single layer that are somewhat inhomogeneous and anisotropic; and the modulus of a single layer that is an equivalent modulus even though the layer is composed of many different materials. However, a fully monitored pavement experiment showed that the multilayered, linear elastic theory was acceptable (5). Several computerized solutions for the analysis of multilayered systems have been developed. This study used CHEVRON N-LAYER, which was developed by the Chevron Research Company (6). A principal reason for its use was that the software was in the public domain.

Asphalt-Bound Material

The modulus of asphalt concrete depends on its material characteristics and testing conditions (loading time and temperature). The relationship between the resilient modulus and temperature for WSDOT Class B asphalt concrete was found as follows (7):

$$\log E_{AC} = 6.4721 - 0.000147362(T_p)^2 \tag{1}$$

where E_{AC} is the resilient modulus of asphalt concrete (psi) and T_p is the pavement temperature (°F).

Unstabilized Materials

The modulus of unstabilized materials depends to a great extent on stress level, dry density, moisture content, degree of saturation, gradation, load duration, and frequency, among which stress level and moisture condition have proven to be the most significant factors. Chou (8) has shown a direct relationship between the modulus and the stress state for unstabilized base materials and subgrade soils.

Several resilient modulus tests were conducted on the granular base material (the unbound bases were all produced to the same specifications; hence, some statewide uniformity). Most of the granular base materials were best represented by the following equation (personal communication between J. P. Mahoney and N. C. Jackson, Feb. 5, 1990):

$$E_{BS} = 8,500\theta^{0.375} \tag{2}$$

where E_{BS} is the resilient modulus of the coarse-grained materials and soils (pounds per square inch) and, θ is bulk stress (pounds per square inch).

STRUCTURAL EVALUATION OF PAVEMENT

The need for information about the in situ pavement layer properties is readily apparent for pavement overlay design and hence the development of optimal pavement rehabilitation strategies. Material properties can be acquired either by laboratory test of samples or by a nondestructive testing (NDT)

evaluation method. Because of the cost and time constraints of the laboratory test, plus the ability to characterize materials as they exist in place, the NDT method is being used more frequently (9). At the time of initial development of the design process, NDT evaluations, which generally use the pavement surface deflection basin, were accomplished by either graphic solution or backcalculation. The latter was felt to be more accurate and robust. Thus, the backcalculation procedure for NDT deflection measurements becomes crucial for pavement rehabilitation, and a significant amount of the reported study resources were devoted to backcalculation development. It is ironic that several other backcalculation programs were under way in other states at about the same time.

Pavement Deflection Analysis Program (EVERCALC)

EVERCALC (10) is a pavement analysis computer program that is based on the multilayered elastic pavement analysis program CHEVRON *N-LAYER*. The program is primarily for the analysis of flexible pavement using FWD deflection measurements. A reverse-solution technique is used to determine elastic modulus from the deflection measurements. (Actually, the pavement surface deflections at a known load and assumed Poisson's ratio and known thickness of each layer are required.) The theoretical deflections are compared with the measured deflections in each iteration. When the discrepancies in the calculated and measured deflections, as characterized by the root mean square error, or the changes in moduli fall within the allowable tolerance, or the number of iterations has reached the specified limit, the program terminates. The current version of the program (EVERCALC 3.3) is capable of evaluating a flexible pavement structure containing up to five layers and can run with or without a "stiff layer." The program makes an initial, rough estimate of modulus ("seed modulus") for each layer using internal regression equations and then backcalculates to determine a "final" modulus for each pavement layer. The program also determines the coefficients of stress sensitivity for unstabilized materials when the deflection data for two or more load levels are available at a given point and then normalizes the asphalt concrete modulus to the WSDOT standard laboratory condition [which is 25°C (77°F)]. The seed moduli are estimated with internal regression equations, which were developed from the relationship among the layer moduli, surface deflections, applied load, and pavement thicknesses (11).

OVERLAY DESIGN PROCEDURE

Traffic load repetitions and environment are two primary factors that induce pavement distress (other factors include construction variation and age). Of the various kinds of distress, fatigue cracking and rutting are the two primary distresses found in flexible pavements in Washington State (mostly fatigue cracking). Numerous studies of pavement distress have shown that pavement performance is related to pavement response parameters (such as strain), which are determined through mechanistic pavement analysis.

This section reviews the design criteria (failure criteria) and a mechanistic, empirically based overlay design procedure computer program, EVERPAVE.

Design Criteria

Investigations have shown that fatigue failure is best related to the horizontal tensile strain at the bottom of the asphalt-bound layer and that rutting can be best related to the vertical compressive strain at the top of the subgrade (12).

The models for fatigue failure criteria generally are a function of the tensile strain and the modulus of the asphalt-bound material. Monismith's laboratory model, one of the most widely used, is as follows (13):

$$\log N_f = 14.82 - 3.291 \log(\epsilon_t) - 0.854 \log(E_{AC}/1,000) \quad (3)$$

where

- N_f = loads to failure,
- ϵ_t = initial tensile strain (10^{-6} in./in.), and
- E_{AC} = modulus of asphalt bound material (psi).

This model was developed for asphalt concrete mixes quite similar to those used by WSDOT. However, the model raises two concerns for overlay design. One is the adjustment of this laboratory relationship to field conditions, and the other is the consideration of the existing asphalt concrete layer.

Because differences exist between the laboratory and actual pavement in the definition of failure and loading mode, laboratory fatigue models need to be adjusted to field conditions. To do this, the laboratory model is multiplied by a shift factor (SF). The resulting predictive equation becomes $N_{field} = (N_{lab})(SF)$. The shift factor depends on asphalt concrete properties such as void ratio, asphalt cement content, and viscosity and other factors such as layer thickness and pavement loading conditions. An investigation of the shift factor, using Monismith's laboratory model for initial pavement performance (i.e., N_{lab}), was attempted at six test sites in Washington State that showed fatigue distress, as shown in Table 1. The service lives of the pavements were 10 to 13 years, and the thicknesses of the asphalt concrete ranged from about 100 to 250 mm (4 to 10 in.). The moduli of the original asphalt concrete were estimated on the basis of engineering judgment and the results of laboratory tests on pavement cores. The moduli of the unbound materials were obtained through backcalculation and seasonal material modulus variations, which will be discussed later. The shift factor ranged from 0.1 to about 6.0, depending on the asphalt-bound layer thickness. However, the lower shift factors were for thick asphalt concrete [about 203 to 229 mm (8 to 9 in.)]. Thus, shift factors of about 6.0 were found for sections with asphalt concrete thickness of 90 to 130 mm (4 to 5 in.). We generally observe that for asphalt concrete pavement thicknesses of about 200 mm (8 in.) or greater, fatigue cracking primarily occurs in the upper wearing course (top-down cracking). For thicker asphalt concrete sections [200 mm (8 in.) or more], structural overlay designs are rarely needed (EVERPAVE is not used for overlay design on thicker asphalt concrete sections). Treatments such as milling and replacement of the distressed surface course are generally recommended.

The second concern is how the performance of the existing asphalt concrete layer is incorporated into the overlay design procedure. This situation poses difficulties because the fatigue failure criteria were developed for new asphalt concrete. Some design procedures consider the strain at the bottom of the new asphalt concrete layer; others consider the strain only at

TABLE 1 Washington State Shift Factors

Test Site	AC Thickness (mm)	ESAL (10^3)	Age (yrs)	Shift Factor
1	132	640	11	5.8
3	213	466	13	0.4
8	185	700	12	2.5
10	229	389	12	0.1
13	244	2,135	12	0.5
15	91	332	10	5.6

Note: The modulus of the original asphalt concrete was assumed to be 2,756 MPa. ESALs accumulated from the original construction date to the time of fatigue cracking.

the bottom of the existing asphalt concrete layer, and others consider both of these strains (14–18). Both strains (bottom of the new overlay layer and the bottom of the existing (pre-overlay) asphalt concrete) were considered in this study and are used in EVERPAVE. The rationale for this is straightforward in that strain (or other movement) in the existing asphalt concrete layer must be controlled to reduce the potential for reflection cracking into the new overlay layer.

Rutting occurs because of permanent deformation of the asphalt concrete layer and unbound layers. However, since the permanent deformation of asphalt concrete is more a construction, materials issue instead of a structural thickness issue, the failure criterion is expressed as a function of vertical compressive strain at the top of the subgrade. The Chevron equation was used to estimate rutting in the subgrade, as follows:

$$N_r = 1.077 \times 10^{18} (\epsilon_{vs})^{-4.4843} \quad (4)$$

where N_r is the number of loads needed to cause a rut depth of approximately 19 mm (0.75 in.) and ϵ_{vs} is the vertical compressive strain at the top of the subgrade (10^{-6} in./in.)

Because there have been no visible signs of rutting in the 16 test site locations, validation of the rutting model has not been possible. In addition, for Washington State, fatigue instead of rutting typically is the controlling pavement failure criteria.

Pavement Environmental Effects in Washington State

The consideration of environmental conditions (as a function of resilient modulus) is essential in mechanistic, empirical pavement design. Seasonal adjustment for asphalt-bound materials is obtained from the relationship between the modulus and temperature. However, for unbound (unstabilized) materials that process is not so straightforward.

Two types of climate prevail in the state of Washington: a marine type in the west and a continental climate in the east. In western Washington, there are two distinct seasons, a warm and dry summer and a wet and mild winter. Eastern Washington experiences a hot and dry summer and a cold winter;

thus spring thaw problems can exist. The predominant roadbed soils are mostly silts and various types of glacial till and clay.

The seasonal variations of soil moduli are primarily induced by variations in soil moisture content, which depend on precipitation, temperature, soil gradation and permeability, surface distress level, and drainage conditions (19). Seasonal variations for each of the two regions were investigated over two distinct seasons (wet or dry) that were based on the back-calculated moduli from 4 years of FWD data and climate data obtained from published climatological information. The ratios of the moduli of various seasons were determined and are indicated in Table 2. The seasonal variations were reevaluated in June 1992 and were found to be unchanged from the values determined in the original study.

Several studies in Washington State have examined the various aspects of seasonal pavement material changes. The observation that the base course changes the most came as no surprise. This change is probably the result of the larger layer moisture changes in the base course layer, compared with those of subgrade layer.

Traffic in Washington State

The equivalent single-axle load (ESAL) concept was adopted for the traffic input [80 kN (18,000 lb)]. The primary concern is how to quantify the mixed traffic for a design period to use in pavement design. FHWA's W-4 loadometer tables were used to determine ESALs for various truck types from 1950 to 1983. Structural numbers of 3.0 and 5.0 were assumed for the pavements built before and after 1963, respectively. A summary of the determined ESAL factors are listed in Table 3.

Overlay Design Program (EVERPAVE)

EVERPAVE (20) is a mechanistic, empirically based overlay design program. The pavement analysis is accomplished through use of EVERSTRS (used as a subroutine), which can account for the stress-sensitive characteristics of the unbound mate-

TABLE 2 Seasonal Variations of Unbound Material Moduli for Washington State

Region	Base		Subgrade	
	Wet/Thaw	Dry/Other	Wet/Thaw	Dry/Other
Eastern Washington	0.65	1.00	0.95	1.00
Western Washington	0.80	1.00	0.90	1.00

TABLE 3 Summary of ESAL Factors

Highway System	Single Units	Combination Units	Buses	Individual Axle	Overall Truck*
Interstate	0.30	1.25	1.30	0.25	1.20
Non-Interstate Rural	0.50	1.50	1.30	0.25	1.40
Non-Interstate Urban	0.25	1.20	1.30	0.25	1.00

* Excludes Buses

rials (8). A flow chart of the EVERPAVE program is presented in Figure 1.

The program can analyze a pavement system up to five layers, including the new overlay. The pavement responses under single or dual wheel loads are determined from the analysis of a pavement system, as shown in Figure 2. The responses include the failure criteria for fatigue and rutting, which are a function of the tensile strains at the bottom of the overlay asphalt concrete and that of the existing asphalt concrete layer, and the compressive strain at the top of the subgrade. The program calculates overlay thickness by comparing the pavement performance lives for fatigue and rutting with the projected design traffic volume (ESALs). When the minimum repetitions of the two failure criteria are greater than the traffic volume, the final overlay thickness is produced. Otherwise, the overlay thickness is increased by increments (an input data requirement) and the analysis is re-

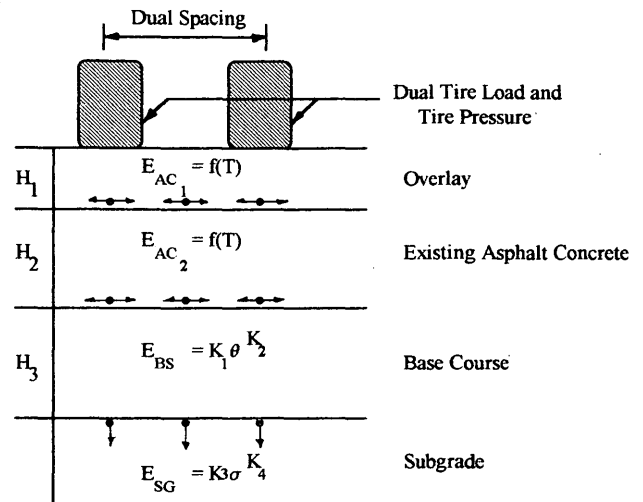


FIGURE 2 Pavement system for overlay design for four layers.

peated. This process continues until the maximum distress performance period exceeds the design traffic volume.

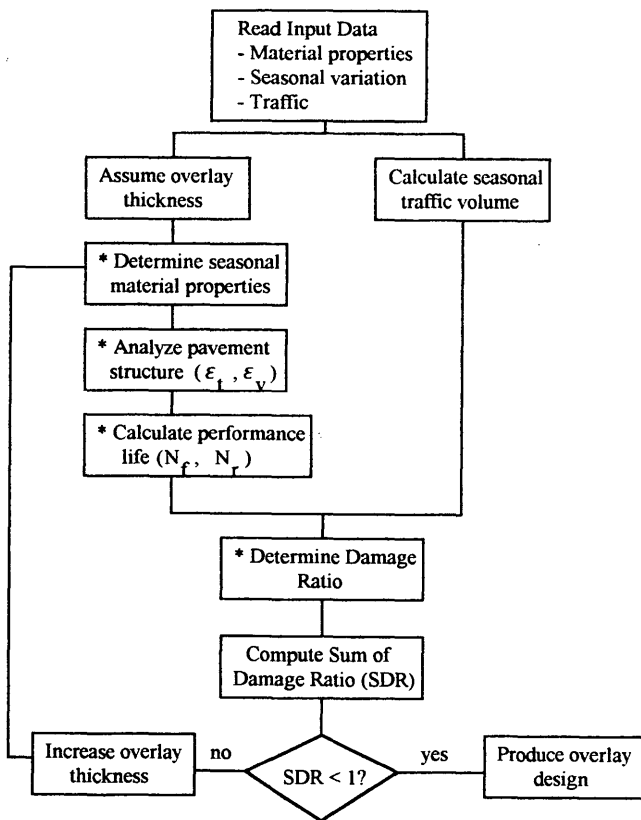
IMPLEMENTATION OF THE PROCEDURE

A resurfacing report is prepared by the district materials engineer for all asphalt concrete (AC) overlays and is even recommended for bituminous surface treatments in which structural problems are evident (21). The resurfacing report includes pavement deflection data (which are collected by the headquarters materials branch), descriptions and photographs of typical pavement conditions, road life history, pavement cores, surfacing and subgrade samples, and a review of drainage features. The resurfacing report is oriented toward analyzing the existing roadway conditions so that a reasonable definition of the special problems and structural needs of the roadway may be defined.

Upon submittal of the resurfacing report to the headquarters materials branch, the materials branch reviews the contents of the report, performs a mechanistic, empirical design analysis (when FWD data are available), and submits a final headquarters overlay design.

The mechanistic, empirical design analysis is composed of two distinct parts: materials analysis and overlay design. Materials analysis, which may include pavement layer backcalculation, has been purposely separated from the overlay design process so that the backcalculated material properties can be characterized before input for overlay design.

A comparison of the overlay thicknesses produced by various methods was used to examine the new overlay design



* Repeat for four seasons

FIGURE 1 Overlay design procedure by EVERPAVE.

procedure (EVERPAVE). Because every overlay design method has its own peculiar design parameters, the comparisons were limited to the revised AASHTO (22) and the Asphalt Institute methods (23). To illustrate how the process works, a typical project is presented as a case study.

CASE STUDY

State Route 500 (Milepost 2.00 to Milepost 3.05) is a section of urban undivided multilane highway located in southwestern Washington (near Vancouver, Washington). The soil consists largely of fluvial deposited (deposited under water) sands and silts. The cuts through this material intercepted considerable perched water flowing in the sandy soils between the silt lenses at varying depths through the cut. The environment is typical of the Pacific Northwest coast, relatively mild temperatures, both in summer and winter, with an annual rainfall of about 1,000 mm (40 in.) per year, mostly occurring from midfall through late spring.

The roadway was constructed in 1983 with 3.7-m (12-ft) lanes and 1.2-m (4-ft) inside shoulders and 3-m (10-ft) outside shoulders. The pavement section consists of 108 mm (4.25 in.) of asphalt concrete, over 70 mm (2.75 in.) of crushed rock base, over 127 mm (5.0 in.) of gravel base. This roadway was a staged construction, which called for placing a second-stage AC overlay 5 to 6 years after the initial construction. The original construction included an extensive system of drains to mitigate erosion and to intercept the perched water before it reached the subgrade. It is clear that the drainage design did not control the subsurface water as well as expected, as was evident when the pavement began to fatigue crack within 4 to 5 years after construction. Subsequent investigations indicated that the sandy subgrade soils have stabilized at a moisture content of about 3 to 5 percent over optimum, resulting in a structurally underdesigned pavement section. As a result of the staged pavement design and the wet subgrade, the pavement began to experience both longitudinal and fatigue cracking in approximately 10 percent of the total area of the wheelpaths by the spring of 1988. The estimated ESALs for the next 10 years is 2 million.

FWD data were collected for this project in April 1988. The average center deflection (D_0) is 508 μm (20.0 mils), with values ranging from 371 to 678 μm (14.6 to 26.7 mils). The subgrade modulus ranges from 79 to 166 MPa (11,537 to 24,100 psi), and averaging 120 MPa (17,351 psi) with a standard deviation of 30 MPa (4,420 psi) (24).

Asphalt Institute's Deflection Procedure

Representative rebound deflection (RRD)

$$= 671 \mu\text{m} (26.4 \text{ mils})$$

$$\text{Overlay thickness} = 0.0 \text{ mm}$$

Asphalt Institute's Effective Thickness Procedure

Effective thickness of existing pavement (108 mm AC)(0.75)

$$= 81 \text{ mm} (3.2 \text{ in.})$$

$$\begin{aligned} \text{Effective thickness of base (197 mm base)(0.20)} \\ = 39 \text{ mm} (1.6 \text{ in.}) \end{aligned}$$

$$\text{Total effective thickness} = 120 \text{ mm} (4.7 \text{ in.})$$

1. Milepost (MP) 2.05

$$M_R = 83 \text{ MPa} (12,000 \text{ psi})$$

$$\text{Design thickness} = 235 \text{ mm} (9.3 \text{ in.})$$

$$\text{Effective thickness} = 120 \text{ mm} (4.7 \text{ in.})$$

$$\text{Overlay thickness} = 115 \text{ mm} (4.5 \text{ in.})$$

2. MP 2.55

$$M_R = 76 \text{ MPa} (11,000 \text{ psi})$$

$$\text{Design thickness} = 241 \text{ mm} (9.5 \text{ in.})$$

$$\text{Effective thickness} = 120 \text{ mm} (4.7 \text{ in.})$$

$$\text{Overlay thickness} = 121 \text{ mm} (4.8 \text{ in.})$$

Revised AASHTO

The overlay was determined using the FWD deflection basins at MP 2.05 and MP 2.55 and using only the NDT method.

1. MP 2.05

$$D_0 = 678 \mu\text{m} (26.7 \text{ mils})$$

$$D_{36} = 140 \mu\text{m} (5.5 \text{ mils})$$

$$C = 1.00, 0.50, \text{ and } 0.33$$

$$D = 305 \text{ mm} (12 \text{ in.})$$

$$p_i = 4.5$$

$$p_r = 2.5$$

$$S_0 = 0.49$$

$$R = 50 \text{ percent}$$

$$M_R = (C = 1.00) 75 \text{ MPa} (10,909 \text{ psi})$$

$$(C = 0.50) 38 \text{ MPa} (5,455 \text{ psi})$$

$$(C = 0.33) 25 \text{ MPa} (3,636 \text{ psi})$$

$$\begin{aligned} \text{Overlay thickness } (C = 1.00) &= 40 \text{ mm} (1.6 \text{ in.}) \\ (C = 0.50) &= 89 \text{ mm} (3.5 \text{ in.}) \\ (C = 0.33) &= 122 \text{ mm} (4.8 \text{ in.}) \end{aligned}$$

2. MP 2.55

$$D_0 = 572 \mu\text{m} (22.5 \text{ mils})$$

$$D_{36} = 158 \mu\text{m} (6.2 \text{ mils})$$

$$C = 1.00, 0.50, \text{ and } 0.33$$

$$D = 305 \text{ mm} (12 \text{ in.})$$

$$p_i = 4.5$$

$$p_r = 2.5$$

$$S_0 = 0.49$$

$$R = 50 \text{ percent}$$

$$M_R = (C = 1.00) 67 \text{ MPa} (9,677 \text{ psi})$$

$$(C = 0.50) 33 \text{ MPa} (4,893 \text{ psi})$$

$$(C = 0.33) 22 \text{ MPa} (3,226 \text{ psi})$$

Overlay thickness ($C = 1.00$) = 28 mm (1.1 in.)
 ($C = 0.50$) = 77 mm (3.0 in.)
 ($C = 0.33$) = 112 mm (4.4 in.)

where

- D_0 = FWD center deflection,
 D_{36} = FWD deflection at 36 in. from the load plate,
 C = adjustment factor: "The recommended method for determination of the design M_R from NDT back-calculation requires an adjustment factor (C) to make the value calculated consistent with the value used to represent the AASHTO subgrade. A value for C of no more than 0.33 is recommended for adjustment of backcalculated values to design M_R values." (23),
 D = actual pavement structure thickness,
 p_i = initial serviceability index,
 p_t = terminal serviceability index,
 S_0 = overall standard deviation of normal distribution of errors associated with traffic prediction and pavement performance,
 R = reliability level, and
 M_R = effective roadbed resilient modulus.

WSDOT Mechanistic, Empirically Based Overlay Design

The EVERCALC backcalculation results (24) were examined and the following conditions were determined:

- Existing AC modulus: 1654 MPa (240,000 psi), which represents a partially cracked AC pavement condition, 3858 MPa (560,000 psi), which represents an unfatigued AC pavement condition.
- Base course modulus conforms to $E_{BS} = 8,500\theta^{0.375}$
- Subgrade modulus (using stiff layer): 76 and 83 MPa (11,000 and 12,000 psi)
- AC overlay modulus: 2756 MPa (400,000 psi)
- Fatigue criterion relationship: $SF = 5$

The results are as follows:

- MP 2.05
 $E_{AC} = 1654$ MPa (240,000 psi)
 $M_R = 83$ MPa (12,000 psi)
 Overlay thickness = 91 mm (3.6 in.)
- MP 2.55
 $E_{AC} = 3858$ MPa (560,000 psi)
 $M_R = 76$ MPa (11,000 psi)
 Overlay thickness = 611 mm (2.4 in.)

The overlay design that was selected for this project is 76 mm (3.0 in.) AC pavement after repairing the worst of the fatigue cracked pavement. Table 4 summarizes the overlay design for this case study.

ADDITIONAL STUDIES

With the development of the mechanistic, empirically based overlay design procedure, the need has evolved for additional

TABLE 4 Summary of Overlay Design Thickness

	MP 2.05	MP 2.55
Asphalt Institute		
Deflection Procedure	0	0
Effective Thickness Procedure	115 mm	121 mm
AASHTO		
$C = 1.00$	40 mm	28 mm
$C = 0.50$	89 mm	77 mm
$C = 0.33$	122 mm	112 mm
WSDOT EVERPAVE	91 mm	61 mm
Constructed Overlay	76 mm	76 mm

studies to validate and modify the various aspects in both the EVERCALC and the EVERPAVE computer programs. Currently, WSDOT, in conjunction with the University of Washington, has conducted several studies to validate program conditions.

DEPTH TO STIFF LAYER

The depth to stiff layer is estimated using the scheme reported by Rohde and Scullion (25) and has been incorporated into the current version of EVERCALC. The original development of this scheme requires the use of one of four separate regression equations that are dependent on ranges of the AC layer thickness [less than 50 mm (2.0 in.)], between 50 and 100 mm (2.0 to 4.0 in.), between 100 and 150 mm (4.0 to 6.0 in.) and greater than 150 mm (6.0). It has been found that the regression equations are not continuous across the AC layer ranges. Therefore, as time allows, this issue (and equations), will be revisited.

The effect that a water table may have on the calculated layer moduli is currently being examined. If the depth-to-stiff-layer option is used, a moduli and Poisson's ratio for the stiff layer must be selected. This layer has a significant effect on the calculated layer moduli and root-mean-square error. Several locations are being evaluated where FWD and boring logs are available. In some cases it has been found that the depth-to-stiff layer is actually the depth to the water table or an area of saturated soils. Generally, it appears that lower moduli are appropriate for the "stiff layer" where this condition exists.

SHIFT FACTOR

The EVERCALC/EVERPAVE process has been in use in Washington State since 1988. WSDOT evaluates about 100 projects a year as part of the basic overlay design process. With some additional work the actual fatigue performance (shift factor) can be estimated. It is the intent of WSDOT to further evaluate these past overlay designs, reevaluate the originally determined shift factors, and build a fairly large and comprehensive data base documenting the range of fatigue performance experienced in the state of Washington.

RELIABILITY

Currently the EVERPAVE program uses a 50 percent reliability. As the modifications to the AASHTO Design Guide

become available and are further evaluated, a range of reliability values will also be incorporated into the EVERPAVE program.

SUMMARY

The mechanistic, empirical flexible pavement overlay design procedure developed for WSDOT has been overviewed. It uses somewhat traditional failure criteria for estimating fatigue cracking and rutting. These criteria were simply adaptations of prior work that were "shifted" to accommodate conditions found in Washington State. Further, the seasonal effects of changing moduli were investigated and incorporated as seasonal moduli ratios.

The required layer moduli for design are assumed (as for the new AC overlay material) or estimated via laboratory tests or NDT analysis. The primary use of the NDT data (from the FWD) is for backcalculation. After several years of experience obtaining and using backcalculated pavement moduli, we believe that this fundamental approach is valid. However, we continue to gain experience mostly through empirical evidence on how to improve our backcalculation process.

The mechanistic, empirical design process has many clear advantages over conventional (empirically based) design processes. Our experience has shown that it is not only a more rational design process; it also more adequately addresses unique conditions, such as the following:

1. Overlays of granular surfacing with thin surface seals, which are very strain critical.
2. Overlays of thick AC in which the existing AC is moisture sensitive and has lower stiffness and tensile strength than normal AC.
3. Overlays with materials that have different fatigue properties from normal AC, such as open-graded emulsion mixes, or some of the new AC mixes with modified AC binders.

The design process is sensitive to the material properties selected for input. Effective use of the design process requires a rigorous and accurate analysis of the in situ material properties. Most of the effort required to use the design process is in analyzing and characterizing the in situ material properties.

The overall goal of designing AC overlay thickness that are appropriate for "early" distress to "extreme" distress was accomplished by the design process described in this paper. The design process is not unlike that developed by numerous other researchers; however, what may be somewhat unique is the development process, whereby WSDOT and the Washington State Transportation Center (University of Washington) worked together, as a team, throughout various research efforts. Early results were trial implemented and subsequently refined. The end results are a fully implemented design system.

ACKNOWLEDGMENT

The authors would like to express their appreciation to the Research Office of the Washington State Department of

Transportation for their continued support and assistance in the completion of this study.

REFERENCES

1. F. N. Hveem and R. M. Carmany. The Factors Underlying the Rational Design of Pavements. *HRB Proc.* 1948.
2. R. V. LeClerc. Flexible Pavement Design in the State of Washington. Presented at 35th Annual Meeting of the Highway Research Board, Washington, D.C., 1956.
3. J. P. Mahoney, S. W. Lee, N. C. Jackson, and D. E. Newcomb. *Mechanistic-Based Overlay Design Procedure for Washington State Flexible Pavements*. WSDOT Research Project GC8286, Task 29, Jan. 1989.
4. D. M. Burmister. The Theory of Stress and Displacements in Layered System and Application to the Design of Airport Runways. *HRB Proc.*, Washington D. C., 1943.
5. W. G. Bleyenbergh, A. I. M. Claessen, F. V. Gorkum, W. Heukelop, and A. C. Pronk. Fully Monitored Motorway Trails in the Netherlands Corroborate Linear Elastic Design Theory. *Proc., 4th International Conference on the Structural Design of Asphalt Pavements*, University of Michigan, Ann Arbor, Vol. 1, 1977, pp. 75-90.
6. J. Michelos. *Analysis of Stress and Displacements in an N-Layered Elastic System Under a Load Uniformly Distributed on a Circular Area*. California Research Corporation, Richmond, Calif., 1963.
7. A. A. Bu-bushait. *Development of a Flexible Pavement Fatigue Model for Washington State*. Ph.D. dissertation. University of Washington, Seattle, 1985.
8. Y. T. Chou. *Engineering Behavior of Pavement Materials: State of the Art*. Report FAA-RD-77-37. U.S. Army Engineer Waterways Experiment Station, Vicksburg, Miss., Feb. 1977.
9. *Summary of the AASHTO Questionnaire on The Guide for Design of Pavement Structures, 1986*. FHWA, Office of Highway Operations, Washington D.C., April 1988.
10. *EVERCALC User's Guide*. Washington State Transportation Center, University of Washington, Seattle, April 1987.
11. D. E. Newcomb. *Development and Evaluation of Regression Methods to Interpret Dynamic Pavement Deflections*. Ph.D. Dissertation. University of Washington, Seattle, 1986.
12. *Research and Development of the Asphalt Institute's Thickness Design Manual (MS-1)*, 9th ed. Research Report 82-2. The Asphalt Institute, College Park, Md. Aug. 1982.
13. C. L. Monismith and J. A. Epps. Asphalt Mixture Behavior in Repeated Flexure. Institute of Transportation and Traffic Engineering, University of California, Berkeley, 1969.
14. R. C. Koole. Overlay Design Based on Falling Weight Deflectometer Measurements. In *Transportation Research Record 700*, TRB, National Research Council, Washington D.C., 1979, pp. 59-72.
15. M. S. Mamlouk and B. E. Sebaaly. Overlay Thickness Design for Flexible Pavements. In *Transportation Research Record 993*, TRB, National Research Council, Washington D.C., 1986, pp. 63-66.
16. R. E. Smith, M. I. Darter, and R. L. Lytton. Mechanistic Overlay Design Procedures Available to the Design Engineer. In *Transportation Research Record 1060*, TRB, National Research Council, Washington D.C., 1986.
17. M. R. Thompson and M. S. Hoffman. Concepts for Developing a NDT Based Asphalt Concrete Overlay Thickness Design Procedure. Presented at 62nd Annual Meeting of the Transportation Research Board, Washington D.C., 1983.
18. J. H. Tenison, Jr. *Proposed New Mexico State Highway Department Elastic-Layered Overlay Evaluation and Design Procedure for Asphalt Concrete Pavements*. Research Report MB-RR-83/2. Materials Laboratory Bureau, New Mexico State Highway Department, Santa Fe, N. Mex., 1983.
19. J. A. Lary, J. P. Mahoney, C. A. Bell, and R. G. Hicks. Seasonal Environmental Effects on the Strength of Pavement Structures. Research Report for the U.S. Forest Service, University of Washington, Seattle, May 1983.
20. *EVERPAVE USER'S GUIDE*. Washington State Transportation Center, University of Washington, Seattle, 1987.

21. Washington State Transportation Commission. *Design Manual*. Washington State Department of Transportation, Olympia, 1987.
22. M. I. Darter, R. P. Elliott, and K. T. Hall. *Revision of AASHTO Pavement Overlay Design Procedures*. Final Report. NCHRP, TRB, National Research Council, Washington, D.C., April 1992.
23. *Asphalt Overlays for Highway and Street Pavement Rehabilitation*. Manual Series 17. The Asphalt Institute, College Park, Md., June 1983.
24. J. P. Mahoney, D. E. Newcomb, N. C. Jackson, and L. M. Pierce. *Pavement Moduli Backcalculation Short Course*. NHI Short Course, Reno, Nev., Sept. 1991.
25. G. T. Rohde and T. Scullion. *MODULUS 4.0: Expansion and Validation of the Modulus Backcalculation System*. Research Report 1123-3. Texas Transportation Institute, Texas A&M University System, College Station. Nov. 1990.

Publication of this paper sponsored by Committee on Pavement Rehabilitation.

Performance Monitoring of Joint Load Transfer Restoration

KATHLEEN T. HALL, MICHAEL I. DARTER, AND JAMSHID M. ARMAGHANI

The most comprehensive load transfer restoration experiment currently in service was constructed on Interstate 10 near Tallahassee, Florida, in 1986. The performance of this experiment has been monitored continuously by the University of Illinois and the Florida Department of Transportation between 1986 and 1992. Fourteen different load transfer restoration treatments were studied. Retrofit dowel factors studied included number of dowels per wheelpath, dowel length, and dowel diameter. Double-V shear device factors studied included core wall grooving and number of devices in the outer and inner wheelpaths. The results of condition surveys, faulting surveys, and falling weight deflectometer deflection load transfer testing of the project are reported. All of the treatments were effective in limiting faulting increases to much lower levels than the faulting increases of the control sections. In addition, they all improved deflection load transfer significantly, and after 5 years in service, deflection load transfer percentages are still similar to initial postconstruction values. The only poor aspect of the project's performance is slab cracking in the vicinity of many retrofit dowels, which appears to be the result of a combination of construction, materials, and climatic factors.

Many jointed concrete pavements have been constructed without mechanical load transfer devices (e.g., dowels) across joints, and significant faulting has occurred on some of these pavements as a result of poor load transfer. Many other jointed concrete pavements have been constructed with dowels, but under heavy traffic the dowels may become loose and significant faulting may result. Transverse cracks in concrete pavements often deteriorate because of poor load transfer.

In an effort to extend the service lives of concrete pavements that exhibit poor load transfer and faulting at joints and cracks, highways agencies have used various devices to restore load transfer. These devices include retrofitted dowels, double-V shear devices, figure-eight devices, and miniature I-beam devices. The devices sometimes are placed in all traffic lanes and sometimes in only the most heavily trafficked (outer) lane. Load transfer restoration is often, but not always, done in conjunction with diamond grinding to remove existing faults at joints and cracks.

The effectiveness of load transfer restoration may be assessed by monitoring the performance of rehabilitated joints and cracks. This monitoring includes measurement of faulting and measurement of deflection load transfer with a heavy-load deflection device such as the falling weight deflectometer (FWD). In addition, condition surveys are useful for identi-

fication of device failure and assessment of future maintenance needs.

Previous field studies have demonstrated the ability of retrofit load transfer devices to improve deflection load transfer and thereby delay the recurrence of faulting (1). However, very few well-designed field experiments that examine a variety of devices and configurations (i.e., number and layout of devices) are in service on jointed concrete highway pavements. Such experiments are extremely valuable in assessing the performance and cost-effectiveness of pavement rehabilitation techniques such as load transfer restoration.

PROJECT DESCRIPTION

The most comprehensive load transfer restoration experiment currently in service was constructed on Interstate 10 near Tallahassee, Florida, in the fall of 1986. The statistically designed experiment was the result of a collaboration between the Florida Department of Transportation (DOT), the Civil Engineering Department of the University of Illinois at Urbana-Champaign under contract to FHWA, and the Dayton Superior Corporation.

The Florida DOT provided the location and construction control and conducted annual FWD testing and faulting surveys. The University of Illinois provided the experimental design and also conducted faulting surveys, visual performance ratings, and data analyses. Dayton Superior provided the load transfer devices, backfill materials, and some of the specialized equipment required for installation. Other pavement restoration operations done in conjunction with the load transfer restoration were slab replacement, slab undersealing, edge drain installation, and joint resealing. Diamond grinding was not done. The rehabilitation work was done between September and December 1986.

Faulting and deflections at joints on the experimental load transfer restoration project on I-10 have been monitored by the University of Illinois and the Florida DOT between 1986 and 1991 (2). This paper presents the results of the analyses of the performance data collected and summarizes the performance of the load transfer restoration experiment. This project offers a rare opportunity for longitudinal study of the progression of faulting and load transfer, which is essential to assessing the long-term performance and cost-effectiveness of this rehabilitation technique.

Project Site

The I-10 experimental project is located on Interstate 10 in Gadsden County, Florida, about 32 to 48 km (20 to 30 mi) east

K. T. Hall and M. I. Darter, Department of Civil Engineering, University of Illinois at Urbana-Champaign, Urbana, Ill. 61801-2352. J. M. Armaghani, Florida Department of Transportation, Gainesville, Fla. 32602-1029.

of Tallahassee. The project begins at milepost 172 and extends eastward about 0.8 km (0.5 mi). The region has a wet, non-freezing climate.

The pavement is a 22.9-cm (9-in.) jointed plain concrete pavement on a cement-treated subbase. The subgrade is predominantly silty gravel or sand (AASHTO classification A-2-4), with clay (A-6) and silty gravel or sand backfill (A-2-4) in some locations. The joints were originally constructed without dowels. The joint spacing is 6.1 m (20 ft). The pavement was constructed with asphalt concrete shoulders and without longitudinal edge drains.

The pavement was opened to traffic in November 1978. Between that time and the time of rehabilitation in 1986, the pavement carried approximately 6 million 18-kip (8.1 metric ton) equivalent single-axle loads (ESALs) in the outer traffic lane. Between 1986 and 1991, the pavement carried approximately 7.5 million ESALs.

Load Transfer Device Test Sections

The project was divided into 14 test sections completely replicated in each direction (eastbound and westbound). Each test section consists of nine joints, so a total of 126 joints in each direction are contained in the test sections. Control sections of nine joints each also exist at the beginning and end of the project in each direction. Eight different retrofit dowel configurations and six different precompressed shear device configurations were used. A diagram of the test section layout is shown in Figure 1. The dowel and shear device factorials are shown in Figure 2. Details of the construction activities were provided previously (2-4).

The retrofit dowels were fitted with expansion caps on one end, mounted on chairs in parallel slots sawed across the joints, and backfilled with a concrete patching material (trade-name HD-50) supplied by Dayton Superior. The positions of the retrofit dowels across the traffic lane for the different configurations are illustrated in Figure 3.

The primary components of the LTD + Plus double-V shear device are two v-shaped plates of stainless steel, welded together and flanged. The interior of the device is filled with polyurethane foam, and the double-V's are wrapped in polyvinyl foam. The double-V's are aligned with the transverse joint to permit horizontal movement of the slabs. The positions of the shear devices across the traffic lane for the different configurations are illustrated in Figure 4.



FIGURE 1 I-10 load transfer restoration test section layout.

DOWEL DEVICE FACTORIAL				
No. of Dowels In Wheelpath	Three		Five	
	14	18	14	18
Dowel Length (in)				
Dowel Diameter (in)				
1.0	D1	D5	D2	D6
1.5	D3	D7	D4	D8

1 in = 2.54 cm

SHEAR DEVICE FACTORIAL				
Grooving of Core Walls	No		Yes	
	1	2	1	2
No. of Devices In Inner Wheelpath				
No. of Devices In Outer Wheelpath				
2	S1	S2	S4	S5
3	--	S3	--	S6

FIGURE 2 Retrofit dowel and shear device factorials.

Installation Costs

The following low bid prices were obtained for the dowel and shear device materials and installation:

Device	1986 Cost (\$)
Dowel	62.00
Shear device	65.00

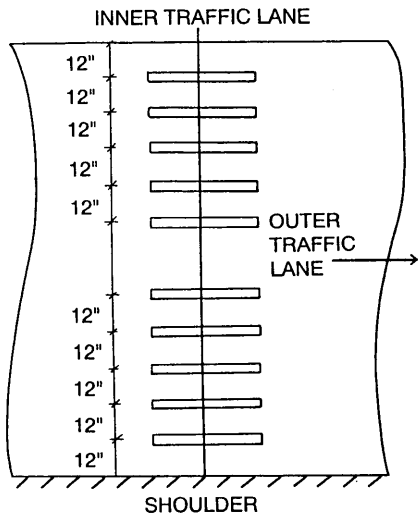
Device	1986 Cost per Lane-Kilometer (164 joints) (\$)	1986 Cost per Lane-Mile (264 joints) (\$)
Dowels		
10 per joint	101,709	163,680
6 per joint	61,025	98,208
Shear devices		
5 per joint	53,315	85,800
4 per joint	42,652	68,640
3 per joint	31,989	51,480

PERFORMANCE MONITORING

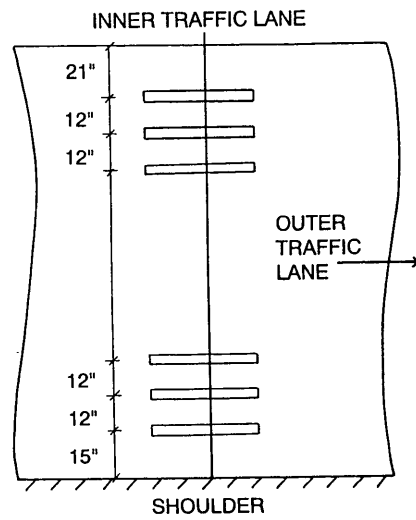
Comparison of 1988 and 1991 Survey Results

Examination of past survey results indicate that the retrofit dowels and shear devices exhibited very little distress from the time of construction through 1988. At the time of the 1988 survey, the major distress affecting the retrofit dowels was multiple hairline cracks in the dowel backfill at many locations. Several of these cracks, spaced an inch or more apart, ran across the dowel slot, parallel to the transverse joint.

D2, D4, D6, AND D8



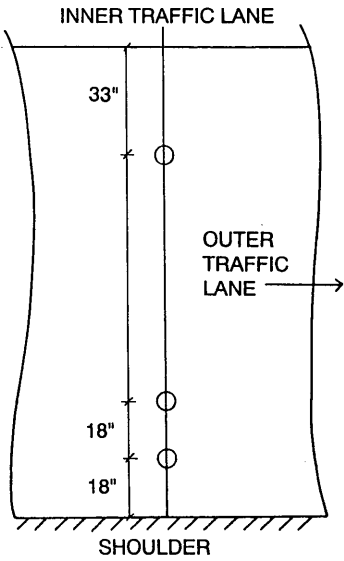
D1, D3, D5, AND D7



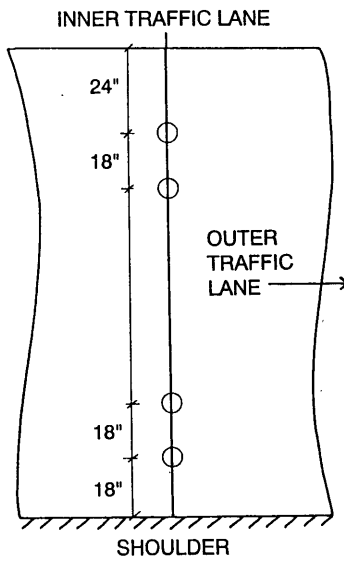
1 in = 2.54 cm

FIGURE 3 Retrofit dowel layouts.

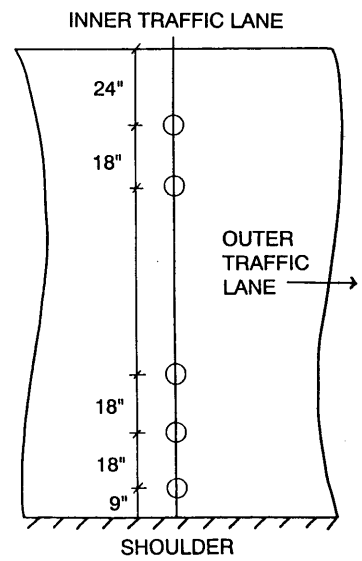
S1 AND S4



S2 AND S5



S3 AND S6



1 in = 2.54 cm

FIGURE 4 Shear device layouts.

These hairline cracks in the dowel backfill were visible during the field survey but were so fine that they are difficult or impossible to see in almost all of the photographs taken at dowel locations in the University of Illinois' (UI) 1988 survey. Neither the field notes nor the photographs from the 1988 UI survey show significant cracking of the slab between the dowel slots or emanating from the dowel slots, although hairline cracks between dowel slots are visible in a few photos.

Between 1988 and 1991, however, the project developed considerable distress, particularly at the retrofit dowels. At many locations, a series of horizontal cracks was observed between the dowel slots, parallel to the joint. Often one or more cracks ran along the side of a dowel slot, and from there extended back into the slab. Some of these slab cracks extended straight from the dowel slot, parallel to the wheelpath, but most of the slab cracks that emanated from dowel slots run diagonally across the slab and intersected the lane edge a few feet from the transverse joint. This type of cracking occurred at dowel installations in both wheelpaths of the traffic lane.

Figure 5 shows Joint 9 in the eastbound D7 test section in 1988 (*top*) and in 1991 (*bottom*). The cracking, which is barely visible in 1988, reached medium severity by 1991.

In the 1988 survey, the most noticeable distress at shear device installations was cracking or spalling in the backfill of

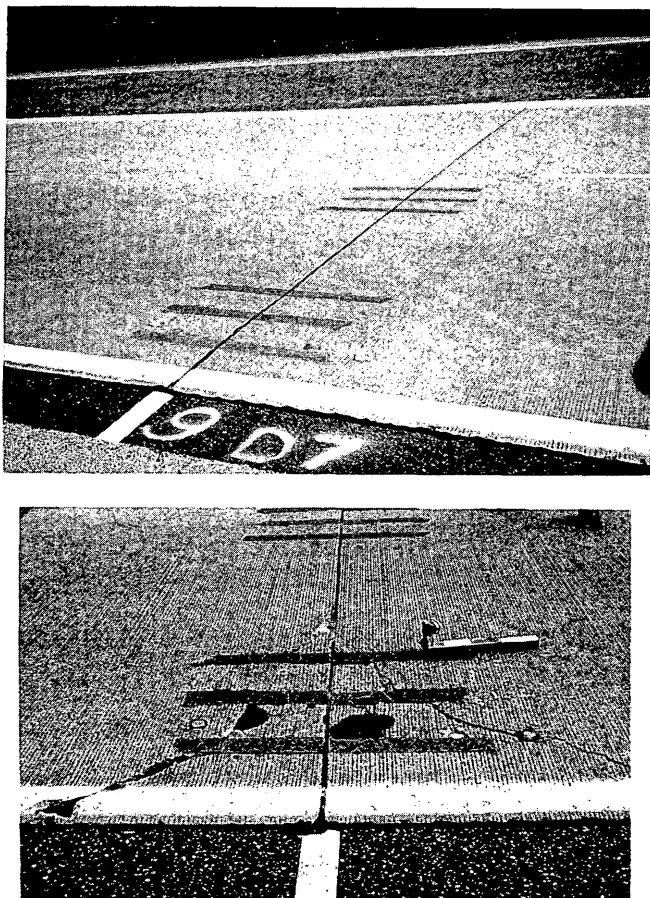


FIGURE 5 Cracking at D7 dowel section, Joint 9 eastbound, 1988 (*top*) and 1991 (*bottom*) surveys.

about a half dozen of the shear devices. At one device the top inch or more of backfill was spalled out and the metal of the shear device was visible. As noted in the previous section, some shear device installations also had slab cracks emanating from the edge of the core hole. These also developed sometime after the 1988 survey.

1991 Condition Survey Results

The number of joints in each section affected by slab cracking or device distress in 1991 is illustrated in Figure 6. For most of the retrofit dowel sections, the slab cracking in the vicinity of the retrofit dowels is more prevalent and more severe in the eastbound direction than in the westbound direction. A striking contrast, for example, is seen between the eastbound and westbound D7 sections. All nine of the eastbound D7 joints have cracking, and this cracking was rated medium or high severity at seven of the nine joints. None of the westbound D7 joints have any cracking. It is worth noting that the eastbound D7 section was one of the first test sections to be constructed (see the test section layout in Figure 1).

For the three shear device treatments without core wall grooving (S1, S2, and S3), slab cracking or device distress is more prevalent in the westbound sections than in the eastbound sections. For the remaining three shear device treatments, the distress levels in the two directions were very similar.

Slab cracking is not limited to the retrofit dowels: a few shear devices also have cracks emanating from their core holes straight back into the slab or diagonally to the slab edge. However, the more prevalent distresses at shear devices were sealant failure, debonding, cracking, or spalling of the backfill on one or both sides of the joint, and/or device failure (broken metal). A total of 18 shear devices in the eastbound direction (18 of 216 total, or 8 percent) and 20 shear devices in the westbound direction (9 percent) showed some distress.

Possible Causes of Retrofit Dowel Distress

Two hypotheses are suggested for the cause of the slab cracking at the retrofit dowels on the Florida I-10 project. One hypothesis is that the dowels are locked up, preventing joints from opening in response to falling temperatures. This would cause high tensile stresses in the dowel backfill material and the surrounding concrete slab.

Two factors point to the likelihood of dowel lock-up as the cause of the cracking. The first factor is the frequent occurrence of cracking at dowel installations in both wheelpaths, which suggests that whatever is causing the cracking is acting across the full slab width, and not just at the outer slab edge. This would be true of longitudinal contraction caused by falling temperatures. However, if the cracking were caused by corner deflections and nonuniform support, one would expect the cracking to be confined largely to the outer wheelpath.

The second factor is the likely decrease in ambient temperatures during construction. The test sections were constructed sequentially, beginning at the west end of the eastbound lane in late September, when daytime temperatures were about 26°C (80°F) and nighttime temperatures were in

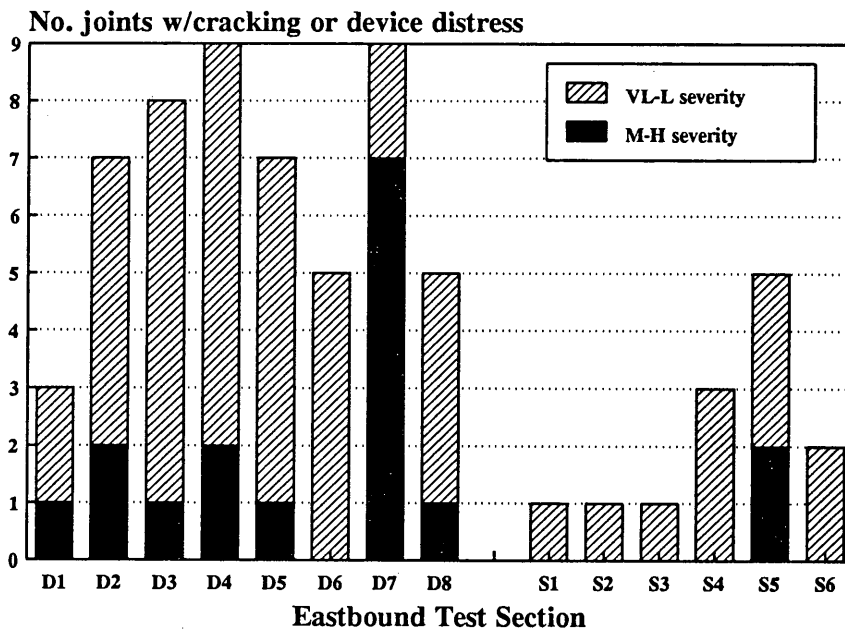
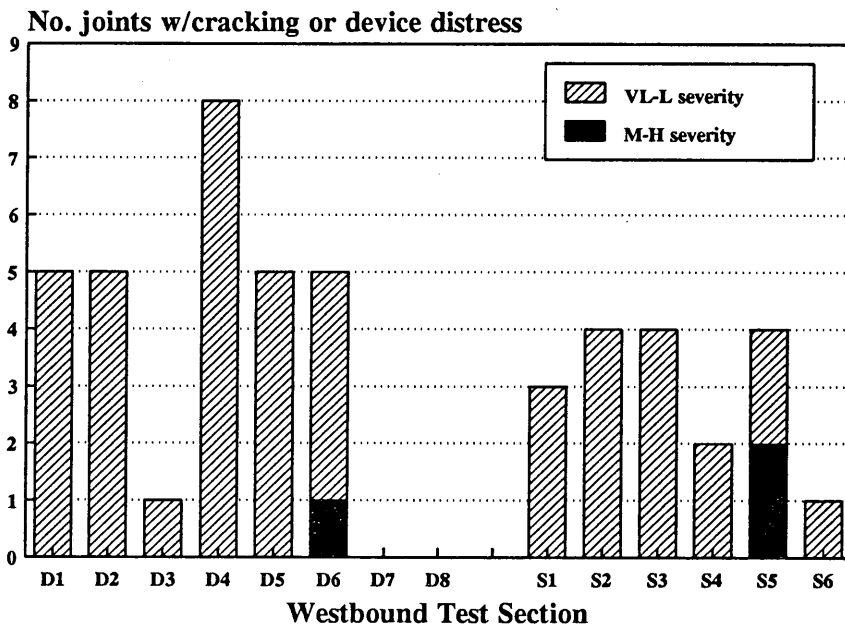


FIGURE 6 Number of joints with slab cracking or device distress.

the range of 10°C to 15°C (50°F to 60°F). Construction of the eastbound sections continued in order, followed by the westbound sections. Construction of the last westbound test sections was completed around mid-December.

It is likely that ambient daytime temperatures were lower during the westbound construction and that, as a result, the joints were open wider when the dowels were installed, and thus lower tensile stresses were induced in the backfill and slabs by further slab contraction in January. This suggestion

is consistent with the greater extent and severity of cracking in the eastbound sections than in the westbound sections.

Dowel lock-up, if it occurred, may have been caused by development of bond between the backfill material and the epoxy-coated dowels. A thin coating of motor oil or some other lubricant is typically used on retrofit dowels to prevent the backfill material from bonding to the dowel. Because the dowels were epoxy coated and because the HD-50 backfill was a high-strength patching material (mean flexural strengths

of 3238 kPa (470 psi) at 2 hr, 4134 kPa (600 psi) at 24 hr, and 9646 kPa (1,400 psi) at 28 days (R. E. Nelson and G. O. Schumacher, personal communication, 1986), a relatively strong bond could have developed between the two since no bond-breaker was used.

Dowel misalignment may also have played a part in locking up the transverse joints. Either the dowel slots or the dowels themselves may have been misaligned, so that the dowels were not positioned parallel to each other and perpendicular to the transverse joint, within the tolerances specified. This would explain the particularly badly deteriorated joints in the eastbound direction where construction started—where the dowel slots were marked individually, before the contractor started using a template to mark all the dowel slots together. However, the same type of cracking is evident, albeit at lower severities, in the westbound lane where the template was used.

A second hypothesis is that high tensile stresses could have developed from a combination of heavy traffic loads, curling at the corners, and the presence of either voids or a non-uniform and stiff grout beneath the slab corners. Stresses in the corner region of the slab under truck wheel loads may be dramatically increased by the presence of the dowel slots, and the corners of the dowel slots may become points of stress concentration.

The slab cracking at retrofit dowels, which appears to have occurred throughout the project, may have been caused by either a combination of the two mechanisms described above, or by some other unknown cause. It is important to note that this type of distress is not typical of retrofit dowels (1). It is strongly recommended that some deteriorated dowel installations be removed for further inspection.

Faulting Survey Results

Since diamond grinding was not done on this product, the effectiveness of the load transfer restoration must be measured not in terms of actual faulting measurements, but rather by increases relative to initial faulting measurements. Pre-construction faulting measurements were taken on all joints, using a faultmeter provided by the University of Illinois. This same device has been used for several previous studies, including the NCHRP 1-19 (COPEs) study (5), and an FHWA study of diamond grinding, retrofit load transfer, and other rehabilitation techniques in several states (1). A description of the faultmeter and its use was given previously (4).

The initial faulting data taken in 1986 represent the average of two to four readings taken at each joint 30.5 cm (12 in.) from the edge. Joint faulting varied considerably along the project (coefficients of variation were 60 and 62 percent, respectively), and the eastbound average faulting was higher than the westbound average [0.262 cm versus 0.221 cm (0.103 in. versus 0.087 in.)].

Subsequent joint faulting measurements were taken by UI personnel in April 1987, November 1987, November 1988, and October 1991. As before, the faulting value obtained for each joint was determined from two to four readings. For each individual joint, the increase in faulting was determined by subtracting the fault measurement obtained from the pre-construction (October 1986) fault measurement. For each test section, the average faulting was determined by averaging the

faulting measurements for the nine joints in the test section, and the average increase in faulting was determined by averaging the fault increases for the nine joints in the test section.

The percent change in average faulting between 1986 and 1991 is illustrated in Figure 7. The 50 percent change for control joints represents the average for all joints in the project's four control sections (36 joints total). The percent changes shown for the various load transfer treatments represent the average of the percent changes for the treatment sections in both directions (18 joints total). The percent change in control section faulting has been much greater than that in any of the load transfer treatments.

Figure 8 illustrates the effects of the retrofit dowel factors and shear device factors studied on faulting performance. In each category the percent change in faulting is much less than the 50 percent change in control section faulting.

The number of dowels does not appear to have been significant: sections with three dowels per wheelpath (D1, D3, D5, and D7) and sections with five dowels per wheelpath (D2, D4, D6, and D8) both had similarly small increases in faulting.

Figure 8 suggests that dowel length may have been significant: the average faulting change of sections with 45.7-cm (18-in.) dowel bars was positive, whereas the average faulting change of sections with 35.6-cm (14-in.) dowel bars was negative. However, these results were actually mixed by section. Of the treatments with 35.6-cm (14-in.) dowels (D1, D2, D3, and D4), one of four showed a percentage increase in mean faulting, and two of four showed a positive average increase in faulting. Similarly, of the treatments with 45.7-cm (18-in.) dowels (D5, D6, D7, and D8), two of four showed a percentage increase in mean faulting and two of four showed a positive average increase in faulting.

The most significant factor in retrofit dowel faulting performance appears to have been dowel diameter. All of the sections with 2.5-cm (1-in.) dowels (D1, D2, D5, and D6) showed a percentage increase in mean faulting and a positive average increase in faulting. All of the sections with 3.8-cm (1.5-in.) dowels (D3, D4, D7, and D8) showed no positive percentage increase in mean faulting, and only D3 showed a slight positive average increase in faulting.

Grooving of the core walls does not appear to have been significant: neither the sections without grooved core walls (S1, S2, and S3) nor the sections with grooved core walls (S4, S5, and S6) showed an overall average percentage increase in faulting. In each group, one treatment (S1 and S4, respectively) showed slight faulting increases, and the other two treatments (S2 and S3 and S5 and S6) did not show positive changes.

Of the three shear device patterns used, the only one to show an increase in faulting was the weakest pattern (two devices in the outer wheelpath and one in the inner wheelpath for S1 and S4). Both of the other patterns (two devices in each wheelpath for S2 and S5 and three devices in the outer wheelpath and two in the inner wheelpath for S3 and S6) showed no positive increases in mean faulting.

Deflection Survey Results

Deflection testing and deflection data analyses were conducted by the Florida DOT before and after installation of

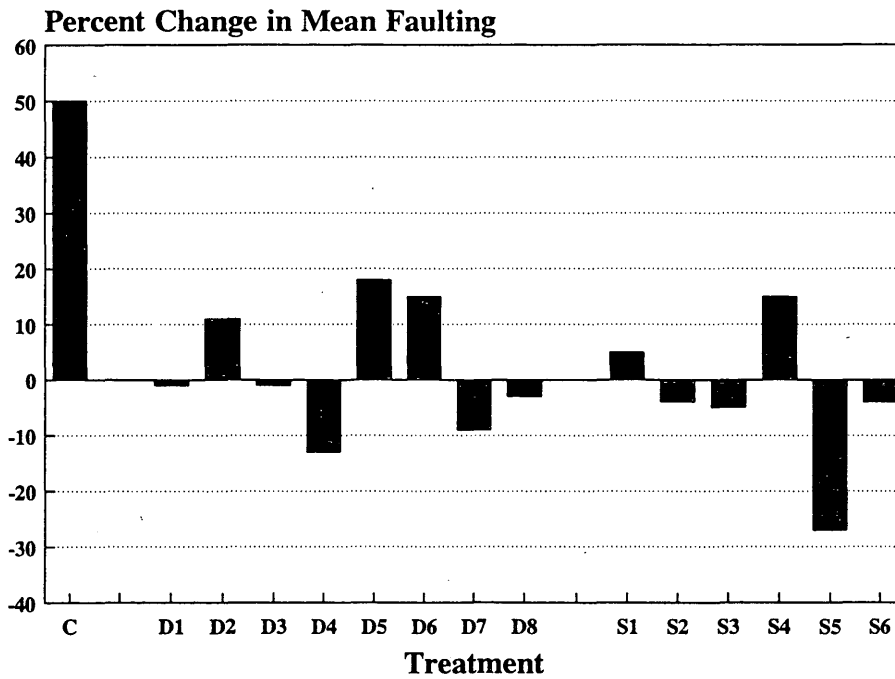


FIGURE 7 Percent change in mean faulting of control sections and load transfer and restoration treatments.

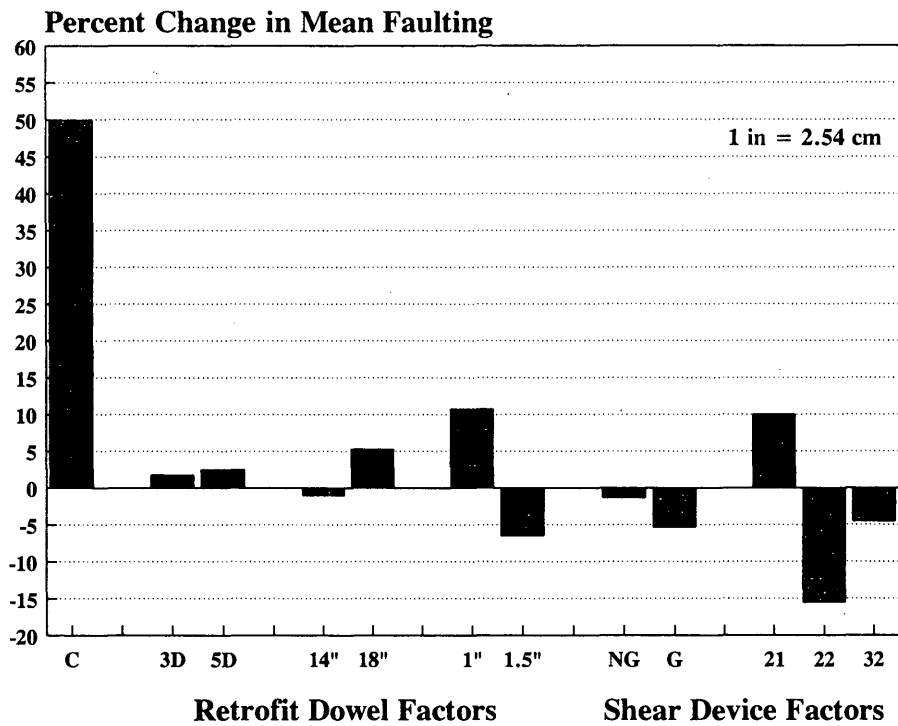


FIGURE 8 Effect of retrofit dowel and shear device factors on faulting.

the load transfer devices, using an FWD. The deflection testing was typically done between the hours of 11:30 p.m. and 2:30 a.m. when slab temperature gradients were low (6). The load plate used for testing was 30 cm (11.8 in.) in diameter, with a deflection sensor at the center of the load plate, 30.5 cm (12 in.) behind the load plate, and 30.5, 61, 91.5, 122, and 152.5 cm (12, 24, 36, 48, and 60 in.) ahead of the load plate. For the purpose of joint load transfer measurement, the FWD load plate was centered in the outer wheelpath approximately 30.5 cm (12 in.) from the longitudinal slab edge, with the edge of the plate close to the transverse joint, so that the joint was approximately midway between the load plate sensor and the sensor 30.5 cm (12 in.) behind the load plate sensor.

The deflection load transfer efficiency of each joint was computed from the ratio of the deflection on the unloaded side to deflection of the loaded side. Before installation of the dowels and shear devices, load transfer was very poor (less than 10 percent in most sections) throughout the project. The retrofit dowels improved load transfer substantially: up to 50 to 80 percent. More than 50 percent generally would be considered good load transfer, and more than 70 percent generally would be considered very good load transfer. The shear devices achieved smaller increases in load transfer: up to 20 to 55 percent, which might be considered fair to poor.

Deflection testing was conducted again by the Florida DOT in early 1992. The load transfer efficiencies of the various test sections are compared with the load transfer efficiencies in 1986 in Figure 9. In general, the results are similar.

The load transfer efficiencies of most of the retrofit dowel sections in 1992 are within 15 percent of their 1986 values. Most of the westbound dowel sections actually have higher mean load transfer efficiencies now, whereas most of the eastbound dowel sections have lower load transfer efficiencies now. In one eastbound dowel section (D7), joint load transfer measurements were not taken, presumably because of excessive joint deterioration.

Dowel length does not appear to have any significant effect on load transfer efficiency: pairwise comparisons of sections in each direction with 35.6-cm (14-in.) versus 45.7-cm (18-in.) dowels show similar results in most cases. The number of dowels has some significance: pairwise comparisons show that in most cases, sections with five dowels per wheelpath have slightly higher load transfer efficiencies than sections with three dowels per wheelpath. An exception to this is D5 (three dowels) versus D6 (five dowels). In both directions the D5 section has a slightly higher mean load transfer efficiency than the D6 section. Dowel diameter also appears to be significant: in most cases in both directions, the section with 3.8-cm (1.5-in.) dowels has higher load transfer than the section with 2.5-cm (1-in.) dowels. An exception is eastbound D2 [2.5-cm (1-in.) dowels], which has higher load transfer than eastbound D4 [3.8-cm (1.5-in.) dowels].

The load transfer efficiencies of most of the shear device sections in 1992 are within about 10 percent of their 1986 values. Two eastbound sections (S2 and S5) appear to have dropped to fairly low load transfer levels (less than 20 percent). Sections without grooved core walls do not have significantly different load efficiencies than corresponding sections with grooved core walls. In the westbound direction, the load transfer efficiency improves with increasing number

of devices: Sections S1 and S4 (2/1 device pattern) have the lowest load transfer levels, Sections S2 and S5 (2/2 device pattern) have higher load transfer, and Sections S3 and S6 (3/2 device pattern) have the highest load transfer. This trend is not repeated in the eastbound direction, however. The 2/2 pattern actually shows the lowest load transfer. It is interesting to note that the trend of higher load transfer with more devices was present in both directions, for both grooved and nongrooved core walls, initially after construction.

Figure 10 illustrates sample load versus deflection plots for representative joints in two dowel sections and two shear sections. The dowelled joints show lower deflections at each load level than the shear joints. Between the two dowelled joints shown, the joint with 3.8-cm (1.5-in.) dowels shows lower deflections than the joint with 2.5-cm (1-in.) dowels. Between the two shear device joints shown, the one with three devices in the outer wheelpath shows lower deflections than the one with two devices in the outer wheelpath.

The trends illustrated in Figure 10 are typical of the load-versus-deflection behavior of joints throughout the project, although there is significant variation from joint to joint within each test section. In general, joints with 3.8-cm (1.5-in.) dowels had about 30 percent lower corner deflections than joints with 2.5-cm (1-in.) dowels. Other retrofit dowel factors did not have any significant effect on corner deflections. Overall, dowelled joints had about 30 percent lower corner deflections than joints with shear devices. Joints with 3.8-cm (1.5-in.) dowels had about 38 percent lower corner deflections than joints with shear devices.

CONCLUSIONS

Condition Results

This pavement section was in very good condition for the first 3 years after installation of the load transfer devices in 1986. Sometime between 1988 and 1991, a considerable amount of cracking developed, mostly at joints with retrofit dowels. This cracking may have been caused by stress concentrations at dowel slot corners or by joint lock-up as a result of a lack of bondbreaker, dowel misalignment, or some other cause. The eastbound direction has many deteriorated joints that must be repaired, and the westbound direction has many joints with lower-severity cracking that is expected to deteriorate in the future.

The deterioration of the retrofit dowel installations, which is not at all typical of retrofit dowel behavior on other projects, has greatly reduced the performance life of the load transfer restoration work. Further investigation of the causes of the dowelled joint deterioration is strongly encouraged.

Faulting Results

All of the load transfer restoration treatments investigated in this project were effective, in combination with undersealing and edge drain retrofitting, in limiting faulting increases to much lower levels than the faulting increases of the control

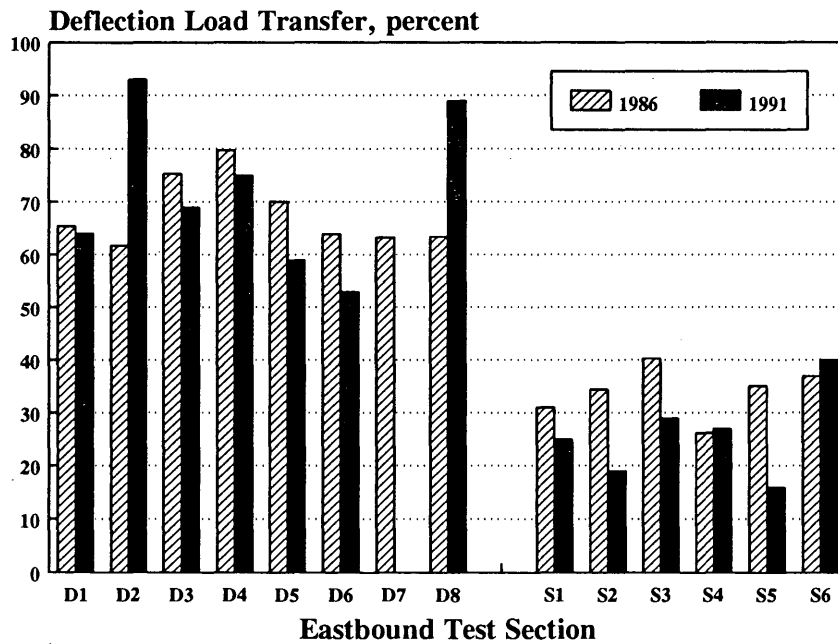
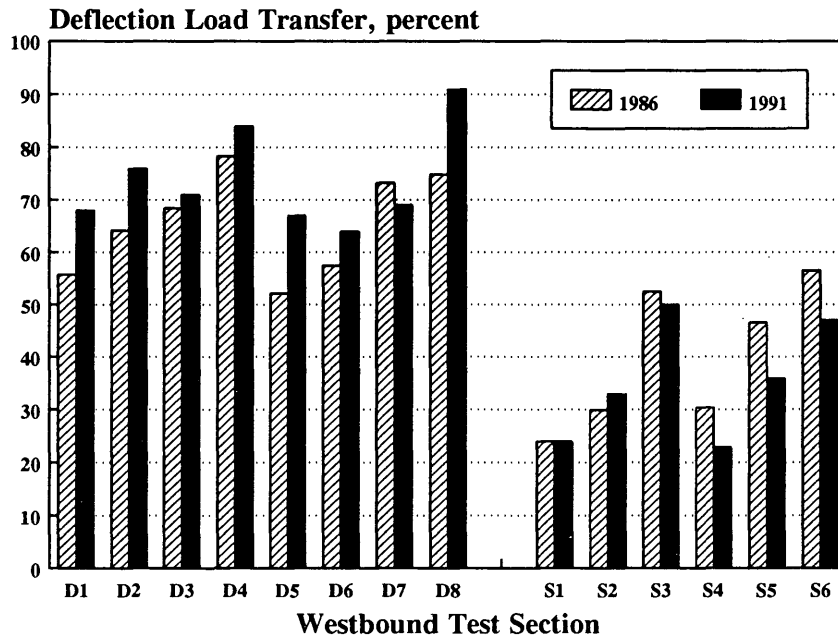


FIGURE 9 Comparison of 1986 and 1991 deflection load transfer efficiencies in test sections.

sections. Several sections actually showed a negative change in faulting from 1986 to 1991, which, within the range of random variation, may be interpreted for practical purposes as prohibiting any increase in faulting. In addition, faulting was not measured at joints that were deteriorated enough to prohibit a valid faulting measurement.

Three dowels per wheelpath and five dowels per wheelpath performed equally well in terms of faulting. Dowel length had

mixed results on faulting. Dowel diameter appeared to significantly affect faulting: sections with dowel bars 2.5 cm (1 in.) in diameter showed increases in faulting, whereas sections with dowel bars 3.8 cm (1.5 in.) in diameter did not.

Grooving core walls did not appear to have any significant effect on faulting of joints with Double-V shear devices. Of the three shear device patterns investigated, the weakest one (two devices in the other wheelpath and one in the inner

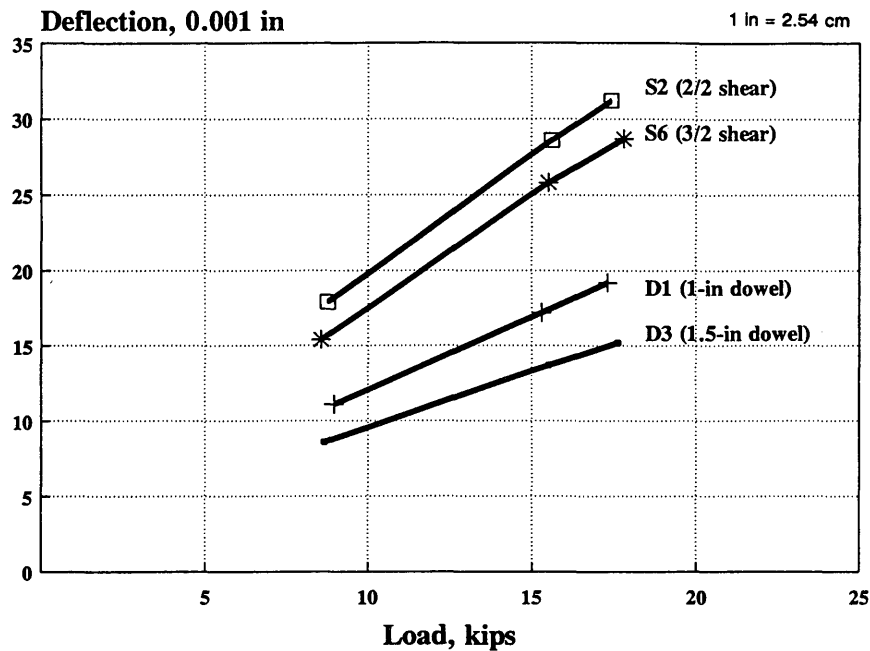


FIGURE 10 Example of load-versus-deflection results at slab corners for dowels and shear devices.

wheelpath) showed an increase in faulting, whereas the other two patterns (two devices per wheelpath, and three in the outer wheelpath, two in the inner wheelpath) did not show an increase.

Deflection Results

Before installation of the load transfer devices, the undowelled joints of this project had very poor deflection load transfer efficiency (less than 10 percent for most test sections). The retrofit dowels improved load transfer dramatically, to between 50 and 80 percent. The shear devices produced more modest load transfer improvements, to between 20 and 55 percent. After more than 5 years in service, both the retrofit dowels and the shear devices exhibit load transfer efficiencies that are similar to those measured initially after installation.

In most but not all cases, sections with five dowels per wheelpath had slightly higher load transfer efficiencies than sections with three dowels per wheelpath. Similarly, in most but not all cases, sections with 3.8-cm (1.5-in.) dowels had slightly higher load transfer efficiencies than sections with 2.5-cm (1-in.) dowels. Dowel length did not appear to affect load transfer efficiency.

Grooving core walls did not appear to affect the load transfer efficiency of joints with shear devices. Joints with three shear devices in the outer wheelpath and two devices in the inner wheelpath had the highest load transfer efficiencies. Only the 3/2 pattern appeared to be able to achieve load transfer efficiencies in the range of 50 percent, and then only in one direction on the project. The shear device pattern with the lowest load transfer efficiency was not consistent by direction.

Joints with 3.8-cm (1.5-in.) dowels had about 30 percent lower corner deflections than joints with 2.5-cm (1-in.) dowels. Other retrofit dowel factors did not have any significant effect on corner deflections. Overall, dowelled joints had about 30 percent lower corner deflections than joints with shear devices. Joints with 3.8-cm (1.5-in.) dowels had about 38 percent lower corner deflections than joints with shear devices.

Despite the fact that joints with retrofit dowels have higher load transfer efficiencies and lower corner deflections than joints with shear devices, the dowels and shear devices appear to have been about equally effective in controlling faulting. However, the higher load transfer and lower corner deflections achieved by retrofit dowels may benefit pavement performance in other ways (i.e., reduction of slab stresses caused by corner loads).

ACKNOWLEDGMENTS

The research reported in this paper was sponsored by FHWA. The authors thank Roger Larson of FHWA for initiating this study and Mark Kaler of the Dayton Superior Corporation for his cooperation.

REFERENCES

1. M. B. Snyder, M. J. Reiter, K. T. Hall, and M. I. Darter. *Rehabilitation of Concrete Pavements, Vol. 1—Repair Rehabilitation Techniques*. Report FHWA-RD-88-071, FHWA, U.S. Department of Transportation, 1989.
2. M. J. Reiter, M. I. Darter, and S. H. Carpenter. Restoration of Joint Load Transfer. In *Transportation Research Record 1183*, TRB, National Research Council, Washington, D.C., 1988.

3. W. N. Lofroos, W. J. Rutledge, Jr., and W. J. Gerry. *Post Construction Report: Jointed Concrete Pavement Load Transfer Restoration, Evaluation of Alternatives on Interstate 10*, Pavement Management and Design, Bureau of Roadway Design, Florida Department of Transportation, Aug. 1987.
4. K. T. Hall, M. I. Darter, and J. M. Armaghani. Performance Monitoring of Joint Load Transfer Restoration: A Report on the Five-Year Performance of Experimental Load Transfer Restoration on Interstate 10 in Florida. Final Report. FHWA, U.S. Department of Transportation, 1992.
5. M. I. Darter, J. M. Becker, and M. B. Snyder. *NCHRP Report 227: Concrete Pavement Evaluation System (COPES)*. TRB, National Research Council, Washington, D.C., 1985.

Publication of this paper sponsored by Committee on Pavement Rehabilitation.

Major Factors Explaining Performance Variability of Seal Coat Pavement Rehabilitation Overlays

MOHAMED-ASEM U. ABDUL-MALAK, D. W. FOWLER, AND A. H. MEYER

A statistical experiment was conducted with the objective of identifying the role of certain factors in explaining the performance variability of seal coat pavement surfaces. Considered factors included the type and properties of the aggregate used in a seal coat surface, the designed construction rate at which the aggregate was spread, and the climatic region in which the highway section was placed. A graphical examination of the effect of each of the considered variables was performed. This examination was followed by statistically testing the significance of the observed effects. A performance model was then formulated, and the usefulness of the model was demonstrated.

This paper reports the results of a statistical experiment conducted as part of a research project undertaken at the Center for Transportation Research, the University of Texas at Austin. The ultimate aim of this research project was to formulate statistical models that can be used for predicting the frictional performance of seal coat pavement overlays. A seal coat overlay is a rehabilitation method for pavements of all classes, used mostly on rural highways. The construction of this method involves the application of asphalt to a road surface, at a range of 1.36 to 3.17 liters/m² (0.3 to 0.7 gal/yd²) of surface, followed by the spreading of cover aggregate, at a range of 77 to 165 m² of surface for each cubic meter of material (70 to 150 yd³/yd³), to form an overlay about 1 in. thick. Multiple successive layers of asphalt and aggregate may be used to achieve thicker seal coat overlays.

The methodology, reported earlier by Abdul-Malak et al. (1,2), involved establishing 59 seal coat test sections in many districts of the state of Texas, including all four environmental regions, and monitoring their performances over time. Many factors, believed to have an influence on performance level and identified in the literature and Texas district surveys (1), were considered in this study. These factors included aggregate physical and mineralogical properties, construction variables, traffic variables, and environment and weather variables.

Frictional performance has been measured by a skid trailer and expressed as a friction number (FN). Eight sets of FN measurements, spanned over about 5 years, were used for the analysis of the statistical experiment. Weather data relevant to the period before field testing were also collected.

M. U. Abdul-Malak, Faculty of Engineering and Architecture, American University of Beirut, Beirut, Lebanon; and 850 Third Ave., 18th floor, New York, N.Y. 10022. D. W. Fowler and A. H. Meyer, Department of Civil Engineering, The University of Texas at Austin, Austin, Tex. 78712-1076.

The performance data were graphed to detect the sources of performance variability and then grouped according to the different considered variables (2). The grouping gave insights into which variables controlled the observed differences in frictional performance. The grouping was followed by extensive statistical modeling that pinpointed the significant variables.

In this paper, the effect of aggregate type, aggregate construction spreading rate, and climatic region on seal coat frictional performance is examined graphically. A statistical experiment that tests for the statistical significance of the considered variables is then analyzed.

BACKGROUND

Parameters of Frictional Resistance

Two components make up the frictional resistance developed between the tire and the pavement surface: adhesion and hysteresis (3). Among the many factors that affect the role of these components, the most important are the microtexture and macrotexture of the pavement surface (4). The microtexture controls the adhesion component, whereas the macrotexture controls the hysteresis component.

In seal coats, the microtexture is the fine-scaled roughness contributed by individual small asperities on the individual coarse aggregate particles. Ideally, for it to sustain a highly favorable microtexture, the aggregate particle should be composed of hard, coarse, angular minerals well bonded into a softer matrix so that gradual differential wear will occur. The macrotexture is the large-scale texture at the surface caused by the size and shape of and the spacing among the coarse aggregate particles. Appropriate angularity, proper maximum size and gradation, and adequate spreading rate of aggregate particles are essential for achieving adequate macrotexture.

The most commonly used laboratory method is the polish value (PV) test (5), in which the friction of the coarse aggregate particles is evaluated with the British portable tester after 9 hr of exposure to accelerated polishing. The four-cycle magnesium sulfate soundness test (6) used to judge the soundness of an aggregate when it is subjected to weathering action (freeze and thaw) gives indications of the strength (or softness) of the cementing matrix that holds the individual grains in the aggregate particles. Recent work has shown that aggregate petrographic properties can be very helpful in ex-

plaining a considerable portion of the variability observed in the frictional performance of seal coat surfaces (7).

Several methods have been developed for evaluating or measuring pavement macrotexture. Of these, the sand patch and silicone putty (volumetric measurements), outflow meter (drainage measurement), and stereo photographic interpretation (topography measurement) methods are most commonly used. Other methods have recently evolved, examples of which are the "Numerisateur," a contactless sensor-based system used in France, and the Transport and Road Research Laboratory Mini-Texture Meter, a laser based monitoring system used in Britain (8).

Variability in Frictional Resistance

Two types of seasonally caused variations have been observed: long-term and short-term. Long-term variations are caused by changes in the microtexture of the exposed aggregates brought about by polishing during long dry periods and roughening caused by the rejuvenating effects of long wet periods (9). As a result of this mechanism, friction measurements made in the wet periods have been reported to be much higher than those made in the dry periods. Superimposed on these long-term (annual) variations are short-term variations attributable to external factors, such as amount and timing of intermittent rainfall, and possibly to contamination from oily films, drippings, and other deposits on the surface (10,11).

Two models, a generalized prediction model and a mechanistic model, were recently developed at Pennsylvania State University (12) to predict seasonal variations in the skid resistance of asphalt pavements associated with rainfall conditions, temperature effects, and time of year. It has been suggested that the models be limited to the geographical area within which the investigation was conducted.

METHODOLOGY

Data Collection

Extensive laboratory testing was performed on the aggregate samples obtained from construction sites. Of the numerous tests performed (2), the following major tests were used for grouping the various types of aggregates encountered: the polish value and insoluble residue tests for measuring the polish susceptibility; the four-cycle magnesium sulfate soundness and freeze-thaw tests for evaluating the resistance to weathering action in natural and synthetic aggregates, respectively; and the Los Angeles abrasion test for determining the resistance to abrasion and impact actions. Other basic tests were also performed on collected aggregate samples, including the sieve analysis (gradation) and the specific gravity and absorption tests.

For each constructed test section, a survey was made that mainly consisted of information on the coarse aggregate material and asphalt type and the rates at which both materials were to be placed; these were the design distribution rate of asphalt (ASDR) and the spreading rate of aggregate (AGSR).

Various aggregate materials and asphalt types were used in the construction of the established sections along with wide ranges of ASDR and AGSR; the AGSR range was from 77 to 142 m² of surface for each cubic meter of aggregate (70 to 130 yd²/yd³), respectively, corresponding to a range of 52 to 20 kg of aggregate per square meter of surface. Typically, aggregates from Grades 3 and 4 were used, with an aggregate maximum size of 1.6 cm (5/8 in.) and 1.3 cm (1/2 in.), respectively. The annual average daily traffic (ADT) counts varied between 300 and 3,500 vehicles per lane.

The skid resistance test has been conducted twice a year in accordance with ASTM E274. Eight sets of skid resistance measurements were used in the analysis to follow.

Detailed climatological data also have been sought. Specifically, the data have been concerned with the length of the last rainfall period, the number of days between the last rainfall that occurred in that period and the day of field testing, and the total precipitation that fell in that period. Data collection also has involved categorizing the testing seasons into either wet or dry.

Design of Performance Experiment

After extensive graphical data manipulation (2), a statistical experiment was designed. It was aimed toward a better understanding of the effects on the performance of seal coat overlays of aggregate properties, aggregate construction spreading rate, and the environment.

The design, shown in Table 1, included the various aggregate groups that were considered (AGGR) and the ranges of the results of the four major laboratory tests obtained for most of the aggregates. Two siliceous gravel aggregates with high percentages of carbonate contents were grouped with the limestone aggregates of the Limestone 2 group. Because the obtained asphalt and aggregate spreading rates were those specified by the highway engineer and to account for the slight expected variations in the actual construction rates, the aggregate spreading rate variable was introduced into this experiment as a three-level variable (LAGSR)—low, medium, and high. With respect to the environment variable, Figure 1 shows a map of the state of Texas with its four climatic regions (I, II, IV, and V) and the districts where test sections were placed. The respective environmental characteristics are wet and no freeze, wet and freeze-thaw cycling, dry and no freeze, and dry and freeze-thaw cycling. However, according to the findings of the graphical data manipulation, only the temperature freeze-thaw division of the climatic regions seemed to matter. Therefore, it was decided to consider two temperature-based classes of region (RGT)—cold and warm—in the experiment. The two classes are delineated by the horizontally dividing line of the map.

The groups of sections with similar characteristics and performance patterns were placed in the appropriate cells of the design. This design represented about three-fourths the total number of friction observations collected for all established sections, amounting to 355 observations. Because of the different number of observations in each cell and because of the presence of empty cells, the design was regarded as unbalanced. Adding more levels of the considered variables, to

TABLE 1 Design of the Experiment for the Environment, Aggregate Type, and Construction Spreading Rate Effects

AGGREGATE GROUPS (AGGR)	AGGREGATE PROPERTIES	LEVELS OF CONSTRUCTION AGSR	REGION (RGT)	
			II & V (COLD)	I & IV (WARM)
LIGHTWEIGHT (A)	PV ^a = 48 to 51 FRTH ^b = 3.00 to 9.53 LA ^c = 18 to 25	77 (LOW)	Group 1 (n=13)	---
		104 to 120 (MED)	Group 3 (n=40)	Group 2 (n=32)
		130 to 142 (HIGH)	---	Group 4 (n=16)
SANDSTONE AND RHYOLITE (B)	PV = 36 to 41 MSS ^d = 0.0 to 15.0 LA = 15 to 28 INRD ^e = 55.00 to 100.00	77	Group 5 (n=8)	---
		104 to 120	Group 6 (n=75)	---
		130 to 142	Group 7 (n=10)	---
LIMESTONE ROCK ASPHALT (C)	PV = 34 to 40 MSS = 7.0 to 14.0 LA = 28 to 34 INRD = 1.28 to 14.71	77	---	---
		104 to 120	Group 8 (n=14)	Group 9 (n=27)
		130 to 142	---	Group 10 (n=16)
LIMESTONE 1 (D)	PV = 33 to 37 MSS = 17.1 to 41.0 LA = 26 to 36 INRD = 0.41 to 4.24	77	---	---
		104 to 120	Group 11 (n=22)	---
		130 to 142	Group 12 (n=10)	---
LIMESTONE 2 (E)	PV = 25 to 29 MSS = 2.7 to 8.6 LA = 22 to 24 INRD = 0.45 to 20.23	77	---	---
		104 to 120	Group 13 (n=18)	Group 15 (n=7)
		130 to 142	Group 14 (n=14)	Group 16 (n=32)

(a: Polish Value; b: Freeze-Thaw resistance; c: Los Angeles abrasion; d: Magnesium Sulfate Soundness; e: Insoluble Residue)

allow for the inclusion of the remaining one-fourth of the collected observations, only would have augmented the problems that are usually encountered with such designs. Table 1 indicates between parentheses the abbreviations used for the different variables in the statistical analyses. It also shows the number of observations occupying each cell.

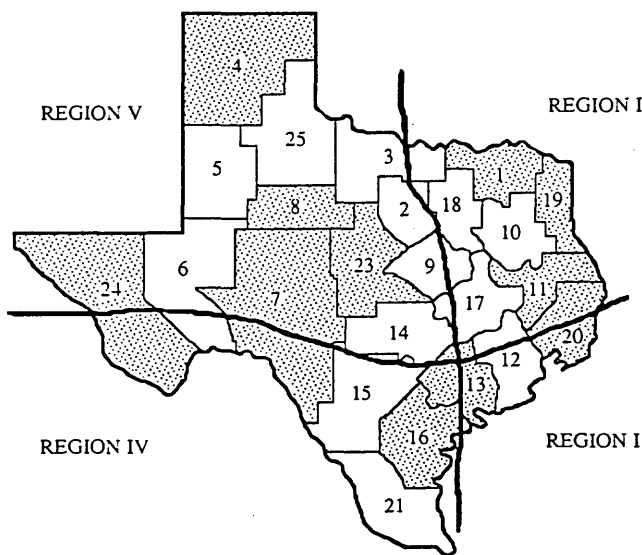


FIGURE 1 Texas map showing the climatic regions and the districts where test sections were placed.

EXAMINATION OF PERFORMANCE VARIABILITY

The performance of each group of sections was judged on the basis of the rate of decrease in FN and the number of accumulated traffic passes withstood by the material before the FNs intercepted with the zone of minimum friction. This zone was assumed to be confining FNs in the range of 30 to 40. The lower boundary, an FN of 30, was that thought by highway engineers to represent the level of friction below which a corrective measure should be considered. The upper boundary was roughly chosen on the basis of a study involving wet-pavement accidents (13), in which a significant decrease in the accident rate was revealed when pavement FNs were greater than about 44.

Variability Associated With Aggregate Type and Properties

Figures 2 and 3 depict the performance of various groups of test sections constructed in the cold and warm regions, respectively, with a medium-level aggregate spreading rate. The scatter in the performance of the five groups (Groups 3, 6, 8, 11, and 13) located in the cold region (Figure 2) was found to be wide. However, much of the scatter appeared to be explained by the type and properties of aggregates constituting each group. As expected, the performance of the lightweight aggregate group was seen to be superior. The sandstone aggregates of Group 6 were found to have maintained

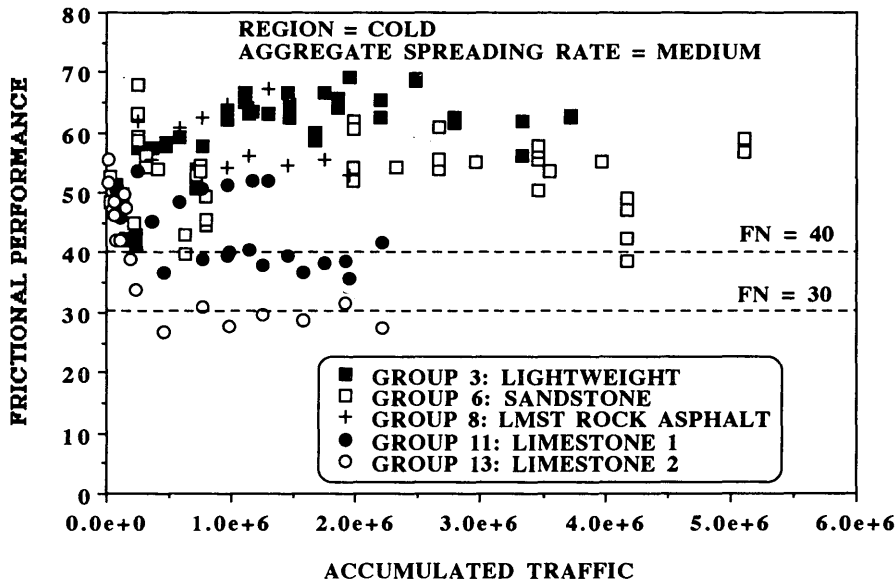


FIGURE 2 Frictional performance of five groups of test sections constructed in the cold region with medium-level aggregate spreading rate—grouped according to aggregate types.

adequate frictional performance. However, the FNs were widely scattered at the early stages of performance, ranging from about 40 to about 70.

Group 8, consisting of a porous limestone rock asphalt aggregate with a PV of 40, showed a steady performance compared with the decrease in performance observed in Group 9 (Figure 3). It is believed that the difference is because the aggregate in Group 8 possesses a constantly rejuvenated microtexture caused by the high number of temperature freeze-thaw cycles that characterize the cold region. Since the aggregate of Group 8 was placed on both the inner and outer

lanes of the same highway section, the variability within the performance data of this group is thought to be attributable to the various levels of ADT the aggregate was exposed to on each of the lanes. Although the accumulated traffic was the basis used in performance evaluation, ADT is thought to control the level of particle embedment during the early years of a section's life, thus controlling the level of macrotexture that may be maintained throughout the remaining useful years.

In the limestone groups, the rate of decrease in the FN was seen to be high, particularly for Group 13, with almost all of the sections intercepting with the zone of minimum friction

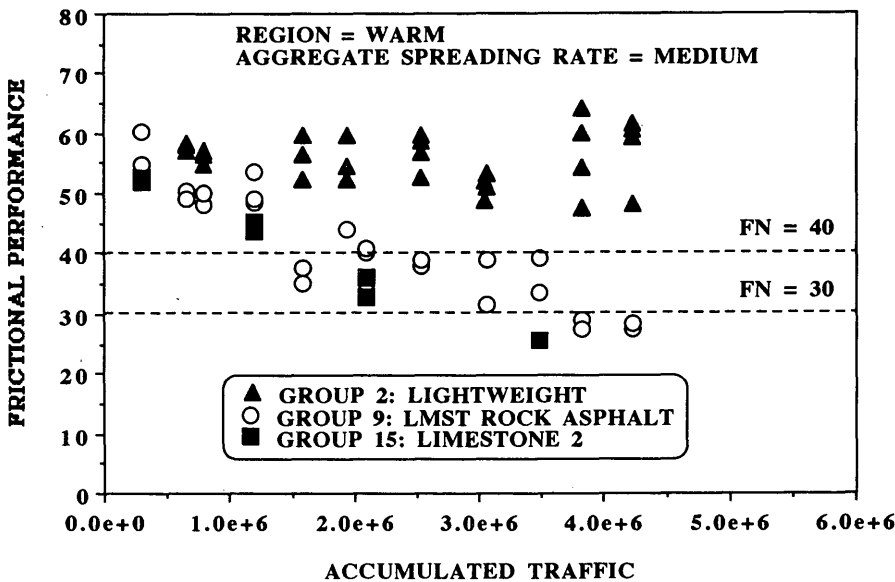


FIGURE 3 Frictional performance of three groups of test sections constructed in the warm region with medium-level aggregate spreading rate—grouped according to aggregate types.

at accumulated traffic of less than 1 million passes. Sections of Group 11 constructed of porous aggregates having higher PVs performed better than those of Group 13 built of dense aggregates having low PVs. However, the data of Group 11 were found to show a considerable variability. The only factor found to explain this variability was the low level of ADT (interacted with the effect of region) on those sections exhibiting a higher level of performance. In the warm region (Figure 3), similar observations could be made about the role that the aggregate type played in explaining performance variability.

Variability Associated with Aggregate Construction Spreading Rate

The clear role of the aggregate construction spreading is illustrated in Figures 4 and 5. The implication was that as the spreading rate increased, the level of frictional performance increased. The phenomenon can be explained as follows. Under the exposure to traffic, the aggregate particles in a seal coat surface are pressed more and more into the asphalt layer, thus displacing some of the asphalt. When the same cubic yard of aggregates is spread over different surface areas, more asphalt will need to be displaced in the smaller areas. The displacement of asphalt results in the asphalt filling much of the volume of the interstices between the aggregate particles. This, in turn, results in a reduction in the macrotexture of the surface that may cause a bleeding distress in the surface. Moreover, when the aggregate particles are spaced so closely that excessive interlocking and overlaying between the particle edges occur, the particles may become crushed. Crushing alters the gradation of the aggregate, thus making the surface unstable and causing bleeding problems.

Variability Associated With Environment

The data included in Figures 6 and 7 were grouped according to the temperature freeze-thaw division of the climatic regions. The effect of region on the performance of Groups 8 and 9 was discussed earlier in this section. The Limestone-2 group consisted of the test sections built with dense aggregates of the poorest polish qualities. As seen in Figure 7, most of its friction data fell within the zone of minimum friction, indicating that its use should not be desirable if other better-quality aggregates can be economically obtained. However, Groups 15 and 16 of the warm region performed much better than Groups 13 and 14 of the cold region. If this performance difference was truly caused by the climatic region variable, the relevant weather components would be moisture and temperature. That is because, in general, chemical decay of minerals in dense rocks is fostered by warm, moist climates (14).

STATISTICAL TESTING

Three-Variable General Linear Model

Because of the unbalance of the experimental design presented in Table 1, the general linear model (GLM) procedure, a capability of the statistical analysis system software, was used for testing the significance of the main three variables constituting the design. The first model generated had the FN as the dependent variable and the three variables and their interaction terms as the main predictors. In addition, accumulated traffic, referred to as CUTR in this analysis, and ADT levels were used as covariates in the model. The ADT variable was thought to influence the degree of aggregate embedment in the asphalt film, especially during the early

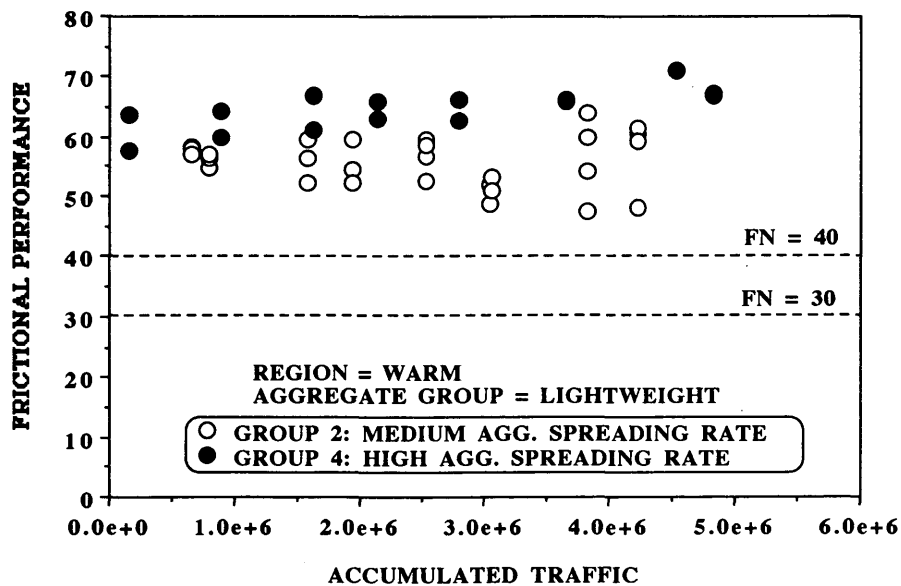


FIGURE 4 Frictional performance of two groups of test sections constructed in the warm region with lightweight aggregates—grouped according to aggregate construction spreading rate.

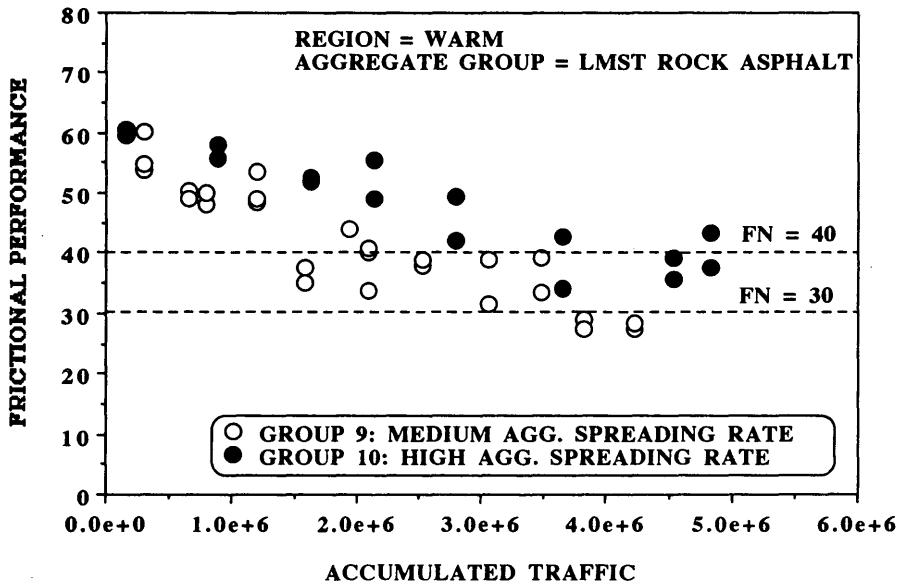


FIGURE 5 Frictional performance of two groups of test sections constructed in the warm region with limestone rock asphalt aggregates—grouped according to aggregate construction spreading rate.

years of a section life, thus affecting the macrotexture depth to be maintained on a seal coat surface. It was also thought to interact with the region variable because both variables control the degree of rejuvenation in the surfaces of aggregate particles. Since the performances of some of the groups were seen to have exhibited logarithmic relationships with traffic, the natural logarithmic function of the CUTR (LGCUTR) was used in this analysis. The model, based on 355 observations, had the following form:

$$\begin{aligned}
 FN = & AGGR + LGCUTR + (AGGR \times LGCUTR) \\
 & + RGT + (AGGR \times RGT) + (LGCUTR \times AGGR \\
 & \times RGT) + LAGSR + (AGGR \times LAGSR) + ADT \\
 & + (ADT \times AGGR)
 \end{aligned}$$

The summarized statistical results are shown in Table 2. The model had an excellent coefficient of determination (R^2) of

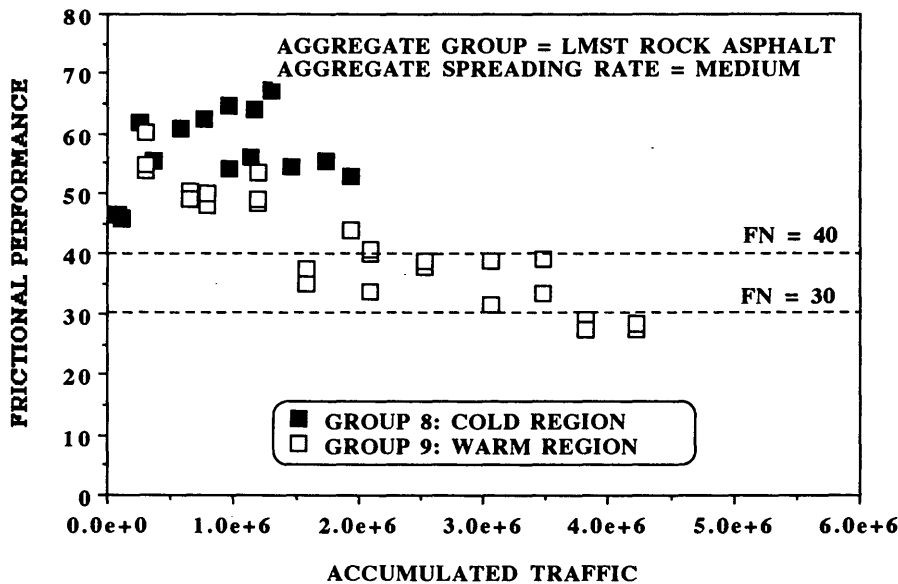


FIGURE 6 Frictional performance of two groups of test sections constructed with limestone rock asphalt aggregates and medium aggregate construction spreading rate—grouped according to region.

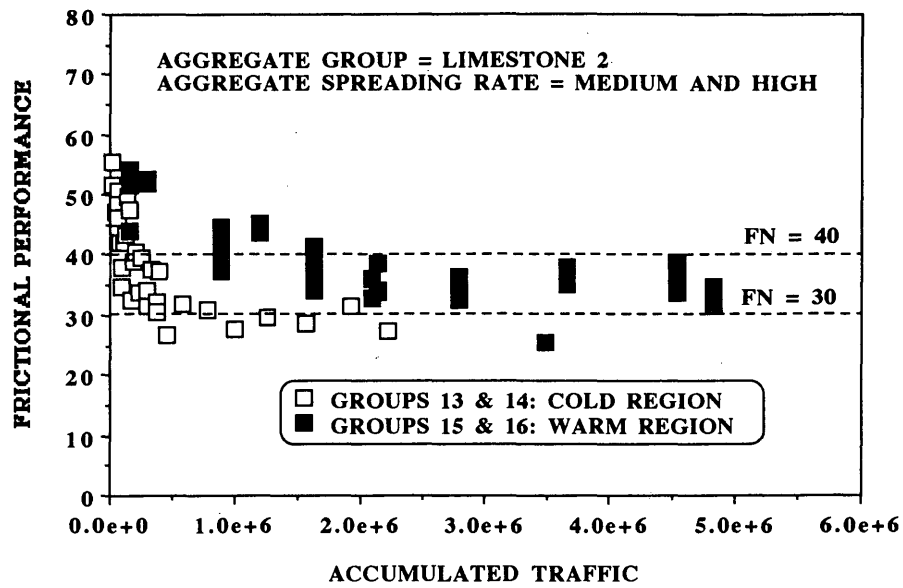


FIGURE 7 Frictional performance of four groups of test sections constructed with limestone aggregates and high and medium aggregate construction spreading rates—grouped according to region.

about 0.84 with each of the considered terms that showed significance at the individual level. Other covariates were then considered in the analysis that included the aggregate sieve analysis results and the asphalt distribution rate as macrotexture parameters and the LRP, DLR, and TPP short-term weather variables. Only the DLR weather variable showed significance at the individual level accompanied by a very slight increase in the model's R^2 . However, because it does not serve any design purposes, this variable was omitted from the model.

The GLM solution of the above model indicated that aggregate Groups A and B had friction means that were higher than those of Groups C, D, and E. It also indicated that Groups A, B, and D had different slopes (with traffic) compared with those of Groups C and E. The effect of region was seen to be significant in Groups A and C, particularly in interaction with traffic. In addition, the LAGSR variable was observed to explain some of the variation in Groups A, B,

C, and D. Finally, the ADT effects was shown to be significant in Groups B, C, and D. The scatter of the residuals against the predicted response was seen to be normal, requiring no transformation of the response.

One-Way General Linear Model

To ensure that any possible bias in the computed estimates was not wholly the result of empty cells being present in the design (because those affect the number of degrees of freedom of the interaction terms), another general linear model was generated in which the groups filling 16 of the cells were considered as 16 levels of a one-way experiment. To avoid over specification in the model, the ADT variable was left out after a small reduction in the R^2 of the first model, which resulted from this action (R^2 decreased to about 0.825), was observed. Using the GLM procedure, the one-way model had

TABLE 2 Three-Variable General Linear Model

SAS									
GENERAL LINEAR MODELS PROCEDURE									
DEPENDENT VARIABLE: FN									
SOURCE	DF	SUM OF SQUARES	MEAN SQUARE	F VALUE	PR > F	R-SQUARE	C.V.		
MODEL	31	30656.11604231	988.90696911	47.92	0.0	0.824122	9.1429		
ERROR	317	6542.41924249	20.63854651	ROOT MSE		FN MEAN			
CORRECTED TOTAL	348	37198.53528479	4.54296671		49.68836390				
SOURCE	DF	TYPE I SS	F VALUE	PR > F	DF	TYPE III SS	F VALUE	PR > F	
LGCUTR	1	0.41149891	0.02	0.8878	1	653.51917951	31.66	0.0001	
GROUP	15	23867.05988307	77.10	0.0	15	5345.54762448	17.27	0.0001	
LGCUTR*GROUP	15	6788.64466032	21.93	0.0001	15	6788.64466032	21.93	0.0001	

the form of

$$FN = LGCUTR + GROUP + (LGCUTR \times GROUP)$$

and an R^2 of about 0.825, the same as that of the first model after dropping ADT. The statistical results are shown in Table 3. Any possible bias in the estimates of the solution of the one-way model is primarily the result of unequal numbers of observations in the filled cells.

Regression Model

To get the prediction equation of the one-way model, a regression analysis [in this case, an analysis of variance (ANOVA)] was performed on the 16 groups. The resulted estimates for the groups and their interactions with LGCUTR are summarized in Table 4. The model had a good adjusted R^2 of 0.77. Because the GROUP variable was dummy coded, the estimates of the intercept and LGCUTR applied directly to Group 16. With 90 percent confidence, the intercepts of Groups 2, 7, 11, 12, 13, and 14 were shown to be not statistically significant compared with that of Group 16. Furthermore, the slopes of Groups 11 through 14 were found to be not statistically significant from that of Group 16.

USE OF THE PERFORMANCE MODEL

The regression equation can be used most appropriately for predicting the mean performance of aggregates that are, based on history, to fall in any of the 16 groups constituting the design in Table 1. Further, the prediction model can be incorporated into a pavement management system, as illustrated in Figure 8. Suppose that a seal coat overlay is to be placed with a medium AGSR on a highway, located in the warm region, with an expected ADT of 2,740 vehicles per lane and that no major rehabilitation project is scheduled for this highway within the next 8 years. For the 8-year period, two overlays of a local limestone rock asphalt aggregate are required, as contrasted with only one overlay of a sandstone

aggregate. If this sandstone aggregate is not available locally, the extra cost incurred from obtaining and hauling this good-quality aggregate should be weighed against the cost of having to lay down a second overlay with the local material.

CONCLUSIONS

A statistical experiment was conducted with the objective of identifying the role of certain factors in explaining the performance variability of seal coat pavement surfaces. Factors found to be statistically significant included the type and properties of aggregates, the aggregate construction spreading rate, and the climatic region. These class variables, along with a short-term weather covariate—the number of days between last rainfall and day of field testing—and the level of ADT exposure, as well as some interaction terms, were found to explain about 84 percent of the observed performance variability. A prediction equation was formulated to describe the performance of the 16 groups of test sections included in the experiment. The following observations were also drawn from the study:

1. The grouping of some of the data according to the various aggregate materials was found to explain, in broad terms, much of the scatter observed in the data. Superior performance was observed in the lightweight and sandstone groups. The limestone rock asphalt and limestone groups experienced different, noticeable rates of decrease in frictional performance.
2. The level of performance of aggregates with high polish values and high soundness losses (carbonate aggregates) was found to be dependent on the level of ADT because the polishing action of this variable interacted with the degree of rejuvenation caused by weathering action.
3. Porous aggregates, particularly some lightweight and limestone rock asphalt ones, were seen to maintain excellent rejuvenated surfaces in the cold region characterized by temperature freeze-thaw cycling.
4. The level of construction aggregate spreading rate was shown to explain much of the variations among many of the

TABLE 3 One-Way General Linear Model

SAS								
GENERAL LINEAR MODELS PROCEDURE								
DEPENDENT VARIABLE: FN								
SOURCE	DF	SUM OF SQUARES	MEAN SQUARE	F VALUE	PR > F	R-SQUARE	C.V.	
MODEL	29	31150.44194538	1074.15317053	57.23	0.0	0.836233	8.7116	
ERROR	325	6100.46552738	18.77066316			ROOT MSE	FN MEAN	
CORRECTED TOTAL	354	37250.90747275				4.33251234	49.73250423	
SOURCE	DF	TYPE I SS	F VALUE	PR > F	DF	TYPE III SS	F VALUE	PR > F
AGGR	4	17293.54896334	230.33	0.0	4	1551.68445536	20.67	0.0001
LGCUTR*AGGR	5	4893.57083960	52.14	0.0001	5	2153.45228166	22.94	0.0001
AGGR*RGT	4	2095.10085401	27.90	0.0001	4	1438.11287015	19.15	0.0001
LGCUTR*AGGR*RGT	4	1394.20094170	18.57	0.0001	4	1704.37329012	22.70	0.0001
LAGSR	2	3063.01791495	81.59	0.0001	2	2390.55288756	63.68	0.0001
AGGR*LAGSR	5	1378.77114586	14.69	0.0001	5	1337.36369584	14.25	0.0001
ADT	1	118.81673852	6.33	0.0124	1	639.85718132	34.09	0.0001
ADT*AGGR	4	913.41454740	12.17	0.0001	4	913.41454740	12.17	0.0001

TABLE 4 Regression or ANOVA Equation of the One-Way General Linear Model

SAS

DEP VARIABLE: FN
ANALYSIS OF VARIANCE

SOURCE	DF	SUM OF SQUARES	MEAN SQUARE	F VALUE	PROB>F
MODEL	31	29509.43407	951.91723	39.717	0.0001
ERROR	323	7741.47340	23.96740991		
C TOTAL	354	37250.90747			

ROOT MSE	4.895652	R-SQUARE	0.7922
DEP MEAN	49.7325	ADJ R-SQ	0.7722
C.V.	9.843969		

PARAMETER ESTIMATES

VARIABLE	DF	PARAMETER ESTIMATE	STANDARD ERROR	T FOR HO: PARAMETER=0	PROB > T	VARIABLE	MEAN	VARIANCE
INTERCEP	1	101.55039	11.71296926	8.670	0.0001	LGCUTR	13.87742571	1.34459076
LGCUTR	1	-4.24198826	0.80939370	-5.241	0.0001	GROUP1	0.03513514	0.03399253
GROUP1	1	-75.89946709	23.87036818	-3.180	0.0016	GROUP2	0.08648649	0.07922068
GROUP2	1	-35.21252122	22.59299120	-1.559	0.1201	GROUP3	0.10810811	0.09668205
GROUP3	1	-119.68286	15.74819426	-7.600	0.0001	GROUP4	0.04324324	0.04148539
GROUP4	1	-69.68385572	20.35115642	-3.424	0.0007	GROUP5	0.03513514	0.03399253
GROUP5	1	-108.47536	26.84568586	-4.041	0.0001	GROUP6	0.18918919	0.15381235
GROUP6	1	-52.94475671	13.77786481	-3.843	0.0001	GROUP7	0.02702703	0.02636783
GROUP7	1	-55.92553587	38.48353356	-1.453	0.1471	GROUP8	0.03783784	0.03650480
GROUP8	1	-88.37051997	21.60586706	-4.090	0.0001	GROUP9	0.08378378	0.07697209
GROUP9	1	84.45210742	20.34597279	4.151	0.0001	GROUP10	0.04324324	0.04148539
GROUP10	1	42.58030511	20.35115642	2.092	0.0372	GROUP11	0.05945946	0.05607559
GROUP11	1	-19.93751604	19.53226906	-1.021	0.3081	GROUP12	0.02702703	0.02636783
GROUP12	1	9.33253706	38.48353356	0.243	0.8085	GROUP13	0.04864865	0.04640738
GROUP13	1	9.22700334	15.15751539	0.609	0.5431	GROUP14	0.04050405	0.03900242
GROUP14	1	5.28029734	28.09984244	0.188	0.8511	GROUP15	0.02702703	0.02636783
GROUP15	1	76.03174979	30.87638883	2.462	0.0143	LGGRP1	0.50979647	7.04757918
LGGRP1	1	5.64484886	1.66759373	3.385	0.0008	LGGRP2	1.27627954	16.93262469
LGGRP2	1	3.53035553	1.55957045	2.264	0.0243	LGGRP3	1.51907548	18.79943111
LGGRP3	1	9.87131565	1.11132988	8.882	0.0001	LGGRP4	0.63487580	8.81553219
LGGRP4	1	6.54326212	1.40816492	4.647	0.0001	LGGRP5	0.29622619	3.92526663
LGGRP5	1	8.36087896	1.96677630	4.251	0.0001	LGGRP6	2.69585683	30.75175868
LGGRP6	1	4.55134506	0.96056646	4.738	0.0001	LGGRP7	0.36438294	4.70853787
LGGRP7	1	5.19284977	2.88481095	1.800	0.0728	LGGRP8	0.51623181	6.69787343
LGGRP8	1	7.54227463	1.57649801	4.784	0.0001	LGGRP9	1.22511119	16.17108453
LGGRP9	1	-5.87541208	1.41790765	-4.144	0.0001	LGGRP10	0.63487580	8.81553219
LGGRP10	1	-2.43635841	1.40816492	-1.730	0.0846	LGGRP11	0.81952484	10.48865524
LGGRP11	1	1.42080995	1.40901508	1.008	0.3140	LGGRP12	0.36438294	4.70853787
LGGRP12	1	-0.47536686	2.88481095	-0.165	0.8692	LGGRP13	0.61050922	7.27357805
LGGRP13	1	-1.57202275	1.12112947	-1.402	0.1618	LGGRP14	0.50759072	6.00945932
LGGRP14	1	-1.45825924	2.22656057	-0.655	0.5130	LGGRP15	0.39129151	5.44124143
LGGRP15	1	-5.56882502	2.20398239	-2.527	0.0120			

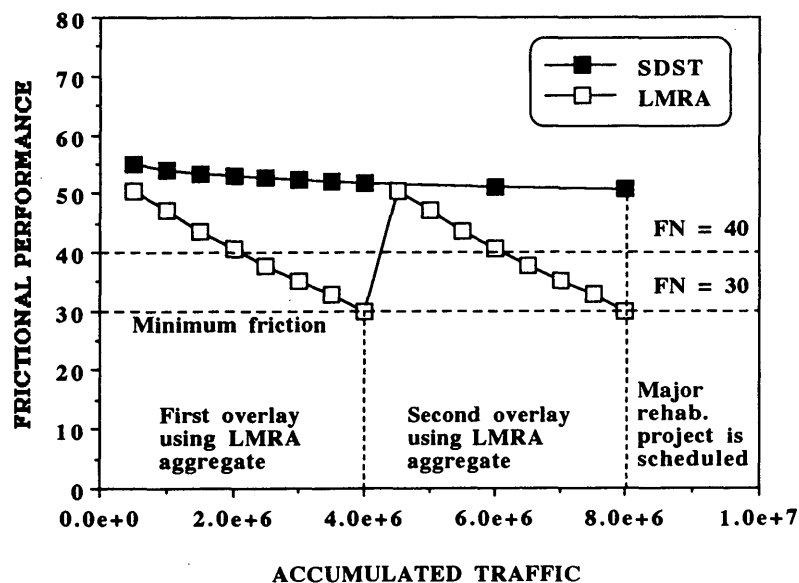


FIGURE 8 Example of how the performance model can be incorporated in a pavement management system.

examined groups. The implication was that as the spreading rate increased, a higher level of frictional performance was achieved.

ACKNOWLEDGMENTS

This study was conducted at the Center for Transportation Research (CTR) of the University of Texas at Austin under the sponsorship of the Texas State Department of Highways and Public Transportation (SDHPT) and in cooperation with FHWA. The authors extend their appreciation to the members of the project executive committee of the Texas SDHPT for their constructive comments and suggestions. Thanks are also due to Virgil Anderson of Purdue University and to Chryssis Papaleontiou of CTR for their helpful insights into the statistical experiment. Finally, thanks are also extended to the University Research Board of the American University of Beirut, who made it possible for the first author to conduct follow-up research on this subject.

REFERENCES

1. M. U. Abdul-Malak, A. H. Meyer, and D. W. Fowler. Research Program for Predicting the Frictional Characteristics of Seal-Coat Pavement Surfaces. In *Transportation Research Record 1217*, TRB, National Research Council, Washington, D.C., 1989, pp. 53-64.
2. M. U. Abdul-Malak. *Implication of Aggregates in the Construction and Performance of Seal Coat Pavement Overlays*. Ph.D. dissertation. The University of Texas at Austin, Austin, 1990.
3. T. D. Gillespie. *Pavement Surface Characteristics and Their Correlation With Skid Resistance*. Report 12, Pennsylvania State University.
4. J. J. Henry and S. H. Dahir. Effects of Textures and the Ag-

- gregates That Produce Them on the Performance of Bituminous Surfaces. In *Transportation Research Record 712*, TRB, National Research Council, Washington, D.C., 1979, pp. 44-50.
5. *Manual of Test Methods: Accelerated Polish Test for Coarse Aggregate*. Test Method Tex-438-A-1983. Texas State Department of Highways and Public Transportation, Jan. 1983.
6. *Manual of Test Methods: Soundness of Aggregate by Use of Sodium Sulfate or Magnesium Sulfate*. Test Method Tex-411-A-1978. Texas State Department of Highways and Public Transportation, Jan. 1978.
7. M. U. Abdul-Malak, D. W. Fowler, and A. H. Meyer. The Mineralogy of Aggregates in Relation to the Frictional Performance of Seal Coat Pavement Overlays: A Petrographic Study. Presented at the 71st Annual Meeting of the Transportation Research Board, Washington, D.C., Jan. 1992.
8. Surface Characteristics. Technical Committee Report 1. Presented at 18th World Road Congress, Brussels, Belgium, Sept. 13-19, 1987.
9. S. H. Dahir et al. *Seasonal Skid Resistance Variations*. Report PA 80/75-10. FHWA, U.S. Department of Transportation, 1979.
10. R. R. Hegmon. Seasonal Variations in Pavement Skid Resistance—Are These Real? *Public Roads*, Sept. 1978, pp. 55-62.
11. B. J. Hill and J. J. Henry. Short-Term, Weather-Related Skid Resistance Variations. In *Transportation Research Record 836*, TRB, National Research Council, Washington, D.C., 1981, pp. 76-81.
12. K. Saito and J. J. Henry. Mechanistic Model for Predicting Seasonal Variations in Skid Resistance. In *Transportation Research Record 946*, TRB, National Research Council, Washington, D.C., 1983, pp. 29-37.
13. J. L. Beaton. Providing Skid Resistant Pavements, Skidding Accidents: Pavement Characteristics. In *Transportation Research Record 622*, TRB, National Research Council, Washington, D.C., 1976, pp. 39-50.
14. H. Williams, F. J. Turner, and C. M. Gilbert. *Petrography: An Introduction to the Study of Rocks in Thin Sections*. W. H. Freeman and Company, San Francisco, 1982.

Publication of this paper sponsored by Committee on Pavement Rehabilitation.

Application of Cracking and Seating and Use of Fibers To Control Reflective Cracking

YI JIANG AND REBECCA S. MCDANIEL

Two methods for reducing pavement cracking on asphalt overlays over concrete pavement on I-74 in Indiana—cracking and seating before overlay and fiber reinforcement in the overlay mixture—were evaluated. The project was constructed in 1984 and 1985 and divided into several experimental sections and control sections. As a performance comparison with the experimental sections, the control sections were overlaid by the conventional method. The study results based on the 7-year pavement performance data indicated that the cracking and seating technique was successful in this project: it delayed most of the transverse cracks for 5 years. The majority of the transverse cracks on the cracked and seated sections were thermal cracks, which were narrower and less severe than the reflective cracks on the control section. It was also found that the type of hammers used for cracking the concrete slabs had strong effects on pavement performance. The use of fibers in the overlay mixture further reduced transverse cracks on cracked and seated sections but did not improve the cracking resistance of the control sections. Fibers improved rutting resistance on both control and cracked and seated sections. However, the sections with fibers exhibited quick decreases in pavement strength and rideability. Thicker overlays increased the construction costs significantly but did not reduce the transverse crack intensities. According to the pavement performance and the cost analyses, it is recommended that the thickness of asphalt overlay be determined only by the pavement strength requirement and not be increased as a means of cracking control.

This study evaluated two methods for reducing reflective cracking of an asphalt overlay over a 12.5-mi (20.1-km) section of reinforced jointed concrete pavement on I-74 in Indiana from the Montgomery/Boone County Line to State Route 39. The first method, cracking and seating, breaks the existing concrete pavement slabs into smaller pieces and then seats these pieces by rolling to achieve uniform contact between the individual slab pieces and the base layer before placement of the asphalt overlay. This process reduces the effective slab length and therefore reduces the slab's horizontal movement caused by temperature or moisture changes, or both. The vertical movements of slabs are also limited because the small pieces of the slabs are in uniform and tight contact with the subbase and there exists some degree of aggregate interlock between the slab pieces. The second method involves the addition of polypropylene fibers to the asphalt overlay to increase the tensile strength of the asphalt mixture.

The project was constructed in 1984 and 1985. The pavement condition has been monitored since then by performing

deflection tests, roughness tests, visual inspections, and rutting measurements. This paper presents the study results based on the 7-year pavement condition data. In this paper, pavement performance in the experimental and control sections in the 7-year period is discussed and the effectiveness of the techniques is determined. The results of a life cycle analysis are also presented to determine the cost-effectiveness of the cracking and seating technique.

SCOPE OF THE STUDY

The concrete pavement in place before rehabilitation was 19 years old. It consisted of concrete slabs 10-in. (25.4 cm) thick over a 6-in.-thick granular subbase. The concrete slabs were 40 ft (12.2 m) long with joints connected by dowel bars. The traffic volume is over 10,000 vehicles per day with about 30 percent trucks. The following eight different treatments were applied on this project:

A—Asphalt underseal with 4.25-in. (11.4-cm) asphalt overlay

Surface: 70 lb/yd² (38 kg/m²)

Binder: 150 lb/yd² (81 kg/m²)

Base: 250 lb/yd² (135 kg/m²)

A1—Same as A with fiber-reinforced asphalt base layer

A2—Same as A with fiber-reinforced asphalt base and binder layers

B—Cracked and seated slab with 5-in. (12.7-cm) asphalt overlay

Surface: 70 lb/yd² (38 kg/m²)

Binder: 150 lb/yd² (81 kg/m²)

Base: 330 lb/yd² (179 kg/m²)

B1—Same as B with fiber-reinforced asphalt base layer

B2—Same as B with fiber-reinforced asphalt base and binder layers

C—Cracked and seated slab with 6.5-in. (16.5-cm) asphalt overlay

Surface: 70 lb/yd² (38 kg/m²)

Binder: 150 lb/yd² (81 kg/m²)

Base: 510 lb/yd² (276 kg/m²)

D—Cracked and seated slab with 8.5-in. (21.6-cm) asphalt overlay

Surface: 70 lb/yd² (38 kg/m²)

Binder: 150 lb/yd² (81 kg/m²)

Base: 700 lb/yd² (380 kg/m²)

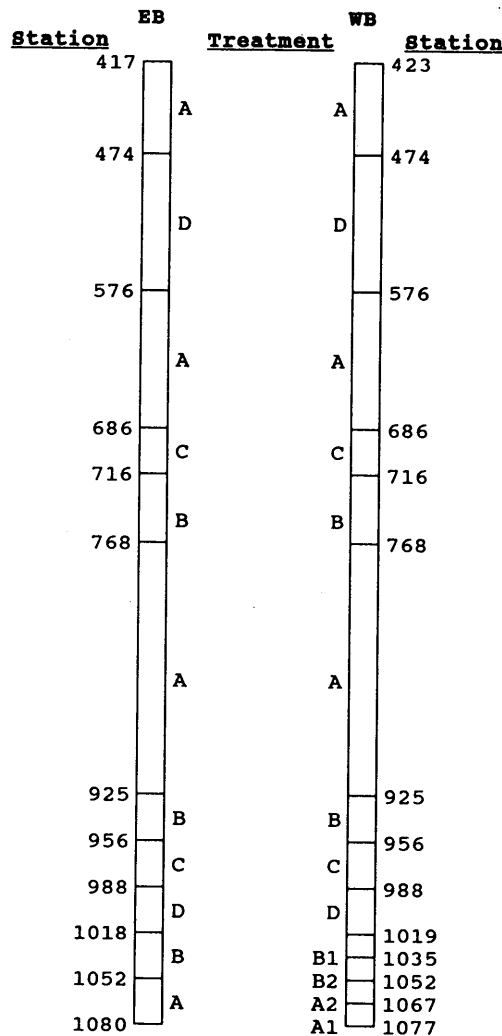
Figure 1 shows the layout of the sections of various treatments along the roadway. Treatments A, A1, and A2 were designated as control sections of this study. Treatments B, B1, B2, C, and D were required to be cracked transversely at 18- to 24-in. spaces. No longitudinal cracks were allowed to develop during the cracking and seating process. Polypropylene fibers were added to the base layer or base and binder layers in sections of treatments A1, A2, B1, and B2. All the rehabilitation work, except for laying the 70-lb/yd² (38-kg/m²) surface layer, were carried out in the summer and fall of 1984. The surface layer was laid the following summer in 1985.

CONSTRUCTION

The cracking process was started in the section between Stations 474 and 576 with a whip hammer manufactured by Wol-

verine Technology. A number of hammer head shapes and blow patterns were tried and it was found that six to eight blows in a large semicircular pattern produced the required transverse cracks. This was verified by removing a portion of a slab with a crane and taking cores at the location of the surface. Two methods were used to detect the presence of cracks at the surface. The first method used water sprinkled on the surface of the slab. As the water evaporated, the water in the location of the cracks could be seen. The second method used flour sprinkled on the surface of the slab. When the slab was struck by the hammer, the flour moved from the cracks showing the locations of the cracks.

Cracking the pavement with the whip hammer was relatively time consuming, since it required approximately six blows across the width of the 12-foot (3.66-m) lane. Also, it did not always produce the desired cracking pattern. Therefore, a second type of cracker was used for other experimental



- Treatments:**
 A: Underseal, 4 1/4 Inch Overlay
 B: Crack & Seat, 5 Inch Overlay
 C: Crack & Seat, 6 1/2 Inch Overlay
 D: Crack & Seat, 8 1/2 Inch Overlay

- 1: Fiber Reinforced Base
 2: Fiber Reinforced Base & Binder

FIGURE 1 Location of various treatments.

sections. The new cracker was a 7-ton guillotine-type drop hammer manufactured by Wirtgen. With the drop hammer, only one blow was required to produce a crack across the full width of the lane, and the cracks were more consistent in pattern than those produced by the whip hammer. The drop hammer needed only about one-sixth of the time required by the whip hammer to produce a transverse crack of full lane width.

After cracking the slabs, a 50-ton rubber-tired roller pulled by a rubber-tired tractor was used to seat the pavement. The seating process was intended to reduce the voids between the cracked slabs and the subbase. The Dynaflect was used to test the pavement deflection before and after cracking of some selected sections in the travel lane. The Dynaflect has five sensors for deflection measurements. Sensor 1 is located between the two loading wheels of the Dynaflect, and Sensors 2 through 5 are spaced at 1-ft (30.5-cm) increments from Sensor 1, with Sensor 5 being the farthest (4 ft or 122 cm) from Sensor 1. In practice, sensor 1 is used as an indicator of slab strength, and sensor 5 is used as an indicator of the base and subbase support strength. To compare the changes of slab and subbase strength, the deflection values before

cracking and after cracking and three passes of the roller are plotted in Figures 2 and 3. The two figures show that the sections cracked with the whip hammer (Figure 3) lost more strength than those cracked with the drop hammer (Figure 2). This indicates that the cracking process with the whip hammer may have disturbed the consolidation of the subbase and damaged the aggregate interlock between the produced small slab pieces. This was evidently related to the fact that too many blows were required for the whip hammer to produce each transverse crack.

The deflections after a various number of roller passes on the whip hammer cracked sections are plotted in Figure 4. Because the seating process was to impress the slab pieces onto the subbase, it was expected that the deflections would decrease with each pass of the roller. However, as shown in Figure 4, the deflections under both sensors did not decrease but increased with the number of passes. That is, both the concrete slabs and the subbase lost, instead of gained, strength in the seating process. The possible reason for this strength decrease was that the heavy roller further weakened the very little remaining aggregate interlock between slab pieces produced by the whip hammer. The rolling process then caused

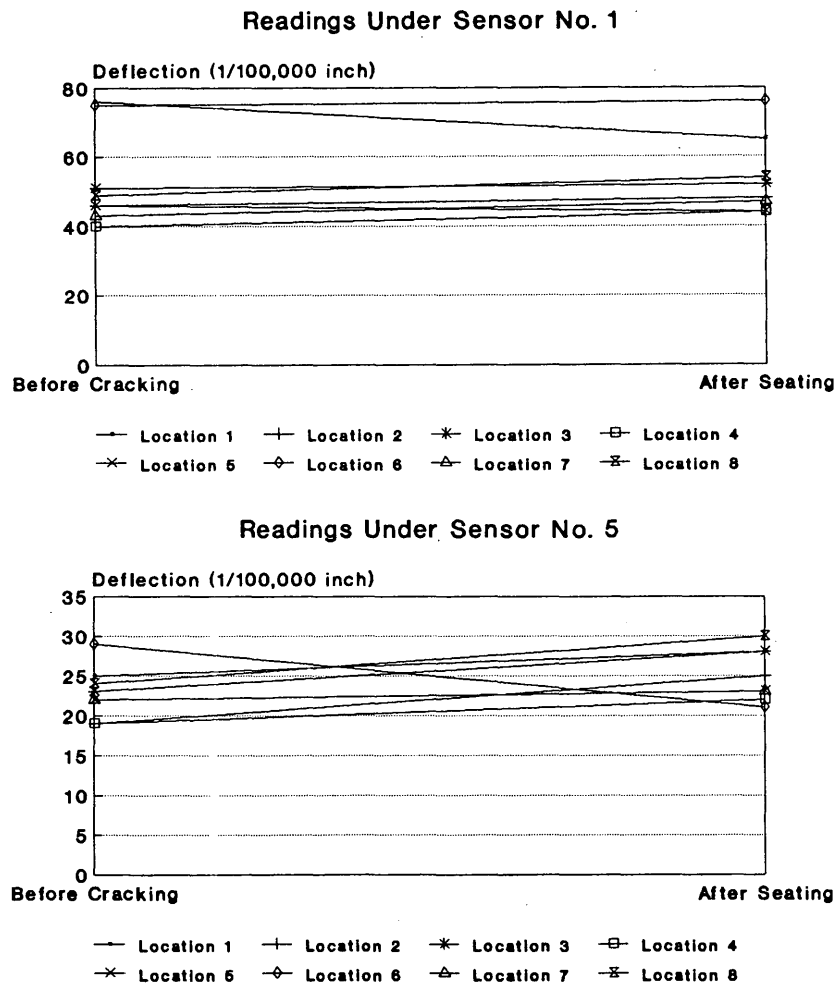


FIGURE 2 Deflections before and after cracking and seating at various locations (on drop hammer-cracked sections).

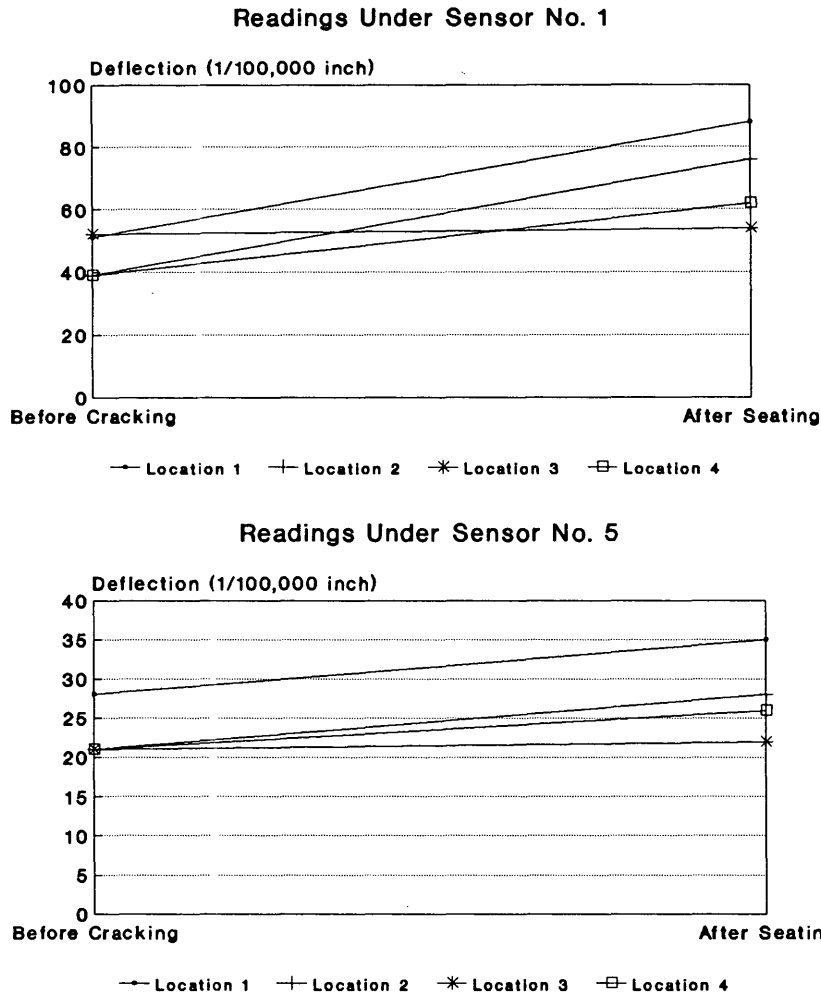


FIGURE 3 Deflections before and after cracking and seating at various locations (on whip hammer-cracked sections).

the slab pieces to rock on the subbase. The slab pieces were unseated instead of seated as was intended. Therefore, the whip hammer was not suitable for the cracking and seating process because it was not only time consuming to use, it also caused significant strength decrease of slabs and subbase support. The drop hammer, however, proved to be efficient and produced the required cracks and maintained aggregate interlock between the slab pieces as desired.

As control sections, treatments A, A1, and A2 were overlaid by the conventional method. Before they were overlaid, the concrete slabs were first undersealed in areas showing high deflections with oxidized asphalt to improve the strength and the uniformity of the subbase support.

The polypropylene fibers were 0.4 in. (1.0 cm) long and were added at the rate of 0.3 percent by weight of the asphalt mixture (approximately 6 lb of fibers per ton of asphalt mixture) to the base layer of sections A1 and B1 and to the base and binder layers of section A2 and B2. The effects of the fibers on the asphalt mixture were assessed by visual inspections of the mixture during construction. The fibers appeared to decrease the segregation of the mixture at the plant and during placement on the roadway, especially for the larger maximum aggregate size base.

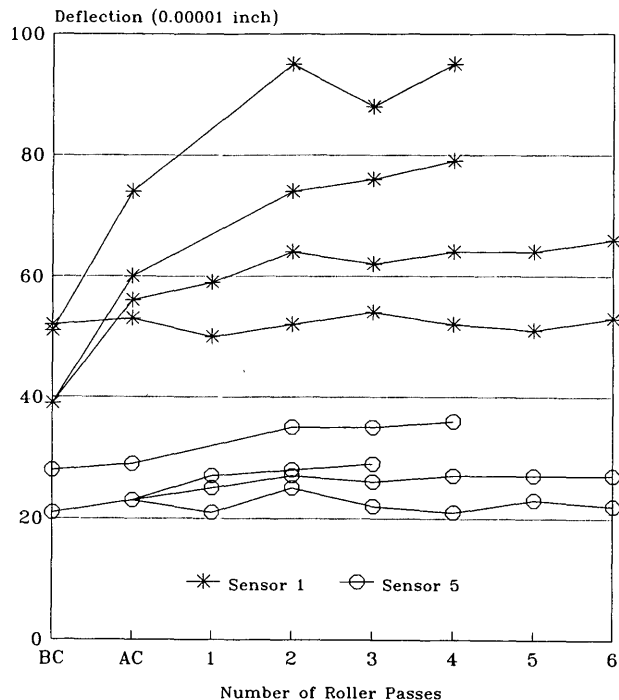
PAVEMENT PERFORMANCE

The pavement condition has been monitored for 7 years since the rehabilitation. The Dynaflect deflection test, a visual survey of reflective cracks, rutting measurements, and roughness tests, was conducted each year. These pavement condition data are summarized in this section to study the performance of each rehabilitation treatment. To examine the effects of cracking equipment, Treatment D is divided into the following two groups:

1. D(drop)—Treatment D cracked with the drop hammer and
2. D(whip)—Treatment D cracked with the whip hammer.

Pavement Strength

Table 1 shows the average deflection values for 6 of the 7 years of the study period (1987 data are missing) for all the treatments. The deflection data were adjusted to the standard temperature of 70°F (21°C) according to the manual for Dynaflect operation (1). Sensor 1 is used as an indicator of pave-



BC = Before Cracking
AC = After Cracking

FIGURE 4 Slab deflections for various numbers of roller passes (on whip hammer-cracked sections).

ment strength, and Sensor 5 is used as an indicator of the base and subbase support strength. Readings of 50×10^{-5} in. (0.0127 mm) or less by Sensor 1 and 30×10^{-5} in. (0.00762 mm) or less by Sensor 5 are indications of adequate pavement strength and good subbase support, respectively.

The data in Table 1 indicate that all the sections have undergone some decrease in strength during the 7-year period.

However, the data show that all the sections still had good pavement strength and subbase support after 7 years in service. To compare the strengths and the strength changes of the treatments, the deflection values under Sensor 1 in 1991 and the percent changes of these values are listed below.

Treatment	Deflection (1991)	Change (1991 Versus 1985) (%)
D(drop)	28	16.7
D(whip)	30	7.1
C	32	10.3
A	32	18.5
B	33	13.8
A1	34	21.4
A2	35	45.8
B1	36	38.5
B2	39	39.3

Because the deflection values are listed in ascending order, it is easy to observe the following:

1. All the sections still had adequate pavement strength with deflection values lower than 50.
2. Comparing Treatments D, C, and B for the cracked and seated sections, the thicker the overlay was, the higher was the pavement strength (or the lower was the deflection value). However, the differences were not significant.
3. The strength of Treatment A (4.25-in. conventional overlay) was equivalent to the strength of Treatment C (6.5-in. cracked and seated overlay).
4. The sections of Treatments A1, A2, B1, and B2 experienced greater loss of strength (with higher percent changes of deflection values) than other sections.

Because it was known that the use of fibers could increase the stiffness and tensile strength of the asphalt mixtures, it was expected that the sections with fibers would have a somewhat higher pavement strength. The deflection data, however, do not support this. The reason for this could not be known without further study of the mixture material, but the

TABLE 1 Average Pavement Dynaflect Deflection Values by Treatments (10^{-5} in.)

Treatment	Year											
	1985		1986		1988		1989		1990		1991	
	S1	S5	S1	S5	S1	S5	S1	S5	S1	S5	S1	S5
A	27	16	30	18	34	18	-	-	33	18	32	17
A1	28	18	36	22	36	22	36	21	37	21	34	18
A2	24	15	32	19	-	-	29	15	32	17	35	19
B	29	17	32	18	34	18	33	18	38	20	33	15
B1	26	15	32	17	-	-	27	15	32	17	36	19
B2	28	16	35	20	-	-	30	16	33	17	39	20
C	29	18	29	19	32	19	30	18	34	20	32	16
D(whip)	28	16	28	18	27	16	-	-	32	17	30	14
D(drop)	24	14	26	16	27	15	25	14	28	17	28	15

Note: S1 -- Sensor No. 1
S5 -- Sensor No. 5
D(whip) -- Sections of Treatment D Cracked with Whip Hammer
D(drop) -- Sections of Treatment D Cracked with Drop Hammer

loss of strength may have been caused by the decrease in bonding between the fiber and the asphalt mixture as the asphalt hardens with time. As the bond in the interface between the fiber and asphalt reduced or disappeared, the fiber could no longer reinforce the mixture but became detrimental to the integrity and the strength of the mixture. This issue should be investigated further.

Pavement Roughness

Pavement roughness testing was performed annually with a PCA Roadmeter. Table 2 gives the average roughness numbers (RN) and the corresponding present serviceability indexes (PSI) for each treatment from 1985 to 1991. A roughness number is a measure of the square of the number of $\frac{1}{8}$ -in. (3.2-mm) movements of the automobile body with respect to the rear axle. The lower the roughness number is, the better is the rideability of the pavement. The roughness numbers have been correlated to PSI values ranging from 0 to 5. A PSI of 2.5 or less is considered unsatisfactory on interstate pavements. Table 2 shows that the PSI values for all treatments were fairly high except in 1988. However, the PSI values for 1988 are suspiciously low compared with the data for the other 6 years. Because no significant changes in pavement condition were observed during the visual inspection in 1988, it is believed that the roughness data for 1988 are not accurate because of some equipment or operational problem.

The PSI values for the other 6 years indicate that the pavement rideability for all sections was good during the study period. The data for 1991 indicate that the pavement was still in good condition with respect to roughness or rideability after 7 years in service. There were no significant differences in pavement roughness between either the control sections and the cracked and seated sections or the sections with and without fibers.

Transverse Cracks

General Observations and Comparisons

Figure 5 illustrates the average transverse crack intensities for various treatments over the 7-year study period. The crack intensities are expressed as the number of transverse cracks per 1,000 ft of pavement section. Each transverse crack across the whole width of the pavement (24 ft or 7.3 m) is counted as one transverse crack, and a crack of a lane width (12 ft or 3.7 m) is counted as one-half transverse crack. This figure shows that the cracked and seated sections had fewer transverse cracks than the control sections in the first 5 years, even though the crack intensities on these sections were not significantly different in the last 2 years. Therefore, the crack-and-seat technique successfully delayed the crack development for 5 years. This deferment of crack development is very desirable because it can prolong the service life of the pavement and reduce maintenance activities.

It was observed that the transverse cracks were spaced in regular intervals of about 40 ft (12.2 m) on control sections but spaced randomly on the cracked and seated sections. The cracks on the control sections apparently developed over the joints of the underlying concrete pavement because the spaces between joints are 40 ft (12.2 m). This indicates that these transverse cracks on the control sections are truly reflective cracks, or they were caused mainly by movement of the concrete slabs beneath the asphalt overlay because of the thermal and moisture changes. However, it is believed that the transverse cracks on the cracked and seated sections were mainly caused by the contraction of the asphalt overlay as a result of low temperatures or hardening of the asphalt mixture.

The difference in crack severity between the control sections and the cracked and seated sections was also noticed during the annual visual inspections. Most of the transverse cracks on the control sections were in the categories of medium and high severities, whereas the cracks on the cracked and seated sections were of low severity. The widths of the

TABLE 2 Roughness Number and Present Serviceability Index Data by Treatments

Treatment	Year													
	1985		1986		1987		1988		1989		1990		1991	
	RN	PSI	RN	PSI	RN	PSI	RN	PSI	RN	PSI	RN	PSI	RN	PSI
A	272	3.96	396	3.64	431	3.54	721	3.10	523	3.38	431	3.54	318	3.80
A1	-	-	-	-	452	3.50	1434	2.51	634	3.21	452	3.50	345	3.73
A2	320	3.79	-	-	-	-	1676	2.34	502	3.41	353	3.71	260	3.97
B	235	4.06	403	3.60	426	3.55	721	3.10	514	3.39	402	3.60	307	3.83
B1	290	3.88	327	3.80	-	-	1390	2.54	446	3.51	397	3.61	260	3.97
B2	251	4.00	398	3.61	584	3.28	1841	2.30	538	3.35	379	3.65	260	3.97
C	181	4.28	330	3.77	426	3.55	730	3.09	457	3.49	379	3.65	314	3.81
D(whip)	251	4.00	388	3.12	386	3.63	2175	2.16	554	3.33	465	3.48	363	3.68
D(drop)	197	4.21	342	3.74	390	3.63	666	3.17	492	3.43	360	3.69	288	3.88

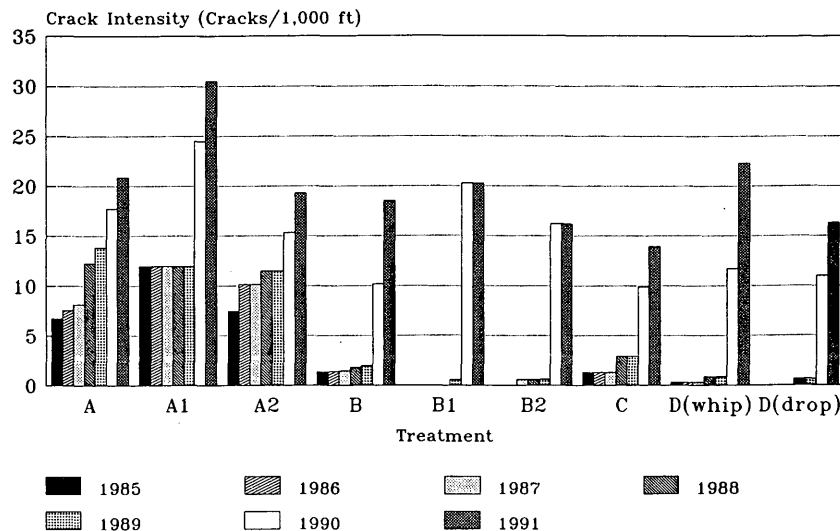


FIGURE 5 Development of transverse cracks with time for all treatments.

crack openings ranged from 0.25 to 2 in. (0.6 to 5.1 cm) on the control sections, but from 0.04 to 0.25 in. (0.1 to 0.6 cm) on the cracked and seated sections. The wide openings of the reflective cracks on the control sections served as entrances for water to get into the pavement and therefore caused the asphalt mixture near the cracks and the concrete joints underneath to deteriorate. The deterioration of the joints then in turn further accelerated the deterioration of the asphalt overlay. On the other hand, the transverse cracks on the cracked and seated sections had much less deterioration, lower severity, and narrower opening. Figure 6 presents a picture of deteriorated pavement around a reflective crack in Treatment A and a picture of a typical transverse crack on a cracked and seated section. Picture A shows that raveling (dislodging of aggregate particles) and weathering (loss of asphalt binder) have occurred on the pavement around the reflective crack on the control section, and a pothole has also developed in the area. Picture B shows that the transverse crack on the cracked and seated section has a much lower severity.

The better conditions of cracks on the cracked and seated sections can be explained as follows. First, the cracking and seating technique reduced the size of concrete slabs and impressed the small pieces onto the subbase, which limited the horizontal and vertical slab movements and, therefore, the reflective cracking. Second, most of the transverse cracks (thermal cracks instead of reflective cracks) emerged 5 years later than the reflective cracks on the control sections. This delay of crack occurrence allowed less time for water penetration and other detrimental effects to damage the pavement through the cracks than on the control sections. Third, the thermal cracks were generally narrower and less than the reflective cracks.

As can be seen in Figure 5, the crack intensities on the cracked and seated sections increased more quickly than those on the control sections during the last 2 years. On the cracked and seated sections, the final crack intensities were almost the same as or even higher than those on the control sections.

It was found during the visual inspections that most of those cracks that did emerge on the control sections in the last 2

years were similar to those on cracked and seated sections—that is, they were most likely thermal instead of reflective cracks. The reason that the control sections did not develop as many transverse cracks in the last 2 years as the cracked and seated sections was probably because many reflective cracks developed in the first 5 years, reducing the effective contraction size of the asphalt overlay. In other words, the reflective cracks on control sections worked as contraction joints to relieve pavement tensile stress and, therefore, limited the development of thermal cracks in the last 2 years.

Effects of Cracking and Seating, Overlay Thickness, and Types of Crackers

The changes in crack intensities with time for Treatments A, B, C, D(whip) and D(drop) are shown in Figure 7. The differences in crack intensities between Treatment A and cracked and seated treatments are clearly illustrated by the figure. Treatment A had much higher crack intensity values consistently during the 7-year period, except for the last year when it had a slightly lower value than Treatment D(whip). In 1989 or the year before the crack intensity values jumped, the crack intensity value for Treatment A was about 5 to 21 times as high as the values for other treatments. It is apparent that the cracking and seating technique was successful in reducing the transverse cracks. In addition, as discussed earlier, this technique also significantly alleviated the severity of cracks and the deterioration of the pavement around the cracks.

Among the cracked and seated treatments, Figure 7 indicates that during the first 5 years the thickest overlay, Treatments D(whip) and D(drop), had lower crack intensities than the thinner overlays. However, comparing Treatments B (5-in. overlay) and C (6.5-in. overlay), the differences in crack intensities were not significant, and Treatment C even had higher crack intensity values in 1988 and 1989. Furthermore, according to the figure, in 1991 Treatment C (6.5 in.), but not D(drop) or D(whip) (8.5 in.), had the lowest final intensity value. These results indicate that the increase of overlay

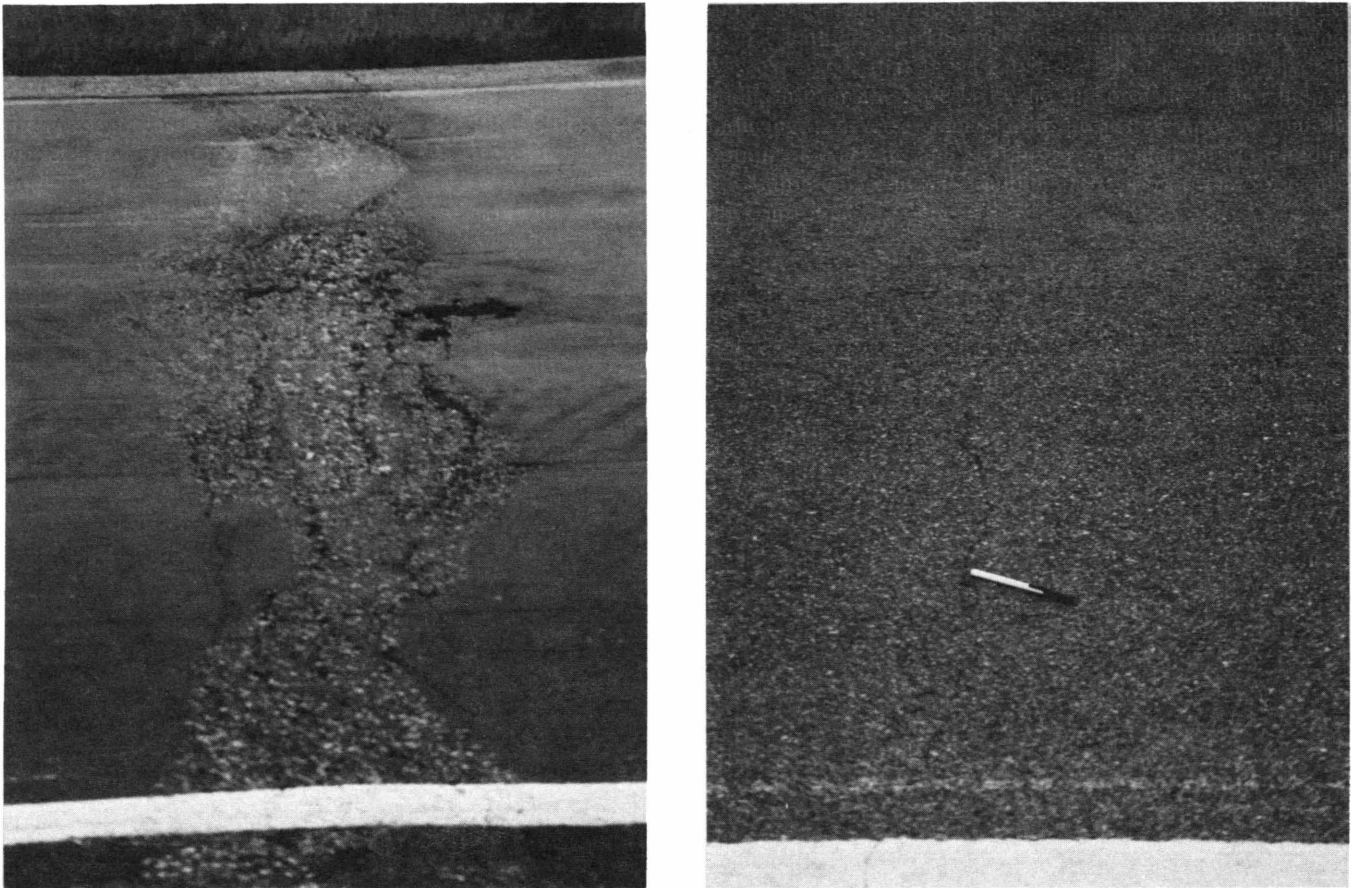


FIGURE 6 Examples of transverse cracks: *left*, deteriorated pavement around a reflective crack on control section; *right*, typical transverse crack on cracked and seated section.

thickness on cracked and seated sections indeed reduced pavement cracking for a while, but the reduction was not consistent or significant. Considering the cost involved, the option of using a thicker overlay to control pavement cracks is not recommended.

As indicated in Figure 7, the crack intensity values for Treatment D(whip) were slightly higher than those for Treatment D(drop) in the first 6 years. However, in 1991, Treatment D(whip) increased its crack intensity at a much greater rate than did D(drop). It has been shown in the previous section that the whip hammer was time consuming to use and caused a significant decrease in strength of the original concrete pavement. With the intensity values, D(whip) once again proved its relative weakness compared with D(drop). It is therefore strongly recommended that whip hammers not be used in the cracking operation.

Effects of Fibers

The crack intensities for Treatments A and B and their corresponding sections with fibers (A1, A2, B1, and B2) are plotted in Figure 8. The figure shows that the control sections (A, A1, and A2) were in much worse condition with respect

to crack intensities for most of the time. Comparing the curves for treatments A, A1, and A2, it can be concluded that use of the fibers in the base layer (Treatment A1) or in both base and binder layers (Treatment A2) did not delay or reduce transverse cracking on the control sections. This is because the majority of the transverse cracks in these sections were reflective cracks caused mainly by the horizontal and vertical movements of the concrete slabs. The movements of the uncracked concrete slabs were significant because of the large slab size and the existence of joints. They produced too great a stress in the asphalt overlay to be offset by the bonding between asphalt and fibers.

On the other hand, Figure 8 also shows that use of fibers further reduced or delayed the transverse cracking on cracked and seated sections (B1 and B2) as compared with Treatment B. Treatments B1 and B2 were not significantly different in crack intensities during the study period, but for most of the time Treatment B1 had the same or lower crack intensities than Treatment B2. This indicates, although contrary to what was expected, that the use of fibers in the binder layer in addition to in the base layer did not provide further help in reducing transverse cracks in this project. It appears that the option of cracking and seating in combination with adding fibers in the base layer should be most appropriate for cracking control.

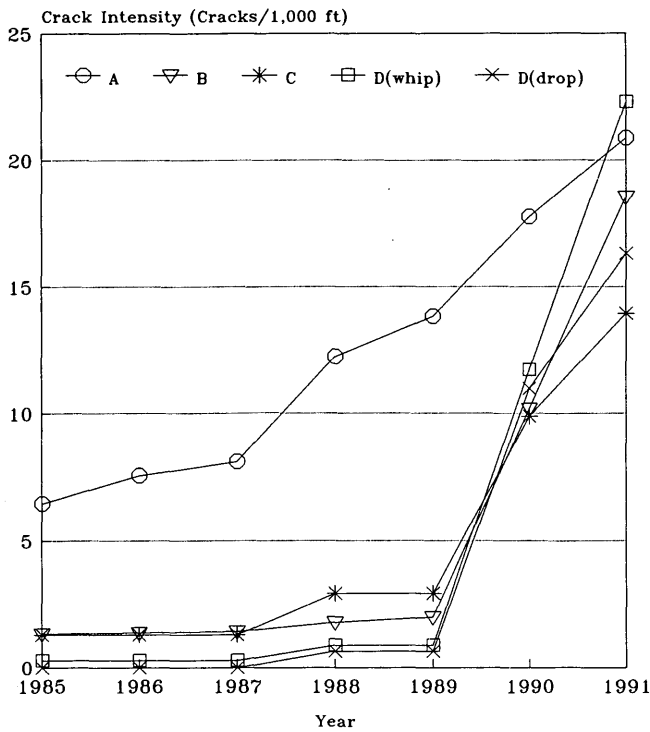


FIGURE 7 Comparison of crack intensities on control and experimental sections.

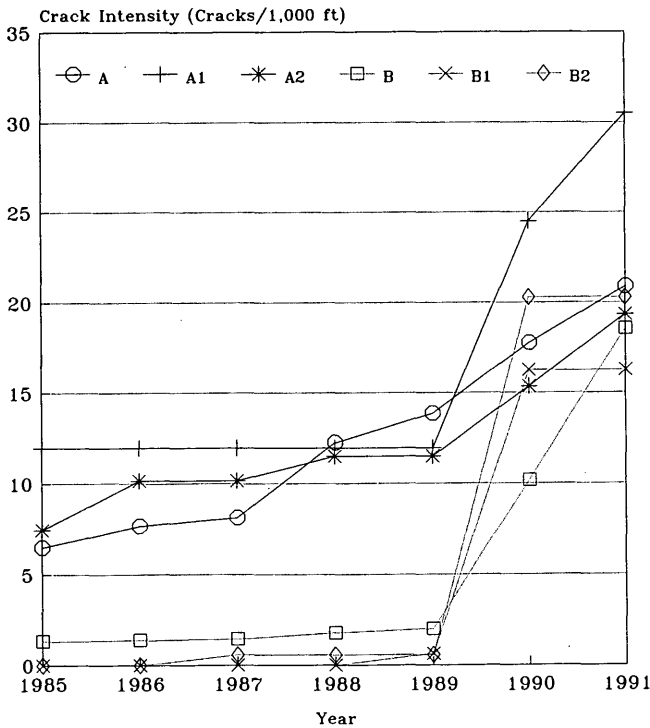


FIGURE 8 Comparison of crack intensities on sections with and without fibers.

Rutting

Ruts were measured in the wheelpath using a 4-ft (1.2-m) straightedge. Rutting on this project was negligible in 1985 and 1986. In 1987 ruts were approximately 1/16 in. (1.6 mm) for all sections with fiber and 1/8 in. (3.2 mm) for all other sections. These ruts did not develop further according to the measurements taken between 1988 and 1991. The slightly reduced rutting in fiber sections was the result of fiber reinforcement. The measurements showed that the cracking and seating technique did not affect pavement rutting.

COST ANALYSIS

The construction cost per mile for each treatment is listed as follows:

Treatment	Cost (\$/mi)
A	247,974
B	272,998
C	340,838
D	431,290

The data show that the increase of overlay thicknesses significantly increased the construction costs on the cracked and seated sections. Because various thicknesses and techniques were involved, the pavement service lives for the treatments are expected to be different. To compensate for the higher costs on the cracked and seated sections, these sections must have longer service lives than the control sections. A life-cycle analysis was conducted on the basis of an interest rate of 7 percent to compare the control sections and the cracked and seated sections. The life-cycle cost of a pavement depends on the service life of the pavement (2). The construction costs for all treatments were converted to equivalent uniform annual costs for different service lives between 10 and 20 years, as shown in Figure 9. The maintenance costs were not available and therefore were not included in the analysis.

A 10-year service life is a reasonable estimation for a conventional asphalt overlay such as Treatment A. If treatment A has a service life of 10 years, then Treatments B, C, and D should have service lives of longer than 10 years to have the same life-cycle cost as that of Treatment A. A dashed horizontal line is drawn in Figure 9 to determine the minimum service lives for these treatments are as cost-effective as Treatment A with a service life of 10 years. The intersections of the horizontal line and the cost curves indicate that the minimum service life required is about 11.5 for Treatment B, and 16.7 for Treatment C. That is, Treatments A, B, and C would have the same uniform annual costs if their service lives were 10, 11.5, and 16.7 years, respectively. The uniform annual cost for Treatment D was so high that even at the 20-year service life it is still much higher than that for Treatment A with a 10-year life. Because the thicker overlays did not improve pavement performance considerably but greatly increased construction costs, it is recommended that the thickness of asphalt overlay be determined only by the pavement strength requirement, but not be increased as a means of cracking control. Considering the cost as well as the performance, Treatment B should be the best choice for this project.

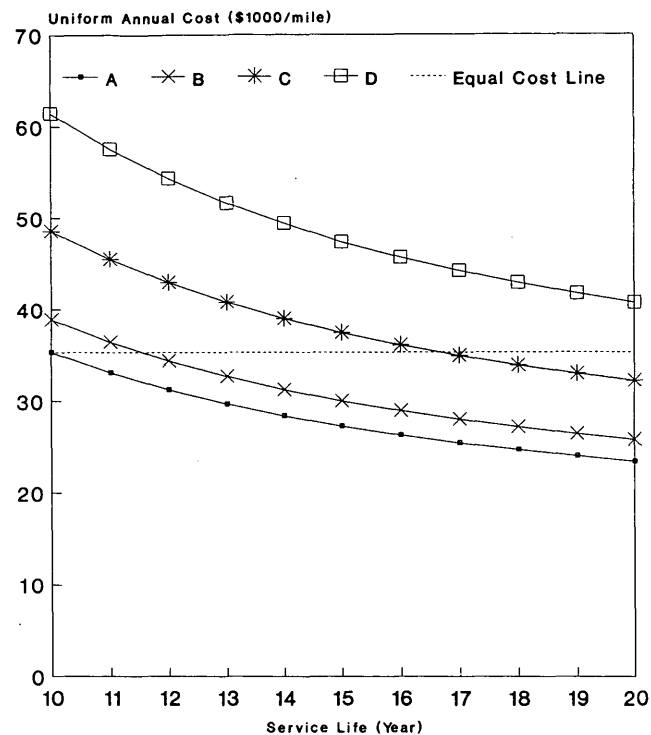


FIGURE 9 Equivalent uniform annual costs with various service lives.

CONCLUSIONS AND RECOMMENDATIONS

This study evaluated two methods for reducing pavement cracking on asphalt overlay over concrete pavement: cracking and seating before overlay and fiber reinforcement in the overlay mixture. On the basis of the analysis of the 7-year data, the following conclusions and recommendations are made.

1. The cracking and seating technique was successful in this project. It delayed most of the transverse cracks for 5 years. The majority of the transverse cracks on the cracked and

seated sections were thermal cracks, which were narrower and less severe than the reflective cracks on the control section.

2. The type of hammers used for cracking concrete slabs had strong effects on pavement strength. The sections cracked with the whip hammer developed more transverse cracks than did the sections cracked with the drop hammer. It is recommended that the whip hammer not be used for cracking and seating projects.

3. Use of fibers in the overlay mixtures further reduced transverse cracks on cracked and seated sections, but did not improve the cracking resistance of the control sections. Adding fibers in the base layer of the asphalt overlay on cracked and seated sections proved to be as effective for cracking control as adding fibers in both base and binder layers.

4. Use of fibers improved rutting resistance on both the control and the cracked and seated sections.

5. Sections including fibers exhibited quicker decreases of pavement strength than did other sections.

6. The increase of overlay thickness improved pavement strength, as expected. However, thicker overlays increased the construction costs significantly but did not reduce the transverse crack intensities. The pavement performance and the cost analysis indicate that Treatment B, the thinnest cracked and seated overlay, should be the best choice for this project. It is recommended that the thickness of asphalt overlay be determined only by the pavement strength requirement and not be increased as a means of cracking control.

REFERENCES

1. K. Majidzadeh and V. Kumar. *Manual of Operation and Use of Dynaflect for Pavement Evaluation*. FHWA/OH-83/004. FHWA, U.S. Department of Transportation, 1983.
2. E. L. Grant, W. G. Ireson, and R. S. Leavenworth. *Principles of Engineering Economy*, 7th ed. John Wiley and Sons, Inc., New York, 1982.

Publication of this paper sponsored by Committee on Pavement Rehabilitation.

Analysis of Crack Resistance of Asphalt Concrete Overlays—A Fracture Mechanics Approach

YEOU-SHANG JENQ, CHWEN-JANG LIAW, AND PEI LIU

Cracking is one of the major distress modes that cause premature failure of asphalt concrete pavements. Formation of cracks in asphalt concrete pavements can be the result of the following: applied traffic loads, temperature-induced thermal stresses, freeze-thaw damage due to water infiltration, aging effects, and so forth. A conceptual framework to characterize (and quantify, if possible) the crack resistance of asphalt concrete pavement systems based on a fracture mechanics theory is presented. A cohesive crack model, which is similar to the Dugdale-Barenblatt type of models proposed for ductile yielding of metals, was used to simulate the progressive crack formation and propagation in asphalt concrete. A parametric study was conducted to study the effects of temperature, fiber reinforcement, and overlay thickness on the crack resistance of asphalt concrete overlays. It was found that a thicker overlay has a much higher temperature crack resistance, which is in agreement with general field observations. Furthermore, although it was found that at lower service temperature the overlay has a much higher temperature resistance, this improvement is not enough to compensate for a much larger temperature differential and contraction displacement caused by the service temperature drop. Fiber reinforcement was found to slightly increase the crack resistance of the asphalt concrete overlays. It was further observed that the temperature crack resistance is proportional to the increase of the tensile strength.

Cracking is one of the major distress modes that cause premature failure of asphalt concrete pavements. Formation of cracks in asphalt concrete pavements can be the result of the following: applied traffic loads, temperature-induced thermal stresses, freeze-thaw damage due to water infiltration, aging effects, and so forth. Because of the complexity involved in the development of cracks in asphalt concrete, there is currently no unique approach accepted by researchers to characterize the crack resistance of asphalt concrete pavement systems. The present paper is an attempt to present a conceptual framework initially to characterize (and quantify, if possible) the crack resistance of asphalt concrete pavement systems based on fracture mechanics theory.

A cohesive crack model, which is similar to the Dugdale-Barenblatt type of models proposed for ductile yielding for metals, is used in the present study to simulate the progressive crack formation and propagation in asphalt concrete. A parametric study of the effects of temperature on the crack resistance of asphalt concrete overlays was performed to demonstrate the feasibility of the proposed approach in characterizing the fracture response of flexible pavement systems.

The theoretical results were found to be in agreement with commonly reported field observations, which indicates that the proposed fracture mechanics approach has its potential in analyzing asphalt concrete pavement systems subjected to more complex service conditions. In addition, it is believed that the material properties associated with the proposed fracture mechanics model can be used as criteria in designing good-quality asphalt concrete mixes with better crack resistance.

PROPOSED COHESIVE CRACK MODEL

In modeling crack formation and crack propagation, the crack can generally be modeled as the Griffith type of traction-free cracks or the Dugdale-Barenblatt type of cohesive cracks. It is believed that the cohesive type of cracks is more suitable in describing the nature of cracks in viscous materials such as asphalt concrete. The cohesive crack concept assumes that when a crack starts to develop in a material, the crack is still able to transfer some forces. The crack zone that is bridged by this cohesive force, which is generally termed the "process zone," is governed by the applied load, structure/sample geometries, and the basic properties of the material. The cohesive crack concept was originally proposed by Dugdale (1) and Barenblatt (2) for metals and by Hillerborg et al. (3) for portland cement concrete to characterize progressive crack development in the materials.

To simulate crack formation and propagation in asphalt concrete, a cohesive crack model that is similar to the Dugdale-Barenblatt cohesive crack model discussed earlier was proposed by Jenq and Perng (4). Because of the viscous nature of asphalt concrete, the cohesive stress was assumed to be time dependent and temperature dependent, and may be modeled using various combinations of nonlinear springs and dashpots (see Figure 1). In addition, several assumptions were proposed in the proposed model:

1. The process zone is assumed to initiate at the point when the first principal stress reaches the tensile strength (f_t ; see Figure 2a and b).
2. The direction of the process zone will be perpendicular to the direction of the first principal stress.
3. The properties of the materials outside the process zone are governed by a stress-strain relationship (Figure 2a), which is dependent on the applied loading rate and service temperature.

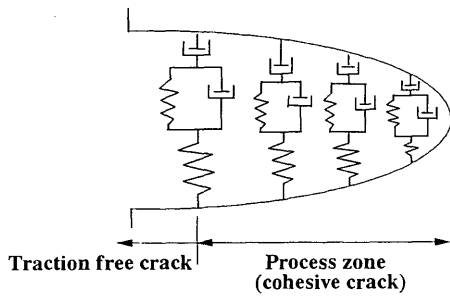


FIGURE 1 Cohesive crack modeled using nonlinear springs and dashpots.

4. The material in the process zone is able to transfer stress, and the stress-transferring capability depends on its opening according to the stress-separation relationship shown in Figure 2b. This stress-separation relationship is a function of loading rate and temperature. The area under the stress-separation curve is defined as fracture energy (G_f), which represents the energy needed to create a unit of traction-free surface.

On the basis of these assumptions, the size of the process zone, the magnitude of the bridging stress, and the applied load can be determined accordingly (4,5). The proposed stress-separation curve concept is the key factor that separates the proposed fracture mechanics model from conventional strain-based or stress-based models. Since strain cannot be objectively defined when there is displacement discontinuity (e.g., a crack), a fracture mechanics model will be more suitable in characterizing fracture mechanisms in a material.

NUMERICAL FORMULATION

For simplicity, a notched beam is used to demonstrate the numerical formulation for the proposed cohesive crack model. Consider a notched beam with a preexisting crack up to Node n subjected to a load P in the midspan, as shown in Figure 3a. It is assumed that the process zone will develop along a straight plane, which is reasonable for Mode I crack propagation. When the beam is loaded, by introducing the closing stresses over the crack, one can analyze the progressive crack development in the beam (5).

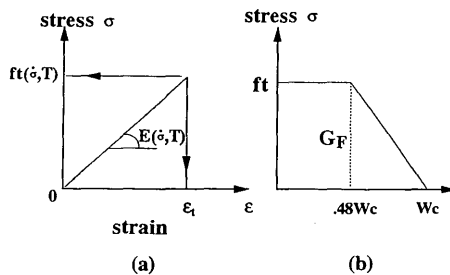
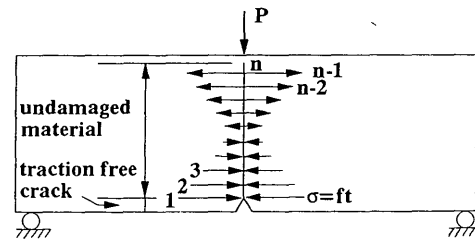
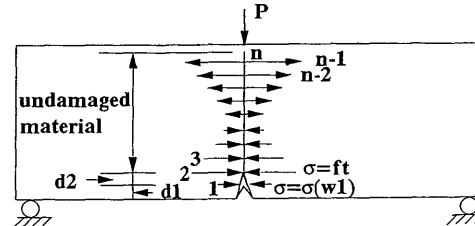


FIGURE 2 (a) Stress-strain curve for asphalt concrete before process zone initiation and (b) proposed σ - w curve for asphalt concrete after process zone initiation.



(a)



d1: traction free crack
d2: cohesive crack

(b)

FIGURE 3 (a) Notched beam subjected to three-point bending and (b) crack propagation to the second point.

In the calculation process, the stresses acting across the cohesive crack were replaced by equivalent nodal forces. These forces can be determined according to the stress-separation curve when the width at the cohesive crack zone is known. As indicated in Figure 3a, when the first node reaches its tensile strength, the opening displacement at the first node is still equal to zero, that is, $\sigma_1 = f_t, w_1 = \dots = w_{n-1} = 0$. From this, one can determine the first point, which corresponds to the crack initiation point, of the load-load line deflection ($P - \delta$) curve and the load-crack mouth opening displacement (P -CMOD) curve.

When the crack starts to propagate, as shown in Figure 3b, the first node is opened and the second node is assumed to reach the tensile strength. At this point the boundary conditions can be expressed as $\sigma_2 = f_t, w_2 = w_3 = \dots = w_{n-1} = 0, w_1 \neq 0$, and $\sigma_1 = \sigma(w_1)$. The system equations are nonlinear because of the stress-separation constraint. Therefore, an iteration process is needed for this step.

Following the same principle, the progress of crack propagation can be analyzed, and complete $P - \delta$ and P -CMOD curves can be generated. On the basis of the proposed cohesive crack model, no tensile stress will be transferred along the crack surfaces when the crack opening displacement is larger than the critical crack opening displacement (w_c), which is equal to $G_f / (0.74f_t)$ for the proposed stress-separation curve, as indicated in Figure 2a. The critical crack opening displacement is about 0.102 and 0.178 cm at 0°C for plain asphalt concrete and fiber-reinforced asphalt concrete, respectively. More detailed numerical formulation was given previously (4,5). The driving force for crack propagation in a pavement system is not limited to the applied load (P). Service temperature differential (T), which is defined as the temperature difference from the surface to a certain depth of the pavement,

can also be the driving force for crack propagation. The principle involved in the numerical formulation, however, is the same for the applied load and service temperature. Thus, one can derive the numerical formulation for temperature loading by replacing the effect of applied load with that of temperature. To obtain the theoretical results using the proposed cohesive crack model, a numerical method such as the finite element method has to be applied.

NUMERICAL EXAMPLE

To demonstrate the applicability of the proposed cohesive crack model, a parametric study on the reflective crack resistance of asphalt concrete overlays to temperature differentials was performed. The reflective cracking in asphalt concrete overlays is mainly the result of the contraction and curling actions of the overlaid old pavements caused by temperature differentials and the applied traffic loads. For the present analysis, only temperature effect is considered, and the pavement system is simulated using a two-dimensional model. Furthermore, only the effect of a single temperature cycle is analyzed in the present study. A complete analysis, of course, should include the effect of temperature cycles (6), which is currently under way and will be reported elsewhere. Although temperature-induced reflective cracking can be modeled as a Mode I crack, mixed mode failure conditions may occur under the application of traffic load, which will generate a much higher compressive stress and shear stress in the overlay.

The pavement system analyzed was a three-layer system in which there is an asphalt concrete overlay over existing concrete slabs. The thicknesses for the concrete slabs and subgrade soil were 22.86 and 203.2 cm, respectively. Three different overlay thicknesses (i.e., 5.08, 10.16, and 15.24 cm) were analyzed. The length of the jointed slabs is 731.52 cm. Material properties such as Young's modulus, coefficient of thermal expansion, and Poisson's ratios for each layer were listed in Figure 4 along with the prescribed boundary condition. Because of the symmetry condition of the pavement, only half of the slab was analyzed. No initial crack or notch was imposed on the asphalt concrete overlay. The existence of the concrete joint, which creates a very high stress concentration at the joint-overlay interface, was simulated as an existing crack. Thus, the reflective crack was assumed to initiate from the bottom of the overlay and propagate upwards.

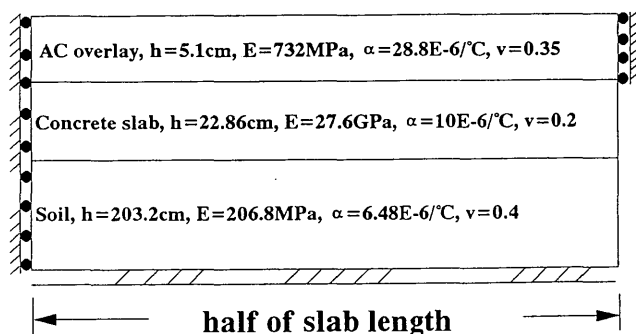


FIGURE 4 Boundary conditions.

Because temperature is the driving force in the present study, temperature distribution in the pavement has to be prescribed first. A parabolic equation was used to describe the temperature distribution along the depth of the pavement. This assumption was based on the results of field temperature measurement (see Figure 5) (7,8). It was further assumed that the temperature differential below 38.1 cm of the pavement surface is zero. A typical unit temperature differential profile is given in Figure 6. Because the material properties such as the fracture energy, modulus of elasticity, and fracture energy values are also dependent on service temperature, for simplicity, material properties associated with the model were also assumed to be the same as those measured at a constant service temperature throughout the analysis. When the temperature profile is known, the effects of temperature differential (*T*) on the crack resistance of the pavement system can be performed.

Based on the same numerical formulation principle discussed earlier, the opening displacement of the crack at each node and at the reference point can be calculated from the following equations:

$$w_i = \sum_{j=1}^{n-1} a_{ij}\sigma_j + c_jT \tag{1}$$

$$w_R = \sum_{j=1}^{n-1} b_j\sigma_j + d_T T \tag{2}$$

$$\begin{bmatrix} a_{11} & a_{12} & \dots & a_{1(n-1)} & c_1 \\ a_{21} & a_{22} & \dots & a_{2(n-1)} & c_2 \\ \dots & \dots & \dots & \dots & \dots \\ a_{(n-1)1} & a_{(n-1)2} & \dots & a_{(n-1)(n-1)} & c_{n-1} \\ b_1 & b_2 & \dots & b_{n-1} & d_T \end{bmatrix} \begin{bmatrix} \sigma_1 \\ \sigma_2 \\ \vdots \\ \sigma_{n-1} \\ T \end{bmatrix} = \begin{bmatrix} w_1 \\ w_2 \\ \vdots \\ w_{n-1} \\ w_R \end{bmatrix} \tag{3}$$

or

$$\{C\}[F] = [\Delta] \tag{4}$$

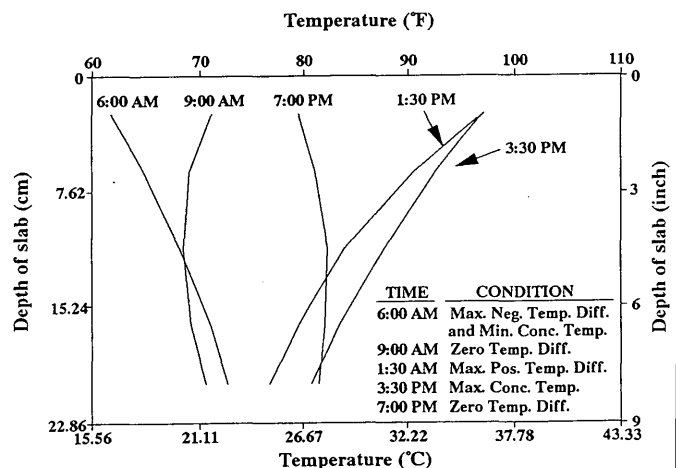


FIGURE 5 Typical temperature gradient for a 22.86-cm slab (7).

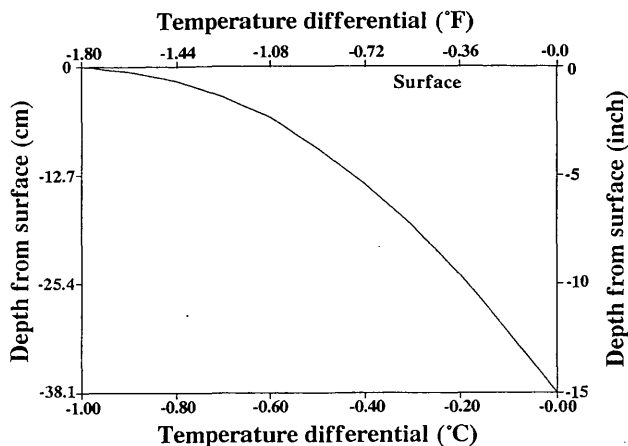


FIGURE 6 Temperature profile used in the present study.

where

- a_{ij} = the opening displacement of the crack at Node i when an equivalent closing force is acting at Node j ,
- c_j = the opening displacement of the crack at Node i when a unit-negative temperature differential is applied,
- b_j = the displacement at the reference point when an equivalent closing force is acting at Node j ,
- d_T = the opening displacement at the reference point when a unit-negative temperature differential is applied,
- σ_j = the closing pressure at Node j , and
- w_R = the displacement at the reference point.

The square matrix, $\{C\}$, in Equation 4 is referred to as the influence matrix. In the influence matrix, except for the last column, the i th column represents the opening displacement at each node and at the reference point when a pair of equivalent unit closing forces acts at the i th node point. The last column represents the openings at each node and the displacement at the reference point when a negative unit temperature differential is applied. ABAQUS finite element package was used to generate the influence matrix, and the finite element mesh used in the analysis is given in Figure 7. The vector $[F]$ represents the closing pressure at each node and the applied temperature differential, and the vector $[\Delta]$ represents the opening displacement at each node and the reference point.

Thus, based on the calculation procedures discussed earlier, a complete temperature differential versus CMOD curve and crack growth development as a result of temperature differential can be generated. The definition of CMOD used here is the same as the joint opening displacement of the concrete slabs (Figure 8).

MATERIAL CHARACTERIZATION

To perform the analysis, proper material properties such as Young's modulus (E), shape of the stress-separation curve, fracture energy (G_f), and the tensile strength (f_t) associated with the proposed model have to be evaluated first. The stress-

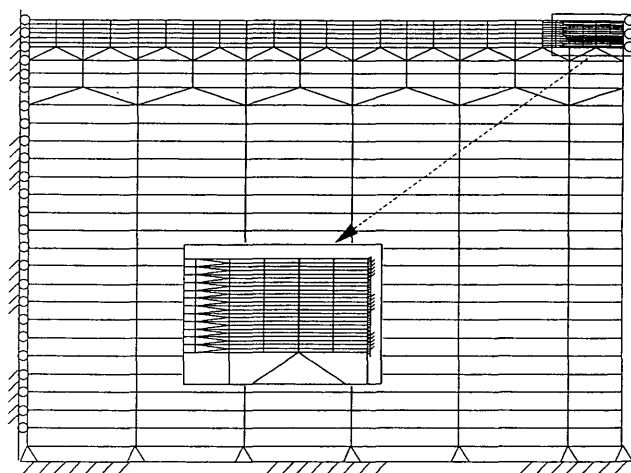


FIGURE 7 Finite element mesh used in the influence matrix generation.

separation relationship reported by Jenq and Perng (4), as shown in Figure 2, was used in the present study. For the post-crack stress-separation relationship, a ductile Dugdale type of bridging stress is first encountered and then the bridging stress decreases as the separation increases. When the crack opening is larger than the critical crack opening displacement (w_c), the bridging stress diminishes. The fracture energy, which has the same value as the area under the stress-separation curve, was determined from a notched half-disk fracture mechanics test, and the tensile strength was obtained from the indirect tensile tests (4,9). Values of E , G_f , and f_t at different temperatures reported by Jenq and Liu (9) were used as the material properties for asphalt concrete overlays. The modulus of elasticity determined using the indirect tensile test, which was used in the present study, is much lower than those determined from the resilient modulus test because of the very low loading rate used in the indirect tensile tests (9). The mix proportions and the associated material properties of plain asphalt concrete and fiber-reinforced asphalt concrete are listed in Tables 1 and 2, respectively. Detailed material properties and testing methods used to determine these values were given previously (9).

In addition to the above-mentioned material properties, to perform the analysis one also has to know the coefficient of thermal expansion, the Poisson's ratios, and the modulus of elasticity of the base material and the soil. For the present

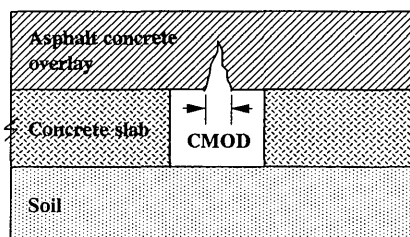


FIGURE 8 Crack mouth opening displacement (CMOD) in the concrete pavement system.

TABLE 1 Mixing Parameters for Various Series of Asphalt Concrete

Series	Fiber type	Fiber weight content (%)	Fiber volume fraction (%)	Asphalt content (%)	Mixing temperature (°C)
A	***	0	0	5.5	152
F	polyester	0.3045	0.593	5.8	152
G	polypropylene	0.2724	0.688	5.8	146

TABLE 2 Material Properties of Various Series of Asphalt Concrete

	Temperature	A ^a	F ^a	G ^a
Young's Modulus E (MPa) ^b	0°C	732.2	784.6	805.3
	23°C	219.7	211.0	196.7
Fracture Energy Gf (N/m) ^c	0°C	5248.3	7815.5	8430.9
	23°C	1270.5	2089.2	1705.7
Tensile Strength ft (MPa)	0°C	1.130	1.235	1.282
	23°C	0.278	0.361	0.325
Poisson's Ratio	0°C	0.25	0.25	0.25
	23°C	0.35	0.35	0.35
Coefficient of thermal expansion (*10 ⁻⁶ /°C)	***	28.8	28.8	28.8

^a Related mix information of series A, F, and G is given in Table 1.

^b 1 Pa = 0.000145 psi.

^c 1 N/m = 0.00571 lbs/in.

analysis, typical values reported by various researchers on these materials were used and given in Figure 4.

PARAMETRIC STUDY

On the basis of the proposed model, effects of overlay thickness, service temperature, fiber reinforcement, and tensile strength on the crack resistance of asphalt concrete overlays were observed. Figure 9 shows the theoretical predictions on the effect of temperature differential on the crack resistance of asphalt concrete overlays of various thicknesses at 0°C

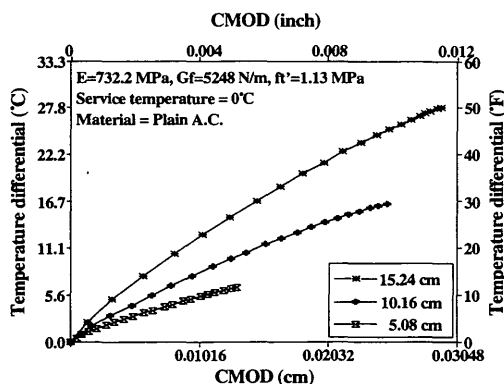


FIGURE 9 Effect of thickness on the crack resistance of plain asphalt concrete overlay at low service temperature (0°C).

service temperature. The *X*-axis represents the joint opening displacement underneath the concrete slabs and the *Y*-axis represents the magnitude of the temperature differentials. Each data point represents a unit element length of crack advancement in the overlay. In the present case, each increment is $\frac{1}{24}$ the depth of the overlay. The peak point associated with each curve in Figure 9 is also the point at which the crack extends from the interface to the top of the overlay (90 percent of the overlay thickness in the present study). The CMOD value at the joint-overlay interface is smaller than the critical crack opening displacement (which is about 0.102 cm for plain asphalt concrete and 0.178 cm for fiber-reinforced asphalt concrete at 0°C). This difference indicates that although the cohesive crack has propagated to the top of the asphalt concrete overlay, the bridging force along the crack surface is still there and a higher opening displacement (or more temperature differential) is needed to create a traction-free crack. Study of the effect of postcohesive process on the temperature crack resistance is still under way. For the present paper, the temperature differential resistance is defined as the peak temperature differential when the cohesive crack reaches the top of the overlay.

Effect of Overlay Thickness

Figure 9 indicates that the thicker the overlays, the better the crack resistance to temperature differentials. This theoretical result also indicates that for the crack to propagate to the top in a thicker overlay, a larger joint contraction displacement (or CMOD), and thus a higher temperature differential, is

needed. This prediction is in agreement with field experience on the formation of reflective cracking; that is, increase of overlay thickness can retard the formation of reflective cracks in asphalt concrete overlays. A similar thickness effect is also predicted for higher service temperatures (i.e., 23°C), as indicated in Figure 10.

Effect of Service Temperature

As discussed earlier, the material properties (i.e., fracture energy, tensile strength, and Young's modulus; see Table 2) of asphalt concrete are highly temperature dependent. At different service temperatures, the material properties of the same mix can be very different. In general, the lower the service temperature, the higher the fracture energy, tensile strength, and resilient modulus. From Figures 9 and 10, it can be concluded that because of higher tensile strength and fracture energy, asphalt concrete overlays have better crack resistance to a temperature differential at a lower service temperature. In the meantime, at a lower service temperature, the magnitude of temperature differential and the contraction displacement of concrete slabs in the pavement also are much higher than those at normal service temperature. As a result, the improvement caused by a temperature-induced material property change may not be enough to compensate for the adverse effects caused by the drop in service temperature.

Effect of Fiber Reinforcement

The addition of fibers to asphaltic mixes in general increases the fracture energy by 50 to 100 percent, which implies that the fiberized mix is tougher and more ductile. Fiber addition, however, does not seem to have a significant effect on the material's modulus of elasticity or its tensile strength (see Table 2). Material properties of plain asphalt concrete (Series A) and fiberized asphalt concrete mixes (Series F and G) (9) were used to investigate the effect of fiber reinforcement. The peak temperature differentials of these three materials for various overlay thicknesses at service temperatures of 0°C and 23°C were reported in Figures 11 and 12, respectively. The

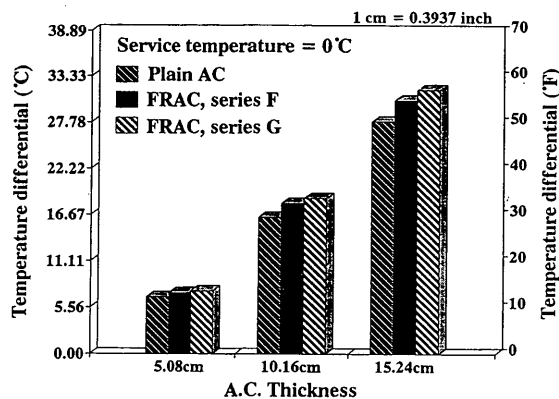


FIGURE 11 Peak temperature differentials of plain and fiberized asphalt concrete overlays at low service temperature (0°C).

fiberized asphalt concrete mixes have slightly better temperature crack resistance than does the plain asphalt concrete. This increase, however, is not very significant. However, because of the larger fracture energy values associated with the fiberized mix, it is expected that a much larger opening displacement is needed to generate a traction-free crack, which may add to the overall durability of the fiberized mix.

Effect of Tensile Strength

The effects of tensile strength on the reflective crack resistance were also analyzed with the other material properties (i.e., fracture energy and Young's modulus) being kept constant. Figures 13 and 14 show the effects of tensile strength on the crack resistance to temperature differentials for overlays of various thicknesses. The theoretical analysis indicates that the higher the tensile strength, the better the crack resistance to temperature differentials. The improvement is almost proportionate to the increase of the tensile strength.

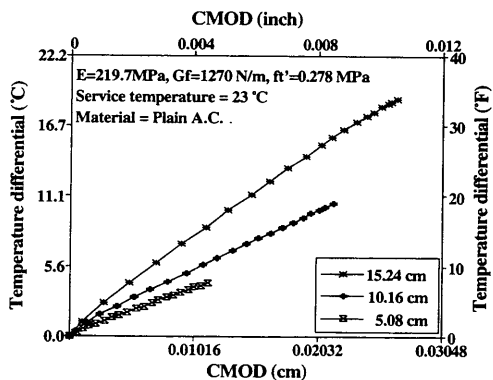


FIGURE 10 Effect of thickness on the crack resistance of plain asphalt concrete overlay at regular service temperature (23°C).

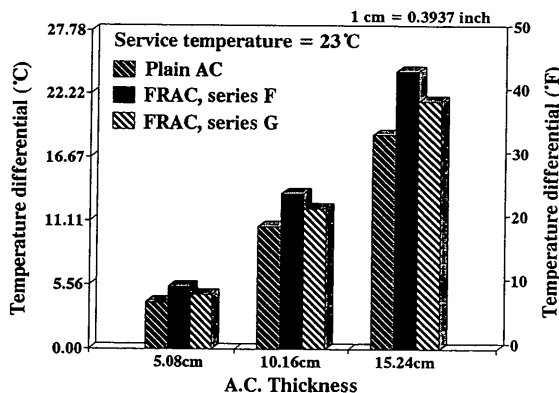


FIGURE 12 Peak temperature differentials of plain and fiberized asphalt concrete overlays at regular service temperature (23°C).

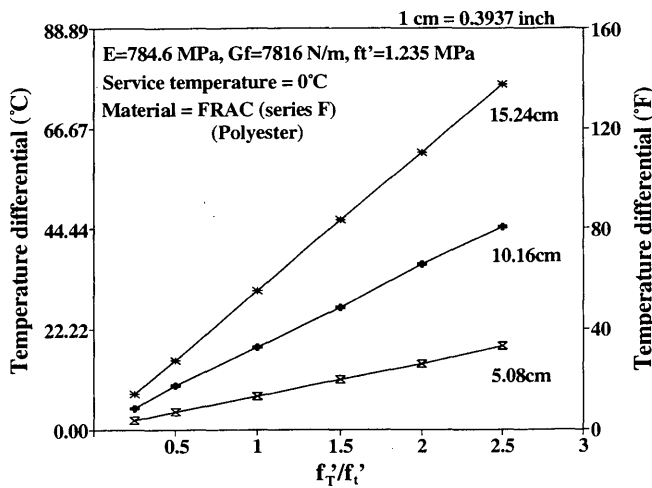


FIGURE 13 Effects of tensile strength on crack resistance of polyester-fiberized asphalt overlay at low service temperature (0°C).

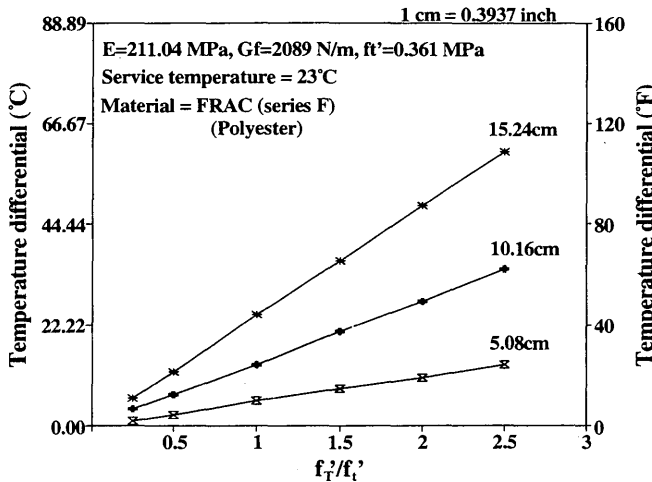


FIGURE 14 Effects of tensile strength on crack resistance of polyester-fiberized asphalt overlay at regular service temperature (23°C).

CONCLUSIONS

The following conclusions can be derived from the present study:

1. When temperature effect is the only consideration, the temperature crack resistance will be higher if a thicker asphalt concrete overlay is applied.
2. Crack resistance to the temperature differential at a lower service temperature was found to be better than that at a

higher service temperature. However, this increase is not enough to prevent the frequently observed low temperature cracking in asphalt concrete caused by larger temperature differentials encountered at a much lower service temperature.

3. Temperature crack resistance of asphalt concrete overlays can be increased if the tensile strength of the asphaltic concrete mix is improved.

4. The proposed model provides a feasible approach to quantifying the crack resistance in asphalt concrete pavement systems. There is, however, a need for more research efforts to include effects, such as applied traffic loads, in the analysis.

ACKNOWLEDGMENTS

The authors appreciate the financial support provided by the Ohio Department of Transportation for the present research.

REFERENCES

1. D. S. Dugdale. Yielding of Steel Sheets Containing Slits. *Journal of the Mechanics and Physics of Solids*, Vol. 8, 1960, pp. 100-108.
2. G. I. Barenblatt. The Mathematical Theory of Equilibrium of Crack in Brittle Fracture. *Advances in Applied Mechanics*, Vol. 7, 1962, pp. 55-129.
3. A. Hillerborg, M. Modeer, and P. E. Petersson. Analysis of Crack Formation and Crack Growth in Concrete by Means of Fracture Mechanics and Finite Elements. *Cement and Concrete Research* 6, 1976, pp. 773-782.
4. Y. S. Jenq and J. D. Perng. Analysis of Crack Propagation in Asphalt Concrete Using A Cohesive Crack Model. In *Transportation Research Record 1317*, TRB, National Research Council, Washington, D.C., 1991, pp. 90-99.
5. J. D. Perng. *Analysis of Crack Propagation in Asphalt Concrete Using a Cohesive Crack Model*. M.S. thesis, The Ohio State University, June 1989.
6. S. H. Carpenter and R. L. Lytton. Procedure for Predicting Occurrence and Spacing of Thermal-Susceptibility Cracking in Flexible Pavements. In *Transportation Research Record 671*, TRB, National Research Council, Washington, D.C., 1978, pp. 39-46.
7. J. M. Armaghani, T. J. Larsen, and L. L. Smith. Temperature Response of Concrete Pavements. In *Transportation Research Record 1121*, TRB, National Research Council, Washington, D.C., 1987, pp. 23-33.
8. J. M. Richardson and J. M. Armaghani. Stress Caused by Temperature Gradient in Portland Cement Concrete Pavements. In *Transportation Research Record 1121*, TRB, National Research Council, Washington, D.C., 1987, pp. 7-13.
9. Y. S. Jenq and P. Liu. Effects of Fiber Reinforcement on the Crack Resistance of Asphalt Concrete. Presented at 71st Annual Meeting of the Transportation Research Board, Washington, D.C., Jan. 12-16, 1992.

Publication of this paper sponsored by Committee on Pavement Rehabilitation.

Analytical Considerations for Thin Concrete Overlays on Asphalt

JAMES W. MACK, LAWRENCE W. COLE, AND J. P. MOHSEN

An analytical study was undertaken to account for the performance of a thin concrete overlay on an asphalt concrete (AC) pavement built in Louisville, Kentucky, in September 1991. Initial investigations and theoretical studies based on conventional concrete theory indicated that the pavement should have failed after its first few loadings. However, this did not happen. After 11 months of use, with very heavy traffic (400 to 600 garbage trucks per day, 5½ days a week), the pavement has provided much better service than was anticipated, suggesting that a bond developed between the concrete overlay and underlying AC that greatly improved the pavement's performance. Some direction for future research is provided.

Concrete overlays on asphalt concrete (AC) pavements (whitotopping) have been successfully used as rehabilitation procedures for deteriorated AC pavements since 1944. In that year, an airfield at the U.S. Air Force Base in Offut, Nebraska, was successfully whitotopped. Since that time, many more whitotopping projects have been built throughout the United States and worldwide. Generally, these concrete overlays are a minimum of 127 mm (5.0 in.) thick and designed with conventional concrete pavement theory that characterizes the AC pavement as a stabilized base using Westergaard's modulus of subgrade reaction (k).

To investigate the performance of a thin concrete overlay [less than 127 mm (5.0 in.) thick] on AC, the Portland Cement Association, the American Concrete Pavement Association, and other industry groups combined to build an experimental project in Louisville, Kentucky, in September 1991. The overlay was constructed on the Waste Management Corporation's Outer Loop Recycling and Disposal Facility access road. This site was chosen because of the high number of trucks that use the facility (400 to 600 trucks per day, 5½ days a week). The existing AC pavement was in relatively uniform condition with some minor surface distortions and mild rutting in the existing AC; however, there were no cracks or structural failures in the test sections. To obtain a uniform overlay thickness, the AC pavement was milled before the concrete overlay was placed. This milling left the AC surface with a rough surface. Initially, the milled surface was believed to be approximately 102 mm (4.0 in.) thick; however, later, it was found to be slightly less.

The experimental project consisted of two sections (Figure 1). The first section consisted of a 89-mm (3.5-in.) pavement cut into 1.83- × 1.83-m (6- × 6-ft) panels. The second section was a 51-mm (2.0-in.) pavement cut into 1.83-; × 1.83-m (6-

× 6-ft) panels and 0.61- × 0.61-m (2- × 2-ft) panels. The concrete was a high early-strength mixture with polypropylene fibers capable of obtaining a laboratory compressive strength of 27.59 MPa (4,000 lb/in.²) in 18 hr. Approximately 3 hr after concrete placement, the 1.83-m (6-ft) spaced control joints were sawed into the overlay. These joints were ¼ the pavement depth. In the 0.61-m (2-ft) panels, saw joints 25.4 mm (1.0 in.) deep were used to ensure that slab interaction would be minimal. None of these joints was sealed. Additional information on the construction of this project may be found elsewhere (1).

ANALYTICAL INVESTIGATION

Concrete and Subgrade Support Characterization

For analysis, the properties of the concrete and AC layers had to be determined. Concrete compression strengths were determined to be 23.6 MPa (3,422 lb/in.²) at 24 hr, 33.74 MPa (4,893 lb/in.²) at 36 hr, 35.32 MPa (5,122 lb/in.²) at 48 hr, 44.50 MPa (6,453 lb/in.²) at 7 days, and 51.07 MPa (7,405 lb/in.²) at 28 days per ASTM C39. Third-point beam flexural strengths were determined to be 5.23 MPa (759 lb/in.²) at 24 hr, 5.77 MPa (837 lb/in.²) at 36 hr, and 7.07 MPa (1,025 lb/in.²) at 28 days per ASTM C78. The modulus of elasticity for the concrete (E_c) was determined by 34 473 MPa (5 million lb/in.²) using the 28-day compressive strength and the following American Concrete Institute (ACI) equation:

$$E_c = 4.73 \sqrt{f'_c} (\text{MPa}) \quad [E_c = 57,000 \sqrt{f'_c} (\text{lb/in.}^2)] \quad (1)$$

where f'_c is the compressive strength.

In addition to the concrete testing, falling weight deflectometer (FWD) measurements were taken on the AC after milling and on the concrete overlay 24 hr after construction. The backcalculation computer programs BISDEF (2) and ILLI-BACK (3) were used to characterize the AC pavement and subgrade support. These analyses determined the AC modulus of elasticity (E_{ac}) to be 3447 MPa (500,000 lb/in.²), the k on top of the AC pavement to be 68.0 MPa/m (250 lb/in.²), and the subgrade modulus of elasticity (E_{sg}) to be in the range of 186.2 to 206.9 MPa (27,000 to 30,000 lb/in.²).

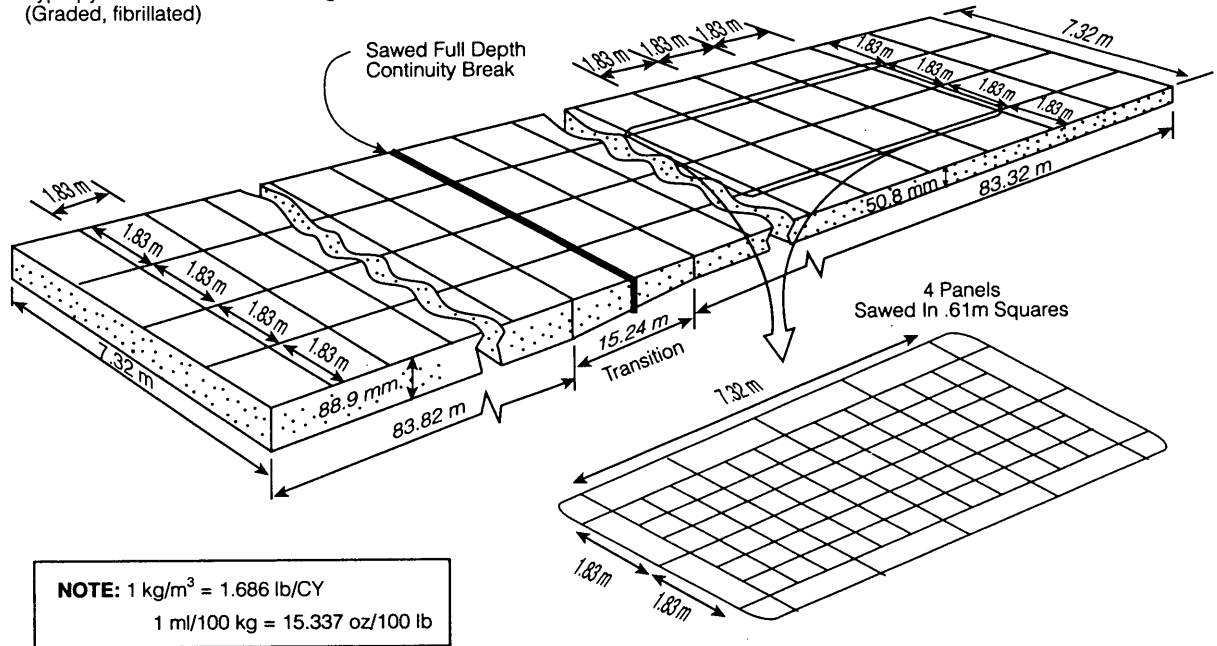
Westergaard Analysis To Determine Stresses and Deflections

An initial analytical investigation of the pavement sections started shortly after the pavement was open to traffic. Most

J. W. Mack and L. W. Cole, American Concrete Pavement Association, 3800 N. Wilke Road, Suite 490, Arlington Heights, Ill. 60004.
J. P. Mohsen, University of Louisville, Louisville, KY. 40208.

Mix Design

Type 1 Cement	474.4 kg/m ³
Coarse Aggregate (#8 crushed limestone)	10688 kg/m ³
Fine Aggregate (Natural sand)	948.2 kg/m ³
Air Content	4%-6%
High Range Water Reducer (ASTM C-494, Type F)	0.9128 ml/100 kg cement
Polypropylene Fibers (Graded, fibrillated)	1.78 kg/m ³



NOTE: 1 kg/m³ = 1.686 lb/CY
1 ml/100 kg = 15.337 oz/100 lb

FIGURE 1 Layout of experimental section.

experiment observers assumed that the pavement would crack shortly after opening to traffic. However, after 4 weeks of truck loading with approximately 43,000 80-kN (18-kip) equivalent single-axle loads (ESALs), only 6 percent of the pavement showed visible distress, with all of the distresses concentrated in the 1.83-m (6-ft) panels. Corner cracking was the primary distress mode. Less than 0.6 percent of the slabs exhibited transverse cracking. The 0.61-m (2-ft) panels had no signs of cracking of any type (4).

The initial analysis used the following Westergaard equations (5) to calculate interior, edge, and corner stresses and deflections caused by a single wheel load.

Maximum stress (lb/in.²):

$$\begin{aligned}
 \text{[Edge stress} &= 3(1 + \mu)P/[\pi(3 + \mu)h^2] \\
 &\quad * [\ln(Eh^3)/(100ka^4) \\
 &\quad + 1.84 - 4\mu/3 + (1 - \mu)/2 \\
 &\quad + 1.18(1 + 2\mu)(a/l)] \quad (2)
 \end{aligned}$$

$$\begin{aligned}
 \text{Interior stress} &= 3P(1 + \mu)/(2\pi h^2) \\
 &\quad * [\ln(2l/b) + 0.5 - \gamma] \\
 &\quad + 3P(1 + \mu)/(64h^2) * (a/l)^2 \quad (3)
 \end{aligned}$$

$$\text{Corner stress} = 3P/(h^2)[1 - (a\sqrt{2l})^{0.6}] \quad (4)$$

Maximum deflections (in.):

$$\begin{aligned}
 \text{Edge deflection} &= P(2 + 1.2\mu)^{0.5}/[(Ek h^3)^{0.5}] \\
 &\quad * [1 - (0.76 + 0.4\mu)(a/l)] \quad (5)
 \end{aligned}$$

Interior deflection

$$= P/(8kF) * [1 + 0.5\pi[\ln(a/2l) + \gamma - 5/4] * (a/l)^2] \quad (6)$$

$$\text{Corner deflection} = [1.1 - 1.24(a/l)]P/(kF) \quad (7)$$

where

- μ = Poisson's ratio;
- P = total load [N (lb)];
- h = thickness [mm (in.)];
- l = radius of relative stiffness [mm (in.)];
- $l^4 = E_c h^3 / [12(1 - \mu^2)k]$;
- $b = a$ if $a > 1.724h$ (which is true in this case);
- $b = -.0675h + (1.6a^2 + h^2)$ if $a < 1.724h$;
- a = equivalent radius of a plate with semiaxis at x and y ,
 $r = (x^2 + y^2)/2$;
- γ = Euler's constant = 0.5772156649;
- E_c = elastic modulus of concrete, MPa (lb/in.²); and
- k = modulus of subgrade reaction, MPa/m (lb/in.²).

This analysis found the maximum stress and deflection in the 51-mm (2.0-in.) overlay to be 18.006 MPa (2,611 lb/in.²) and 3.69 mm (0.1453 in.), respectively. For the 89-mm (3.5-in.) overlay, the maximum stress and deflection were 8.160 MPa (1,183 lb/in.²) and 2.19 mm (0.0863), respectively. These maximum calculated stresses for single-wheel load were well above the 36-hr flexural strength of the pavement when it was opened to traffic and indicated that the pavement should have cracked in the transverse direction.

Finite Element Analysis

Because the Westergaard analysis failed to explain the pavement's performance, an additional analysis was performed using finite element procedures with the finite element computer program ILLI-SLAB (6,7). ILLI-SLAB calculates deflections and stresses in jointed slabs-on-grade pavements, with and without load transfer, for various subgrade support conditions. For this analysis, the pavement was modeled as a one-layer and two-layer system on a Winkler foundation. The k value for the one-layer system was set to 68.0 MPa/m (250 lb/in.²/in.), the k value on top of the AC. For the two-layer system, k was altered between 27.2, 40.8, and 54.4 MPa/m (100, 150, and 200 lb/in.²/in.) and E_{ac} was set to 3,447 MPa (500,000 lb/in.²). The load was modeled as a dual tire load on 279- × 228-mm (11- × 9-in.) wheels. This roughly corresponds to a tire aspect ratio of 0.8. The modeled load was 36.0 kN (8,100 lb) per tire, which was the average test load used at the Louisville experimental project. The majority of the analysis work was done on the 1.83- × 1.83-m (6- × 6-ft) slabs, which were modeled as single slabs. Only one slab could be modeled at a time because of the mesh fineness required by ILLI-SLAB to get accurate values for stresses and deflections. Analysis work was also done on the 0.61- × 0.61-m (2- × 2-ft) slabs. These slabs were modeled with the same mesh patterns used for the 1.83- × 1.83-m (6- × 6-ft) slabs, except that joints were placed at 610 mm (24 in.) and 1220 mm (48 in.), which created a multislabs model with three slabs extending in both the x and y directions.

Single-Layer Analysis

The single-layer analysis model for the 51-mm (2.0-in.) and 89-mm (3.5-in.) pavements used the stiff subgrade [$k = 68.0$ MPa/m (250 lb/in.²/in.)] determined from the FWD testing and the concrete material properties (E_c) described earlier. This analysis calculated a maximum stress of 20.182 MPa (2,926 lb/in.²) and a maximum deflection of 6.01 mm (0.2366 in.) for the 51-mm overlay and 10.104 MPa (1,465 lb/in.²) and 3.78 mm (0.1567 in.), respectively, for the 89-mm (3.5-in.) pavement. Although these values generally were in close agreement with the values obtained from the single layer Westergaard analysis, they still failed to explain the pavements' behavior.

Two-Layer Analysis

The two-layer analysis had the pavement modeled as concrete over a 102-mm (4-in.) AC pavement on top of a subgrade

with k values of 27.2, 40.8, and 54.4 MPa/m (100, 150, and 200 lb/in.²/in.). These k values were chosen as a representative range of values underneath the AC layer. Because the k on top of the AC was 68.0 MPa/m (250 lb/in.²/in.), it was deduced that the k underneath it had to be some lesser value. The AC layer was modeled with an E_{ac} of 3447 MPa (500,000 lb/in.²) and a Poisson's ratio of 0.3. Interface conditions were modeled as bonded and unbonded. The loading conditions modeled were at the interior, corner, and edges of the slab. The analysis results for maximum calculated stresses and deflections are presented in Figures 2 and 3.

Figure 2 indicates the significant effect of bond between the concrete overlay and AC pavement on the maximum calculated stresses in the concrete overlay. By bonding the upper concrete layer to the lower AC layer, much of the load is transferred down into the pavement structure, keeping the stresses in the concrete well within acceptable limits. Figure 2 also shows the relative insensitivity of the calculated stresses to the various subgrade support conditions or k values. This is opposite of what happens with the deflections for the bonded and unbonded systems. As indicated in Figure 3, deflection is somewhat insensitive to the bonding conditions between the layers and more sensitive to the subgrade k value. Although bond does decrease the deflections, the k value of the subgrade has a much larger impact on decreasing the deflections.

It is important to note the magnitude of the deflections obtained for these pavements. Most concrete pavements usually do not deflect more than about 0.8 mm (0.03 in.). However, for both the bonded and unbonded thin concrete overlays on the soft subgrade [$k = 27.15$ MPa/m (100 lb/in.²/in.)], the calculated deflections are much higher than this. For corners, where deflection is the highest, the deflection may be over 5 mm (0.2 in.) for both conditions. Such high deflections on soft subgrades must be considered in the design of such pavement structures because they may lead to permanent subgrade deformations and early failures.

One unexpected anomaly is found when comparing the stress values of the bonded 51-mm (2.0-in.) overlay to the stresses of the bonded 89-mm (3.5-in.) overlay. As shown in Figure 2, the calculated bonded stresses in the 51-mm (2.0-in.) concrete pavement are actually lower than the stresses in the bonded 89-mm (3.5-in.) pavement. This is the opposite

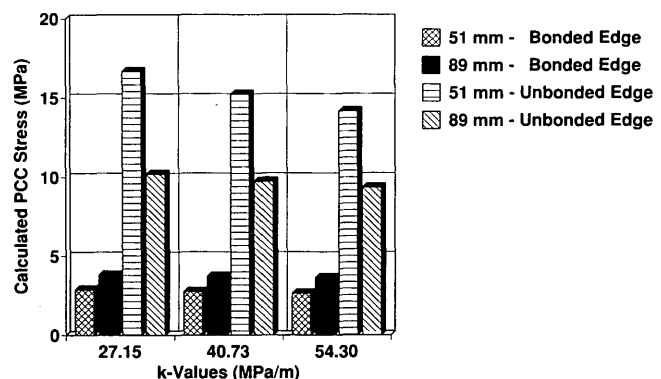


FIGURE 2 Maximum calculated edge stresses.

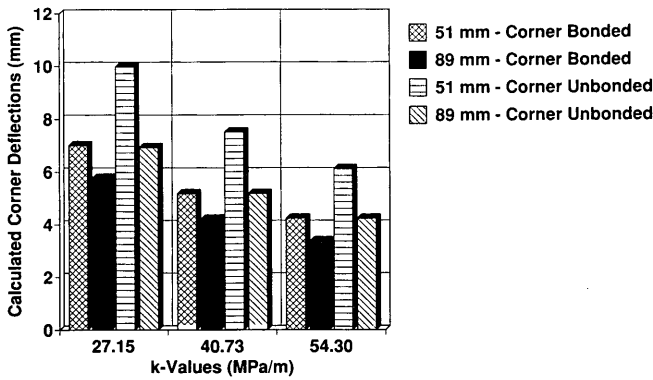


FIGURE 3 Maximum calculated corner deflections.

of what happens in the unbonded systems and goes against conventional concrete pavement theory.

This phenomenon can be explained by examining the location of the neutral axis with respect to the bottom of the concrete slab. Figure 4 shows stress diagrams for both the 51-mm (2.0-in.) and 89-mm (3.5-in.) pavement in the bonded condition. This figure shows that although the neutral axis stays in the bottom half of the concrete slab, its location from the bottom of the slab increases as the slab gets thicker. As the neutral axis gets farther away from the bottom, the flexural stress at the bottom of the concrete increases as more of the load is carried by the concrete slab. Also shown in Figures 4 and 5 is the decrease in the AC layer stresses caused by an upward shift of the neutral axis. Basically, in the 51-mm (2.0-in.) pavement, more load is carried by the lower layer, as shown by the higher AC stress value. As the concrete thickens to 89 mm (3.5 in.), the neutral axis shifts up, more load is absorbed by the concrete, and the stresses in the AC layer decrease.

Both the 51-mm (2.0-in.) and the 89-mm (3.5-in.) systems carry the same total load; however, the shifting of the neutral axis changes the amount of the load carried by each individual layer. As the neutral axis gets lower, more of the total load is carried in the AC layer and less by the concrete, and as the neutral axis gets higher, more of the total load is carried by the concrete and less by the AC. Eventually, as the concrete overlay thickness increases, the effect of shifting the neutral axis is offset by the overlay thickness itself; that is, the stresses will start to decrease as the thickness increases.

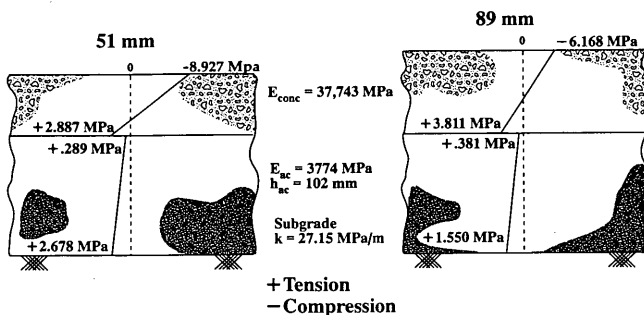


FIGURE 4 Stress distribution for bonded overlay.

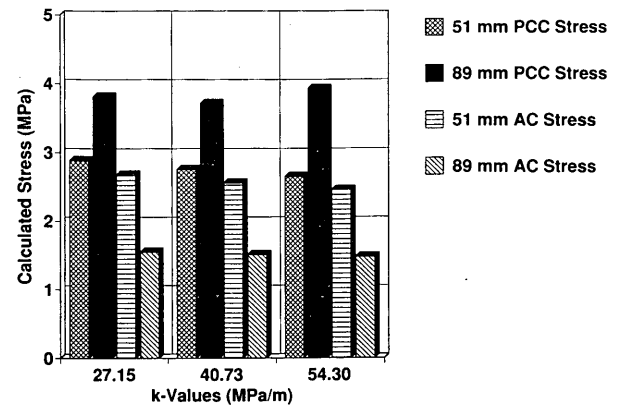


FIGURE 5 Calculated stresses in bottom of PCC and AC layers for bonded condition at edge loading.

This phenomenon is indicated in Figure 6, in which a 127.0-mm (5.0-in.) pavement section, using the same mesh, material properties, and loading conditions as the 51-mm (2.0-in.) and 89-mm (3.5-in.) pavements, was evaluated using ILLI-SLAB. As shown, the calculated stresses in the 127.0-mm (5.0-in.) overlay are lower than the stresses from the 89-mm (3.5-in.) overlay because the upward shift of the neutral axis is offset by the thickness.

Conceptually, this phenomenon is shown in Figure 7 for a given AC thickness. As the location of the neutral axis moves further from the bottom of the slab, or to the right, the stresses at the bottom of the concrete increase because of the shifting of the load from the AC to the concrete. Conversely, as the concrete overlay thickness increases, the stresses decrease because of the increase of the load-carrying capacity of the slab. At the point where the two lines cross, the neutral axis is high enough and the slab thickness is thin enough to produce maximum stresses in the slab bottom. An increase in concrete overlay thickness will lower the stresses associated with concrete slab thickness, and a decrease in thickness will decrease the stresses associated with the lowering of the neutral axis.

Although only one AC thickness value was used at Louisville, the effect of the underlying AC layer thickness on the location of the neutral axis was also evaluated. As the AC layer thickens, it becomes stiffer, and the neutral axis shifts

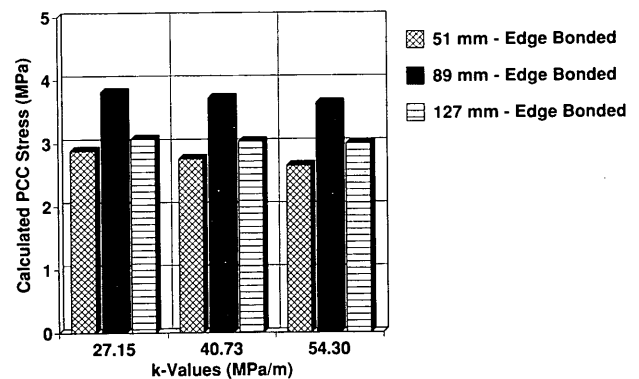


FIGURE 6 Calculated edge stresses for various PCC thicknesses.

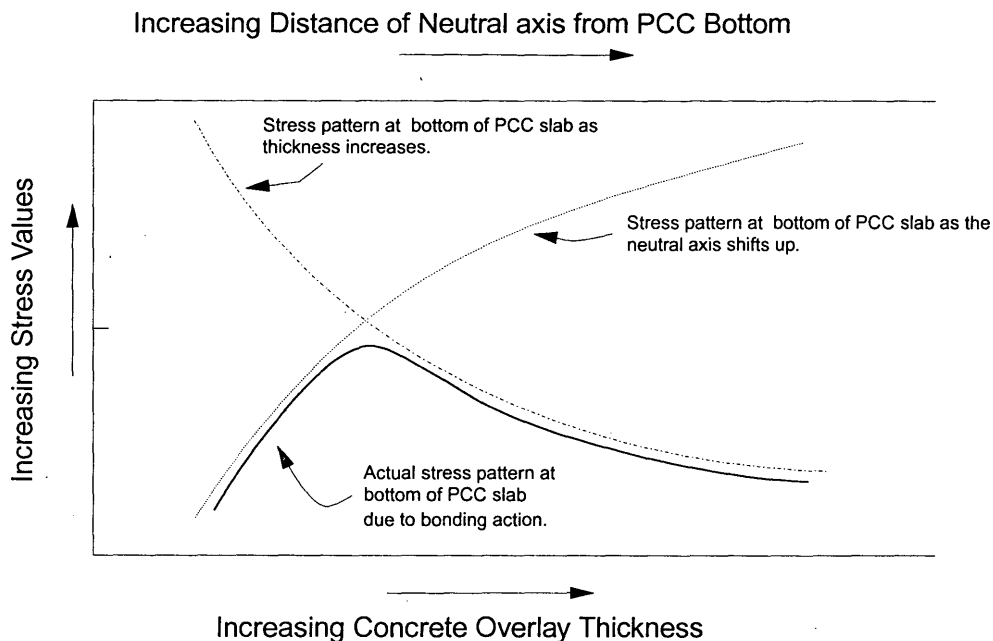


FIGURE 7 Conceptual stress pattern at PCC slab bottom caused by location of neutral axis and thickness of slab for a bonded system with a constant AC thickness.

down. Likewise, as the AC layer gets thinner, it carries less of the applied load and the neutral axis shifts up. A diagram similar to that in Figure 7 could be developed for constant concrete thickness that would show when the neutral axis was at its most critical location for various AC thicknesses. Figures 8 and 9 show how the concrete and AC stresses are affected by the concrete overlay and AC thicknesses.

Theoretically, the effect of concrete and AC thickness can be explained by the stiffness or flexural rigidity of the two layers. Flexural rigidity of a layer (D) is defined as

$$D = \frac{Eh^3}{12(1 - \mu^2)} \quad (8)$$

where

- E = modulus of elasticity,
- h = thickness, and
- μ = Poisson's ratio.

Simply put, as the rigidity of a layer increases, the load-carrying capacity of the layer increases. In a bonded system, changing the rigidity of a single layer by changing the thickness changes the rigidity of the entire system and shifts the neutral axis. Note that the layer with the larger rigidity value will take the larger portion of the load. As the concrete slab thickness increases, the effects of the AC thickness increase become less pronounced. Although it has not been tested here, it is believed that changes in the modulus values will have a similar, but smaller, effect. This is a very critical concept because the neutral axis will be in a different location for every concrete and AC modulus value and every concrete and AC thickness. If a pavement happens to be built at a thickness that is near the intersection of the two lines in Figure 7, it will fail earlier than if it was built thicker or thinner.

Expanding this rigidity concept, it would be possible to describe any portland cement concrete (PCC)/AC system as an equivalent single layer with an equivalent modulus and

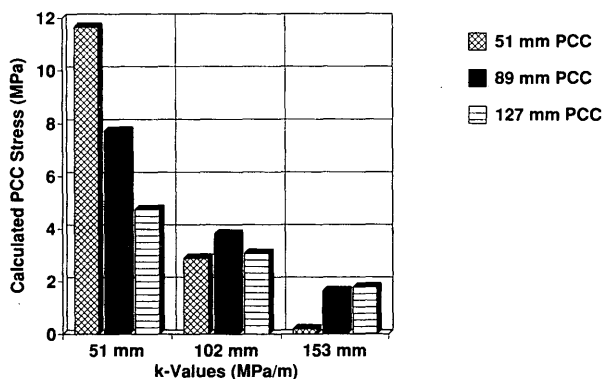


FIGURE 8 Calculated PCC stresses for various AC and PCC thicknesses.

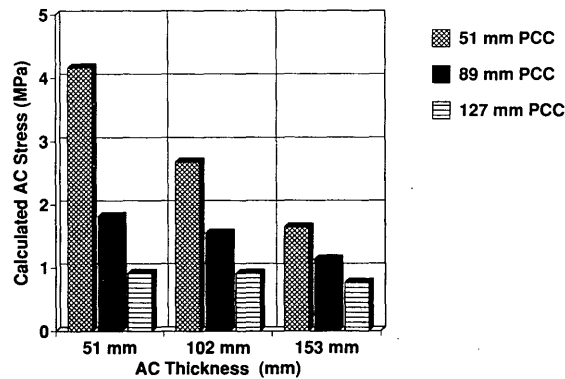


FIGURE 9 Calculated AC stresses for various AC and PCC thicknesses.

equivalent thickness. Although Odemark (8), Packard (9), and Ioannides et al. (10) have proposed similar concepts for other types of pavement systems, we believe that this concept has never been used to specifically address concrete bonded to underlying AC layers.

Slab Studies

The slabs built in Louisville [0.61×0.61 m (2×2 ft)] were also modeled using the finite element program ILLI-SLAB. In this model, the mesh for the 1.83-m (6-ft) edge slabs was used with joints added at 610 mm (24 in.) and 1220 mm (48 in.). No interior or corner loadings were modeled because, at any wheel placement, an edge would be only a couple of inches away. Load transfer between the panels was modeled at 100, 80, 40, and 0 percent. Although it was not measured at Louisville, the load transfer is believed to be low because the 25.4-mm- (1-in.-) deep joint saw cuts in the 51-mm (2-in.) overlay left only a nominal amount of concrete for aggregate interlock. Interface conditions were modeled as bonded and unbonded. Even though at Louisville only the 51-mm (2.0-in.) overlay was cut into 0.61-m (2-ft) sections, both the 51-mm (2.0-in.) and 89-mm (3.5-in.) pavements were modeled in ILLI-SLAB. Figures 10 and 11 give the stresses and deflections for both the unbonded and bonded systems for 0 percent load transfer efficiency.

Figure 10 again shows the considerable effect bond has on stress. By bonding the layers, the computed flexural stresses decrease from about 7.16 MPa (1,039 lb/in.²) to about 1.03 MPa (149 lb/in.²) for the 51-mm (2.0-in.) section and from about 3.69 MPa (535 lb/in.²) to 1.29 MPa (187 lb/in.²) for the 89-mm (3.5-in.) section. Plots using other load transfer efficiencies would show similar results. Again, it is interesting to note that the stresses in the 51-mm (2.0-in.) bonded overlay are lower than the stresses in the 89-mm (3.5-in.) bonded overlay. Although not tested, it is again assumed that at some thickness, stress will start to decrease with thickness. Notice that even though the bonding decreased the stresses in the 89-mm (3.5-in.) section, the stresses in the unbonded system are still low and well within the limits of a normal concrete

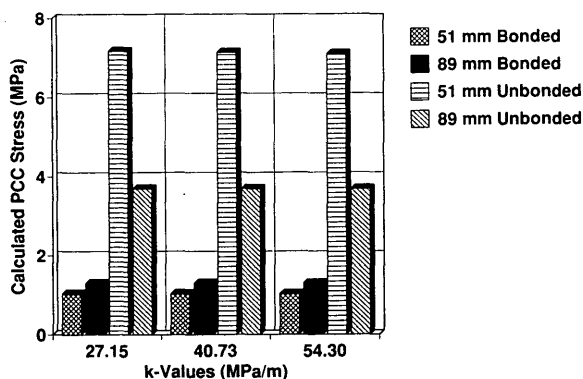


FIGURE 10 Calculated edge stresses for 0.61-m panels with 0 percent load transfer.

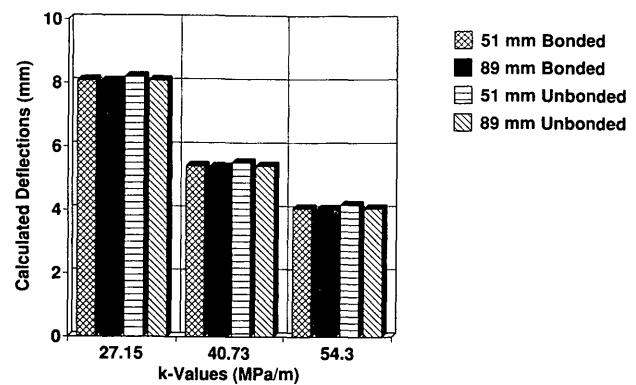


FIGURE 11 Calculated deflections for 0.61-m panels for 0 percent load transfer.

pavement. Understanding this, it should be recognized that small slab sizes may be used to counteract any possible debonding that may occur between the concrete and the AC.

Figure 11 shows the effect bond has on deflections. As with the 1.83-m (6-ft) panels, bond does not have as great an effect on deflections, and in both bonded and unbonded systems deflections are high. Again, it was found that subgrade support had a much larger impact on the deflections.

COMPARISON WITH THE LOUISVILLE PROJECT

After 28 days and approximately 43,000 80-kN (18-kip) ESAL's, the project in Louisville has shown only a small amount of distress. About 6 percent of the slabs have shown visible signs of cracking, which was mainly concentrated at the corners of 1.83- \times 1.83 m (6- \times 6-ft) panels. Less than 0.6 percent of the overlay had transverse cracking. The one section of the 1.83-m (6-ft) panels that had longitudinal cracking occurred at a location that inadvertently had the entire AC layer removed during the milling process—that is, the concrete was sitting on a granular base. As of 28 days, no distresses were noted in the 0.61-m (2-ft) panels. In fact there were still no cracks in the 0.61-m (2-ft) panels after 1 year of use and over 500,000 80-kN (18-kip) ESALs (4).

It is believed that the corner cracking in the 1.83-m (6-ft) panels is the result of two actions: (a) the upturning of the corners mainly from moisture warping and (b) the high deflections at the corner. It is believed that the combination of moisture warping and high corner deflections is causing the bond between the AC and concrete to fail. Then as the corners are loaded the slab cracks as a result of the high induced concrete stresses.

Originally, it was thought that both temperature and moisture could be causing the upturning of the corners. However, using Bradbury's (11) equations to determine interior and edge curling stresses and the maximum temperature differential between the top and the bottom of the slab taken during the first 72 hr of pavement life [2.2°C (4°F) for the 88.9-mm (3.5-in.) overlay], it was found that the maximum interior curling stress would be 0.145 MPa (20.96 lb/in.²) and 0.147 MPa (21.23 lb/in.²) for the 51-mm (2.0-in.) and 89-mm (3.5-

in.) pavements, respectively, whereas the maximum edge curling stress would be 0.246 MPa (35.63 lb/in.²) and 0.430 MPa (62.34 lb/in.²), respectively. Meanwhile, moisture studies by Janssen (12) from the University of Washington and Stark (13) from Construction Technologies Laboratories have shown that drying occurs in the top 12 mm (0.5 in.) of the pavement, and this drying has been calculated to cause moisture warping stresses as high as 5.52 MPa (800 lb/in.²) for a 203-mm- (8-in.-) thick pavement. Such high moisture warping stresses could cause debonding of the slab and would have a significant effect on slab dimensioning and pavement performance. Clearly this area needs more research.

CONCLUSIONS AND RECOMMENDATIONS

This paper presented an analytical and theoretical study of the performance of a thin concrete overlay on asphalt concrete pavement built in Louisville, Kentucky. In this investigation, it was concluded that bond was critical to the pavement's performance. If bond did not exist, this pavement would fail. The second item found to be critical was the location of the neutral axis of the bonded system compared with the bottom of the concrete slab. Factors affecting the neutral axis location are concrete and AC thickness. Although this aspect was not investigated, it is believed that the modulus values of the concrete and AC will also have a critical effect on neutral axis location, which may be significant because of the temperature dependence of the AC modulus (E_{ac}). Also found to be influential on stresses and deflections were the subgrade support conditions. Although it did not greatly affect stresses, increased subgrade support did have a large effect on deflections.

If design procedures for thin concrete overlays on AC pavements are to be developed, they must recognize that the flexural stresses in the thin concrete overlay are not the only critical item. AC radial strain and panel deflections must also be checked to ensure that they are within allowable limits. Clearly, design criteria need to be developed for AC strain and deflection, which requires much more research. Other important items for research include, but are not limited to, slab size effects and jointing requirements, bond strength and durability, concrete and AC thickness and modulus (rigidity) requirements, interaction with neighboring slabs, moisture warping and temperature curling, permanent deformation characteristics in the AC and subgrade, fatigue effects in AC and PCC and at the PCC/AC interface, and load magnitude and tire effects.

ACKNOWLEDGMENTS

This project was sponsored by the Portland Cement Association, the American Concrete Pavement Association, and over 40 other allied industry groups and companies. The authors would like to thank all those who supported this experiment.

REFERENCES

1. L. W. Cole and J. P. Mohsen. Construction and Instrumentation of a Thin Concrete Overlay of Asphalt Pavement. Presented at the American Concrete Institute Spring Meeting, Washington, D.C., March 1992.
2. A. J. Bush and D. R. Alexander. Pavement Evaluation Using Deflection Basin Measurements and Layered Theory. In *Transportation Research Record 1022*, TRB, National Research Council, Washington, D.C., 1985, pp. 16-29.
3. A. M. Ioannides. Dimensional Analysis in NDT Rigid Pavement Evaluation. *ASCE Journal of Transportation Engineering*, Vol. 116, No. 1, Jan. 1990, pp. 23-36.
4. High Strength Whitetopping Performance Evaluation. Preliminary Final Report. Portland Cement Association, July 1992.
5. A. M. Ioannides, M. R. Thompson, and E. J. Barenberg. Westergaard Solutions Reconsidered. *Transportation Research Record 1043*, TRB, National Research Council, Washington D.C., 1985.
6. A. M. Tabatabaie-Raissi. *Structural Analysis of Concrete Pavement Joints*. Ph.D. thesis. University of Illinois, Urbana, 1977.
7. A. M. Ioannides, M. R. Thompson, and E. J. Barenberg. Analysis of Slabs-on-Grade Pavement Systems Using a Variety of Support Models. *Proc. 3rd International Conference on Concrete Pavement Design and Rehabilitation*, Purdue University, April 23-25, 1985, pp. 309-324.
8. N. Odemark. *Investigation of the Elastic Properties of Different Soil Types and Theory for Calculation of Pavements According to the Theory of Elasticity*. Bulletin 77, State Highway Commission, Stockholm, Sweden, 1949.
9. Robert G. Packard. Structural Design of Concrete Pavements with Lean Concrete Lower Course. *Proc., 2nd International Conference on Concrete Pavement Design and Rehabilitation*, Purdue University, April 14-16, 1981, pp. 119-131.
10. A. M. Ioannides, L. Khazanovich, and J. L. Becque. Structural Evaluation of Base Layers in Concrete Pavement Systems. Presented at 71st Annual Meeting of the Transportation Research Board, Washington, D.C., 1991.
11. R. D. Bradbury. *Reinforced Concrete Pavements*. Wire Reinforcement Institute, Washington, D.C., 1938.
12. D. J. Janssen. Moisture in Portland Cement Concrete. In *Transportation Research Record 1121*, TRB National Research Council, Washington D.C., 1987.
13. D. C. Stark. Moisture Condition of Field Concrete Exhibiting Alkali-Silica Reactivity. *Proc., 2nd CANMET/ACI International Conference on Durability of Concrete*, Montreal, Quebec, Canada, 1991.

Publication of this paper sponsored by Committee on Pavement Rehabilitation.

Breaking and Seating of Concrete Pavements: Kentucky's Experience

R. CLARK GRAVES, DAVID L. ALLEN, AND GARY W. SHARPE

Breaking and seating has been utilized extensively in Kentucky for rehabilitation of portland cement concrete pavements for the past 10 years. To date, 1345 lane-km (836 lane-mi) of Interstate pavements and 470 lane-km (292 lane-mi) of parkway pavements have been rehabilitated. Overlay thicknesses have ranged from 114 to 240 mm (4.5 to 9.5 in.). The sections that have been overlaid generally have performed well. Localized areas of distress generally have been observed in the wheel tracks of the driving lane. Research is currently being conducted to relate this type of distress to areas of poor drainage. Kentucky is currently conducting a survey of all broken and seated concrete pavements on Interstate highways and parkways throughout the state. This survey includes a detailed visual survey and falling weight deflectometer testing to determine the in situ condition of the pavement structure. These data, combined with rideability index and condition points, will be used to analyze performance of this type of rehabilitation. Information gained from this study may be used to modify the current design and construction procedures if necessary. On the basis of the experience gained, Kentucky will continue to use breaking and seating of concrete pavements as a rehabilitation alternative.

Rigid [portland cement concrete (PCC)] pavements have been used extensively on the Interstate and parkway system throughout Kentucky. Many of these pavements are nearing the end of their design lives and are beginning to show signs of deterioration, spalling, cracking, joint deterioration, and faulting at joints.

Breaking and seating has been used extensively in Kentucky for rehabilitation of PCC pavements for the past 10 years. To date, 1345 lane-km (836 lane-mi) of Interstate pavements and 470 lane-km (292 lane-mi) of parkway pavements have been rehabilitated. Several test sections have been constructed to evaluate construction techniques to use and appropriate factors to consider in design procedures. Projects have been constructed with overlay thicknesses ranging from 114 to 240 mm (4.5 to 9.5 in.).

In general, all sections that have been rehabilitated are performing well. To date, no large-scale resurfacing has been conducted on any of the projects. Localized areas of distress that have been observed generally are in the wheel tracks of the driving lane.

The relationship between the size of the broken particles and the behavior of the rehabilitated pavement has been studied for some time. Small particles will reduce or possibly eliminate reflective cracking in the overlay but will use the

least structural potential of the existing concrete pavement. Very large particles may maximize the structural potential of the existing pavement but will permit increased movements of the broken slab, thereby increasing the potential for reflective cracking.

Previous research in Kentucky indicated that, generally, an effective modulus of 62 to 278 MPa (9,000 to 30,000 lb/in.²) may be associated with concrete broken into 75- to 150-mm (3- to 6-in.) particles; an effective elastic modulus of 345 to 6800 MPa (50,000 to 1 million lb/in.²) may be associated with fragments of 457 to 610 mm (18 to 24 in.), and an effective elastic modulus of 4100 to 13700 MPa (600,000 to 2 million lb/in.²) may be associated with 762- to 915-mm (30- to 36-in.) particles (1).

Other research has indicated various relationships relating broken particle size and effective elastic modulus. Models have been developed for rubblized concrete and crack and seat concrete. No model was developed for broken and seated concrete because of the large variation in effective moduli that were backcalculated (2).

A research study is currently being conducted to evaluate all broken and seated concrete pavements in Kentucky. Falling weight deflectometer (FWD) measurements are being obtained on each project to evaluate the in situ structural condition of the pavement. Effective broken concrete moduli will be evaluated and compared with values currently in use. Detailed visual survey data combined with rideability index and condition points will be used to analyze performance of this type of rehabilitation. The results of this study will provide a means to evaluate the total performance of these pavements and modify the current design and construction procedures if necessary.

DESIGN CONSIDERATIONS AND SPECIFICATIONS

Current Kentucky construction specifications were developed through experience gained during the past 10 years of constructing break and seat projects. Table 1 summarizes the various aspects of the specifications and how they have changed since 1982.

The initial specifications, in March 1982, required 80 percent of the broken particles to be 152 to 304 mm (6 to 12 in.) in size and all particles to be less than 456 mm (18 in.). In June 1982, the particle size specifications were changed requiring 80 percent of the broken particles to be 456 to 608 mm (18 to 24 in.) in size and all particles to be less than 760 mm (30 in.).

R. C. Graves and D. L. Allen, Transportation Research Building, Kentucky Transportation Center, University of Kentucky, Lexington, Ky. 40506-0043. G. W. Sharpe, Division of Design, Kentucky Transportation Cabinet, Frankfort, Ky. 40622.

TABLE 1 Specification Comparison

	Specification Date					
	March 1982	June 1982	August 1984	April 1986	January 1987	February 1990
Particle Size	80% 152 - 304-mm, All < 456 mm	80% 456 - 608-mm, All < 760-mm	80% 456 - 608-mm, All < 760-mm	80% 456 - 608-mm, All < 760-mm	80% 456 - 608-mm, All < 760-mm	80% 456 - 608-mm, All < 760-mm
Breaking Equipment	Impact Hammer	Impact Hammer	Impact Hammer	Impact Hammer	Impact Hammer	Impact Hammer
Test Section	Not Required	Not Required	Required	Required	Required	Required
Extent of Breakage	Use of Water to Detect Cracks	Use of Water to Detect Cracks	Use of Water to Detect Cracks	Water Not Permitted to Detect Cracks	Water Not Permitted to Detect Cracks	Water Not permitted to Detect Cracks
Roller (seating)	7.3-metric ton Vibratory Roller or 45-metric ton Pneumatic Tire Roller	7.3-metric ton Vibratory Roller or 45-metric ton Pneumatic Tire Roller	45-metric ton Pneumatic Tire Roller	45-metric ton Pneumatic Tire Roller	32-metric ton (7 passes) or 45-metric ton (5 passes) Pneumatic Tire Roller	32-metric ton (7 passes) or 45-metric ton (5 passes) Pneumatic Tire Roller
Limits of Breaking	< 1,524 m Ahead of Paving	< 1,524 m Ahead of Paving	< 1,524 m Ahead of Paving	< 1,524 m Ahead of Paving	< 1,524 m Ahead of Paving	< 24 Hours Ahead of Paving
Miscellaneous						Vertical Displacement Limited to Less Than 13 mm

1 in = 25.4 mm
 1 ton = 0.907 metric ton
 1 ft = 0.30480 m

The specifications remained unchanged until 1984, when the use of vibratory rollers for seating was eliminated. The requirement of a test section for verification of breaking and seating was also added at that time. Until 1986, water was used to detect cracks resulting from the breaking operation. This procedure was eliminated because of inspection problems. The wetted surface exposed cracks that were present before the breaking operation. In some cases, these cracks could not be distinguished from the full-depth cracks that resulted from the breaking.

In 1987 specifications were modified to allow for the use of a pneumatic tire roller weighing 32 metric tons (35 tons) with seven passes across the pavement or one weighing 45 metric tons (50 tons) using five passes. The current specifications were last modified in 1990. In 1990 the amount of vertical displacement of the pavement surface during the breaking and seating operation was limited to 13 mm (0.5 in.). In addition, the contractor must allow overnight curing of each course of bituminous overlay before opening to traffic. The contractor must also limit the breaking to less than 24 hr ahead of the paving operation.

LONG-TERM PERFORMANCE

The first broken and seated concrete rehabilitation projects were opened to traffic in 1983. These projects contained test sections that had various breaking patterns [76 to 304 mm (3 to 12 in.), 456 to 608 mm (18 to 24 in.), and 760 to 912 mm (30 to 36 in.)]. Extensive research was conducted during the

construction of these projects. Road Rater deflection measurements were obtained before, during, and after the breaking operation to evaluate the effectiveness of the breaking and seating operation (1). On the basis of this study, a relationship (previously mentioned) was developed relating the effective stiffness of the broken PCC to the average dimension of the broken particle. This relationship is shown in Figure 1.

The evaluation of long-term performance will be limited to three of the oldest projects. These projects include Interstate 71, Interstate 64, and Bluegrass Parkway. Overlay thicknesses were 178 mm (7 in.) of asphaltic concrete for both Interstate projects and 121 mm (4.75 in.) of asphaltic concrete for the Bluegrass Parkway. The performance evaluation included rideability index (RI), pavement condition rating, detailed crack survey, and Road Rater and FWD deflection measurements. The pavement condition data and rideability index were obtained from normal pavement management activities conducted by Kentucky Transportation Cabinet personnel. The detailed crack survey and deflection measurements were conducted as a portion of the research study for evaluation of broken and seated pavements. The pavement condition rating form used by the Pavement Management Branch of the Kentucky Transportation Cabinet is shown in Figure 2. Pavements are visually inspected to evaluate conditions according to six types of distress and are assigned condition points (demerits) for each. Condition points are assigned for both extent and severity of each distress. The condition points are summed to obtain the pavement condition rating. The total scale ranges from 0 to 100, with 0 being a pavement

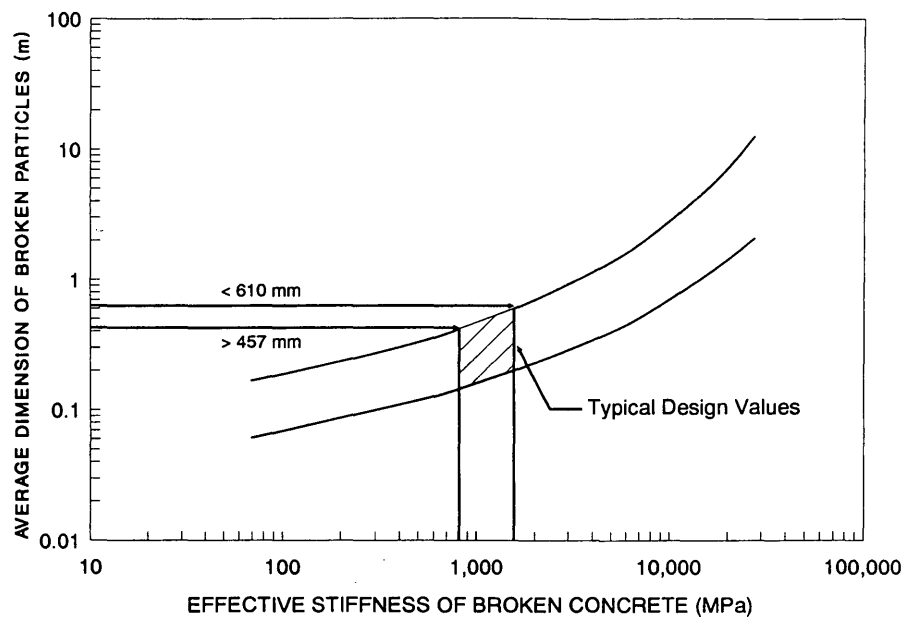


FIGURE 1 Effective modulus of broken concrete.

having no observed distresses. The rideability index is determined using a Mays ride meter.

Interstate 71

The Interstate 71 project was the first large-scale breaking and seating rehabilitation project conducted in Kentucky. The project contains particle sizes of 76 to 304 mm (3 to 12 in.), 456 to 608 mm (18 to 24 in.), and 760 to 912 mm (30 to 36 in.). In addition, there was a control section that was not broken. Each section was approximately 1.6 km (1.0 mi) in length. An asphaltic concrete overlay of 178 mm (7 in.) was placed on each section.

Each breaking pattern has been evaluated separately to determine the effects of the broken particle size on the long-term performance of the pavement. Rideability measurements have been conducted on a yearly basis since construction. The rideability of each section is shown in Figure 3. This figure indicates that the RI before rehabilitation ranged from 2.5 to 3.0. After overlay, all sections had an RI of approximately 4.0. This figure indicates further that there has been very little decrease in RI since construction. There also appears to be no significant difference in performance between the various sections comparing RI values.

Annual condition ratings also have been conducted on each section. The condition ratings for each section plotted as a function of testing year are shown in Figure 4. This figure shows an accelerated deterioration in the unbroken section when compared with the broken sections. Until 1989, all sections were performing in a similar manner. From 1989 through 1991, the condition of the control section deteriorated rapidly—probably the result of an increase in the number of reflective cracks. Since reflective cracking is the primary disease that normally occurs on broken and seated concrete pavements, a detailed crack survey was conducted on these sections in 1990. The results of this survey are shown in Figure 5. This

figure expresses the amount of transverse cracking in feet per lane-mile of pavement. It is clear that the control section has considerably more transverse cracking than the other sections. This observation is not unexpected because the pavement was not broken.

Deflection measurements were conducted in 1985 on each section using the Model 400B Road Rater. In 1992, deflection measurements were conducted using a JILS-20 FWD. To compare the deflections from these two test dates, the FWD deflections were converted to Road Rater deflections using correlations developed during previous research in Kentucky. The comparison is limited to the deflections taken at distances of 0, 305, 610, and 915 mm (0, 12, 24, and 36 in.) from the load because the Road Rater has only four sensors. These deflections were then adjusted to a reference temperature of 21°C (70°F) (3). The adjusted deflections were then converted to equivalent 40-kN (9,000-lb.) FWD deflections. These comparisons are shown in Figures 6 through 9. These figures show that in each case the 1992 deflections have increased, indicating a decrease in structural condition. The magnitude of each deflection in the deflection bowl has increased, indicating a decrease in strength of the base layers. In addition the deflection bowl has become steeper, which indicates deterioration of the asphaltic concrete layer. The visual survey information also indicates a deterioration of the asphaltic concrete layer, denoted by the increase in the condition index.

Interstate 64

The Interstate 64 project was constructed in 1983 and 1984 and is the second oldest project in Kentucky. The project contains sections with particle sizes of 152 to 304 mm (6 to 12 in.), 456 to 608 mm (18 to 24 in.), and 760 to 912 mm (30 to 36 in.). A 178-mm (7-in.) asphaltic concrete overlay was placed on all sections. The annual performance evaluation was not conducted for each breaking size; however, subse-

PAVEMENT CONDITION EVALUATION FORM
INTERSTATE AND PARKWAYS

0990

ROAD NO: _____ ROAD NAME: _____
 COUNTY: _____ DISTRICT: _____
 FROM: _____ MP: _____
 TO: _____ MP: _____
 ADT(90): _____ LENGTH: _____
 CONSTRUCTED DGA: INCHES CBR: JOINT SPACING: _____
 CONTRACTOR FOR ACTION:

DATE ACTION PAVEMENT SURFACE _____
INCHES TYPE TYPE REMARKS

VISUAL CONDITION SURVEY (DEMERIT POINTS)	MAXIMUM		LANE					
	EXT	SEV	EXT	SEV	SUM	EXT	SEV	SUM
CRACKING	18	13	_____	_____	_____	_____	_____	_____
BASE FAILURES - FAULTING	9	9	_____	_____	_____	_____	_____	_____
RAVELING - WEAR SPALLING	6	6	_____	_____	_____	_____	_____	_____
OUT OF SECTION	6	6	_____	_____	_____	_____	_____	_____
PATCHING	12		_____	_____	_____	_____	_____	_____
APPEARANCE	_____	15	_____	_____	_____	_____	_____	_____
>---- TOTAL ---->	51	49	_____	_____	_____	_____	_____	_____

REMARKS: _____

GUARDRAIL: POOR FAIR GOOD SHOULDER: _____ : POOR FAIR GOOD

NUMBER OF LANES: _____ INN OUT _____ INN OUT
 PREVIOUS RI (89): _____
 RI (90): _____
 DECREASE IN RI: _____
 RUTTING (INCHES): _____
 SKID NUMBER: _____

RECOMMENDATIONS: OVERLAY MILL GRIND YEAR: _____
 OTHER _____

RATERS: RIZENBERGS BURCHETT DADE DATE: ____/____/90

REMARKS: _____

RANKING

FIGURE 2 Pavement condition rating form.

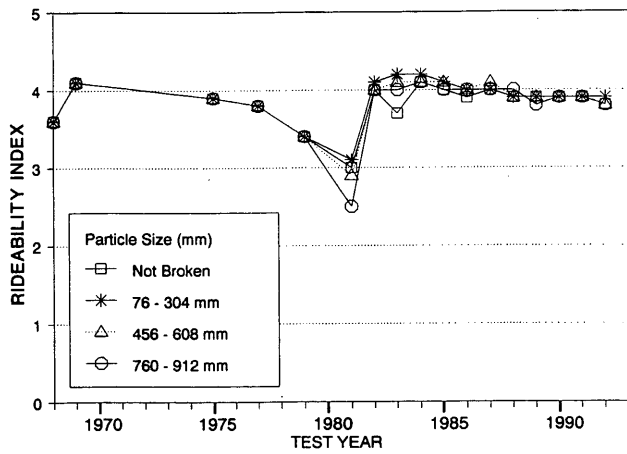


FIGURE 3 Rideability index, Interstate 71.

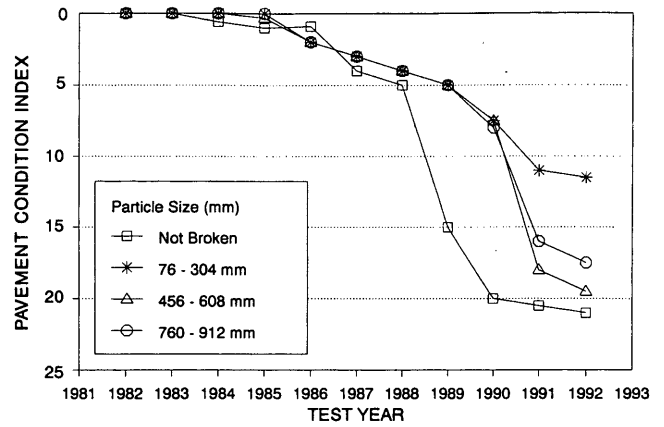


FIGURE 4 Pavement condition index, Interstate 71.

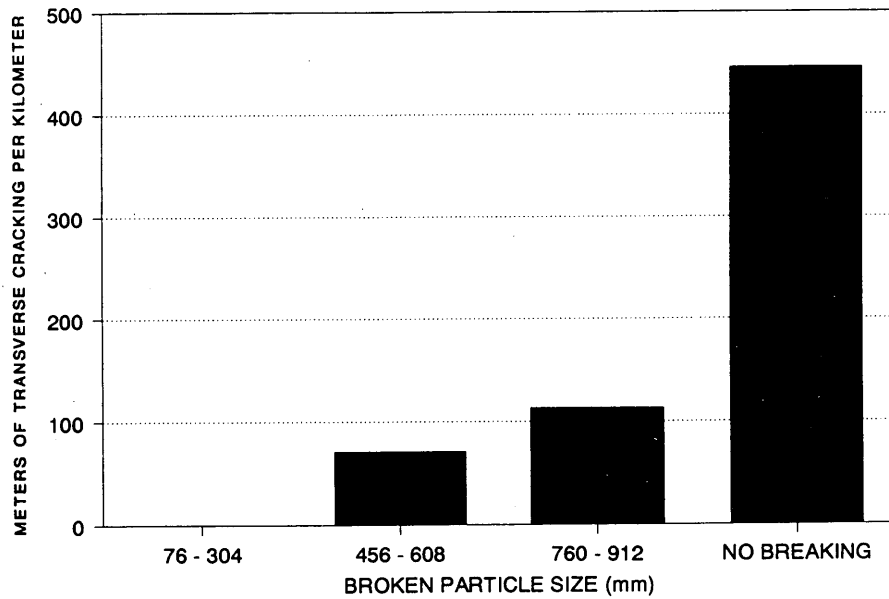


FIGURE 5 Comparison of reflective cracking, Interstate 71.

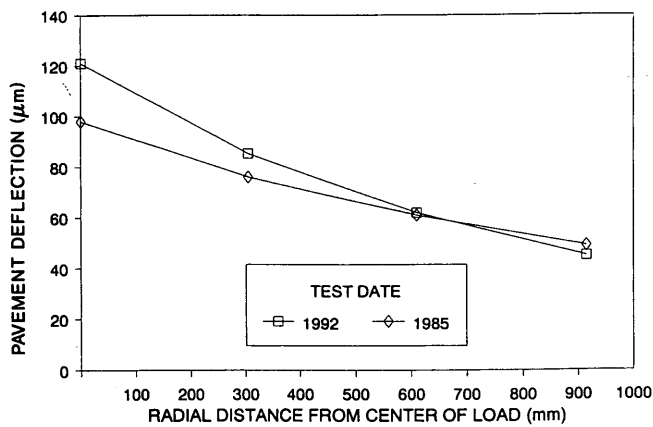


FIGURE 6 Deflection bowl comparison: particles of 76 to 304 mm (3 to 12 in.), Interstate 71.

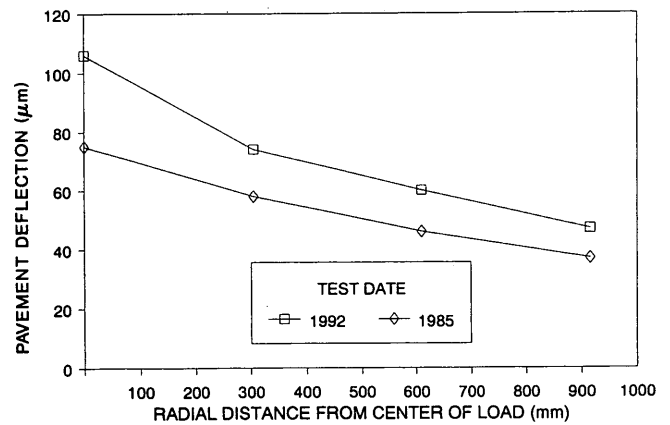


FIGURE 7 Deflection bowl comparison: particles of 456 to 608 mm (18 to 24 in.), Interstate 71.

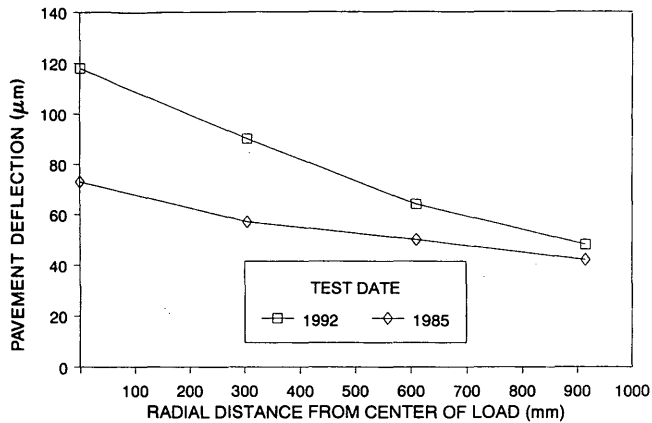


FIGURE 8 Deflection bowl comparison: particles of 760 to 912 mm (30 to 36 in.), Interstate 71.

quent visual surveys indicate that all sections are performing in a similar manner. This pavement has remained in good condition since its construction. Figure 10 contains the rideability history for the pavement since rehabilitation of all sections combined. This figure indicates that the RI had dropped to a low of 1.7 after 23 years of service before rehabilitation. After reconstruction, the RI has remained almost constant. The pavement condition rating has decreased since rehabilitation, as seen in Figure 11; however, the pavement is still in good condition. Deflection measurements obtained in 1985 and 1992 indicate little change in the pavement structural condition.

Bluegrass Parkway

The Bluegrass Parkway project was constructed in 1985 using a thin overlay of 121 mm (4.75 in.). The pavement is currently showing signs of deterioration. The breaking pattern for this project consisted of particle sizes of 456 to 608 mm (18 to 24 in.). Alligator cracking has been observed in numerous areas, indicating base failures. Reflective cracking is evident throughout the project. The observed distresses indicate that rehabilitation will be necessary in the near future.

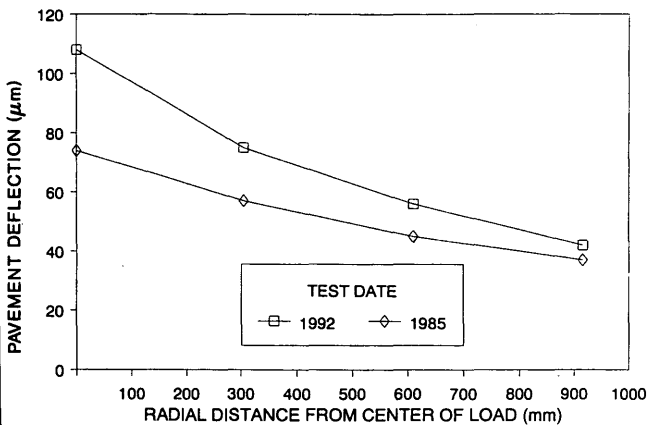


FIGURE 9 Deflection bowl comparison: control section, Interstate 71.

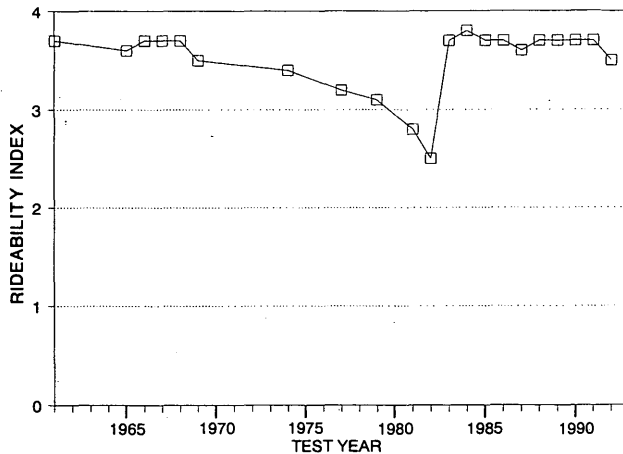


FIGURE 10 Rideability index, Interstate 64.

The pavement condition history of the project is shown in Figure 12 for the eastbound and westbound lanes. This figure indicates a steady decline in condition since rehabilitation. The condition rating for the eastbound lanes is approximately 40. In comparison, the condition ratings are 10 and 20 for Interstate 64 and Interstate 71, respectively. There has been

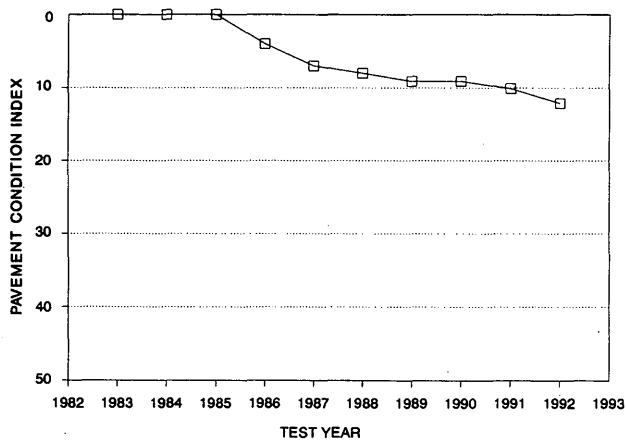


FIGURE 11 Pavement condition index, Interstate 64.

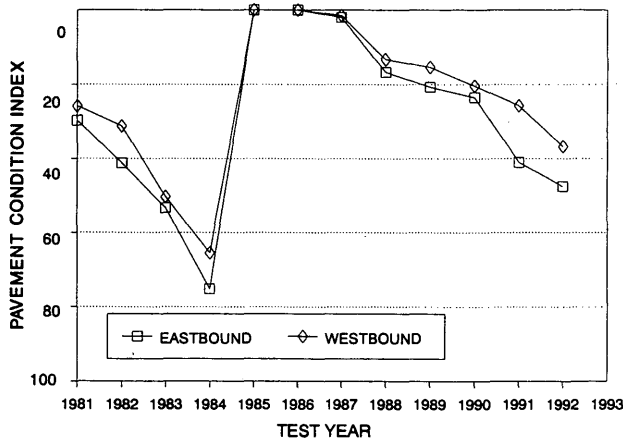


FIGURE 12 Pavement condition index, Bluegrass Parkway.

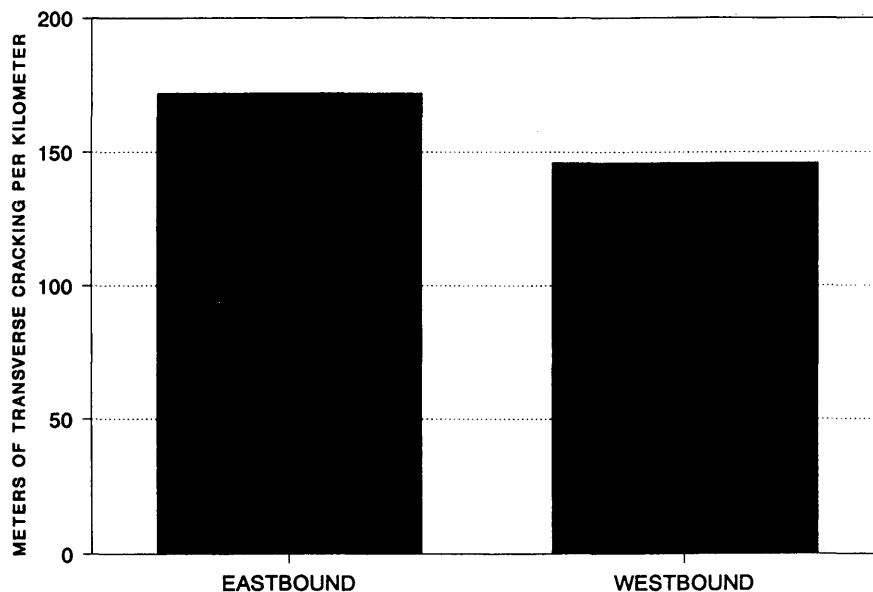


FIGURE 13 Comparison of reflective cracking, Bluegrass Parkway.

a large increase in distress in the eastbound lanes from 1990 to 1991. The westbound lanes do not show as large an increase. A detailed crack survey was also conducted, and the results are shown in Figure 13. These data also indicate that the eastbound lanes have more transverse cracking than the westbound lanes. This supports the difference in condition rating between the two directions. The rideability index for each direction is shown in Figure 14. This figure indicates a decrease in RI since rehabilitation; however, it has not decreased in the same proportion as the condition points.

CONTINUING RESEARCH

Kentucky is currently involved in several research projects relating to broken and seated concrete pavements. Kentucky is participating in FHWA Special Project 202, which is evaluating the effects of various breaking sizes on joint movement. In addition to the instrumentation installed by FHWA, Ken-

tucky has installed electronic measuring devices in each breaking pattern. These devices provide a continuous record of joint movement over an evaluation period, normally 30 days.

Kentucky continues to survey all the broken and seated pavements in the state. This effort continues to provide valuable information regarding the performance of these pavements. Kentucky has recently rehabilitated a continuously reinforced concrete pavement by rubblizing of the existing concrete slab followed by an unbonded PCC overlay. The concrete was rubblized, and the reinforcing steel was removed. The rubblized material was then overlaid with an asphalt-treated drainage layer followed by conventional PCC pavement. The long-term performance of this project is currently being evaluated.

SUMMARY AND CONCLUSIONS

Information in this paper documents the procedures that have been used in Kentucky with good success with regard to performance of broken and seated concrete pavements. This type of rehabilitation has been performed routinely for several years; in some isolated areas remedial action has been required. The majority of these areas were base type failures in the wheel tracks of the driving lane. Research is currently being conducted to relate this type of distress to that in areas of poor drainage. These areas may be associated with problems in the pavement drainage system, because all of these projects contain pavement edge drains.

Data collected from Interstate 71 illustrate that the breaking pattern of 76 to 304 mm (3 to 12 in.) would provide the best performance (on the basis of the amount of observed reflective cracking and analysis of condition points). The current Kentucky specifications require the breaking pattern of 457 to 609 mm (18 to 24 in.). This pattern has been chosen on the basis of Kentucky's experience in the construction of these

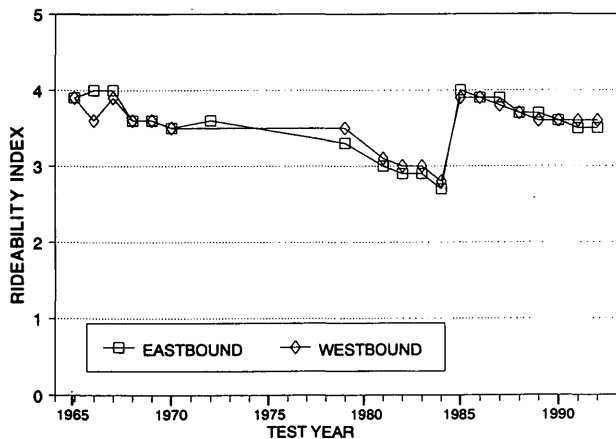


FIGURE 14 Rideability index, Bluegrass Parkway.

types of pavements. This pattern provides for good constructibility and overall performance.

This method of rehabilitation is considered to be a cost-effective means of extending the service life of the pavement structure. These procedures have been developed through experience in Kentucky. Therefore, conditions in other states may not yield the same type of performance. Kentucky's successful experience with this type of rehabilitation may provide other states with guidelines for development of specifications based on their own experience. On the basis of its experience over the last 10 years, Kentucky will continue to use breaking and seating of concrete pavements as a rehabilitation alternative.

ACKNOWLEDGMENTS

The study reported herein was funded by FHWA and the Kentucky Transportation Cabinet through the University of Kentucky Research Foundation.

REFERENCES

1. G. W. Sharpe, M. Anderson, and R. C. Deen. *Breaking and Seating of Rigid Pavements*. Research Report. Kentucky Transportation Research Program, University of Kentucky, Lexington, Oct. 1987.
2. *Guidelines and Methodologies for the Rehabilitation of Rigid Highway Pavements Using Asphalt Concrete Overlays*. Pavement Consultancy Services, Division of Law Engineering, Inc., Beltsville, Md., June 1991.
3. H. F. Southgate, G. W. Sharpe, R. C. Deen, and J. H. Havens. *Structural Capacity of In-Place Asphaltic Concrete Pavements from Dynamic Deflections*. Research Report. Kentucky Transportation Research Program, University of Kentucky, Lexington, Aug. 1981.

The contents of this paper reflect the views of the authors, who are responsible for the facts and accuracy of the data presented here, and do not necessarily reflect the official views or policies of the sponsoring agencies. This paper does not constitute a standard, specification, or regulation. The inclusion of manufacturer names and trade names are for identification purposes and are not to be considered as endorsements.

Publication of this paper sponsored by Committee on Pavement Rehabilitation.

Direct Tension and Simple Stiffness Tests—Tools for the Fatigue Design of Asphalt Concrete Layers

JAMES M. MATTHEWS AND CARL L. MONISMITH

A design strategy with fatigue as the major concern and with a check on rutting was developed using creep and direct tension tests as simple tools. This design is appropriate for the heavy-duty asphalt concrete pavements subject to the environmental and traffic conditions that exist in the state of California. Two types of asphalt cements (AR 4000 and AR 8000) with the California standard 0.5-in. maximum size, medium grade, granite aggregate were used. Hveem stabilometer tests were used to derive the design asphalt contents. Uniaxial unconfined creep tests were conducted to determine the stiffness of the mix. The environments in the state of California were divided into five groups. Full-scale fatigue and direct tension tests were conducted for three temperatures. From these test results equations were developed to predict the fatigue life through the direct tensile stress and simple stiffness. Thus the fatigue testing program, which is time consuming and costly and requires special equipment, was eliminated. Finally several pavement case studies were designed, and the best of these were selected for each of the environmental groups.

With increasing frequency, user agencies in developed and developing countries have been reporting problems with fatigue and rutting distress in the performance of highways at all agency levels—city, county, state, and federal. To minimize these pavement distresses, mixture and pavement design methods should be considered together.

PURPOSE AND SCOPE

The objective of this paper is to present the development of a design strategy, with fatigue as the major concern, using simple tools such as direct tension and uniaxial creep tests. The design system is appropriate for heavy-duty asphalt concrete pavements (AC) subject to traffic and environmental conditions such as those in the state of California. This work concentrates on the development of solutions to mitigate fatigue with a check on rutting. This paper does not cover the design procedure for rutting; however, a check on rutting was done for the sake of completeness of the design procedure. Other forms of distresses (for example, thermal cracking and raveling) are not included in this study. This study is limited to hot-mixed asphalt concrete, excluding, for example, open-graded friction courses and drainage layers.

J. M. Matthews, Department of Civil Engineering, Temple University, Philadelphia, Pa. 19122. C. L. Monismith, Institute of Transportation Studies, University of California, Berkeley, Calif. 94720.

There are no design charts that cover all the temperature conditions in California available to field engineers for designing highways with fatigue as the major concern; full-scale fatigue testing for at least two or three temperature conditions is necessary. Fatigue testing is time consuming and costly and requires special equipment. The materials studied in this investigation are commonly used in the state of California. Therefore, the development of a design procedure for heavy-duty asphalt concrete pavements that does not require fatigue testing and that incorporates charts that cover the traffic and environmental conditions in the state would be a significant benefit to the field engineer.

MATERIALS AND MIXTURE PROPERTIES

The aggregates and asphalt use, requisite properties, test methods, and criteria to define these properties were given previously (1). The properties of the desired mixture, with some of the factors that influence these properties, were also given before (1). Past experience at the University of California indicated that AR 4000 and AR 8000 asphalt cements with the properties given in Table 1 and Watsonville granite aggregate with 0.5-in., maximum-size medium gradation (California standard) would pass these standards and requirements for the preparation of asphalt concrete mixes for constructing heavy-duty pavements.

The Hveem stabilometer method was used to determine the design asphalt content (Figure 1). For Class A concrete, California standard (2) stipulates a minimum relative stability of 37. Figure 1 indicates that a 5.5 percent asphalt content meets this requirement. To reflect the quality control during the construction, a lean of 0.3 percent asphalt content should be provided (2). Therefore an average design asphalt content of 5.2 percent (by weight of aggregate) was selected for both asphalts.

SAMPLE PREPARATION, TESTING EQUIPMENT, AND TESTING TECHNIQUES

Sample Preparation

Two types of mixes were prepared using Watsonville granite aggregate and AR 4000 and AR 8000 asphalt cements for the gradation selected. All the samples were compacted using the Triaxial Institute kneading compactor. For creep tests, cylin-

TABLE 1 Properties of Asphalts Used in Study

	AR-8000 CR88R-5009	AR-4000 CR88R-5020
Penetration at 77F. dmm	46	72
Viscosity at 140F. poise	3786	2125
Viscosity at 275F. cSt.	425.8	350.8
RTFC Residue		
Penetration at 77F. dmm	29	37
Viscosity at 140F. poise	8764	4882
Viscosity at 275F. cSt.	620.8	501.4

(Tests are performed by Chevron Research Corporation)

dricul specimens 4 in. in diameter and 9 in. in height were initially compacted. Then the material at the ends was trimmed off with a diamond saw to produce the final specimens about 8 in. in height. The top and bottom surfaces were then capped with a thin layer of hydrostone to obtain smooth surfaces for load application. Fatigue beams 4 × 3.75 in. in rectangular sections and 15 in. in length were cast in three layers. Then specimens 1.5 × 1.5 × 15 in. were cut using a diamond saw after freezing the sample for 8 hr at 5°F. From one fatigue sample, two direct tension specimens, each 1.5 × 1.5 × 6 in., were cut by the diamond saw.

Test Procedure

Specific gravity and air void content were determined and cross-sectional measurements were taken for all specimens

before testing. The air void contents for the 6 and 5.2 percent asphalt content samples were 4.8 and 6.5 percent with coefficients of variation of 0.1 and 0.1, respectively.

Creep Tests

Creep tests were performed in axial compression in the unconfined condition. The detailed procedure followed in conducting the creep test is beyond the scope of this paper and is given elsewhere (3). Tests were performed at temperatures of 77°F, 100°F, 120°F, and 140°F. The pressures applied were 22 lb/in.² on AR 4000 specimens at 140°F; all other specimens were tested at 30 lb/in.². AR 4000 coarse aggregate samples were not tested at 140°F because the mix is unsuitable for withstanding this high temperature. An IBM personal com-

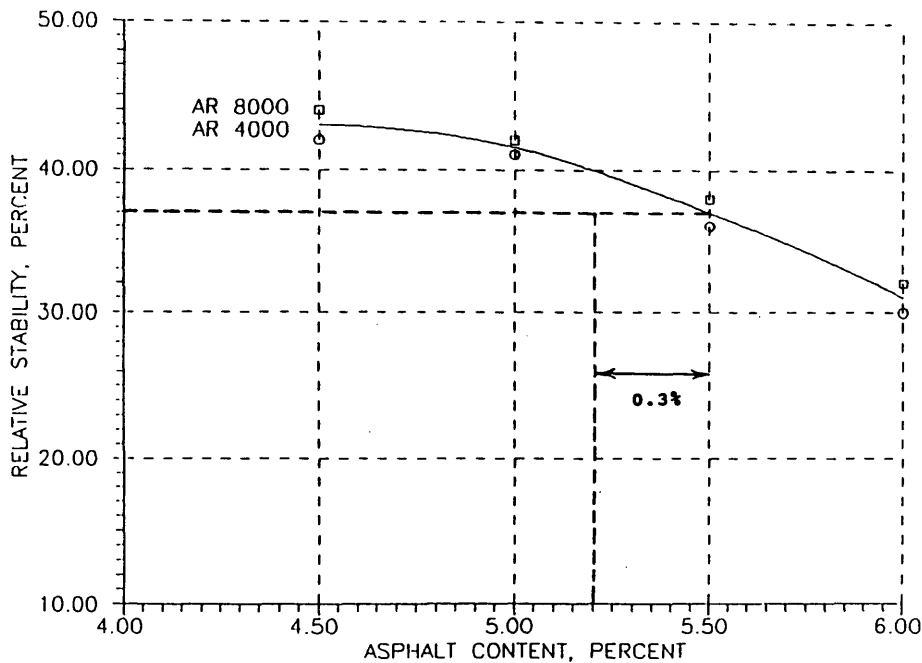


FIGURE 1 Stability versus asphalt content.

puter was used to control the load, record both the load and the deformation, and determine the compliance as a function of time. Creep moduli as a function of time were calculated as the quotient of applied stress divided by total strain at a particular time. A total of 24 creep tests were conducted. Three specimens were tested for each test condition, and the average value was computed. The results of the tests are given in Figure 2. From these results the relationship between the temperature and stiffness at 0.1-sec loading time was derived as shown in Figure 3.

Fatigue Tests

Equipment used by Epps (4) was used for conducting fatigue tests. For heavy-duty asphalt pavements controlled fatigue tests are applicable, as suggested by Monismith et al. (1). Therefore fatigue tests were conducted under controlled stress conditions. A total of 56 specimens were tested with groups of seven specimens representing one test condition. The test conditions consisted of two stress levels, two types of asphalts, and two temperatures. The two temperatures were 90°F and 110°F. Epps (4) tested the same materials at 68°F. The remaining test conditions were the same in both cases [Epps (4) and the present study]. Results of Epps were used for 68°F. The loading duration was 0.1 sec with a rest period of 0.5 sec. Although the tests were done at the design asphalt content (5.2 percent) and 0.8 percent more than the design asphalt content (6 percent), the results of 6 percent asphalt content were used for further analysis, for reasons explained in the section entitled Design Implications. Figure 4 (stress-versus-fatigue life relationship) and Figure 5 (strain-versus-fatigue relationship) show the results of 6 percent asphalt content. The stress-versus-fatigue life relationship had better sensitivity with respect to the temperature than that of the strain-

versus-fatigue relationship (4). This is consistent with the well-established concept of the strain criterion. Therefore the stress-versus-fatigue life relationship was used in the analysis. The influence of temperature on the fatigue bending stress for various repetitions is shown in Figures 6 and 7.

Direct Tension Tests

The testing system similar to the one developed by Epps (4) was used in this study. Temperature control was achieved by placing the samples, well packed with two layers of 1-in. thick fiberglass sheets, in the control cabinet. The required temperature was maintained within an accuracy of 1°F. Each test was completed within 5 sec after removing the sample from the temperature control cabinet. While the test was being conducted the insulation remained intact on the sample. Because obtaining complicated test parameters [e.g., the linearity loss of the stiffness of the LCPC (5)] is not feasible for the field engineer, the objective of this paper is to use simple tests for the design of highways. A simple parameter in the direct tension test is the tensile stress at break; hence, this parameter was selected in the present study. Epps (4) also studied the behavior of asphalt concrete mixes under direct tensile stresses for similar materials with a deformation rate of 0.3 in./min. This rate would produce tensile failure in the specimen in about 0.1 sec, which corresponds to the same timing of loading in fatigue tests. Hence, all the tests were done at a constant strain rate of 0.3 in./min. Tensile stress at break was computed for each specimen for the same variables as those used to define the fatigue test results. The air void content and coefficient of variation were the same for fatigue and direct tension specimens. Two asphalt contents (5.2 and 6 percent) were tested and, as in the case of fatigue, a total of 84 direct tension tests were conducted for each asphalt content (see Figure 8).

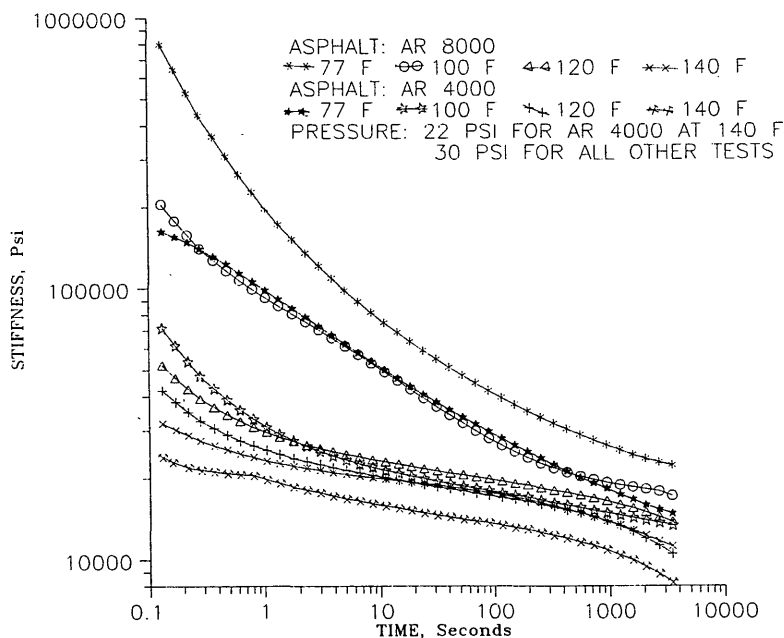


FIGURE 2 Axial creep test results for medium grade aggregates.

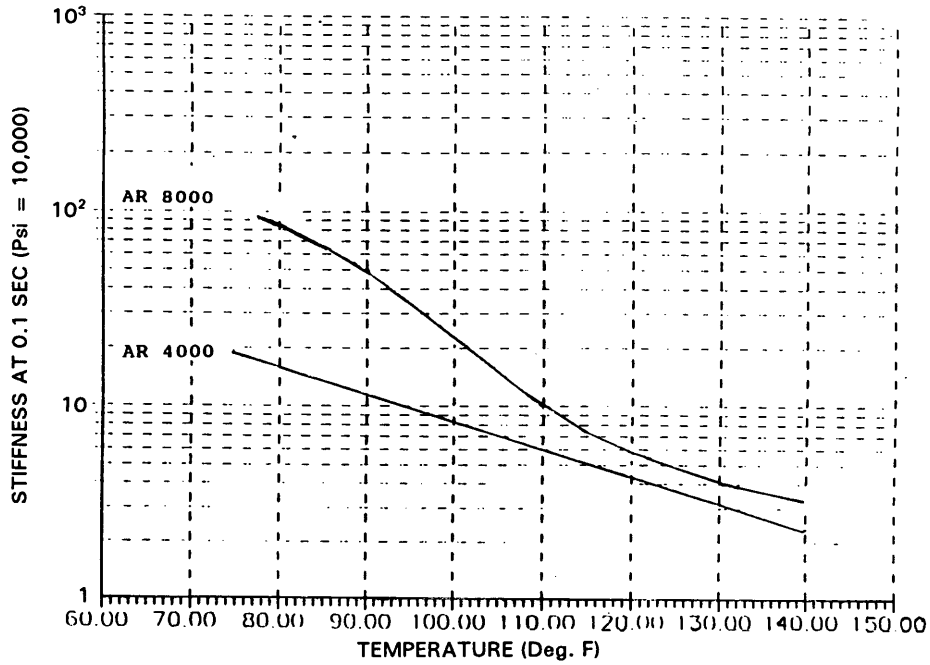


FIGURE 3 Temperature versus stiffness at 0.1 sec; pressure = 30 lb/in.²

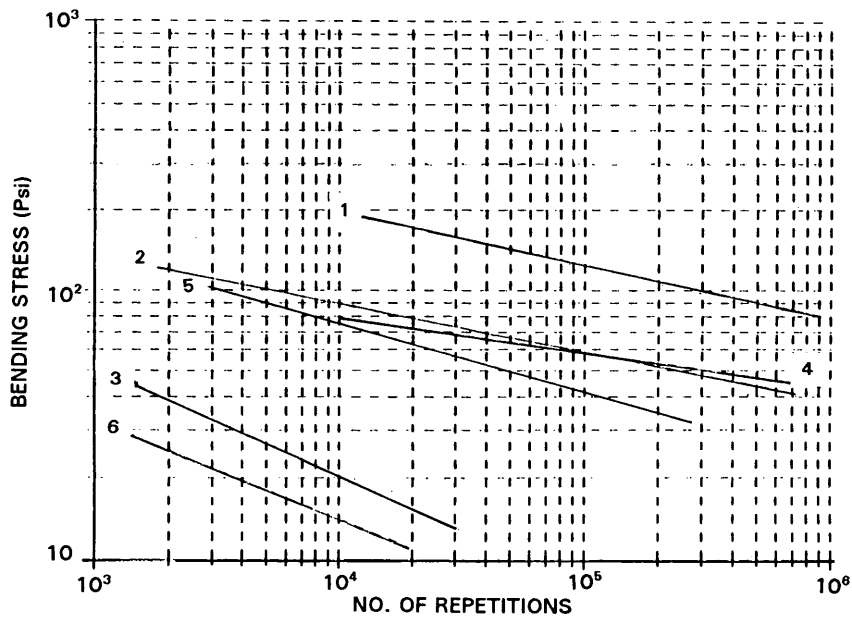


FIGURE 4 Influence of asphalt type and temperature on fatigue life (medium aggregate; 6.0 percent asphalt content; solid lines, AR 8000 [(1), 68°F; (2), 90°F; (3), 110°F]; dashed lines, AR 4000 [(4), 68°F; (5), 90°F; (6), 110°F].

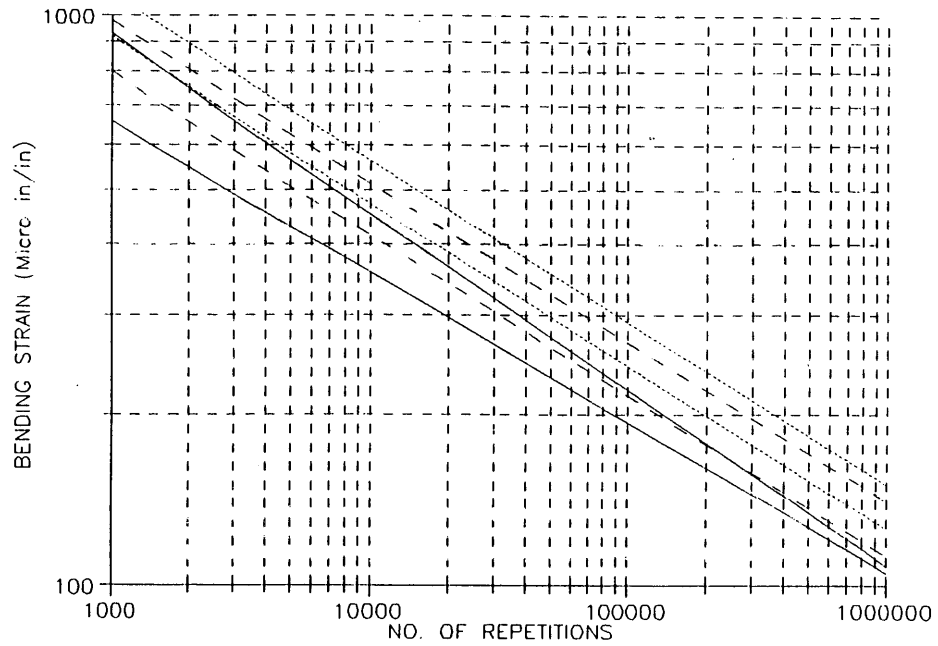


FIGURE 5 Fatigue life versus bending strain: solid lines, 68°F; dashed lines, 90°F; dotted lines, 110°F. In each case, upper line represents AR 4000 and lower line represents AR 8000.

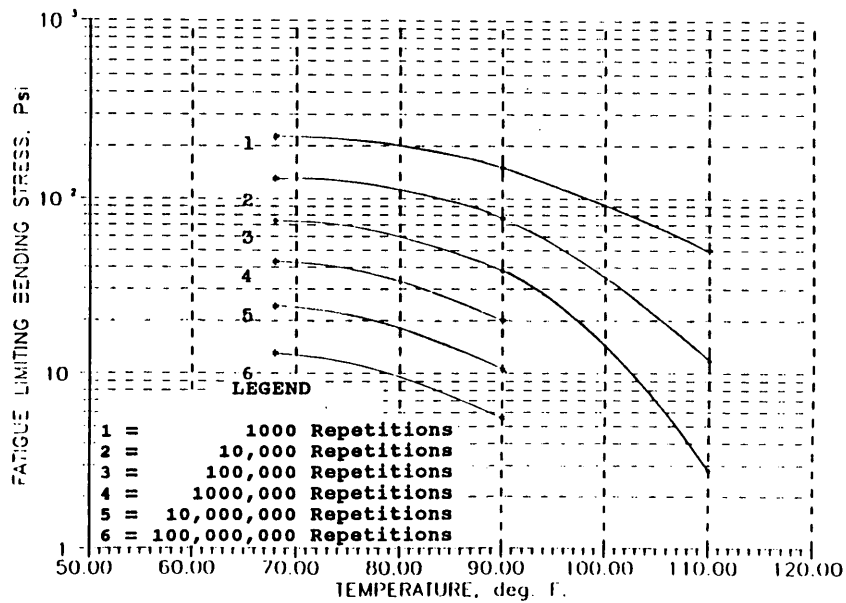


FIGURE 6 Influence of temperature on fatigue limiting bending stress for various repetitions (AR 4000; aggregate, granite, Cal.; asphalt content, 6.0 percent; std. 0.5 in. medium).

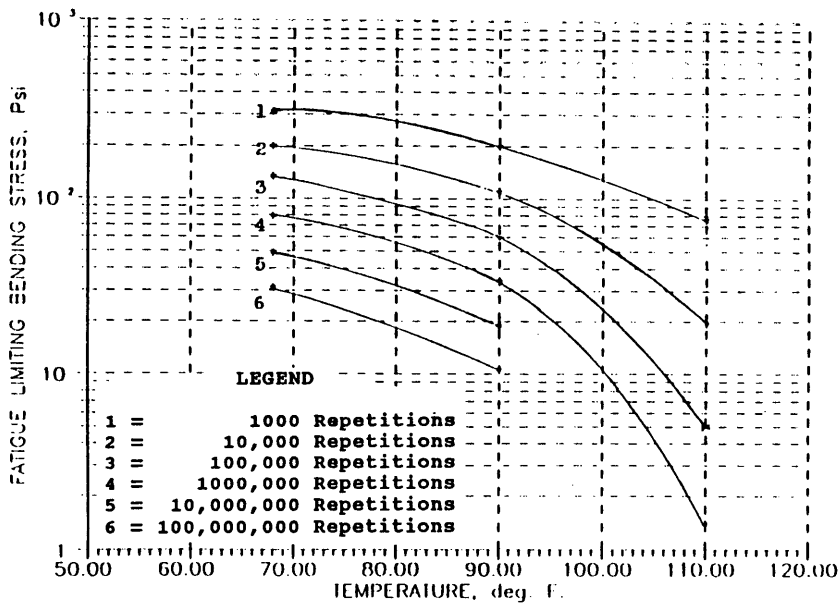


FIGURE 7 Influence of temperature on fatigue limiting bending stress for various repetitions (AR 8000; aggregate, granite, Cal.; asphalt content, 6.0 percent; std 0.5 in. medium).

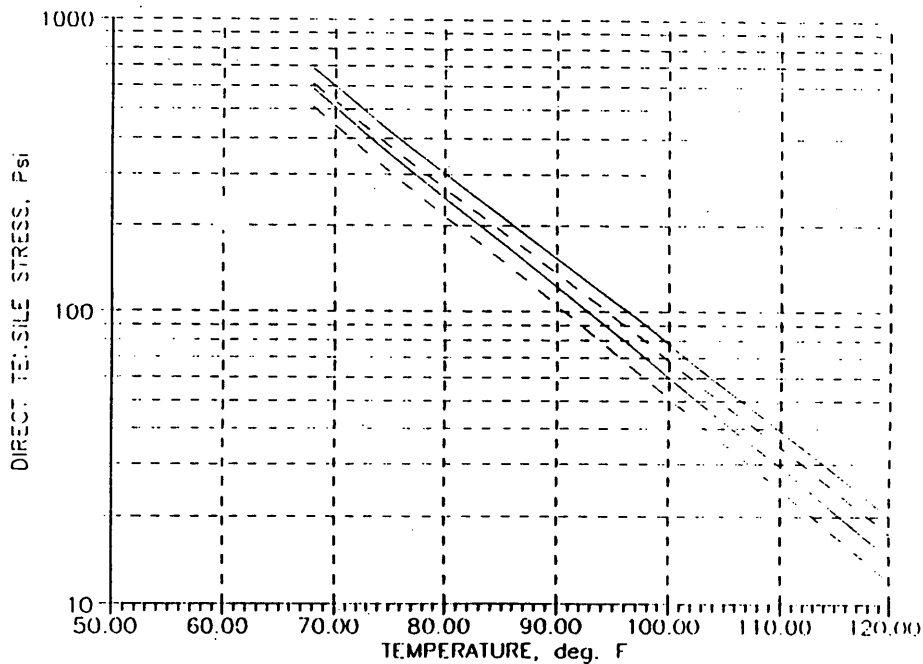


FIGURE 8 Influence of temperature on direct tensile stress (solid lines, 6 percent asphalt content; dotted lines, 5.2 percent asphalt content). In each case, upper line represent AR 8000 and lower line represents AR 4000.

DEVELOPMENT OF DESIGN STRATEGY WITH FATIGUE AS THE MAJOR CONCERN

Influence of Maximum Tensile Stress on Thickness of AC Layer

A multilayer linear elastic analysis was conducted using the ELSYM computer program. About 300 case studies of pavement structural sections were studied, and tensile stresses at the bottom of the AC layer were determined for a set of six variables with the following ranges. These ranges are fairly typical of those usually found in traffic and environmental conditions in the state of California for heavy-duty pavements.

1. Subgrade stiffness, 5,000 to 20,000 lb/in.²;
2. Base stiffness, 10,000 to 40,000 lb/in.²;
3. AC stiffness, 20,000 to 800,000 lb/in.²;
4. Thickness of base, 0 to 24 in.;
5. Thickness of AC layer; 3 to 40 in.; and
6. Tensile stress (bottom of AC), 0 to 450 lb/in.²

The ELSYM computer program consisted of a dual-wheel configuration. Each wheel weighing 4,500 lb had a tire pressure of 100 lb/in.² and a radius of contact of 3.79 in. There was a free space of 3.79 in. between the two wheels. Typical results are shown in Figures 9 and 10.

Relating Direct Tensile and Fatigue Bending Stresses

From the laboratory test results, charts were developed that related the direct tensile stress and the fatigue bending stress for various wheel load repetitions ranging from 1,000 to 100 million, for the temperature range 68°F to 110°F in 5°F in-

crements. Typical graphs are shown in Figures 11 through 13; detailed results were given previously (3). The results shown in Figures 6 and 8 were used to develop graphs in Figures 11 through 13. From Figure 8 one can obtain 570 lb/in.² as the direct tensile breaking stress for (a) 6 percent asphalt content, (b) AR 4000 asphalt, and (c) 68°F. From Figure 6 for the same data, one can obtain 225 lb/in.² as the fatigue limiting bending stress for 1,000 repetitions and obtain a point (abscissa, 225 lb/in.² bending stress; ordinate, 570 lb/in.² direct tensile stress) of Curve 1 in Figure 12. Similarly Curve 1 is completed by varying the asphalt content, and Curves 2 and 5 are plotted by changing the load repetitions. A total of 84 fatigue tests consisting of two asphalt contents were conducted in this study. An enormous increase in the repetitive work could produce a slight improvement in the accuracy of the results by increasing the amount of asphalt content. However, this is considered beyond the scope of this paper.

To account for the differences between laboratory and field responses, shift factors are necessary to translate laboratory fatigue characteristics into those considered to be representative of in situ performance. Because of mix age, stiffness of in-service pavements increases for a considerable duration. However, once microcracks start (when the major portion of pavement life is consumed) the stiffness starts decreasing. For thick asphalt pavements (controlled stress fatigue tests) an increase in stiffness increases the fatigue life. Although the influence of age hardening on the fatigue life of individual pavement varies, this phenomenon leads to a conservative design. For tests in which there are rest periods between load applications, usually a factor less than 20 is used (6). Finn et al. (7) suggested a factor of 13 for predicting up to 10 percent cracking in the wheelpath area for California-type mixtures. This factor was used in the present study because the materials used herein are commonly used in the state of California for

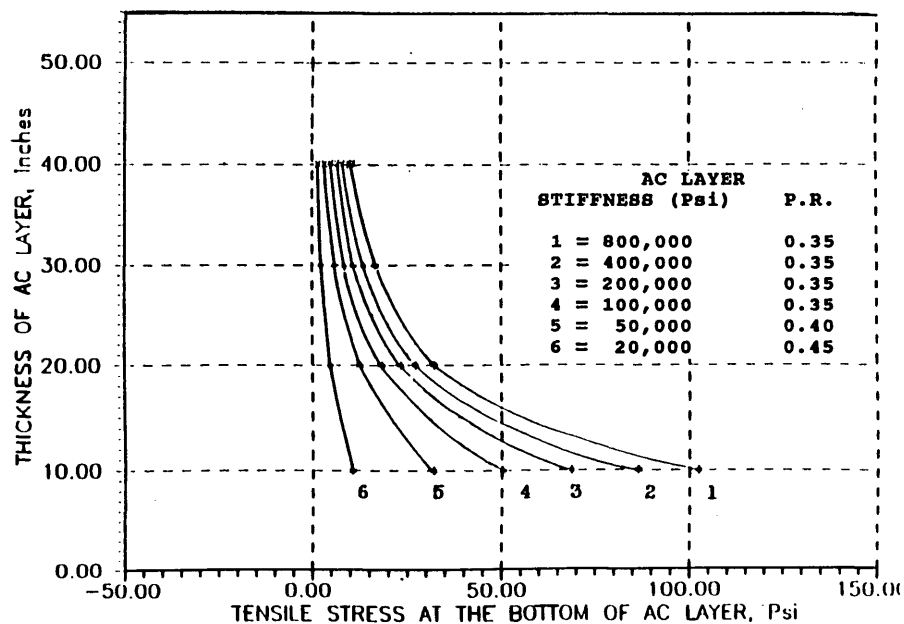


FIGURE 9 Full-depth AC pavement thickness versus tensile stress in AC layer (base thickness, 0 in.; subgrade, E = 10,000 lb/in.²; P.R. = 0.35).

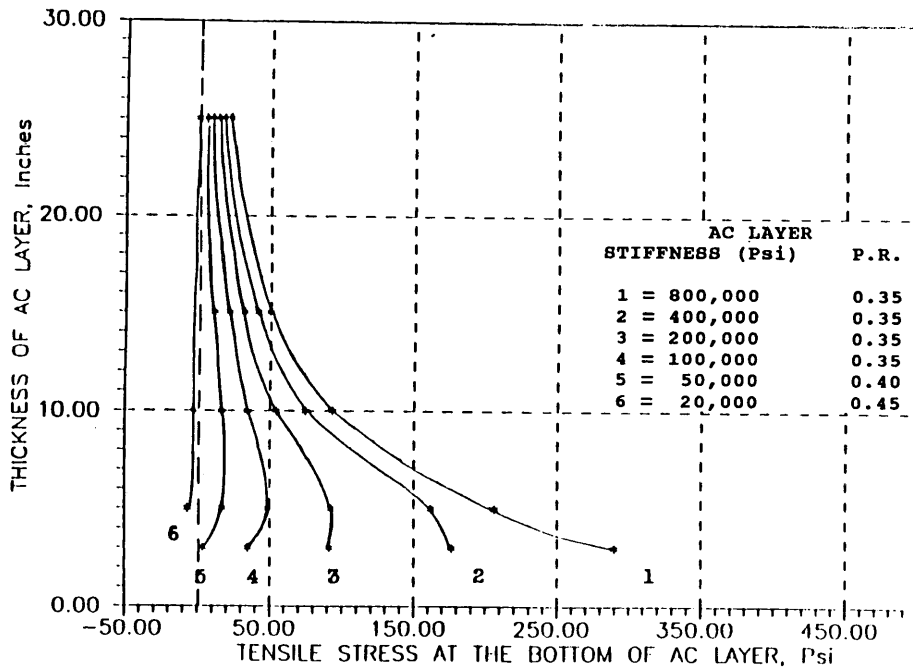


FIGURE 10 Thickness versus tensile stress in AC layer. Base: $h = 12$ in.; $E = 20,000$ lb/in.²; P.R. = 0.35. Subgrade: $E = 10,000$ lb/in.²; P.R. = 0.35.

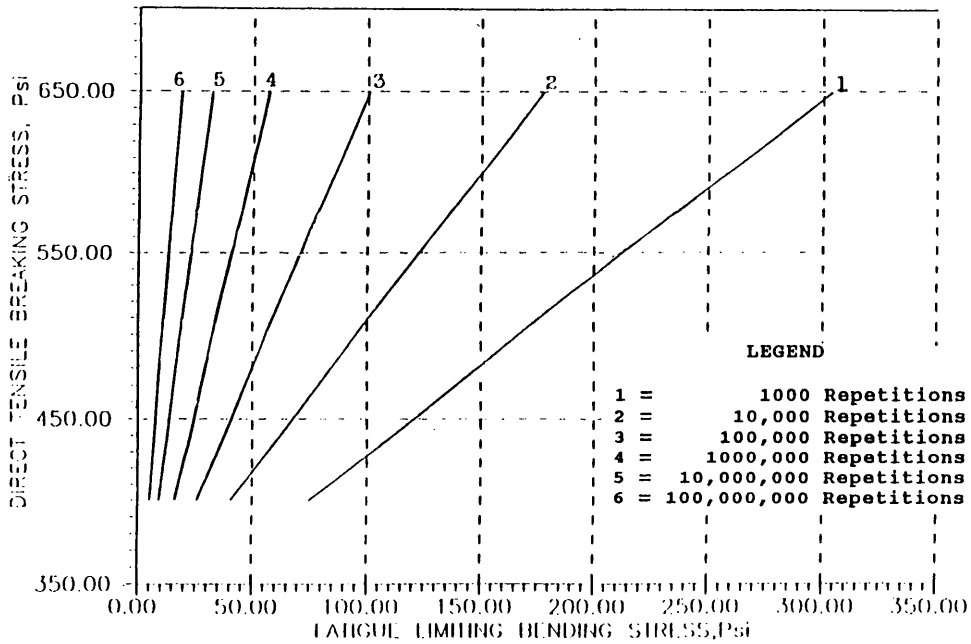


FIGURE 11 Direct tensile stress versus fatigue bending stress for various repetitions (AR 4000; aggregate, granite; 68°F; Cal. std. 0.5 in. medium).

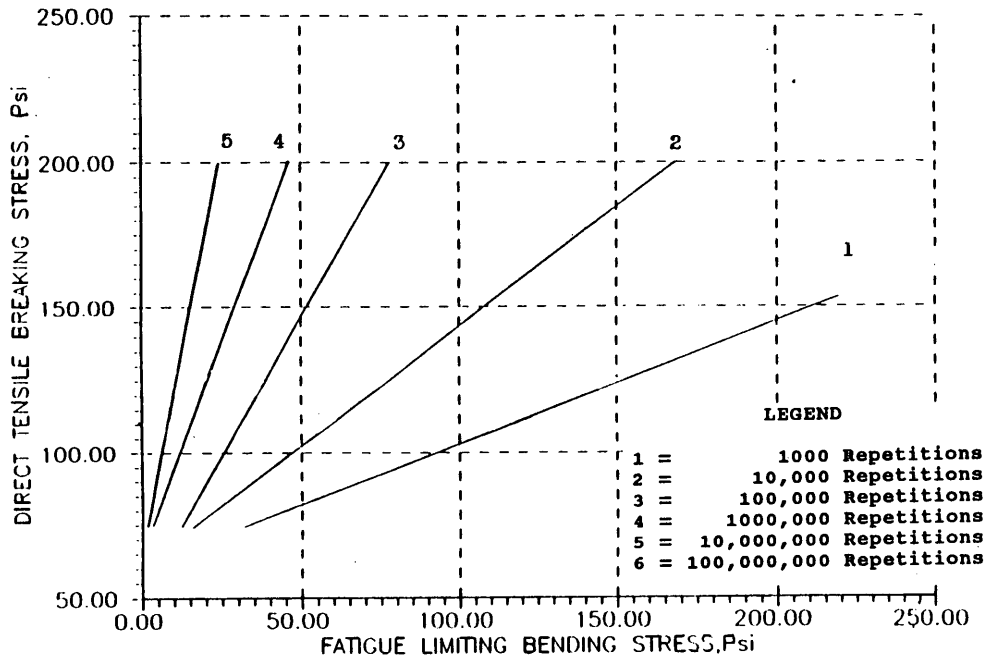


FIGURE 12 Direct tensile stress versus fatigue bending stress for various repetitions (AR 4000; aggregate, granite; 90°F; Cal. std. 0.5 in. medium).

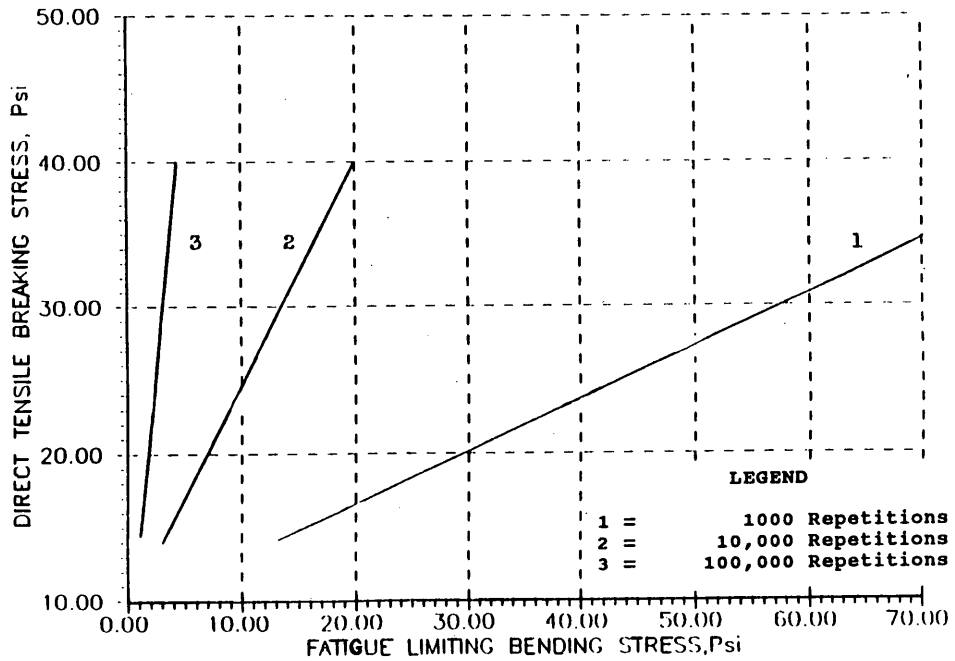


FIGURE 13 Direct tensile stress versus fatigue bending stress for various repetitions (AR 4000; aggregate, granite; 110°F; Cal. std. 0.5 in. medium).

the construction of heavy-duty asphalt pavements. The number of load repetitions in Figures 11 through 13 represent the laboratory fatigue load repetitions. In selecting the design traffic (in terms of cumulative standard axles), the load repetitions of Figures 11 through 13 are multiplied by the factor 13.

Categorization of Environmental Conditions of California

Table 2 gives a summary of the five categories with a typical example city in California. For these zones the mean monthly air temperatures (MMAT) were averaged from data taken during the past 30 years (8). The mean monthly pavement temperatures (MMPT) were calculated according to Witzak's equation (9).

First Trial Thickness

Once the location and design traffic are selected, trial thickness can be calculated using the charts shown in the design manual of the Asphalt Institute (10). An example chart is shown in Figure 14. From this chart AC layer thickness can be obtained if equivalent single-axle load (EAL), subgrade resilient modulus (MR), aggregate base thickness, and MMAT are known.

Tensile Strength of Mix

The relationships between tensile stress at break and temperature are shown in Figure 8. Alternately, field engineers can use the results of direct tension tests of their mixes.

Stiffness of Mix

The stiffness of the mix was obtained from the results of the creep tests as shown in Figure 3, or field engineers can use the results of creep tests of their mixes.

Determination of Fatigue Bending Stress

For the highest MMPT (usually this occurs in July), the fatigue bending stress can be found from Figures 11 through 13 for the appropriate values of direct tensile stress and design traffic.

Second Trial Thickness

For a selected type of pavement structure (e.g., a pavement with a 24-in. thick untreated aggregate base), with the stiffness of the mix and the fatigue bending stress obtained as described above, the AC layer thickness can be obtained from Figures 9 and 10. The fatigue bending stress corresponds to the highest

TABLE 2 Classification of Overall Temperature Conditions

CITIES BY GROUPS	AVERAGE	AVERAGE			RANGE
	YEARLY AIR TEMP. °F	YEARLY AIR TEMP. FOR THE GROUP °F	AIR TEMP. JAN. MIN. °F	TEMP JULY MAX. °F	
I VERY HOT					
Death Valley	75.3				
Needles FAA Airport	73.2	73.2	52.1	97.2	
(This is taken as Representative city for group I)					
Barstow	69.0				
II HOT					
Bakersfield	63.3				
Modesto	61.4				
Fresno	63.9	63.9	43.0	86.0	
(This is taken as Representative city for Group II)					
III MODERATELY HOT					
Sacramento Airport	59.9	59.9	42.4	77.0	
IV COASTAL					
San Diego	64.5				
(Extreme South)					
Eureka	52.4				
(Extreme North)					
San Francisco	58.6	58.6	50.0	64.1	
(This is taken as Representative city for Group IV)					
V COLD					
Eureka	52.4	52.4	47.9	58.6	

MAAT 75°F

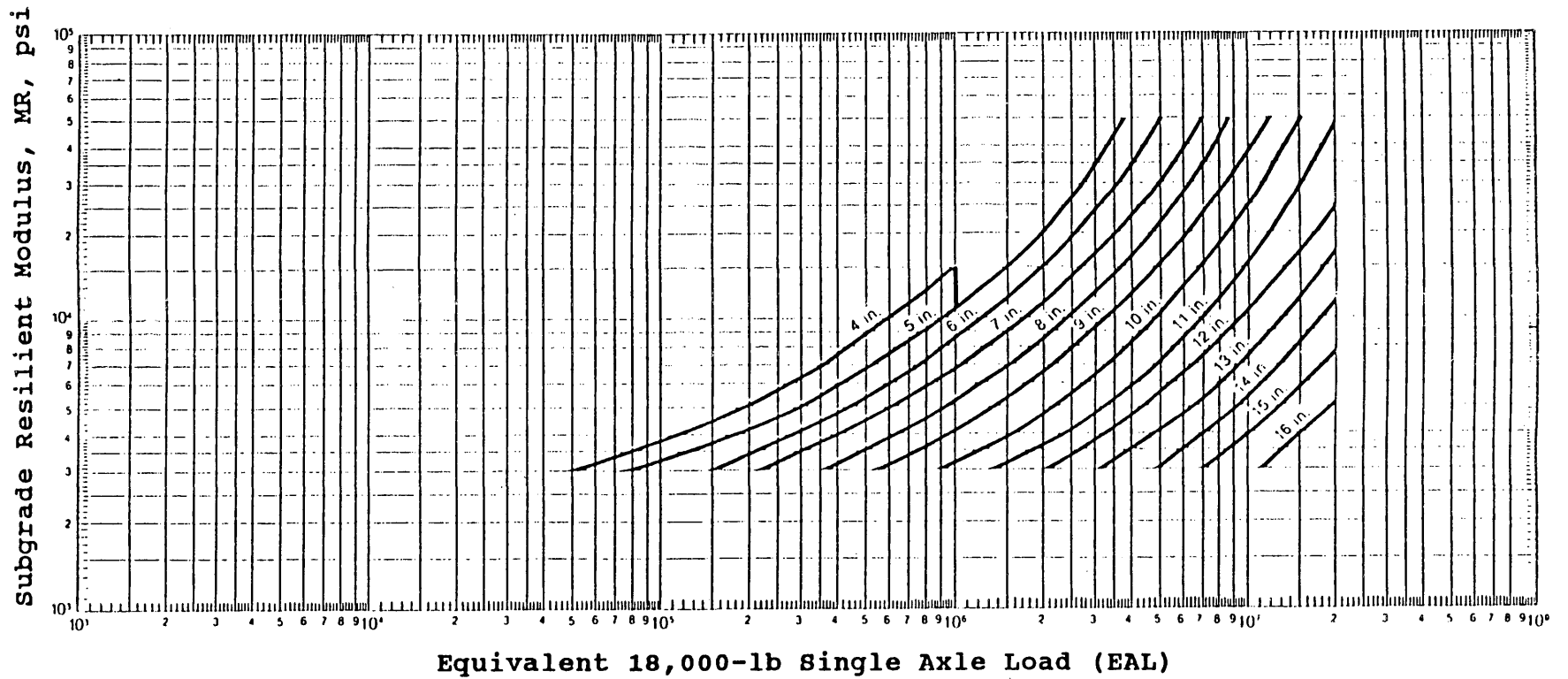


FIGURE 14 Asphalt Institute chart for determining trial thickness (*I*₀) (untreated aggregate base, 12-in. thickness).

MMPT value. Because an increase in temperature reduces the viscosity of asphalt (hence the stiffness of mix) logarithmically, a major portion of the life of the pavement is consumed in the hottest month. Therefore, the second trial thickness targets the performance of the AC layer during the hottest month. The thickness obtained during that month will be modified to reflect the fractions of damage to the life of the pavement during the other months, as shown in the third trial thickness. This thickness is sufficient to carry traffic during the hottest month in every year during the design period. Experience has shown that the final design thickness usually is within a range of 1 and 1.5 times the second trial thickness.

Third Trial Thickness

The third trial thickness involves an iterative process. The second trial thickness was multiplied by a factor of 1.25. Using Figures 9 and 10 for the values of the second trial thickness and the stiffness of the AC layer obtained earlier, the tensile stress at the bottom of the AC layer was found. From the set of MMPT values and the direct tensile and fatigue bending stresses, the cumulative number of standard axles that possibly can pass were obtained each month (Figures 11 through 13).

By applying the cumulative damage hypothesis (the ratio of the actual number of axles that need to pass divided by the

possible number of axles that can pass) the fraction of design life consumed was calculated for each month of the design period.

If the sum of the fractions of life consumed was less than unity, then the third trial thickness became the final design thickness; otherwise further iterations were continued until the cumulative damage fraction became less than unity.

Subgrade Vertical Strain Criterion

The subgrade vertical strain criterion was verified by using the Asphalt Institute's equation, and it was found that all the sections satisfied the criterion.

Case Studies for Fatigue Design

A total of 19 case studies consisting of various pavement structural compositions, asphalt types, traffic intensities, and temperature levels were analyzed. These case studies represent a variety of conditions and are appropriate for the design of heavy-duty asphalt concrete pavements in California. Detailed calculations were conducted for full-depth AC and AC with 4, 8, 12, and 24 in. of base for all the environmental conditions. As an example, the detailed calculations are shown in Tables 3 and 4 for Environmental Condition 3.

TABLE 3 Design of Full-Depth AC Layer for Group 3 Conditions

MONTH	MMPT °	DIRECT TENSILE BREAKING PSI	STIFFNESS AT 0.1 SEC PSI	LIMITING BENDING STRESS PSI	# AXLE REPETITIONS POSSIBLE = LIFE * 10 ⁵	FRACTION OF LIFE CONSUMED
J	52.0	>1000	440,000	>25.0	>>8.3	Negligible
F	57.3	>1000	410,000	25.0	>>8.3	Negligible
M	60.9	940	390,000	24.5	>8.3	<0.01
A	66.4	640	330,000	23.5	>8.3	<0.01
M	73.4	390	260,000	22.5	190	0.04
J	80.3	240	180,000	21.3	60*	0.138
J	85.3	170	170,000	21	25	0.33
A	83.8	185	175,000	21.2	60	0.14
S	81.1	240	195,000	21.5	97	0.09
O	72.2	465	270,000	22.6	480	0.017
N	60.7	950	395,000	24.6	>8.3	<0.01
D	52.8	>1000	450,000	>25.0	>>8.3	Negligible

Fraction of life consumed = 0.785

1st trial thickness = 14 inches

2nd trial thickness = 19 inches

Design thickness = 21 inches

TABLE 4 Design of AC Layer with 12-in. Base for Group 3 Conditions

MONTH	LIMITING BENDING STRESS psi	NO. OF AXLE REPETITIONS POSSIBLE * 10 E5	FRACTION OF LIFE CONSUMED
J	>30.0	>>8.3	Negligible
F	30.0	>>8.3	Negligible
M	28.1	>>8.3	Negligible
A	23.3	550	0.015
M	20.4	180	0.046
J	20.3	65	0.128
J	20.0	27	0.307
A	20.2	65	0.128
S	20.9	98	0.085
O	23.7	440	0.019
N	28.3	>>8.3	Negligible
D	30.0	>>8.3	Negligible

Fraction of life consumed = 0.728

Design thickness = 19

Development of Equivalency Factors

The influence of base thickness, ranging from 0 to 24 in., on the thickness of the AC layer is shown in Figure 15. From these graphs equivalency factors were developed describing the relationships between the thicknesses of the AC and the base layers for all the environmental conditions, as shown in Table 5.

Determination of Optimal Thickness of the AC Layer

For each location and type of material used, there exists a cost relationship between the thickness of the AC layer and that of the base layer. Assuming a cost ratio of 3.5 (i.e., the cost of 1 in. of AC layer is equal to the cost of 3.5 in. of base), the thickness of the AC layer was determined from Table 6 for each environmental condition. For example, from Figure 14 and Table 5 it is seen, in the case of Environmental Condition 1, that 1 in. of base can reduce the design thickness of AC layer by about 1 in. for the first 4 in. of base thickness. Since the cost differs by a factor of 3.5, this is the largest saving and hence the strongest argument for the AC to be replaced by the base. Using a similar justification, up to 9 in. of base can be provided. In developing countries an AC layer is usually several times costlier than that of the base (because of the high cost of asphalt and cheap manual labor); therefore, a cost ratio of 1:10 (AC:base) might be appropriate. Table 6 also shows the design results with an optimal base for this cost ratio. A summary of the design results with fatigue as the major concern is provided in Table 7.

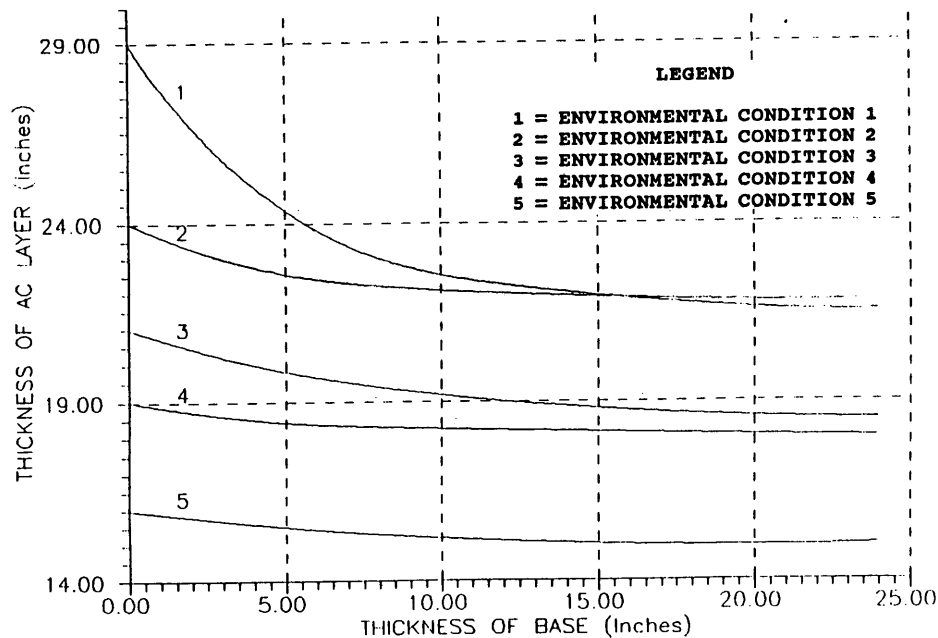


FIGURE 15 Influence of base thickness on thickness of AC layer for the five environmental conditions.

TABLE 5 Development of Equivalency Factors of AC Thickness for 1-in. Base Thickness (1 in. AC = 10 in. UTB)

Environmental Group	RANGE OF BASE THICKNESS			
	0-4	4-8	8-12	12-24
I (one in. of AC is reduced by one)	1.0	0.5	0.175	0.058
		two	six	seventeen inches of base)
II (one in. of AC is reduced by two & half)	0.375	0.1	0.025	0.017
		ten	forty	sixty inches of base)
III (one in. of AC is reduced by four)	0.25	0.15	0.1	0.04
		six & half	ten	twenty-four inches of base)
IV (one in. of AC is reduced by eight)	0.125	0.05	0.03	0.015
		twenty	twenty-three	sixty-six inches of base)
V (one in. of AC is reduced by ten)	0.10	0.07	0.035	0.025
		fourteen	twenty-eight	forty inches of base)

Equations For Predicting Fatigue Life

For each environmental condition, during the four most influential months (June, July, August, and September, which account for about 97 percent of the consumed life) seven data sets of MMATs were obtained for alternate years from 1976 through 1988 (11). From these MMATs, using Witczak's equation (9), MMPTs were calculated. Direct tensile stress, stiffness value, and fatigue life of the asphalt concrete were also calculated using the procedure explained in previous sections. Multiple regression equations were derived from about

28 data observations, and a summary of the statistical analysis is given in Table 8. Large correlation coefficients ranging from 0.82 through 0.93 were obtained between the independent and dependent variables, as shown in Table 8. The correlation coefficients are statistically significant at the 95 percent confidence interval.

$$\text{Log } N_f = 0.112 * T + 0.036 * S_{\text{mix}} + 0.292 \tag{1}$$

(Environmental Condition 1)

TABLE 6 Optimum Base and AC Thicknesses for 10-in. Base = 1 in. AC and 3.5-in. Base = 1 in. AC

Environmental Group No.	One inch of AC =			
	10 inches of Base		3.5 inches of Base	
	Base (in.)	AC (in.)	Base (in.)	AC (in.)
I	14	22	9	22.8 say 23
II	8	23	5	22.4 say 23
III	12	19	4	20.0
IV	3	19	2	18.7 say 19
V	4	16	Full Depth	16.0

All AC thicknesses are rounded off to next inch.

TABLE 7 Summary of Design Results with Fatigue as the Major Concern

Env. Design Cond. Traffic Std. Axles	Stiffness of Subgrade Base (Millions) (Psi)	Stiffness of Base (Psi)	Max. MMPT (°F)	Asphalt Type	Design Thicknesses			
					Full Depth AC (1" In)	With Opt. Base AC = 3.5" In)	Base AC (In)	
1	13	20,000	40,000	107.6	AR8000	29	9	23
	1	20,000	40,000	107.6	AR8000	15	4	14
2	130	10,000	20,000	92.2	AR8000	24	5	23
	10	10,000	20,000	92.2	AR8000	16	4	15
3	130	10,000	20,000	85.3	AR4000	21	4	20
	10	10,000	20,000	85.3	AR4000	14.5	2	14
4	130	5,000	10,000	70.4	AR4000	19	2	18.6 (rounded to 19)
	10	5,000	10,000	70.4	AR4000	14	2	13.8 (rounded to 14)
5	130	5,000	10,000	65.4	AR4000	16	0	16
	10	5,000	10,000	65.4	AR4000	13	0	13

$\log N_f = 0.0068 * T + 0.0274 * S_{mix} - 0.961$ (2)

(Environmental Condition 2)

$\log N_f = 0.0021 * T + 0.0968 * S_{mix} - 0.177$ (3)

(Environmental Condition 3)

$\log N_f = 0.0023 * T + 0.0447 * S_{mix} + 0.541$ (4)

(Environmental Condition 4)

$\log N_f = 0.00023 * T + 0.00116 * S_{mix} + 1.236$ (5)

(Environmental Condition 5)

where

N_f = wheel load repetitions (on the highway) in 0.13 million for Equation 1 and 1.3 million for Equations 2 through 5;

T = tensile breaking stress (lb/in.²); and

S_{mix} = stiffness of the mix.

The stiffness of the mix was obtained in uniaxial creep tests conducted at the design asphalt content. The creep tests were needed for checking the rutting distress. Therefore, the results of the creep tests at the design asphalt content were used. The results of creep tests at 6 percent asphalt content could also be used. This would change the coefficients in the regression equations and require extra work on the part of the field engineer.

TABLE 8 Summary of Statistical Analysis of Fatigue Equations

Environmental Condition	R-Squared	Std. Error of Y-est.	T- Values		Degrees of Freedom	
			Calculated	Critical		
			Ten. Stress	S_{mix}		
1	0.824	0.243	2.168	2.684	2.064	21
2	0.913	0.238	2.141	2.283	2.064	21
3.	0.898	0.122	2.135	3.722	2.048	25
4.	0.934	0.068	7.068	2.178	2.052	24
5.	0.934	0.014	3.225	5.116	2.048	25

Check for Rutting

Using the results of the creep tests, rut depths were verified for the pavement sections by the procedure originally developed by the Shell researchers (12) and modified by Monismith et al. (1). The rut depths were found to be within acceptable limits, as shown in Table 9.

WORKED-OUT EXAMPLE

Given

The following conditions are assumed: Environmental Condition 3; maximum MMPT = 85.3°F; MMAT = 74.3°F; MMPTs for each month given in Table 3; asphalt, AR 4000; aggregate, California standard medium gradation, 0.5-in. maximum size; base, untreated aggregate 12 in. thick; traffic, 10 million standard axles; subgrade stiffness: 10,000 lb/in.²; base stiffness, 20,000 lb/in.²

Procedure

1. First trial thickness is 12 in. (from Figure 14).
2. Second trial thickness is computed as follows: direct tensile breaking stress at an MMPT of 85.3°F, 155 lb/in.² for 6 percent asphalt content and AR 4000 asphalt (from Figure 8); S_{mix} , 130,000 lb/in.² (from Figure 3); fatigue bending stress, 42 lb/in.² (from Figure 12, for 155 lb/in.² direct tensile stress and from Curve 5). Therefore, second trial thickness = 19 in. (from Figure 10), for the S_{mix} of 130,000 lb/in.² and the fatigue bending stress of 42 lb/in.²
3. Design thickness is 21 in. (from Table 3).

STRATEGY DEVELOPED IN THIS STUDY COMPARED WITH THAT OF OTHER METHODS

LCPC Method

In the LCPC (France) procedure the tensile strain corresponding to 1 million applications is estimated from a regres-

sion equation (5). The data indicated excellent correlation between the estimated strain and that measured in controlled strain fatigue tests at 10°C (50°F) conducted at a frequency of 25 Hz (5). With the data obtained from the test program, an elastic quality indicator was calculated. This elastic quality indicator is the thickness of asphalt concrete required to sustain 1 million repetitions (using the estimated strain at 1 million repetitions from the tensile test sequence) of a 130-kN axle load when the modulus of the subgrade is 100 MPa and the stiffness of the mix is determined from the test data at 10°C and at a time of loading 0.02 sec.

Modifications Incorporated into this Study

Effect of Temperature

In this study the effect of temperature, ranging from 68°F to 110°F (which covers the state of California), on the design of asphalt concrete layers can be determined with fatigue as the major concern.

Mode of Loading

Monismith et al. (1) have shown that controlled stress type of loading is more appropriate for thick asphalt pavements, whereas a controlled strain mode of loading is more suitable for thin asphalt pavements. In the LCPC method, controlled strain tests were followed, whereas in the present study controlled stress tests were conducted because in this investigation only thick asphalt pavements were considered.

Asphalt Institute Method

Effect of Temperature and Asphalt Type

There is a provision, to some extent, in the Asphalt Institute's method of thickness design for estimating the effect of temperature on the design thickness (10). The charts of the MS-1 manual show the influence of mean annual air temperature (MAAT) for a limited range of 45°F to 75°F on the thickness of AC layer for a given subgrade modulus. In this (the Asphalt Institute's) method, MAAT has to be averaged for the entire 1-year period.

The present study can account for the influence of air temperature for each month. In most of the cases, about 75% of the design life of the highway is consumed in the two hottest months. The Asphalt Institute's method does not account for the asphalt type, whereas the present study can determine the influence of two types of asphalts that are used in the state of California (AR 4000 and AR 8000) on the design thickness of the AC layer. Table 10 compares the AC layer thicknesses obtained in the present investigation with those designed by the Asphalt Institute's method. Results from this study at the moderately high air temperature of 75°F using AR 8000 asphalt and at the low air temperature of 60°F using AR 4000 asphalt agree closely with those obtained by the Asphalt Institute's method.

TABLE 9 Summary of Rut Depth Predictions

Sl. No.	Environmental Condition	Asphalt Type	Rut Depth Inches	mm
1	1	AR8000	0.053	1.3
2	1	AR4000	0.067	1.7
3	2	AR8000	0.042	1.0
4	2	AR4000	0.055	1.4
5	3	AR8000	0.040	1.0
6	3	AR4000	0.051	1.3
7	4	AR8000	0.030	0.7
8	4	AR4000	0.036	0.9

TABLE 10 Comparison of AC Layer Thicknesses Obtained by Study and Asphalt Institute Method (Traffic = 10 million, Subgrade E = 10,000 lb/in.²)

ASPHALT INSTITUTE METHOD			PRESENT STUDY					
MMAT (°F)	AC THICKNESS		Max. Asphalt MMPT Type (°F)	Tensile Stress (Psi)	Bending Stress (Psi)	AC THICKNESS		
	Full Depth AC (In)	12 In. Base (In)				Full Depth AC (In)	12 In. Base (In)	
75	15	13	83	AR8000	255	45	16.5	16
60	14	12	68	AR8000	700	92	8.5	8
				AR4000	580	52	13.5	13

Influence of Base Thickness on Design Thickness of Asphalt Concrete

The Asphalt Institute's method cannot identify the effect of base thickness on the design thickness of the asphalt layer. The design strategy of the present study determines the optimal base thickness and corresponding AC thickness so that the total project cost is minimized. The maximum base thickness that could be used by the Asphalt Institute's method is only 18 in. whereas, in this study, up to 24 in. of base can be analyzed.

DESIGN IMPLICATIONS

The maximum resistance to permanent deformation without the loss of the required stability can be obtained by designing the AC layer with an asphalt content that is obtained by the Hveem procedure. Epps (4) showed that optimal fatigue performance for the dense-graded mixes occurs at an asphalt content (by weight of aggregate) about 0.8 percent higher than that of the stability requirement. For all the cases analyzed in this study the minimum thickness of AC layer was 16 in. For this thickness the vertical stress (100-lb/in.² tire pressure and 4,500-lb dual wheel load) at the bottom of the AC layer would be on the order of 3 to 5 lb/in.², and the pavement temperature would be on the order of 92°F (Environmental Condition 4 has the maximum temperature among all the conditions). For such a low vertical stress and temperature, a slight increase in asphalt content would be justified to obtain the benefit of increased fatigue performance without losing the resistance to permanent deformation. Therefore, only at the bottom 2 in. of the AC layer might the design asphalt content be increased to 5.7 percent (the target content of 6.0 percent was reduced by 0.3 percent because of construction quality control considerations).

SUMMARY

1. Hveem stabilometer tests were used to derive the design asphalt contents.

2. Optimal resistance to fatigue with a check on rutting was obtained by recommending a design asphalt content of 5.2 percent (obtained by the Hveem method) in the AC layer, except in the bottom 2 in. where 5.7 percent asphalt content is recommended.

3. Tables were prepared for the design of heavy-duty pavements with fatigue as the dominant concern for the environment and traffic conditions that exist in the state of California. These tables enable the field engineer to design highways without conducting the fatigue tests, which are costly and time consuming and require special equipment, and with materials commonly used in the state of California (Watsonville granite aggregate and AR 4000 and AR 8000 asphalt cements). The two parameters needed by the field engineer are tensile strength and stiffness of the mix.

4. Equations were derived to predict the fatigue life of the AC layer for each environmental condition by using the direct tensile stress and stiffness of the mix. These equations had large coefficients of correlation between the independent and dependent variables. The correlation coefficients are statistically significant at the 95 percent confidence interval.

REFERENCES

1. C. L. Monismith, F. N. Finn, and B. A. Vallerga. A Comprehensive Asphalt Concrete Mix Design System. Presented at ASTM Symposium, Ball Harbor, 1987.
2. *Test Methods 366, Materials Manual*, Vol. 2. California Department of Transportation, Sacramento, 1978.
3. C. S. Rao. *Development of Asphalt Aggregate Mixture and Analysis System*. Ph.D. dissertation. University of California, Berkeley, 1989.
4. J. A. Epps. *Influence of Mixtures Variables on the Flexural Fatigue and Tensile Properties of Asphalt Concrete*. Ph.D. dissertation, University of California, Berkeley, 1968.
5. J. Bonnot. Asphalt Aggregate Mixtures. In *Transportation Research Record 1096*, TRB National Research Council, Washington, D.C., 1986, pp. 42-51.
6. C. S. Rao, J. Crause, J. A. Deacon, and C. L. Monismith. *Summary Report on Fatigue Response of Asphalt Mixtures*. TM-UCB-A-003A-89-3. ITS, University of California, Berkeley, 1990.
7. F. N. Finn, C. Saraf, R. Kulakarni, K. Nair, W. Smith, and A. Abdullah. The Use of Distress Prediction Subsystems for the Design of Pavement Structures. *Fourth International Conference of the Structural Design of Asphalt Pavement*, Vol. 1, Ann Arbor, Mich., 1977, pp. 3-38.

8. *Monthly Normals of Temperature, Precipitation and Heating and Cooling Degree Days: 1951-80*. U.S. Environmental Data Service, Department of Commerce, 1982.
9. M. W. Witzak. Design of Full Depth Asp. Airfield Pavements. *Proc. 3rd International Conference on the Structural Design of Asphalt Pavement*, Ann Arbor, Mich., Vol. 1, 1972, pp. 550-567.
10. Thickness Design—Asphalt Pavements for Highways and Streets. MS-1. The Asphalt Institute, College Park, 1981, pp. 39-195.
11. *Climatological Data, California*. U.S. Weather Bureau, 1988-1974.
12. *Shell Pavement Design Manual*. Shell International, London, 1977.

Publication of this paper sponsored by Committee on Flexible Pavement Design.

Rehabilitation Procedures for Faulted Rigid Pavement

LUIS JULIAN BENDAÑA AND WEI-SHIH YANG

Faulting of transverse joints in rigid pavements generally has not been a problem in New York, but a change in load-transfer devices (LTDs) between 1960 and 1972 produced significant faulting in pavements with high-volume truck traffic. The results of an 8-year study conducted on Interstate 84 are described. Constructed in the late 1960s, I-84 is a four-lane, 23-cm-thick concrete highway with 18.55-m joint spacing. As a result of failure of LTDs and heavy commercial traffic, faulting became a significant problem in the 1970s. In 1980 a study was begun to determine the most efficient method of removing the faults. After the first 2 years of field study, it was determined that where truck traffic is heavy, it is absolutely necessary to restore load-transfer capability with retrofitted LTDs to minimize pumping and loss of support that result in faulting. In 1983 the study was extended to establish criteria for effective procedures of fault removal and load-transfer restoration. By 1985 the magnitude of faulting at joints not retrofitted was already as great as when faults had been corrected. A second phase of the study thus was initiated to evaluate the effectiveness of LTD replacement in keeping faults from recurring. Two LTDs—the University of Illinois retrofit (the double-V device) and I-beam dowel bars—were installed from 1982 to 1985, retrofitting 289 joints at various locations on I-84. Their performance was evaluated by comparing (a) the rate of faulting return, (b) magnitude of differential joint movement, and (c) distress indexes. Construction and field testing of the LTDs are described, and their effectiveness in removing faulting and restoring load transfer is compared. From the findings, rehabilitation strategies are suggested.

The New York State portion of Interstate 84 was constructed under 16 contracts let between 1962 and 1968. The pavement is 23-cm-thick portland cement concrete with transverse joints spaced at 18.55-m intervals. Each joint had a two-component, malleable-iron load-transfer device (LTD) (Figure 1). The highway is an important connector for traffic flowing to and from New England and the South—the only Interstate route in the area that bypasses the New York City area and thus a heavily used truck route. By the mid-1970s, traffic counts along its length showed annual average daily traffic (AADT) of 8,000 to 17,000 vehicles, with 20 to 32 percent trucks.

In 1976 maintenance personnel observed significant faulting problems at transverse joints in various locations on I-84; in many cases the faulting was more than 2.5 cm. After an average of 10 years of service, faulting had grown so great that trucks were driving in the passing lane to avoid the discomfort of dropping at each faulted joint. The result was a good pavement surface and bad joints.

Engineering Research and Development Bureau, New York State Department of Transportation, State Campus, Albany, N.Y. 12232.

In 1977 a task force was formed to investigate causes of the transverse joint faulting problem and determine inherent implications for future rehabilitation work. In 1978 they recommended (1) that

1. The pavement not be overlaid,
2. The pavement not be "slabjacked" by contract,
3. Faulted joints be milled,
4. All transverse joints be resealed when restoration or alleviation work was done, and
5. Edge drains be designed into all plans for restoration or alleviation work.

In 1980 a study was initiated to determine the most efficient method of removing faults. The first phase investigated two methods of removing faulting at transverse joints: (a) lifting the slabs and then filling the underlying voids in the subbase and (b) grinding the pavement surface. In 1983 the study was extended to evaluate effective fault removal and load-transfer restoration procedures. A total of 289 joints were retrofitted using various LTDs between 1982 and 1985. The restoration methods were evaluated by comparing

1. Rate of faulting return,
2. Magnitude of differential vertical joint movements (DVJMs),
3. Magnitude of differential horizontal joint movements (DHJMs), and
4. Distress indexes.

This paper contains a description of the construction and field testing of those methods, and the performance of each rehabilitation technique is documented. The work is more fully discussed in Research Report 158 of New York's Engineering Research and Development Bureau (2).

In jointed reinforced-concrete pavements, LTDs are provided to transfer loads applied by traffic from one slab to the next and to minimize vertical deflection at the joint. Insufficient load transfer at the joint increases the potential for faulting and pumping by magnifying vertical deflections. Because of the importance of LTDs in maintaining pavement service life, their performance has been a major concern in New York State.

Inadequate horizontal slab movement, joint lockup, concrete cracking, and loss of load transfer experienced with steel dowels led in 1960 to introduction of two-component, malleable-iron devices (Figure 1). However, these new devices proved to be less efficient than the dowels, eventually losing metal because of corrosion and wear and thus failing

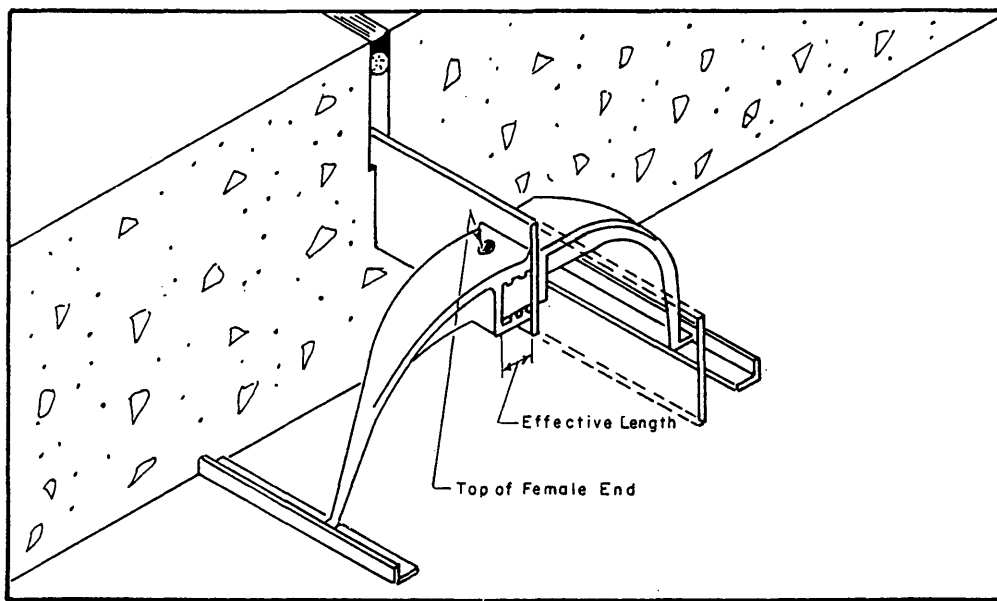


FIGURE 1 Configuration of two-component load-transfer device.

in load-transfer capability. As these problems became apparent, use of these devices was discontinued and plastic-coated or epoxy-coated dowels and I-beams were substituted. The problem now was how to restore load-transfer capability to the two-component devices that were reaching the stage at which they became ineffective, resulting in severe faulting and related distress.

In the past, faulting occurred slowly and coincided with other forms of distress; the general remedy was to overlay the pavement with asphalt concrete. More recently, however, the combination of relatively rapid loss of LTD efficiency and increasingly heavy truck traffic—both in volume and in weight—led to earlier and more severe faulting. Frequently the concrete slabs remained in fairly good condition, but the faulting appeared relatively early in life of the pavement. The New York State Department of Transportation (NYSDOT) began considering alternatives to overlaying the concrete. Two problems were involved: (a) repairing distress to restore riding quality and (b) developing procedures to retard recurrence of the distress.

INVESTIGATION

First-Phase Evaluations (1977)

In 1977 the task force formed to investigate I-84 pavement condition began collecting data. Several indexes of deterioration were measured—faulting, differential vertical and horizontal movements, and pavement cracking. Truck traffic data were also collected.

Faulting Measurements

All faulting data were collected in the travel lane, because field inspection showed little or no faulting in the passing lane. Faulting was measured to the nearest 1.6 mm and joint sealer condition was recorded for both lanes at more than 700 joints. Previous work had shown that faulting became noticeable to the motorist when it averaged 3.2 mm and objectionable at 4.8 to 6.4 mm. Faulting measurements are given in Table 1,

TABLE 1 1977 Condition Survey of I-84 Transverse Joints

Range of Faulting, 1/16 in.	Total Readings (two/joint)	Actual Average Faulting, 1/16 in.	% of Readings Showing Faulting	% of Joints With Faulting \geq Range Shown
1.1-2.0	111	1.5	7.85	100.00
2.1-3.0	243	2.6	17.20	92.15
3.1-4.0	603	3.3	42.60	74.95
4.1-5.0	24	4.8	1.70	32.30
5.1-6.0	330	5.3	23.30	30.60
6.1-7.0	17	6.2	1.20	7.30
>7.1	86	10.3	6.10	6.10

(1 mm = 0.04 in.).

where it can be noted that 92 percent of the readings were over 3.2 mm by 1977, putting the faulting in the noticeable range and 75 percent were greater than 4.8 mm, making the faulting objectionable.

Differential Vertical Joint Movements

DVJMs of adjacent slabs across a transverse joint were measured using a truck with a 100-kN axle load, which was then the legal maximum single-axle load in New York State. Table 2 summarizes results of measuring DVJMs across transverse joints for four different faulting ranges to the nearest 25.4 μm . None of these movements were large (over 0.5 mm). Weather records showed no appreciable rainfall for nearly 2 weeks before these measurements, which meant that the pavement sections had received little infiltration of surface water. Table 2 data showed no trend between average faulting and DVJMs.

Pavement Cracking

The number of slabs with transverse, longitudinal, and corner cracks was recorded for the faulted sections. Table 3 is a summary of the number of slabs having such cracking and corresponding ranges of joint faulting. The most prevalent type is transverse cracks, appearing in close to 25 percent of the slabs in two of the faulting ranges. No trend appears between transverse faulting magnitude and percent of slabs with transverse cracking. However, a trend is evident between faulting and years of service (Table 4). A linear relationship appears between the first three faulting ranges and years of service of about 1.6 mm of faulting annually, but for the last two ranges the relationship is nonlinear with a higher rate of deterioration.

Truck Traffic

The most important and most difficult data to obtain concern traffic to which the pavement is subjected. Performance of a pavement such as I-84 with a high volume of trucks greatly depends on that traffic; that is, the number and configuration of axle loads that the pavement experiences will control its service life. A Viatic axle-weight analyzer was used to measure traffic loading. This device determines weights of moving

TABLE 2 Effects of Faulting on DVJM

Range of Faulting, 1/16 in.	Average Faulting, 1/16 in.	DVJMs, mils
1.1-2.0	1.7	0.3
3.1-4.0	3.5	0.3
6.1-7.0	6.6	12.1
>10.0	10.5	2.5

(1 mm = 0.04 in.).

axles and classifies them in 900-N categories. Measurements were made at several locations where significant changes in traffic volume were expected; counts were taken for 18 to 22 hr. The data were then converted to 24-hr periods and numbers of 80-kN equivalent single-axle loads (ESALs). Total ESALs for the years in service was determined with the following equation: $\text{ESAL} = \text{number of 80-kN ESALs/truck} \times \text{total truck traffic} + \text{number of 80-kN ESALs/car} \times (\text{total traffic} - \text{truck traffic})$. Table 4 summarizes these counts and gives faulting averages. A trend appears between faulting and total axle loads, but it seems less significant than that for increased faulting with age.

Visual Inspection from Test Pit

Once faulting begins, erosion of material under the slabs and inadequate load transfer across the joint contribute to a faster rate of faulting. Deflections induced by heavy wheel loads continue to increase faulting unless corrective measures are taken. To investigate magnitude of the settlement under the slab and corrosion of the LTDs, visual inspection was attempted from a test pit. At six locations, joint assemblies were removed from the right edge of the travel lane adjoining the shoulder. Pavements were sawcut and 60- by 90-cm rectangles were removed across transverse joints to include bearing portions of the LTDs. The test showed that at joints with little or no faulting, bearing surfaces remained in good-to-excellent condition. Otherwise, either or both portions of the sleeve-and-butt devices were corroded or sheared away, eliminating part or all of the load-transfer capability. In all instances, a ridge of soil material was found directly below the joint assembly, suggesting that pumping had occurred. The neoprene joint sealers were compressed and had lost much of their original shape.

TABLE 3 Faulting, Cracking, and Years in Service

Range of Faulting, 1/16 in.	Total Slabs	% of Slabs Having			Total Slabs With Cracks		
		Transverse Cracks	Years in Service		Transverse	Longitudinal	Corner
1.1-2.0	99	25	7	25	2	1	
2.1-3.0	247	19	8	47	1	4	
3.1-4.0	98	12	9	12	3	4	
4.1-5.0	659	8	11	49	9	25	
5.1-6.0	120	24	13	29	0	10	

(1 mm = 0.04 in.).

TABLE 4 Faulting, ESALs, and Years in Service

Range of Faulting, 1/16 in.	Actual Average Faulting, 1/16 in.	18-kip ESALs, millions	Years in Service
1.1-2.0	1.9	4.1	7
3.1-4.0	3.8	5.0	9
4.1-5.0	4.3	6.7	11
5.1-6.0	5.9	5.2	13
6.1-7.0	6.2	7.8	13

(1 mm = 0.04 in., 1 N = 0.225 lbf).

Second-Phase Evaluations (1979-1991)

Project Contracts

Test sections for this later study involved 116 km of I-84, covering 232 lane-km of the eastbound and westbound driving lanes (Figure 2). The project was divided into five contracts:

1. Contract 1 was located near Port Jervis, in Orange County, and had a total length of 7.4 km, including 3.5 km in the town of Deer Park and 3.9 km in the town of Greenville. Rehabilitation began in June 1979 because the I-84 task force survey had previously shown that joints in the driving lane were

badly faulted over most of the highway in both directions. The cause was determined to be the malleable-iron LTDs used from 1960 to 1972, the period during which most of I-84 was built. To correct the faulted pavement, various rehabilitation techniques were attempted, including full-width, full-length grinding of slabs, mechanical lifting and pump grouting, edge drains, resealing, and subsealing.

2. Contract 2 was located near Fishkill in Dutchess County on 7.66 km in the town of Fishkill. It called for a full-width, full-length grinding and subsealing with a fly-ash grout.

3. Contract 3, near the village of Ludingtonville in Putnam County, was awarded in May 1983, including 5.8 km eastbound in the towns of Kent and Patterson. It called for partial-length slab grinding at the rate of 38 cm/mm of faulting, edge drains, crushed-stone weeps, and resealing. The pavement was retrofitted with I-beam dowels and University of Illinois (UI) LTD devices (to be discussed later).

4. Contract 4 was called the "Penn-Conn" (Pennsylvania to Connecticut) contract. Awarded in May 1983, it covered all of I-84 from the western to eastern state lines, a length of 63.6 km in Orange County, 27.55 km in Dutchess County, and 15.10 km in Putnam County, with a total contract length of 106.25 km.

5. Contract 5 was used for administrative convenience to describe installation and monitoring of a group of improved mechanically precompressed retrofit LTDs supplied by the Dayton-Superior Corporation (manufacturer of the Illinois LTDs). As a result of early failure of previous retrofit LTDs

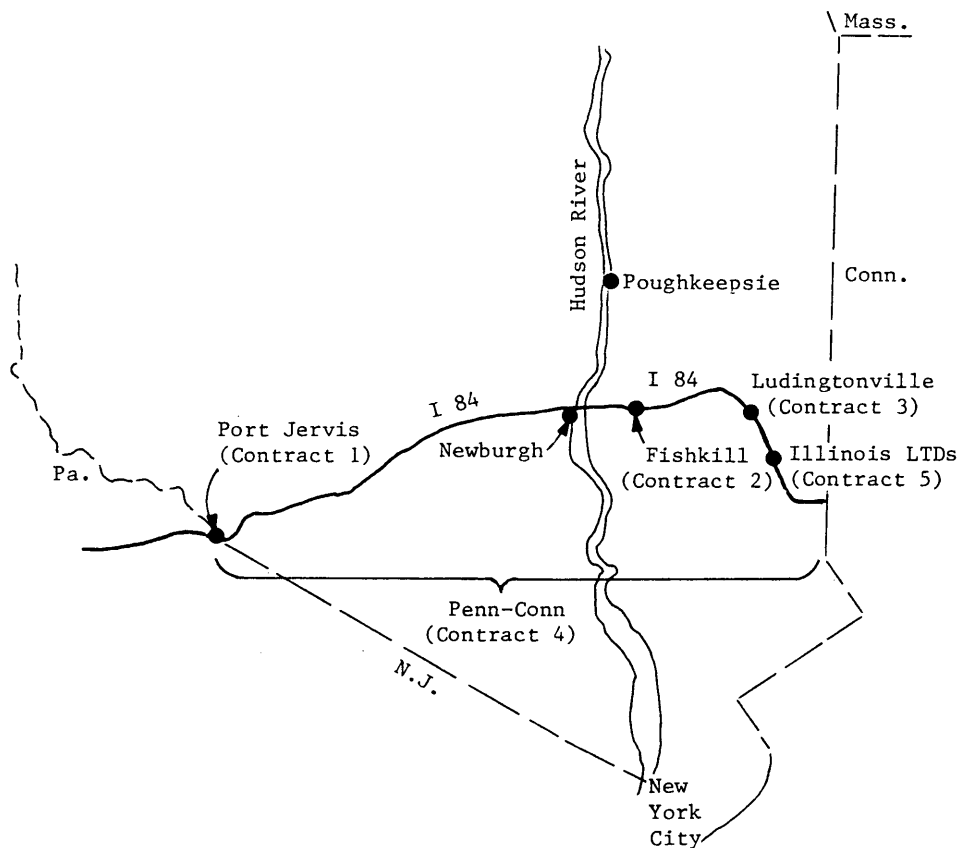


FIGURE 2 Locations of I-84 contracts and test sections.

of the Illinois design, the manufacturer developed a mechanically compressed version to replace it, which was to compensate for the wide joint openings experienced in winter. In 1985, 100 of these factory-compressed LTDs were installed, four per joint.

Rehabilitation Procedures

Fault Removal Without Restoration of Load Transfer For the first part of this later study two procedures were used to remove faulting at transverse joints without trying to restore load transfer across the joints: (a) lifting the slabs and then filling the underlying voids in the subbase and (b) grinding the pavement surface. The first method was achieved by lifting the slabs mechanically using several lifting procedures tested in the field. After the slabs were raised to the height of the adjoining slabs, a cement grout was pumped beneath them (1). The second method was grinding the pavement surface with a drum consisting of closely spaced diamond sawblades. The desired longitudinal profile was maintained by carrying the drum in an extended wheelbase. A vacuum-collecting device picked up the cooling water and fine particles during grinding. These two methods effectively reduced the magni-

tude of faulting without attempting to treat its cause. One problem encountered using lifting was that the slabs settled below the desired level when the jacks were released, forcing grout (thought to have set) from beneath them along the sides and into the transverse joint. Experience also showed that when grout is used to jack slabs, it is difficult to determine when all voids are filled and support is adequate.

Retrofitted LTDs In the second part of the study, two devices were installed and evaluated: University of Illinois (IU) LTDs [epoxy-coated (E), stainless steel (S), and pre-compressed (C)] and epoxy-coated I-beam dowel bars. The Illinois devices (Figure 3) were placed either three or four per joint. The retrofitted I-beam dowel bars (Figure 4) were in two configurations, four or eight per joint. Installation of the Illinois devices involved drilling a 15.25-cm core hole across the joint, applying polymer primer, inserting the device, and backfilling the hole with polymer concrete; the transverse joints were sawcut to remove the fiberboard bond breaker and form a sealer reservoir. The procedure for the I-beams consisted of making longitudinal grooves (slots) at least 7.6 cm wide and 46 cm long, preparing the slots using the same procedures as for the Illinois devices, installing the I-beams,

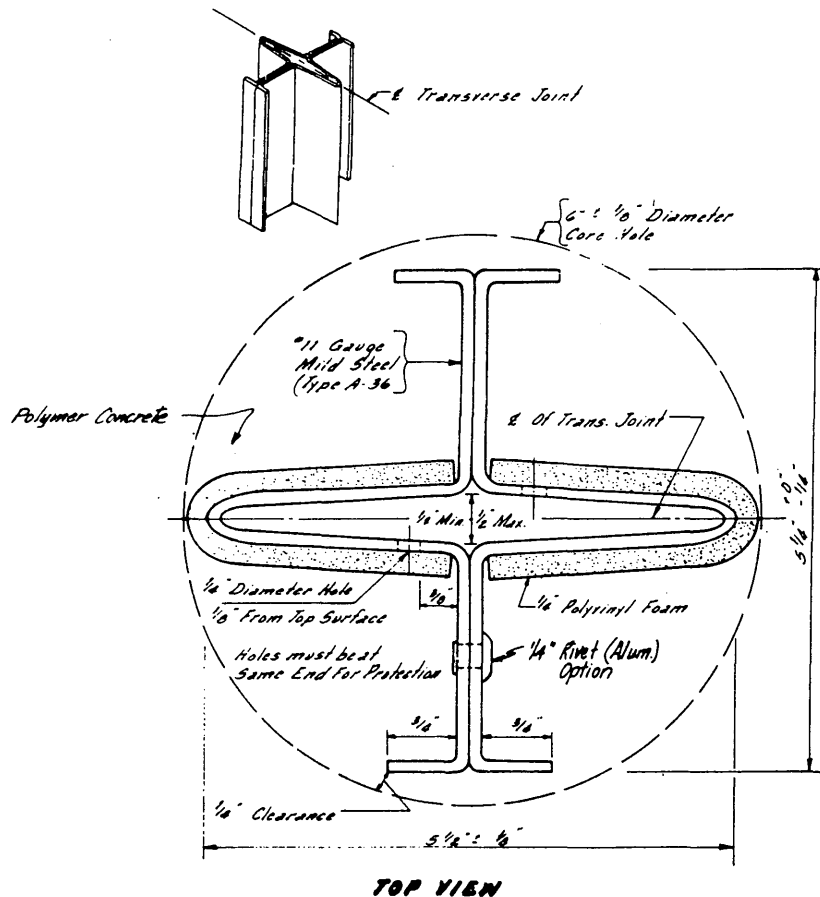


FIGURE 3 Configuration of University of Illinois double-V retrofit LTD (1 mm = 0.04 in.).

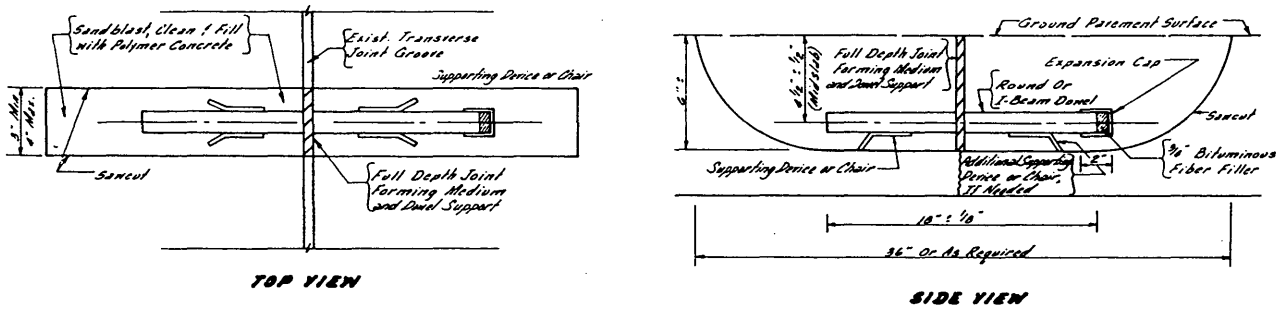


FIGURE 4 Configuration of I-beam retrofit LTD (1 mm = 0.04 in.).

filling the slots with polymer concrete, and sawcutting the transverse joints. Construction for these two LTDs followed two NYSDOT specification items [Contract for F.A. Project I-84-1 (I-84), March 3, 1983, Items 18502.3401 and 18502.3402] and was documented by Bernard (3). Spacing and orientation of the double-V and I-beam devices as used in this study are shown in Figure 5. They were installed while traffic was maintained in adjacent lanes, and the retrofitted lanes were opened to traffic after the polymer concrete cured for about 2 hr.

RESULTS AND DISCUSSION

Faulting

Because faulting was the major cause for the poor functional performance of I-84, all rehabilitation techniques studied were focused on its correction. Because of concern that too much concrete would be removed by grinding, it was decided to limit grinding to sections where average faulting was less than 2.5 cm and to lift joints that had greater faulting. However, for some joints exceeding this limit, grinding was permitted for uniform sections. Grinding and lifting effectively reduced the magnitude of faulting but failed to restore load transfer. Figure 6 shows faulting from 1980 to 1987 before and after

grinding. Grinding removed all faulting in 1980, but by 1985 average faulting was larger than before grinding. Fault return at joints that were lifted was about equal to that at joints that were ground. Final faulting at lifted joints was greater than that at ground joints, lifting having left some faulting (both positive and negative) that contributed to greater fault return.

Epoxy-coated Illinois (IUE) retrofit LTDs were installed in four joints in August 1982, an operation that was labor-intensive and time-consuming. It was hoped to gain experience installing the new devices and then monitor their performance. Average faulting for three- and four-Illinois-LTD installations (3UI and 4UI) was compared using a *t*-test; no significant difference was found. Thus, 3UI and 4UI were combined into a single Illinois group. Figure 6 compares these three approaches and shows the effectiveness of LTDs in retarding fault recurrence.

The Ludingtonville project (Contract 3) was specifically designed to solve the long-term faulting problem. To do this, the project scope was changed on the basis of information obtained during construction as well as postconstruction evaluation of the first two projects and availability of funds. The first two projects had included grinding the entire pavement, subsealing, underdraining, and sealing joints. In contrast, this contract called for partial grinding in the passing and driving lanes, selective subsealing, selective underdraining, sealing

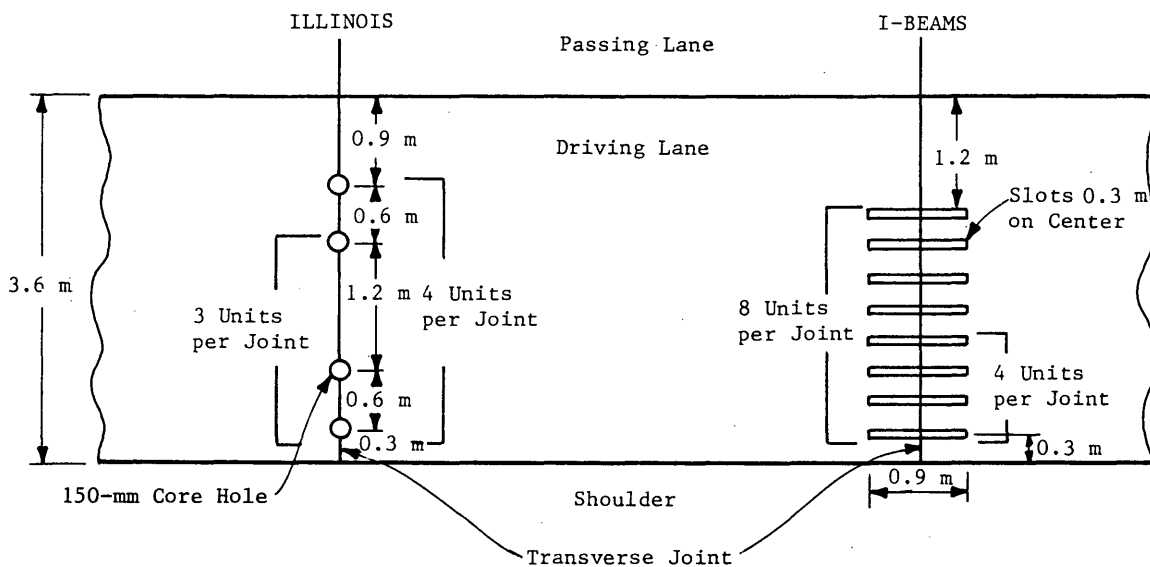


FIGURE 5 Spacings and orientations of Illinois and I-beam LTDs.

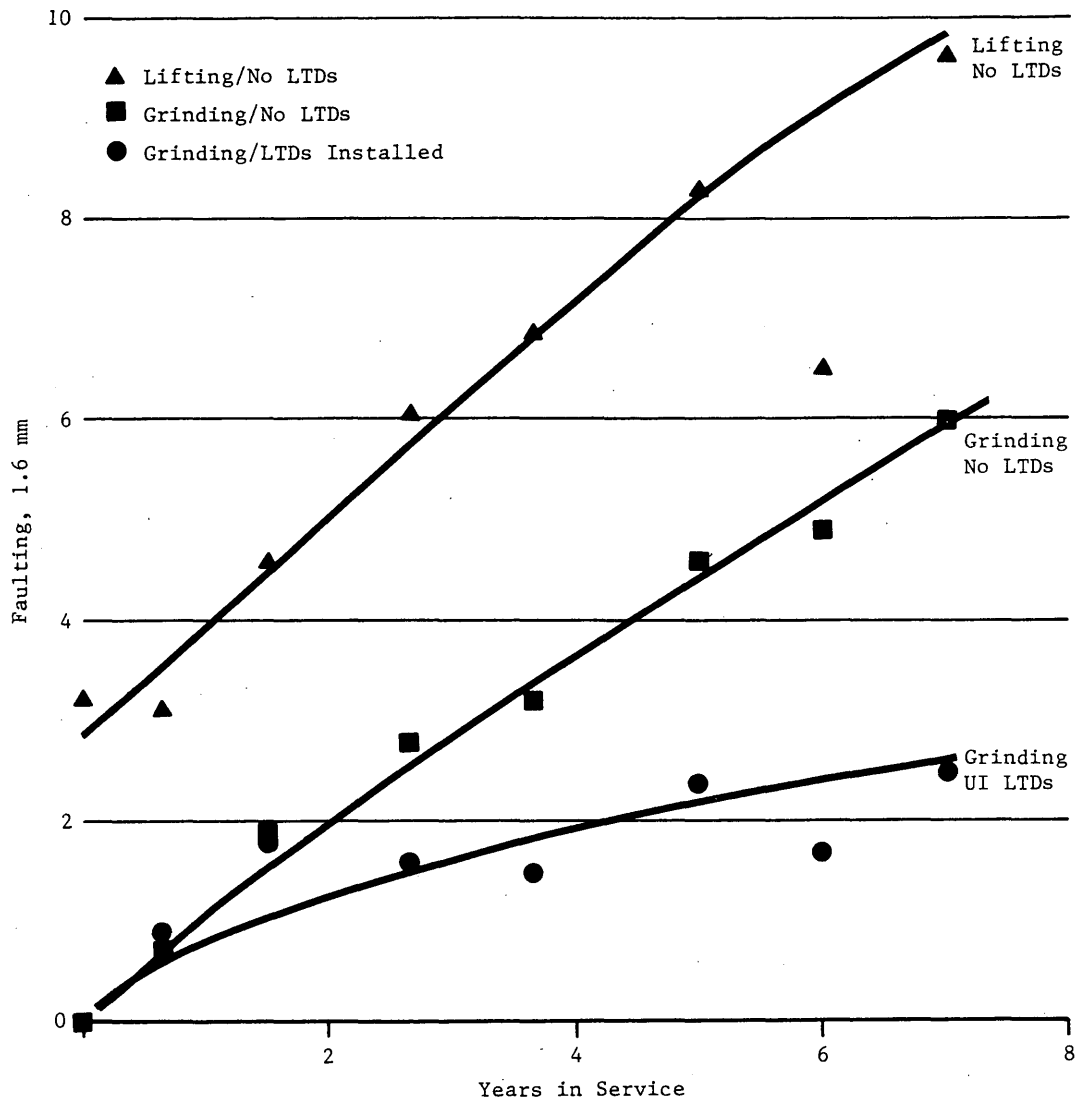


FIGURE 6 Contract 1 faulting with and without LTDs.

joints, and retrofitting LTDs. As in the previous two projects, construction was very difficult and labor-intensive.

Statistical analysis of Contract 3 faulting data showed no significant difference between 3UIE and 3UIS joints, which were thus combined for analysis into a single 3UI group. Four LTD groups could then be compared: 3UI, 4UI, four I-beam, and eight I-beam. Figure 7 summarizes faulting before and after grinding. In a comparison of the 3UI and 4UI joints, the former performed better, with an annual fault return of less than 0.8 mm. Paradoxically, the 4UI performed worse, with an annual fault return of 1.9 mm. Inadequate compaction of polymer concrete and improper aggregate gradation were two construction and materials problems noted, which caused poor performance of the 4UI joints.

The Penn-Conn project (Contract 4) had the same objectives as Contract 3, including partial slab grinding (38 cm horizontally per millimeter of fault), joint sealing, and retrofitting Illinois and I-beam LTDs along the entire highway length (except the road near Ludingtonville treated under Contract 3). Driving and passing lane joints with more than

4.8 mm of faulting were to be ground. To preserve earlier test sections at Port Jervis and Fishkill, several groups of joints were not to be ground even if faulting equaled or exceeded 4.8 mm. Annual survey results showed that performance of joints with retrofitted LTDs varied significantly from joints without them. In general, faulting of joints without LTDs had an annual return of about 2.4 mm compared with less than 1.6 mm for those with LTDs.

In Penn-Conn Contract 4, as at Ludingtonville (Contract 3), no significant difference was observed between the epoxy and steel Illinois LTDs, and they were combined into a single 3UI group. Penn-Conn faulting data for 3UI and 4UI were compared using a *t*-test; no significant difference was found. These two types had annual fault returns of about 1 mm after more than 3 years of service. Penn-Conn faulting data are shown in Figure 8.

In a comparison of the performance of the four and eight I-beam joints, the latter performed better, but the results also showed no proportionality between number of LTDs and annual fault return values. At Ludingtonville, increasing the

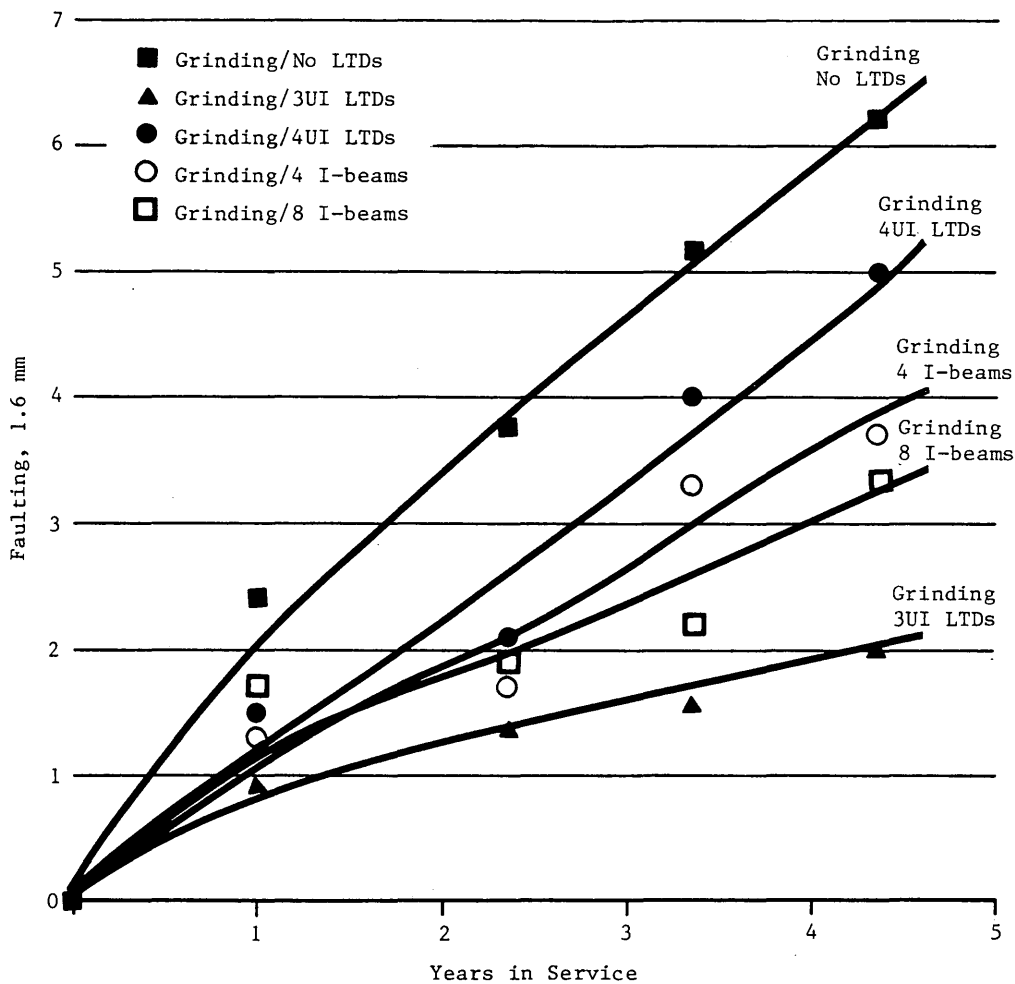


FIGURE 7 Contract 3 faulting with and without LTDs.

number of LTDs by 100 percent (from four to eight I-beams) improved performance by only 7 percent, from an annual fault return of 1.36 mm to 1.2 mm. In Contract 4 the same increase in total LTDs accounts for a 33 percent improvement, from an annual fault return of 1.06 to 0.67 mm. For the Illinois devices, the 33 percent increase in number of LTDs (from three to four) had no noticeable effect on performance. Quality of the patching material seemed to have the greatest effect on performance of Illinois LTDs.

In 1985, 100 factory-compressed Illinois LTDs were installed, four each in 25 joints in the eastbound lanes just east of Ludingtonville. Overall, this device performed better than any other tested, with an annual fault return of 0.42 mm, although only the first 2½ years of service was monitored.

Life-Cycle Cost Analysis

A simplified analysis compared cost-effectiveness of Illinois devices and I-beams. Five treatments were considered: joints with three or four epoxy-coated or stainless steel Illinois devices, joints with four precompressed Illinois devices, and joints with four or eight I-beams. A 4 percent discount rate

was used to compute life-cycle cost, using the following costs associated with rehabilitation work:

Retrofit (per mile)	Cost/Lane-Mile (\$)
Illinois device (each)	13,840
Dowels (each)	17,300
Grinding	23,252
Resealing	43,306

Life-cycle costs reported here were based on two failure criteria: faulting index and distress index. These were selected on the basis of the assumption of a proportionality between (a) faulting and performance and (b) distress and performance. For faulting it was assumed that a joint failed when average faulting reached 6.2 mm. For distress, if 50 percent of the LTD system showed such distress as cracking or debonding, the joint was considered to have failed. A rating scale from 0 to 100 (with 100 a perfect pavement) was used in computing faulting and distress indexes. Threshold values for both indexes were set at 70. The equations are as follows:

$$FI = 100 - 30 \times (\text{millimeters of faulting} \div 6.4)$$

$$DI = 100 - 30 \times (\text{percent cracked area} \div 50)$$

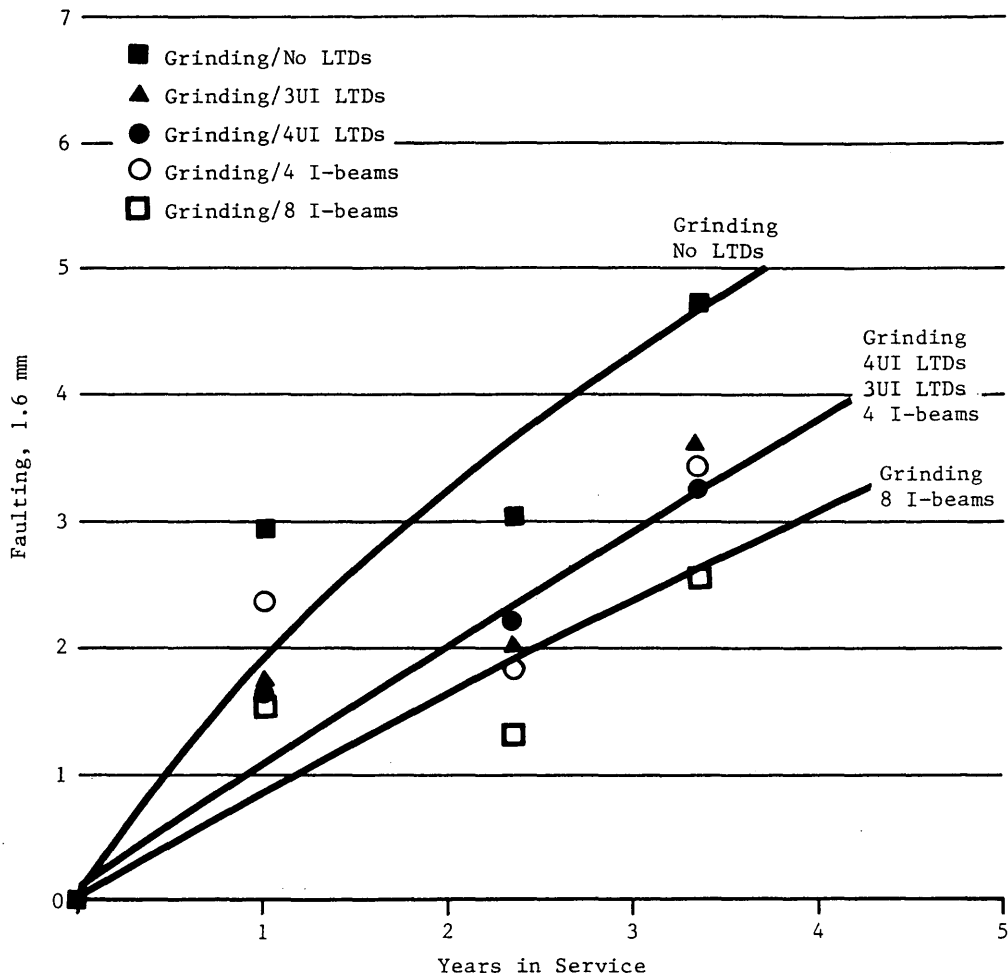


FIGURE 8 Contract 4 faulting with and without LTDs.

Contract 3 (Ludingtonville)

For Contract 3, faulting and distress indexes were used to determine the life of the various treatments. Based on the field data, the estimated life associated with the four treatments (2) for an FI of 70 was as follows (each treatment type includes grinding and subsealing):

Treatment Type	Years in Service
3UI	8
4UI	3
Four I-beams	5
Eight I-beams	6

Using the present worth method and the costs shown in the previous section, the results indicated that 3UI was the most cost-effective treatment, followed by four and eight I-beams, with 4UI last.

For a DI of 70, the years in service were as follows (each treatment type includes grinding and subsealing):

Treatment Type	Years in Service
3UI	3.5
4UI	2
Four I-beams	4
Eight I-beams	6

Using the present worth method and the same costs, the results again indicated that 3UI was the most cost-effective treatment, followed by four and eight I-beams, with 4UI last.

Contracts 4 and 5

For Contracts 4 and 5, faulting was the only factor used in determining the life of the various treatments. Besides the four treatments discussed for Contract 3, a fifth, the precompressed Illinois device (UIP), was included for the faulting analysis. Estimated years of service associated with those five treatments were as follows (each treatment type includes grinding and subsealing):

Treatment Type	Years in Service
3UI	4
4UI	4
4UIP	6
Four I-beams	4
Eight I-beams	5

The results indicated that 4UIP was the most cost-effective, followed by 3UI, 4UI, and four I-beams, with eight I-beams last.

Subsealing

This procedure restores the structural integrity of slab support by filling voids and providing an even surface. In Contract 1 (Port Jervis), subsealing with limestone grout was inadequate. Angularity of the limestone increased the mixture's viscosity, reducing its ability to flow freely beneath the slabs. This could have caused uneven support for the slabs, resulting in poor performance. Contract 2 (Fishkill) called for subsealing the entire project with a fly-ash grout, which flowed more freely than the limestone grout at Port Jervis and consequently performed far better.

Fishkill faulting data (grinding and subsealing without retrofitting LTDs) were compared with Penn-Conn data (grinding without LTDs) to investigate effectiveness of subsealing in retarding faulting recurrence. Since construction and material qualities were adequate at Fishkill and both contracts were without LTDs, the comparison is technically correct. At Fishkill after 6 years of service, the magnitude of faulting was 7.85 mm, with an annual fault return of 1.32 mm versus Penn-Conn with 7.6 mm of faulting and an annual fault return of 2.16 mm after almost 3½ years. This indicates that subsealing, done properly, does reduce fault return.

Differential Vertical Joint Movements

In this study DVJM values were directly measured using a truck with a 100-kN single-axle load. Since with this method the deflections of the approach and leave slabs are unknown, load-transfer efficiency could not be computed. The magnitude of the DVJM values thus may result from such other factors as humidity, temperature, and aggregate interlock, but not necessarily from load-transfer efficiency. DVJM values were used here to compare degree of load transfer between adjacent slabs for the different procedures tested, using engineering judgment to account for environmental conditions.

At Port Jervis (Contract 1), DVJM was measured at transverse joints before and after LTD installation. On the average, DVJM values changed from 660 μm at 19 C without retrofitted LTDs to 162 μm at 12 C with them, indicating good load transfer.

Distress Survey and Construction Problems (Contract 3)

During the surveys each LTD system was visually inspected after installation. The concern was to establish whether LTD system performance was affected solely by the devices themselves or by other factors (such as quality control during construction and quality of patching material). The types of distress recorded were circle and hairline cracks, crushing of the patch over the retrofit device, and debonding between patching material and old concrete.

Polymer primer and polymer concrete were used to bond the retrofitted Illinois and I-beam devices to the concrete slab. Dowel performance in bonding was good, with no I-beam debonding found 10 months after installation. A 16 percent

debonding rate, however, was recorded for the Illinois devices. After a review of construction procedures, it was determined that poor polymer concrete consolidation and insufficient primer adhesion were the primary reasons for the high debonding rate. It was concluded that under no circumstances should polymer primer be used on a wet concrete surface.

A field inspection on October 19, 1983, showed that 8 of 85 Illinois LTDs were displaying cracks at joints between polymer and old concrete. By October 26, the number had increased to 24. A follow-up inspection on November 14 indicated that about 40 were showing cracks. Coring revealed that the polymer concrete was not consolidated and that many voids existed between LTD flanges and the core hole walls. In 1984 a condition survey reported that 46 of 304 Illinois LTDs were showing cracks, with 44 of these 46 failing on the leave slab. Thirty of those 46 had been placed on the first day, the same day that wrong aggregate size and wrong type of primer application brush were noted.

To compare effectiveness of the LTD systems in preventing fault recurrence, it was necessary to include in the analysis the quality of construction materials and quality control during construction. The latter was assessed by computing the percent of LTDs showing distress. If quality control and material quality are the same for both LTD types, it thus is technically correct to compare them on the basis of fault return alone. Figure 7 shows faulting for the 4UI and 3UI LTDs. An erroneous conclusion could be drawn from this graph if distress is not considered. It is reasonable to expect that 4UI LTDs will perform far better than 3UI LTDs if both are subjected to the same number of stress repetitions. However, looking at the fault return rate, the 4UI has a higher rate than the 3UI but more failures, reflected by their poor performance. Data collected for the 4UI thus cannot be used to quantify effectiveness of only the LTD, but rather the entire LTD system, since poor construction practices and material quality were found to control its behavior.

Long-term performance of a load-transfer system depends on adequate performance of all its components. For retrofitting, these include

1. Construction quality control,
2. Good patching material quality,
3. Sound concrete slabs, and
4. Adequate load-transfer devices.

The system can be represented by a series of models. Failure of any component causes the system to fail. This model is a reasonable and convenient approximation of actual performance of a load-transfer system. For example, the patching material component has the reliability function $R_i(t)$. Then the probability that the system will survive to time t is the probability that all the components simultaneously will survive to time t . Probability of system survival is the product of the individual probabilities of survival. The reliability function of the system is

$$R_{\text{system}} = R_{\text{construction quality control}} \times R_{\text{good patching material}} \times R_{\text{sound concrete slabs}} \times R_{\text{adequate LTDs}}$$

Differential Horizontal Joint Movements

For a joint to perform adequately, its LTDs should accommodate expansion and contraction movements due to temperature change. If horizontal movement is restricted, slabs may crack. In this study, DHJMs were measured to determine if LTDs under consideration allowed horizontal expansion and contraction at joints. DHJM data (2) indicate that all LTDs in this experiment did permit horizontal movement.

CONCLUSIONS AND RECOMMENDATIONS

The following conclusions and recommendations can be drawn from these results:

1. Interstate 84 restoration proved that concrete pavement joint retrofitting is appropriate when slabs are in good-to-excellent condition and distress is mostly due to LTD deficiencies at the joints. On the other hand, when a pavement has lost its structural integrity, retrofitting is not recommended.

2. Total traffic loading is the major factor that accelerates or decelerates failure. This study proved that retrofitting is essential to retard fault recurrence when a pavement is subjected to such heavy traffic loading as there is on I-84.

3. The faulting mechanism implies that voids are present under the leave slab. Thus, if there is faulting, subsealing is recommended before any LTDs are placed, to prevent a rapid breakup of the slab. However, careful attention to construction practice is important because insufficient grout may not reduce deflections and too much grout could easily result in more broken slabs by providing an uneven support. Excessive grout also fills the transverse joints, which may cause blowups.

4. Other researchers (4) have indicated that at least four dowels should be used in each wheelpath for adequate load transfer between slabs. However, results from this study in-

dicate that using fewer than four dowels in each wheelpath may be satisfactory. The gain in performance by using four rather than two dowels per wheelpath was not significant. Additional field experimentation is needed to determine the optimum combination of size and spacing.

5. Patching material for the I-beams was found to be less critical than for the Illinois shear devices.

6. Results of life-cycle cost analyses indicate that Illinois LTDs are the most cost-effective method of load-transfer restoration if good construction quality control and good quality patching material are provided.

ACKNOWLEDGMENT

The research reported here was conducted in cooperation with the Federal Highway Administration, U.S. Department of Transportation.

REFERENCES

1. *Portland Cement Concrete Pavement Performance, Interstate 84: Pennsylvania State Line to Connecticut State Line*. Soil Mechanics Bureau, New York State Department of Transportation, Albany, March 1978.
2. L. J. Bendaña and W-S. Yang. *Rehabilitation Procedures for Faulted Rigid Pavement*. Research Report 158. Engineering Research and Development Bureau, New York State Department of Transportation, Albany, Nov. 1992.
3. D. W. Bernard. *A Construction Report on Reestablishing Load Transfer in Concrete Pavement Transverse Joints*. Technical Report 84-6. Materials Bureau, New York State Department of Transportation, Albany, Sept. 1984.
4. K. W. Heinrichs, J. J. Liu, M. I. Darter, S. H. Carpenter, and A. M. Ioannides. *Rigid Pavement Analysis and Design*. Report FHWA-RD-88-068. Department of Civil Engineering, University of Illinois, Urbana-Champaign, June 1989.

Publication of this paper sponsored by Committee on Pavement Rehabilitation.